FLUTTER TESTING TECHNIQUES

A conference held at
RYDEN FLIGHT RESEARCH CENTER
Edwards, California
October 9-10, 1975

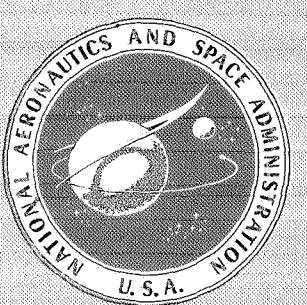

NATIONAL AERONAUTICS AND SPACE ADMINISTRATION

FLUTTER TESTING TECHNIQUES

The proceedings of a conference held at the Dryden Flight Research Center in Edwards, California, on October 9–10, 1975

Prepared by Langley Research Center

Scientific and Technical Information Office 1976
NATIONAL AERONAUTICS AND SPACE ADMINISTRATION
Washington, D.C.

For sale by the National Technical Information Service
Springfield, Virginia 22161
Price – $12.50

FOREWORD

This document is a compilation of 19 technical papers and comments from a panel discussion presented during a symposium on Flutter Testing Techniques that was held at the NASA Hugh L. Dryden Flight Research Center, Edwards, California, October 9-10, 1975. Sponsored jointly by the NASA Hugh L. Dryden Flight Research Center and the NASA Langley Research Center in conjunction with the U.S. Air Force Wright Aeronautical Laboratory, the U.S. Navy Air Systems Command, and the Aerospace Flutter and Dynamics Council, the symposium focused on recent developments in flutter testing in flight and on the ground and on new methods and techniques for improving flutter testing and data analysis.

The idea for this symposium germinated during the 1974 fall meeting of the Aerospace Flutter and Dynamics Council. There were several reasons for holding a symposium on flutter testing; among them was the lack of a comprehensive forum on flutter testing since the Flight Flutter Testing Symposium held May 15-16, 1958. In addition, major advances have been made in equipment and facilities since that date. These advances have led to the creation of new techniques for testing and analysis that have been evaluated during the development of new aircraft from the testing of models during design to the flutter clearance of the flight vehicles. Thus, this symposium provided an opportunity to discuss and evaluate the state of the art for flutter testing. The symposium should also serve to encourage research in the field, resulting in further improvements in the methods used and safer and less costly testing techniques.

On behalf of the symposium committee, I would like to thank the authors for their fine papers, the session chairmen for their invaluable assistance, and the panel members for sharing their experience and insight into flutter technology.

The papers contained in this compilation have been edited only for clarity and format. Technical contents and views expressed are the responsibility and opinions of the individual authors.

Eldon E. Kordes
Chairman

COMMITTEES

SYMPOSIUM COMMITTEE:

Eldon E. Kordes, General Chairman
NASA Flight Research Center

Wilmer H. Reed III
NASA Langley Research Center

Walter J. Mykytow
Air Force Wright Aeronautical Laboratory

George P. Maggos
Naval Systems Command

Clarence H. Perisho
Aerospace Flutter and Dynamics Council

TECHNICAL PROGRAM COMMITTEE:

Clarence H. Perisho, Chairman
McDonnell Douglas Corporation

Mike H. Abla
Gates Learjet Company

Jack B. Bartley
Boeing Commercial Airplane Company

William F. Grosser
Lockheed Georgia Company

Robert A. Ormiston
U.S. Army Mobility R&D Laboratory

Raymond P. Peloubet
Convair Aerospace Division, General Dynamics Corporation

Wilmer H. Reed III
NASA Langley Research Center

Jing G. Yen
Bell Helicopter Company

PUBLICATION:

Wilmer H. Reed III
NASA Langley Research Center

LOCAL ARRANGEMENTS AND GENERAL ASSISTANCE:

Trudy Tiedemann
NASA Flight Research Center

B. Lyle Schofield
Air Force Flight Test Center

CONTENTS

ON IDENTIFYING FREQUENCIES AND DAMPING IN SUBCRITICAL FLUTTER TESTING

John C. Houbolt

Aeronautical Research Associates of Princeton, Inc.

SUMMARY

A review is given of various procedures that might be used in evaluating system response characteristics as involved in subcritical flight and wind-tunnel flutter testing of aircraft. Emphasis is given to the means for eliminating or minimizing the contamination effects produced by an unknown noise in the input. Results of a newly developed procedure for identifying modal frequency and damping values, and a possible way for making a detailed evaluation of system parameters, are also given.

INTRODUCTION

The purpose of this report is to give a review of various procedures that might be used in evaluating system response characteristics as involved in subcritical flight and wind tunnel flutter testing of aircraft. The aim in such testing is generally to evaluate modal damping and frequencies as a function of flight speed. In some cases, studies aim to identify the system parameters in greater detail, such as identifying the coefficients of a modelled differential equation of motion.

In practical subcritical flutter testing three main problems arise: (1) there usually is an unknown noise input, such as that due to turbulence, and this contamination makes the system response evaluation very difficult, uncertain, or impossible; (2) time for a test run must often be kept short, such as less than 10 seconds (for example, to achieve a given speed the airplane may have to be put in a shallow dive and the interval of time over which test conditions are reasonably constant is therefore limited), shortness of records in turn aggravates the noise problem; and (3) an underlying desire is to be able to perform rapid analyses of the records so that the tests may proceed almost immediately to the next test run. The procedures presented herein represent various attempts to cope with these problems, with emphasis being given to means for minimizing or obviating the noise problem.

Much of the material in this report is covered in reference 1, which contains a number of references to other work; no other reference is therefore cited. Some new findings are included.

RELEVANT EQUATIONS

Let the general governing differential equation for response for the airplane subcritical flutter system be given by

$$D_1 y = D_2 P \tag{1}$$

where D_1 and D_2 are differential operators, and y is the response to the forcing function P. The force P may be a prescribed force, as obtained from a shaker, or it may be some unknown quantity, such as due to atmospheric turbulence, and these forces may be acting singly or in combination.

If the input force is a Dirac function $\delta(0)$ at $t = 0$, equation (1) defines the impulse response function h as follows

$$D_1 h = D_2 \delta(0) \tag{2}$$

For a unit sinusoidal input, $P = e^{i\omega t}$, and with

$$y = He^{i\omega t}$$

equation (1) yields the frequency response function

$$H(\omega) = A(\omega) + iB(\omega) \tag{3}$$

according to the equation

$$(\Delta_1 + i\Delta_2)(A + iB) = N_1 + iN_2 \tag{4}$$

where Δ_1, N_1 and Δ_2, N_2 are the real and imaginary parts that are associated with the operators D_1 and D_2. The A component of H is symmetrical with respect to the frequency ω, the B component is antisymmetrical.

The h and H functions are related by the Fourier transform pair

$$H = \int_0^\infty he^{-i\omega t}\, dt \tag{5}$$

$$h = \frac{1}{2\pi} \int_{-\infty}^{\infty} He^{i\omega t}\, d\omega \tag{6}$$

By the superposition theorem, the solution of equation (1), for any general forcing function P, is given by

$$y = \int_{-\infty}^{\infty} P(\tau)h(t - \tau)d\tau \tag{7}$$

The Fourier transform of this equation is

$$F_y(\omega) = H(\omega)F_P(\omega) \tag{8}$$

from which H follows as

$$H = \frac{F_y}{F_P} \tag{9}$$

Equation (8) also leads to the well-known spectral result

$$\phi_y = |H|^2\phi_P \tag{10}$$

If P is equal to $P + Q$, where P is a known force, and Q is an unknown "noise" force, equation (8) would appear

$$F_y = H(F_P + F_Q)$$

The multiplication through the complex conjugate $\bar{F}_P$ leads in turn to the spectral equation

$$\phi_{Py} = H(\phi_P + \phi_{PQ}) \tag{11}$$

where ϕ_{Py} is the cross spectrum between P and y, ϕ_P is the spectrum of P, and ϕ_{PQ} is the cross spectrum between P and Q. If P and Q are uncorrelated, $\phi_{PQ} = 0$, and thus equation (11) yields the important cross-spectrum equation

$$H = \frac{\phi_{Py}}{\phi_P} \tag{12}$$

which appears as a completely noise-free result.

Reference 1 gives some significant special solutions to equation (1), as follows.

I:

$$D_1 R_h = D_2 h(-t) \tag{13}$$

where

$$R_h = \int_{-\infty}^{\infty} h(\tau)h(t + \tau)d\tau \tag{14}$$

Thus, the autocorrelation function of h is the response of the system to a force input of $h(-t)$.

II:

$$D_1 y_n = D_2 Q_n \tag{15}$$

where Q_n is white noise. For this situation, it can be shown that $R_{y_n} = R_h$; thus, the correlation function of the response to white noise is the same as the autocorrelation function of the impulse function h .

III:

$$D_1 R_{Py} = D_2 R_P \tag{16}$$

Thus, if the autocorrelation function of an input P is applied to the system as an input force, the response is the cross-correlation function between P and the response y due to P .

CLASSIFICATION OF THE SWEPT SINE FUNCTION

Forcing inputs are achieved by several means, such as inertial shakers or aerodynamic vane exciters, explosive charges, stick raps, and the natural turbulence of the atmosphere. Of all these means, vane exciters or shakers are most commonly used. For the forcing function, the swept sine wave has become a popular choice, mainly because it covers a sizable frequency band in a short period of time and because the spectral content of this function resembles white noise. The rate of sweep and total duration are prime variables; with some tests the sweep rate is fast, in others the rate is quite slow. For discussion and testing purposes, it appears desirable to make a classification of the duration of sweep. The rate of change of frequency depends of course on the frequency range covered and the duration required to make the sweep. For the testing of most aircraft systems, however,

it appears that classification can be based mainly on duration alone. The following classification is suggested:

1) Fast sweep - one made with a duration of about 5 to 10 seconds

2) Moderate sweep - duration of around 1 minute

3) Slow sweep - duration of around 5 minutes

Each of these sweeps has certain advantages and certain deficiencies, depending on the application. The slow sweep is the best for minimizing noise, but the drawback is long testing and record analysis times. In many instances, though, test conditions dictate the use of fast sweeps.

DAMPING AND FREQUENCY EVALUATION FOR THE IDEAL CASE

Figure 1 indicates three basic ways for evaluating the damping and frequency of a mode. It is assumed that a test has been made, such as through application of a swept sine wave forcing function, and that the response has been analyzed to obtain H (equation (9)), which yields B and A, $C^2 = |H|^2 = A^2 + B^2$, and h (equation (6)). The situation depicted by this figure is ideal; that is, there is no noise present in the input and only a single mode is involved. The top sketch depicts the transfer loci or admittance plot involving A and B. The resonant frequency f_o is identified at the point where there is the greatest rate of change of arc length with respect to a change in the frequency. The damping ratio $\frac{\beta}{\beta_{cr}}$ is given by the equation shown. In the second scheme involving $C^2 = A^2 + B^2$ plotted against f, the modal frequency is identified by the location of the peak, the damping by the width at 1/2 power. In the third scheme, involving damped unforced motion after some excitation, frequency is identified by the period T, damping by the log decrement equation.

Note, the offhand appearance of a peak (second sketch of figure 1) may at first cause a misinterpretation of damping. In figure 2, for example, the peaks on the right visually seem to indicate more damping than the peaks on the left; all peaks on the same line have the same damping, however, as measured in terms of percent of critical damping. Likewise, the three peaks on the right of the middle sketch have the same damping, even though the shortest peak seems to suggest a larger damping than the tallest peak.

Other means for deducing frequency and damping involve curve-fitting procedures, such as fitting the experimentally derived frequency response function H, or fitting the impulse response function h, and then deducing the roots from the fitted curves.

When modes are close together, or when noise is present in the input, the techniques of figure 1 break down. It is towards handling the situation of the presence of a number of modes and the contamination due to an unknown noise source that the remainder of this report is devoted.

THE USE OF EXCITERS AND TRANSDUCERS IN COMBINATION

It is odd that little in general has been done in using transducers in pairs as a way of helping to solve the closely spaced mode situation, particularly in separating the symmetrical and antisymmetrical modes which have frequencies close together. Figure 3 serves as a reminder of what practices should be followed in general. With one shaker, say on the right, the use of only the signal from point 1 makes it very difficult to distinguish the symmetric mode from the antisymmetric mode. The addition of the signals from point 1 and point 2, however, identifies the symmetric mode and virtually eliminates the antisymmetric mode. The subtraction of the signals, on the other hand, identifies the antisymmetric mode to the exclusion of the symmetric mode. This subtraction scheme also provides for good rejection of symmetric excitation due to noise.

For two shakers, one on the left and one on the right, use of y_1 or $y_1 + y_2$ for in-phase excitation gives symmetric mode isolation. If the two shakers are 180° out of phase, y_1 or $y_1 - y_2$ gives good antisymmetric mode isolation. Again, in this case, $y_1 - y_2$ also gives good rejection of symmetric excitation due to noise.

The use of two pick-ups in a different chordwise position, such as at points 3 and 4, also should be considered as a way of helping to isolate closely spaced modes; the idea here is that excitation of different modes appears in a different relative sense according to the closeness to the nodal lines.

Figure 4 depicts results obtained for a three-mode system, with two symmetric modes of 3 Hz and 10 Hz and one antisymmetric mode of 9.8 Hz; thus, the antisymmetric mode had a frequency only 2 percent different from one of the symmetric modes. With one shaker, a swept sine wave excitation, and only one pick-up, the deduced results for A, B, C^2, B vs A, and h, indicate that only two modes are present, one around 3 Hz and one around 10 Hz.

Figure 5 applies to one-shaker excitation of the same system, but the signals from a right and a left transducer are subtracted. The marked change in the results is a clear indication that two modes are present near 10 Hz. For figure 6, the situation is the same as for figure 5, except that a strong symmetric excitation due to noise is also present. The results, in spite of the noise, gives a tip-off that there are two closely spaced modes around 10 Hz. Thus, with one shaker operation, the technique of adding the signals from two opposite transducers and of subtracting the signals and comparing the deduced results appears as a good way to establish whether two modes with frequencies close together - one symmetric, one antisymmetric - are present. Two shakers, first used symmetrically then antisymmetrically, provide an even better way to isolate symmetric and antisymmetric modes.

INITIAL SEQUENCE OF DATA ANALYSIS

Some of the first data analysis checks that should be made are often overlooked in a testing sequence. A review of certain initial steps that should be performed is thus considered worthwhile.

It is assumed that tests are being made with a swept sine force input. The first analysis that should be made is to make an attempt to identify modal frequencies roughly, to classify the modes as to whether they are symmetrical or antisymmetrical, and to see if the apparent modes can be identified with ground vibration modes. Suggested first steps are as follows:

1) Combine signals as indicated in the previous section.

2) Scan the combined time history signals and look for "bursts" in the response; the object here is to obtain a rough idea of the modal frequencies and to establish whether the mode is symmetric or antisymmetric and whether primarily bending or torsion.

3) From the signals, establish raw H values (equation (9)) and in turn h values (equation (6)). Clear h, according to the cleared h procedure discussed subsequently, transform back to first improved H, and form $C^2 = |H|^2 = A^2 + B^2$. Examine the C^2 function to obtain a second check on the modal frequencies (verify those established by scanning the time history signals, pick up others that may have been missed) and to obtain a first estimation of modal damping where possible.

4) From the appearance of the C^2 functions, an assessment of the noise problem can be made, and a judgment can be

rendered as to what type procedures should be used subsequently to minimize the noise problem.

Essentially, the idea behind these steps is to do something quite simple at first so as to obtain a quick insight as to what the frequencies might be and to obtain a quick appraisal of the severity and nature of the noise problem.

TECHNIQUES FOR MINIMIZING OR ELIMINATING INPUT NOISE EFFECTS

Use of Both Input and Output Information

Six schemes for coping with the problem of having noise in the input are presented in brief fashion in this section. (See reference 1 for more detail.) It is assumed that one or more shakers are used to drive the system, such as by a swept sine wave, and that an unknown excitation noise force, such as due to buffeting or atmospheric turbulence, is also present.

Clearing h.- Figure 7 is typical of the results that are obtained for H and h, by means of equations (9) and (6), when a large input noise is present along with the swept sine wave excitation. One way to eliminate much of the noise contamination is simply to clear or erase the results for h beyond a point where useful information no longer seems to appear, such as point a in figure 7, and then to transform this truncated h back to H (eq. (5)). Example results are given in figure 8. The remarkable improvement that is obtained for the A and B values by doing this simple expedient is seen.

Weighting h.- Another technique is shown in figure 9. Here the raw h is weighted by an exponential function; the weighted result is then transformed back to give refined A and B values. This technique, as with figure 8, reduces noise effects greatly. With this weighting technique, a correction to the deduced values of damping must be made to correct for the apparent damping that is added by the weighting function used.

Use of cross correlation between input and output.- Figure 10(a) applies to the raw results as obtained by use of equation (9). By contrast, the results shown in figure 10(b) were obtained by use of equation (12), which involves the cross spectrum between the measured output and the known shaker force input. This cross-correlation technique is seen to give a marked improvement in the deduced A and B values. In general, the longer the record, the better is the noise minimization by this technique.

Peak shifting.- Figure 11 is used to describe the peak shifting technique for eliminating noise effects. The top sketch depicts the swept sine wave input force, the bottom sketch the noise-contaminated response. First, select a peak such as a . Then select peak b and shift the entire record so as to make peak b fall on peak a . Next, take peak c and shift the record to make peak c fall on a . Do this for a number of peaks in succession, and then add all the results to form a composite input force designated by

$$P_T = \sum P_n$$

The output response is handled in the same way, but using the same shifts as used for the input; the composite response is designated as

$$y_T = \sum y_n$$

Now deduce H from P_T and y_T , using equation (9). The concept in this technique is that a single short record may be used and that the shifting and adding operations cause the meaningful or intelligent part of the record to be enhanced, amplified, or reinforced, while the noise level remains the same (or the signal-to-noise ratio increases). Figure 12 gives results obtained in a particular case where only 19 shifts were made. In the main frequency range of interest, around 10 Hz, it is seen that practically noise-free results are obtained. A feature of the peak shifting scheme is that it is possible to concentrate on various frequency ranges even with the use of a single record. For example, in figure 11, two "bursts" in the output response are noted, suggesting two frequencies of possible concern. To concentrate on the lower frequency, peaks in the vicinity of peak a are shifted to fall at peak a ; to concentrate on the higher frequency, peaks in the vicinity of peak p are shifted.

Ensemble averaging.- In ensemble averaging, the concept is to deduce, by repeat runs, a number of raw estimates for the function h , and then to add all the raw functions together. The idea is that this averaging-type operation will "average out" noise effects and leave only the meaningful signal. Example results, involving an ensemble average of 20 raw functions, are shown in figure 13. It is seen that virtually noise-free results are obtained. This is one of the best schemes for eliminating noise, but the main drawback is that it requires making a number of repeat runs.

Sweep over limited frequency band.- Figure 14 is given as a help to describe a limited sweep approach. Suppose that test sweeps are made to cover the range of 3 Hz to 25 Hz in 10 seconds, and consider that the analysis of the results indicate some modal

information in the range of 10 Hz but that the results are too noisy to be interpreted with confidence. A good way to improve the situation is to sweep over only the frequency range of concern, say, in this case, from 8 Hz to 12 Hz in the 10 seconds of sweep time. Generally, a vast improvement in the deduced results will be noted. The disadvantage, of course, is the problem of resetting the sweep range and of having to make another run.

Use of Output Information Only

There are at least two ways to derive system response characteristics by consideration of the output response alone. The procedures apply in general whether the response is due to a forced swept excitation with an unknown noise input or whether the response is due to noise excitation alone.

One procedure involves the establishment of the auto-correlation function R_y of the output response. Each side or half of this symmetric function has characteristics of the h function. The Fourier transform of R_y is the spectrum ϕ_y of the response. Examination of this spectrum gives an indication of the frequency and damping of the system modes. Ensemble averaging of the R_y functions is found to be a powerful way to minimize noise by this approach, reference 1. Other ways to use the R_y function and minimize noise will be indicated in the subsequent section.

A second procedure for deriving system response characteristics using response information alone is the formation of the "randomdec" signature. The essentials of one type of construction for this approach are shown in figure 15. It can be reasoned that the sum of all the individual signals should form a pure signal which resembles or has characteristics of the h function. Damping and frequency follow from the resulting summed signal. A main difficulty of the approach is that the summation must often involve hundreds of functions before converged values of the sum are achieved. Another difficulty is in identifying closely spaced modes.

SUCCESSIVE CORRELATIONS OF CORRELATION RESULTS - A PROMISING SOLUTION TO THE NOISE PROBLEM

Under a contract effort for AFFTC/AFSC, Edwards AFB, the author has developed additional techniques for treating the noise problem - techniques which appear remarkable and in a way unbelievable. This section summarizes some of the results

obtained. The procedures involved are quite versatile and represent subsequent manipulations for improving the quality of the results that are obtained by most all the procedures described earlier in this report. Two figures are presented first as a way to describe the procedures involved. In figure 16, the top sketch refers to autocorrelation of the raw h function (see eq. (14)) that has been deduced by any of the procedures discussed previously, or it refers to the autocorrelation R_y, obtained by considering only the response (due to noise alone, due to a swept sine wave alone, or due to these forcing functions acting in combination). Note, the raw h should always be cleared as discussed in connection with figures 7 and 8. Likewise, if the autocorrelation function is used, the "noisy" tails (the tail portions on either side which appear to be due to noise only) should be erased. Then the following steps are performed:

1) Make R_1 one-sided; call it r_1

2) Form R_2, the autocorrelation of r_1

3) Form ϕ_2, the Fourier transform of R_2; look at this function for improvement (reduction in noise content) and for mode identification

4) Go back to R_2

5) Make R_2 one-sided; call it r_2

6) Repeat these steps as often as necessary until the spectrum ϕ_n appears without distortion due to noise.

In the application of these steps, the following will occur:

1) The modes which show up with low power will first disappear (means for recovering these modes will be discussed subsequently).

2) The mode with the next lowest power (actually a combination of power and damping) will then disappear, and so on, until finally only one mode remains.

3) With each iteration, the results become more and more noise-free.

4) Sometimes, depending on modal power and damping and on mode closeness, noise-free results will occur with perhaps two or three modes still remaining.

5) The reading of the frequency and damping of these remaining modes, by the second scheme of figure 1, will be

an accurate indication of the frequency and damping of these modes.

Figure 17 illustrates a companion type manipulation. In this case, the correlation functions are kept in their two-sided form; thus, a correlation function of a correlation function is found, in succession. In this case, the following should be observed.

1) The modes with the lowest power lose more and more power with each iteration and finally disappear.

2) The peaks become more and more spiked; damping is lost, but frequency is more and more sharply pinpointed.

Although the theory is not given here, it should be noted that the consequences of the two types of manipulation described can be explained on a theoretical basis.

Means for recovering any lost mode are as follows. Go back to the original spectrum type function ϕ_1. In figure 16, peak a would probably have remained to the end. But, suppose it was desired to identify the mode inicated by b more precisely. In this case, simply erase the ϕ_1 function above frequency ω_2 and below ω_1 (in this case, erasing above ω_2 is all that is required); application of the steps described earlier will then bring out mode b in a pure form.

Figure 18 shows results as obtained by the one-sided procedure, using h as established from a raw or contaminated H. The experiment involved use of an analog simulation of a system; excitation was by means of a linear swept sine wave, and an unknown random noise. In part (a), we see frequencies around 3 Hz and 10 Hz, but the precise location and damping cannot be established. In part (b), which represents the first iteration, mode 1 has just about disappeared, and the rest of the function is much more noise-free. By 5 iterations, mode 2 has become very pure; damping and frequency are nearly precisely the values set in the analog set up (in this case, $f_o = 10$ Hz, $\frac{\beta}{\beta_{cr}} = 0.05$).

Figure 19 gives results using the response only, and its autocorrelation, for the same run of figure 18. The raw spectrum indicates the two modes in the vicinity of 3 Hz and 10 Hz. By three iterations, the 10 Hz mode is identified purely.

In figure 20, end results are shown for convergence to the mode near 3 Hz. In this case, strain response rather than acceleration response was used, and convergence went automatically to the lowest mode (no spectrum erasing had to be performed).

Note, displacement or strain emphasizes the lower modes, while acceleration response, due to the ω^2 weighting, emphasizes the higher modes.

Figure 21 serves to show the remarkable power of the procedure to regenerate correct frequency and damping information when severe truncations in the frequency plane are made. Figure 21(a) is the original spectrum of h obtained for a one-mode system and without noise in the input. The shaded areas were then erased; after several iterations, starting with this truncated spectrum, the spectrum as indicated by figure 21(b) was found. Frequency and damping of the mode is still intact. The experiment was repeated, truncating figure 21(a) to the severe form shown by figure 21(c); here truncation is within the half-power limits. After several iterations, the results shown in figure 21(d) were obtained. Damping and frequency are still the same as the original, even though the only information used was that given by figure 21(c).

Figure 22 shows results that were obtained with a system having frequencies of 9 and 10 Hz, both with $\frac{\beta}{\beta_{cr}} = 0.05$. Figure 22(a) represents the raw or contaminated spectrum of h . After several iterations by the one-sided approach, the result shown in figure 22(b) was obtained; the frequency and damping are in excellent agreement with the model values. Figure 22(c) represents the spectrum as obtained by considering the response only. Figure 22(d) is the result obtained by the one-sided approach after information beyond f_c was erased; this erasing was done to bring out the lower mode. The damping and frequency indicated by figure 22(d) for this mode is in good agreement with the correct values, even though the information contained in peak 1 was all that was used. Figure 22(e) is the result obtained by applying the two-sided approach to the R_y function; the tendency to form sharp spikes is shown by this sketch.

Figure 23 applies to a system having modes fairly close together as follows:

Mode	f,Hz	β/β_{cr}
1	8	0.05
2	9	0.05
3	10	0.02

Figure 23(a) is the raw spectrum of h . If no erasing is made, application of the sequence of steps would result in the 10 Hz mode coming out in pure form. Clearing beyond f_a yielded the result shown by figure 23(b) by the one-sided approach; clearing

before f_a and beyond f_b yielded the result shown by figure 23(c). Damping and frequencies for both modes are very good. Thus, both lower modes were extracted, in spite of the closeness of another mode having a much lower value of damping.

SYSTEM PARAMETER IDENTIFICATION - POSSIBILITIES OF A NEW APPROACH

A number of different schemes have been studied as means for obtaining a more detailed identification of system parameters. These schemes generally fall under three categories:

1) Curve fitting of the frequency response function

2) Fitting of time plane information, such as the h function

3) Difference-equation approaches in which the coefficients of a difference-equation model are evaluated, from which system roots may in turn be extracted

Collocation procedures are sometimes used for the curve-fitting operations but, more generally, the approaches are based on the use of least-squares concepts. Some of the system identification approaches are reviewed and developed in reference 1 and the references contained therein. Thus, they will not be discussed further herein. Instead, the notions of a possible new approach will be outlined.

A commonly used concept in subcritical flutter testing of an aircraft is to make a plot of damping g versus V, figure 24. The basic idea is to establish the trend of the damping curves and to extrapolate forward to estimate the flight speed at which the damping vanishes (or reduces to some stipulated lower level). This procedure is reasonably satisfactory for a mild approach to the critical flutter speed, curve a, but is quite treacherous when an explosive flutter situation is encountered, curve b, for in this situation the damping can deteriorate very quickly with only a small increase in speed. A way to obviate this problem is sought. Reference 1 suggests one possible procedure. The idea is to derive the coefficients of the assumed governing differential equation model and to watch how these coefficients vary with air speed. Figure 25, taken from reference 1, depicts results for the situation of a mild approach to flutter. The nature of the extrapolation is known by analytical considerations; for example, the coefficients a_3, a_2, a_1, and a_0 are known to vary in a quadratic manner. Extrapolation to higher speeds seems straightforward. With the extrapolated coefficients, system

roots for higher speeds may be evaluated, from which an estimate of the critical flutter speed may be made. Figure 26 shows the behavior of the coefficients for a system which has explosive flutter characteristics. In figure 25 the variation of the coefficients appears gradual, while in figure 26 two of the coefficients, specifically a_2 and a_3, are changing quite markedly with V. This rapid, but not abrupt, change in the coefficients with speed appears as a tip-off that the situation may be of the explosive flutter variety.

We now combine the thoughts associated with figures 25 and 26 with the procedures discussed in the previous section. Suppose that the procedures outlined in the previous section stand the test of more extensive study and that the procedures indeed are reliable in establishing the frequencies and damping of the various modes of the system under study. With the frequencies and damping established, the governing differential equation can then be formed. As an example, consider that three modes are identified; roots may then be written as

$$p_1 = \left(\frac{g_1}{2} + i\right)\omega_1$$

$$\bar{p}_1 = \left(\frac{g_1}{2} - i\right)\omega_1$$

$$p_2 = \left(\frac{g_2}{2} + i\right)\omega_2$$

$$\bar{p}_2 = \left(\frac{g_2}{2} - i\right)\omega_2$$

$$p_3 = \left(\frac{g_3}{2} + i\right)\omega_3$$

$$\bar{p}_3 = \left(\frac{g_3}{2} - i\right)\omega_3$$

where $g_n = 2\left(\frac{\beta}{\beta_{cr}}\right)_n$. From these roots, the governing differential equation follows as

$$(p - p_1)(p - \bar{p}_1)(p - p_2)(p - \bar{p}_2)(p - p_3)(p - \bar{p}_3) = 0$$

Expansion of this equation yields the characteristic equation

$$p^6 + a_5p^5 + a_4p^4 + a_3p^3 + a_2p^2 + a_1p + a_o = 0$$

which in turn defines the coefficients a_n of the governing differential equation. In accordance with figures 25 and 26, we watch how these coefficients vary with air speed.

We note that curve fitting in the frequency plane or time plane, or any other evaluation of coefficients through use of least-squares procedures, is precluded in this suggested approach. The success depends simply on the reliable estimation of the mode frequency and damping values.

CONCLUDING REMARKS

Which one of the procedures outlined herein for minimizing noise effects is the best? No specific choice can really be made. A systematic study is needed to try each procedure in a number of different applications and circumstances. The choice of which is best will undoubtedly depend on the situation encountered. Nevertheless, some comment about certain features or drawbacks of the procedures can be made.

The procedure of clearing the impulse response function h (rectangular truncation) should always be used, no matter how h has been derived. The exponential weighting of the raw h is not suggested in general, since the cleared h process serves just about as well. The use of the cross-spectrum approach is considered one of the best but generally is more applicable for the longer sweep times. The peak shifting technique is very attractive but of course requires the intermediate step of shifting and summing the record portions. Ensemble averaging is perhaps the best but is probably precluded in most instances because of the necessity for making a number of repeat runs. Randomdec is not advocated unless a swept sine wave forming function is used (with a noise input alone, too many terms are required in the summation in general). Where response information only is available, the autocorrelation approach (or equivalently, the spectrum of the response) should, of course, be used. In this approach, care should be taken to erase the "noisy" tails of the correlation function, as mentioned in the body of the report. Also, in this approach it is likely that fairly long record lengths are available; this works to the favor of the approach because, on the whole, the longer the record the better the results (as in the general rule for most all approaches).

As a general comment, while there is a science to the procedures for minimizing the noise problem, there is also an art in their applications. Depending on the circumstances and the type

of analysis equipment available, little "tricks" can be inserted at appropriate places to gain an improvement in the end results.

REFERENCE

1. Houbolt, John C.: Subcritical Flutter Testing and System Identification. NASA CR-132480, August 1974.

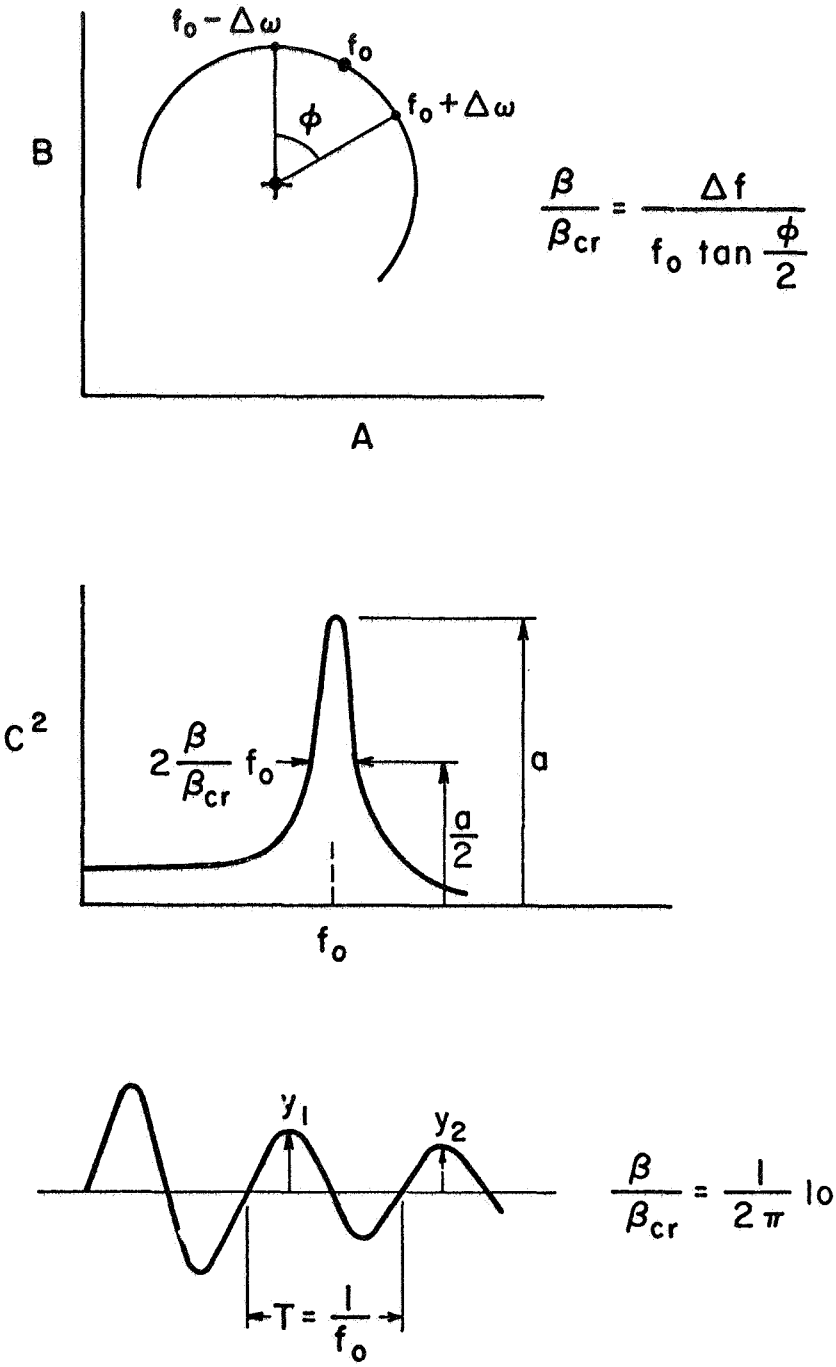

Figure 1.- Three basic ways for estimating modal frequencies and damping.

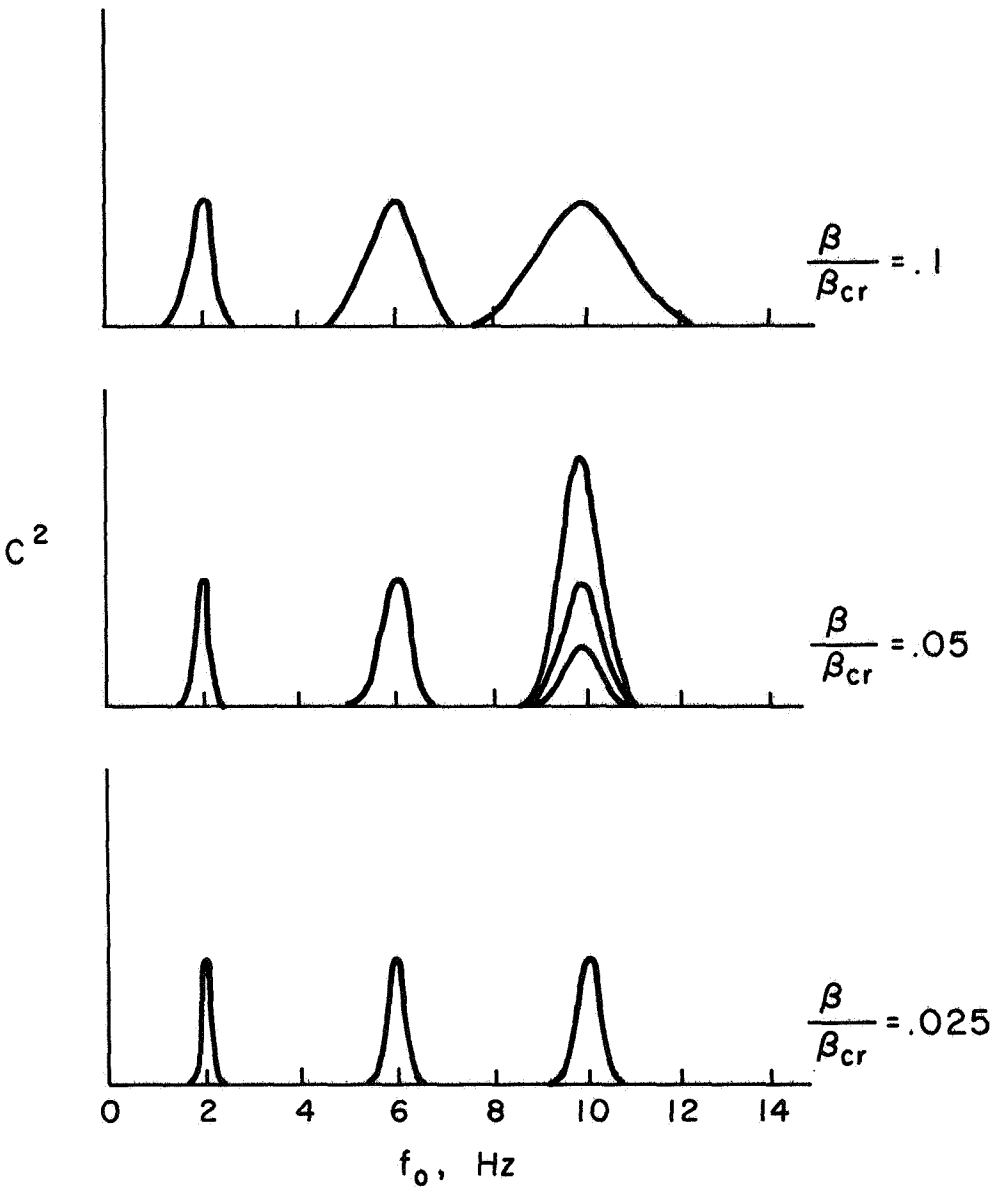

Figure 2.- Appearance of resonance peaks of different damping.

One Shaker:

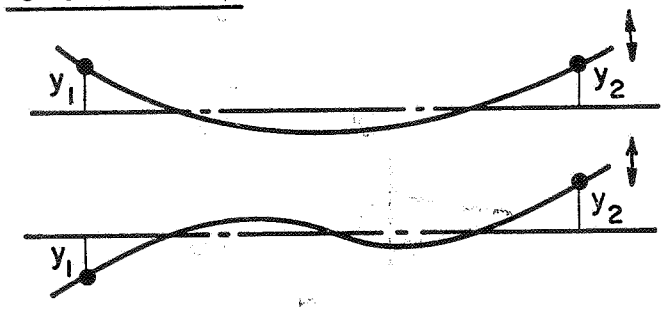

$y_1 + y_2$

$y_1 - y_2$ — good elimination of symmetric excitation due to noise

Two Shakers:

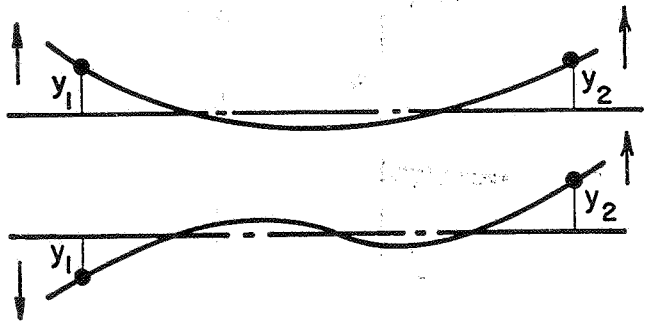

y_1 or $y_1 + y_2$

y_1 or $y_1 - y_2$, for better elimination of symmetric excitation due to noise

also for y_3 & y_4

Figure 3.- Combining response signals to identify symmetric and antisymmetric modes.

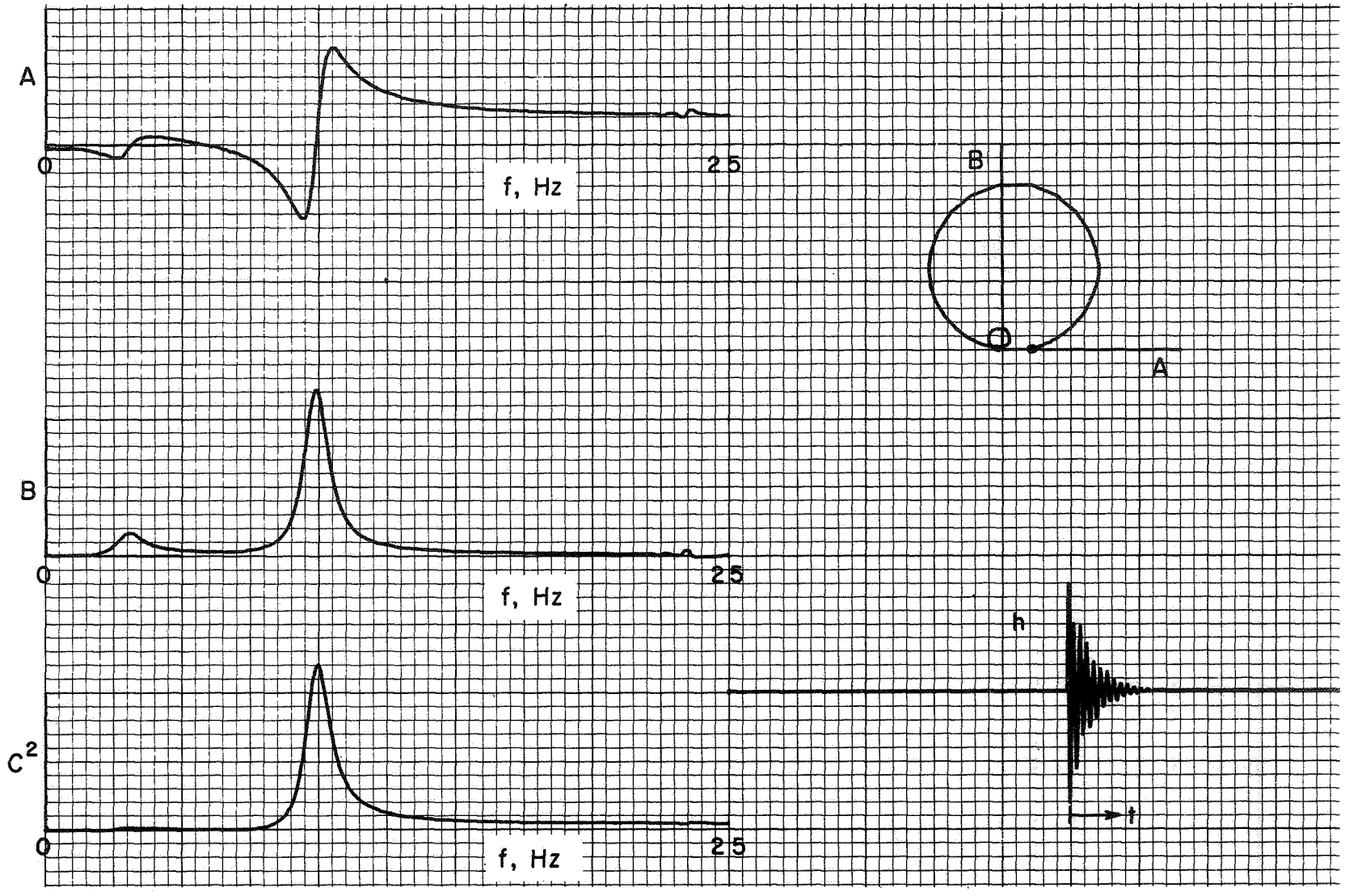

Figure 4.- Response results for three-mode system, one shaker, adding tip responses.

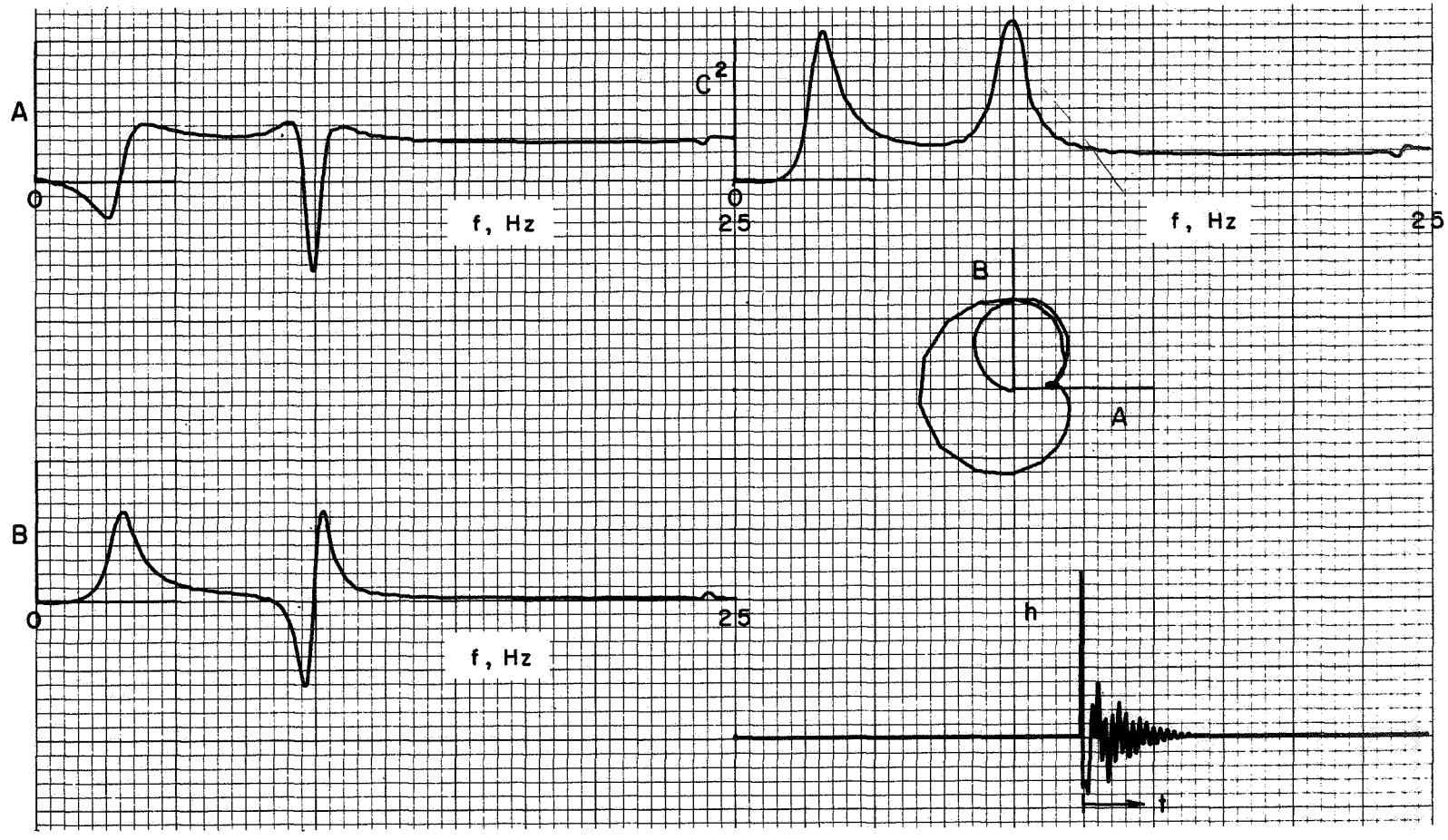

Figure 5.- Response results for three-mode system of figure 3, one shaker, subtracting tip responses.

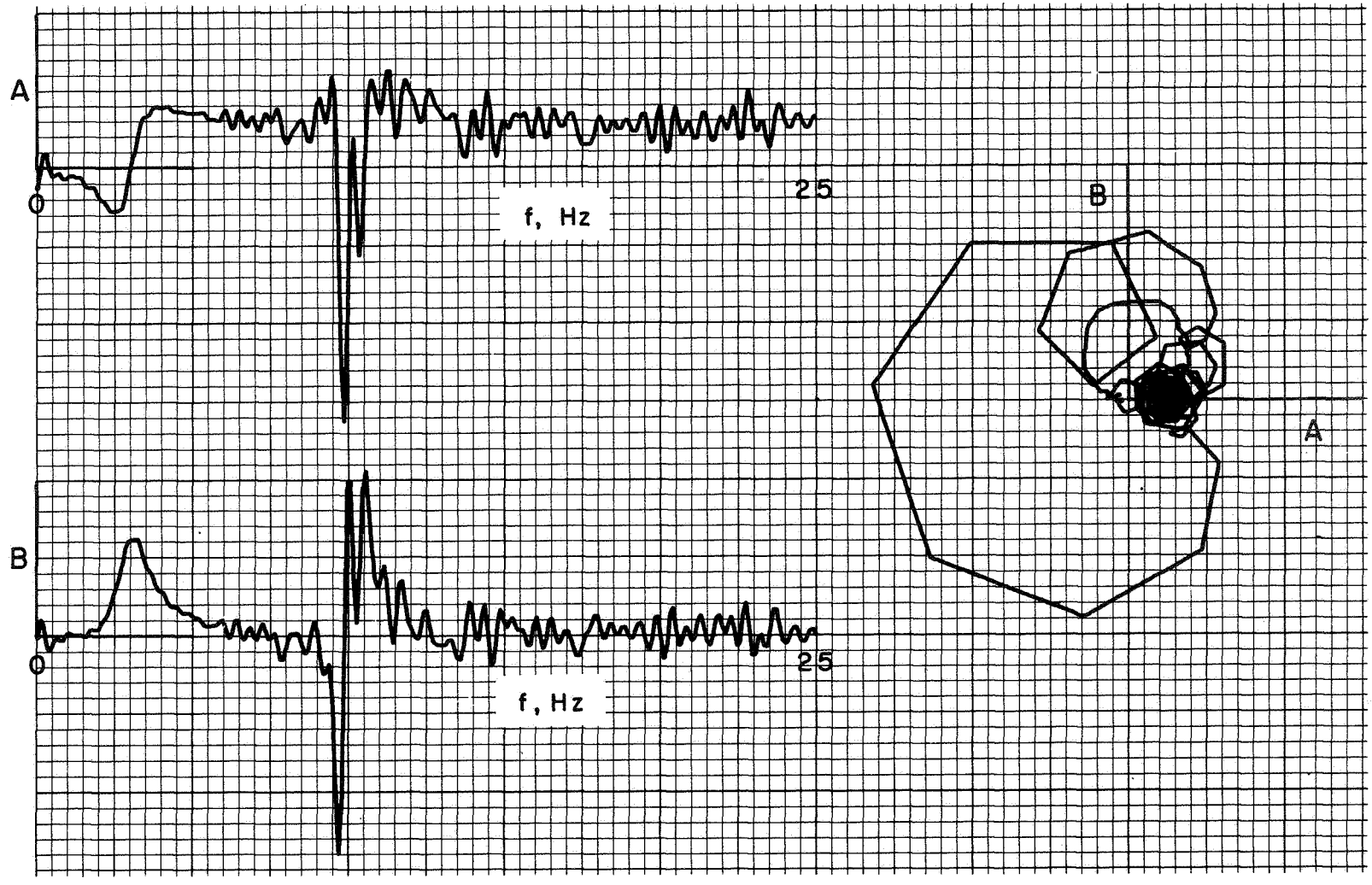

Figure 6.- The situation of figure 5 with noise in the input.

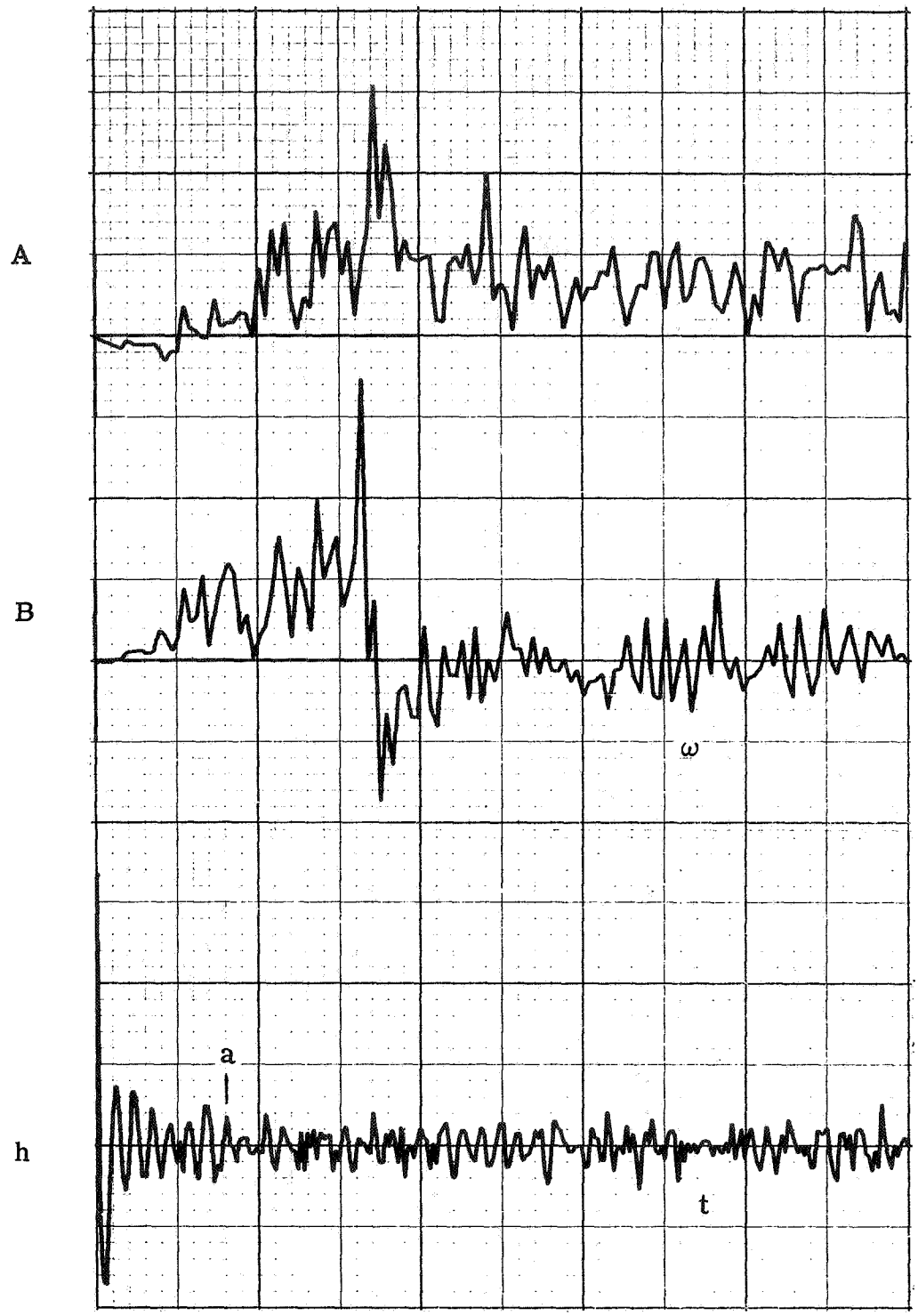

Figure 7.- Frequency response and h functions obtained by single swept sine run with noise in input.

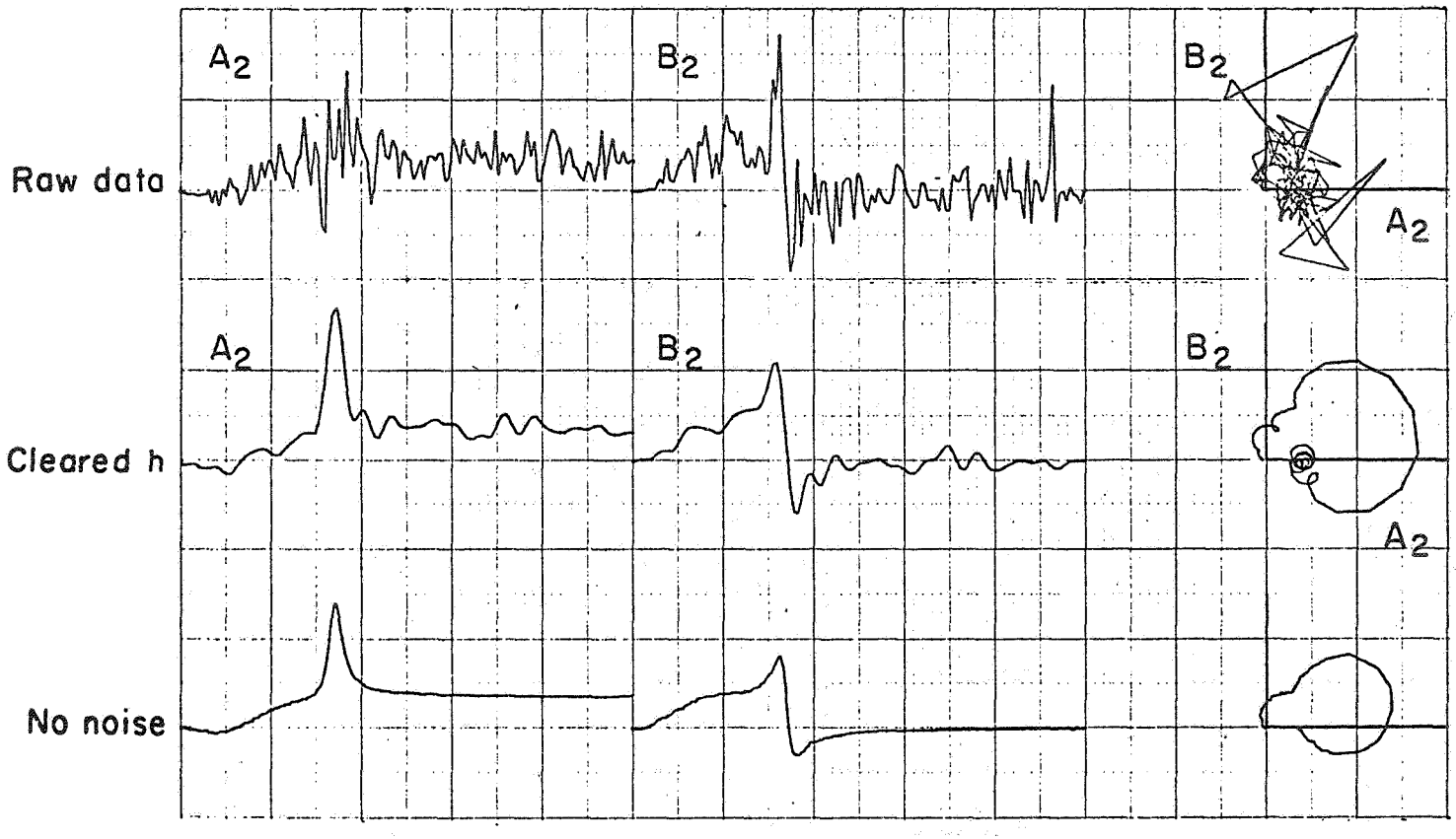

Figure 8.- Improved frequency response function by clearing h function.

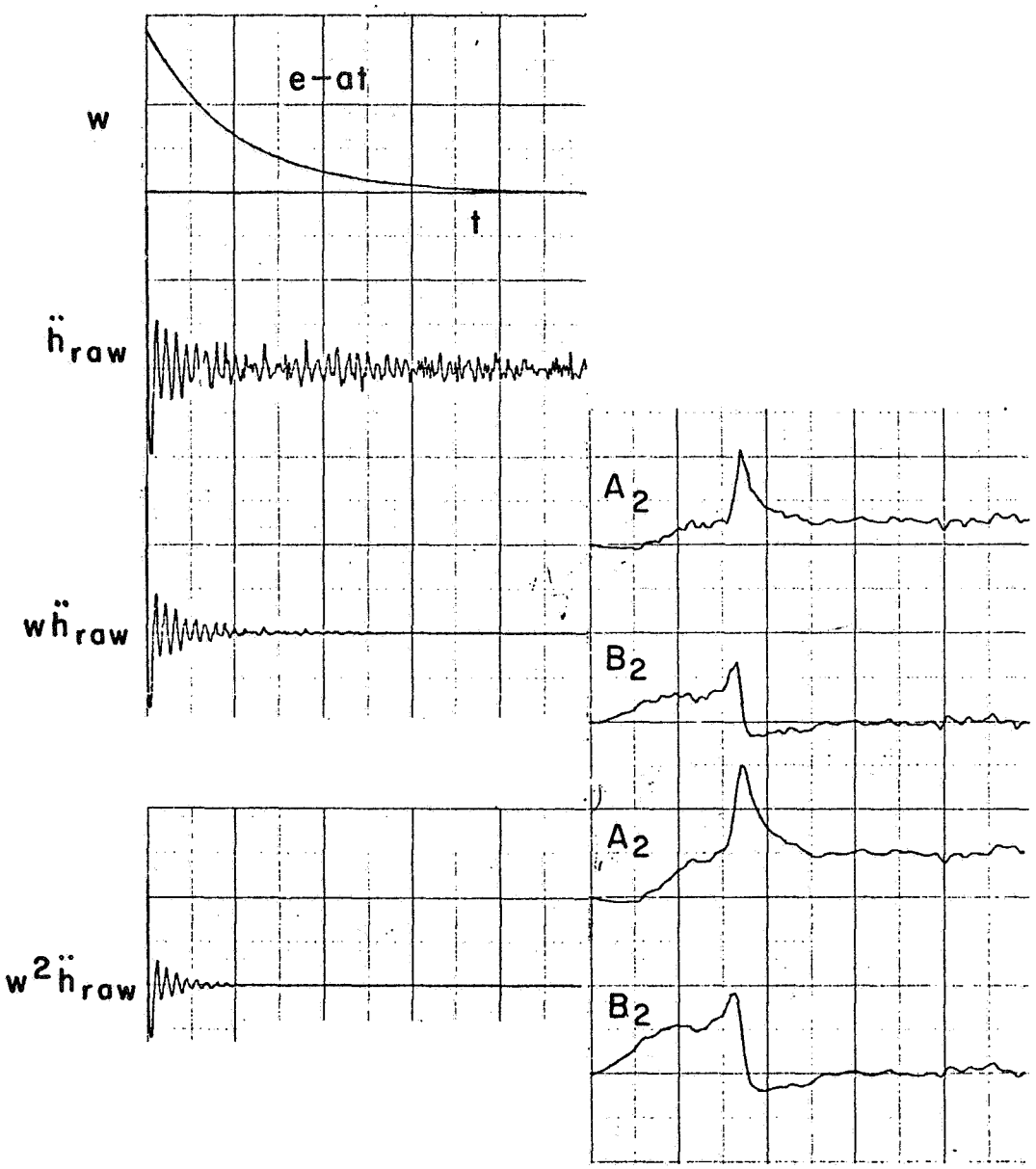

Figure 9.- Improved frequency response function by exponential weighting of h function.

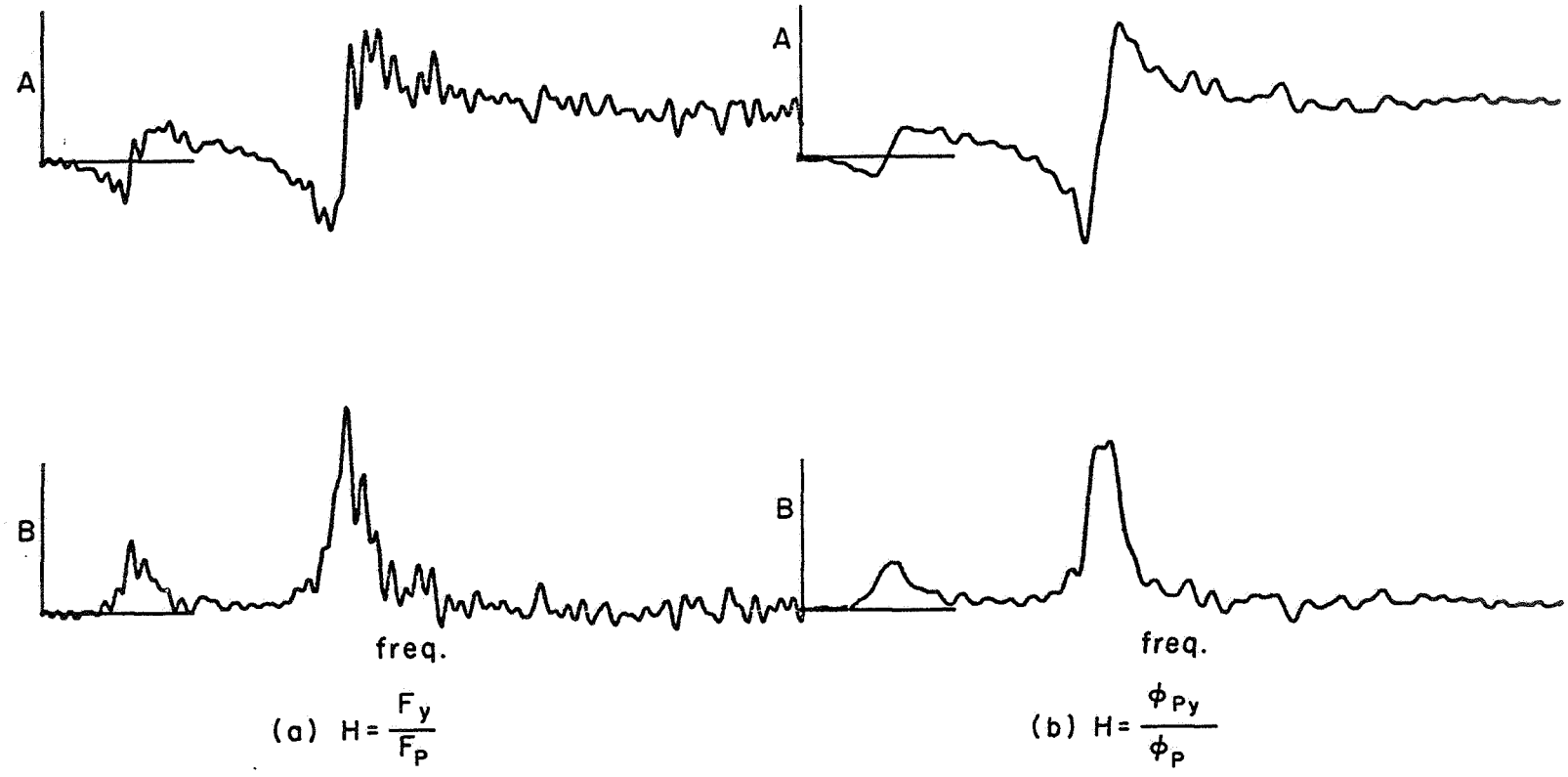

Figure 10.- Improvement in the deduction of H through use of cross-spectrum between input and output.

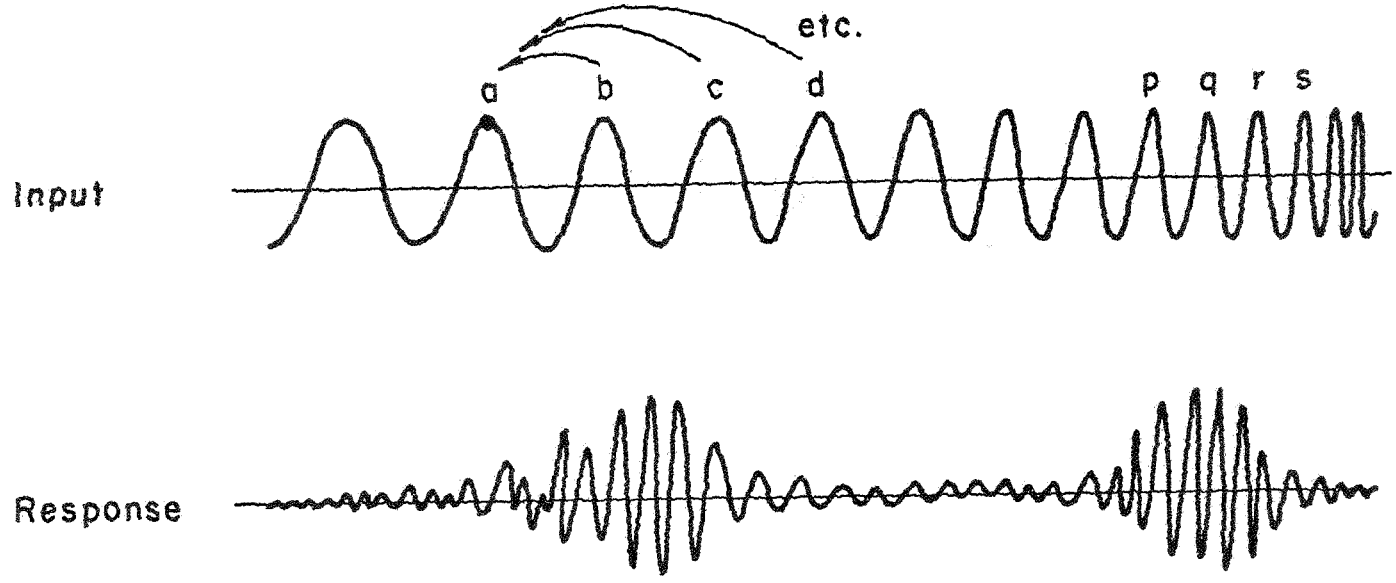

Figure 11.- Peak shifting to minimize noise effects.

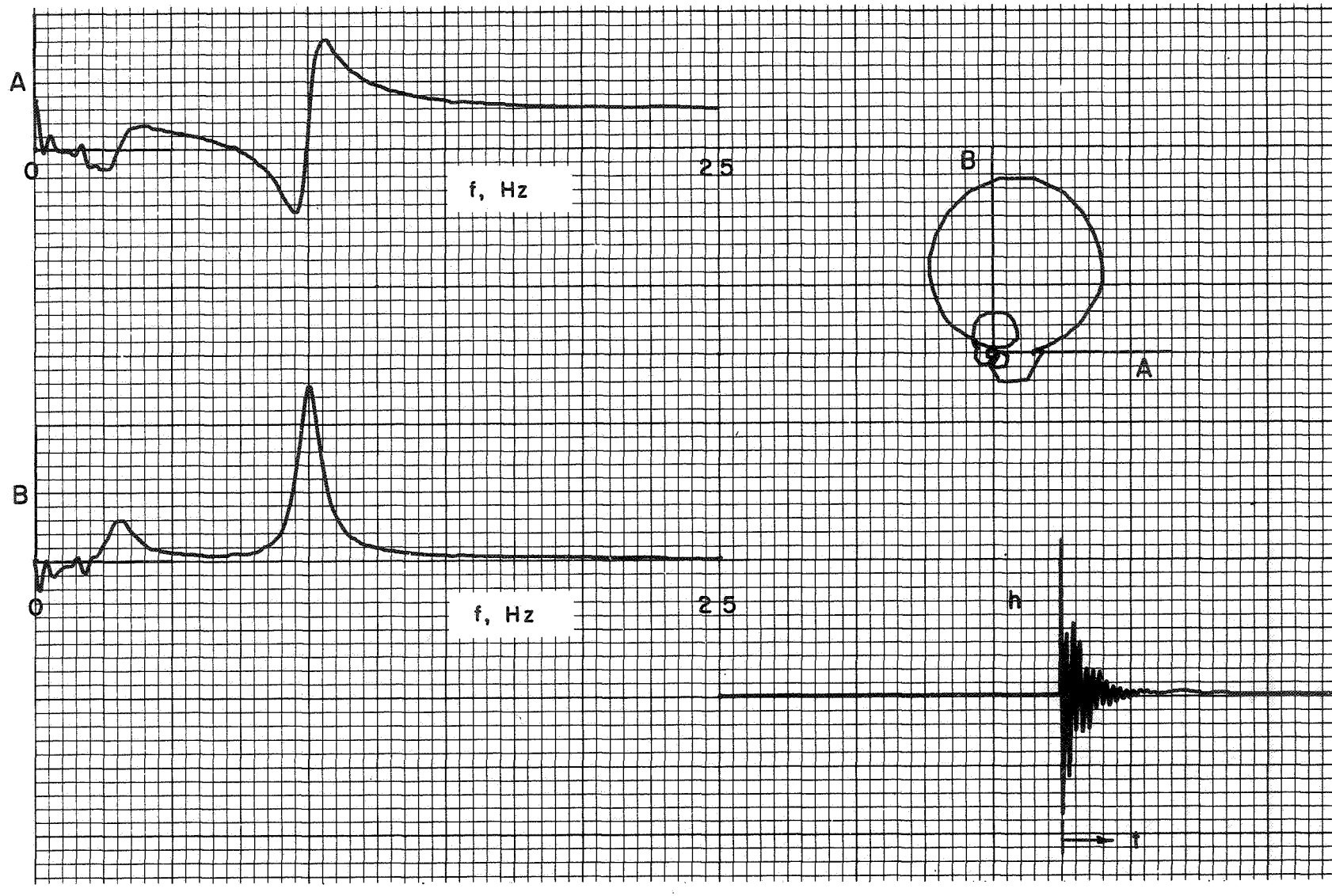

Figure 12.- Results obtained by peak shifting technique (19 shifts); original results very contaminated by noise.

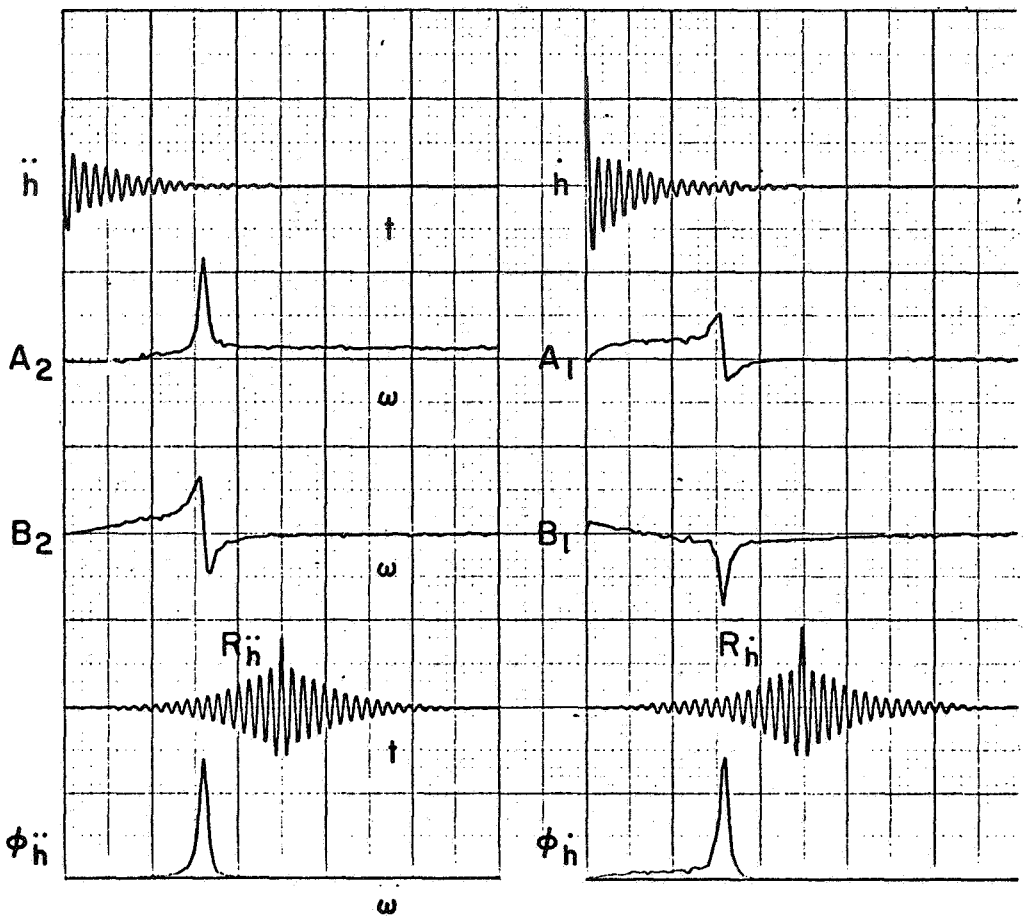

Figure 13.- Use of ensemble averaging of sine sweep runs to eliminate noise.

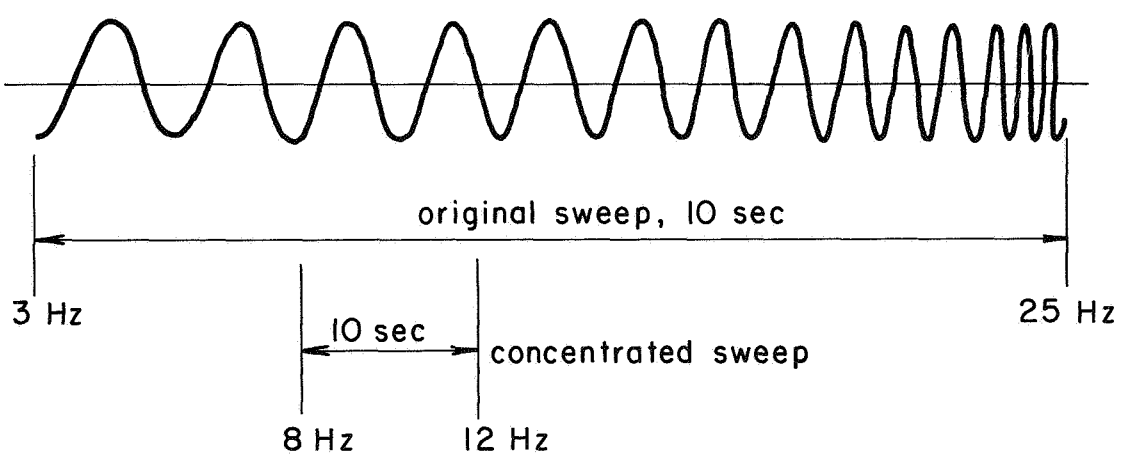

Figure 14.- Use of sweep over narrow frequency band.

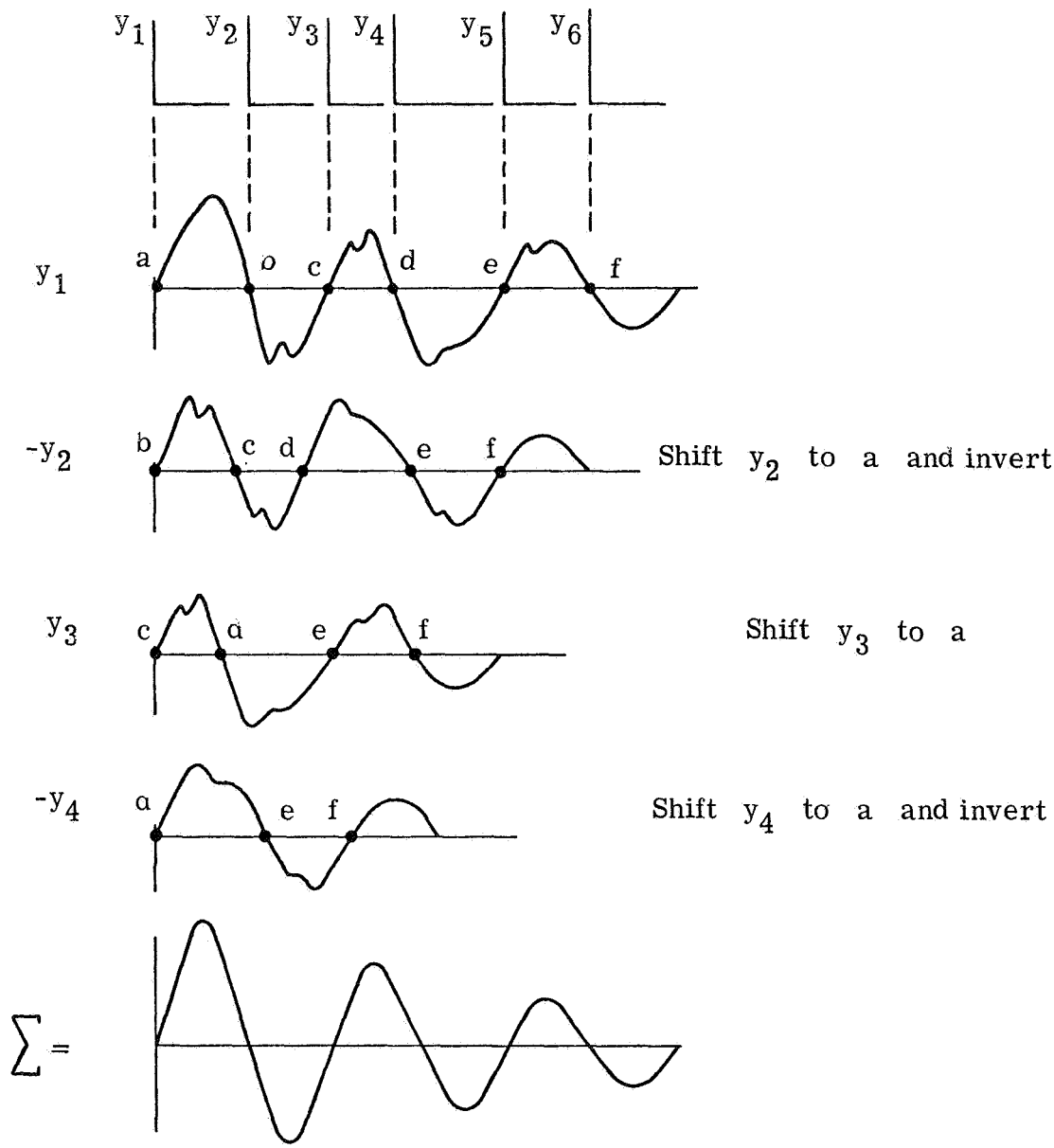

Figure 15.- "Randomdec" process to derive h-type function.

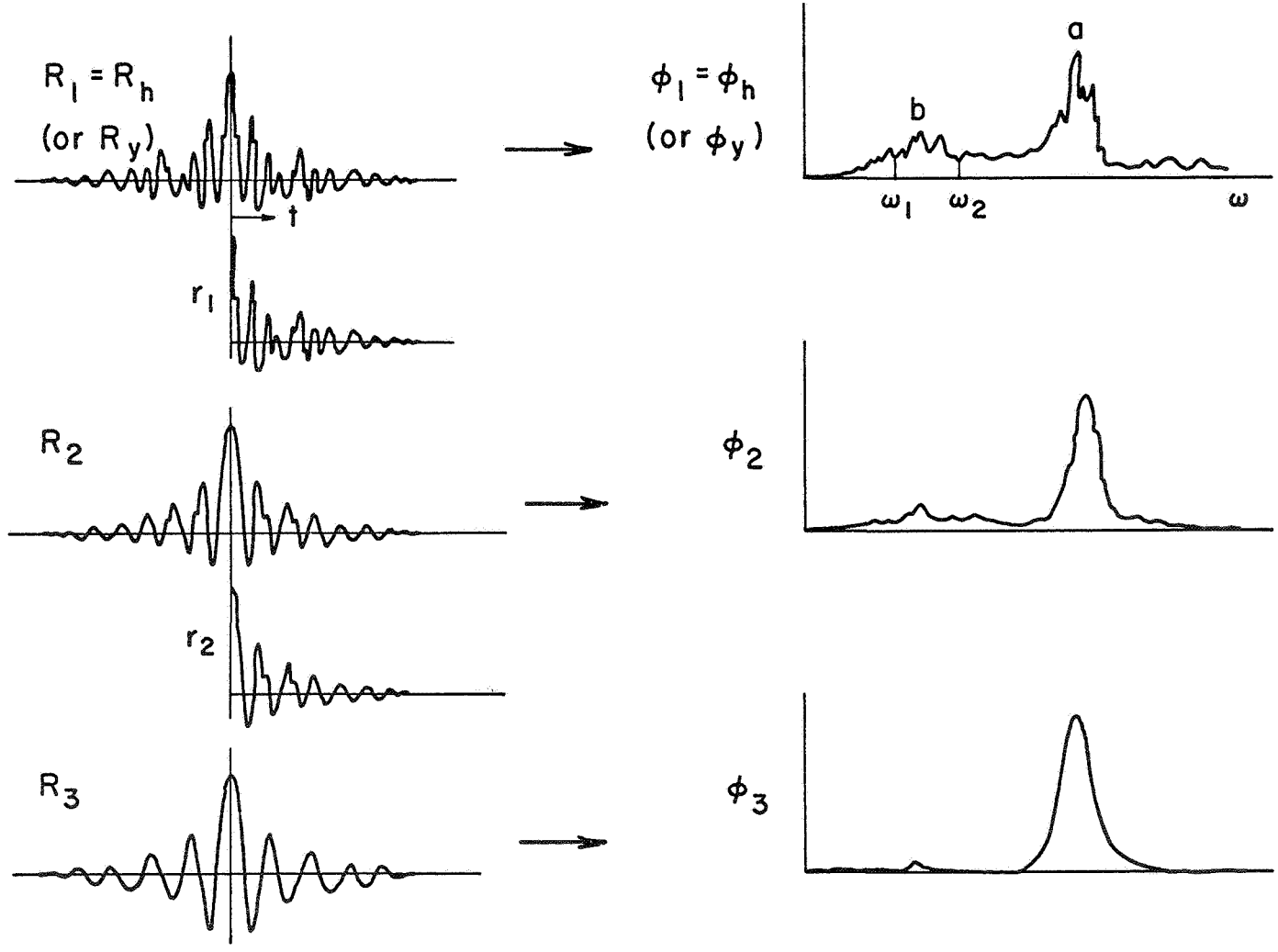

Figure 16.- Successive autocorrelations of one-sided correlation functions.

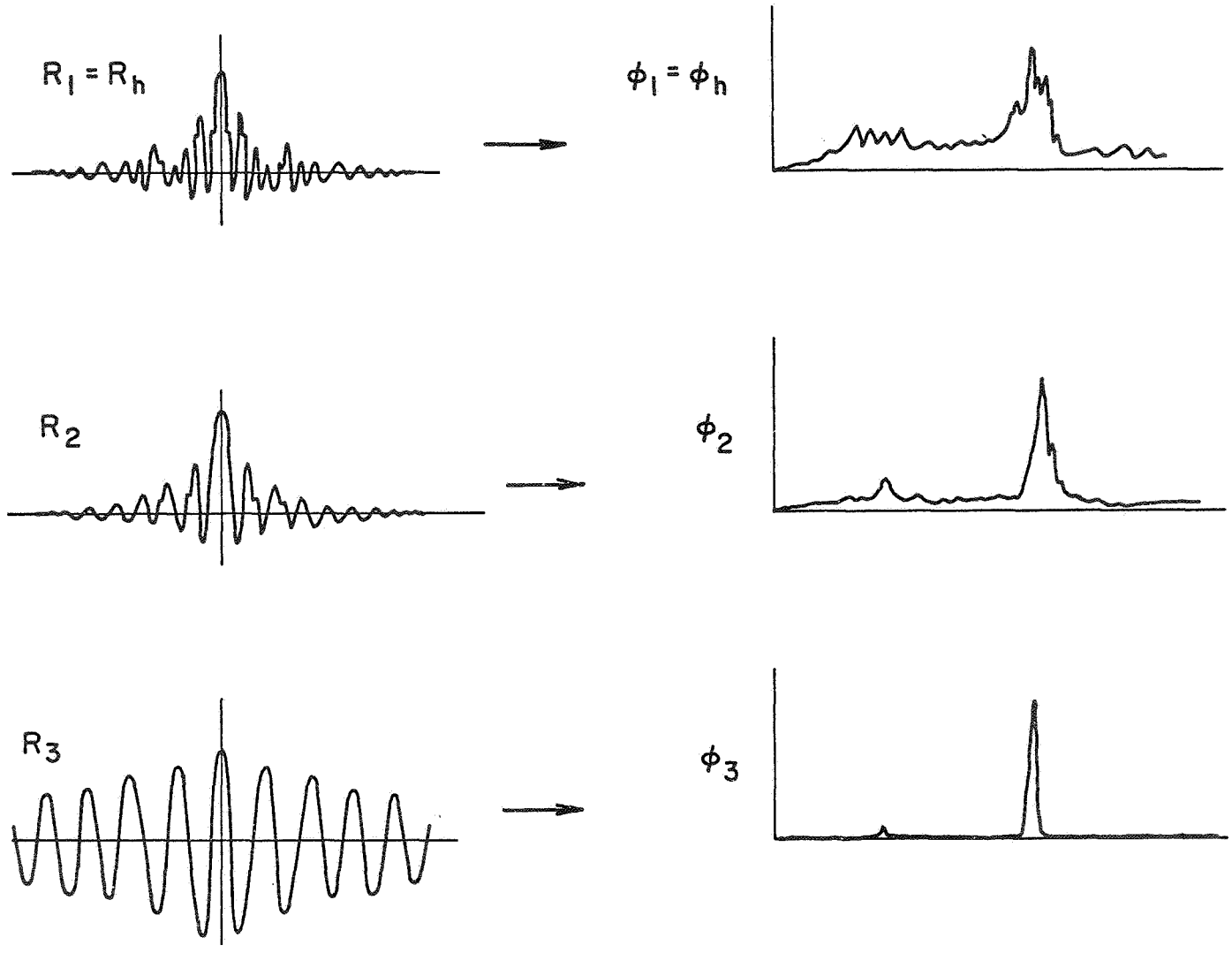

Figure 17.- Successive autocorrelations of two-sided correlation functions.

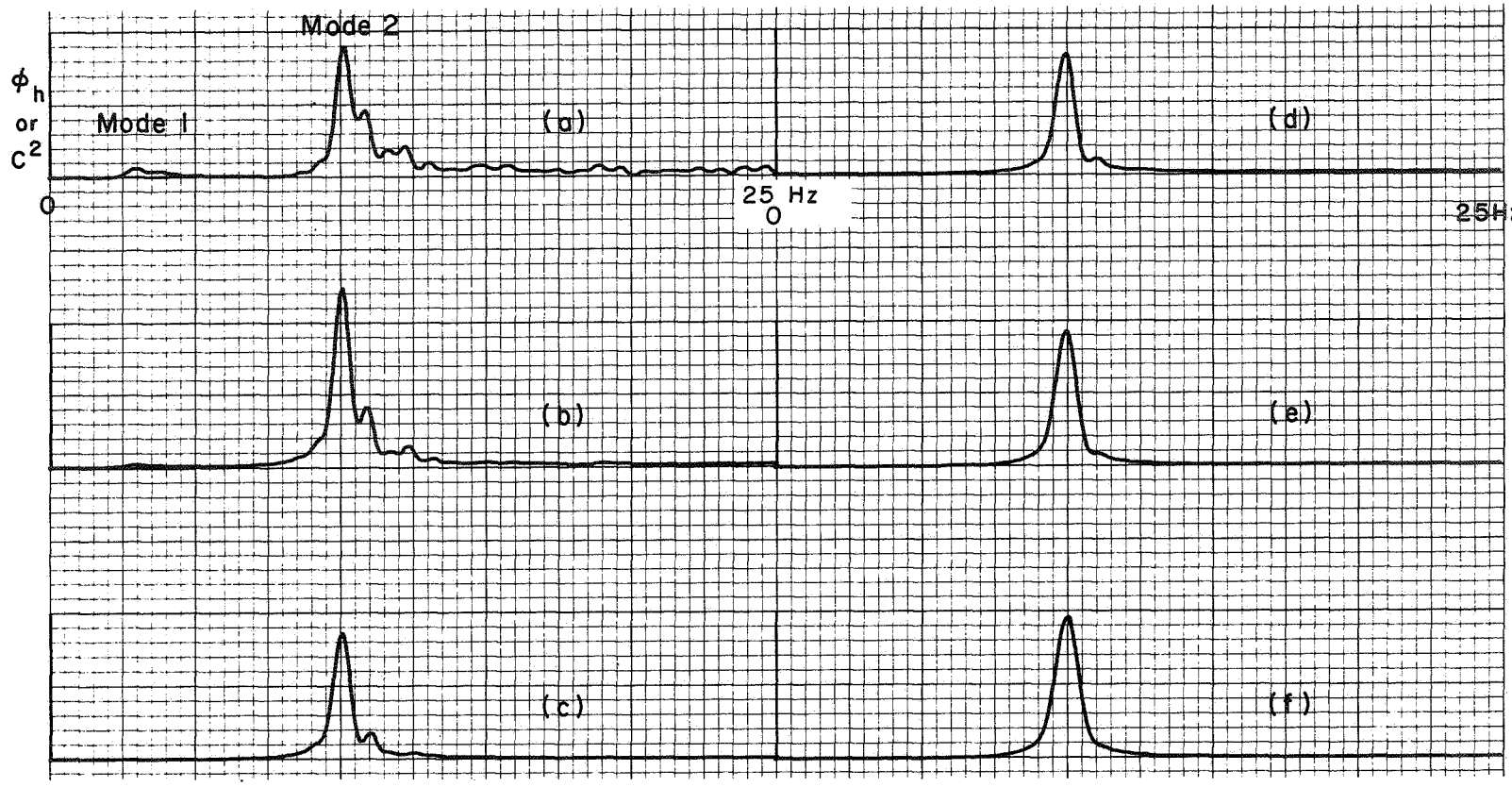

Figure 18.- Results obtained by successive correlations of one-sided correlation functions, starting with h as determined from raw H.

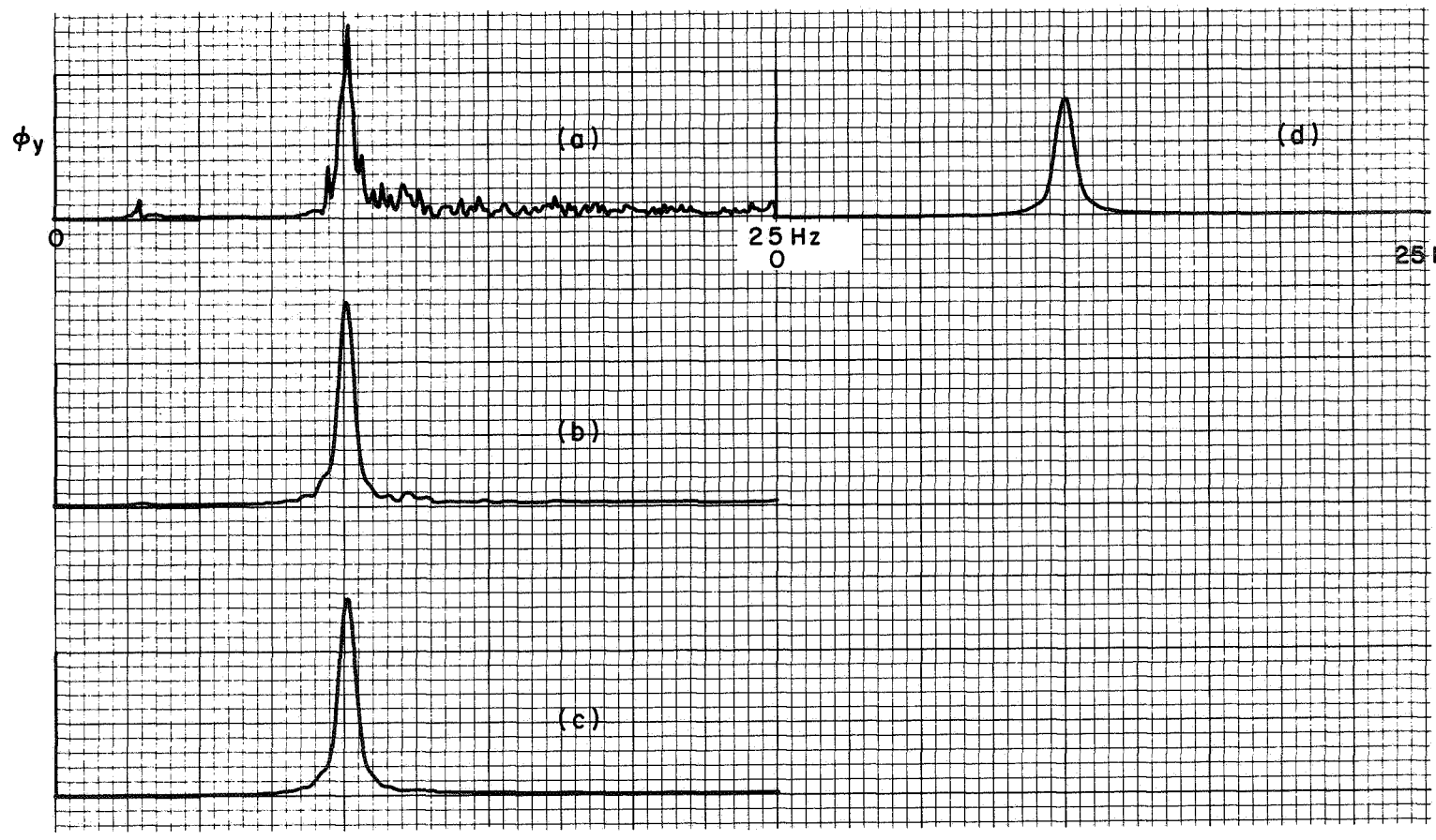

Figure 19.- Results obtained by successive correlations of one-sided correlation function, starting with R_y of the response only.

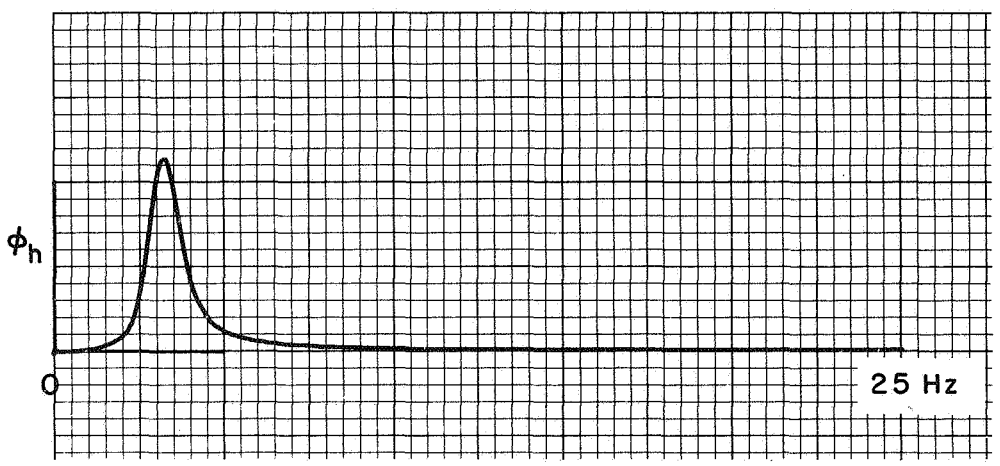

Figure 20.- Pure results for the low-frequency mode obtained by successive correlations of the one-sided correlation function.

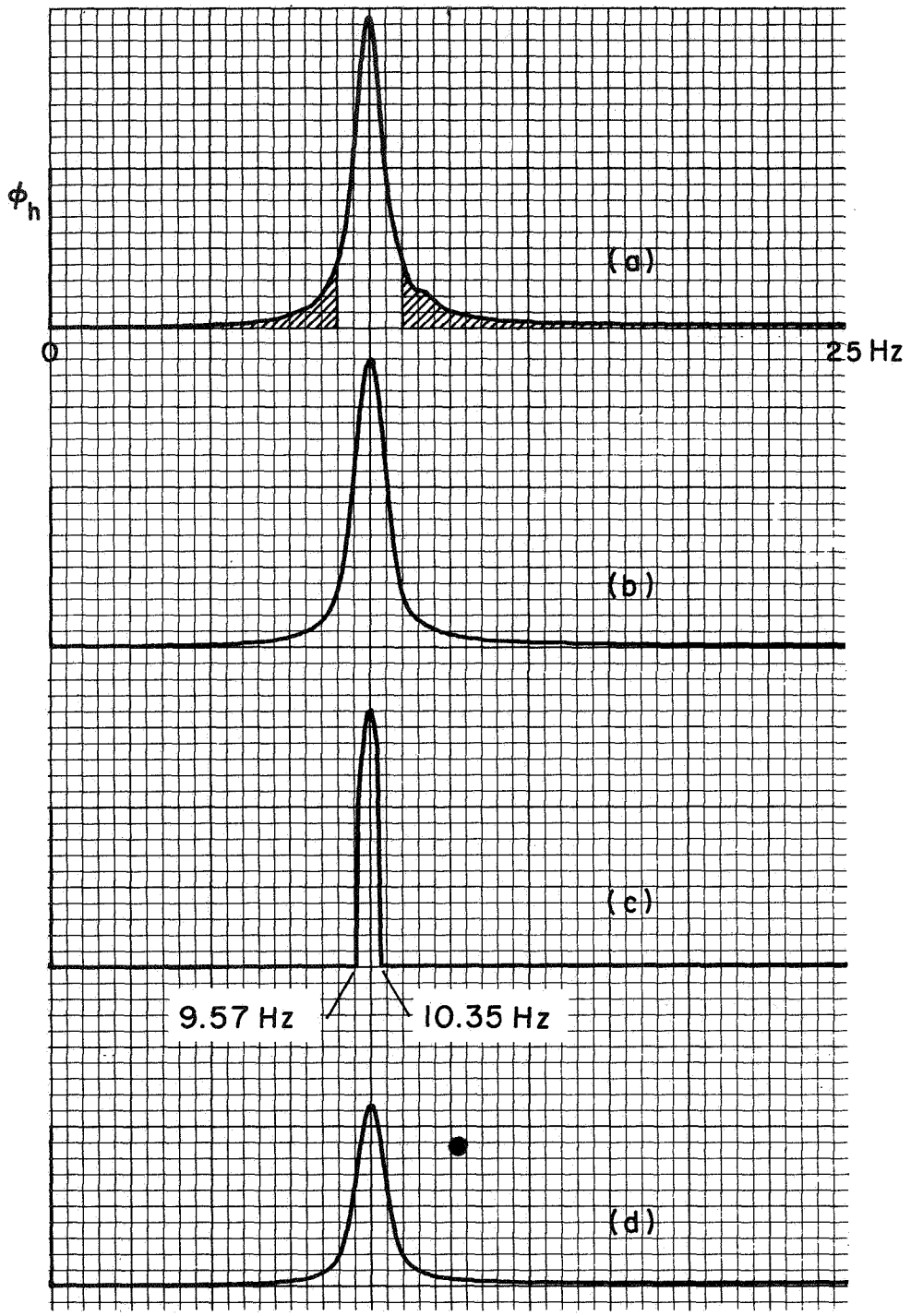

Figure 21.- Regeneration of modal response characteristics after truncation in the frequency plane.

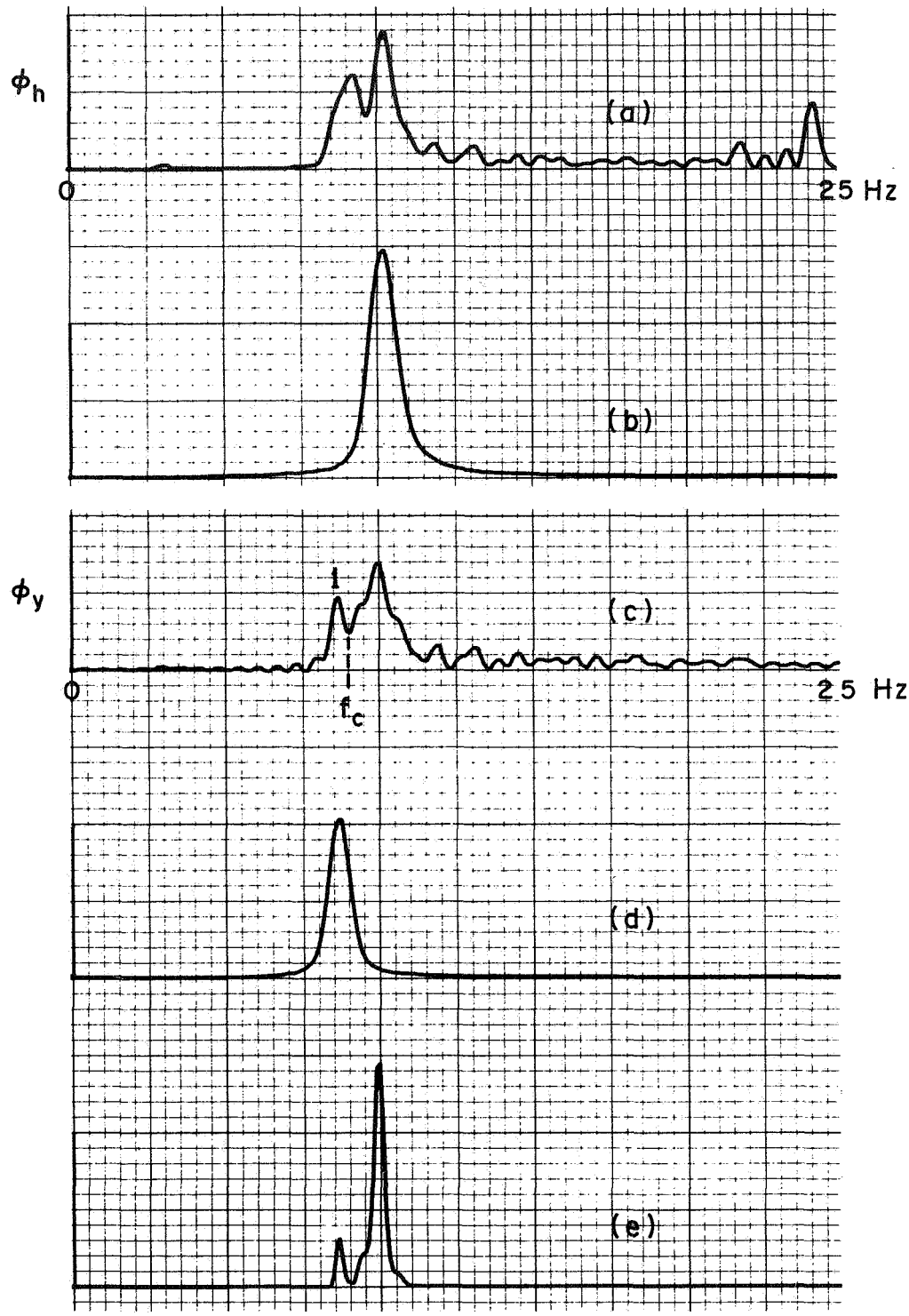

Figure 22.- Isolation of modes by frequency plane erasing, two-mode system.

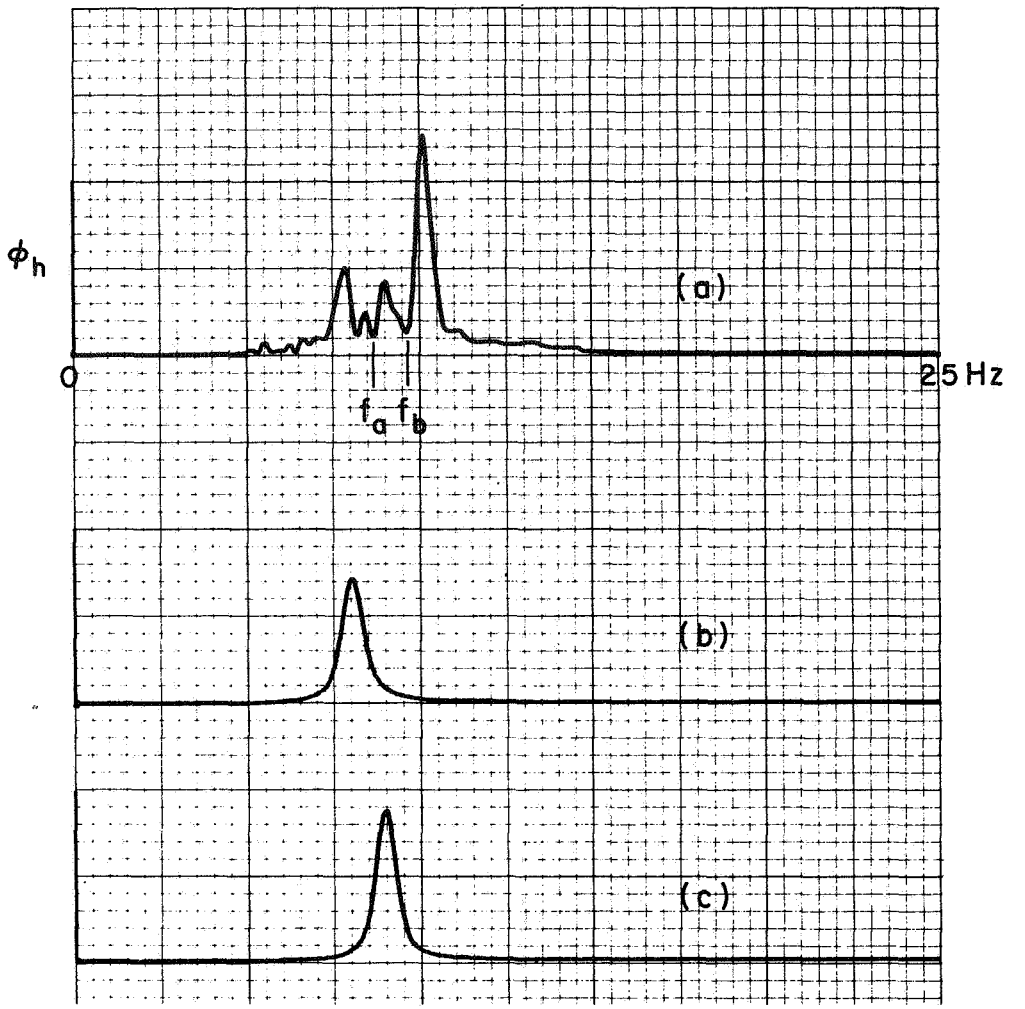

Figure 23.- Isolation of specific modes by frequency plane erasing, three-mode system.

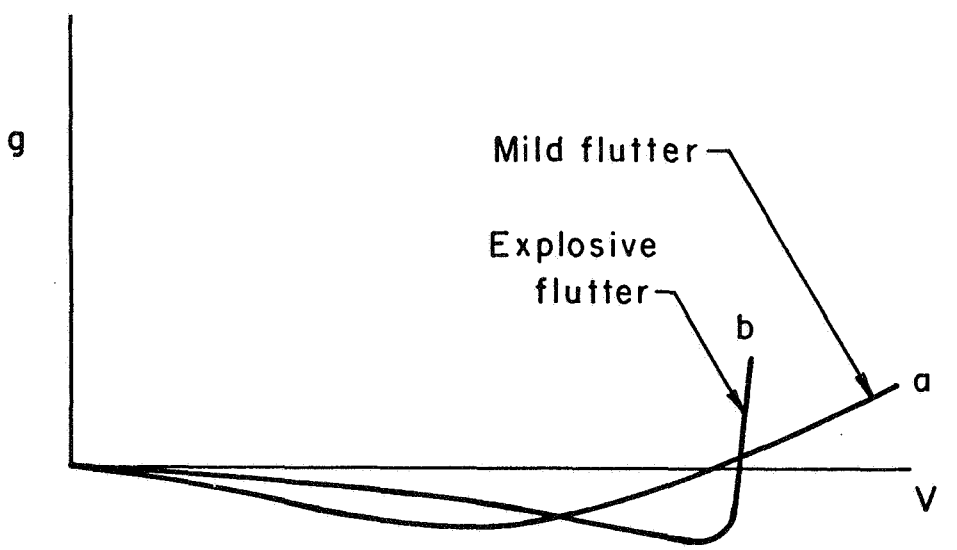

Figure 24.- Damping curves for mild and explosive flutter cases.

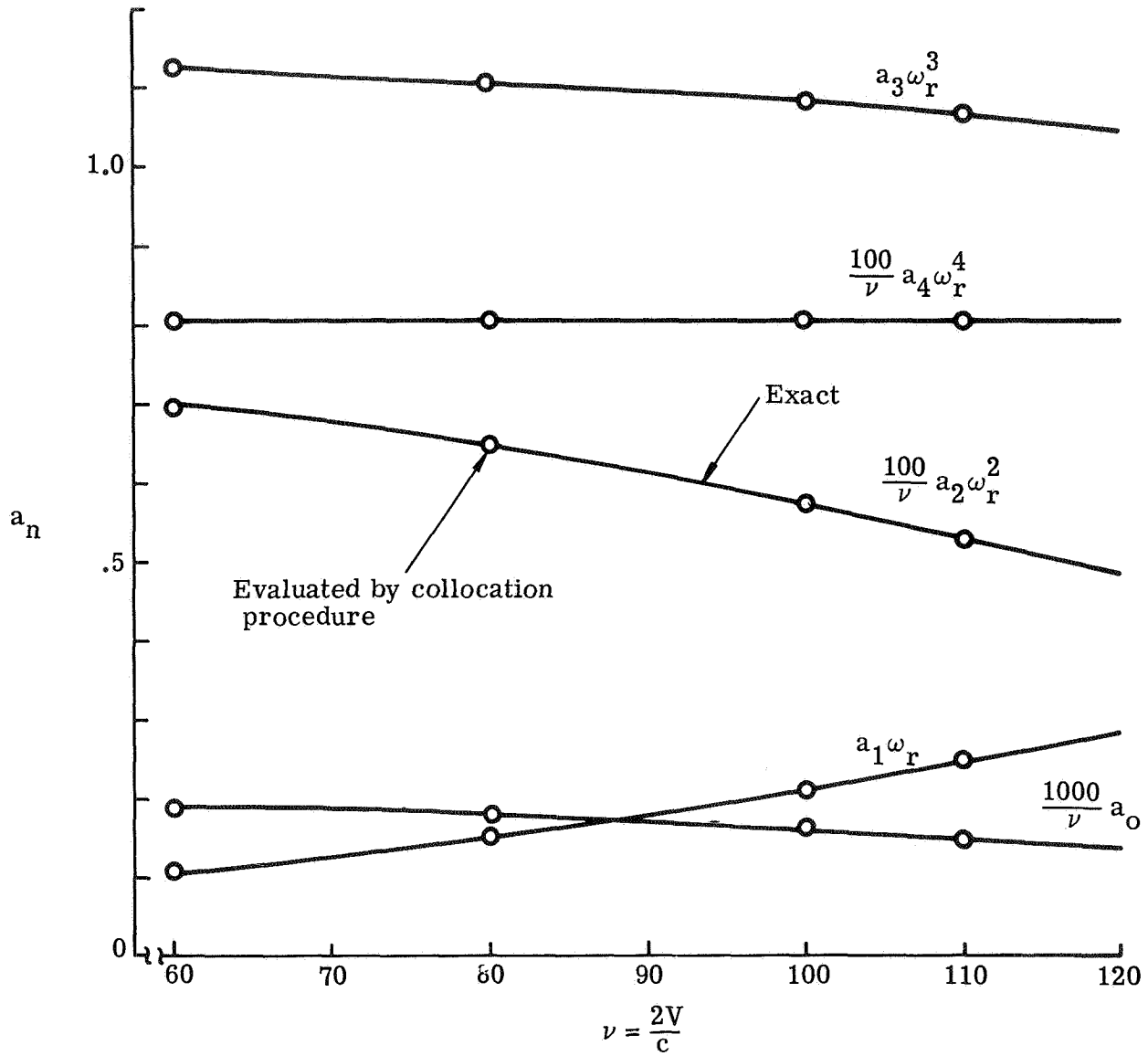

Figure 25.- Variation of differential equation coefficients with airspeed, mild flutter.

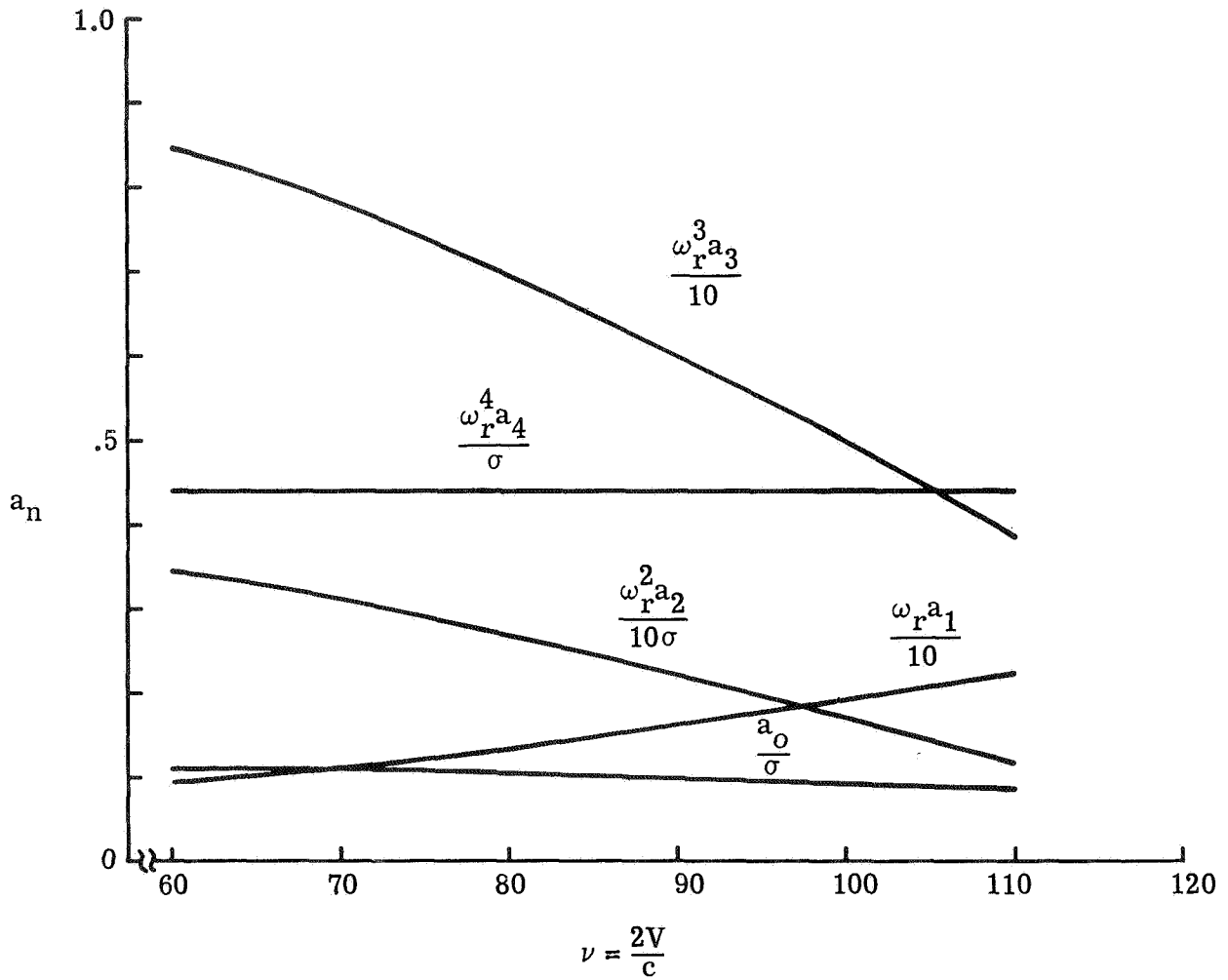

Figure 26.- Variation of differential equation coefficients with airspeed, explosive flutter.

CURVE FITTING OF AEROELASTIC TRANSIENT RESPONSE DATA WITH EXPONENTIAL FUNCTIONS

Robert M. Bennett and Robert N. Desmarais

NASA Langley Research Center

2

SUMMARY

The problem of extracting frequency, damping, amplitude, and phase information from unforced transient response data is considered. These quantities are obtained from the parameters determined by fitting the digitized time-history data in a least-squares sense with complex exponential functions. The highlights of the method are described and the results of several test cases are presented. The effects of noise are considered both by using analytical examples with random noise and by estimating the standard deviation of the parameters from maximum-likelihood theory.

INTRODUCTION

One of the fundamental tasks in flutter testing is the determination of the frequency and damping of aeroelastic modes. Transient response or free decay records are often used for extracting this information and may be generated directly by a method such as the resonant dwell and cut (e.g., see ref. 1), or indirectly through the use of autocorrelation or randomdec types of data-reduction techniques (refs. 2 and 3). Graphical or manual techniques have often been used to determine frequency and damping, but, with the widespread use of automated data-reduction procedures, numerical curve-fitting techniques of complex exponential functions or damped sine waves are frequently used. There may be strong interactions between the curve-fitting method and the data-collection process, especially in the areas of record length requirements and specifications of noise level and distortion. Several procedures are currently available for the curve-fitting process (refs. 4 to 6). The purpose of this paper is to describe a method that takes a somewhat different approach from the previous works. The emphasis here is on developing a nearly real-time digital technique that is not only computationally fast but is also stable in the presence of real-world noise or contamination effects. A simple direct search technique for obtaining a least-squares fit using exponential functions has been developed and is presented. The application to several test cases is presented and discussed. Some effects of measurement noise are evaluated by comparing test-case results for different signal-to-noise ratios, and by developing estimates of the standard deviations of the parameters from maximum-likelihood theory (ref. 7, e.g.).

It should be kept in mind that although in a practical engineering sense the use of exponential functions for the analysis of data may be satisfactory, the aeroelastic equations are not strictly constant-coefficient ordinary

differential equations (ref. 8) and may involve other functions. Furthermore, the extrapolation of damping measured at subcritical conditions to flutter may also have shortcomings. For example, a case presented in reference 9 indicated a slope and curvature away from a flutter crossing in a plot of damping against velocity, even up to within 2 percent of the flutter speed.

SYMBOLS

a_0	coefficient in curve fit, the offset or static value (eq. (1))
a_k	coefficient of kth cosine term in curve fit (eq. (1))
b_k	coefficient of kth sine term in curve fit (eq. (1))
E	mean-squared error (eq. (2))
$\hat{E}$	expected value (eq. (3))
f	frequency, Hz
f_i	ith data point of digitized time history
i	data point index, 1 to N
j	parameter index
K	number of modes in curve fit
k	modal index, 1 to K
N	number of data points in digitized time history
R_1	output error covariance matrix
$\hat{S}$	parameter sensitivity matrix
t	time, seconds
V	velocity
V_f	flutter velocity
Y	curve-fitting expression (eq. (1))
ζ	fraction of critical damping
η	damping coefficient (eq. (1))
ω	frequency, rad/sec

ANALYSIS

Least-Squares Fitting Procedure

Given a free decay record containing the response of one or more vibration modes in the form of a digitized time history, the problem is to determine the modal damping, frequency, amplitude, and phase of each mode. A least-squares curve fit is made with complex exponential functions (or damped sine waves) in the form

$$Y(t) = a_0 + \sum_{k=1}^{K} e^{-\eta_k t} (a_k \cos \omega_k t + b_k \sin \omega_k t) \tag{1}$$

by minimizing the squared-error difference between the output fit $Y(t_i)$ and the input time history f_i. The error is given by

$$E = \sum_{i=1}^{N} [Y(t_i) - f_i]^2 \tag{2}$$

Inspection of equation (1) shows that if η_k and ω_k are preassigned, it is possible to compute a_0, a_k, and b_k by solving a linear least-squares problem. The nonlinear parameters η_k and ω_k must be determined by some type of search algorithm. Although this is a standard nonlinear, unconstrained optimization problem for which several methods are available for trial, for simplicity a direct search technique is used to search the coordinate space (η_k,ω_k) until the values that minimize equation (2) are obtained. At each step, values for η_k and ω_k are determined, the small linear system solved, and the error recomputed.

The technique has been programed for the Xerox Sigma 5 digital computer. In the program, the coordinate stepping process proceeds as follows:

(1) A starting set of coordinates η_k,ω_k (k = 1, . . ., K) and a starting step size are furnished to the program.

(2) The error E is computed at (η_k,ω_k) and at 4K additional points obtained by adding and subtracting the step size to or from each value of η_k and ω_k. If the central error E is less than any of the 4K peripheral values of E, the step size is reduced by 75 percent, and the calculations are repeated.

(3) Otherwise, the point that gave the lowest value of E is taken to be the new central point, and the step size is increased by 10 percent.

(4) The procedure is terminated when either the step size has been reduced below a preassigned threshold or a preassigned number of steps have been executed.

The method requires starting values for η_k and ω_k. For a single mode the starters can be arbitrary. However, for the multiple-mode case, the computer time can be significantly reduced by choosing good starters. The following procedure has been found to be a reasonable way of getting starters for multiple-mode cases:

(a) Generate a one-mode solution using arbitrary starters.

(b) Compute the difference between the one-mode solution and the input data, that is, the output error. Then generate a one-mode fit to the error.

(c) Use the η_k and ω_k values from steps (a) and (b) as the starters for the two-mode solution.

(d) For higher modes, steps (b) and (c) are repeated using the difference between the current multiple-mode solution and the original data to estimate the next higher mode.

Although this procedure is cumbersome, it appears to be stable and, at least for the single-mode case, surprisingly fast. It would also be very helpful to set the method up on an interactive basis similar to the technique described in reference 10.

One of the schemes in the literature is referred to as Prony's method (ref. 4). It computes η_k and ω_k by solving a 2K-order polynomial equation whose coefficients are determined from a least-squares process. The solution for the coefficients a_0, a_k, and b_k is then determined by a linear least-squares procedure, as is done here. Since this method is elegant and computationally efficient, it was examined during the present study. However, it has been the authors' experience that although Prony's method works well for perfect data, it is so sensitive to real-world noise that it is essentially useless even for generating starters for the search algorithm.

Uncertainty Levels of Estimated Parameters

The standard deviations of the estimated parameters, or uncertainty levels, can be determined from maximum-likelihood theory (ref. 7, e.g.). This type of estimate has provided some useful results in the field of stability and control (e.g., ref. 11). Assuming only measurement noise that is Gaussian and white, the expected variance of the parameter vector is

$$\hat{E}[\Delta\vec{p}\ \Delta\vec{p}^T] = \left\{ \sum_{i=1}^{N} \left[\hat{S}^T(t_i) R_1^{-1} \hat{S}(t_i) \right] \right\}^{-1} \tag{3}$$

where $\hat{S}$ is the parameter sensitivity matrix, R_1 is the output error covariance matrix, here a constant, and T denotes matrix transpose. The parameter vector $\vec{p}$ is made up of a_0, a_k, b_k, η_k, and ω_k, and the sensitivity matrix is given by $S_j(t_i) = \dfrac{\partial Y(t_i)}{\partial p_j}$. These elements of the sensitivity matrix can be

calculated by directly differentiating equation (1), and the variance is a normal output parameter. Thus, for a single channel of data, as considered here, these parameter uncertainty levels can be readily calculated after the curve-fitting process is completed.

RESULTS AND DISCUSSION

The curve-fitting method has been applied to three sets of data as test cases. The first case is a calculated damped sine wave with noise added with a random-number generator. The true answer is thus known. The second case is wind-tunnel data from the dynamic calibration of an aircraft gust vane. The third case is a set of data consisting of the subcritical randomdec signatures of the response to input noise of a two-dimensional flutter model that was implemented on an analog computer.

Analytical Test Case

The calculated data for the analytical test case with no added noise are shown in figure 1(a) and are compared with the fitted curve, which is exact in this case. For this case, the analytical input function was a single mode with offset and is given by

$$Y(t) = 1 - e^{-5t} \cos 30t$$

The curve fits for various levels of random noise are shown in figures 1(b) to 1(d). The noise level is defined as the rms level of the Gaussian noise and is given as the fraction of the maximum amplitude of the mode that is 1. The results of the curve fit are summarized in figure 2. Only modest degradation of the results is shown for reasonable values of noise level of up to 0.10 or 0.20. Also shown, as brackets on the points, are the standard deviations of the parameters, or uncertainty levels, calculated from equation (3) using the results output from the curve-fit procedure. In this case the exact modal parameters are known and it is possible to calculate a predicted uncertainty level from the exact parameters by assuming that the output error covariance is the value for the noise only. These predicted levels are shown as dashed lines. Both results give a good indication of the actual scatter, and thus the confidence level, with noise level. It might be noted that the effect of noise is larger on the coefficients a_1 and b_1 than on the damping, frequency, or offset. Thus, one must be more cautious in using the magnitude and phase information from such procedures.

These results amply demonstrate that the algorithm works well in the presence of random measurement noise. It has been the authors' experience, however, that a test case of this type does not indicate that a method will be satisfactory in practice. The noise here is random with zero mean, whereas in the real world, the effects of frequency drift, meandering means, and harmonic distortion are more severe.

Gust Vane Data

The two cases considered are from a wind-tunnel dynamic calibration of a light balsa vane used to sense atmospheric turbulence on an aircraft. The vane was mechanically displaced and released repetitively. Since the response to tunnel turbulence was a sizable fraction of the total response and the release conditions somewhat ill defined, the transients were ensemble averaged. The background noise was thus diminished, but a pure step response was not obtained. The two cases considered are called the low-damping case and the high-damping case (although the low-damping case is relatively highly damped by structural standards). The data for the low-damping case and the one-mode fit are shown in figure 3(a). The fit is reasonable, but there is some systematic deviation, particularly near the rightmost portion of the data. A two-mode fit was computed and, as shown in figure 3(b), gives a significantly improved result. The results of the one- and two-mode fits are summarized as follows:

One-mode fit

$$Y(t) = 0.0444 - e^{-39.9t}(0.239 \cos 140t - 0.452 \sin 140t)$$

Two-mode fit

$$Y(t) = 0.0450 - e^{-35.1t}(0.137 \cos 133t - 0.372 \sin 133t) - e^{-34.6t}(0.086 \cos 190t - 0.026 \sin 190t)$$

As compared with the one-mode results, the two-mode data indicate that the offset is nearly the same, the frequency of the first mode is reduced by about 5 percent, and the damping is reduced by about 10 percent, along with sizable changes in the coefficients of the first mode. The physical significance of the second mode is not clear in this case; it may be low-frequency noise that has not completely averaged out in the ensembling process. However, it is thought that the results for the first or principal mode obtained in the two-mode fit are more representative of the system response.

The results for the highly damped case are presented in figures 4(a) and 4(b). The results and trends are similar to those of the low-damping case. This case is a particularly difficult one to analyze, as it has high damping, a large offset, and a low-frequency distortion. The algorithm of this paper appears to give a reasonable result for this case.

Randomdec-Analog Flutter Data

Some subcritical randomdec signatures of the response of a two-dimensional, two-degree-of-freedom flutter model to input noise on an analog computer are also treated. The mathematical model and test setup were the same as those of the investigation of reference 9. The signatures and a one-mode curve fit are

shown in figures 5(a) to 5(d) as the velocity approaches flutter. As flutter is approached the signatures show little scatter or distortion, in contrast to the lower velocities. The signatures contain two modes, but the lower frequency mode is apparently unconverged in the randomdec procedure and could not be adequately resolved by the curve-fit procedure. The results for the flutter mode are compared with the exact solution in figure 6. The agreement is quite good in both frequency and damping, with the flutter speed underpredicted by less than 1 percent, which is within the expected accuracy of the analog setup. Thus, the curve-fit procedure appears to be a practical means of analyzing randomdec signatures.

CONCLUDING REMARKS

A least-squares curve-fitting procedure to extract frequency, damping, amplitude, and phase information from free decay records has been presented. The method appears to be stable and to give reasonable results in the presence of noise. Some of the effects of noise on the parameter estimates can be assessed by calculating the uncertainty levels from maximum-likelihood theory. The method is relatively fast for a one-mode fit, generally requiring 5 to 15 seconds on a Xerox Sigma 5 computer (which would be about 1 second on a CDC 6600 computer) and thus is a candidate for a real-time method. The two-mode solution, however, requires 2 to 5 minutes, and a three-mode solution is very long to calculate. Further work is needed to accelerate the multiple-mode calculations. It would also be very helpful to set the method up on an interactive basis. Currently, the only multiple-channel capability is to fit each channel of data separately, determine a weighted mean for frequency and damping, and then recalculate the coefficients for each channel. This procedure may be satisfactory for engineering purposes, but the development to a true multiple-channel method may be desirable.

REFERENCES

1. Rosenbaum, Robert: Survey of Aircraft Subcritical Flight Flutter Testing Methods. NASA CR-132479, 1974.

2. Cole, Henry A., Jr.: On-Line Failure Detection and Damping Measurement of Aerospace Structures by Random Decrement Signatures. NASA CR-2205, 1973.

3. Brignac, W. J.; Ness, H. B.; and Smith, L. M.: The Random Decrement Technique Applied to YF-16 Flight Flutter Tests. AIAA Paper No. 75-776, May 1975.

4. Hildebrand, F. B.: Introduction to Numerical Analysis. McGraw-Hill Book Co., Inc., 1956.

5. Wilcox, Phillip R.; and Crawford, William L.: A Least Squares Method for the Reduction of Free-Oscillation Data. NASA TN D-4503, 1968.

6. Chang, C. S.: Study of Dynamic Characteristics of Aeroelastic Systems Utilizing Randomdec Signatures. NASA CR-132563, 1975.

7. Grove, Randall D.; Bowles, Roland L.; and Mayhew, Stanley C.: A Procedure for Estimating Stability and Control Parameters From Flight Test Data by Using Maximum Likelihood Methods Employing a Real-Time Digital System. NASA TN D-6735, 1972.

8. Richardson, J. R.: A More Realistic Method for Routine Flutter Calculations. AIAA Symposium on Structural Dynamics and Aeroelasticity, Aug.-Sept. 1965, pp. 10-17.

9. Houbolt, John C.: Subcritical Flutter Testing and System Identification. NASA CR-132480, 1974.

10. Hammond, Charles E.; and Doggett, Robert V., Jr.: Determination of Subcritical Damping by Moving-Block/Randomdec Applications. NASA Symposium on Flutter Testing Techniques, Oct. 1975. (Paper No. 3 of this compilation.)

11. Iliff, Kenneth W.; and Maine, Richard E.: Practical Aspects of Using a Maximum Likelihood Estimator. Methods for Aircraft State and Parameter Identification, AGARD-CP-172, May 1974, pp. 16-1 — 16-15.

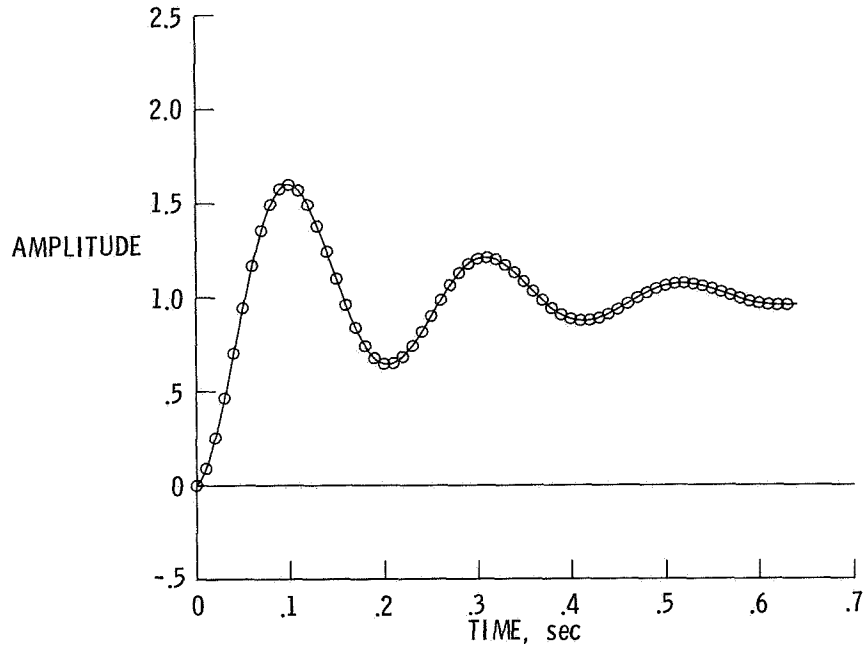

(a) No added noise.

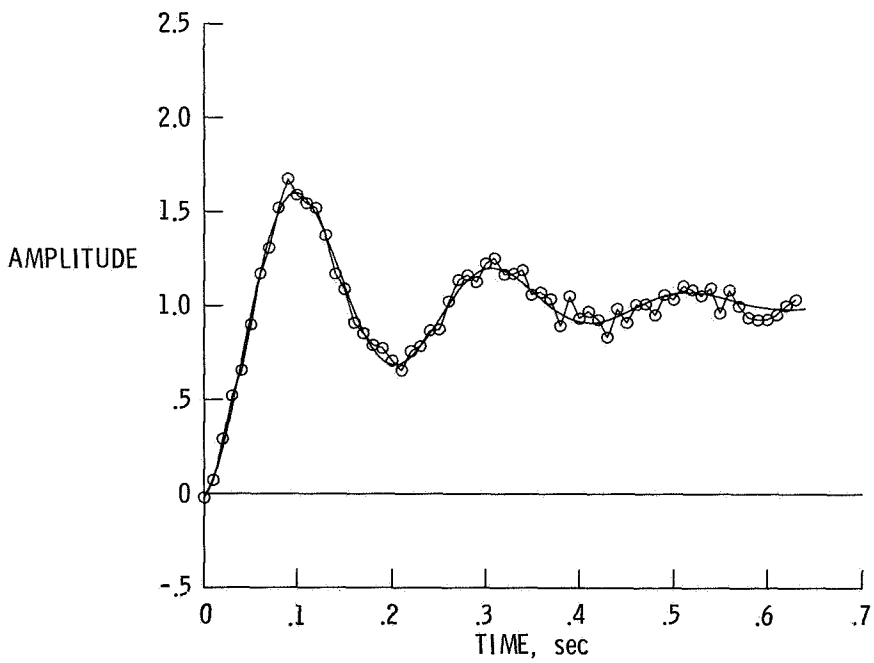

(b) Noise, 0.05.

Figure 1.- Curve fit for analytical case with random noise.

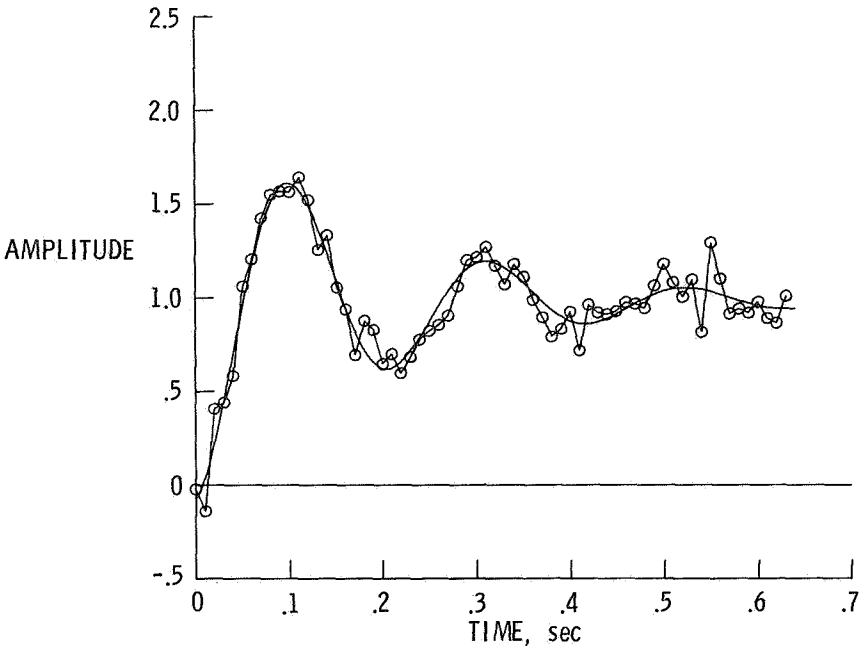

(c) Noise, 0.10.

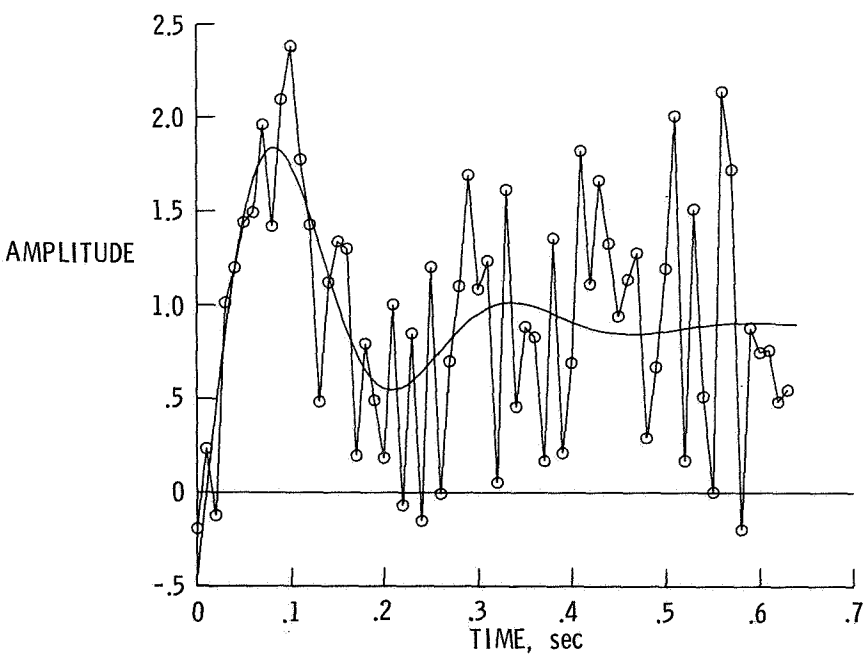

(d) Noise, 0.50.

Figure 1.- Concluded.

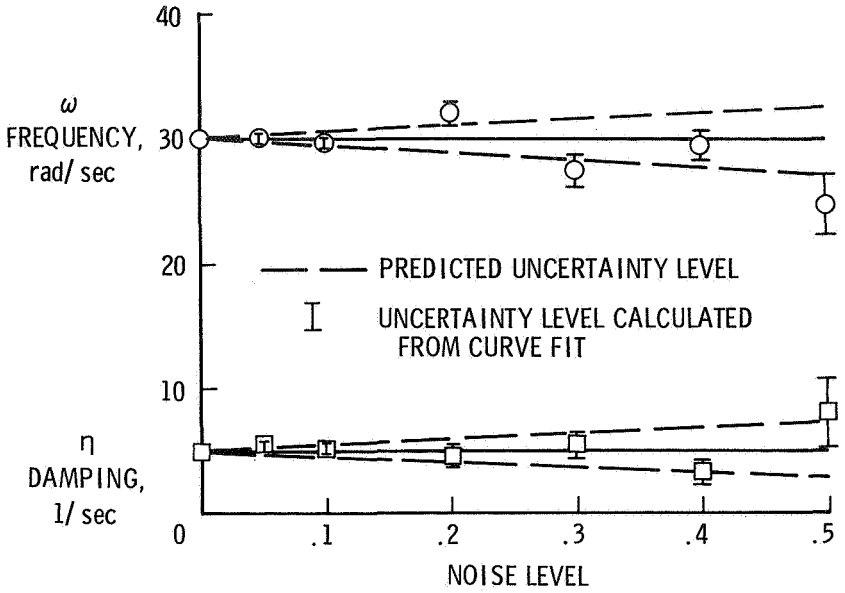

(a) Frequency and damping.

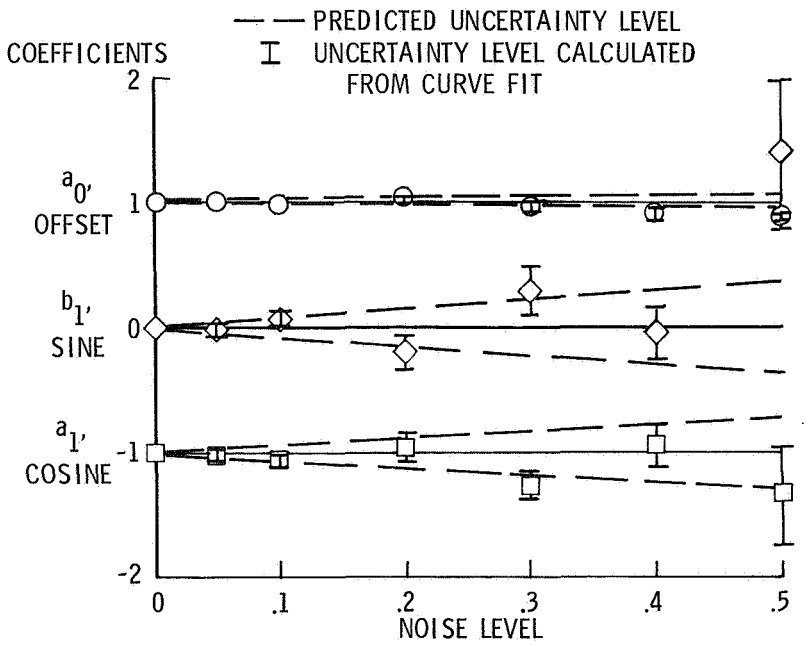

(b) Amplitude coefficients.

Figure 2.- Results of analytical case with random noise.

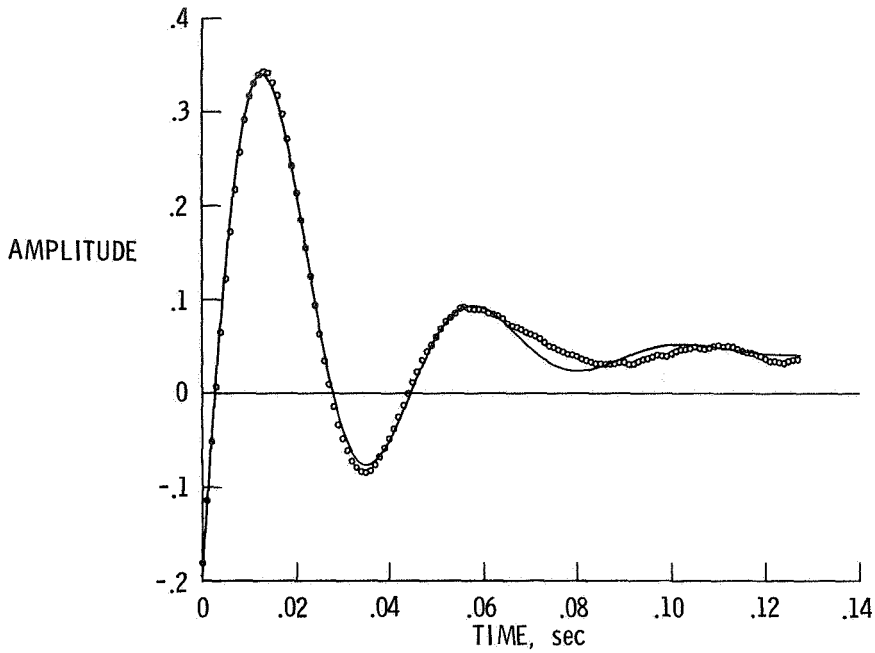

(a) One-mode fit.

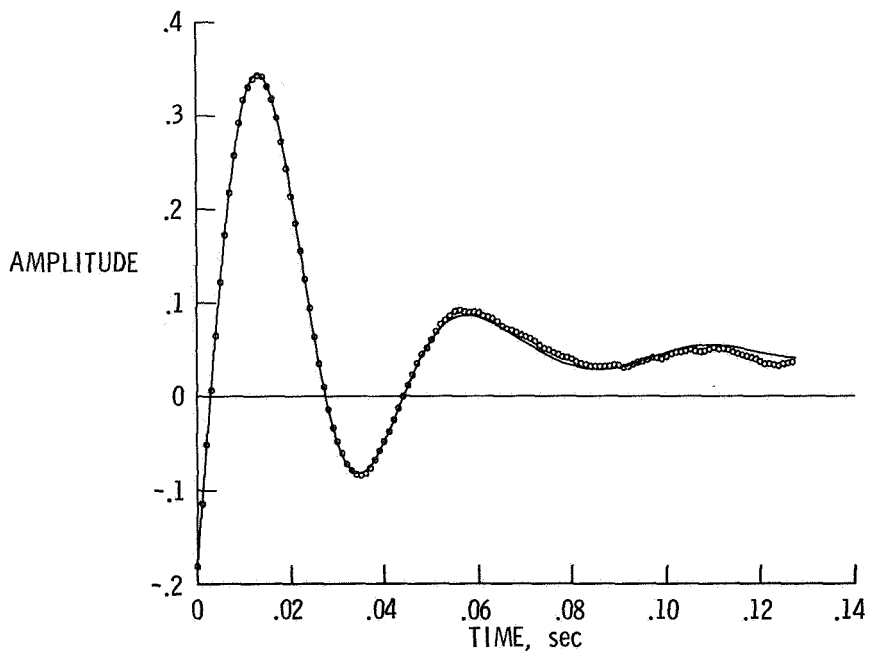

(b) Two-mode fit.

Figure 3.- Gust-vane curve fit for low-damping case.

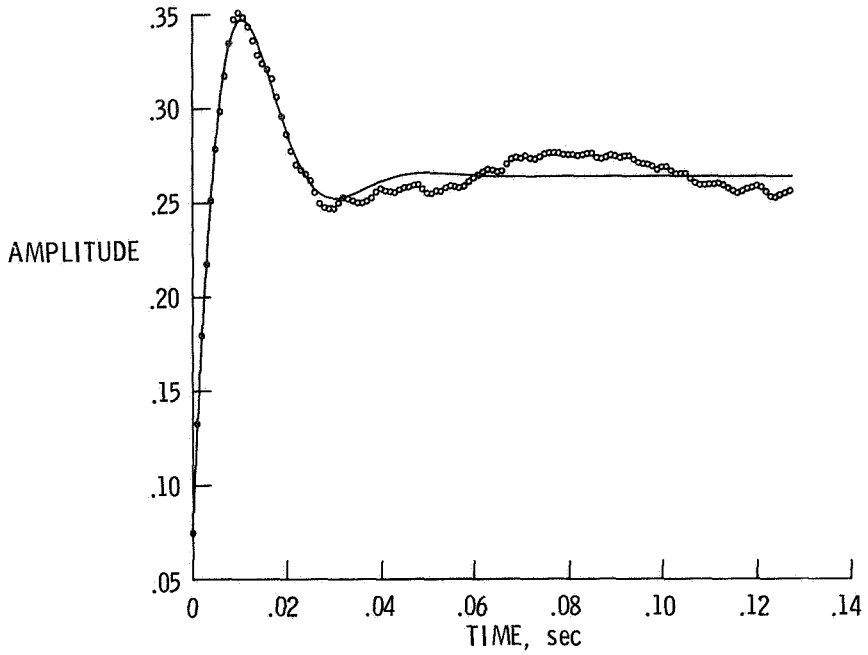

(a) One-mode fit.

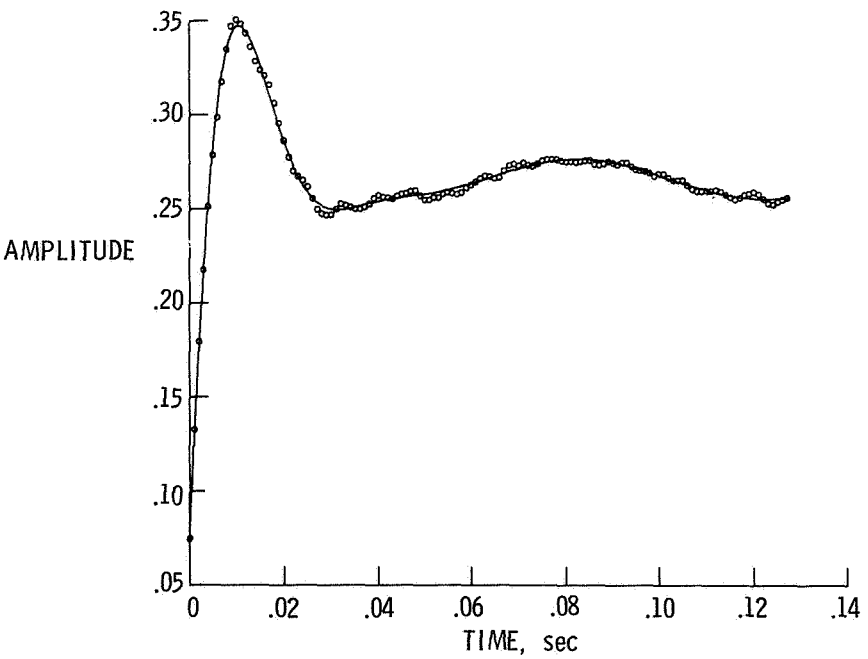

(b) Two-mode fit.

Figure 4.- Gust-vane curve fit for high-damping case.

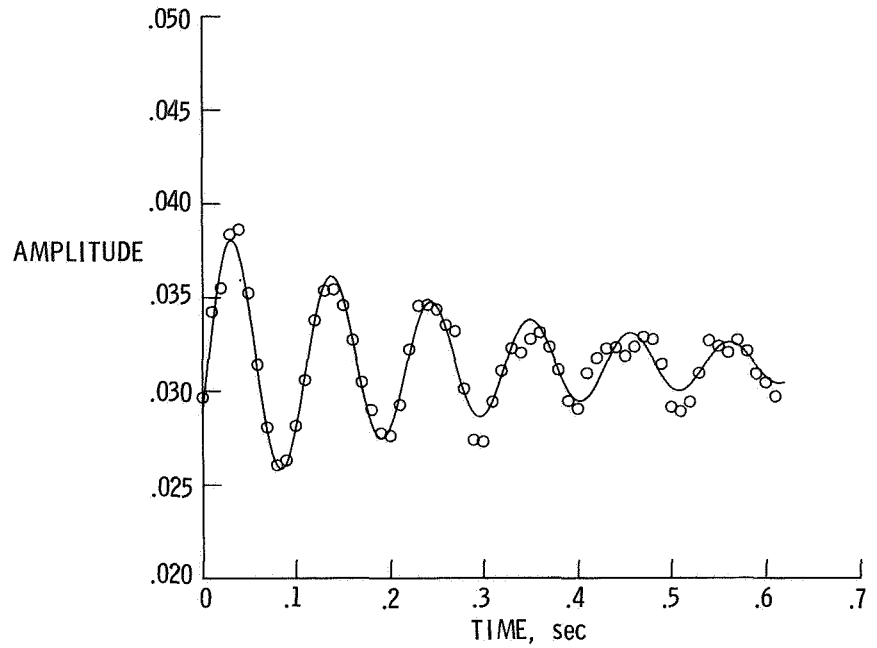

(a) $V/V_f = 0.684$.

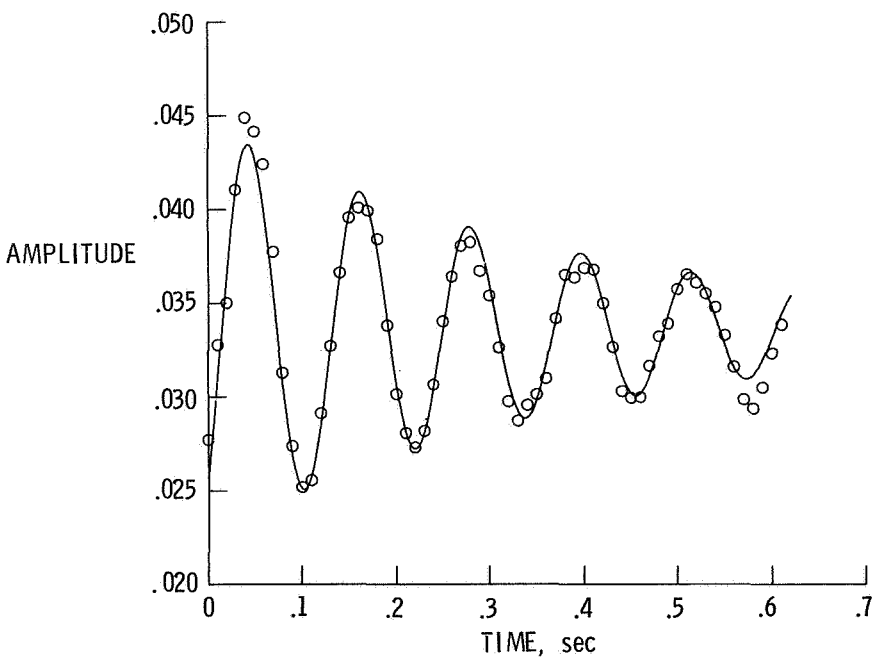

(b) $V/V_f = 0.855$.

Figure 5.- Curve fit of randomdec-analog data.

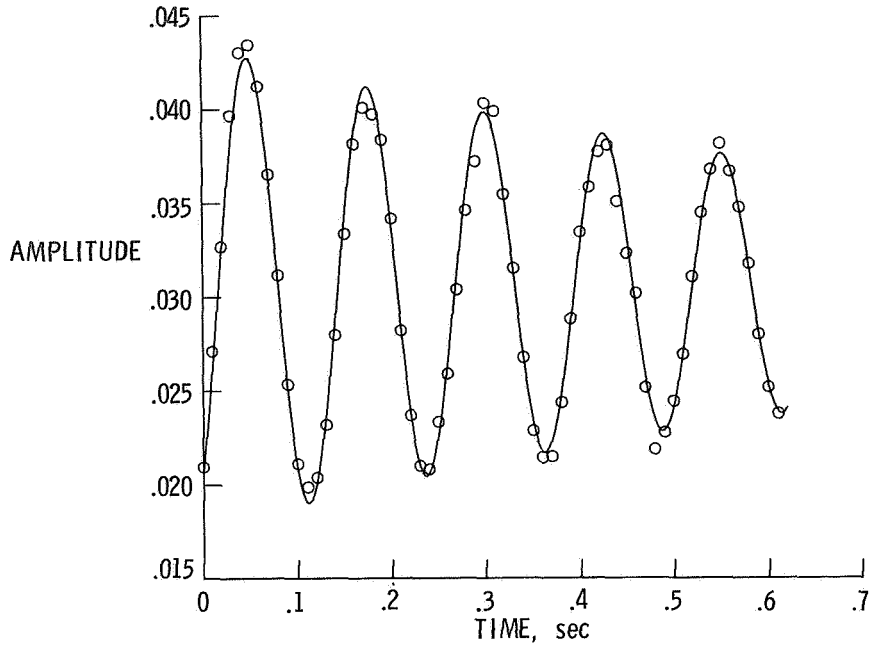

(c) $V/V_f = 0.941$.

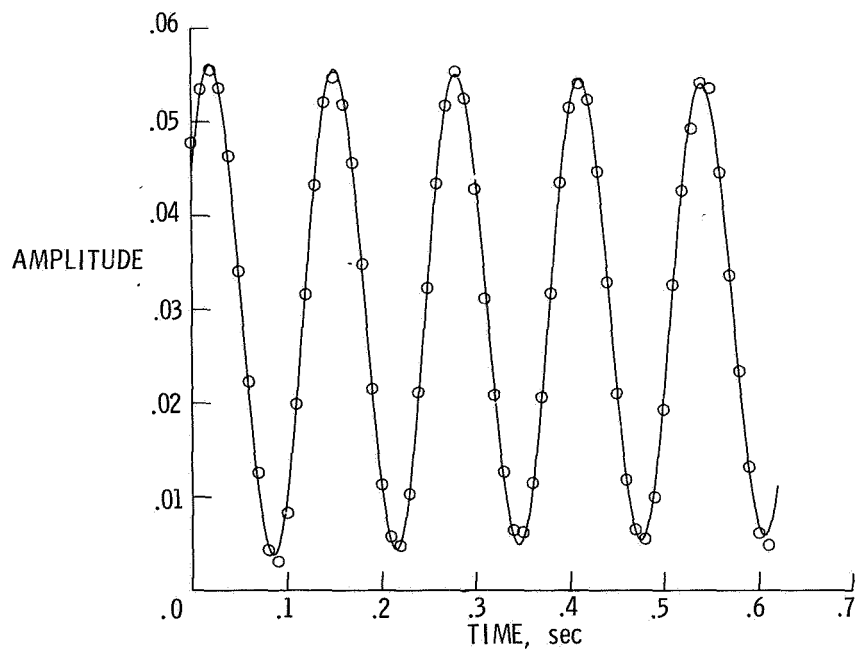

(d) $V/V_f = 0.992$.

Figure 5.- Concluded.

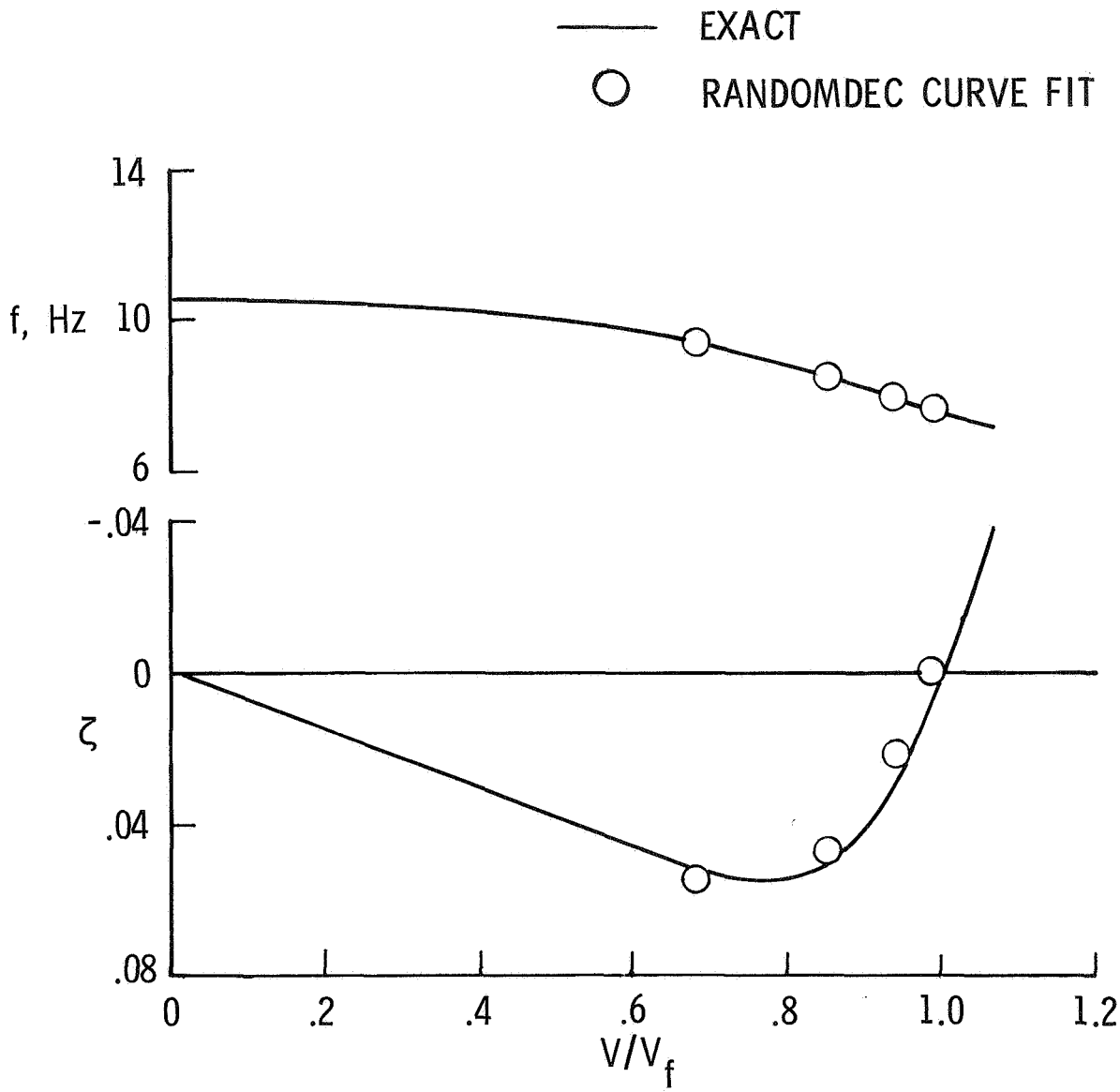

Figure 6.- Comparison of curve fit of randomdec-analog data with exact calculations.

DETERMINATION OF SUBCRITICAL DAMPING BY MOVING-BLOCK/RANDOMDEC APPLICATIONS

Charles E. Hammond
Langley Directorate, U.S. Army Air Mobility R&D Laboratory

Robert V. Doggett, Jr.
NASA Langley Research Center

3

SUMMARY

Two techniques are described which allow the determination of subcritical dampings and frequencies during aeroelastic testing of flight vehicles. The two techniques are the moving-block technique and the randomdec technique. The moving-block technique is shown to have the advantage of being able to provide damping and frequency information for each mode which might be present in a signal trace, but it has the disadvantage of requiring that the structure be excited transiently. The randomdec technique requires only random turbulence for excitation, but the randomdec signature is difficult to analyze when more than one mode is present. It is shown that by using the moving-block technique to analyze the randomdec signatures the best features of both methods are gained. Examples are presented illustrating the direct application of the moving-block method to model helicopter rotor testing and application of the combined moving-block/randomdec method to flutter studies of two fixed-wing models.

INTRODUCTION

Determination of subcritical damping during flutter tests both in wind tunnels and in flight is a subject which is currently receiving widespread attention. Since flutter is a potentially dangerous aeroelastic instability which can lead to catastrophic structural failure, it is desirable to obtain the flutter boundary without actually experiencing flutter. Traditionally, wind-tunnel flutter model test procedures have been to treat flutter as an event that either occurs or does not occur. The models are actually taken to the flutter condition, and by varying tunnel parameters (Mach number and dynamic pressure), sufficient flutter points are obtained to define the flutter boundary. This practice has in the past led to the total destruction of some very expensive models. Although the need for subcritical damping data has long been recognized, obtaining these data is not an easy task, and subcritical damping techniques have not been routinely used in the past. A large part of the difficulty has been associated with the inability to reduce, analyze, and display model damping data in near real time so that the damping can be continuously monitored during approach to the flutter boundary. The installation of the computer controlled data acquisition system has now made it practical to apply subcritical damping methods to flutter tests in the Langley transonic dynamics tunnel.

This paper describes two techniques which are currently being used in wind-tunnel aeroelastic model tests of both helicopter rotors and fixed wings. The two techniques to be described are the so-called moving-block technique and the randomdec technique. Although neither of the techniques is new, it is felt that the combined application of the two analyses is unique, particularly with respect to fixed-wing flutter testing.

SYMBOLS

A	amplitude of transient response
$F(\omega)$	Fourier transform at frequency ω
i	imaginary number, $\sqrt{-1}$
k	an integer in equation (14)
N	an integer in equation (10); total number of data samples in equation (13)
$\bar{N}$	number of data samples in block used for frequency optimization
T	period of boxcar function
t	time
Δt	time between discrete data samples
$u(t)$	boxcar function, equation (2)
$y(t)$	transient response of single-degree-of-freedom system, equation (1)
ζ	damping ratio
τ	start time of boxcar function
ϕ	phase angle
ω	damped natural frequency
ω_n	undamped natural frequency

MOVING-BLOCK TECHNIQUE

The moving-block technique was originally developed by the Lockheed-California Company, and its use in rotary wing aeroelastic stability testing has been reported in references 1 and 2. A formulation of this technique has

been developed at the Langley Research Center, and it has been implemented on the recently installed data acquisition system for the Langley transonic dynamics tunnel.

The moving-block technique is a method which allows the determination of modal dampings and frequencies from a response signal of a structure which has been excited transiently. The transient excitation may consist of a sinusoidal input which has been abruptly terminated or it may be an impulsive excitation. In any event, if the damping and frequency of a particular mode are desired, it is necessary that this mode be excited by the type of excitation chosen. This requirement that the structure be excited and then be allowed to decay freely is one of the disadvantages of the method, but for many applications it is not an overly burdensome requirement. This is particularly true in helicopter applications where the existing control system can be used to supply the necessary excitation of the rotor system.

In order to illustrate how the moving-block technique works, consider the transient response of a single-degree-of-freedom system which may be written as

$$y(t) = Ae^{-\zeta\omega_n t} \sin(\omega t + \phi) \tag{1}$$

where

$$\omega^2 = \omega_n^2(1 - \zeta^2)$$

Now compute the finite Fourier transform of this response at the damped frequency ω from time τ to time $\tau + T$. This is the same as multiplying the response by the boxcar function

$$u(t) = \begin{cases} 0 & \text{for } t < \tau \\ 1 & \text{for } \tau \leq t \leq \tau + T \\ 0 & \text{for } t > \tau + T \end{cases} \tag{2}$$

as shown in figure 1 and computing the infinite transform. The significance of the starting time τ is discussed subsequently. The finite transform is given by

$$F(\omega) = \int_{\tau}^{\tau+T} Ae^{-\zeta\omega_n t} \sin(\omega t + \phi)\, e^{-i\omega t}\, dt \tag{3}$$

This integration may be performed in closed form and the result is

$$F(\omega) = \frac{A}{\zeta\omega_n(\zeta\omega_n + i2\omega)} \left(e^{-(i\omega+\zeta\omega_n)\tau} [(i\omega + \zeta\omega_n) \sin(\omega\tau + \phi) + \omega \cos(\omega\tau + \phi)] \right.$$

$$\left. - e^{-(i\omega+\zeta\omega_n)(\tau+T)} \{(i\omega + \zeta\omega_n) \sin[\omega(\tau + T) + \phi] + \omega \cos[\omega(\tau + T) + \phi]\} \right) \tag{4}$$

After a considerable amount of algebraic manipulation the amplitude of this transform may be written as

$$|F(\omega)| = \frac{Ae^{-\zeta\omega\tau}}{2\zeta\omega} \{1 - 2e^{-\zeta\omega T} + e^{-2\zeta\omega T} + (1 - e^{-\zeta\omega T})\zeta \sin 2(\omega\tau + \phi)$$

$$- e^{-\zeta\omega T}(1 - e^{-\zeta\omega T})\zeta \sin 2[\omega(\tau + T) + \phi]\}^{1/2} \tag{5}$$

In obtaining this expression, it has been assumed that $\zeta << 1$ and thus $\omega_n \approx \omega$. Also, terms involving ζ^2 have been deleted as being small compared to unity. It is convenient to write this expression in the form

$$|F(\omega)| = \frac{A}{2\omega} e^{-\zeta\omega\tau} \left[\frac{1 + f(\zeta)}{\zeta^2}\right]^{1/2} \tag{6}$$

where

$$f(\zeta) = - 2e^{-\zeta\omega T} + e^{-2\zeta\omega T} + (1 - e^{-\zeta\omega T})\zeta \sin 2(\omega\tau + \phi)$$

$$- e^{-\zeta\omega T}(1 - e^{-\zeta\omega T})\zeta \sin 2[\omega(\tau + T) + \phi] \tag{7}$$

Taking the natural logarithm of equation (6) yields

$$\ln|F(\omega)| = - \zeta\omega\tau + \ln\left(\frac{A}{2\omega}\right) + \frac{1}{2} \ln \left[\frac{1 + f(\zeta)}{\zeta^2}\right] \tag{8}$$

The last term in equation (8) may be expanded in a Maclaurin series to yield

$$\ln|F(\omega)| = - \zeta\omega\tau + \ln\left(\frac{A}{2\omega}\right)$$

$$+ \frac{1}{2} \ln \left((\omega T)^2 + (\omega T) \{\sin 2(\omega\tau + \phi) - \sin 2[\omega(\tau + T) + \phi]\}\right)$$

$$- \frac{\zeta}{4} \omega T \left\{\frac{2\omega T + \sin 2(\omega\tau + \phi) - 3 \sin 2[\omega(\tau + T) + \phi]}{\omega T + \sin 2(\omega\tau + \phi) - \sin 2[\omega(\tau + T) + \phi]}\right\} \tag{9}$$

From this expression it can be seen that if a plot of $\ln|F(\omega)|$ versus τ is made, the resulting curve will be the superposition of a straight line with slope $-\zeta\omega$ and an oscillatory component which oscillates about the straight line with a frequency of 2ω. This fact can be more easily seen if it is assumed that T is an integral multiple of the basic period of oscillation. That is,

$$T = \frac{2\pi N}{\omega} \qquad (N = 1, 2, 3, \ldots) \tag{10}$$

With this assumption, equation (9) becomes

$$\ell n|F(\omega)| = -\zeta\omega\tau + \frac{1}{2}\zeta \sin 2(\omega\tau + \phi) + C \tag{11}$$

where C is a constant given by

$$C = \ell n\left(\frac{A}{2\omega}\right) + \ell n(\omega T) - \frac{\zeta\omega T}{2} \tag{12}$$

Thus if the boxcar shown in figure 1 is started at $\tau = 0$ and successive discrete transforms at frequency ω are performed for increasing values of τ, a plot can be made from which the damping can be determined. It is precisely this process which is used in the moving-block analysis.

This analytical background has, for simplicity, dealt with the response of a single-degree-of-freedom system. The basic strong point of the moving-block method is, however, its ability to provide frequency and damping information for each of the modes in a multimode response signal. If a multimode response is thought of in terms of a Fourier series representation, then the response is simply a summation of several single-degree-of-freedom responses, and the Fourier transform effectively provides the means for isolating the various components of the response.

IMPLEMENTATION OF MOVING-BLOCK TECHNIQUE

The moving-block technique described previously has been implemented on the data acquisition system of the Langley transonic dynamics tunnel. The data system consists of a Xerox Sigma 5 digital computer coupled with a 60-channel analog front end. The system is equipped with a graphics display unit which allows data reduction to be accomplished with as much interaction by the engineer as desired. A more detailed description of the data system is presented in reference 3.

The moving-block technique is set up as a completely interactive program. The sequence of events which are incorporated in the analysis is depicted in figure 2. The first step in the process is to obtain the signal to be analyzed. This signal may be digitized directly from the data stream coming from the model which has been transiently excited, or the signal may be a randomdec signature which is passed from the randomdec analysis to be described subsequently in this paper.

Once the signal to be analyzed is obtained, a fast Fourier transform (FFT) of the signal is computed. This transform is solely for the purpose of providing the analyst with information relative to the frequency content of the signal. The transform also allows the analyst to determine whether or not the mode of interest has been excited. From the FFT results the analyst selects the frequency for the mode to be analyzed. The peak in the FFT results may not correspond to the actual frequency in the signal because of the fact that the frequency resolution available from the FFT is dependent upon both digital sampling rate and number of points in the sample as given by

$$\Delta f = \frac{1}{N\ \Delta t} \tag{13}$$

Thus a scheme to optimize the selected frequency has been included in the analysis. In accomplishing this optimization a segment, or block, of the input transient response signal is first selected. Generally, the block length is chosen to be one-half the total number of points in the data sample. Let the number of samples in the block be denoted by $\bar{N}$. The algorithm used by FFT analyses for determining the frequencies at which the transform is computed is

$$f = \frac{k}{\bar{N}\ \Delta t} \qquad (k = 0,\ 1,\ 2,\ \ldots) \tag{14}$$

By using the frequency selected from the original FFT results, the sampling rate, and $\bar{N}$, a value for k can be calculated. Then, if k is held constant and $\bar{N}$ is changed by one data point, a small change in the computed frequency occurs. The optimization then proceeds as follows. Compute the discrete transform at the following three frequencies:

$$\left.\begin{aligned} f_{\bar{N}-1} &= \frac{k}{(\bar{N} - 1)\ \Delta t} \\ f_{\bar{N}} &= \frac{k}{\bar{N}\ \Delta t} \\ f_{\bar{N}+1} &= \frac{k}{(\bar{N} + 1)\ \Delta t} \end{aligned}\right\} \tag{15}$$

Note that the block size is different for each computation. By observing the amplitude of the transform from these three calculations, one can determine how to continue changing the block size to cause the magnitude of the transform to reach a peak. When this peak is reached, the frequency corresponding to that peak is the optimized frequency at which the damping calculations are made.

The damping calculation is made by using the optimized frequency and the block size which resulted in this frequency and by computing successive discrete Fourier transforms as the block is moved down the data record. The block is first positioned at the beginning of the record, the transform is computed, and the logarithm of the transform amplitude is plotted. The block is then moved down the data record one data sample and this process repeated. When the block reaches the end of the data record a plot equivalent to a plot of equation (9) has been made. The damping in the mode being analyzed is obtained from the slope of a linear least-squares fit to this curve.

HELICOPTER TRANSIENT RESPONSE APPLICATION

The moving-block technique was originally implemented at Langley to facilitate subcritical aeroelastic testing of model helicopter rotors in the Langley transonic dynamics tunnel. An in-house model, termed the generalized rotor aeroelastic model (GRAM), is used to test rotors up to 3.4 m (11 ft) in diameter. The model is shown in the left part of figure 3 with the Bell Helicopter Company flex-hinge rotor installed. The right part of figure 3 shows the hydraulic control system of the model which is used both for quasi-static control of the rotor and for transient excitation of the rotor for subcritical damping measurements.

In conducting the rotor tests, the rotor is first trimmed to the desired operating condition, and then the excitation is started either manually or under computer control. The type of excitation, amplitude, frequency, and number of cycles of excitation are options which are manually selectable by the engineer. The computer is programed to begin digitizing data from the channel of interest two or three cycles before the termination of the excitation. The digitized data are then plotted on the graphics display unit (GDU) so that the analyst may select the point on the signal trace where he would like to start the damping analysis. It has been found desirable to have the analyst select the starting point rather than have the computer determine when the excitation terminates and then begin digitizing data because of certain time lags inherent in the system. The analyst also generally feels more confident about the data if he can see some of the forced response in the trace just prior to termination of the excitation.

The Bell Helicopter Company flex-hinge rotor was recently tested on the GRAM. One of the objectives of this test was to examine the amount of in-plane damping available in the rotor system. Figure 4 is a typical GDU display from this particular test. The data trace in the lower left quadrant of this figure was taken from one of the blade chordwise bending gages. Note that this plot begins at the starting point previously selected by the analyst. The plot in the upper left quadrant of the figure is the FFT amplitude plotted out to the Nyquist frequency. Since the frequency of interest may be obscured on this plot, the analyst is provided the capability of interactively changing the frequency range over which the FFT amplitude is plotted. The plot in the lower right quadrant of figure 4 is an expanded scale version of the plot in the upper left quadrant. The frequency of interest is selected by the analyst from either of the FFT plots by use of a light gun. This selected frequency is optimized automatically, and the damping plot is displayed in the upper right quadrant. After the analyst selects the start and stop times for the least-squares fit, the least-squares calculations are made, and the computed frequency and damping are displayed at the bottom of the GDU screen. Options are provided for changing the block size and repeating the analysis at the same frequency and for selecting a new frequency for which the modal damping is desired.

A word of explanation is in order concerning the damping plot in the upper right quadrant of figure 4. The plot is seen to have a portion which approximates a straight line and a later portion which deviates considerably from the

straight line. This deviation from the straight line occurs when the mode being analyzed damps out rapidly. Once the mode of interest damps out, the calculations are influenced by other modes in the signal as well as by noise. This behavior of the damping plot illustrates the desirability of an interactive formulation of this technique.

RANDOMDEC TECHNIQUE

Since a detailed description of the randomdec method is presented in reference 4, only the highlights of the method are described. Simply stated, the randomdec technique provides a means for obtaining damping and frequency information by performing an ensemble average of segments of a random time history of the structural response. The underlying assumption in the method is that the structural response is the linear superposition of the responses to a step force (initial displacement), an impulsive force (initial velocity), and a random force. If the segments used in the ensemble average are chosen so that the initial displacement is the same for all segments and the initial velocities of alternating segments have opposite signs, then the resulting ensemble average, called the randomdec signature, represents the response to a step force, since the averages of the impulse force and random force components approach zero as the number of segments used in the ensemble average increases.

For a single-degree-of-freedom system the damping and frequency can be determined directly from the randomdec signature. The dampings and frequencies of the individual modes of a multi-degree-of-freedom system can be determined either by bandpass filtering the response signal before determining the randomdec signature so that only one mode is present or by further processing of the signature to separate it into its individual frequency components. For example, in the latter case a curve fitting procedure has been presented in reference 5 for determining the individual frequency components of a randomdec signature that contains the responses of several modes.

The randomdec method is very attractive for use in flutter investigations, since no discrete forced excitation is required. The almost always present wind-tunnel turbulence in the case of model tests and atmospheric turbulence in the case of flight tests are sufficient to provide the needed random excitation. Some results from wind-tunnel model studies are presented in reference 6, and some results from a flight flutter clearance study are presented in reference 7.

One of the disadvantages of the randomdec method to date has been the difficulty in determining the damping when more than one mode is present in the randomdec signature. The great advantage of the moving-block technique is, on the other hand, the ability to analyze signals which may have several modes present and to allow the analyst to determine the damping present in each of the modes. It seemed only natural, then, to use the moving-block technique to analyze randomdec signatures. That is, the randomdec signature is used as the transient response input to the moving-block analysis. Some results of applications of the combined moving-block/randomdec method are discussed in the subsequent section.

MOVING-BLOCK/RANDOMDEC FLUTTER APPLICATIONS

The combined moving-block/randomdec method has been used during several wind-tunnel model studies in the Langley transonic dynamics tunnel. Some results from two of these applications are described in the following discussion.

The first application to be described was in the testing of a high-aspect-ratio subsonic-transport wing model. A photograph of this cantilever-mounted model is shown in figure 5. The flutter boundary for this model was determined during testing and also is shown in figure 5. Some subcritical damping data were obtained as the flutter boundary was approached along the path indicated by the dashed line in the figure. The conditions at which damping and frequency were evaluated are indicated by the circle symbols on the figure. At these six conditions the wind-tunnel conditions were held constant, and a randomdec signature was determined and then processed through the moving-block analysis to determine the damping and frequency. One of the randomdec signatures from this test and the results of applying the moving-block analysis to this signature are shown in figure 6. The resulting subcritical damping results are presented in figure 7 in the form of the variation of damping in the critical flutter mode with Mach number and dynamic pressure. It was necessary to plot the damping versus both of these parameters since both were being varied as the flutter boundary was approached. The actual flutter point is indicated by the square symbols on the figure. Note that the flutter point predicted by extrapolating the subcritical damping results is very close to the actual flutter condition.

The second application described was to a low-aspect-ratio arrow-wing model. A photograph of this model is presented in figure 8. Some subcritical damping and frequency data were obtained for this model by using the moving-block/randomdec method as the flutter boundary was approached in a manner similar to that described for the transport-type wing model. Subcritical damping data for the arrow-wing model are presented in figure 9 in the form of the variations of damping ratio with dynamic pressure and Mach number. The measured flutter condition is indicated by the square symbols on the figure. Here again an extrapolation of the subcritical damping results predicts a flutter condition that is very close to that determined experimentally.

As the results presented show, the flutter conditions for both the subsonic-transport wing and arrow-wing models were predicted with sufficient accuracy by extrapolating moving-block/randomdec subcritical damping data. However, it should be pointed out that the method is still in a developmental stage and has not yet replaced the traditional method of actually determining flutter points in defining the flutter boundary during model tests in the Langley transonic dynamics tunnel.

CONCLUDING REMARKS

Two techniques have been discussed for determining damping and frequency information during subcritical aeroelastic testing of fixed-wing aircraft and helicopters. The moving-block technique has the advantage of being able to determine the damping and frequency for each of the modes which might be present in a response signal, but it has the disadvantage of requiring that the structure be excited transiently. This disadvantage has not presented any particular difficulties in the helicopter rotor tests conducted to date, however, since the helicopter control system may be used to provide the necessary excitation. In a fixed-wing test the requirement for transient excitation could be rather troublesome. The randomdec technique has the distinct advantage of providing frequency and damping information with random turbulence being the only excitation required. The disadvantage of the randomdec method is that frequency and damping data for a particular mode are difficult to obtain if the randomdec signature is made up of more than one mode. In order to capitalize on the strong points of each of these powerful methods, the two techniques have been used in series. That is, the moving-block technique has been used to analyze the randomdec signatures. The two examples presented to illustrate the application of this combined procedure indicate that the procedure can, in fact, be used for subcritical flutter testing. The method is, however, still in a developmental stage and it has not yet replaced the traditional method of actually determining flutter points in defining the flutter boundary during model tests in the Langley transonic dynamics tunnel.

REFERENCES

1. Anderson, William D.: Investigation of Reactionless Mode Stability Characteristics of a Stiff Inplane Hingeless Rotor System. American Helicopter Soc. Preprint No. 734, May 1973.

2. Johnston, J. F.; and Conner, F.: The Reactionless Inplane Mode of Stiff-Inplane Hingeless Rotors. Rep. No. LR 26214 (Contract No. DAAJ01-73-C-0286), Lockheed-California Co., Dec. 1973.

3. Doggett, Robert V., Jr.; and Hammond, Charles E.: Application of Interactive Computer Graphics in Wind-Tunnel Dynamic Model Testing. Applications of Computer Graphics in Engineering, NASA SP-390, 1975, pp. 325-353.

4. Cole, Henry A., Jr.: On-Line Failure Detection and Damping Measurement of Aerospace Structures by Random Decrement Signatures. NASA CR-2205, 1973.

5. Chang, C. S.: Study of Dynamic Characteristics of Aeroelastic Systems Utilizing Randomdec Signatures. NASA CR-132563, 1975.

6. Foughner, Jerome T., Jr.: Some Experience Using Subcritical Response Methods in Wind-Tunnel Flutter Model Studies. NASA Symposium on Flutter Testing Techniques, Oct. 1975. (Paper No. 7 of this compilation.)

7. Brignac, W. J.; Ness, H. B.; and Smith, L. M.: The Random Decrement Technique Applied to the YF-16 Flight Flutter Tests. AIAA Paper No. 75-776, May 1975.

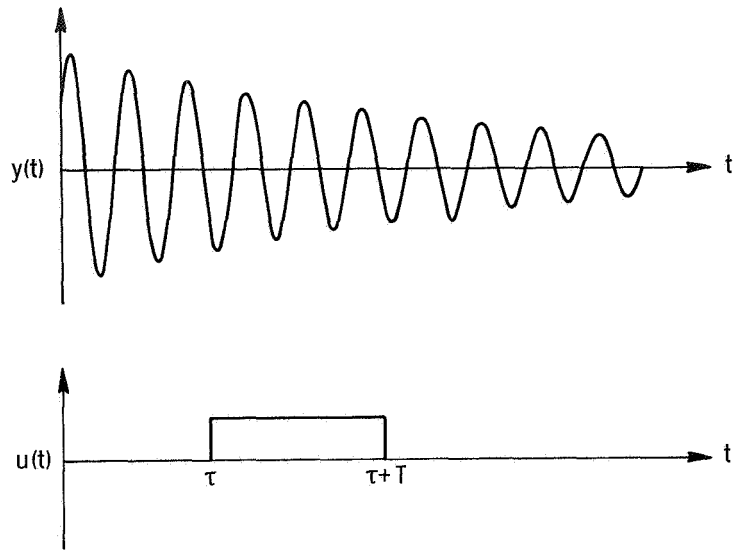

Figure 1.- Single-degree-of-freedom response function and boxcar function used in finite Fourier transform.

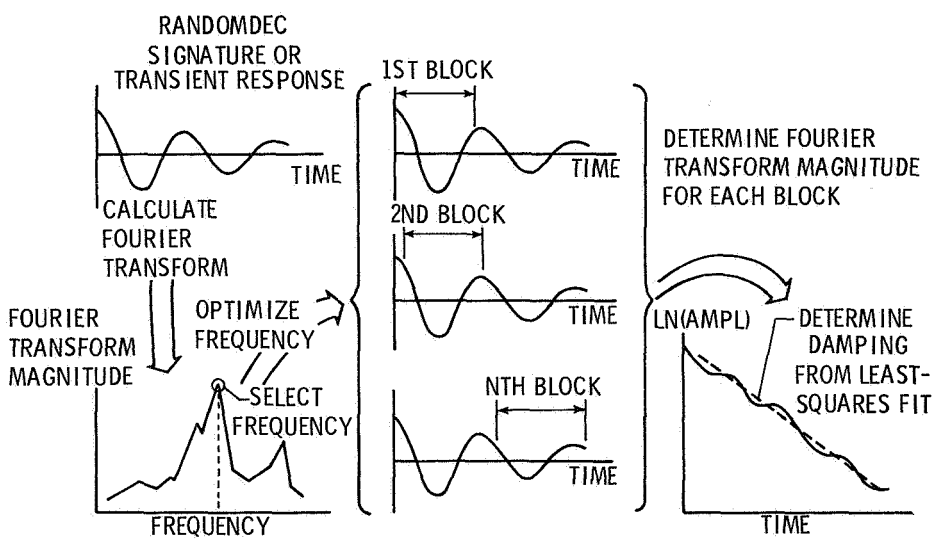

Figure 2.- Moving-block schematic illustration.

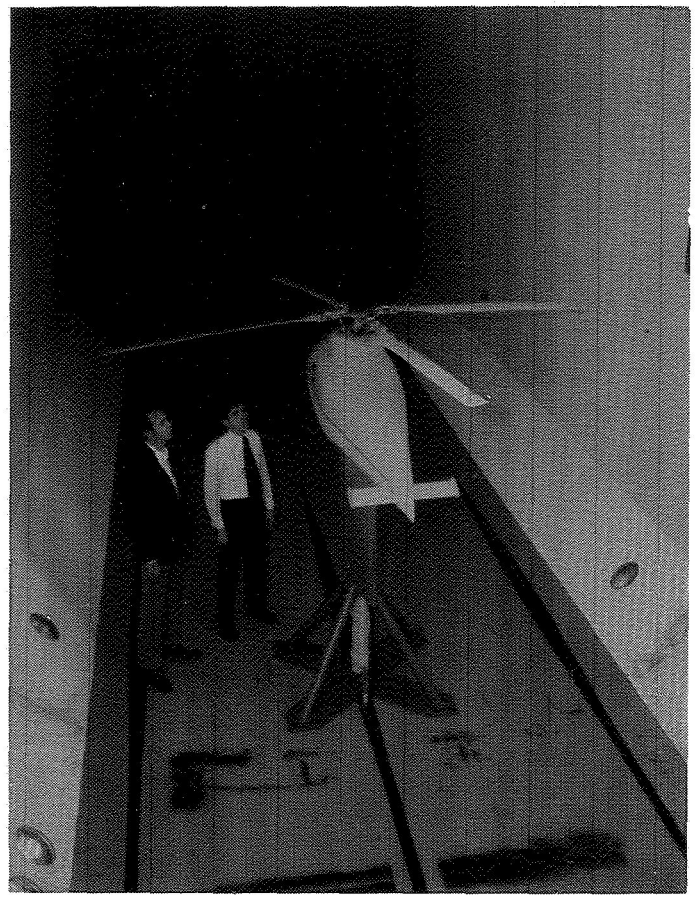

(a) GRAM with Bell Helicopter Company flex-hinge rotor installed.

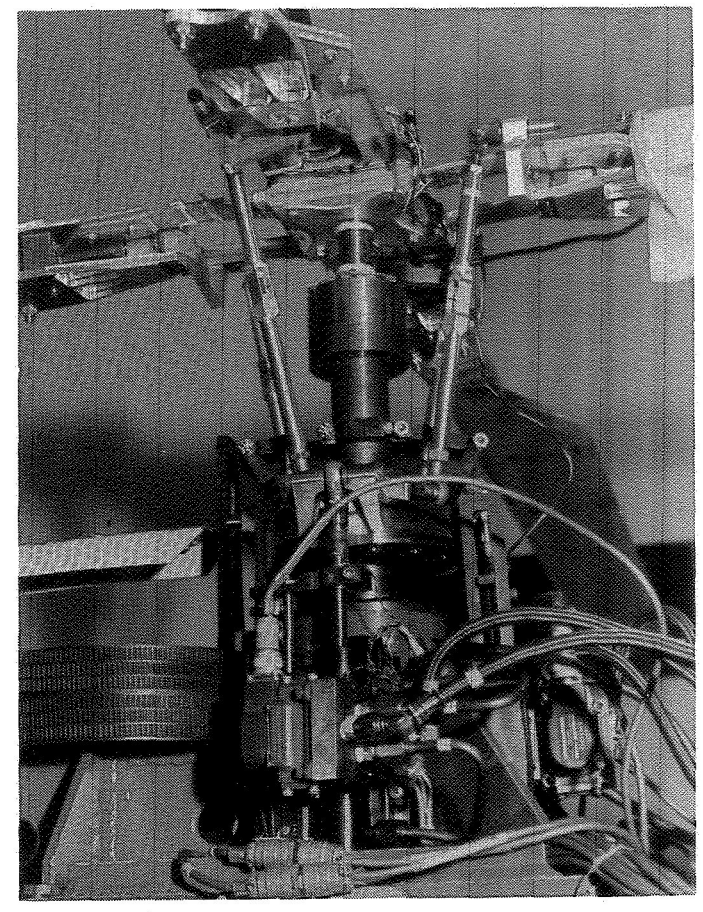

(b) GRAM hydraulic control system.

Figure 3.- The generalized rotor aeroelastic model (GRAM) used for rotor aeroelastic studies in the Langley transonic dynamics tunnel.

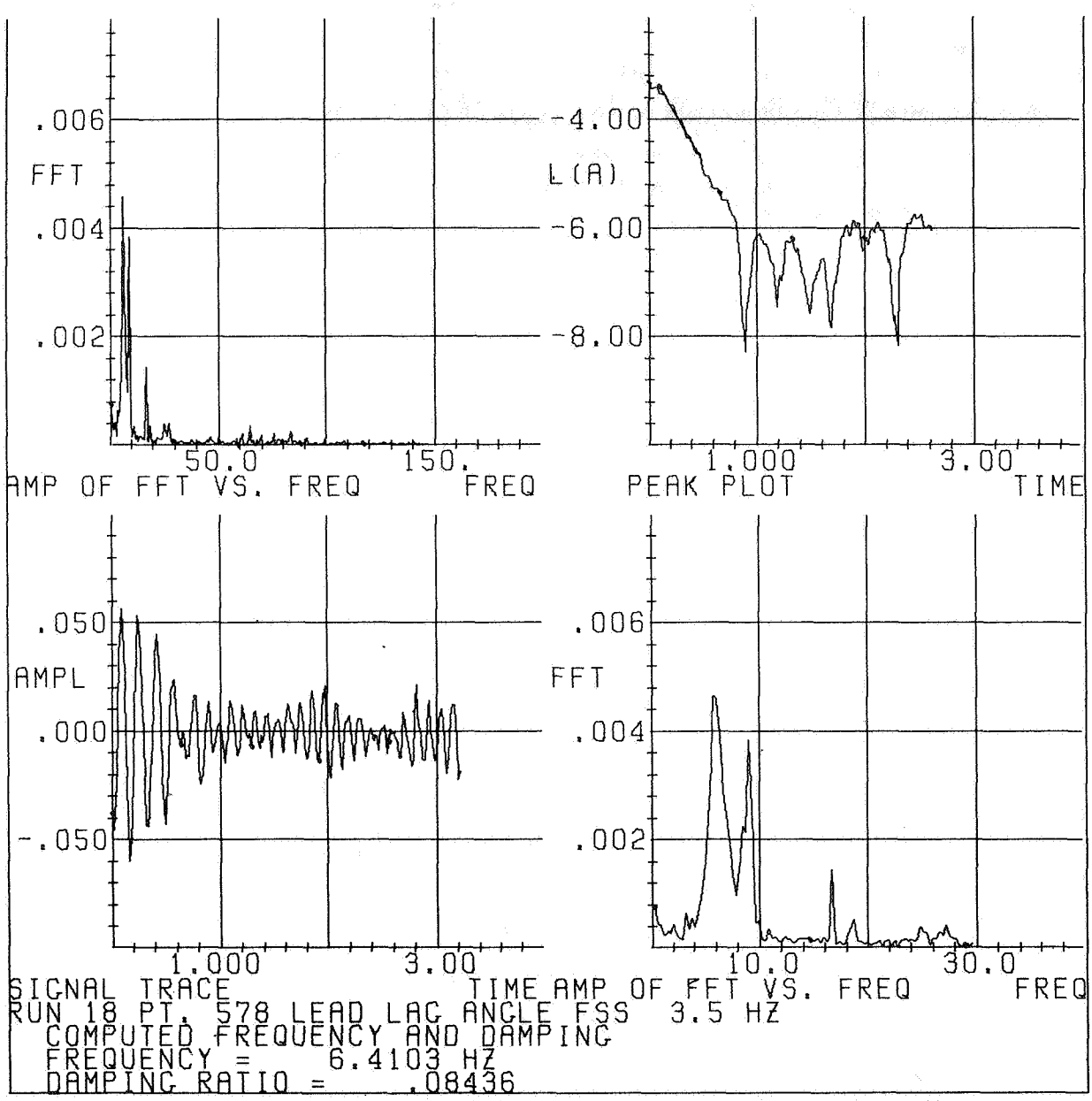

Figure 4.- Typical subcritical response data from GRAM flex-hinge rotor tests.

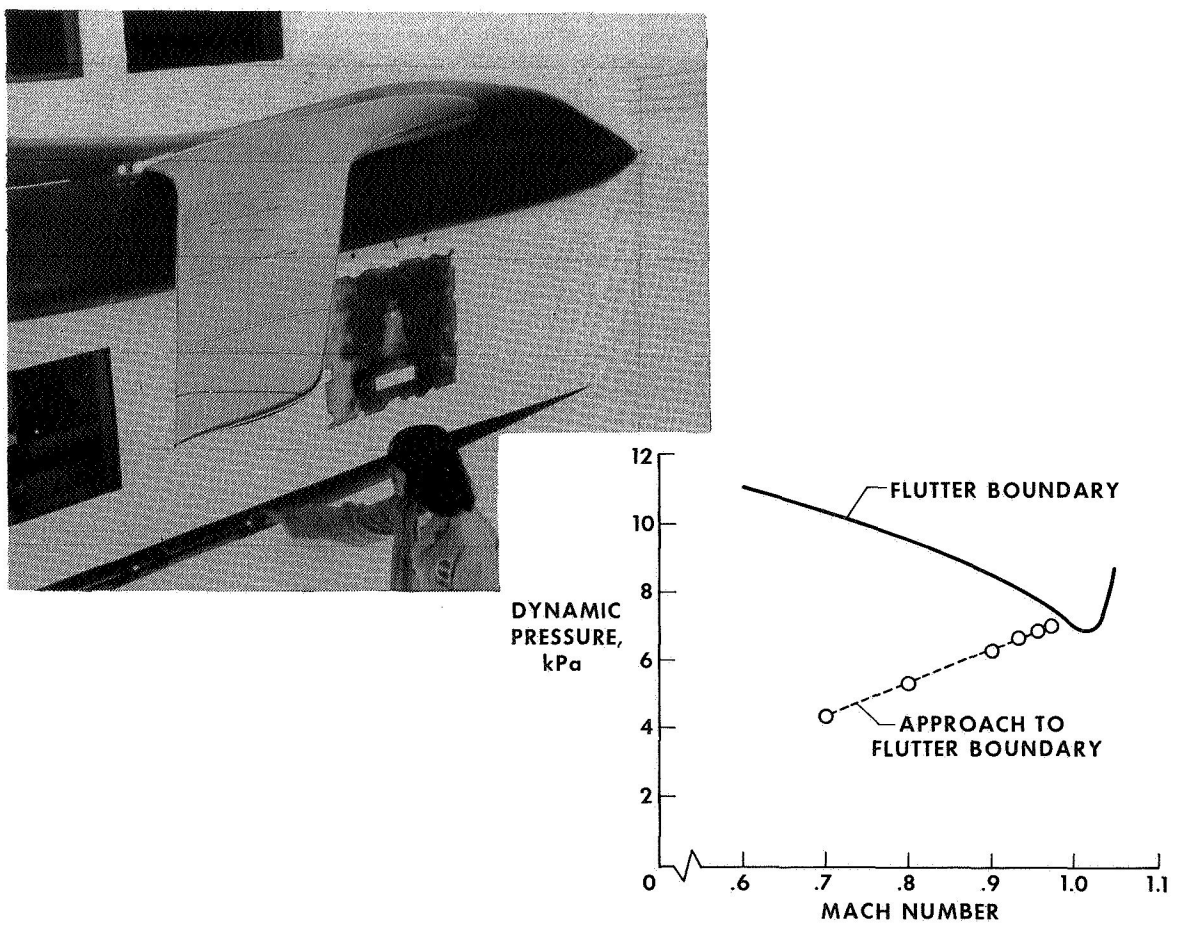

Figure 5.- Flutter boundary and subcritical approach to flutter boundary for the subsonic-transport wing model.

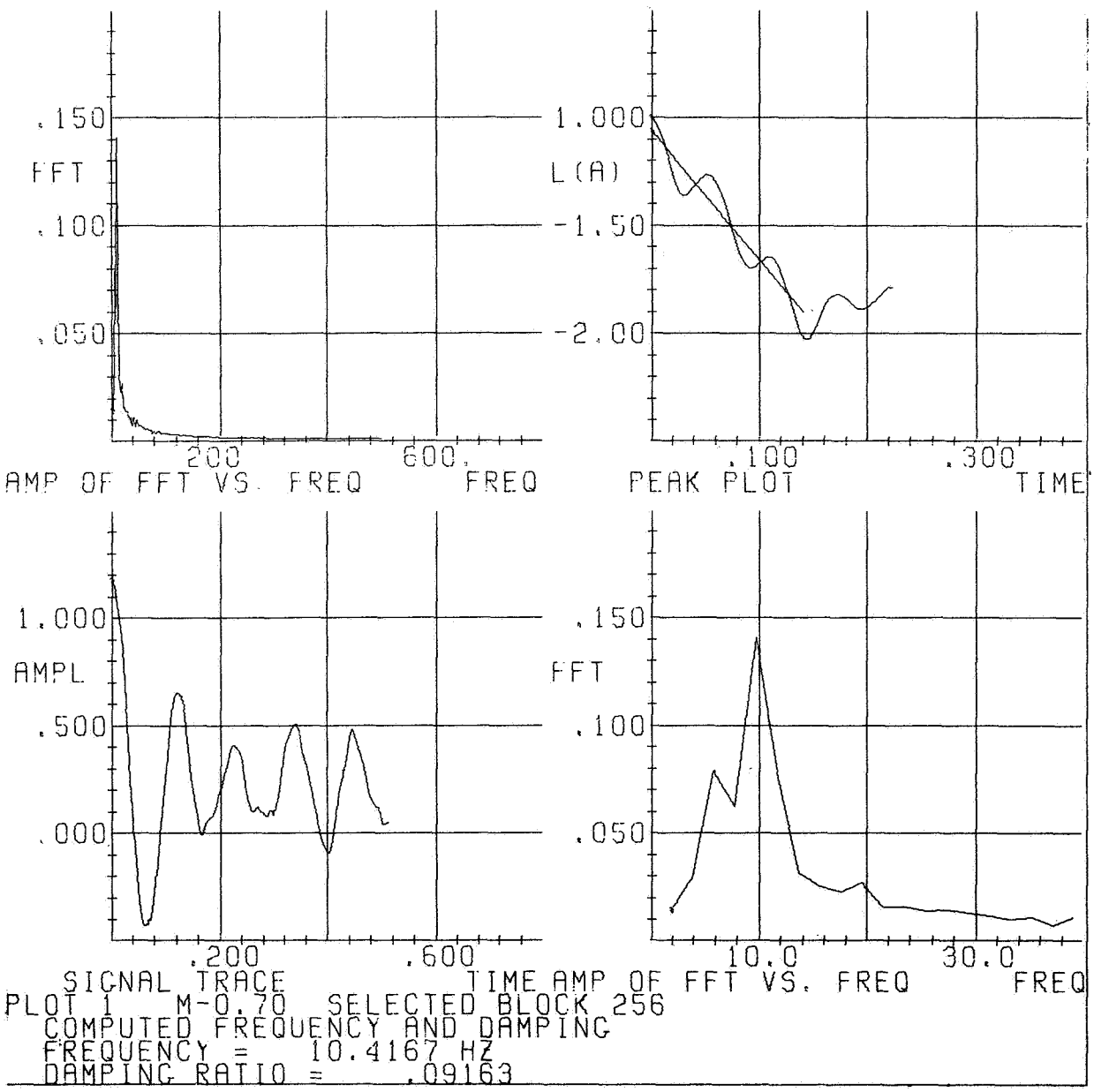

Figure 6.- Sample moving-block/randomdec analysis results for subsonic-transport wing model.

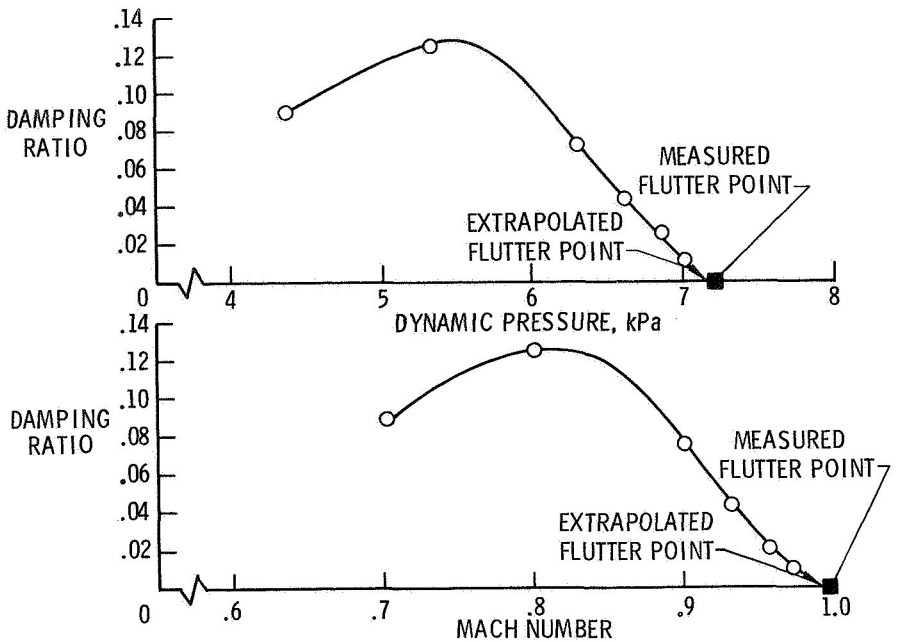

Figure 7.- Moving-block/randomdec subcritical damping results for subsonic-transport wing model.

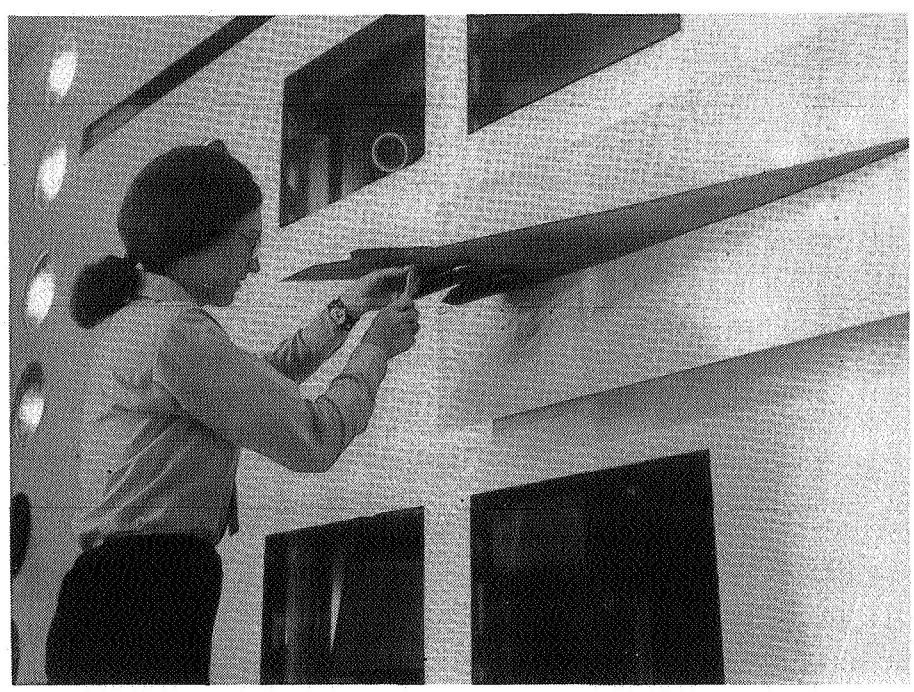

Figure 8.- Photograph of arrow-wing model mounted in wind tunnel.

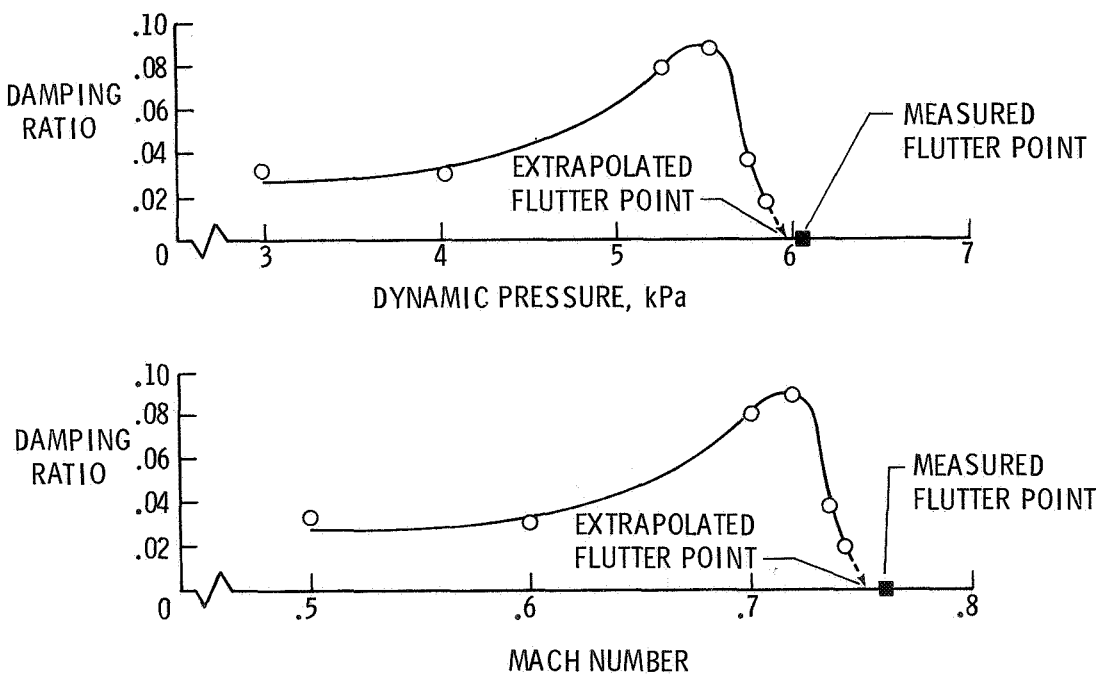

Figure 9.- Moving-block/randomdec subcritical damping results for arrow-wing configuration.

TRANSIENT EXCITATION AND DATA PROCESSING TECHNIQUES EMPLOYING THE FAST FOURIER TRANSFORM FOR AEROELASTIC TESTING

W. P. Jennings, N. L. Olsen, and M. J. Walter

Boeing Commercial Airplane Company

SUMMARY

This paper presents the development of testing techniques useful in airplane ground resonance testing, wind tunnel aeroelastic model testing, and airplane flight flutter testing. Included is the consideration of impulsive excitation, steady-state sinusoidal excitation, and random and pseudorandom excitation. Reasons for the selection of fast sine sweeps for transient excitation are given.

The use of the Fast Fourier Transform Dynamic Analyzer (HP-5451B) is presented, together with a curve fitting data process in the Laplace domain to experimentally evaluate values of generalized mass, modal frequencies, dampings, and mode shapes. The effects of poor signal-to-noise ratios due to turbulence creating data variance are discussed. Data manipulation techniques used to overcome variance problems are also included.

The experience is described that was gained by using these techniques since the early stages of the SST program. Data measured during 747 flight flutter tests, and SST, YC-14, and 727 empennage flutter model tests are included.

INTRODUCTION

In choosing a test method to approach an airplane flight flutter test, the implied ground rules, composed of flight safety, historical constraints, available equipment, test costs, test time, original or derivative model, etc., usually have a large impact on the procedures ultimately used. Until recently, flight flutter tests at Boeing used two forms of excitation; impulsive and slow swept sine wave (steady-state response).

Transient testing techniques have been employed from the earliest times in the form of impulsive testing such as control surface kicks to excite aircraft during flutter tests. Modal frequency and damping have generally been determined by evaluating the logarithmic decrement of a decaying response signal. Hand analyses in the time domain of control surface kick responses are limited to those modes which fall within the bandpass of the control surface; i.e., as long as the assumption that the forcing function was effectively a unit impulse or delta function over the frequency range of interest, a transfer function can be inferred by analyzing the response. The log decrement manual analysis of the response time history can yield excellent results if there is a single mode of interest and the frequency-damping product of that mode is small relative to that of the other modes. Also, the eigenvector for that mode at the spacial point of measurement must be of the same relative scale

as adjacent modes. If there are several modes with roughly equal vectors having similar frequency-damping products, it becomes extremely difficult, if not impossible, to obtain meaningful damping information. The differences in the frequencies of the two modes can be obtained from the beat frequency, but the damping of either mode is difficult to evaluate using the log decrement method. These anomalies in the past generated the requirements to obtain swept frequency (steady-state response) measurements.

These steady-state techniques, coupled with the use of Kennedy-Pancu's vector plot method (ref. 1), provided a means of identifying and tracking the frequencies and dampings of vibration modes during flutter test programs. As usual, this increased the understanding of the dynamics of the system but required a considerable increase in flight test time over that previously used for control surface kicks.

In 1969, a small improvement in swept sine test times was achieved through the use of pseudosteady-state methods and a vector-plotting analysis system (refs. 2 and 3). This system produced results with the structure reaching approximately 90% of steady-state response and was based on the principle that the damping in a system is directly proportional to the number of cycles of oscillation for a given vector phase swing when sweeping through a resonance using a sweep rate $\dot{\omega} = R\omega^2$ (refs. 3 and 4). This method gave reasonable insight into the damping of the modes and approximate modal frequencies; however, the test time required was still too long for the method to be used more than sparingly.

In late 1969, transform methods using the Fast Fourier Transform began to appear practical on digital machines. Experiments into their use were initiated (ref. 5), reevaluating all forms of excitation.

TRANSFORM METHODS

Impulse Excitations

Initial experiments were based upon impulsive excitations; i.e., band-limited delta functions obtained from exponential decaying time domain forcing functions. The initial choice of this function was based upon the idea that if the forcing function could be assumed to be a delta function (over the frequency range of interest), then only the response would have to be transformed, thus, saving on-line computational time. Using this forcing function to excite a multiple degree-of-freedom system presents some problems. As the bandwidth of the pulse increases, the time duration has to decrease; if the peak force remains the same, the total energy has to decrease. Signal-to-noise ratios soon become the most significant consideration. Increasing the peak force to gain some energy soon results in concern because nonlinearities result from local structural deformations. Using a peak force level that avoids questions of nonlinearities with sufficient bandwidth to excite the principal modes will usually result in the response signal being significantly influenced by background noise from acoustical, mechanical, and electrical sources. In the case of flight flutter tests, the atmospheric turbulence can impart more energy than the controlled excitation source.

Considering other waveforms, such as rectangular, trapezoidal, or sin (X)/X time histories, results in small gains in available energy over their effective bandwidths if the comparison is performed with equal peak force and equivalent bandwidth. These small gains are of little significance when orders of magnitude are needed to overcome signal-to-noise ratio problems. The sensitivity to noise using transform methods is the penalty paid for obtaining considerably less time domain data.

Nonimpulse Excitations

Forcing functions that can be employed to overcome signal-to-noise ratio problems are random, pseudorandom, and fast sine sweeps. Random excitation can be considered from two points of view. Since atmospheric turbulence exists, it may be taken advantage of, and the resulting response signal can be processed. To do so requires assumptions to be made about the spectrum of the atmospheric turbulence forcing function. Since this forcing function is a global source of energy to the airplane in flight, it does not lend itself to measurement or analysis, so the assumption must be made that the amplitude spectrum has to be flat or at least well behaved in that it contains no zeros in the frequency band of interest. If airplane response measurements are made during the time a wave front (such as a step function) is being penetrated by the vehicle, then another problem exists due to the time delays as the wave front imparts energy to the airplane. These time delays can cause the energy stored in the vehicle to be reinforced or cancelled as the input energy propagates along the airplane. To approach the problem by recording many independent time histories to enable performing power spectral densities with large degrees of freedom brings back the disadvantages of steady-state sine wave techniques—too much measurement time is consumed making the analysis. If power spectral density (PSD) analysis is performed, then no assumption need be made as to the phase spectrum of the excitation. The disadvantage is that no phase information is contained in the resultant PSD. This makes the problem of system identification more difficult when several modes are overlapping. The Hilbert transform can be used to obtain phase information from the PSD. However, the assumption of minimum phase must be made. Minimum phase indicates no zeros in the right hand Laplace (s) domain.

Assumptions leave targets for stones to be thrown at, independent of whether the assumptions are correct. Therefore, the best approach might be the use of analysis techniques employing minimum assumptions.

The approach of actually measuring the causal relationship between some known input (force) and an output (acceleration) would seem the optimum. In this method, the coherence function is also available as a measure of the causal relationship between input and output. An alternate approach is to use random excitation, hopefully uncorrelated with the turbulence source, to excite the airplane. One problem with the random excitation approach is that if both the random forcing function along with some response signal is measured so that the transfer function can be calculated, the problem of leakage in the frequency domain has to be dealt with. Prior to Fourier transforming the data, some window function (such as Hanning) has to be applied to the time domain data to minimize leakage. The window can effectively reduce the leakage problem; however, the transfer function needs to be corrected for the effects of the particular window used. This is not a straight forward correction, since the window affects both the apparent frequency and the damping, and it is frequency dependent.

If the forcing function is chosen to be a periodic time domain signal, then windowing and the associated problems are eliminated. Both pseudorandom and the fast sine can fall in this category. Of these two forcing functions, the sine sweep has provided better results when systems that exhibit nonlinearities such as a stiffening spring are encounted. This form of excitation has assisted in the understanding of such nonlinear effects. Some insight might come from a look at the amplitude probability distributions of these functions. Another factor favoring the fast sine sweep is that the signal-to-noise ratios of the response signal are improved. Using the fast sine sweep, a given mode will reach a higher percentage of its steady-state response compared with random excitation, especially when systems are lightly damped.

In some systems, limits are imposed on the peak force that can be used. More energy can be imparted to the specimen using the fast sine sweep in these systems. If the 3σ peaks of the random

signal are kept at the same peak value of the fast sine sweep, more energy is available from the fast sine sweep to improve signal-to-noise ratio of the response. Figure 1 portrays this comparison.

Fast Sine Sweeps

Several points need to be made if the discussion is limited at this time to fast sine sweeps. On first thought, a linear sweep rate might seem an obvious candidate for use in testing, since its amplitude spectrum is flat. With a flat spectrum, it seems reasonable to just measure the response and use Fourier transform techniques to obtain an estimate of the transfer function. This, of course, is invalid since the phase spectrum of the force has been ignored. In the case of the swept sine, the phase spectrum is a very rapidly rotating vector. When the transfer function calculation is made by either the response transform divided by the force transform or the cross-power spectrum divided by the auto-spectrum of the force, the effect of this rapidly rotating phase vector is accounted for. Of the three fundamentally different sweep rates, linear, log, and exponential, the log seems to represent the best compromise for a lightly damped multiple degree-of-freedom mechanical system with roughly the same damping in each mode. The exponential sweep would impart equal energy into each mode (approximately), but the dynamic range requirements of the analog-to-digital converter to measure the forcing function would be severe when attempting to cover a large swept bandwidth. Likewise, a linear sweep rate would require a large dynamic range to measure the response, since the high frequency modes would reach a much larger percentage of steady-state response.

Better experimental results have been obtained using the periodic log swept sine-forcing function by actually making the function a true transient signal. Since timing is critical in making a truly periodic forcing function in the Fourier analyzer's sample time (T), a transient signal that allows time for the response to die out before the time sample T has been taken is sometimes used. This is accomplished by stopping the sweep typically at 85% of the total time sample taken. The modal damping values of the system under test will dictate this value. Lightly damped systems may require stopping the sweep at 70%. In any event, the sweep is stopped, allowing enough time for the system to decay out to roughly 10% or less of its peak response. To soften startup and shutdown transients, the amplitudes of the sweep time history are also linearly ramped using a 5% ramp time at the beginning and end of the sweep.

Relative to the time domain measurements, the swept sine has an appealing nature over random in that as each resonance is traversed, the response blossoms, giving a quick intuitive feel as to signal-to-noise ratios and system dampings. Data dropouts and other anomalies are much easier to recognize using sine versus random.

Variance Reduction

For measurements made in very noisy environments such as wind tunnel subcritical response tests, the transfer function is composed of a series of swept sine tests (ensembled) averaged together. The coherence function has been used to obtain a measure of the quantity of ensemble averages that should be taken. Wind tunnel testing is considered the worst case for the method, since the ratio of energy input via the sine sweep to the energy input from turbulence is not very high, typically only 2 to 1. To keep the test times under control, usually not more than ten ensembles are used. The resulting transfer functions contain considerable noise or variance on the measurement. This variance problem has now been significantly reduced by the application of an exponential window applied to the raw, measured, system impulse response. The transfer function is obtained and inverse transformed to obtain the system impulse response. Conceptually, this windowing process arises from the characteristics of a systems impulse response, in that it approaches zero with increased time. Because

of the effects of turbulence, the measured impulse response contains extraneous information out beyond the point where, for all practical purposes, the energy within the system has decayed out. These extraneous data produce the major component of the variance observed in the raw transfer function measurement. The multiplication of the raw impulse response by an exponential window suppresses this extraneous information, significantly reducing the variance in the transfer function when the windowed impulse response is inverse transformed. The choice of an exponential window arises from the ease of calculating the correction factor to back out the effects of the window.

Window Correction Derivation

As a starting point, consider a single degree-of-freedom system mapped in the s-plane:

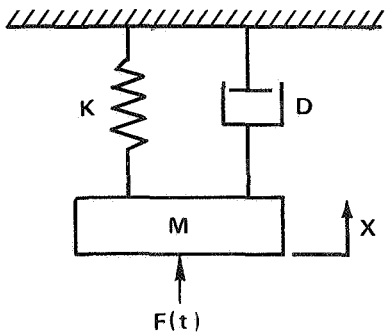

The differential equation of this system is:

$$M\ddot{X} + D\dot{X} + KX = F(t)$$

Using Laplace transform representation with all initial conditions equal to zero:

$$(Ms^2 + Ds + K)\, X(s) = F(s)$$

The transfer function is:

$$H(s) = \frac{X(s)}{F(s)} = \frac{1}{Ms^2 + Ds + K} = \frac{1/M}{s^2 + \frac{D}{M}s + \frac{K}{M}}$$

For convenience, let:

$$A = 1/M,\ B = D/M,\ C = K/M$$

then:

$$H(s) = \frac{A}{s^2 + Bs + C}$$

The roots of this system for the under damped case are:

$$s = -\frac{B}{2} \pm j\sqrt{C - \frac{B^2}{4}}$$

let:

$$\frac{B}{2} = \alpha \qquad \sqrt{C - \frac{B^2}{4}} = \beta$$

then:

$$H(s) = \underbrace{\frac{a}{s + \alpha + j\beta}}_{\text{Negative pole}} + \underbrace{\frac{a^*}{s + \alpha - j\beta}}_{\text{Positive pole}}$$

where:

j	=	the imaginary operator
a	=	a complex constant (residue)
*	=	denotes conjugate

Evaluating the constant a:

$$a = \left.\frac{A}{s + \alpha - j\beta}\right|_{s=-\alpha-j\beta} = \frac{A}{-j2\beta} = j\frac{A}{2\beta}$$

then, in partial fraction form:

$$H(s) = \frac{j\frac{A}{2\beta}}{s + \alpha + j\beta} + \frac{-j\frac{A}{2\beta}}{s + \alpha - j\beta}$$

This system then gives a conjugate pair of poles.

The system parameters are then completely described by three constants; α, β, and the residue (complex constant in the numerator). The natural frequency of the system is:

$$\omega_N = (\alpha^2 + \beta^2)^{1/2} \text{ rad/sec}$$

The damped natural frequency is:

$$\omega_{N_d} = \beta \text{ rad/sec}$$

The damping factor or ratio is:

$$\gamma = \frac{\alpha}{\omega_N}$$

The eigenvector is associated with the residue.

Repeating the Laplace domain description of a single degree-of-freedom system in partial fraction form:

$$H(s) = \frac{j\frac{A}{2\beta}}{s + \alpha + j\beta} + \frac{-j\frac{A}{2\beta}}{s + \alpha - j\beta}$$

where:

A = 1/M

B = D/M

C = K/M

α = B/2

β = $(C - B^2/4)^{1/2}$

M = Mass

D = Damping

K = Stiffness

Taking the inverse Laplace transform of the above equation results in the systems impulse response, $f(t_i)$:

$$f(t_i) = \epsilon^{-\alpha t}\left[\frac{A}{\beta}\sin \beta t\right] \quad t > 0$$

Multiplying the impulse response by the exponential window results in the following:

$$f(t_i) = \epsilon^{-(\alpha+\alpha')t}\left[\frac{A}{\beta}\sin \beta t\right]$$

The only effect the window has on the single degree of freedom is that of increasing the apparent system damping.

In a typical application of this window using the Fourier analyzer:

$$\Delta t = T/N$$

where:

Δt = time between samples in the analog-to-digital sampling, sec

T = total length of time samples, sec

N = total number of samples (channels)

$\epsilon^{-\alpha' t}$ is made equal to 0.1 at channel 1000 (1000 times Δt); therefore:

$$\ell n\,[\epsilon^{-\alpha' t}] = \ell n\,[0.1]$$

$$\alpha' t = 2.30258$$

$$\alpha' = \frac{2.30258}{t_{1000}}$$

where t_{1000} = 1000 times Δt.

The damping ratio of the system without the window is:

$$c/c_0 = \frac{\alpha}{\omega_N}$$

The apparent damping ratio of the system with the window is:

$$c'/c_0 = \frac{\alpha + \alpha'}{\omega_N}$$

since:

$$c/c_0 = \frac{\alpha}{\omega_N}$$

$$\alpha = (c/c_0)\,\omega_N$$

and:

$$c'/c_0 = \left[(c/c_0)\,\omega_N + \alpha'\right]\frac{1}{\omega_N}$$

$$c/c_0 = c'/c_0 - \frac{\alpha'}{\omega_N}$$

$$c/c_0 = c'/c_0 - \frac{(2.30258)}{\Delta t\,(1000)\,(\omega_N)}$$

If the window is applied n times; i.e., the impulse response of the system is multiplied by the window n times,

then:

$$c/c_0 = c'/c_0 - \frac{n\ (2.30258)}{1000\ (\Delta t)\ \omega_N}$$

In the practical application of this windowing technique to reduce the effect of variance due to turbulence, some undesirable effects arise. In a multiple degree-of-freedom system with closely spaced modes (i.e., a pair of roots nearly identical), the application of this window tends to smear the modes together, so that their individual identity tends to merge into what appears to be only one mode. A second practical problem arises because of the truncation of the measured transfer function. In a typical measurement, the transfer function is defined from zero frequency to an upper frequency of interest. When the higher frequency cutoff point coincides with a system antiresonance, no significant problem develops if this antiresonant point has a small magnitude relative to the midband magnitude value. If the upper frequency point coincides with a resonance point, a problem arises due to the truncation of the transfer function. The effect of this truncation is a convolution of the impulse response with a sync function (sin (X)/X). A physical interpretation of this transfer function truncation would be a system impulse response that begins responding before it is excited. This unrealizable impulse response is what would analytically be required to produce the unrealizable truncated transfer function.

In a case where the truncation of the transfer function would produce such an effect, the application of the exponential window would eliminate the tail or convolution product so that when the inverse transform was taken (on the windowed impulse response), the discontinuity in the original transfer function (truncation) would not be reproduced. A modified window is used in such cases to overcome the dominate effects of this problem and allow the tail to be unmodified by the window.

Figure 2 presents a typical transfer function as measured in the wind tunnel on a flutter model. The variance problem makes the measurement a questionable value. This particular measured transfer function also has a truncation problem, since the magnitude is not near zero at the highest frequency in the analysis.

Figure 3 is the calculated impulse response from the raw transfer function measurement of figure 2. The tail at the end is the result of the truncation of the transfer function. Figure 4 presents the exponential window used. The modified window used is dependent upon an observation of the raw impulse response tail. The number of channels (time samples) at which the modified window is at a constant value of unity is arrived at by engineering judgment after observing the raw impulse response. It has been found that there is considerable leeway without any noticeable change in the final windowed transfer function. Figure 5 presents the final transfer function after windowing using the modified window. By whatever method is used to obtain the system frequencies and apparent dampings, the corrected damping could be obtained by using the procedures of this report.

System Identification

With respect to the problem of obtaining a measurement of the complex structural transfer function either in a laboratory environment or a wind tunnel or flight environment, the Fourier analyzer has demonstrated its speed and dynamic range superiority over sine steady-state test methods. The remaining problem, common to both test methods, is that of interpretation of the measured results. Generally, this remaining problem is the methodology used to decompose the measured complex plane transfer function $H(j\omega)$ to separate the total vector response into a set of

linear independent single degree-of-freedom systems so that, when all the individual single degree of freedoms are added together frequency by frequency, the result matches the original measured complex plane measurement. In the past, the methods of Kennedy-Pancu have been used in an attempt to reduce the complex plane plots into a set of modal frequencies and dampings. This method has been reasonably successful when the modes are not too closely spaced. Modes that have become highly damped cannot be tracked by this method either.

The determination of mode shapes from these complex plane plots also becomes invalid for systems having complex eigenvectors. Complex eigenvectors (nonorthogonal vectors) arise when the system damping matrix is not proportional to the stiffness and/or mass matrix. The Laplace transform offers a convenient method whereby both real and complex systems can be analyzed, and it offers a procedure whereby the transfer function measurements can be reduced to modal coordinates of frequency, mode shape, and modal mass, stiffness, and damping.

An airplane in flight exhibits complex modal response due to the aerodynamic forcing terms. Better system identification can thus be realized if the normal assumption of orthogonality is removed.

Laplace Transform

The Fourier transform is basically a two-dimensional representation or picture of a three-dimensional Laplace transform. Consequently, when a transfer function $H(j\omega)$ is obtained and it is desired to identify the system's natural frequencies, dampings, etc., the missing third dimension has to be inferred. The Kennedy-Pancu technique inferrs the third dimension (indirectly), based upon some rather severe assumptions. In many cases, these assumptions are violated, making the technique of limited value. The problem of transfer function interpretation would disappear if a three-dimensional measurement was made. This three-dimensional representation appears via the Laplace transform (fig. 6). The Fourier transform is the plane through $\sigma = 0$ on the $j\omega$ axis of the three-dimensional Laplace (s) domain. If a Laplace transform representation was obtainable from measured data, a complete linear description of the dynamics of the system could be obtained.

A program exists on the Hewlett Packard 5451B Fourier Analyzer (HP) entitled "Modal Analysis System" (refs. 6, 7, 8, and 9), which takes the measured transfer functions (Fourier descriptions) and obtains a Laplace description via a least squares fit. The use of this program has shown encouraging results. For systems which are not too highly damped and for which reasonable measurements of the transfer function have been made, results have been excellent.

Figure 7 contains results of using the modal analysis system on transfer functions measured in flight. The fit was initially performed on the windowed transfer function (fig. 7a) to obtain a better feel as to the quality of the fit (fig. 7b). The results of the fit from the windowed data were used as starting values for the fit on the raw transfer function (fig. 7c). The fit of the raw data is shown in figure 7d. Table 1 presents the comparison of system identification using Kennedy-Pancu's methods on the windowed data, the HP modal analysis on the windowed data, and the HP modal analysis on the raw data. This particular data set was obtained using only one sweep ensemble. The results compare favorably.

An intriguing aspect of obtaining a Laplace description of an airplane transfer function in flight is that, if it were possible, this result coupled with the measured zero airspeed Laplace description could result in a measured Laplace description for the aerodynamic forcing function.

The Laplace approach is still left with some assumptions; i.e., we still can only handle linear systems, and the system under test cannot as yet have multiple roots—more than one mode with the same frequency *and* damping. The modal analysis system has handled systems with identical damped natural frequencies (same value for $j\omega$), if the damping values are considerably different.

EXPERIMENTAL STUDIES

Early Tests

In the first applications of the Fast Fourier Transform (FFT) techniques, existing off-line data processing with existing computing facilities was employed. In these early trials, existing or modified computer programs were used to compare the analytically and experimentally determined transfer functions of simple analogue systems. This work was then expanded to use available dynamic models where the practical problems of nonlinear structural effects and uncorrelated forcing functions (atmospheric turbulence) could be studied.

The first application of the FFT techniques on a Boeing aircraft came in a ride improvement program for the 747 (ref. 10). The objective of this testing was to develop an active control system to improve the ride qualities of the aircraft by suppressing the response of the aircraft's flexible modes of vibration. To aid in this work, the FFT techniques were used to derive the transfer functions between the motions of various locations in the aircraft and forcing functions applied through the aircraft's yaw damper servo units. Both pseudorandom and sinusoidal fast sweep excitation signals were initially employed in this testing; but, because of the greater energy input from the sinusoidal sweep excitation, this form of excitation rapidly became the only one used in later tests.

A typical plot generated from the testing is shown in figure 8. Despite testing in turbulent air and the lack of experience in variance reduction techniques, the tests generated sufficient data to enable the definition of the required transfer functions and the successful development of an active control system.

The results of this testing were also sufficiently encouraging for the technique to be used as a primary analysis system in the AWACS Brassboard ground vibration test where, by a microwave link to a remote computer, data reduction was achieved in a near real-time manner by personnel at the test site. However, since at this time the analysis systems were only capable of generating transfer function plots, considerable manual data reduction was necessary to generate modal frequencies, damping, and mode shapes of the structure from such plots.

Following this work and as a part of the SST Follow-On program conducted by The Boeing Company, a low-speed flutter model was used to demonstrate transient testing techniques that might be developed for wind tunnel and flight flutter testing of future aircraft. This work (ref. 11) considered the use of both fast sinusoidal sweep and pseudorandom noise excitation in comparison with steady-state excitation.

As previously discussed, the fast sinusoidal sweep excitation enables more energy to be input to a system within the same maximum excitation level. The results of this testing demonstrated in a practical manner the superiority of the fast sinusoidal form of excitation and also marked the first use of Hewlett Packard's Fourier analyzer for on-line data reduction.

More recently a series of data recorded during testing as the tunnel airspeed was increased toward the flutter speed has been reanalyzed using the current system capabilities of windowing the

data (fig. 9). A comparison of these results with those presented in reference 11 allows more modes to be identified from the data, providing a greater understanding of the system.

YC-14 Low-Speed Flutter Model

Vibration testing of a low-speed flutter model, both in still air and during wind tunnel testing using the current system capabilities, has been conducted as part of a test program to verify analytical flutter predictions for the aircraft. The use of the system during still air testing enabled a rapid identification of the natural frequencies and damping of the vibration modes, while mode shapes were generated from measurement of the responses at a large number of points across the model. A comparison of the test and analysis frequencies is given in table 2.

In the wind tunnel testing of a cantilevered empennage model (fig. 10), a floor-mounted electrodynamic exciter was used to provide the necessary excitation force, while accelerometers within the model recorded the model's response. On-line production of the model's transfer functions were then generated as test speeds were increased up to the flutter speed. Figure 11 shows the progressive change in such a set of transfer functions as the tunnel speed was increased. From these transfer functions, modal frequencies and damping were manually reduced, and their variations with airspeed were obtained (fig. 12). The use of this approach enabled a large amount of data to be gathered within a realistic time period for a large number of model configurations. One configuration involving a free mass balanced elevator was tested to high speeds before subcritical testing was conducted at low tunnel speeds to reduce some data scatter. The excitation system here provided the energy to initiate flutter, since tunnel turbulence was very small at these speeds. Figure 13 shows the results for this configuration.

727 Transonic Empennage Flutter Model

The fast sine sweep excitation and FFT data analysis techniques have recently been employed in ground vibration and wind tunnel testing of a 727 transonic flutter model. This test program was conducted to experimentally determine the complete dynamic characteristics of this model for use in theoretical flutter calculations.

During ground vibration testing of the model, the modal frequencies, damping, and mode shapes were reduced on-line using the full capabilities of a Hewlett Packard Dynamic Analyzer (HP-5451B). This system employed the previously discussed Laplace mathematical model fitted to the experimental transfer functions to enable a system's dynamic properties to be extracted.

Mode shapes of all model modes below 75 Hz were determined by making a series of measurements over the model and allowing the analyzer to reduce and plot the natural model modes (fig. 14).

To determine the generalized masses of these modes, the technique of using added incremental masses to the model and observing the change in modal frequency and mode shape was used. This technique is summarized in appendix A. The technique assumes that the model's modes are not complex; i.e., monophase.

Accurate evaluation of modal generalized masses is dependent on accurate determination of the mode shapes. Triaxial mode shapes were carefully measured at the incremental mass location and at a reference location on the model for each mode. Total vector mode shapes were evaluated from the triaxial measurements and were used in the generalized mass evaluation.

The incremental masses were varied in magnitude and location to allow two or three separate determinations of generalized mass for each mode. A comparison of resulting values of generalized mass for individual modes showed an average variation in experimental results of 5%. Table 3 presents the measured modal frequencies and generalized masses.

The experimental values of generalized mass and modal frequencies were used in conjunction with calculated oscillatory aerodynamic coefficients to complete a flutter analysis to predict model behavior. The oscillatory coefficients were calculated using the measured modal displacements as input to Doublet-Lattice Oscillatory Aerodynamics theory.

During wind tunnel testing of the model (fig. 15), sine sweep excitation from 2.5 to 50 Hz of the model was accomplished using an electrohydraulic-actuated aerodynamic vane located at the fin tip leading edge. Model response was monitored and recorded for 12 separate accelerometers located on the model structure.

Each sinusoidal sweep from 2.5 to 50 Hz required approximately 20 sec, and an ensemble of 10 sweeps was completed at each wind tunnel Mach number and pressure condition. The resulting input-to-output response transfer functions were ensemble averaged and windowed to reduce variance in data due to model response from sources other than the sinusoidal aerodynamic vane force. Table 4 compares data reduced by using both the Kennedy-Pancu and the modal data analysis techniques.

Complex vector amplitude plots (fig. 16) were produced in a near-to-real time manner and were evaluated using the methods of Kennedy-Pancu (ref. 1) to provide model response frequency and damping. This data reduction was readily accomplished between wind tunnel conditions and plots of damping; frequency versus wind tunnel dynamic pressure were recorded. The damping magnitude and trends as displayed by continuous (between tunnel condition) plotting were reviewed prior to changing wind tunnel conditions.

Figure 17 presents the damping and frequency trends measured during the 727-300 T-tail flutter model test. The last recorded entry was at 34.5 kPa (720 lb/ft^2) dynamic pressure. While on condition and recording data at 38.3 kPa (800 lb/ft^2) dynamic pressure, a fatigue failure in the fin root structure occurred, and the empennage was separated from the model.

Posttest analyses of the data recorded at this final test condition of 38.3 kPa (800 lb/ft^2) have been conducted using the data analysis system with individual sweep records. Figure 18 shows the variation in the T-tail mode frequency experienced as the fatigue failure progressed. During this time, the transient excitation analysis techniques proved invaluable. A complete understanding of the events resulting in the model destruction would not have been realized if the transient excitation and data processing technique had not beem employed.

747 Derivative Tests

Recently, several derivatives of the Boeing 747 aircraft have been tested using current transient testing techniques. These techniques were used to gather data during the ground vibration tests on the 747SP aircraft, where the closely spaced modes of the aircraft were separated by posttest analysis. Posttest data analysis minimized the impact on the manufacturing production flow of the aircraft.

Flight flutter testing of 747 derivative aircraft has also been conducted using the yaw damper servo on the rudder actuator as a means of excitation at low frequencies. Once again, good results have been obtained in an on-line data reduction mode of operation (fig. 19).

CONCLUSION

The steady development of transient testing techniques employing fast sinusoidal sweep excitation forces in conjunction with Fourier and Laplace transform techniques has generated a powerful test capability for use in the many forms of system identification of which flight flutter testing is a small part.

The experience gained with these techniques has shown them capable of providing a wealth of data to the dynamics engineer. These techniques have also increased the safety of flight testing while also enabling test times to be reduced.

While the analysis system meets present requirements, development continues to increase its capabilities in the bulk of data that can be processed and also in determining the generalized air forces that act on an aircraft in flight.

APPENDIX A

EXPERIMENTAL EVALUATION OF GENERALIZED MASS USING THE INCREMENTAL MASS MEASUREMENT TECHNIQUE

Reference: AGARD, Part IV, section 8.1, pp 24 through 27.

$$S = I\omega^2$$

where:

S = generalized modal stiffness

I = generalized modal mass

ω = modal frequency

With the addition of a small incremental mass (δm) to the structure at a point p:

$$S = (I + \Delta I)\omega_1{}^2$$

where:

ΔI = generalized modal mass increment

ω_1 = modal frequency with incremental mass added

Since the structural stiffness is unaffected by the addition of an incremental mass:

$$I\omega^2 = (I + \Delta I)\omega_1{}^2$$

or

$$\llcorner\phi\lrcorner [J] \{\phi\} \omega^2 = \left[\llcorner\phi\lrcorner [J] \{\phi\} + \phi_p{}^2 \delta m\right]\omega_1{}^2$$

where:

$\{\phi\}$ = modal displacement matrix

ϕ_p = modal displacement vectors at point p

$[J]$ = mass matrix

Rearranging the above equation gives:

$$\llcorner\phi\lrcorner [J] \{\phi\} = I = \frac{\phi_p{}^2 \delta m \omega_1{}^2}{\omega^2 - \omega_1{}^2}$$

showing that the generalized modal mass (I) is a function of the incremental mass (δm); the modal displacement (ϕ_p) at the location δm is attached; and the modal frequencies are evaluated with and without δm in place (ω_1 and ω).

REFERENCES

1. Kennedy, C. C. and Pancu, C. D. P.: Use of Vectors in Vibration Measurement and Analysis. Journal of the Aeronautical Sciences, November 1947.

2. Small, E. F.: Evaluation of Vibration Methods to Separate Closely Spaced Modes. The Boeing Company, D6-9447, TN, May 1968.

3. Olsen, N. L.: Flight Flutter Measurements Using The Analog Aeroelastic Modal Analysis System (AMAS). The Boeing Company, D6-33241, INF., February 1972.

4. Winter, W. A.: Flutter Testing of Aircraft in Flight. British Communications and Electronics, April 1963.

5. White, R. G.: Dynamic Analysis of Structures by Transient Excitation. Thesis, Institute of Sound and Vibration, University of Southampton, March 1970.

6. Olsen, N. L.: Vibration Testing Methods and Techniques–Technical Notes. The Boeing Company, D6-6597, INF., June 1975.

7. Hewlett Packard 5451B Fourier Analyzer System Manuals.

8. Richardson, M. and Potter, R.: Identification of Modal Properties of an Elastic Structure From Measured Transfer Junction Data. 20th International Instrumentation Symposium, Albuquerque, N.M., May 1974.

9. Potter, R. and Richardson, M.: Mass, Stiffness, and Damping Matrices From Measured Modal Parameters. International Instrumentation–Automation Conference, New York, October 1974.

10. Cohen, G. C., Cotter, C., and Taylor, D. L.: Use of Active Central Technology to Improve Ride Qualities of Large Transport Aircraft. NASA Symposium on Active Control Technology, July 1974.

11. Ryneveld, A. D.: Transient Excitation Techniques for Wind Tunnel and Flight Flutter Testing of SST Configurations. SST Technology Follow-On Program–Phase II, FAA-SS-73-14, May 1974.

Table 1.– Comparison of system parameters derived from figure 7.

KENNEDY-PANCU[a]			MODAL ON WINDOWED DATA[a]		
MODE	FREQUENCY, Hz	DAMPING, c/c_0	MODE	FREQUENCY, Hz	DAMPING, c/c_0
1	1.76	0.048	1	1.772	0.0427
2	2.27	0.030	2	2.224	0.0386
3	2.44	0.049	3	2.432	0.0544

MODAL ON RAW DATA

MODE	FREQUENCY, Hz	DAMPING, c/c_0
1	1.768	0.0420
2	2.217	0.0342
3	2.44	0.0528

[a]CORRECTED FOR THE WINDOW.

Table 2.– YC-14 low-speed flutter model comparison of test and analysis results.

MODE	EXPERIMENTAL RESULTS		ANALYTICAL RESULTS, Hz	DESCRIPTION
	FREQUENCY, Hz	DAMPING, c/c_0		
SYMMETRIC MODES				
1	5.68	0.005	5.44	FUNDAMENTAL WING BENDING
2	8.62	0.007	8.47	FUNDAMENTAL WING TORSION
3	10.70	0.002	10.61	NACELLE PITCH
4	13.09	0.001	12.84	WING CHORDWISE, NACELLE SIDE BENDING
5	15.15	0.017	15.07	STABILIZER BENDING
6	15.82	0.003	15.62	
7	16.33	0.006	15.77	
ANTISYMMETRIC MODES				
1	5.41	0.002	5.48	AFT BODY TORSION, STABILIZER ROLL
2	6.93	0.005	6.75	FIN TORSION
3	7.72	0.001	7.69	WING BENDING/TORSION
4	10.49	0.003	10.42	WING BENDING, NACELLE PITCH STABILIZER ROLL
5	11.80		11.85	SECOND WING BENDING STABILIZER ROLL
6	15.42		15.16	NACELLE SIDE BENDING
7	17.45	0.002	17.43	OUTERWING TORSION, WING CHORDWISE STABILIZER BENDING

Table 3.– 727 T-tail model ground vibration test.

MODE	FREQUENCY, Hz	GENERALIZED MASS. kg cm^2 (LB-IN-SEC^2)
1	3.68	388.66 (4.13)
2	8.79	7.067 (0.0751)
3	16.57	1.120 (0.0119)
4	25.40	0.285 (0.00303)
5	34.28	1.223 (0.0130)
6	40.13	5.092 (0.0541)
7	53.21	0.863 (0.00917)
8	65.21	0.882 (0.00937)

Table 4.– Comparison of modal parameters for 727-300 empennage model data (fig. 16).

KENNEDY–PANCU[a]

MODE	FREQUENCY, Hz	DAMPING, c/c_0
1	3.8	0.0162
2	9.3	0.0397
3	16.7	0.0335

MODAL ON RAW DATA

MODE	FREQUENCY, Hz	DAMPING, c/c_0
1	3.77	0.016
2	9.22	0.0371
3	16.765	0.0312

[a]CORRECTED FOR THE WINDOW.

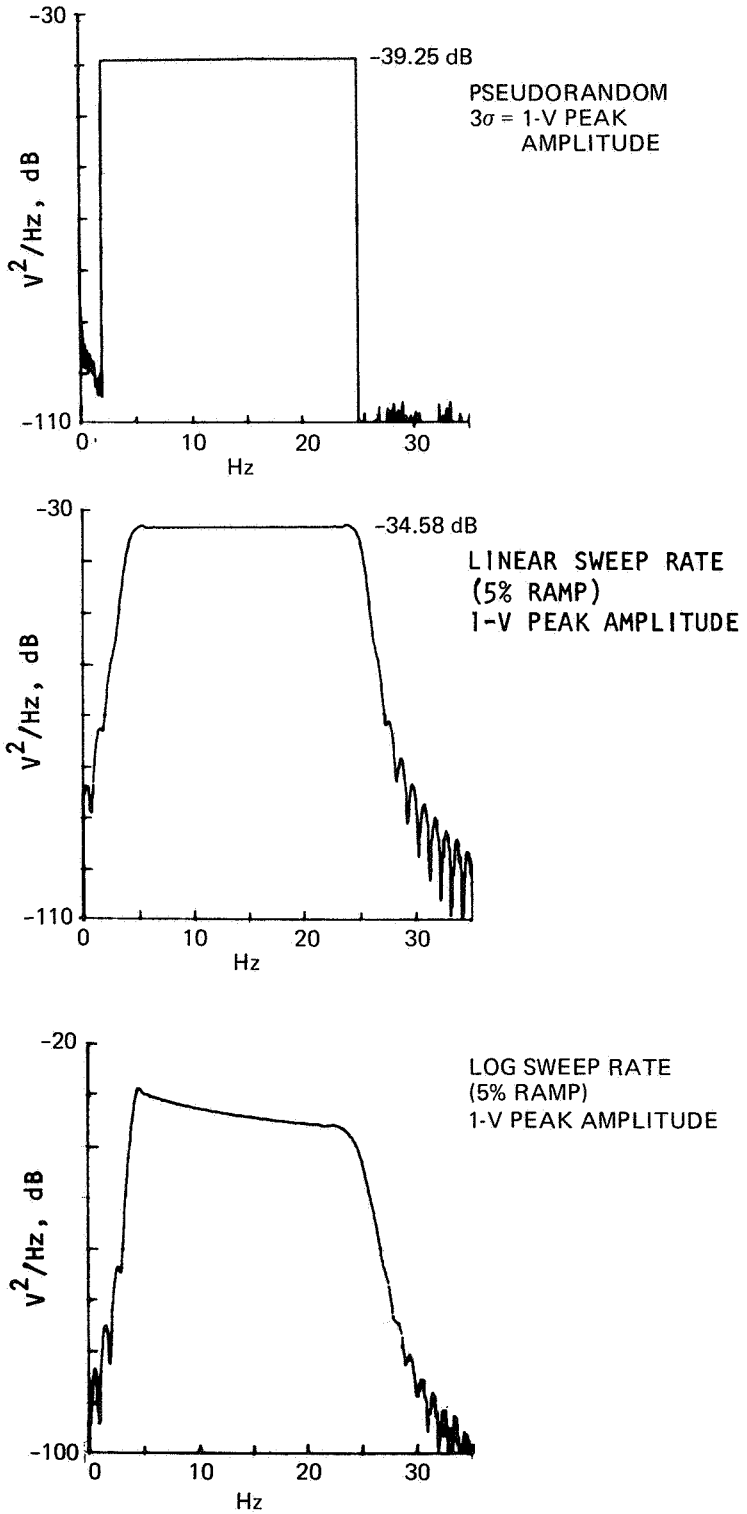

Figure 1.–Comparison of excitation signal input powers, dB.

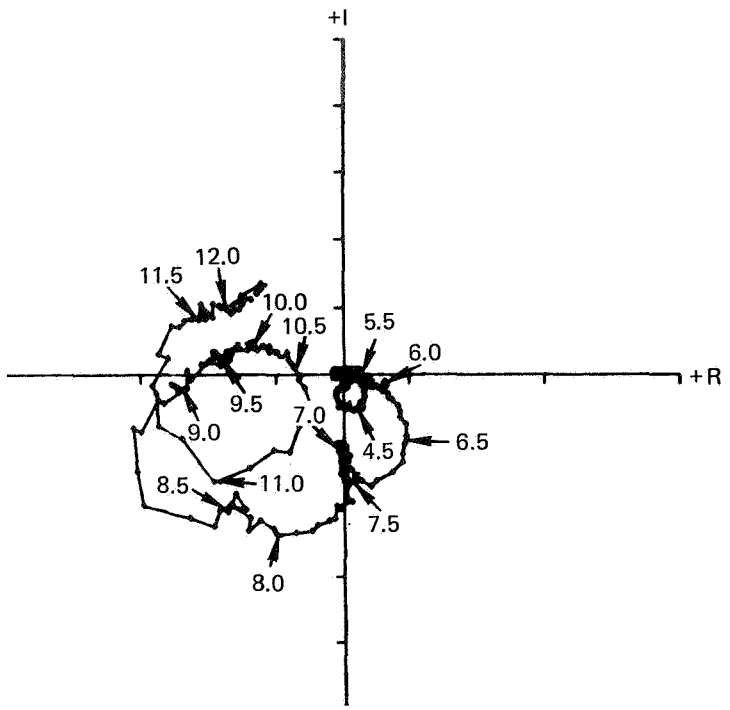

Figure 2.– Raw transfer function from a wind tunnel test.

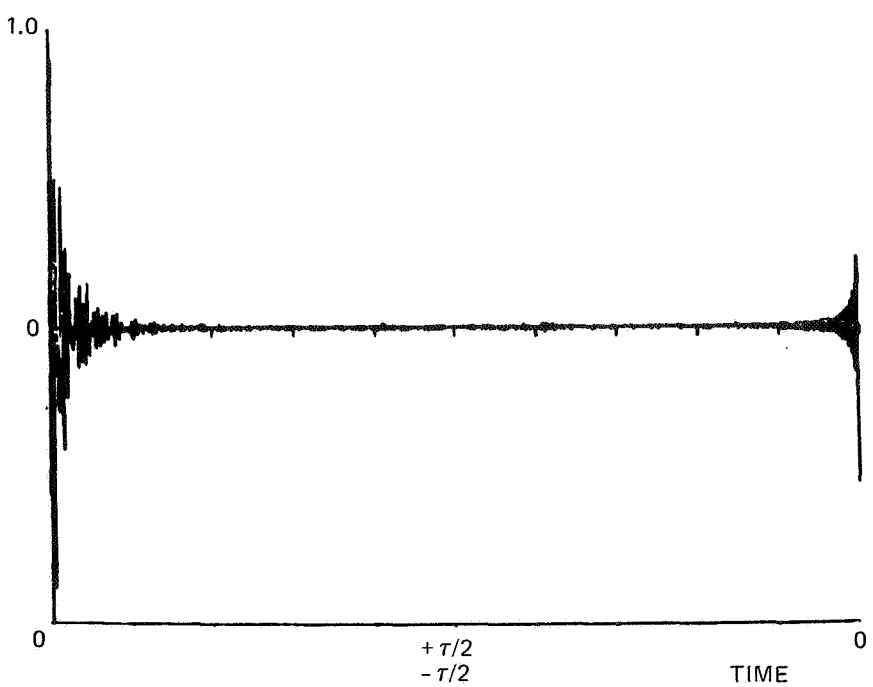

Figure 3.– Impulse response of figure 2.

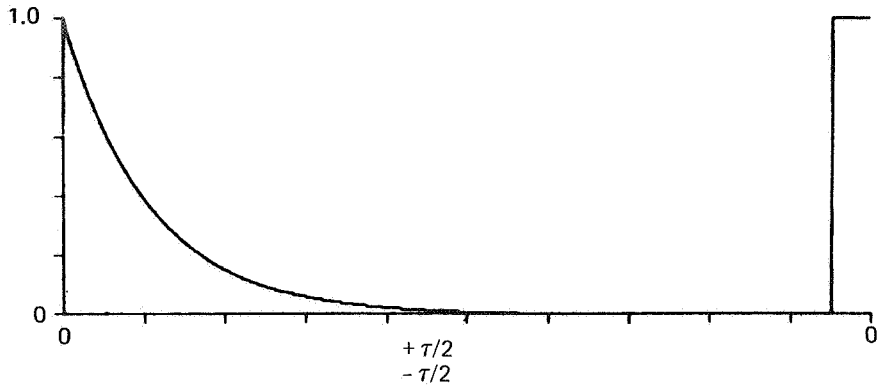

Figure 4.– Typical window function.

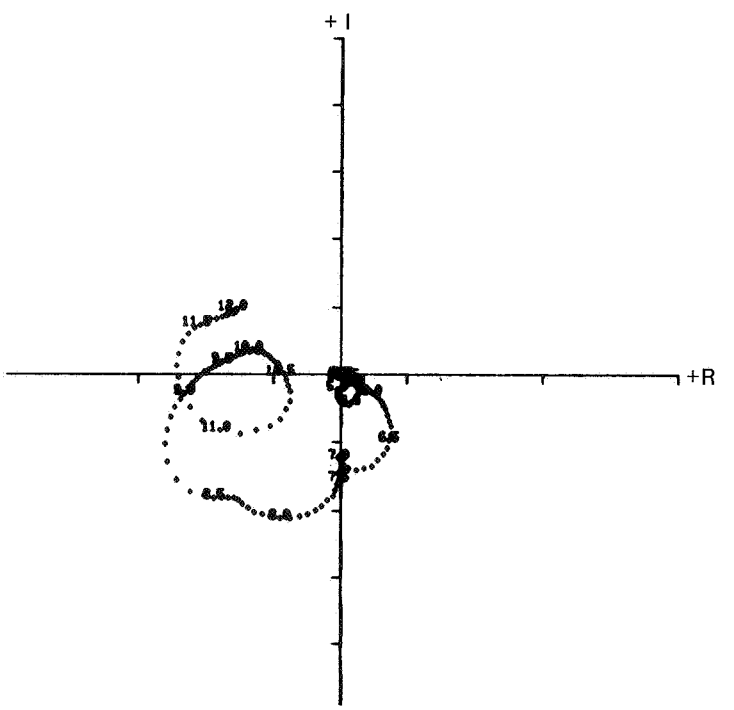

Figure 5.– Windowed transfer function.

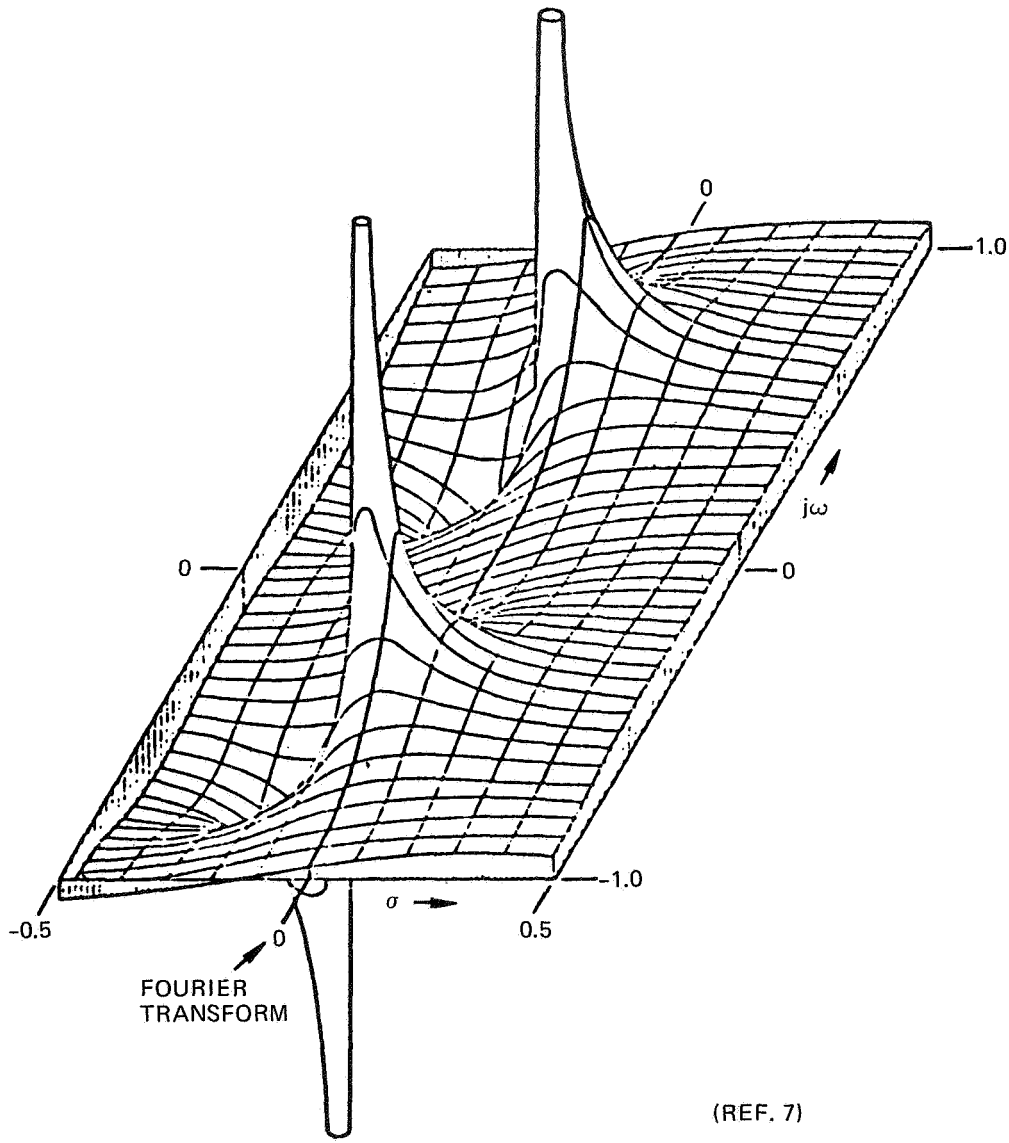

Figure 6.– The imaginary part of the transfer function of a simple resonator with poles at s = -0.1 ±j0.5.

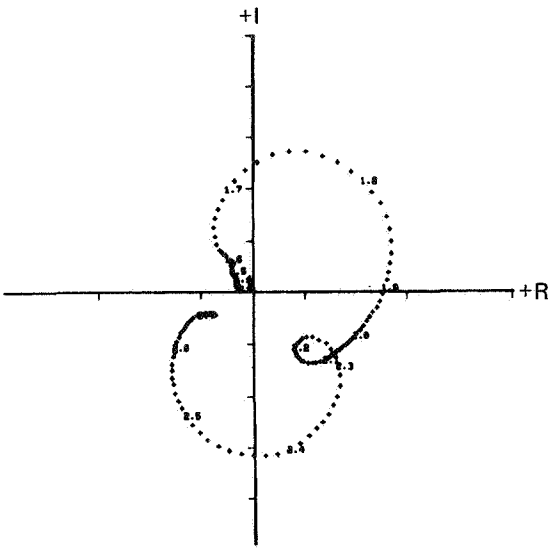

a. Windowed Data

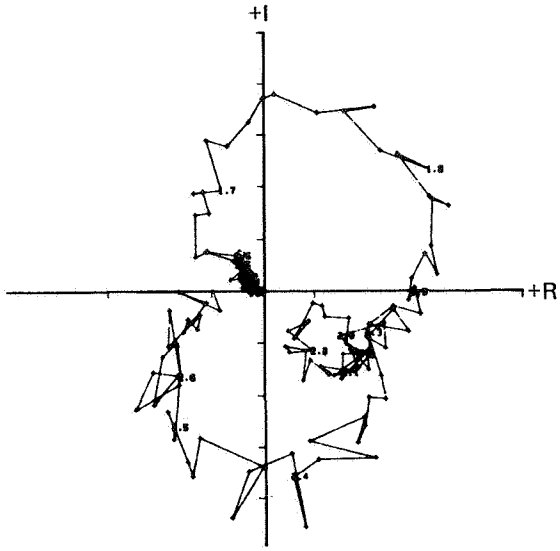

c. Raw Data

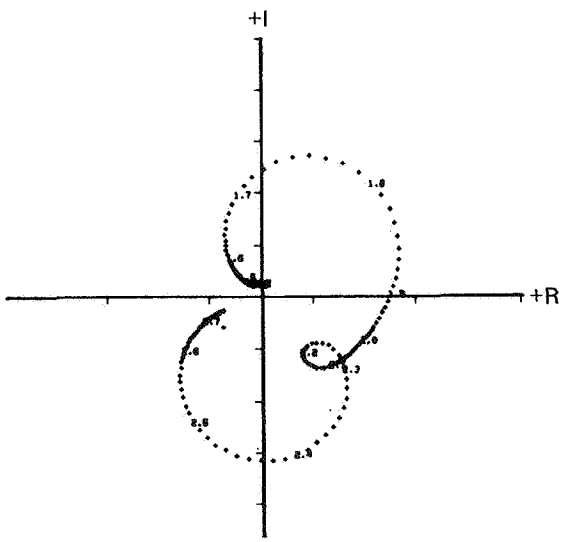

b. Fit of Windowed Data

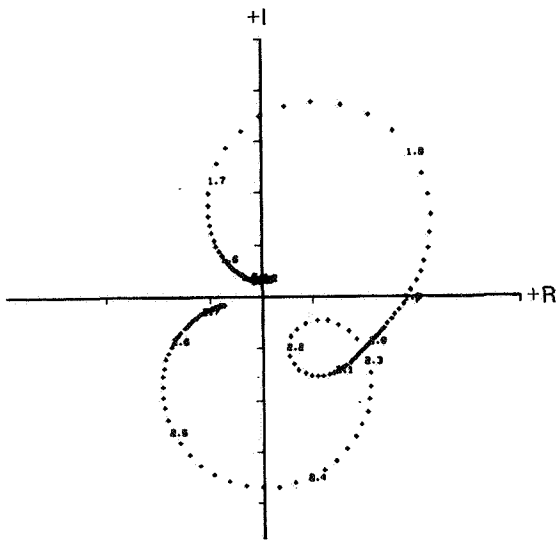

d. Fit of Raw Data

Figure 7.– 747 Flight flutter test–R.H. wingtip/rudder position.

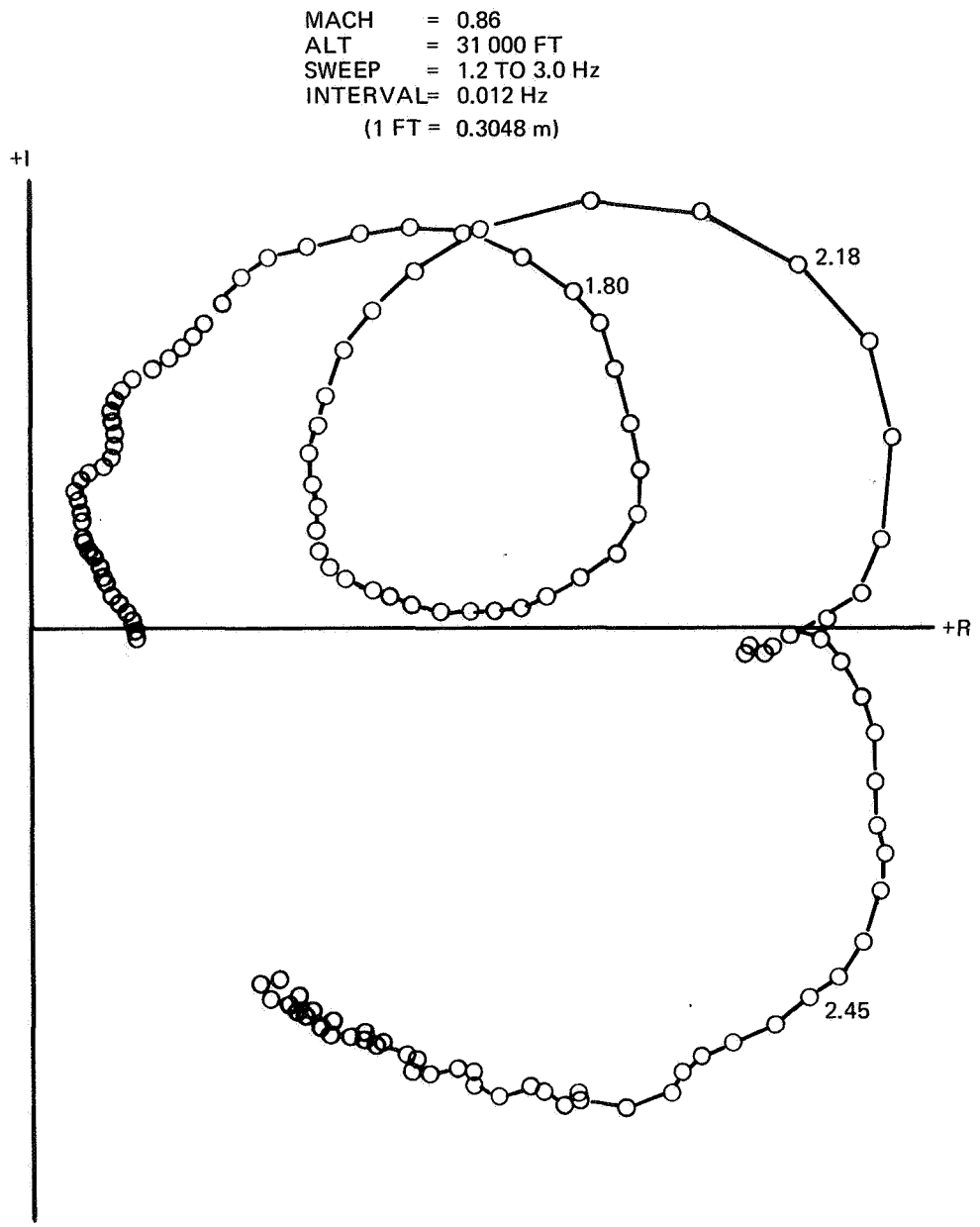

Figure 8.– 747 flight test–Lateral fuselage response to lower rudder yaw damper actuator command signal.

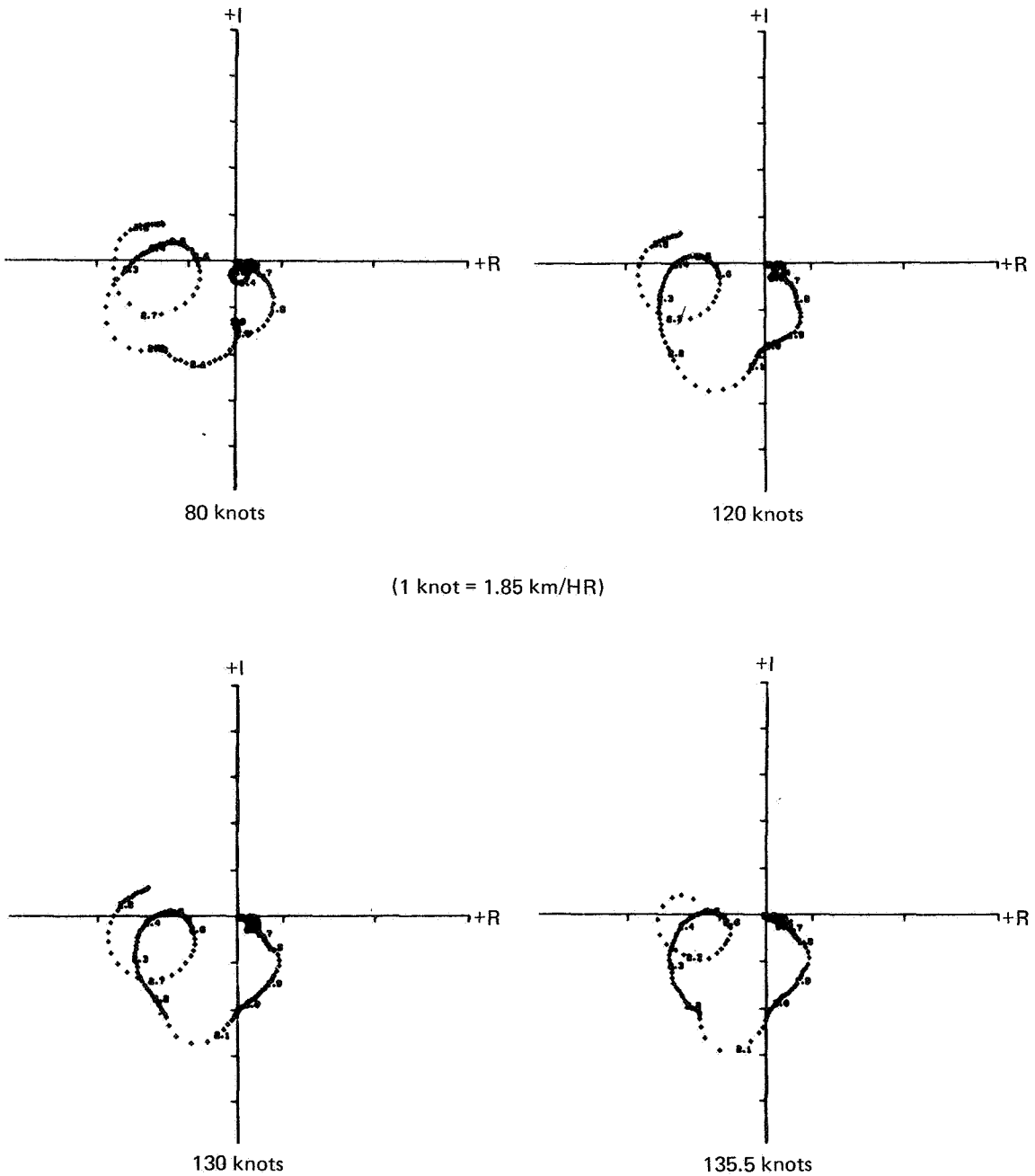

Figure 9.– Transfer functions for windowed data of SST low-speed flutter model (ref 11).

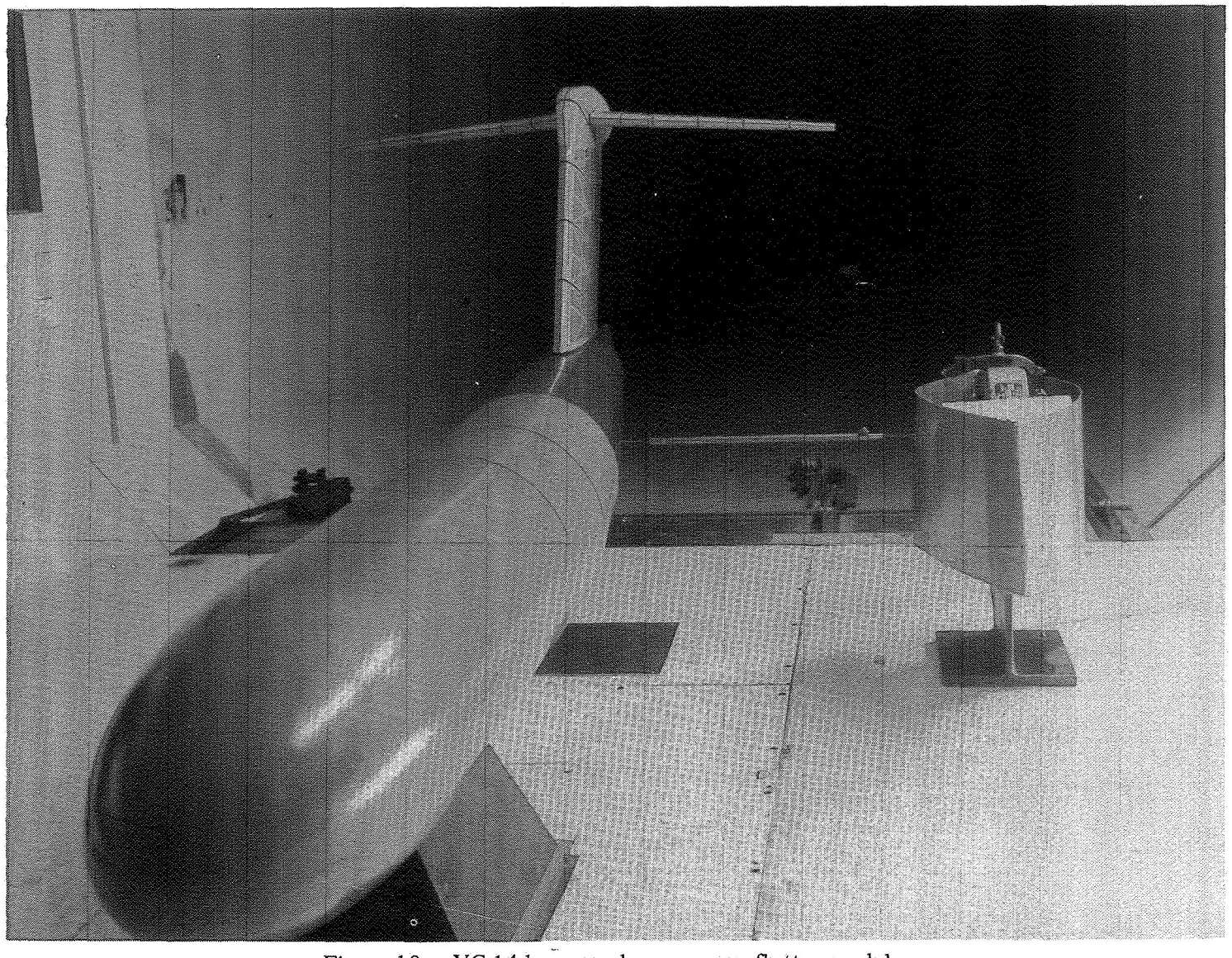

Figure 10.– YC-14 low-speed empennage flutter model.

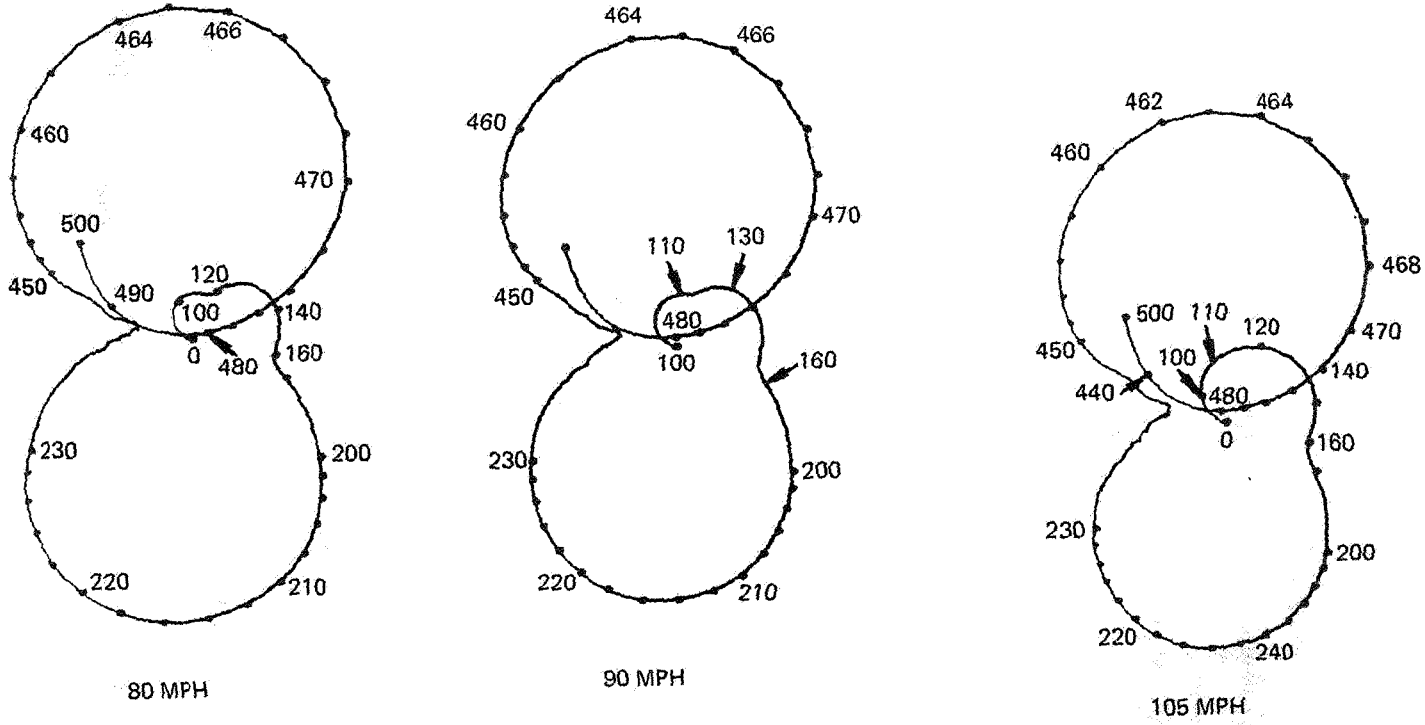

NOTE: FREQUENCY = SCALE NUMBERS X 0.05
(1 MPH = 1.61 km/HR)

Figure 11.– Transfer functions for low-speed YC-14 flutter model at increasing speeds.

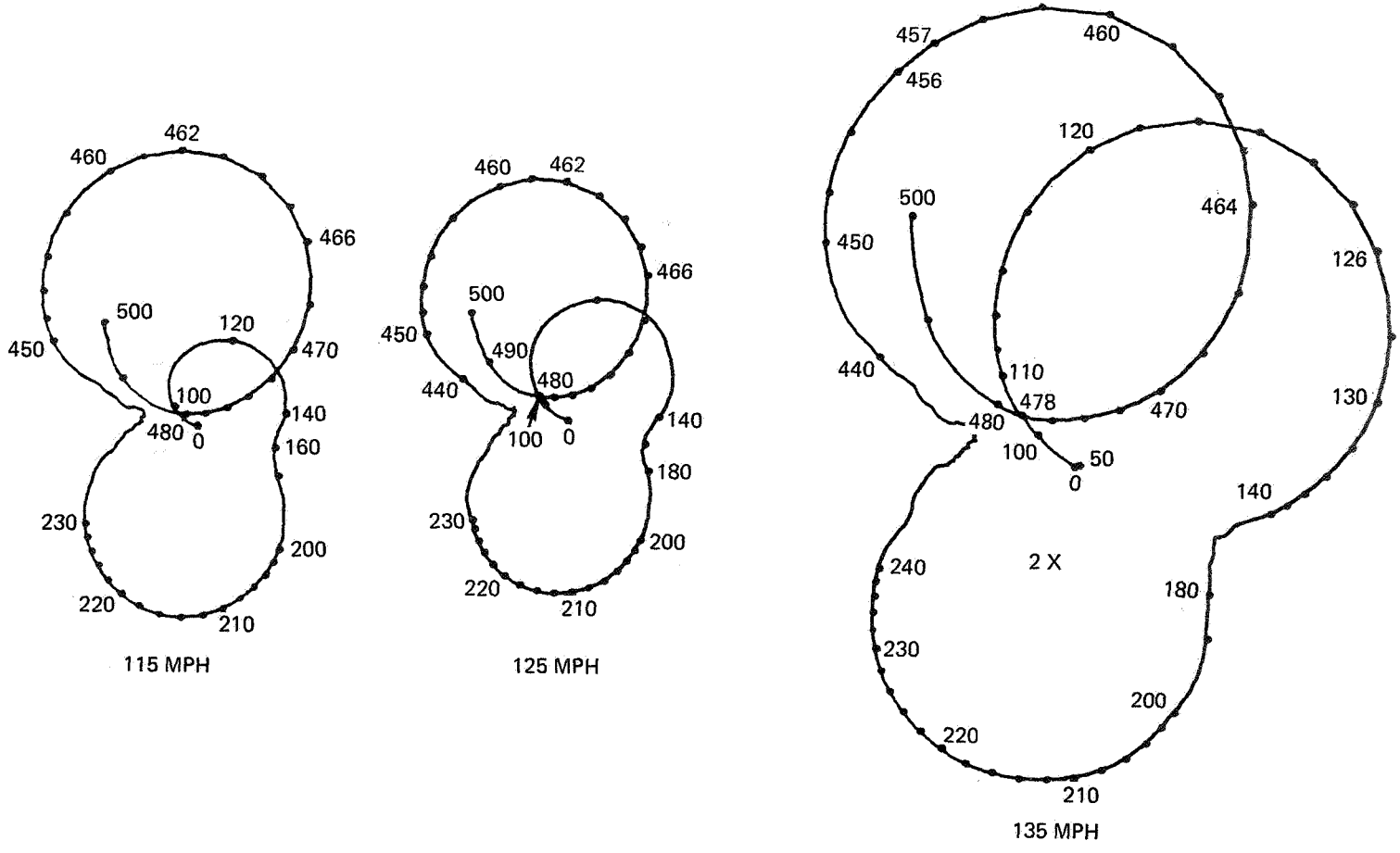

Figure 11.– (Concluded).

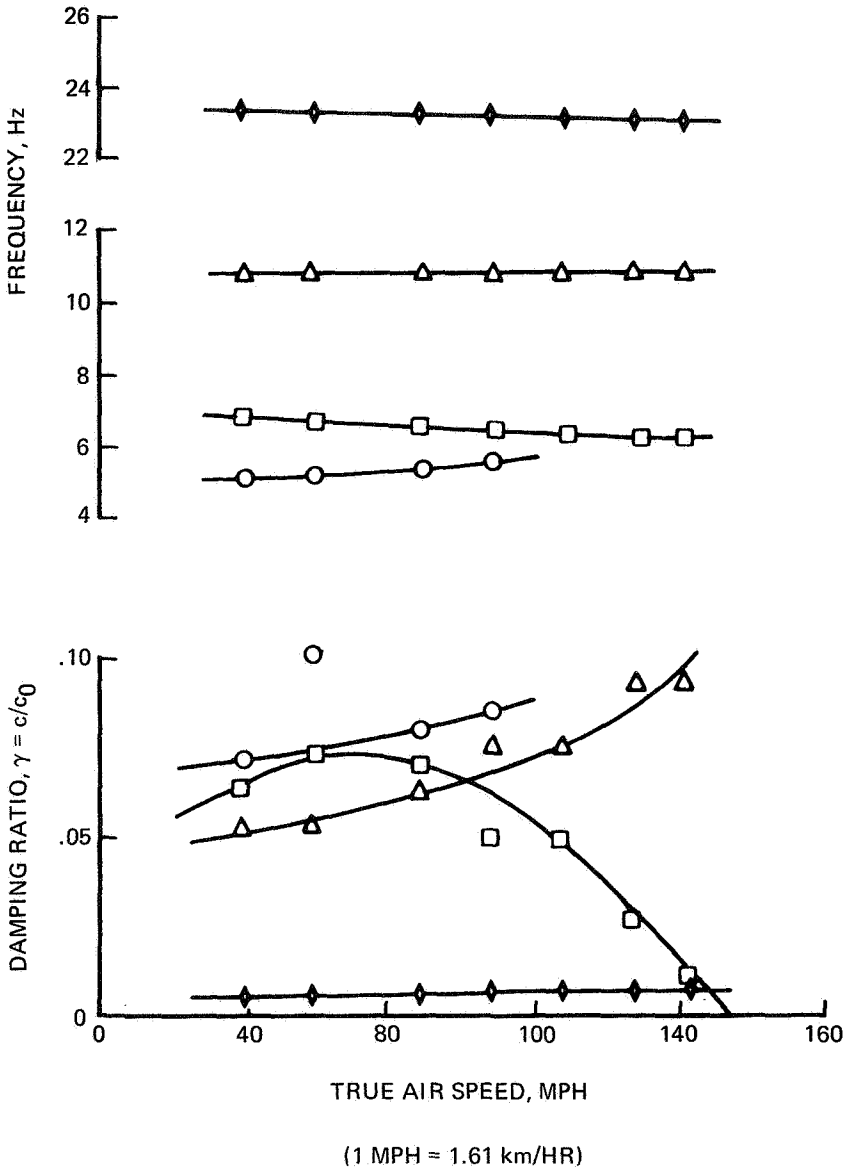

Figure 12.– Variations in modal frequencies and damping derived from figure 11.

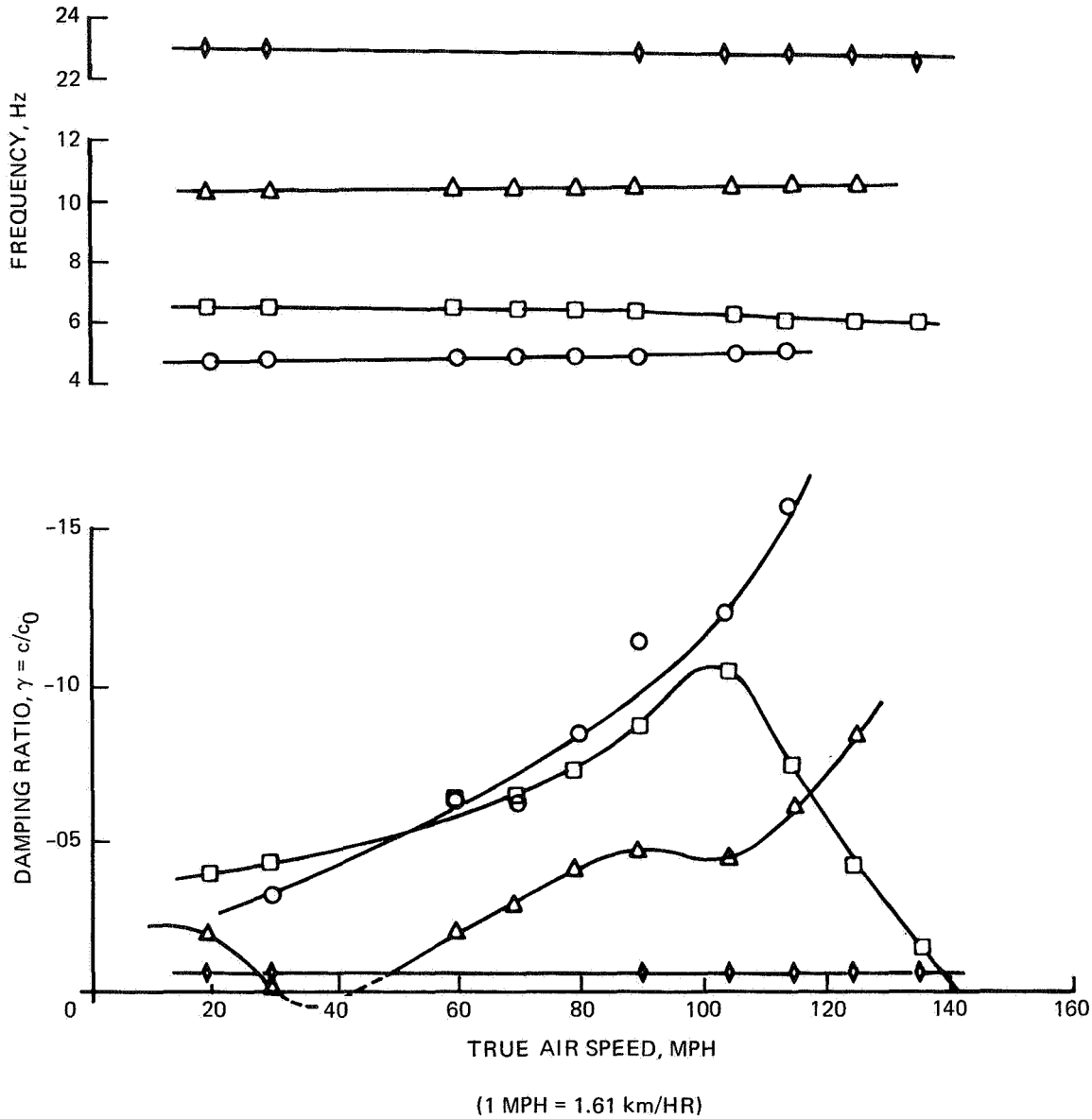

Figure 13.– Frequency and damping variations for model with free elevators.

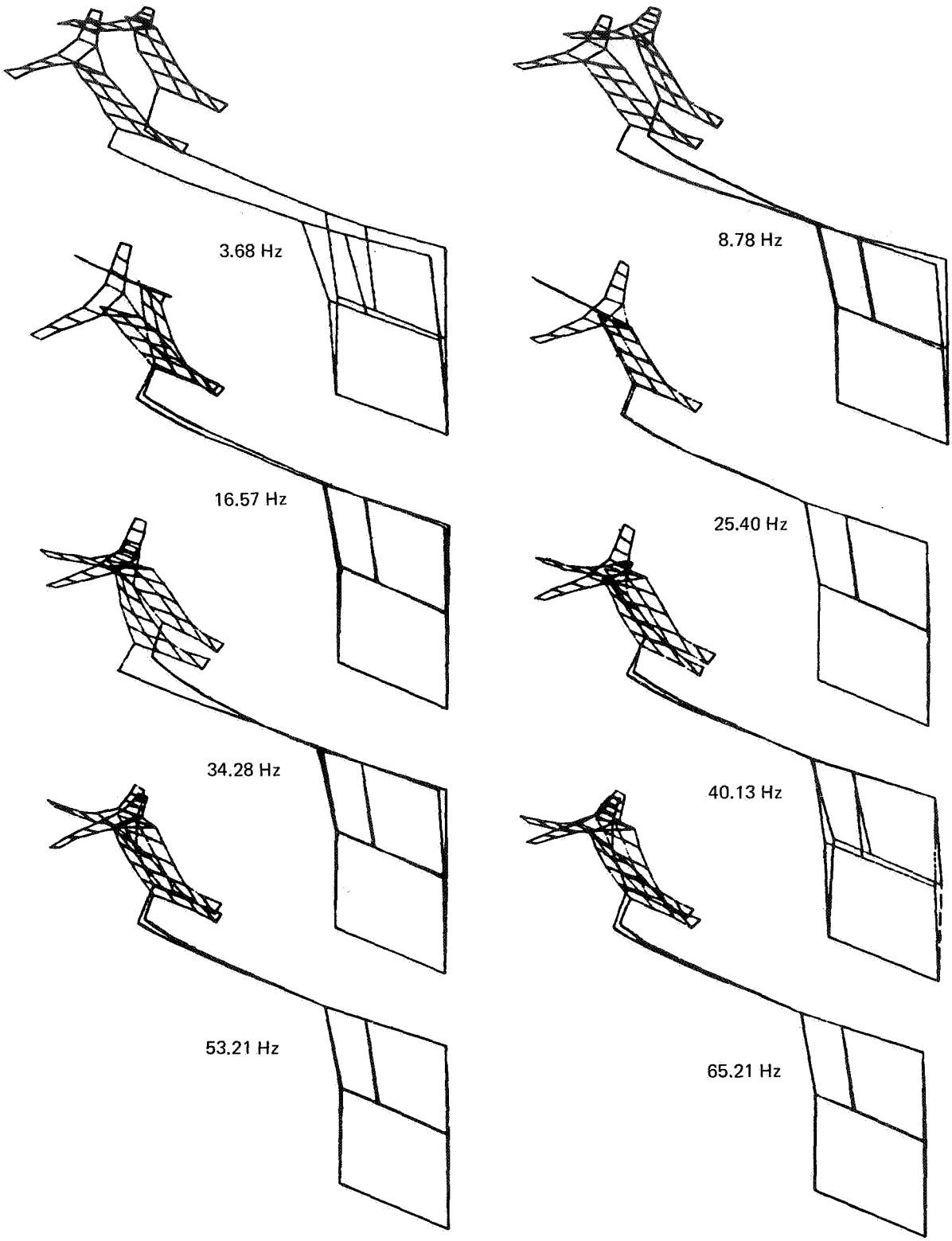

Figure 14.– Still air antisymmetric mode shapes of 727-300 transonic empennage model.

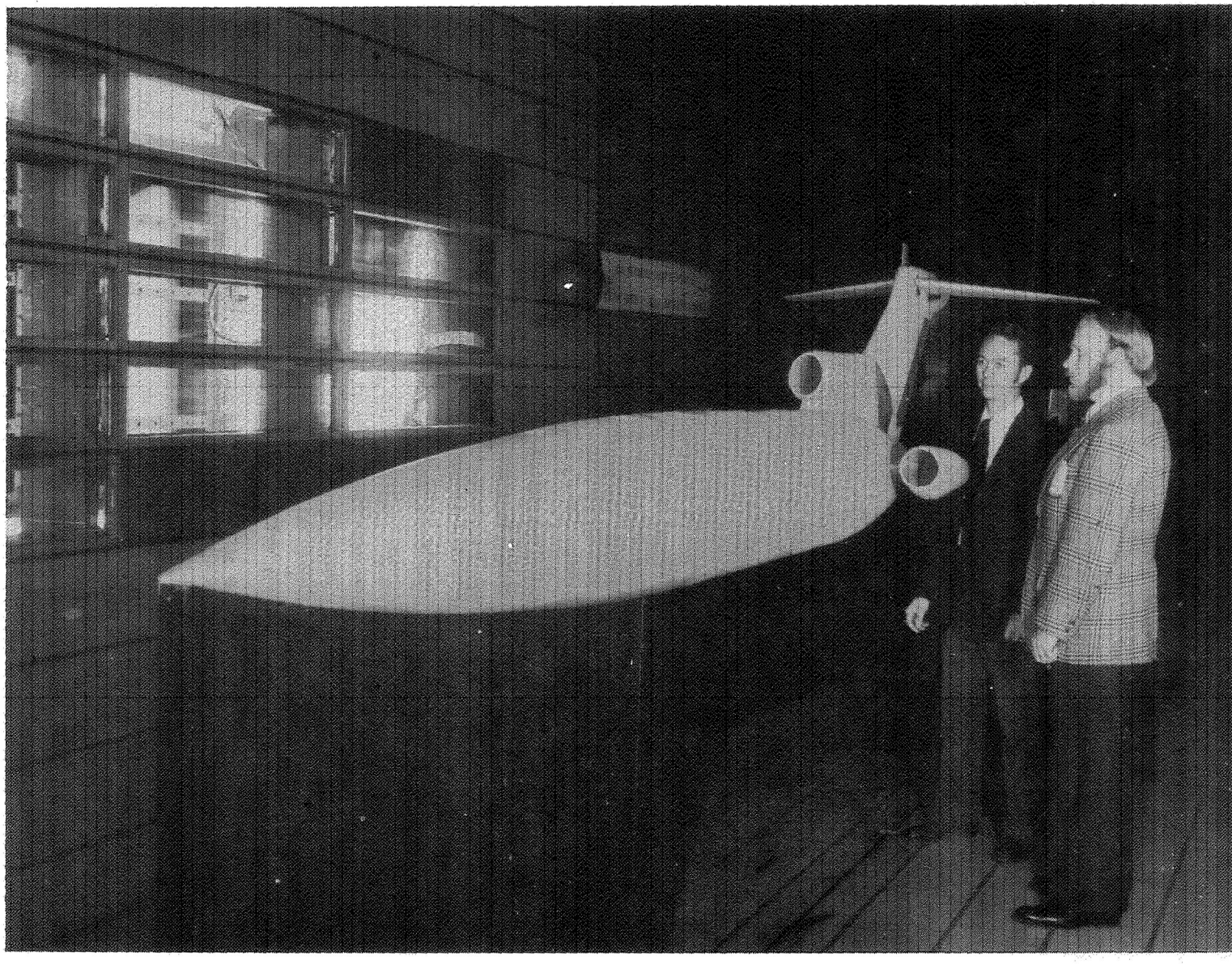

Figure 15.– 727-300 transonic empennage flutter model.

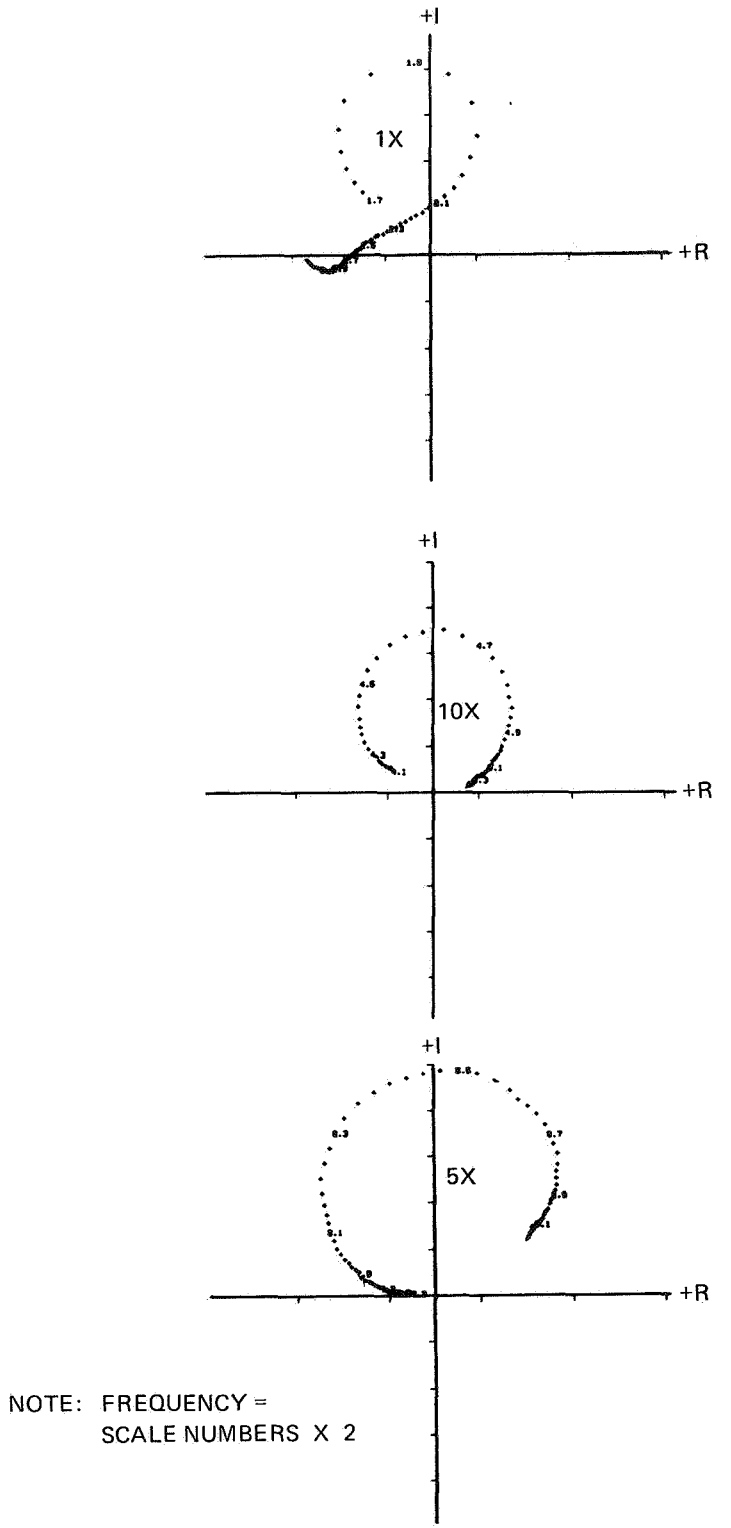

Figure 16.–Typical transfer function plots from transonic empennage model test.

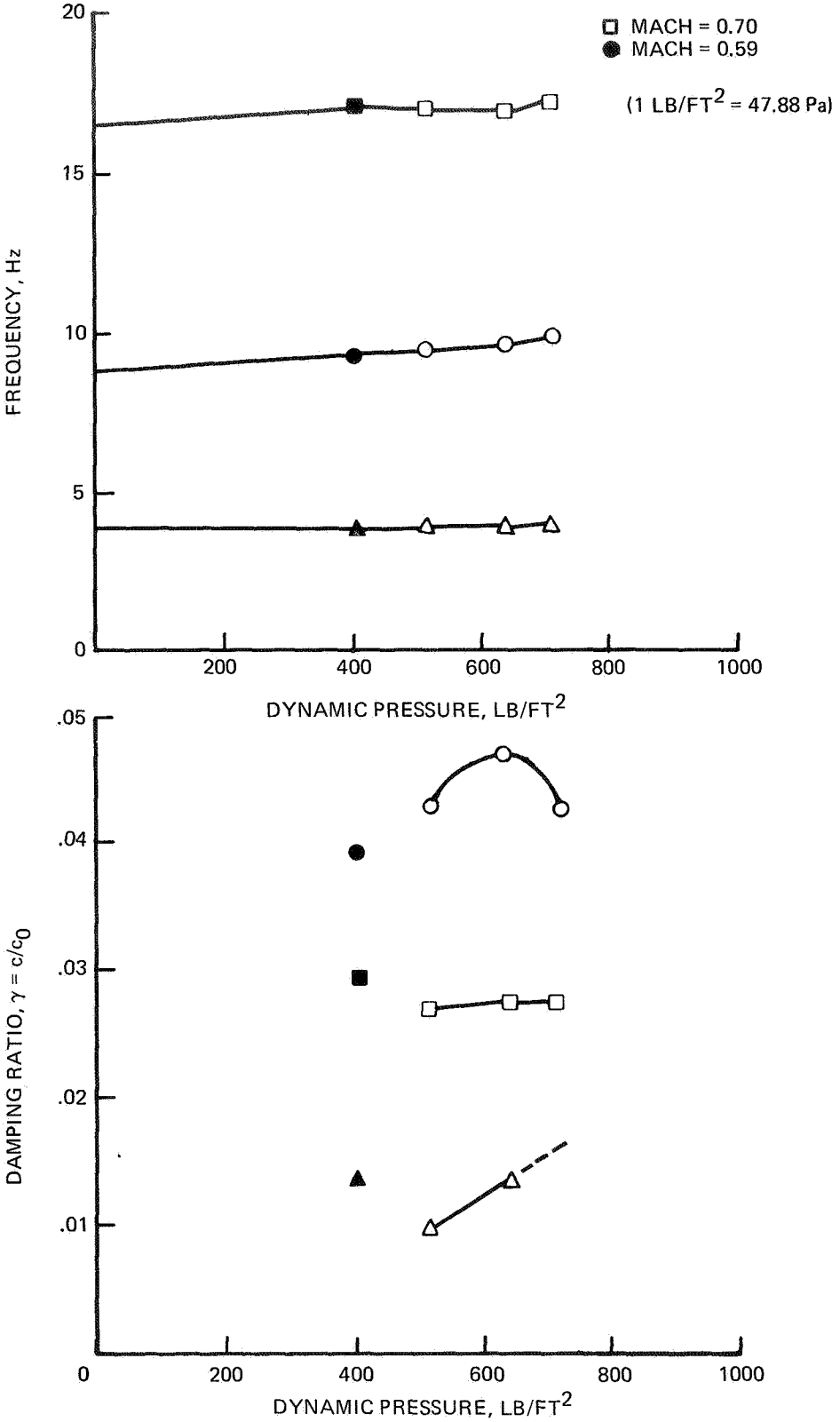

Figure 17.– Dynamic pressure versus damping and frequency.

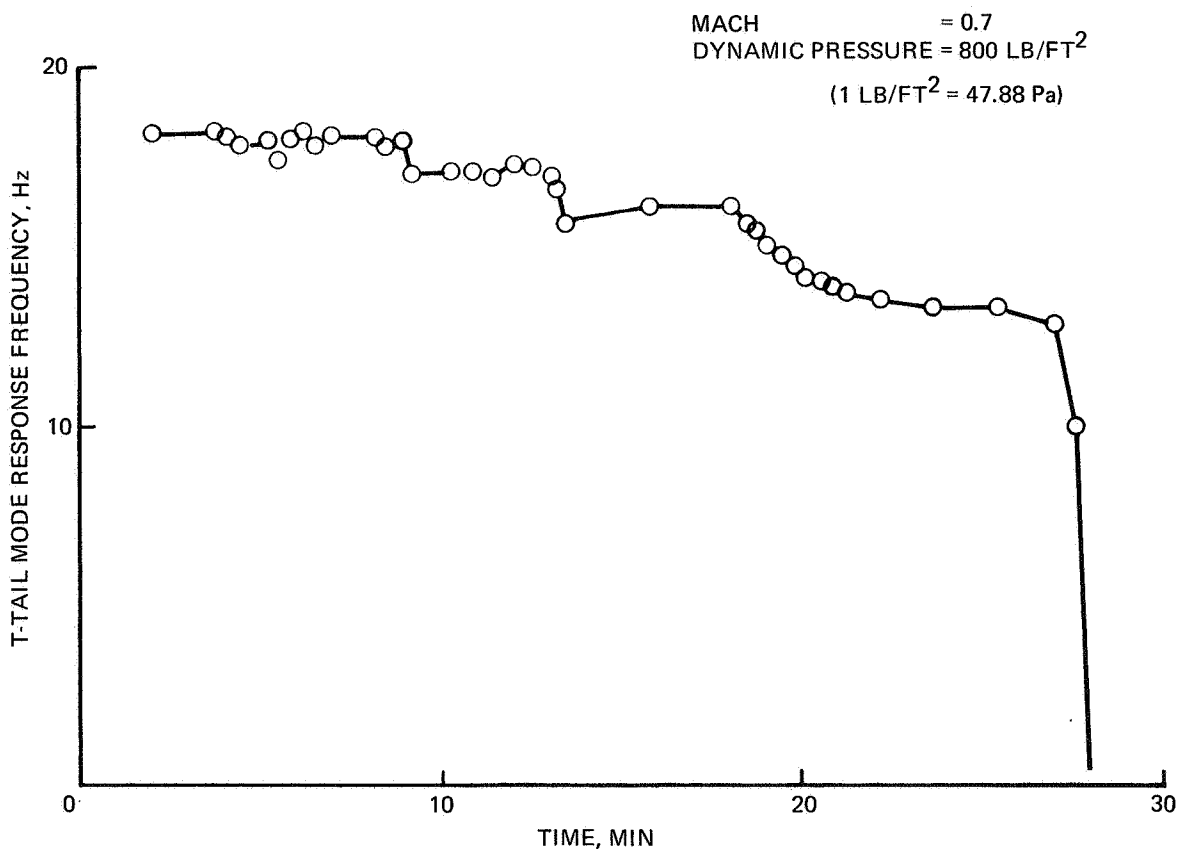

Figure 18.– 727-300 T-tail flutter model.

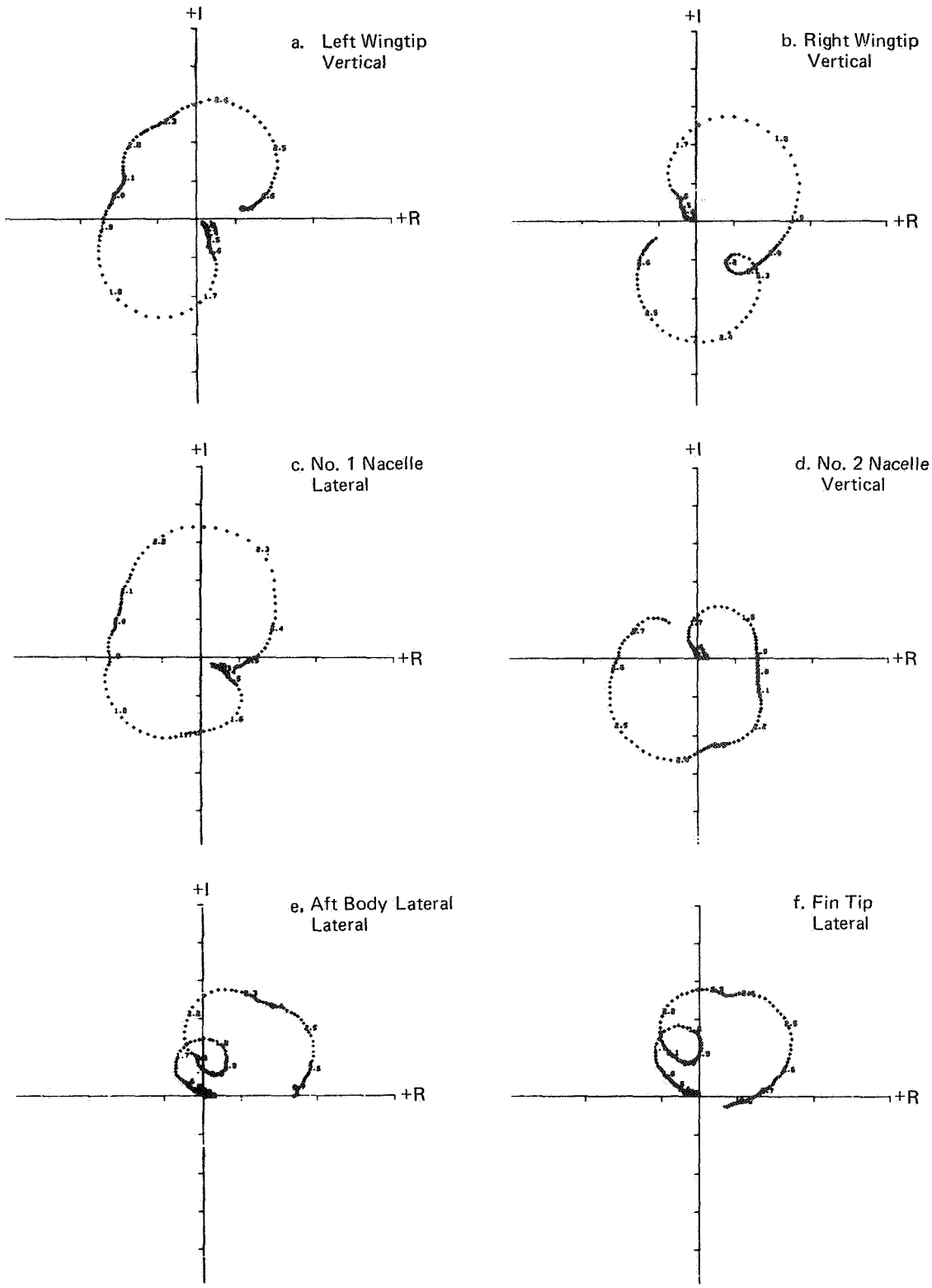

Figure 19.– 747-200 with JT9D-70 engines–Transfer functions relative to rudder excitation.

TURBULENCE EXCITED FREQUENCY DOMAIN DAMPING MEASUREMENT AND TRUNCATION EFFECTS

Jaak Soovere

Lockheed-California Company

SUMMARY

Existing frequency domain modal frequency and damping analysis methods are discussed. The effects of truncation in the Laplace and Fourier transform data analysis methods are described in detail. Methods for eliminating truncation errors from measured damping are presented. Implications of truncation effects in fast Fourier transform analysis are discussed. Limited comparison with test data is presented.

5

INTRODUCTION

Flight flutter testing is generally a time-consuming procedure. It involves the installation of complex excitation generators such as vanes, inertia exciters, or impulsive devices (ref. 1) as well as the response transducers and the associated electronic equipment. During flight testing, many flights are required to fully explore the aircraft critical flight spectrum, producing a large amount of test data which must be subsequently analyzed.

Considerable simplification in equipment installation may be obtained if turbulence excitation can be used instead of mechanical excitation. In any event, atmospheric turbulence and buffet degrade the response data from all types of mechanical excitation, except for random excitation, where it would most probably help more than hinder (ref. 2). Thus, the availability of suitable random response analysis methods, in addition to the existing harmonic analysis methods, would be a great advantage. The random analysis methods, like the current harmonic analysis methods, place the burden of data reduction on the computer, which, when used in the interactive mode with the test engineer, can provide a basis for real-time flutter testing.

The exciter installation and data acquisition and analysis problems are further compounded in space shuttle type vehicles, where weight is of paramount importance and the cost of exploring the entire critical flight spectrum with many flights prohibitive. The nonstationary nature of the flight environment and the relatively short duration of each flight within the atmosphere place a premium on the need for transmitting as much response data as possible,

and as quickly as possible, to the ground station. An increase either in the rate of sampling of the transducers, or in the number of transducers, is possible, if the data sample length can be reduced without a loss in the accuracy of the analysis.

A reduction in the sample length of the random response data is accompanied by a reduction in the statistical accuracy of the frequency domain modal response spectra. The statistical accuracy can be restored at the expense of resolution through a corresponding increase in the effective analysis bandwidth. This increase in analysis bandwidth produces a truncation effect in the response spectra. The truncation effect can occur in the frequency domain modal analysis derived from the Fourier transform of not only the impulse response time history but also the cross- and auto-correlation functions of response due to random and impulse-type excitations.

The effect of truncation is studied by using a single-degree-of-freedom system. Existing frequency domain harmonic analysis methods are briefly discussed as an introduction to the truncation effect and to illustrate the format of the data presentation.

HARMONIC ANALYSIS

The simplest method for obtaining aircraft modal frequency and damping data is through stick pulse generated free decay data (figs. 1 and 2). However, narrow band filtering is required both to isolate each mode in turn and to minimize noise due to the presence of turbulence. Computerized least squares fit methods such as the Moving Block Analysis (ref. 3) can be used to obtain damping data from the log decrement of the decay once the resonant frequencies have been identified by spectral analysis.

Stick pulses, in general, may not excite all the modes of interest and may produce an unconservative estimate of the damping. For close resonances, narrow band filtering may not isolate each mode, resulting in a beating decay response (fig. 1). Under such circumstances, it is possible to extract meaningful data only if the modal damping and amplitudes are comparable in each of the modes. It is, however, possible, through the Fourier transform, to transform the decay data into the frequency domain (figs. 3 and 4) and thereby resolve the modes.

This Fourier transform process can be illustrated mathematically by considering the relationship between the response $y(t)$ of a linear system and a general force $x(t)$, given by

$$y(t) = \int_{-\infty}^{\infty} h(\tau)\, x\,(t-\tau)\, d\tau \qquad (1)$$

where $h(\tau)$ is the impulse response function of the system at time τ. For a single-degree-of-freedom system, the impulse response function is given by

$$h(\tau) = \frac{e^{-\delta\omega_r \tau}}{m\,\omega_r\sqrt{1-\delta^2}} \operatorname{Sin}\omega_r\sqrt{1-\delta^2}\;\tau \qquad (2)$$

where:

- m is the generalized mass,
- ω_r is the angular resonant frequency, and
- δ is the viscous damping coefficient.

If the force is of sufficiently short duration that it can be considered to be an impulse $I\delta(t)$, where $\delta(t)$ is the delta function, then the response time history reduces to

$$y(t) = h(t)\,I \qquad (3)$$

The response spectrum $y(i\omega)$, obtained from Fourier transform of the time history (eq. (1)), is related to the force spectrum $x(i\omega)$ by

$$y(i\omega) = H(i\omega)\,x(i\omega) \qquad (4)$$

where $H(i\omega)$ is the frequency response function of the system. For a single-degree-of-freedom system,

$$H(i\omega) = \frac{1}{m\,(\omega_r^2 - \omega^2 + 2i\delta\omega_r\omega)} \qquad (5)$$

The Fourier transforms of the response $y(t)$ and the force $x(t)$ are defined by

$$y(i\omega) = \frac{1}{2\pi}\int_{-\infty}^{\infty} y(t)\,e^{-i\omega t}dt \qquad (6)$$

and

$$x(i\omega) = \frac{1}{2\pi}\int_{-\infty}^{\infty} x(t)\,e^{-i\omega t}dt \qquad (7)$$

respectively. Again, if x(t) can be considered an impulse $I\delta(t)$, then the force spectrum reduces to

$$x(i\omega) = \frac{I}{2\pi} \tag{8}$$

and the response spectrum to

$$y(i\omega) = \frac{H(i\omega)\, I}{2\pi} \tag{9}$$

which is simply the system frequency response function multiplied by a constant.

Two formats can be used in the presentation of the frequency domain response data. In the response modulus vs frequency presentation (fig. 3), the resonant frequency is located approximately at the peak response, and the viscous damping coefficient, which is twice the structure damping, is obtained by dividing the half power point bandwidth by twice the resonant frequency.

It is accurate for well-separated modes. For close modes, as the modulus represents the total response vector from the origin and not necessarily the modal vector, errors in the measured modal frequency and the viscous damping coefficient may result. The extraction of modal damping may even be prevented by the failure to resolve the half power points (fig. 3).

To overcome these limitations, both amplitude and phase are retained and presented in a format of a Nyquist plot (fig. 4) in which the real part of the response is in phase and the imaginary part is out of phase relative to the excitation. This method of modal analysis was first suggested by Kennedy and Pancu (ref. 4). The resonant frequency is located at the point on the curve where the rate of change in arc length with frequency is at a maximum. The viscous damping coefficient is obtained from the half power points as previously described or by first measuring the angle ϕ subtended at the modal origin, by the arc between any frequency point f and the resonant frequency point f_r, and then using the relationship

$$\delta = \frac{f_r - f}{f_r} \operatorname{Cot}(\phi) \tag{10}$$

A strong feature of the Nyquist plot response data representation is that mode shapes can be identified by means of the modal response vector.

The more common method of generating the response Nyquist plots is by means of a slow sine sweep using mechanical in-flight excitation, such as inertia exciters, in which the force output is used as reference. This method has been computerized for multimodal analysis (ref. 5), employing a least

squares curve fit technique to minimize the effect of extraneous noise and used in a computer/test engineer interactive mode for flutter testing.

In transforming the free decay data as previously discussed, no truncation effects were observed due to the relatively high modal damping and the need for including one beat as a minimum in the decay sample. In the second example of a stick pulse excited decay (fig. 2), the decay was prematurely truncated after one and five seconds to illustrate the effect on the frequency domain response (fig. 5). The Nyquist plots of the response become more oval in appearance as the decay sample duration is progressively reduced. If the Nyquist plots are analyzed by the conventional method described above, unconservative estimates of the damping are obtained. (See table 1.) In order to obtain useful damping data from these Nyquist plots, a method eliminating the effect of truncation from the damping must first be developed.

TRUNCATION THEORY

Due to the similarity between the cross-correlation and the impulse-response functions with the auto-correlation function Ryy (τ) of a single-degree-of-freedom system excited by a constant spectrum force, S_p (ref. 2) and defined by

$$Ryy(\tau) = \frac{\pi S_p \, e^{-\delta\omega_r\tau}}{2m^2\omega_r{}^3\delta}\left(\text{Cos } \omega_r \sqrt{1-\delta^2}\,\tau + \frac{\delta}{\sqrt{1-\delta^2}} \text{ Sin } \omega_r \sqrt{1-\delta^2}\,\tau\right) \qquad (11)$$

it is only necessary to describe the equations for any one of the above functions. The impulse-response function and the cross-correlation function of a single-degree-of-freedom system, when excited by constant spectrum force, exist only for positive time.

If the Laplace transform or the single-sided Fourier transform of the autocorrelation function of the response Ryy (τ) is used, with limits of integration from zero to infinity, instead of the full Fourier transform, phase information is retained in the response spectrum (ref. 2). The resulting response spectrum $S(i\omega)$ is given by

$$S(i\omega) = \frac{S_p}{4m\omega_r{}^2\delta}\left(\frac{i\omega}{\omega_r} H(i\omega) + 2\delta H(i\omega)\right) \qquad (12)$$

The characteristic response function $\frac{S(i\omega)}{S_p}$ has properties similar to the frequency response function $H(i\omega)$. This method provides a powerful tool in

modal response analysis of random as well as impulse response data in the frequency domain. The previously described methods for extracting the modal damping and frequency can be employed as long as no truncation effect is present.

If we let $y(t)$ represent any of the above time functions, with the understanding that they exist only for positive time, the complex response spectrum $y(i\omega)$ is obtained from Fourier transform of $y(t)$.

$$y(i\omega) = \frac{1}{2\pi}\int_{-\infty}^{\infty} y(t)\, e^{-i\omega t}dt \qquad (13)$$

$$\text{where} \quad y(t) = 0 \quad \text{for} \quad t < 0$$

In reality, the response time history is truncated at some finite time τ_m. The resulting estimated response spectrum $\hat{y}(i\omega_1)$ (ref. 6) is given by the relationship

$$\hat{y}(i\omega_1) = \frac{1}{2\pi}\int_{0}^{\tau_m} y(t)\, e^{-i\omega_1 t}dt$$

$$= \frac{1}{2\pi}\int_{-\infty}^{\infty} D(t)\, y(t)\, e^{-i\omega_1 t}dt \qquad (14)$$

where $D(t)$ is the weighting or the truncation function.

Three weighting functions (ref. 7) are considered in this paper. They are the "do-nothing" or the boxcar weighting, generally defined by

$$D(t) = 1 \quad \text{for} \; -\tau_m < t < \tau_m$$
$$= 0 \quad \text{elsewhere} \qquad (15)$$

the Hanning weighting function defined by

$$D(t) = \frac{1}{2}\left(1 + \text{Cos}\,\frac{\pi t}{\tau_m}\right) \quad \text{for} \; -\tau_m < t < \tau_m$$
$$= 0 \quad \text{elsewhere} \qquad (16)$$

and the Bartlett weighting function defined by

$$D(t) = \left(1 - \frac{|t|}{\tau_m}\right) \quad \text{for} \; -\tau_m < t < \tau_m$$
$$= 0 \quad \text{elsewhere} \qquad (17)$$

The reverse Fourier transform for the response is given by

$$y(t) = \int_{-\infty}^{\infty} y(i\omega)\, e^{i\omega t} d\omega \tag{18}$$

On substituting for y(t) in equation (14) and rearranging the order of the integration, the estimate of the spectrum becomes

$$\begin{aligned} \hat{y}(i\omega) &= \frac{1}{2\pi} \int_{-\infty}^{\infty} \int_{0}^{\tau_m} D(t)\, e^{-i(\omega_1 - \omega)t}\, dt\, y(i\omega) d\omega \\ &= \int_{-\infty}^{\infty} Q(\omega_1 - \omega)\, y(i\omega)\, d\omega \end{aligned} \tag{19}$$

where

$$Q(\omega_1 - \omega) = \frac{1}{2\pi} \int_{0}^{\tau_m} D(t)\, e^{-i(\omega_1 - \omega)t} dt \tag{20}$$

$Q(\omega_1 - \omega)$ is referred to as the spectral window. The weighting functions defined by equations (16) to (18) and the corresponding spectral windows are illustrated in figure 6. In the application discussed in this paper, the spectral windows are complex (ref. 6 and 8) since the weighting functions are one sided and exist only in positive time from zero to τ_m.

TRUNCATED DATA REDUCTION

For a linear system excited by random force (or impulse) of constant spectral density, the response spectrum $y(i\omega)$ is proportional to the frequency response function of the system. Equation (19), with $y(i\omega)$ replaced by the frequency response function of a single-degree-of-freedom system and a constant force spectrum, has been integrated by using contour integration for the "do-nothing" and the Bartlett weighting in references 6 and 8, respectively. It has recently been solved by the author for the Hanning weighting. A typical effect of the truncation due to the Hanning weighting is illustrated in figure 7. The single-degree-of-freedom response plots have been normalized relative to the untruncated plot. The other two weighting functions differ only in the degree of truncation effect. The "do-nothing" weighting function, while exhibiting the smallest truncation effect, suffers from the undesirable side lobes (fig. 5) which may be mistaken for modes or may interfere with other nearby modes. The Bartlett weighting function suffers a greater resolution loss, as can be seen by comparing figure 8 with figure 5.

The resonant frequency is still identified by the peak rate of change of arc length with frequency, but the procedure for estimating the damping from the truncated curves is different from the methods previously described. At

first (ref. 6 and 8), the damping coefficient was extracted with the assistance of a nondimensional parameter defined by the peak rate of change of arc length with frequency, divided by the radius of curvature at the resonant frequency, from theoretically predicted curves. In these curves, the above parameter is plotted as a function of the resonant frequency multiplied by the true damping coefficient. These curves were originally developed for use in high frequency structural response studies and consequently are unsuitable for flutter data analysis due to the relatively low aircraft response frequencies.

A more useful graphical format, which provides direct damping readout, is presented in this paper and illustrated in figure 9 for the Hanning truncation. The measured damping coefficient δ^* is plotted against the true damping coefficient δ as a function of the ratio of the effective data analysis bandwidth Δf divided by the resonant frequency. The effective analysis bandwidth Δf is related to the maximum truncation time τ_m by

$$\Delta f = \frac{1}{2\tau_m} \tag{21}$$

The measured damping coefficient δ^* is defined by

$$\delta^* = \frac{2\rho}{ds}\left(\frac{df}{f_r}\right) \tag{22}$$

where ρ is the radius of curvature at resonance, and

ds is the arc length at resonance contained within the frequency interval of df

It can be observed that as the maximum truncation time becomes large, the measured viscous damping coefficient approaches the true value.

This method of obtaining the damping from the truncation-affected single-degree-of-freedom system Nyquist plots has been computerized for potential use in real-time analysis. The number of iterations required to converge to the correct damping from the estimated damping is illustrated in figure 10. The convergence is carried out in two or three sequences and is very rapid. The number of steps in the initial sequence is selected to speed up the iteration, especially in cases of severe truncation.

The damping of the free decay record (fig. 2) as obtained by the computerized method for the "do-nothing", Hanning, and Bartlett truncations, a least squares fit to the free decay, and the restored Nyquist plot method (fig. 11) are summarized in table 2. The method of restoring the Nyquist (ref. 9) plot involves the weighting of the decay with a known exponential weighting to meet the required 55 dB dynamic range criteria (ref. 10) for the decay. Analysis is thereafter carried out conventionally and the damping

corresponding to the exponential weighting is subtracted from the measured damping to arrive at the true modal damping. It is more common to apply the exponential weighting function to the correlation function. This method has been used in flight flutter testing in England (ref. 11). The results from the analysis of the one-second decay record indicate the existence of a lower bound on the accuracy for the above frequency domain analysis methods.

TRUNCATION IN POWER SPECTRAL DENSITY

A method based on the cross-spectral analysis previously discussed was developed to predict the truncation effect in power spectral density (PSD) analysis. The effect of the truncation on the normalized PSD is illustrated in figure 12 for the Hanning weighting. A computer program was developed to obtain the damping from the 3 dB points by using the quadratic curve fit. A graphical method for obtaining the true damping coefficient δ from the measured damping coefficient $\hat{\delta}$ for various ratios of effective analysis bandwidth to resonant frequency is illustrated in figure 13.

A Hanning smoothed power spectral density plot of a typical aircraft response to high-speed buffet is illustrated in figure 14. Due to the very high speed, no reliable flutter test data are available for comparison. The analysis bandwidth of 0.5 Hz produces a truncation error in the two predominant modes at 10.2 Hz and 14.6 Hz. On allowing for the truncation effect, the viscous damping coefficients from the measured 3 dB point values of 0.11 and 0.044 are reduced to 0.068 and 0.02 for the two frequencies, respectively. This method suffers from the same inaccuracies as the modulus method previously discussed. It does, however, provide an indication of the damping where none previously existed.

FAST FOURIER TRANSFORM AND TRUNCATION

The above methods have been basically developed for the Blackman and Tuckey type of analysis (ref. 7). Truncation effects occur also in the fast Fourier transform (FFT) method of analysis. An indication as to the type of truncation present in FFT analysis of cross spectra is obtained from reference 12. The expected cross-spectral estimate $E\left[Sxy(f,T,k)\right]$ is given by

$$E\left[Sxy(f,T,k)\right] = \frac{1}{2\pi}\int_{-T}^{T}\left(1 - \frac{|\tau|}{\tau_m}\right) Rxy(\tau)\, e^{-i\omega\tau} d\tau \qquad (23)$$

As the cross-correlation function of a single-degree-of-freedom system excited by white noise is one sided, as previously discussed, it is concluded that the estimated cross spectrum obtained from FFT analysis is subject to Bartlett truncation errors.

The effect of truncation on the normalized PSD and cross spectral peak response is illustrated in figure 15 as a function of the resonant frequency multiplied by the maximum time delay and the viscous damping coefficient, $f_r \tau_m \delta$. It is observed that for the "do-nothing" truncation, the curve reaches unity near $f_r \tau_m \delta = 1$. This corresponds not only to the damping criteria for cross-spectral analysis established in reference 9, but also to the rule of thumb for PSD resolution for the analysis bandwidth to be one-fourth of the 3 dB point response bandwidth.

Attention is drawn to the fact that the Bartlett truncation curve converges to unity very slowly. Thus the use of cross-correlation functions obtained from the indirect method of first computing the spectra using the FFT and then transforming to time domain, will not only have the Bartlett truncation error but also an additional truncation error in transforming from the frequency domain to the time domain. These truncation errors in correlation functions are discussed in references 13, 14 and 15. Thus a very large number of transformation points must be used in determining the correlation function through the indirect method.

CONCLUSION

Methods for eliminating truncation errors from modal frequency and damping data have been presented for the cross- and power-spectral analysis. These methods have the potential for use in a computer/test engineer interactive mode, for random and impulsive-type response data analysis. Future work will include an evaluation of the methods against simulated and real flutter test data with buffet and turbulence excitation and the study of truncation effects in FFT-type analysis involving multiple Fourier transform operations.

REFERENCES

1. Baird, E. F., and Clark, W. B.: Recent Developments in Flight Flutter Testing in the United States. AGARD Report No. 596, Dec. 1972.

2. Kandianis, F.: Frequency Response of Structures and the Effects of Noise on its Estimates from the Transient Response. J. Sound Vib. 15(2), 1971.

3. Hurley, S. R.: The Application of Digital Computers to Near-Real-Time Processing of Flutter Test Data. NASA Symposium of Flutter Testing Techniques, Oct. 1975. (Paper No. of this compilation)

4. Kennedy, C. C., and Pancu, C.D.P.: Use of Vectors in Vibration Measurement and Analysis. J. Aero. Sci., 1947.

5. Gaukroger, D. R., Skingle, C. W. and Heron, K. H.: Numerical Analysis of Vector Response Loci. J. Sound Vib. 29(3), 1973.

6. Clarkson, B. L., and Mercer, C. A.: Use of Cross Correlation in Studying the Response of Lightly Damped Structures to Random Forces, AIAA J. 3, 1965.

7. Blackman, R. B., and Tukey, J. W.: Measurement of Power Spectra. Dover Publications, 1959.

8. Soovere, J., and Clarkson, B. L.: Frequency Response Function from Cross Correlation: Bartlett Weighting Function. AIAA J. 5, 1967.

9. White, R. G.: Evaluation of the Dynamic Characteristics of Structures by Transient Testing. J. Sound Vib. 15, 1971.

10. White, R. G.: Use of Transient Excitation in the Dynamic Analysis of Structures. R. Ae. S. J. 73, 1969.

11. Baldock, J. C. A., and Skingle, C. W.: Flutter Technology in the United Kingdom. AIAA Dynamics Specialist Conference, Williamsburg, 1973.

12. Bendat, J. S., and Piersol, A. G.: Random Data: Analysis and Measurement Procedures. Wiley-Interscience, 1971.

13. Mercer, C. A.: Note on Digital Estimation of Correlation Functions. J. Sound Vib. 27(2), 1973.

14. Holmes, P. J.: On the Practical Estimation of Spectra and Correlation Functions of Transient Signals. J. Sound Vib. 32(4), 1974.

15. Brownlee, L. R.: Comment on "Note on Digital Estimation of Correlation Functions." J. Sound Vib. 32(4), 1974.

TABLE 1. VISCOUS DAMPING COEFFICIENT OF TRUNCATED PLOTS DETERMINED BY USING EQUATION (10).

Decay Time, Seconds	"Do-Nothing" Truncation	Hanning Truncation	Bartlett Truncation
1	0.186	0.336	0.248
5	0.048	0.073	0.068

TABLE 2. COMPARISON OF VISCOUS DAMPING COEFFICIENT BY VARIOUS METHODS.

Decay Time, Seconds	Least Square Decay	Restored Nyquist Plot	TRUNCATION THEORY		
			"Do-Nothing"	Hanning	Bartlett
1	0.045	0.092	0.037	-	0.035-0.059
5	0.038	0.040	0.030	0.037	0.044

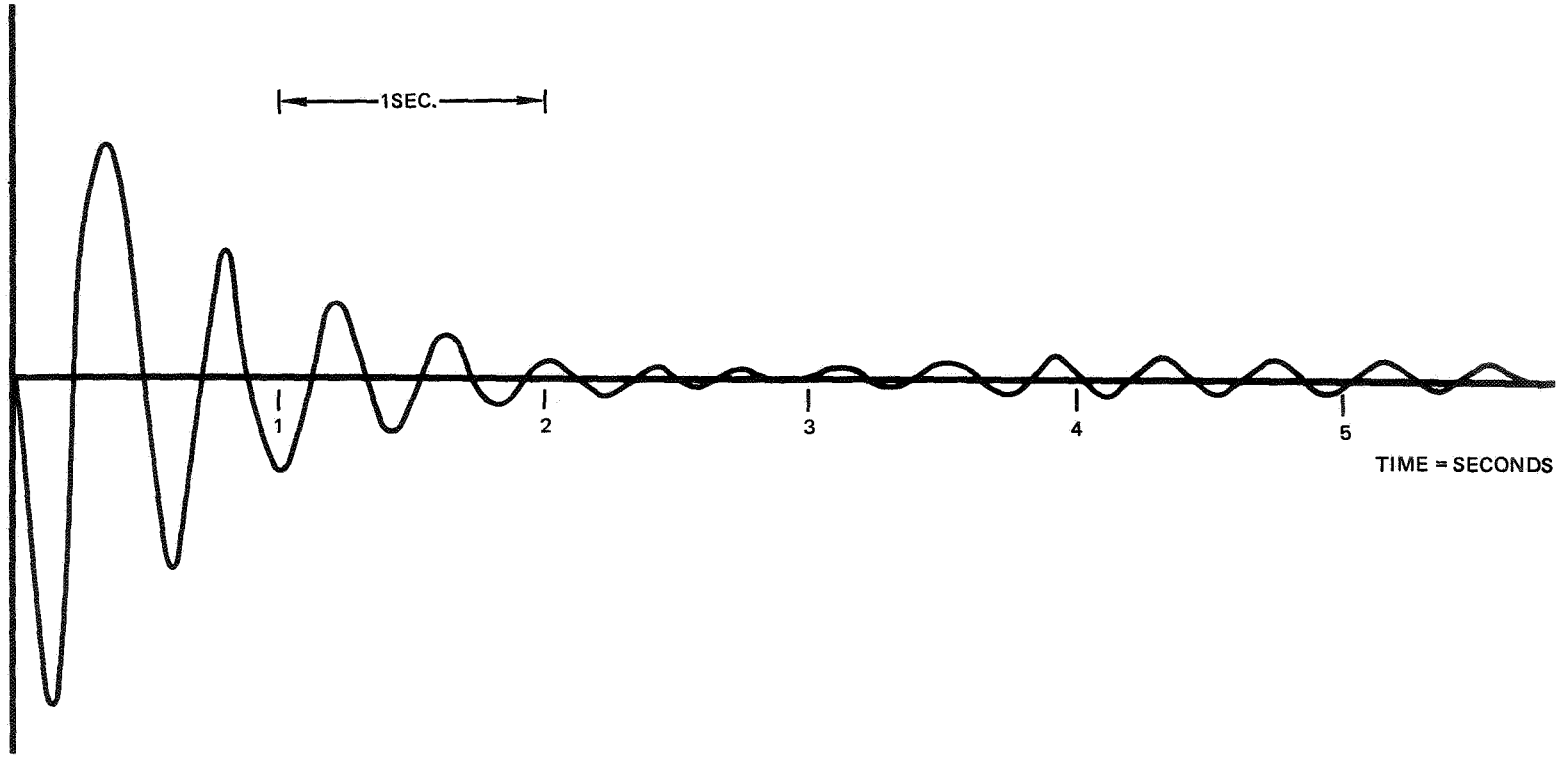

Figure 1. Typical Filtered Stick Pulse Excited Delay with Beating.

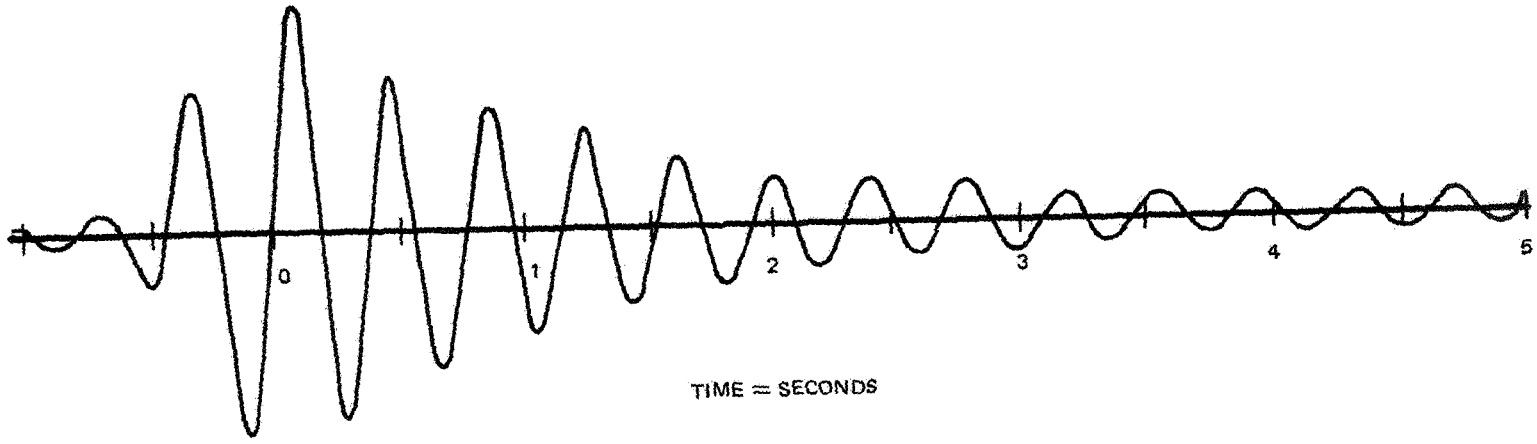

Figure 2. Typical Filtered Single Mode Stick Pulse Excited Decay.

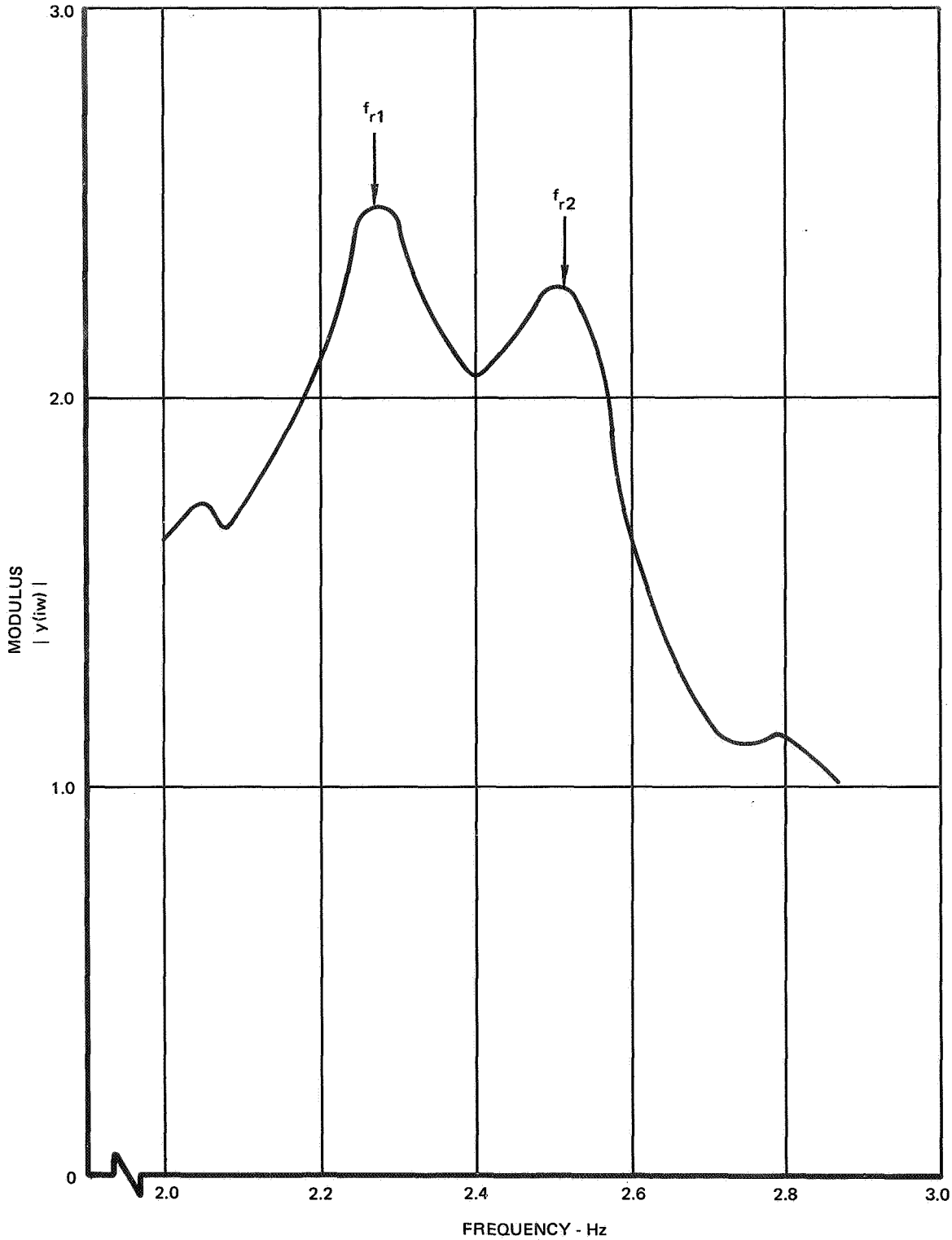

Figure 3. Modulus of the Fourier Transform of Beating Stick Pulse Excited Decay.

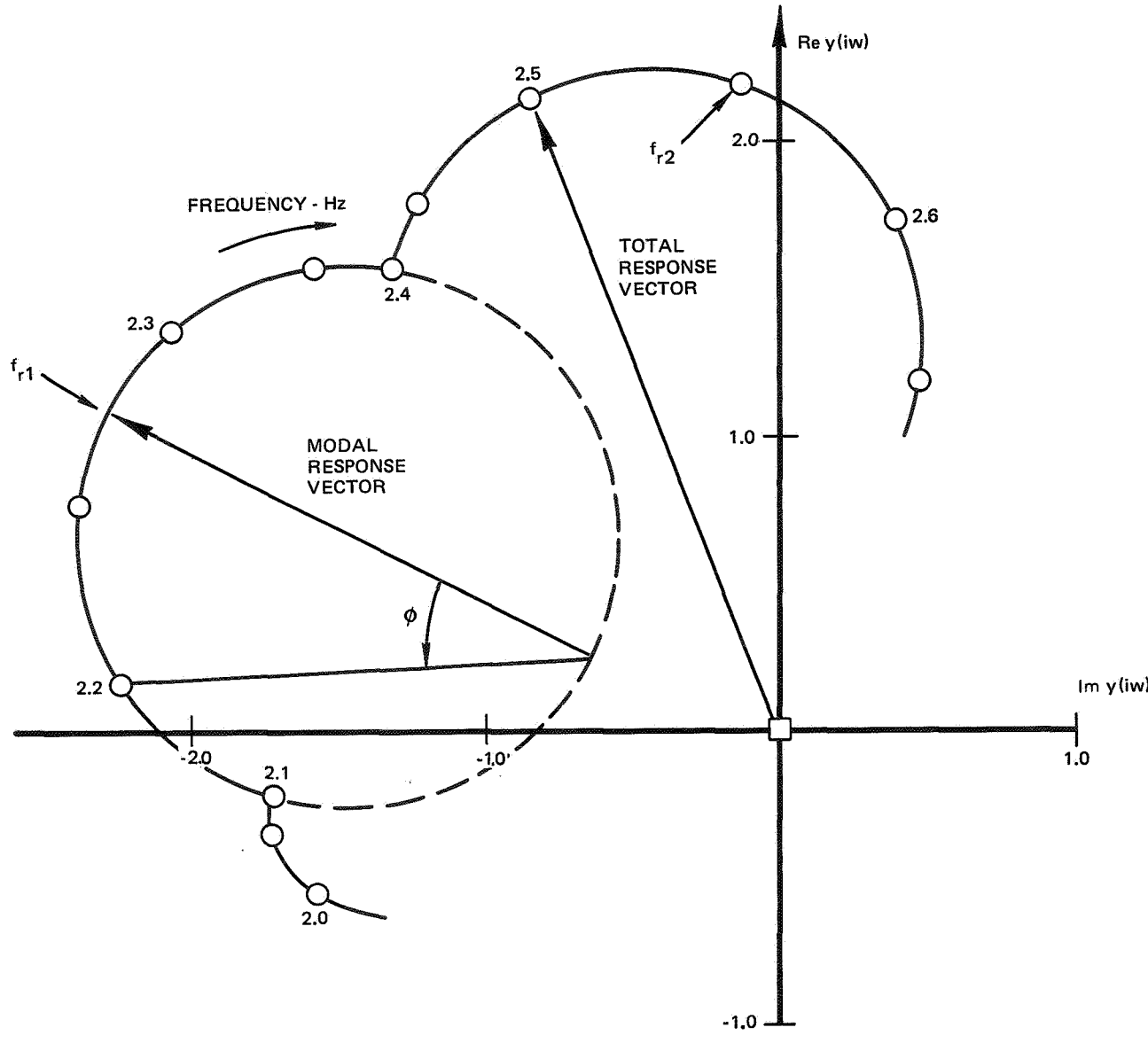

Figure 4. Fourier Transform of Beating Stick Pulse Excited Decay.

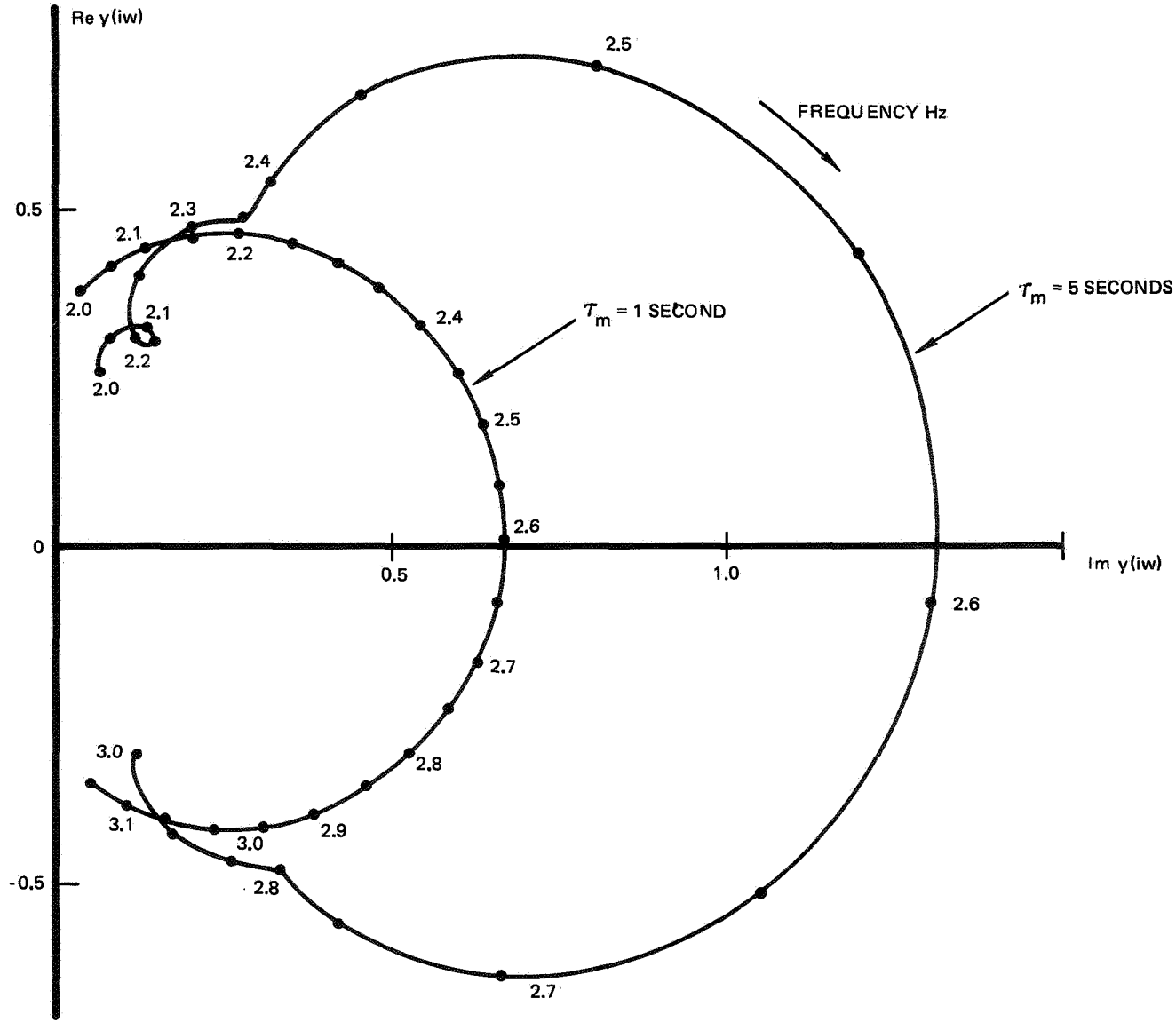

Figure 5. Fourier Transform of Stick Pulse Excited Single Mode Decay Showing Truncation Effect.

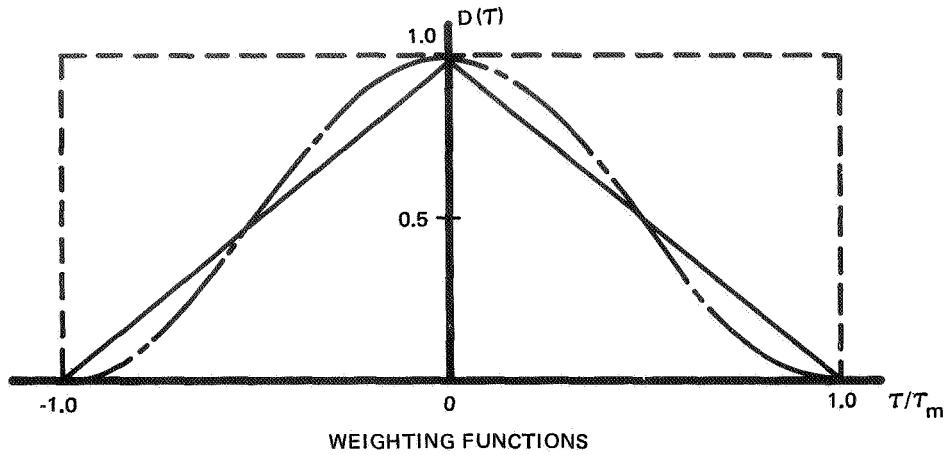

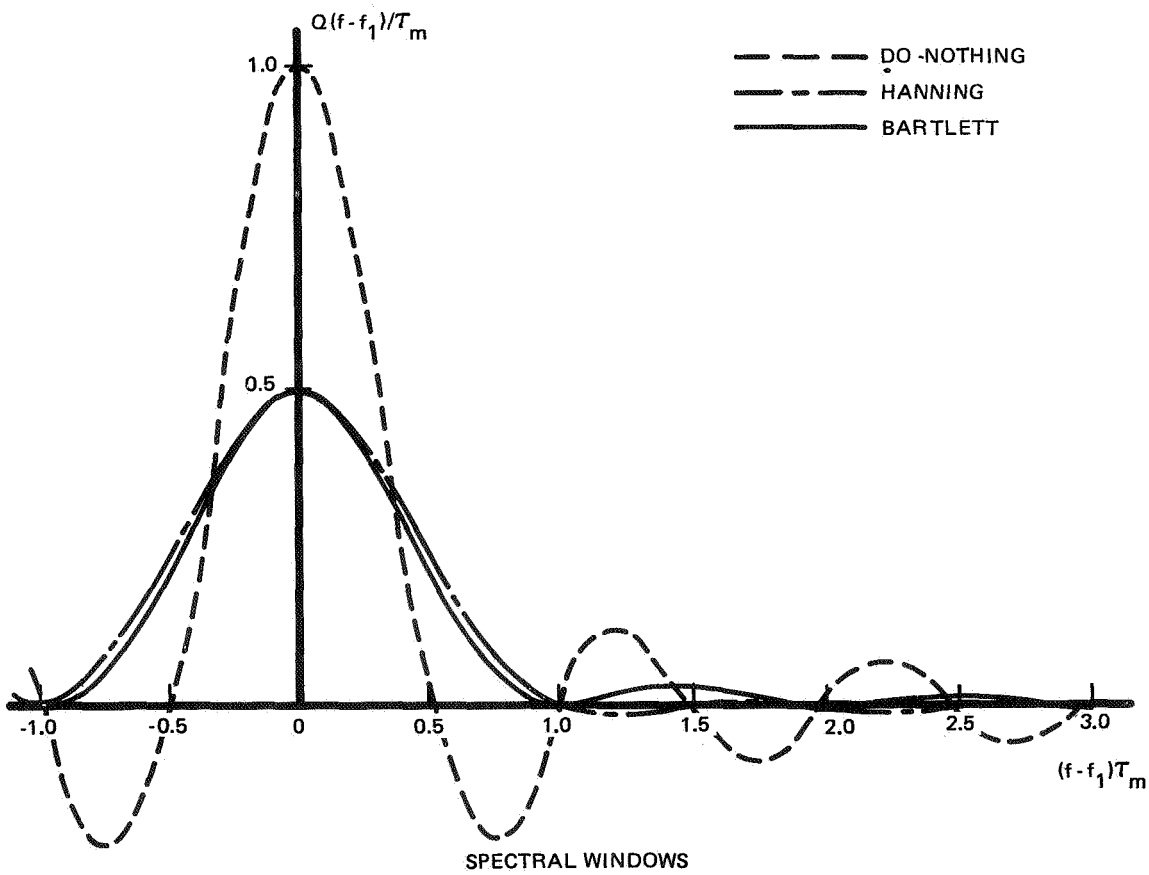

Figure 6. Spectral Windows and Weighting Functions.

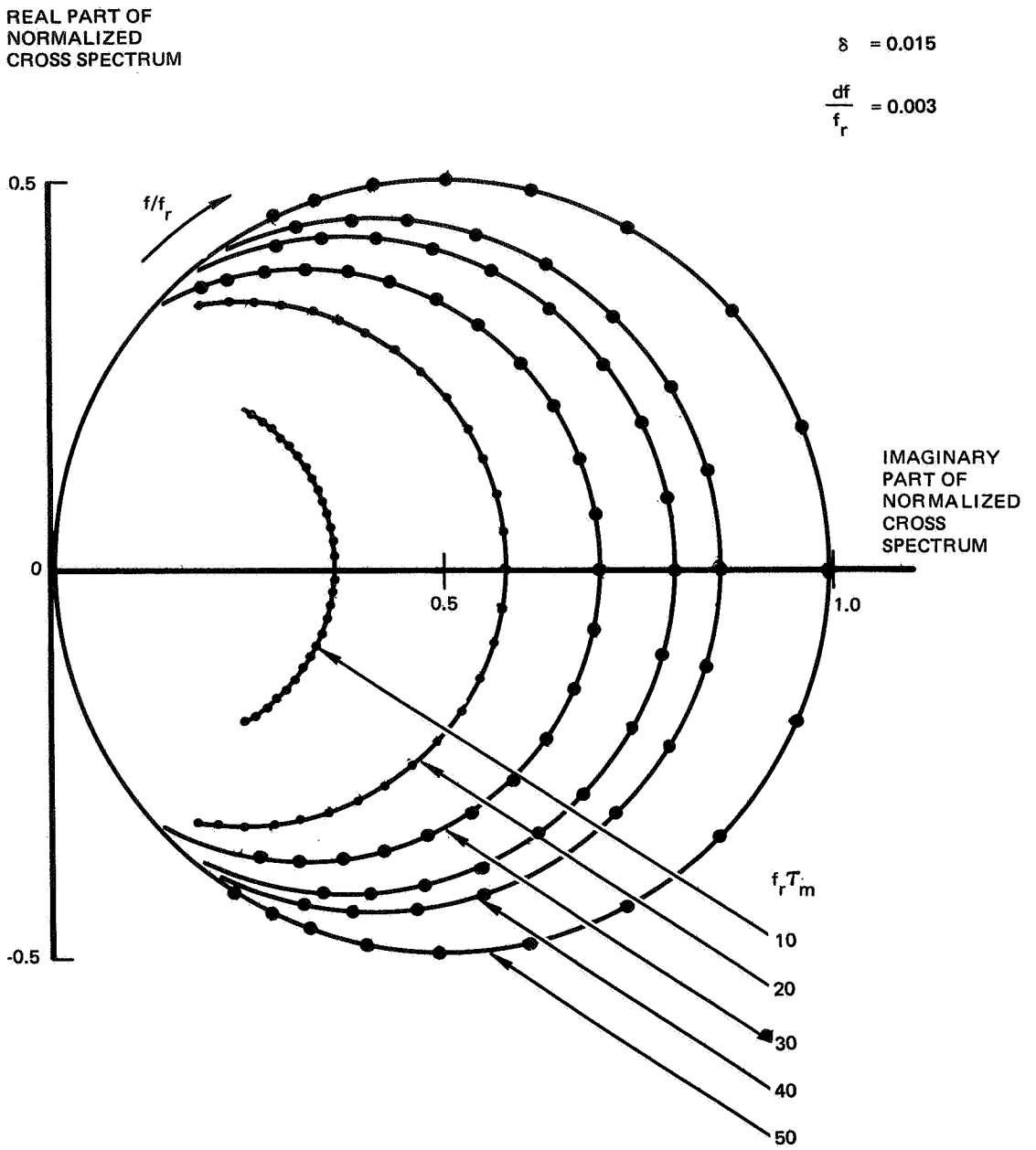

Figure 7. The Effect of Truncation on the Normalized Cross Spectrum of a Single-Degree-of-Freedom System Excited by White Noise - Hanning Weighting.

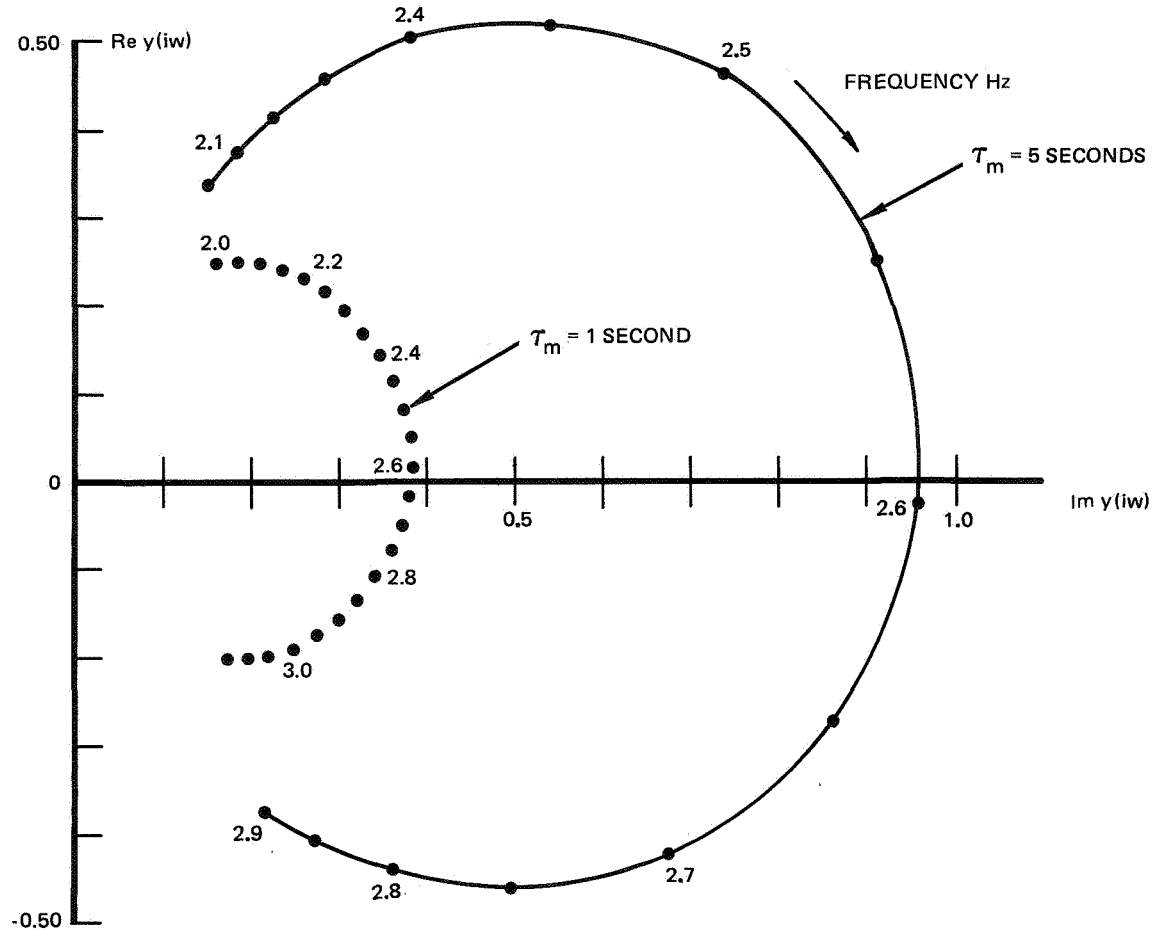

Figure 8. Fourier Transform of Stick Pulse Excited Decay with Bartlett Weighting.

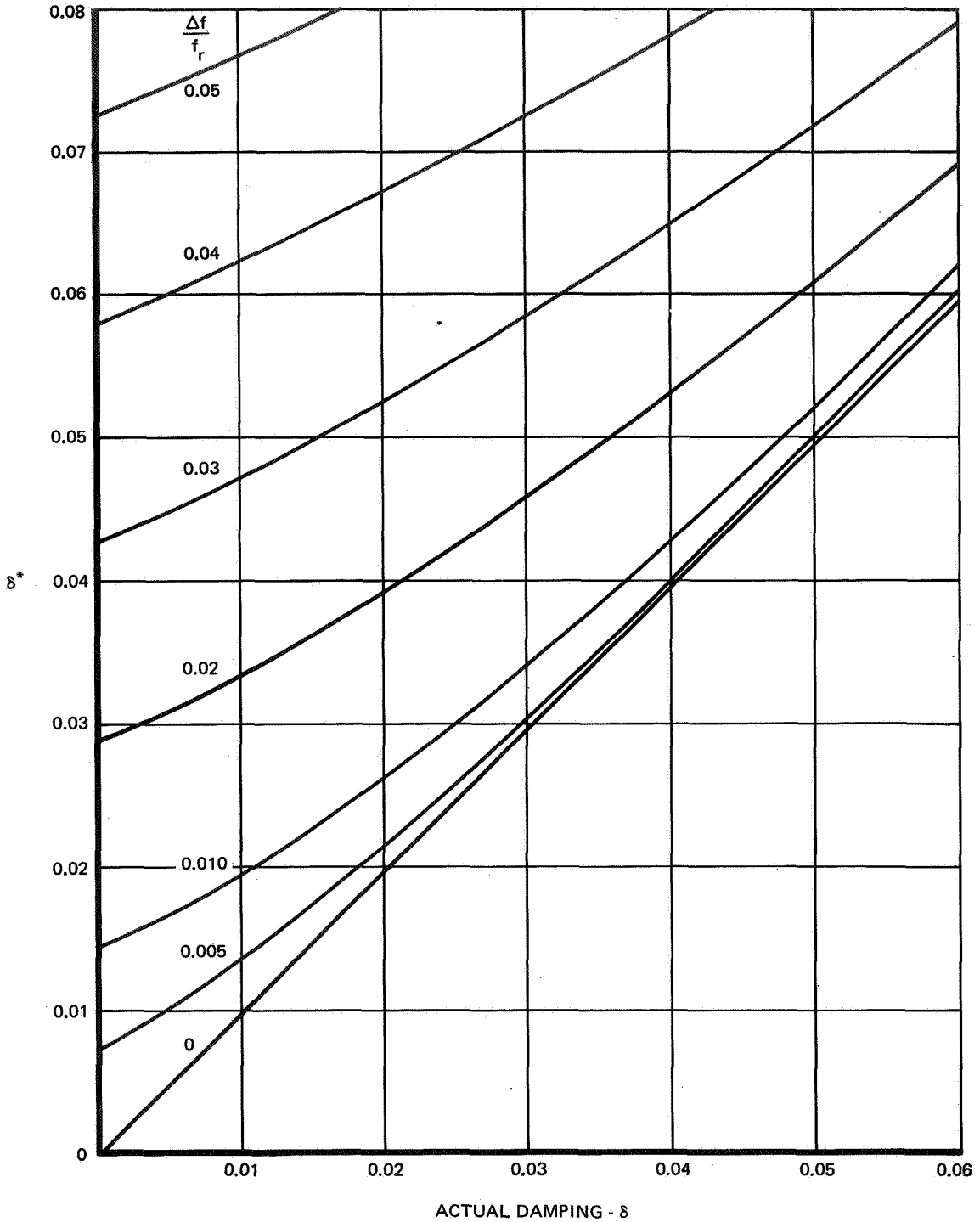

Figure 9. Method for Obtaining Damping from Truncation Affected Cross Spectra of a Single-Degree-of-Freedom System - Hanning Weighting.

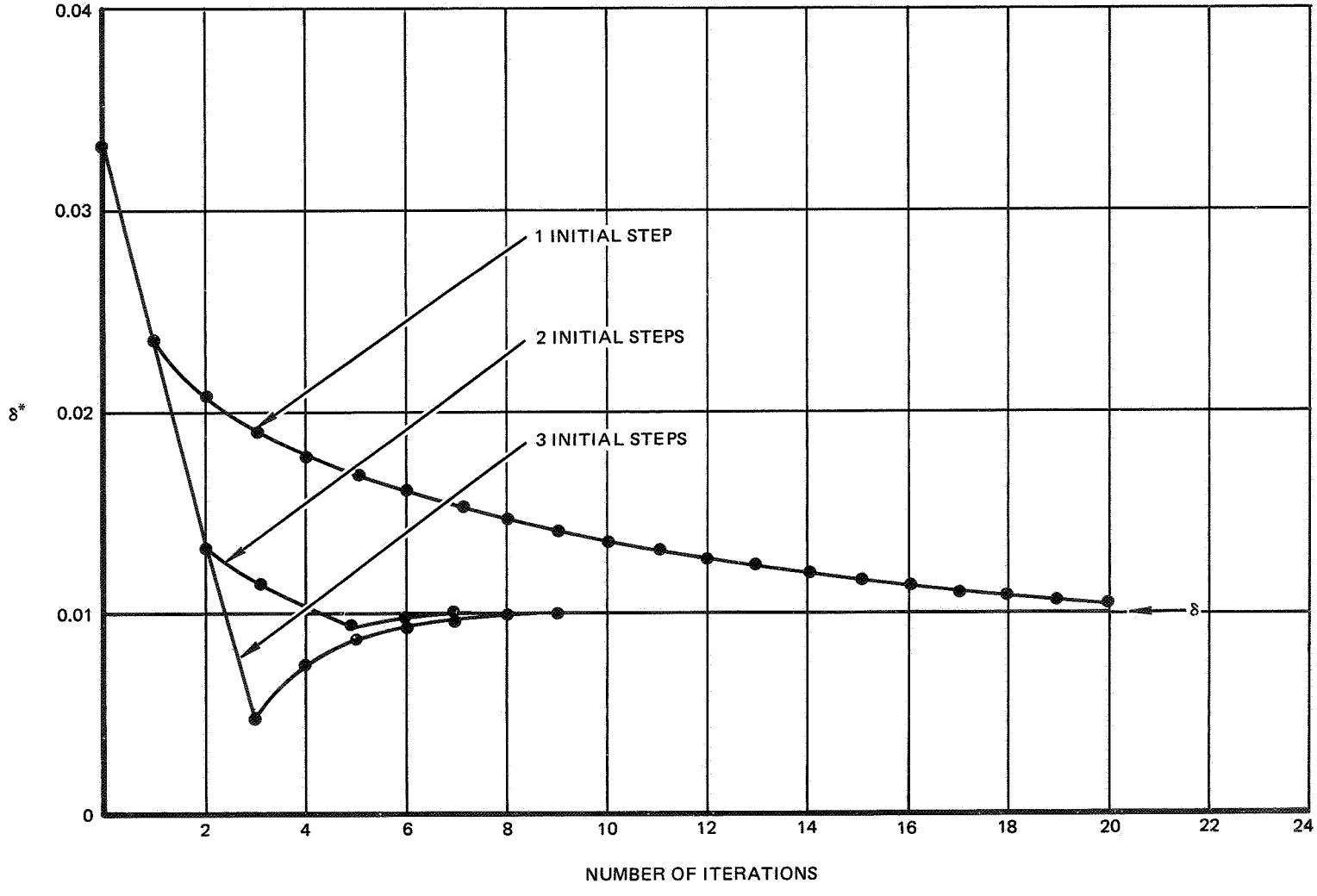

Figure 10. Typical Iteration Patterns - Hanning Truncation.

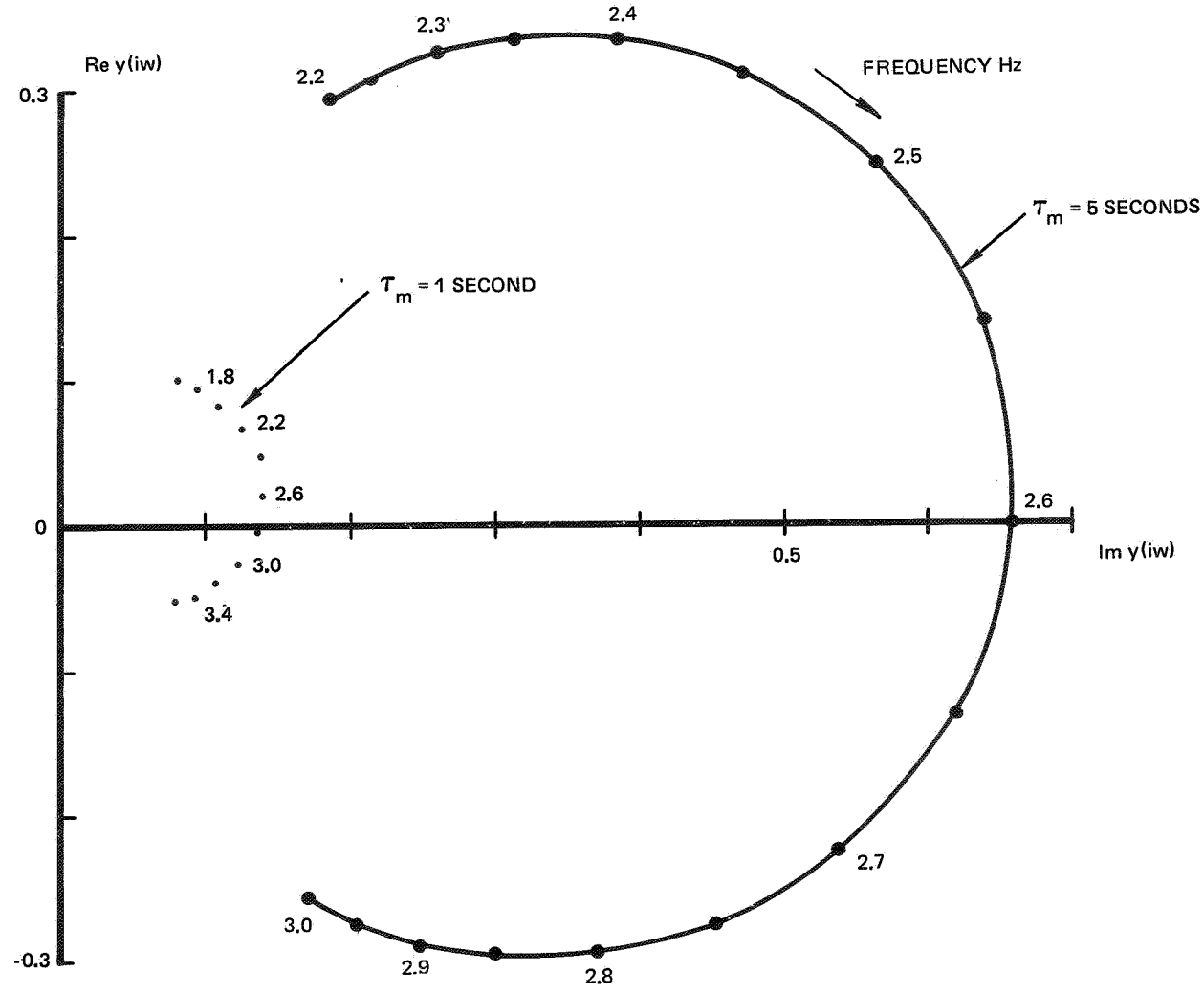

Figure 11. Restored Fourier Transform of Stick Pulse Excited Single Mode Decay Using Exponential Weighting Function.

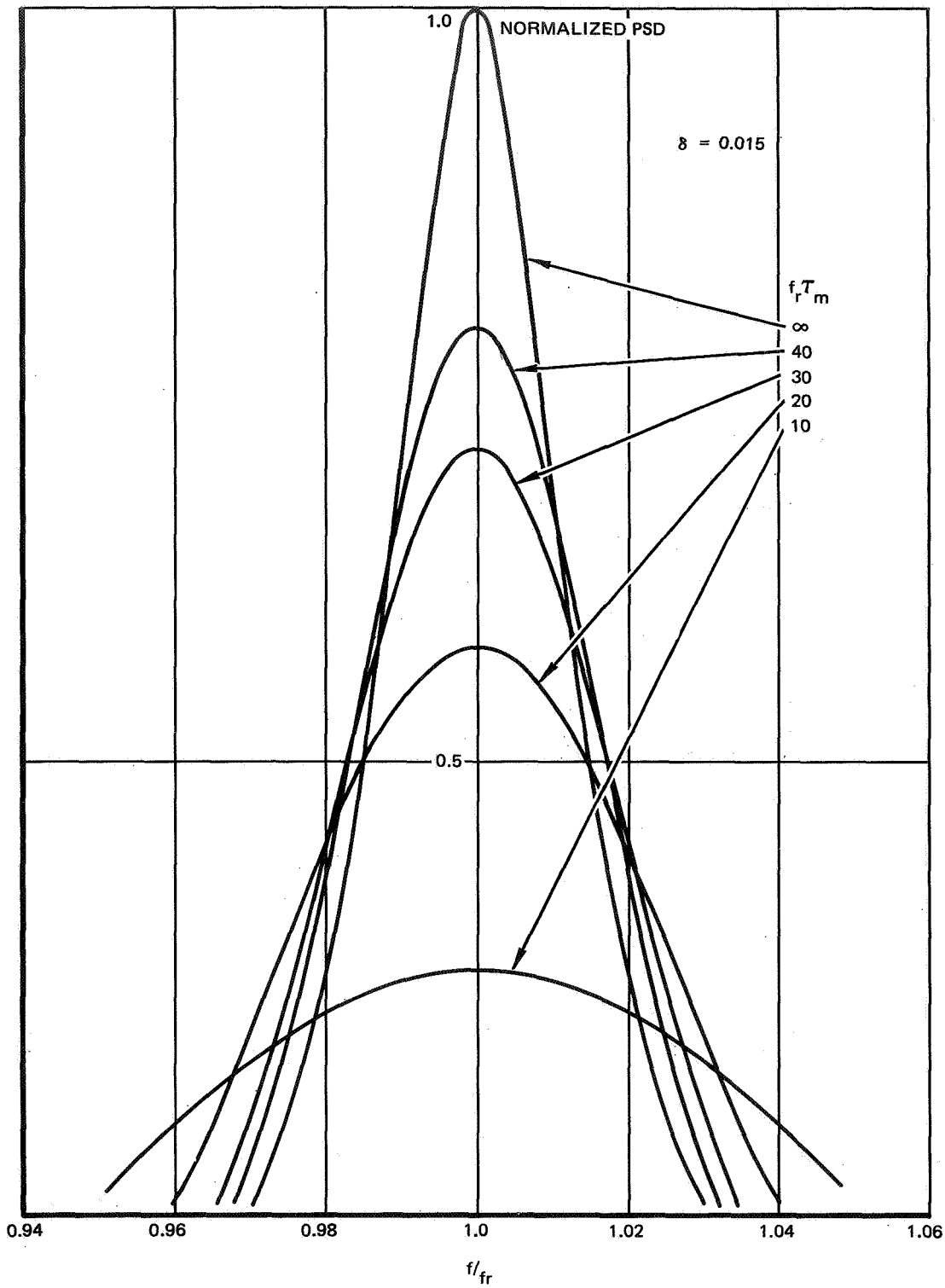

Figure 12. The Effect of Truncation on the Normalized PSD of a Single-Degree-of-Freedom System Excited by White Noise - Hanning Weighting Function.

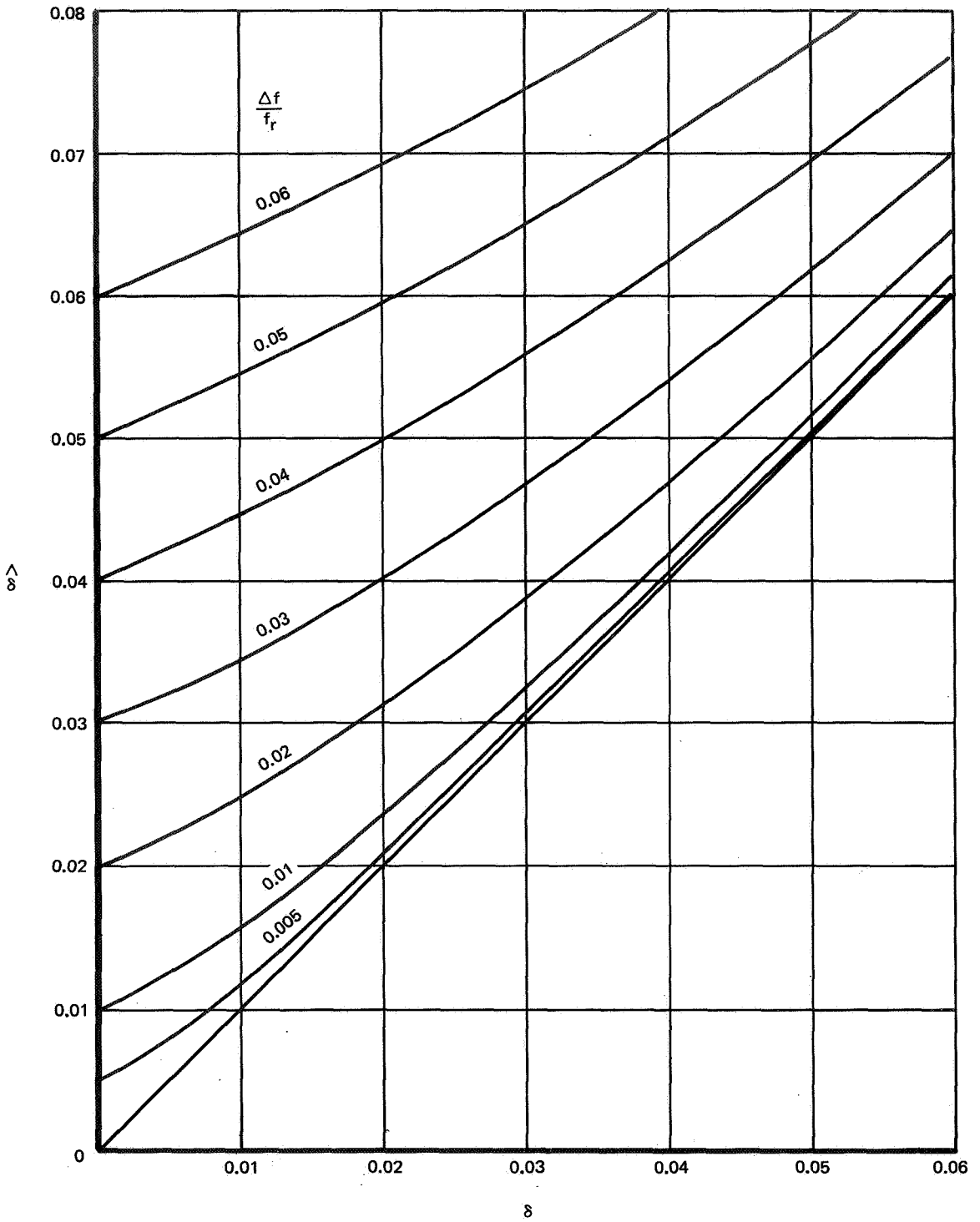

Figure 13. Correction to 3 dB Point Measured Damping from Single-Degree-of-Freedom System Response PSD - Hanning Weighting.

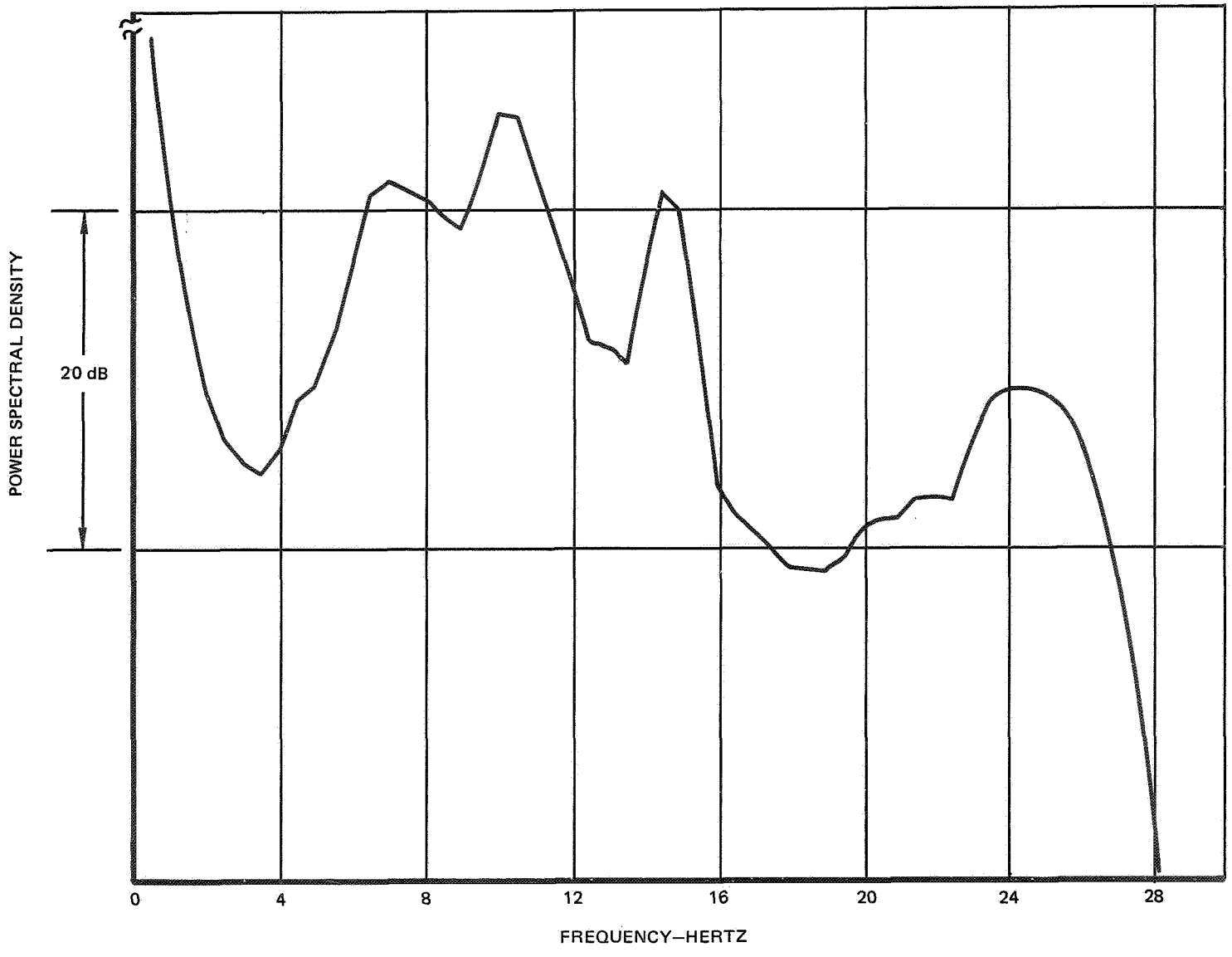

Figure 14. Typical Response Spectrum for Aircraft Excited by High-Speed Buffet.

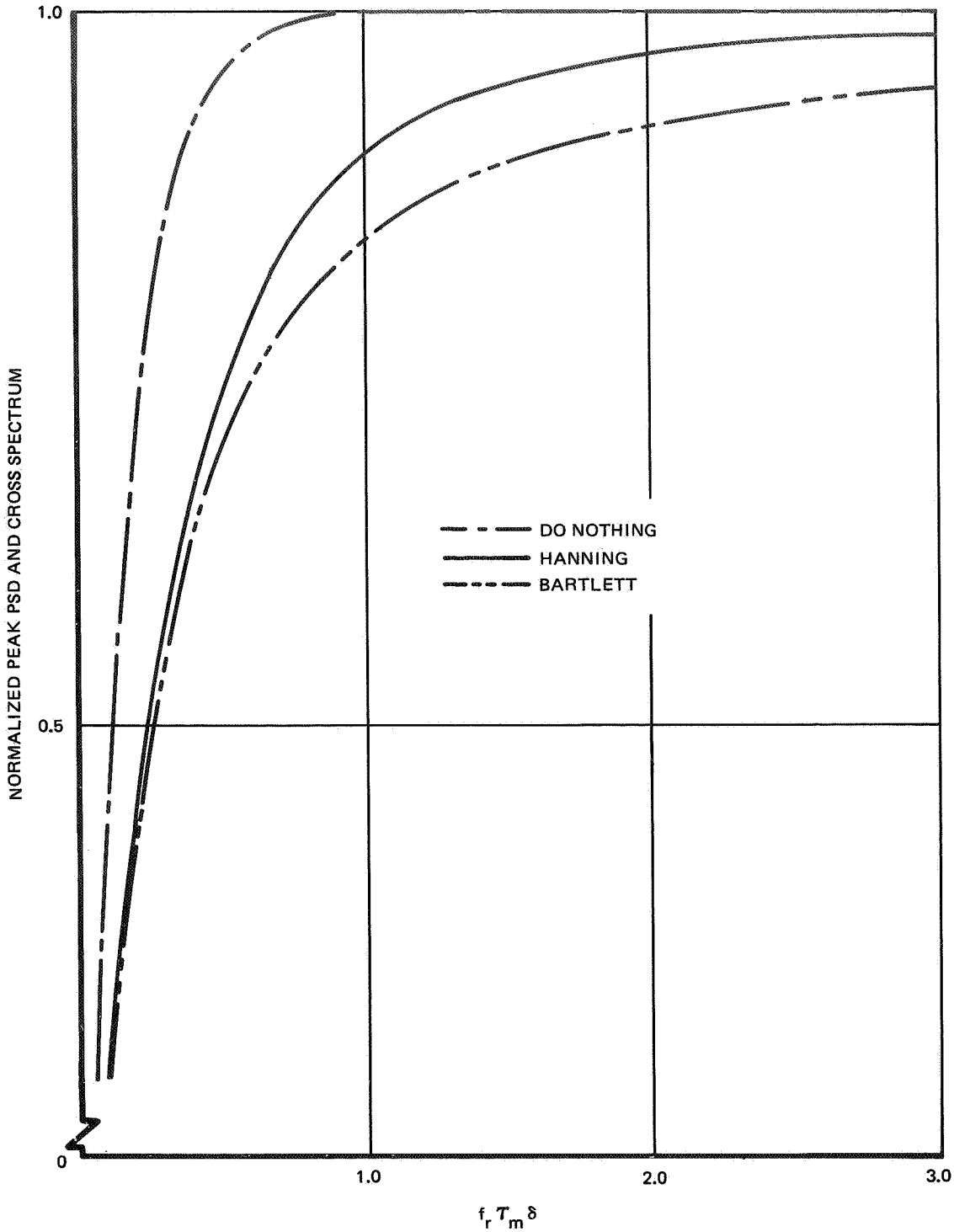

Figure 15. Effect of Truncation on the Peak PSD and Cross Spectral Response Resolution of a Single-Degree-of-Freedom System Excited by White Noise.

SPECIFICATION OF INPUTS AND INSTRUMENTATION FOR FLUTTER TESTING OF MULTIVARIABLE SYSTEMS

Narendra K. Gupta and W. Earl Hall, Jr.
Systems Control, Inc.

SUMMARY

This paper deals with the application of system identification methods in flutter testing of aeroelastic structures. The accuracy with which flutter parameters are estimated depends upon the test plan and on the algorithms used to reduce the data. The techniques for selecting the kinds and optimal positions of inputs and instrumentation, under typical test constraints, are presented. Identification results for both the input/output transfer function and the values of physical parameters are presented. Numerical results on the optimal input spectrum and the accelerometer location for estimating flutter parameters of a two dimensional wing are obtained using these algorithms. Current work on applying system identification methods to high order three dimensional aeroelastic structures is discussed.

INTRODUCTION

The objective of flutter analysis is to quantify the critical points or boundaries of flutter and the stability margins associated with subcritical responses. While it is true that analytical predictive techniques have become increasingly useful to this objective, actual testing and data analysis is always required for verification of these analyses, or to provide results where analytical assumptions are suspect. Thus, flutter test analysis techniques are being developed which use experimental data (usually noisy) to provide accurate estimates of both subcritical stability margins as well as aid extrapolation to the critical points (refs. 1 and 2). To be most useful, these techniques should provide real time (or near real time) estimates to keep test times at a minimum.

Further requirements on these test analysis techniques are emerging due to new aircraft concepts. New structural concepts, such as light weight composites technology, and control concepts, such as the active control of maneuver loads and flutter margins, will require multivariable testing analysis methods. These multivariable analysis techniques are necessary to define the modal frequencies and damping of many interactive structural components in complex aerodynamic regimes.

To meet the challenging requirements of estimating accurate subcritical flutter test parameters and to use these results to effectively predict flutter boundaries for multivariable systems, a systematic approach must be adopted. This approach should integrate the specification of test instrumentation and inputs with multiinput/multioutput data analysis procedures.

The key elements of such an aeroelastic integrated testing analysis of a model or of a prototype vehicle are shown in figure 1. First, the test objective must be quantified. Historically, this test objective has progressed from finding the flutter boundary to more current determination of the frequency and damping of the subcritical stability margin. The need to be able to better use subcritical data to predict the boundary requires determination of the parameters of a flutter model which may contain two or more states of the system. Of course, accuracy specifications for these various levels must be set. Second, the operating points (of a wind tunnel or flight regime) must be set to provide the basis for meeting the objectives within test safety constraints.

To implement the test objectives at the required points, an extensive analysis of test inputs and instrumentation will minimize the probability of ineffective results due to the improper excitation of critical modes and low signal/noise ratios. With the test configuration specified, the data are collected and analyzed using either a spectral analysis technique (e.g., fast Fourier transform (FFT, ref. 3) or Randomdec (ref. 4)) or an advanced parameter identification algorithm.

This paper focuses on the specification of test inputs and instrumentation. Specifically, the three major elements of the test configuration are:

(a) Choice and location of instruments (e.g., accelerometers, strain gages, gyros).
(b) Choice of inputs with respect to type (e.g., sinusoidal, swept sines, random), and location of inputs and frequencies, and energy of inputs.
(c) Required capability of test analysis procedures.

Analytical methods for input design and instrument selection to obtain the most accurate estimates of parameters in models describing the flutter behavior of aerodynamic structures are developed. The methods, based on system identification technology, minimize the expected covariance of errors in estimates of unknown parameters. The locations of the instruments and the inputs (if variable) may also be optimally selected.

This paper describes a simple model of an aeroelastic wing. The dynamics of the wing can be formulated as a state variable model. The analytical formulation of the input design problem for state variable models with unknown parameters is given, along with a description of the methods used for selecting the kind, accuracy, and locations of instruments. Some results on the selections of instruments and inputs to accurately identify the flutter characteristics of a two dimensional wing are described. Finally, the techniques are applied to large aerodynamic structures and the conclusions drawn from this work are discussed.

STATE SPACE EQUATIONS FOR A TWO DIMENSIONAL WING IN FLUTTER

Flutter is an interaction between nonsteady aerodynamic forces and elastic forces in a structural component. To study the experimental design techniques for flutter testing, a reference model for the flutter of a two dimensional wing is given based on the work of Houbolt (ref. 5). The symbols used follow those of reference 5.

An oscillating two dimensional airfoil in an incompressible flow can be modeled as shown in figure 2. Various forces acting on the airfoil are: (a) lift L_1 at quarter chord and lift L_2 at three-quarter chord, (b) restoring force and moment through the elastic axis located at (a), (c) force and moment associated with the inertia of the substance constituting the medium (these will be neglected), and (d) external forces and/or moments, used to excite flutter or inadvertently transmitted through the structure. The lifts L_1 and L_2 are modeled with appropriate delays. Houbolt (ref. 5) shows that the aeroelastic equations for the wing can be written in terms of nondimensional variables as follows (see also fig. 2):

$$\begin{bmatrix} \mu s^2 + \mu\bar{\omega}_y^2 & -\mu r s^2 - \frac{1}{2}s & -1 \\ -\mu r s^2 & \mu\frac{k_m^2}{c^2}s^2 + \frac{1}{2}r_2 s + \mu\frac{k_m^2}{c^2}\bar{\omega}_\phi^2 & -r_1 \\ 2a_2 s^2 + 2b_2 s & -2r_2 a_2 s^2 - (a_2 + 2b_2 r_2)s - b_2 & s + b_2 \end{bmatrix} \begin{bmatrix} w \\ \phi \\ u \end{bmatrix} = \begin{bmatrix} 1 \\ r_f \\ 0 \end{bmatrix} \bar{F} \qquad (1)$$

By defining

$$w_1 \triangleq \dot{w}$$

$$\phi_1 \triangleq \dot{\phi}$$

equation (1) becomes

$$\begin{bmatrix} \mu & -\mu r & 0 \\ -\mu r & \mu \frac{k_m^2}{c^2} & 0 \\ 2a_2 & -2r_2 a_2 & 1 \end{bmatrix} \begin{bmatrix} \dot{w}_1 \\ \dot{\phi}_1 \\ \dot{u} \end{bmatrix} = - \begin{bmatrix} \mu\bar{\omega}_y^2 & 0 \\ 0 & \mu \frac{k_m^2}{c^2} \bar{\omega}_\phi^2 \\ 0 & -b_2 \end{bmatrix} \begin{bmatrix} w \\ \phi \end{bmatrix}$$

$$- \begin{bmatrix} 0 & -\frac{1}{2} & -1 \\ 0 & \frac{1}{2} r_2 & -r_1 \\ 2b_2 & -(a_2+2b_2 r_2) & b_2 \end{bmatrix} \begin{bmatrix} w_1 \\ \phi_1 \\ u \end{bmatrix} + \begin{bmatrix} 1 \\ r_f \\ 0 \end{bmatrix} \bar{F}$$

or

$$A_1 \begin{bmatrix} \dot{w}_1 \\ \dot{\phi}_1 \\ \dot{u} \end{bmatrix} = A_2 \begin{bmatrix} w \\ \phi \end{bmatrix} + A_3 \begin{bmatrix} w_1 \\ \phi_1 \\ u \end{bmatrix} + A_4 \bar{F} \qquad (2)$$

Therefore

$$\frac{d}{dp} \begin{bmatrix} w_1 \\ \phi_1 \\ u \\ w \\ \phi \end{bmatrix} = \begin{bmatrix} A_1^{-1}A_2 & A_1^{-1}A_3 \\ I & 0 \end{bmatrix} \begin{bmatrix} w_1 \\ \phi_1 \\ u \\ w \\ \phi \end{bmatrix} + \begin{bmatrix} A_1^{-1}A_4 \\ 0 \end{bmatrix} \bar{F} \qquad (3)$$

where I is an identity matrix. This is the state space representation of an aeroelastic wing and can be written compactly as

$$\dot{x} = Fx + Gu \tag{4}$$

where x is the state vector, u is the input vector, and F and G are transition matrices which contain unknown parameters. An accelerometer placed at e_o will measure

$$\begin{aligned} y &= \ddot{w} + \frac{e_o}{c}\ddot{\phi} \\ &= \dot{w}_1 + \frac{e_o}{c}\dot{\phi}_1 \end{aligned} \tag{5}$$

The quantities $\dot{w}_1$ and $\dot{\phi}_1$ can be expressed in terms of x using equation (3). Then

$$y = Hx + Du \tag{6}$$

The transfer function between y and u is

$$\begin{aligned} \frac{y(s)}{u(s)} &= H(sI-F)^{-1}G + D \\ &= \frac{b_4 s^4 + b_3 s^3 + b_2 s^2 + b_1 s + b_o}{s^5 + a_4 s^4 + a_3 s^3 + a_2 s^2 + a_1 s + a_o} + D, \quad s = j\omega \end{aligned} \tag{7}$$

This transfer function can be written again into a state space form, often referred to as a canonical form.

OPTIMAL SELECTION AND LOCATION OF INPUTS AND INSTRUMENTS

As shown above, the flutter equations of a wing can be written in either the state variable form or the transfer function form. The multivariable state equations and measurement equations are equations (4) and (6). In practice, the measurements, y, are corrupted by additive noise, v, so that

$$y = Hx + Du + v \tag{8}$$

where v is assumed to be a white noise source with power spectral density matrix R. The unknown parameters and some control parameters (locations of inputs and instruments) are imbedded in the matrices F, G, and H. The unknown parameters, whose estimated we are interested in, will be denoted by θ.

The accuracy of the parameter estimate θ is expressed in terms of the bias and covariance properties of the estimate. It is assumed that an unbiased and efficient estimation procedure is used so that the input design and instrument selection can be carried out independently of the estimation procedure. This makes it possible to compute errors in the parameter estimates based on the Cramer-Rao lower bound. This bound is computed around an a priori value θ_o for the parameters θ. The information matrix M is related to the error in estimated by the following relation

$$\text{cov}(\theta - \hat{\theta}) \geq M^{-1} \tag{9}$$

where $\hat{\theta}$ is the estimate of θ.

The information matrix depends upon the input energy distribution and its location and instrument accuracies and their locations. The design procedures presented here will work with the properties of the information matrix. For physical reasons, a quadratic constraint is placed on the inputs and the state variables

$$\lim_{T\to\infty} \frac{1}{T} \int_o^T (x^T A x + u^T u) \, dt \leq E \tag{10}$$

where A is a symmetric positive semidefinite matrix. An equation for the information matrix, under the constraint of equation (10), in the frequency domain is now obtained.

Information Matrix in the Frequency Domain

The relation between y and u in frequency domain is

$$y(\omega) = \{H(j\omega I - F)^{-1} G + D\} \, u(\omega)$$

$$\triangleq T(\omega, \theta) \, u(\omega) \tag{11}$$

where $T(\omega,\theta)$ is the transfer function from the input, $u(\omega)$, to the measurement $y(\omega)$.

Equation (10) is written in the frequency domain as

$$\int_0^\infty \{u(\omega)\ u^*(\omega) + \mathrm{Tr}(Ax(\omega)\ x^*(\omega))\}\ d\omega \leq E \tag{12}$$

where Tr is the trace operator and '*' denotes conjugate transpose. If $S(\omega,\theta)$ is the transfer function between x and u, equation (12) may be written as

$$\int_0^\infty \{1 + \mathrm{Tr}(A\ S(\omega,\theta)\ S^*(\omega,\theta))\}\ u(\omega)\ u^*(\omega)\ d\omega \leq E$$

or

$$\int_0^\infty \lambda(\omega,\theta)\ u(\omega)\ u^*(\omega)\ d\omega = E \tag{13}$$

The inequality sign can be removed for linear systems because increasing the input amplitude will increase the accuracy of all parameters. The information matrix for parameters θ from measurements y, per unit time, is as follows (see refs. 6 and 7 for details):

$$M = \mathrm{Re}\int_0^\infty \frac{\partial T}{\partial \theta}^*\ R^{-1}\ \frac{\partial T}{\partial \theta}\ u(\omega)\ u^*(\omega)\ d\omega \tag{14}$$

Defining

$$\bar{u}(\omega) \triangleq \lambda^{\frac{1}{2}}(\omega,\theta)\ u(\omega) \tag{15}$$

Equations (13) and (14) become

$$\int_0^\infty \bar{u}(\omega)\ \bar{u}^*(\omega)\ d\omega = E$$

$$M = \mathrm{Re} \int_0^\infty \frac{\partial T}{\partial \theta}^*\ R^{-1}\ \frac{\partial T}{\partial \theta}\ \frac{1}{\lambda(\omega,\theta)}\ \bar{u}(\omega)\ \bar{u}^*(\omega)\ d\omega \qquad (16)$$

The information matrix, M, serves as the basic quantity upon which the input and instrumentation requirements are to be determined. Maximizing M by appropriate input and instrumentation design parameters leads to output data which have a high information content on the system parameters. That is, the sensitivity of the outputs to parameters, for example, is maximized by exciting the modes which are most affected by the parameters. Basing the design on M, though mathematically simpler, has some disadvantages in practice. If the trace of M (e.g., the sum of diagonal elements) is maximized, an almost singular information matrix may result. The inverse of M is the lower bound on the parameter covariance matrix. If M is nearly singular, its inverse may contain large diagonal elements, leading to large errors in the estimates.

For this reason, it is more desirable to work directly with the inverse of the information matrix, M^{-1}. This matrix can be viewed as the ellipsoid of uncertainty of the parameters. Though mathematically more difficult to minimize, this matrix gives useful results since we are minimizing the parameter covariances directly. Two types of methods can be used to minimize M^{-1}. These are based on the following functions of M^{-1}:

(1) Minimize Det (M^{-1}): This method will minimize the volume of the uncertainty ellipsoid. This also minimizes maximum error in the estimate of the transfer function.

(2) Minimize Tr (WM^{-1}): This method minimizes a weighted sum of the parameter estimate covariances (W is the weighting matrix which penalizes certain estimate errors more heavily than others). The weighting matrix serves two purposes. Since the covariances of different parameters have different units, the weighting matrix converts each term in the sum to the same units. Secondly, the weighting matrix offers tremendous flexibility because it is possible to assign varying importance to parameters through weights on their nondimensional covariance. This is considered to be one of the most suitable performance criteria, since it works with parameter estimate covariances directly.

Choice and Location of Optimal Input

The optimal input possesses certain properties which are quite important. They are presented here without proof (ref. 6):

(1) The optimal input has a discrete spectrum (or point spectrum). The number of frequencies with nonzero power does not exceed $\frac{m(m+1)}{2}$ where m is the number of parameters.

(2) If the spectrum of u contains fewer than m/(2p) frequencies, the information matrix is singular (i.e., all the parameters cannot be identified).

(3) The optimal input which minimizes $\mathrm{Det}(M^{-1})$ satisfies a minimum output error criterion. In other words, this input gives the best estimate of the transfer function.

(4) They satisfy two important theorems (see refs. 6 to 8), which convert this complex nonlinear problem into a computation technique.

It has been demonstrated that the computation procedure summarized in appendix A can be applied to select the input spectrum which gives the desired minimum of M^{-1}.

Practical considerations in the computation of optimal input.- The algorithm of appendix A will produce an optimal input design with a sufficient number of iterations. However, at each iteration, the procedure adds one point to the spectrum of the input. For practical implementation, it is desirable to have as few frequencies in the optimal input as possible. During the computation, a few steps can be taken to reduce the number of points in the spectrum. Suppose the normalized input at any stage has k frequencies ω_i with power α_i (i=1,2,...,k). Then:

(a) Frequencies less than $\Delta\omega$ apart can be lumped into one frequency. Suppose q frequencies ω_i^* are within a band $\Delta\omega$ wide. Then they can be replaced by one frequency ω^* with power α^* where

$$\alpha^* = \sum_{i=1}^{q} \alpha_i^*$$

and

$$\omega^* = \frac{1}{\alpha^*} \sum_{i=1}^{q} \alpha_i^* \omega_i^* \tag{17}$$

(b) From this new input, all frequencies ω_i with power less than a threshold α' are dropped. The remaining frequencies do not satisfy the constraint of equation (13), so the design is renormalized.

Steps (a) and (b) should be carried out to ensure that the design does not become degenerate. This "practicalization" requires judgment of $\Delta\omega$ and α.

Choice of location of input.- The transfer functions $T(\omega,\theta)$ (the input-to-output transfer function) and $S(\omega,\theta)$ (the input-to-state transfer function) are both linear functions of the control distribution matrix G. The location of the input affects G in a linear fashion. Therefore, if β is an input location parameter, the transfer functions $T(\omega,\theta)$ and $S(\omega,\theta)$ can be written as

$$\begin{aligned} T(\omega,\theta) &= T_1(\omega,\theta) + \beta T_2(\omega,\theta) \\ S(\omega,\theta) &= S_1(\omega,\theta) + \beta S_2(\omega,\theta) \quad , \quad 0 \leq \beta \leq 1 \end{aligned} \tag{18}$$

Equations (13) and (14) can, therefore, be written as

$$\int_0^\infty \{1 + \mathrm{Tr}(A(S_1(\omega,\theta) + \beta S_2(\omega,\theta))\ (S_1(\omega,\theta) + \beta S_2(\omega,\theta))^*)\}\ u(\omega)u^*(\omega)d\omega = E$$

i.e.,

$$\gamma(1 + C_1\beta + C_2\beta^2) = E \tag{19}$$

and

$$M = \gamma[M_{11} + 2\beta M_{12} + \beta^2 M_{22}] \tag{20}$$

γ is a scalar which adjusts the energy in the input to satisfy the quadratic constraint on the input and the states. Equations (19) and (20) can be combined into one equation,

$$M = \frac{E}{1 + C_1\beta + C_2\beta^2}\,[M_{11} + 2\beta M_{12} + \beta^2 M_{22}] \quad , \quad 0 \leq \beta \leq 1 \tag{21}$$

β can be selected to minimize $|M^{-1}|$ or $\mathrm{Tr}(WM^{-1})$. In fact, an algorithm similar to that of appendix A for input frequency and power selection can be developed.

In a more general case, when there is more than one input and each input may be placed over any point in two or more dimensions, the number of parameters β which must be selected optimally is more than one. The optimization becomes somewhat more difficult, but the basic approach remains the same.

Choice and Location of the Instruments

In addition to selecting the location and type of the excitation signal, there are two other design considerations in planning a flutter test. These are the determination of the kind of instruments which must be used to record flutter response and the choice of instrument location (if there is a choice). Though the problem of instrument selection and location can be treated simultaneously, for sake of simplicity we treat them separately.

Selection of instruments.- The selection of instruments is a tradeoff between dynamic range, accuracy, and cost. The dynamic loads are often limited by structural constraints, and it will be assumed that the instruments cover this range. The accuracy with which the parameters may be estimated is then determined by the accuracy of the instruments. It is clear from equation (14) that the information matrix has an inverse relationship with the measurement noise covariances.

$$M = \mathrm{Re} \int_0^\infty \frac{\partial T^*}{\partial \theta} R^{-1} \frac{\partial T}{\partial \theta} u(\omega)\ u^*(\omega)\ d\omega \tag{22}$$

For the purpose of instrument selection in general, the measurement noise covariance matrix is diagonal, i.e.,

$$R^{-1} = \mathrm{diag}[r_{11}, r_{22}, \ldots, r_{pp}] \tag{23}$$

where $1/r_{11}$ is the covariance of random noise in the ith instrument. The total cost of the p instruments is a sum of the cost of individual instruments

$$C = \sum_{i=1}^{p} C_i(r_{ii}) \tag{24}$$

The total cost of the instrument package is assumed to be fixed. Either of the criteria of equation (17) may be minimized under the cost constraint and

$$r_{ii} \geq 0 \qquad i=1,2,\ldots,p. \tag{25}$$

The Lagrange multiplier approach may be used for optimization. For example, if the criterion requires the minimization of $|M^{-1}|$, the modified cost function is

$$\bar{J} = |M^{-1}| + \sum_{i=1}^{p} (\lambda_i r_{ii} - \mu C_i(r_{ii})) + \mu C \tag{26}$$

where λ_i, $i=1,2,\ldots,p$, and μ are Lagrange multipliers. The following optimization equations result:

$$r_{ii} = 0 \quad , \quad \text{or} \quad \lambda_i = 0$$

$$|M|^2 \, \mathrm{Tr}\left\{M^{-1} \frac{\partial M}{\partial r_{ii}}\right\} + \lambda_i - \mu \frac{\partial C_i}{\partial r_{ii}} = 0 \quad , \quad i=1,2,\ldots,p \, . \tag{27}$$

Equations (24) and (27) are 2p+1 equations in 2p+1 unknowns λ_i, r_{ii} and μ. Note that if any r_{ii} is zero, the corresponding instrument has infinite error; in other words, this instrument should not be used.

The optimal value of r_{ii} would act as a guideline in selecting the instrument. Often, it is not possible to obtain an instrument with mean square error of $\frac{1}{r_{ii}}$ exactly and cost $C_i(r_{ii})$.

Location of instruments.- The transfer function $T(\omega,\theta)$ is a linear function of the measurement distribution matrix H, and, therefore, the position of the instrument. For this reason, optimal choice of instrument location can be determined in the same was as the optimal positioning of inputs.

RESULTS

To demonstrate the application of the methods described above to multivariable flutter problems, a two dimensional wing is considered. The values of the parameters are as follows: $\mu = 10$, $(k_m^2/c^2) = \alpha = 0.1$, $a/c = 0.35$, $r_1 = 0.1$, $r_2 = 0.4$, $a_2 = 0.6$, and $b_2 = 0.3$. The velocity is taken as 15.25c meters/sec (50c ft/sec) and the natural frequencies of the rotational and ver-

tical motions are 10 hertz and 2 hertz, respectively. This gives the system matrices for the nondimensional state equations as

$$F = \begin{bmatrix} 0 & 0.05 & 0.1 & -0.01579 & 0 \\ 0 & -0.2 & 0.1 & 0 & -0.3948 \\ -0.6 & 0.684 & -0.372 & 0.01895 & 0.1105 \\ 1 & 0 & 0 & 0 & 0 \\ 0 & 1 & 0 & 0 & 0 \end{bmatrix} \tag{27}$$

and

$$G^T = [0.1 \ , \ \frac{e_f}{c} \ , \ -0.12 \ -0.48 \frac{e_f}{c} \ , \ 0 \ , \ 0] \tag{28}$$

The measurement distribution matrices are

$$H = [0 \ , \ 0.5 - 0.2 \frac{e_o}{c} \ , \ 0.1 + 0.1 \frac{e_o}{c} \ , \ -0.01579 \ , \ -0.3948 \frac{e_o}{c}] \tag{29}$$

$$D = (0.1 + \frac{e_f}{e_c} \cdot \frac{e_o}{c})$$

where $\frac{e_f}{c}$ and $\frac{e_o}{c}$ are parameters which define the locations of the input actuator and the accelerometer. The noise in the accelerometer is assumed to be white, with a standard deviation of 0.02 in dimensionless units (this corresponds to about 0.61 meters/sec/sec (2 ft/sec/sec)) and a sampling interval of 4 milliseconds. It is assumed that we are interested in estimating the parameters $\bar{\omega}_y^2$, $\bar{\omega}_\phi^2$, r_2, a_2, b_2, α.

The poles and zeros of the transfer function between the measurement and the input $\frac{e_f}{c}$ and $\frac{e_o}{c}$ both equal to 0.1, are, in radians per second (the nondimensional values are multiplied by 100)

$$
\begin{array}{ll}
\text{Poles} & -5.76 \pm 55.6j \\
 & -19.4 \pm 16.6j \\
 & -6.83 \\
\text{Zeros} & -0.163 \pm 76.2j \\
 & -30.0 \\
 & -5.68
\end{array}
\tag{30}
$$

Input Design

As mentioned before, the inputs are designed to maximize the identifiability of flutter parameters from output. The test duration was selected as 2 seconds. This is a fairly short test, but in terms of the natural frequency of the wing in flutter, it is long enough so that the steady state input design can be applied. In the design procedure, the locations of the excitation and the accelerometer are kept fixed, and the input frequency spectrum and power in each frequency of the spectrum are selected.

To simplify the procedure, the parameters in the F, G, and H matrices are identified directly (D does not contain any unknown parameter). The input is designed to produce the most accurate estimates of the underlined parameters in equations (27) and (28) in the sense of minimizing the determinant of the inverse of the information matrix. Starting from the topmost spectrum of figure 3 with available power distributed equally among five frequencies at 2, 4, 6, 8, and 10 cycles per second, the iterative design procedure gives the results shown in the figure. In every iteration, the design procedure adds a new frequency or increases the power at a frequency already included in the spectrum. This leads to a large number of frequencies in the computed spectrum. As mentioned above, this design can be simplified. When frequencies with relative power less than 5 per cent or closer than 0.4 hertz are merged with the neighboring frequencies, the resulting design is shown in figure 4. There are eight frequencies in the optimal spectrum--three each clustered around the two oscillatory modes and one each at a low and an intermediate frequency. Of the three frequencies around the oscillatory modes, one is below, one is above, and one is close to the natural frequency. This characteristic seems to be quite general and substantiates Gerlach's intuitive choice of input frequencies for the identification of the short period parameters of an aircraft (ref. 9). A 2 second time trace for this input spectrum with initial phases selected at random is shown in figure 5.

Choice of Accelerometer Location

In the flutter analysis of a two dimensional wing, typically only one accelerometer is used. It is generally desired that the best accelerometer within the test budget be selected. There may be a possibility of using two poorer quality accelerometers. This tradeoff was not studied.

The location of this accelerometer is an important parameter. The following performance index is considered:

$$J = \sum_{i=1}^{m} \left(\frac{\sigma_{\theta_i}}{\theta_i} \right)^2 \tag{31}$$

where θ_i (i=1,2,...,m) is the set of parameters of interest and σ_{θ_i} is the standard deviation of estimation error in the ith parameter. Figure 6 shows the values of the performance index for constant input rms value and constant output rms value as a function of the accelerometer position. The minimum of the curves gives the positions of the optimal location of the accelerometer under the two constraints.

Simulation and Maximum Likelihood Identification

The flutter equations for the transition matrices of equations (27) to (29) are simulated with the input of figure 5. Both $\frac{e_o}{c}$ and $\frac{e_f}{c}$ are taken as 0.1, and the accelerometer rms random error is 0.02 in the nondimensional units. The transfer function between the input and the output is as follows:

$$-0.0155 \frac{(s^4 + 0.360s^3 + 0.599s^2 + 0.208s + 0.0099)}{(s^5 + 0.572s^4 + 0.457s^3 + 0.158s^2 + 0.0292s + 0.00139)} \tag{32}$$

Three identification runs were made:

(a) The underlined parameters in equations (27) and (28) are estimated. Note that H is a linear combination of the first two rows of F. The estimated and the measured time histories are shown in figure 7.

(b) The input/output relation is represented as a five pole, four zero transfer function. The coefficients of the transfer function are identified directly. This requires estimation of 10 parameters. The measured and estimated time histories of the accelerometer response are shown in figure 8. The match between the two time histories is comparable to that in figure 7. The identified transfer function is

$$-0.0137 \frac{(s^4 + 0.432s^3 + 0.593s^2 + 0.229s + 0.00844)}{(s^5 + 0.525s^4 + 0.451s^3 + 0.145s^2 + 0.0297s + 0.00116)} \tag{33}$$

Certain identifiability problems were indicated by the analysis of the information matrix. This, together with the fact that one zero is very close to a pole (eq. (30)), indicated that a lower order model may be more useful.

(c) The input/output relationship is represented by a four pole, three zero model. The coefficients of the fourth order transfer function are identified by using the maximum likelihood method. The time history plots are shown in figure 9, and the identified transfer function is as follows:

$$-0.0157 \frac{(s^3 + 0.250s^2 + 0.569s + 0.139)}{(s^4 + 0.467s^3 + 0.400s^2 + 0.119s + 0.0195)} \tag{34}$$

Though the fit to the time history responses is poorer than before, no identifiability problems are indicated, implying that the fourth order transfer function is an adequate representation for the accelerometer output/shaker input relationships. This is also indicated by the plots of the gains and the phases of the fifth order and fourth order identified transfer functions in figures 10 and 11.

The poles and zeros of the transfer function used in the simulation and the identified transfer functions in each of the three cases given above are shown in figures 12 and 13. The closeness of poles and zeros in every case indicates that the poles and zeros of the transfer function can be identified quite accurately and that often lower order models may give as good or better results. It should also be noted that the mode which is poorly damped is identified more accurately than the mode which has higher damping.

APPLICATION TO LARGE AEROELASTIC STRUCTURES

A major application of the input design and instrument selection procedures is the estimation of the flutter characteristics of large three dimensional structures. In general, the dynamic flutter behavior of such structures is described by partial differential equations in space and time. For the evaluation of dynamic stability and structural loads, however, a modal analysis or a finite element analysis is sufficiently accurate and converts the more complex partial differential equations into ordinary differential equations. The differential equations describing the flutter characteristics of large structures can be written as follows:

$$M\ddot{x} + C\dot{x} + Kx = Du \tag{35}$$

where M is the generalized mass matrix, C is the damping matrix, K is the spring constant matrix, and D is the input or force distribution matrix. In the vector x, each term corresponds to a linear or angular displacement of one of the modes. The vector u is a vector of deterministic or random inputs. There may be unknown parameters in M, C, K, and D. An accelerometer measures acceleration at one point, which, in general, is a linear combination of several components of $\ddot{x}$, i.e.,

$$y_a = H_a \ddot{x} \tag{36}$$

where H_a represents the parameters which determine the locations of the accelerometers. The strain gages measure displacements, so that their outputs are linear combinations of x, as follows:

$$y_s = H_s x \tag{37}$$

Again, H_s determines the locations of various strain gages. The locations of the inputs are determined by certain parameters in the matrix D. The transfer function between y_a and u is

$$y_a(s) = s^2 H_a \, (Ms^2 + Cs + K)^{-1} D \, u(s) \tag{38}$$

and the transfer function between y_s and u is

$$y_s(s) = H_s \, (Ms^2 + Cs + K)^{-1} D \, u(s) \tag{39}$$

This multivariable problem can be solved in much the same way as described and demonstrated above. It is currently being applied to a 19-mode model of tilt rotor vehicle for tunnel test.

CONCLUSIONS

This paper describes how techniques of system identification can be applied to the problem of determining accurate estimates of certain critical parameters in aeroelastic structures.

It was shown that information theoretic approaches can be used for the selection of input spectra and instruments. In particular, various functionals of the inverse of the information matrix provide useful measures of the accuracy of the parameter estimates. The parameter estimation accuracy depends upon both the input spectra and the points where the inputs are applied. The functionals of the inverse of the information matrix can be minimized under practical con-

straints of total cost, the cost versus the accuracy of various available instruments and certain location constraints, the set of instruments which must be used, and the positions at which they should be located can be optimized. In some cases, the instruments are already installed, but the maximum number of channels is fixed because of telemetry, recording, computer capacity, and many other reasons. A tradeoff can be made between various instruments and the possibility of having two or more instruments share one channel.

In the application of system identification methodology to aeroelastic structures, the importance of an efficient parameter identification program cannot be overestimated. A good method based on the maximum likelihood approach that utilizes an eigenvalue analysis of the information matrix provides not only efficient parameter estimates but also important diagnostics regarding the identifiability of various model parameters and the relevance of various models. An aeroelastic analysis of a two dimensional wing, for example, showed that a lower order transfer function may be adequate to represent the input/output relationships.

Maximum utilization of these techniques will, of course, be realized in large aerodynamic structures where identifiability could be a serious problem. Further work in the development of these techniques is under way.

APPENDIX A

ALGORITHM FOR CHOOSING OPTIMAL INPUT SPECTRUM

The following procedure may be used to determine the optimal input spectrum:

(a) Choose a nondegenerate input $f_o(\omega)$ (i.e., consisting of more than $\frac{m}{2p}$ frequencies, with a finite power in each frequency).

(b) Compute the function $\psi(\omega,f)$ where

$$\psi(\omega,f) = \mathrm{Re}[\mathrm{Tr}\ R^{-1} \frac{\partial T}{\partial \theta} M^{-1}(f) \frac{\partial T^*}{\partial \theta}] \quad \text{to minimize } |M^{-1}(f)| \tag{A1}$$

$$= \mathrm{Re}[\mathrm{Tr}\ R^{-1} \frac{\partial T}{\partial \theta} WM^{-2}(f) \frac{\partial T^*}{\partial \theta}] \quad \text{to minimize } \mathrm{Tr}(M^{-1}(f)W) \tag{A2}$$

Find its maximum at ω_o under the constraint of equation (13).

(c) Evaluate the information matrix $M(\omega_o)$ at ω_o.

(d) Update the design

$$f_1 = (1-\alpha_o)\ f_o + \alpha_o f(\omega_o) \qquad 0 < \alpha_o < 1 \tag{A3}$$

α_o is chosen to minimize $|M^{-1}(f)|$ or $\mathrm{Tr}(M^{-1}(f)W)$, where

$$M(f_1) = (1-\alpha_o)\ M(f_o) + \alpha_o M(\omega_o)\ , \quad 0 < \alpha_o < 1 \tag{A4}$$

It can be shown that such an α_o exists.

(e) Repeat steps (b) through (d) until desired accuracy is obtained.

In the procedure described above, the function ψ has many local maxima. It is computationally time consuming to find ω_o where $\psi(\omega,f)$ is maximum. In the computer implementation of the algorithm, we consider finite number of values ω_i and search through all values of $\psi(\omega_i)$ to find the maximum. Most stable systems of interest are low pass filters. Thus, in most cases it is possible to find a subset of $[o,\infty]$, where the search need be carried out.

There are several ways to see if the input design is close to optimal. These methods use the following criteria:

(a) The information matrix does not change substantially from one step to the next, or the optimizing function does not improve significantly with iterations.

(b) The value of α_i which optimizes the value of the desired function approaches zero. In other words, little power is placed at newly chosen frequencies.

(c) The maximum value of the function ψ_i is not much higher than the maximum value for the optimum design (i.e., m if we maximize $|M|$ and $Tr(M^{-1}(f^*)W)$ if we minimize $Tr(M^{-1}W)$.

In our implementation, (a) and (b) are used as the termination criteria and (c) is used as a check.

APPENDIX B: SYMBOLS
(All Units Are Metric)

a	Elastic axis position from leading edge
a_1	Gain coefficient of lift response to step change in angle of attack
a_2	$=1-a_2$
a_i (i=1,2...)	Coefficients of transfer function denominator
A	State weighting matrix
$A_1,...A_4$	Coefficient matrices defined by equation (2)
b_1	Time constant of lift response to step change in angle of attack
b_2	$=b_1 c/2V$
b_i (i-1,2...)	Coefficients of transfer function numerator
c	Wing chord
C	Cost function of all instruments; generalized damping
C_i	Cost coefficient of a single instrument
d	Derivative
D	Control distribution matrix to measurements; control matrix (equation (35))
e	Position of c.g., relative to elastic axis
e_f	Distance of force application from elastic axis (positive forward)
e_o	Distance of accelerometer from elastic axis (positive forward)
E	Energy constraint
$f(\omega)$	Nondegenerate input function
$f_o(\omega)$	Starting guess of $f(\omega)$ for design algorithm
$f_1(\omega)...$	Intermediate values of $f_i(\omega)$
F	System dynamics matrix; total section lift, input force
$\bar{F}$	$=F/2\pi qS$

G	Control distribution matrix
H	Measurement distribution matrix
H_a	Accelerometer measurement state distribution matrix
H_s	Strain gage measurement state distribution matrix
j	$=\sqrt{-1}$
J	Cost functional
k	Reduced frequency, $k=\omega c/2V$
k_y	Vertical spring rate
k_ϕ	Torsional spring rate
k_m	Mass radius of gyration
K	Generalized spring rate
L_1	Quarter chord lift
L_2	Three quarter chord lift
m	Mass; number of parameters in θ
m_1	Virtual mass
M	Information matrix; generalized mass
M_{ij} (ij=1,2...)	Elements of information matrix
p	Nondimensional distance = $2Vt/c$; number of measurement
q	Dynamic pressure = $1/2\rho V^2$; number of frequencies
r	Nondimensional elastic axis position, $r=e/c$
r_o	Nondimensional location of accelerometer, $r_o=e_o/c$
r_f	Nondimensional input force location, $r_f=e_f/c$
r_1	$=a/c - 1/4$
r_2	$=3/4 - a/c$
r_{ij} (i=1,2...)	Diagonal elements of measurement noise power spectral density matrix

R	Measurement noise power spectral density matrix
R_e	Real part
s	Laplace operator, $\mathcal{L}(d/dp)$
S	Wing area = cb
$S(\omega,\theta)$	State transfer function
$S_1(\omega,\theta)$	Specification parameter independent part of $S(\omega,\theta)$
$S_2(\omega,\theta)$	Specification parameter dependent part of $S(\omega,\theta)$
t	Time
T	Time interval (equation (10))
$T(\omega,\theta)$	Output transfer function
$T_1(\omega,\theta)$	Specification parameter independent part of $T(\omega,\theta)$
$T_2(\omega,\theta)$	Specification parameter dependent part of $T(\omega,\theta)$
u	Lift coefficient, $L_1/2\pi qS$; control variable
v	Measurement noise
V	Velocity
w	Nondimensional vertical displacement, y/c
$\dot{w}$	$\hat{y}/c$
W	Information matrix weighting matrix
x	State
y	Measurement vector (p x 1), vertical deflection
y_a	Accelerometer measurement
z	Deflection at accelerometer location
α^*	Power at frequency ω_i^*
α'	Cutoff power
α_o	Interpolation coefficient for update of the input design
β	Input locator parameter

γ	Scalar adjustment factor
θ	Parameter set
θ_i	Parameter of the set
$\hat{\theta}$	Parameter estimate
$\lambda(\omega,\theta)$	$=1+\mathrm{Tr}(AS(\omega,\theta)S^*(\omega,\theta))$
λ_i	Lagrange multiplier
μ	Mass parameter
μ_i	Lagrange multiplier
ρ	Air density
ϕ	Angular displacement
ϕ_1	Section pitch rate, $\dot{\phi}$
ϕ_i	Standard deviation of $\hat{\theta}_i$
$\psi(\omega,f)$	Optimization function
ω	Circular frequency
ω_o	Undamped frequency; starting frequency for design algorithm
ω_ϕ	Torsional natural frequency = $\sqrt{\frac{k_\phi}{mk_m^2}}$
$\bar{\omega}_y$	Vertical natural frequency = $\sqrt{\frac{k_\phi}{m}}$
$\bar{\omega}_y$	$=\omega_y c/2V$
ω_ϕ	$=\omega_\phi c/2V$
ω_i^*	Frequencies within $\Delta\omega$
ω_i	Power weighted average of frequencies ω_i^*

REFERENCES

1. Baird, E. F.; and Clark, W. B.: Recent Developments in Flight Flutter Testing in the United States. Supplement to the Manual on Aeroelasticity, Volume 4, Chapter 10. AGARD Rept. 596, 1972.

2. Rosenbaum, Robert: Survey of Aircraft Subcritical Flight Flutter Testing Methods. NASA CR-132479, Aug. 1974.

3. Waisanen, P. R.; and Perangelo, H. J.: Real Time Flight Flutter Testing Via Z-Transform Analysis Techniques. AIAA Paper 72-784, Aug. 1972.

4. Cole, Henry A., Jr.: On-Line Failure Detection and Damping Measurement of Aerospace Structures by Random Decrement Signatures. NASA CR-2205, Mar. 1973.

5. Houbolt, John C.: Subcritical Flutter Testing and System Identification. NASA CR-132480, Aug. 1974.

6. Gupta, Narendra K.; and Hall, W. Earl, Jr.: Input Design for Identification of Aircraft Stability and Control Derivatives. NASA CR-2493, Feb. 1975.

7. Mehra, Raman K.: Optimal Input Signals for Parameter Estimation in Dynamic Systems - Survey and New Results. IEEE Trans. on Automatic Control, vol. AC-19, Dec. 1974, pp. 753-768.

8. Mehra, Raman K.; and Gupta, Narendra K.: Status of Input Design for Aircraft Parameter Identification. Methods for Aircraft State and Parameter Identification. AGARD-CP-172, Nov. 1974.

9. Gerlach, O. H.: The Determination of Stability Derivatives and Performance Characteristics From Dynamic Manoeuvres. Presented at 38th Meeting of AGARD Flight Mechanics Panel, Toulouse, France, May 1971.

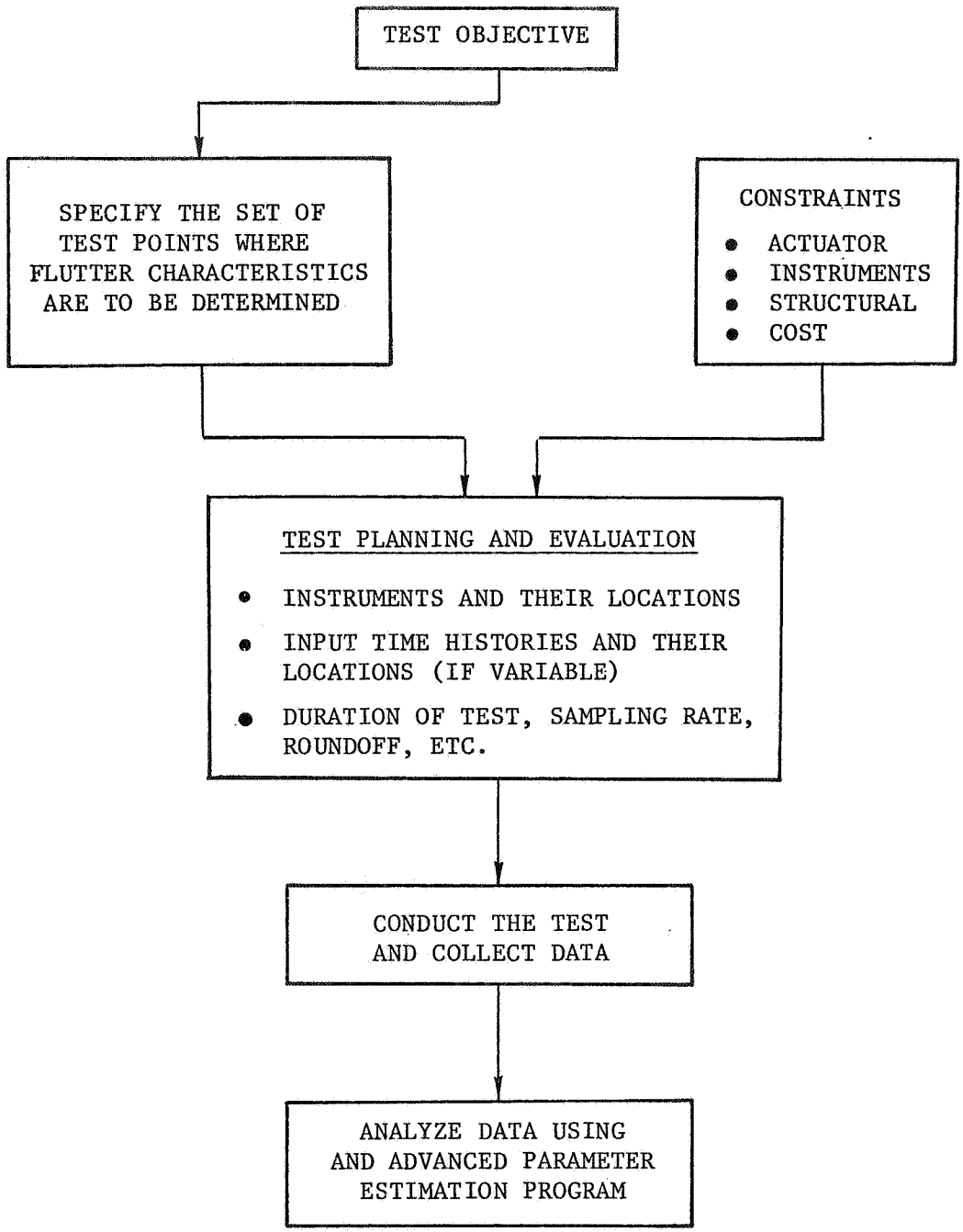

Figure 1. Various steps in aeroelastic testing.

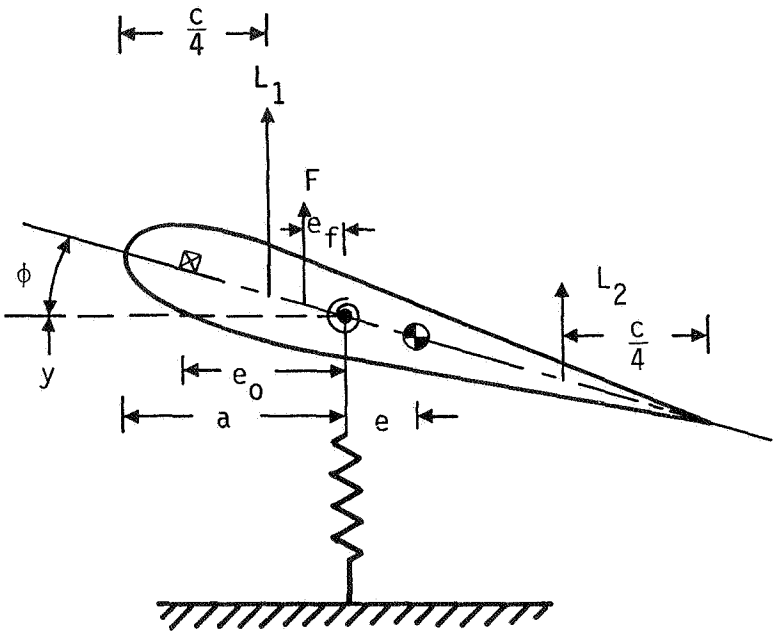

Figure 2. Model of a two dimensional wing in flutter.

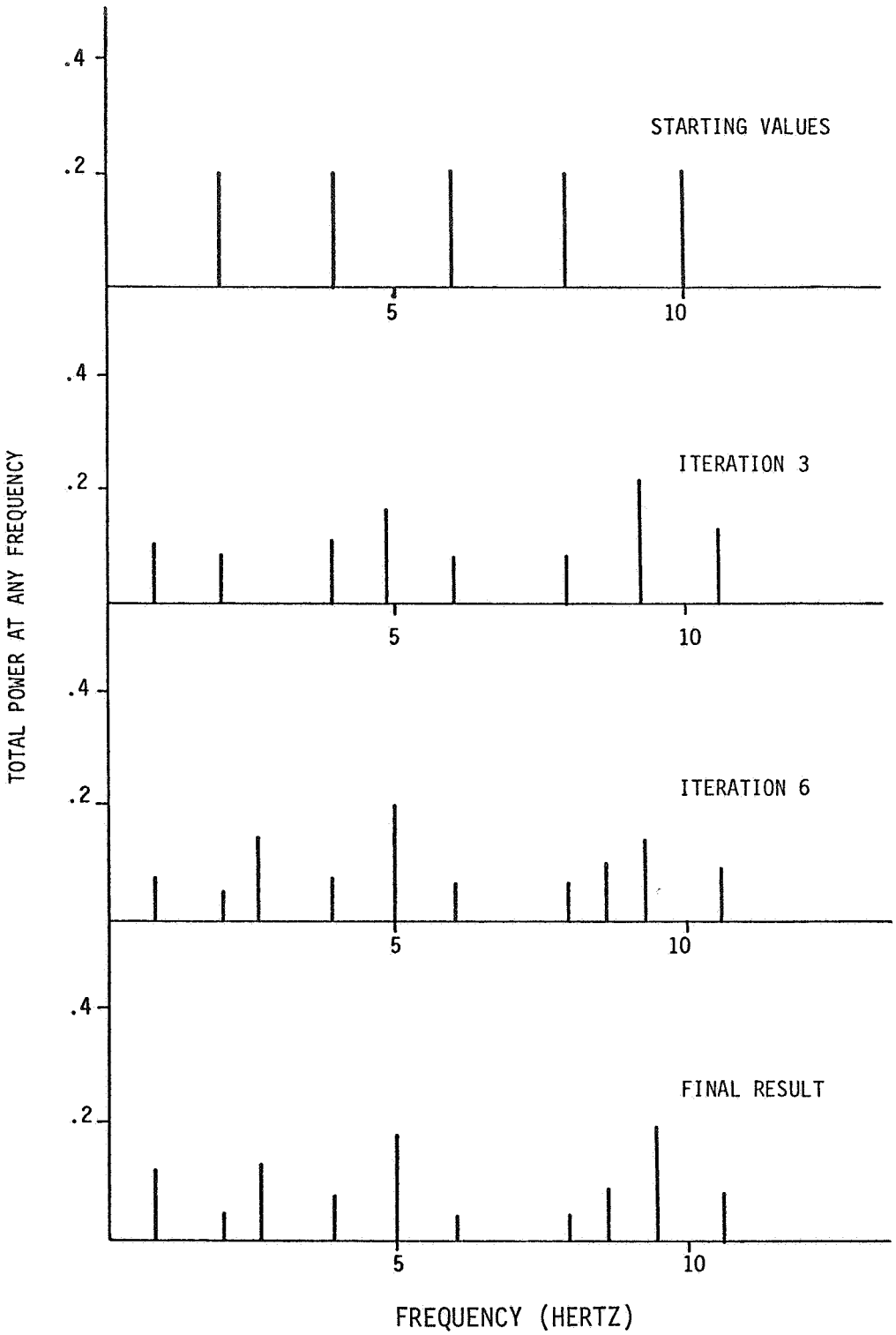

Figure 3. Optimal input design for the identification of flutter parameters.

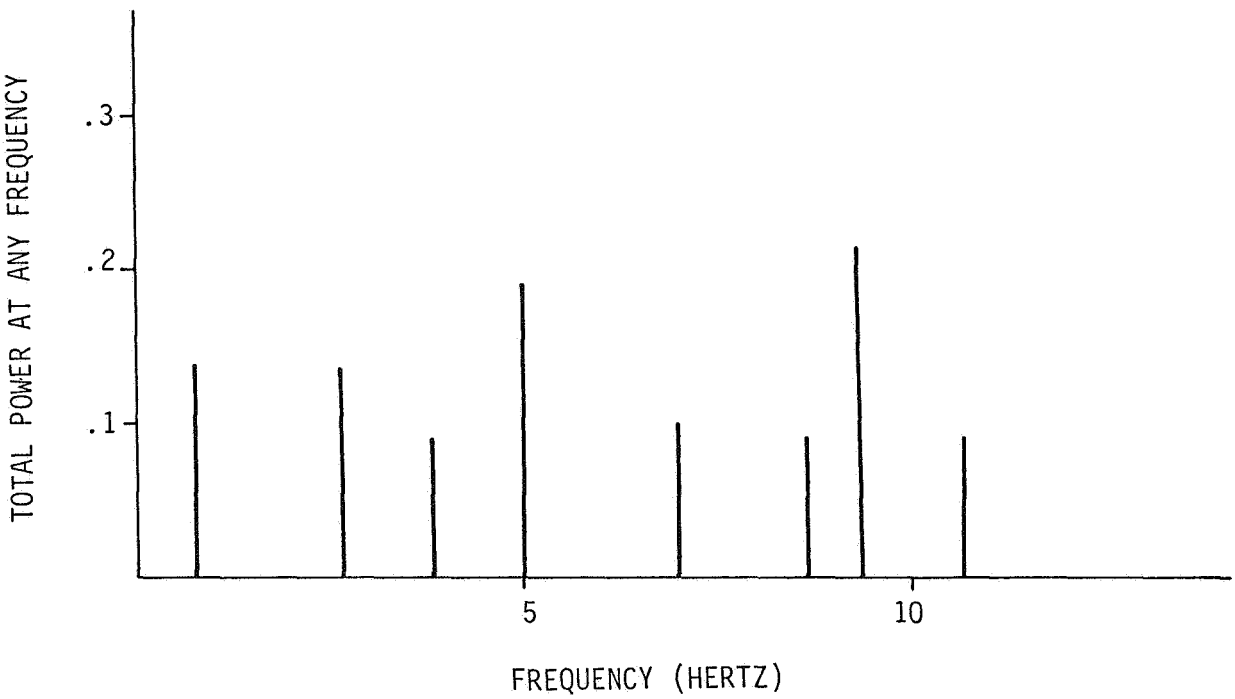

Figure 4. Simplified optimal input spectrum for identification of flutter parameters.

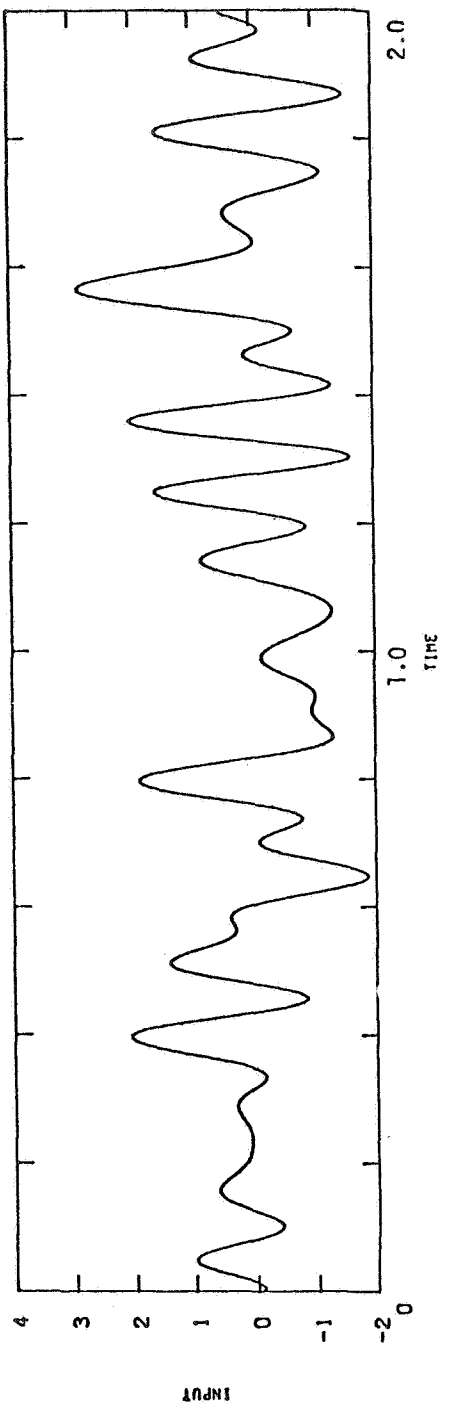

Figure 5. Time history trace of the optimal input.

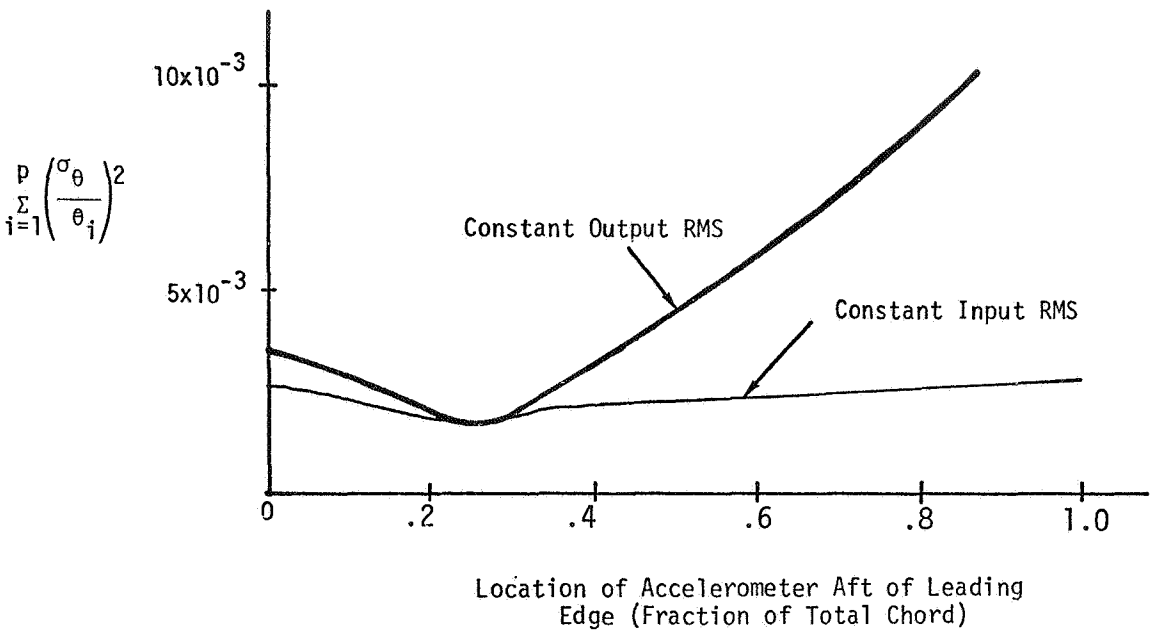

Figure 6. Parameter estimation error as a function of accelerometer position.

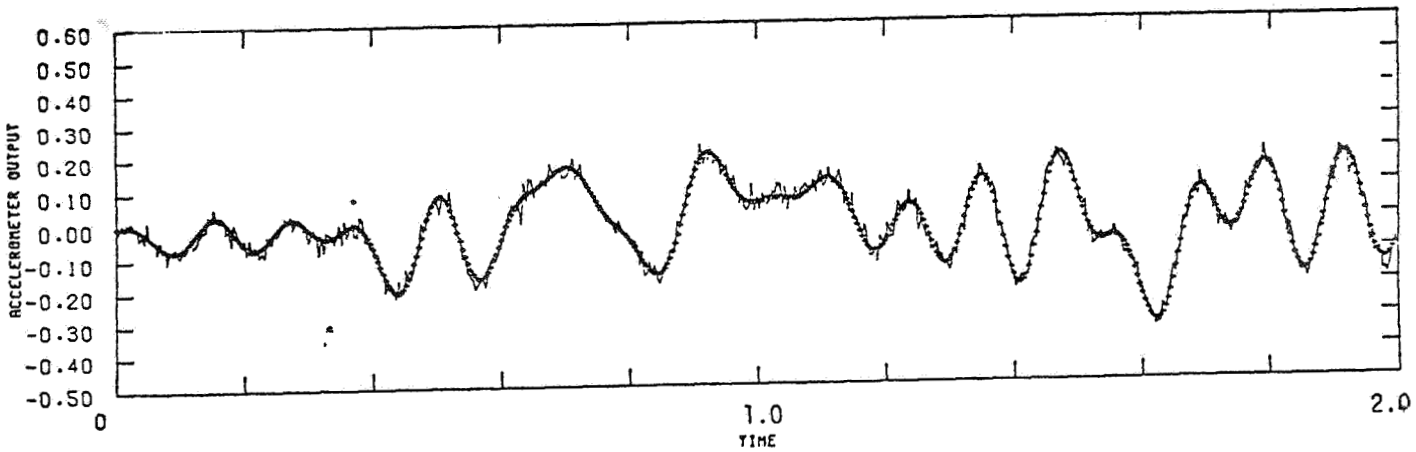

Figure 7. Simulated and estimated time history of the accelerometer output (physical parameters identified).

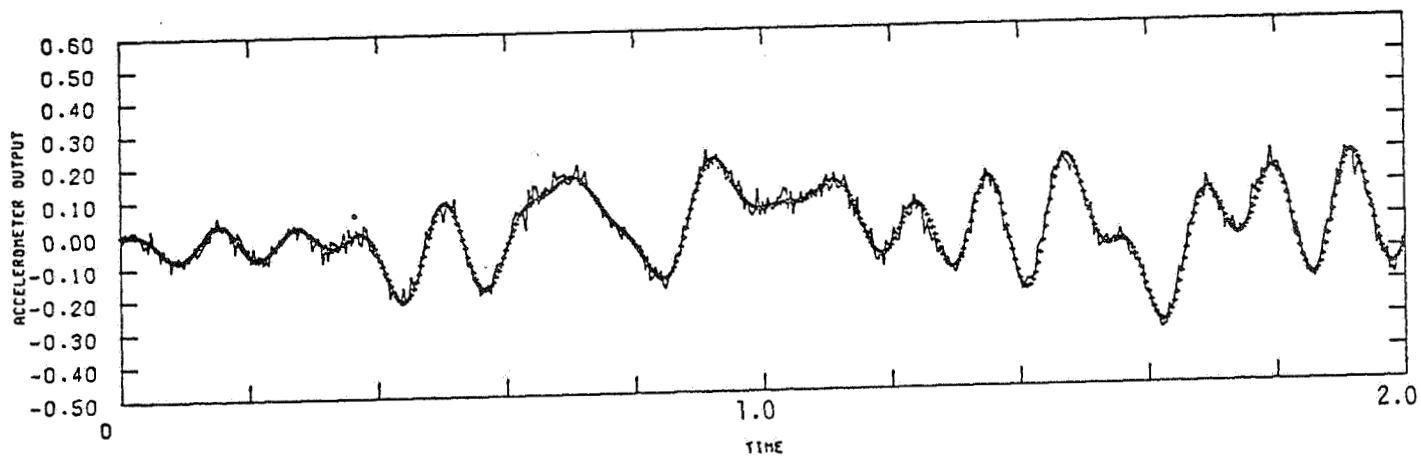

Figure 8. Simulated and estimated time history of the accelerometer output (fifth order transfer function model identified).

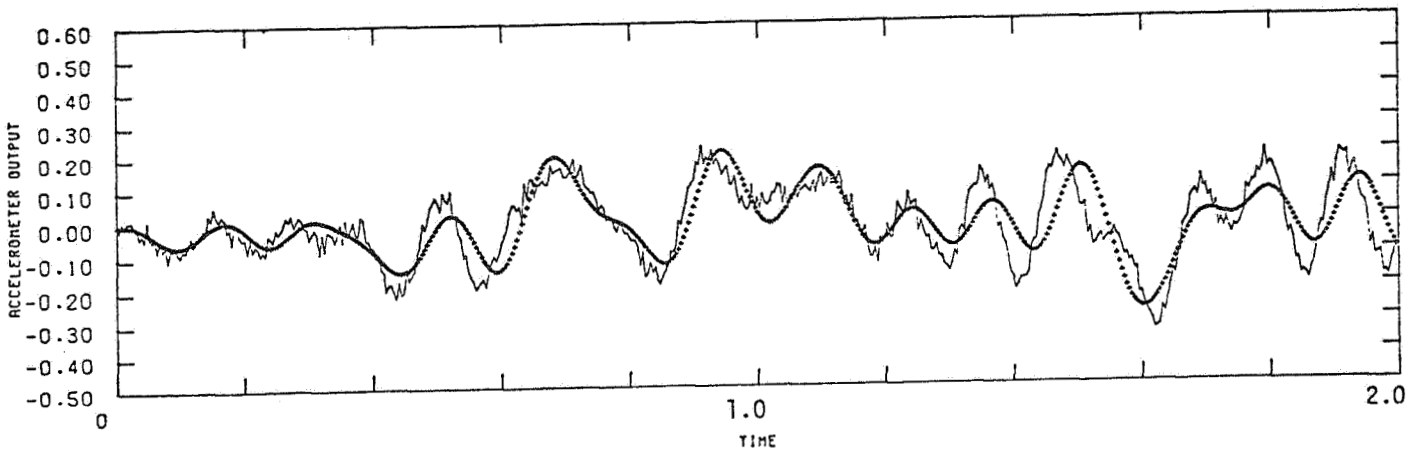

Figure 9. Simulated and estimated time history of the accelerometer output (fourth order transfer function model identified).

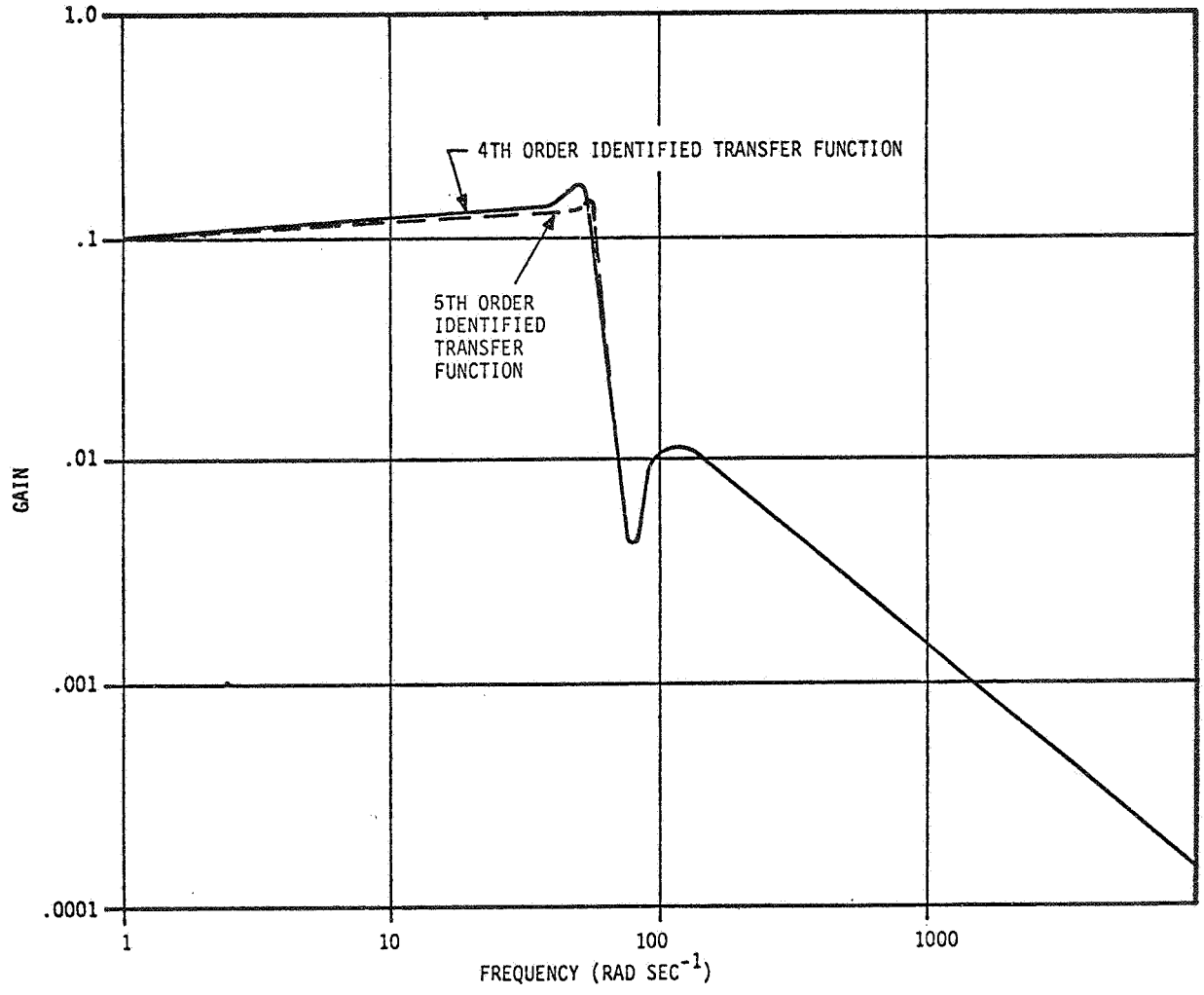

Figure 10. Gain comparisons of fifth order and fourth order identified transfer functions.

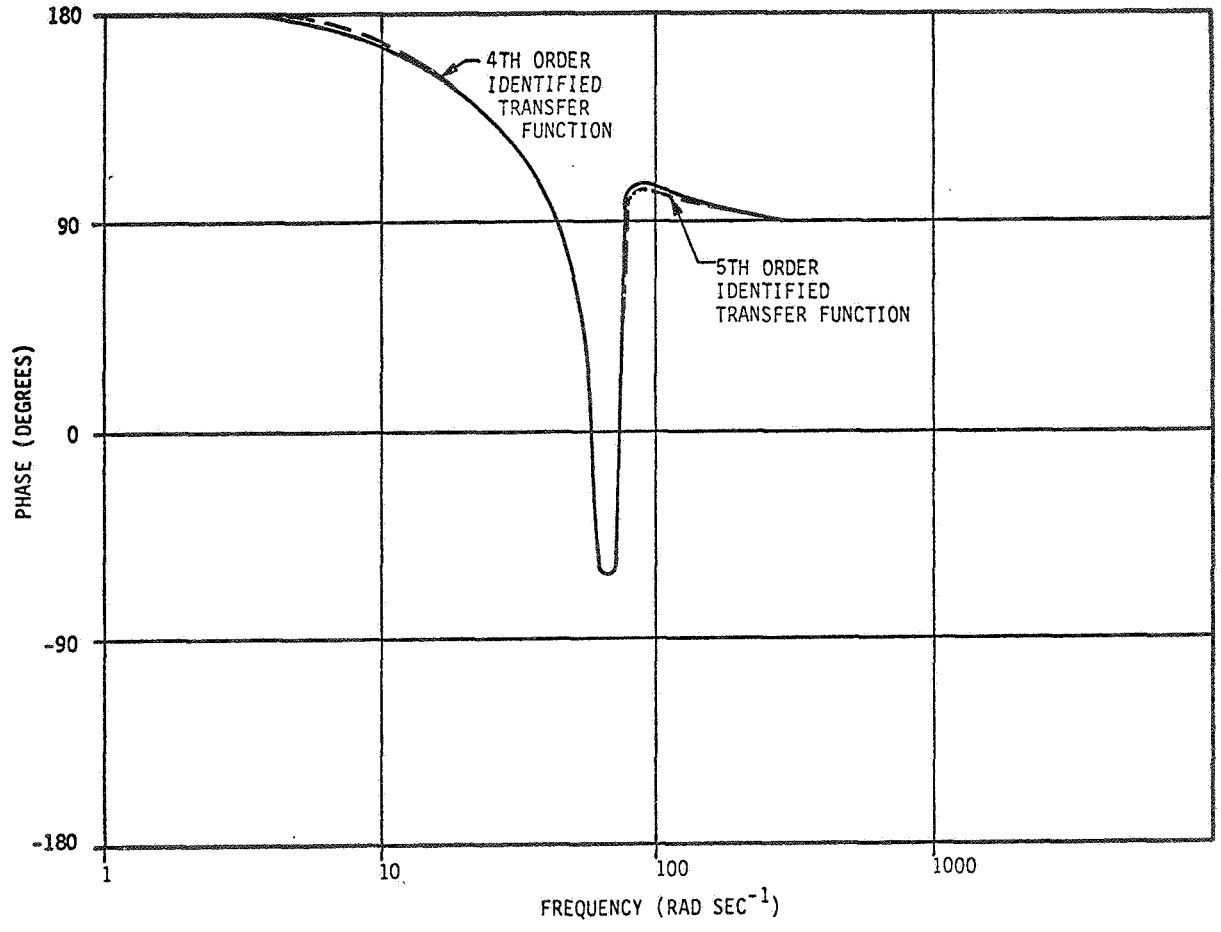

Figure 11. Phase comparisons of fifth order and fourth order identified transfer functions.

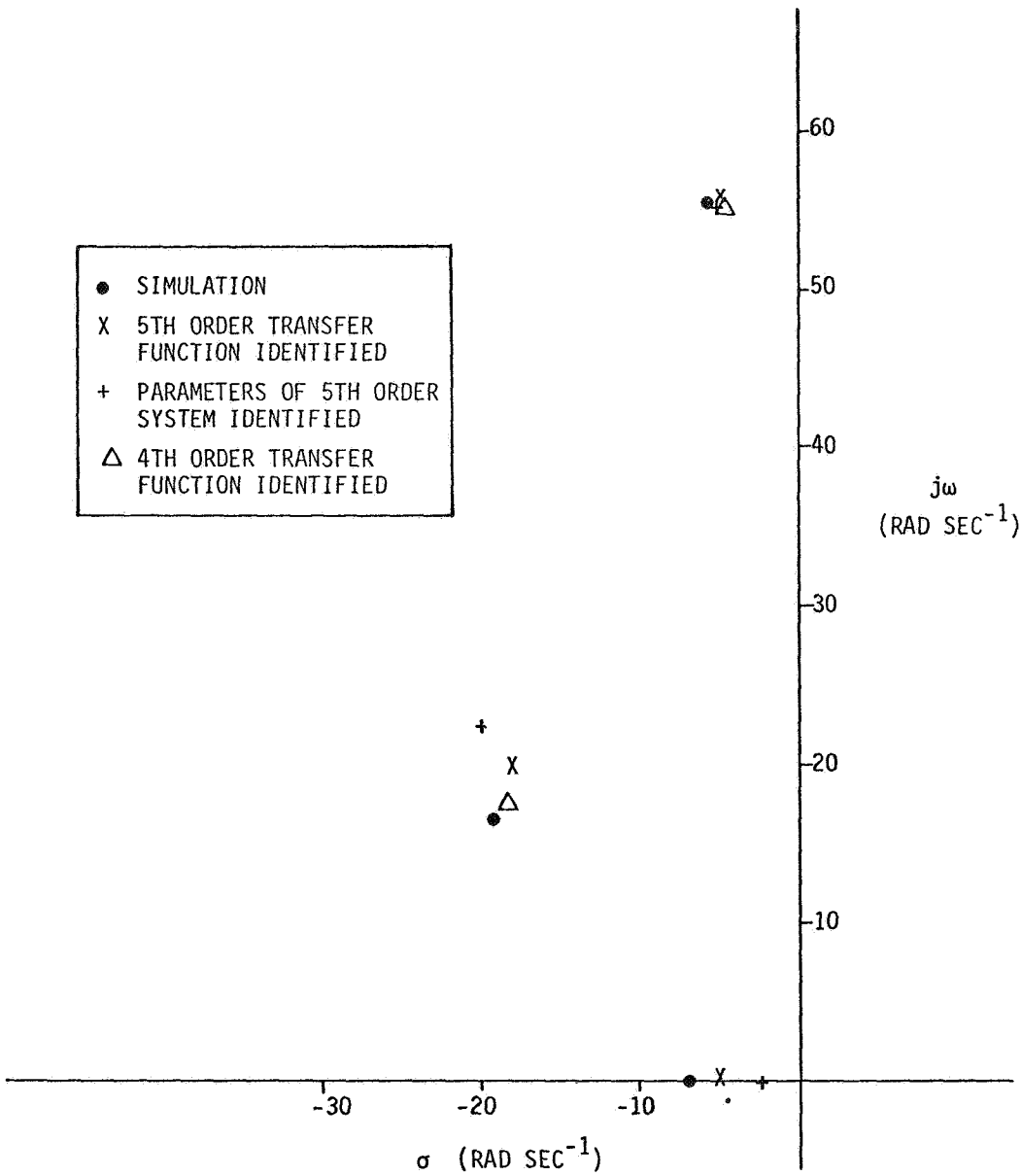

Figure 12. Poles of the simulation transfer function and identified transfer function.

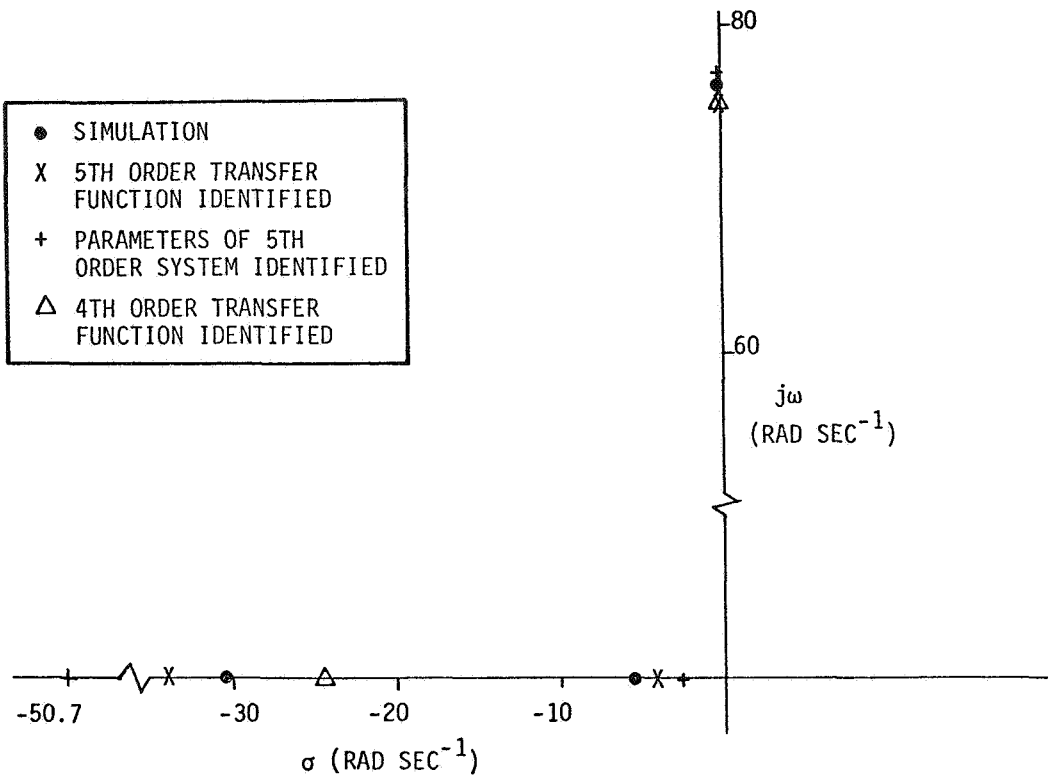

Figure 13. Zeros of simulation transfer function and identified transfer function.

SOME EXPERIENCE USING SUBCRITICAL RESPONSE METHODS IN WIND-TUNNEL FLUTTER MODEL STUDIES

Jerome T. Foughner, Jr.

NASA Langley Research Center

SUMMARY

Experiences obtained with four methods to predict flutter of wind-tunnel models from subcritical response data are described. The four methods are: co/quad, randomdec, power spectral density, and the peak-hold spectrum. Model excitation techniques included both forced (sinusoidal sweep) and random (tunnel turbulence). These methods were successfully used to measure the frequency and damping (or an inverse response amplitude proportional to the damping) in the predominant flutter modes. Implementation and application of each method are discussed. Some results and comparisons between methods are presented.

INTRODUCTION

Transonic flutter model testing has become an integral part of the development of high-speed aircraft such as the Grumman F-14, Rockwell B-1, Boeing 747, and Lockheed C-5A. Wind-tunnel studies to establish transonic flutter clearances and to provide data for correlation with analysis and with flight tests are made using dynamically scaled aeroelastic models. Some examples of correlation between flight and wind-tunnel model tests in the Langley transonic dynamics tunnel (TDT) are given in reference 1. These models simulate the complete aircraft under near free-flying conditions and are quite sophisticated and expensive. Since flutter can be an explosive-type, destructive instability, there is a substantial risk of damaging the model when flutter is encountered. Consequently, there is a need to develop methods to predict the flutter condition without having to actually experience flutter. The requirements are similar to those in flight flutter testing, namely, to identify the vibration modes critical to flutter and to measure and track the frequency and damping in these modes as the test conditions are varied, and the flutter boundary is approached.

The state of the art of subcritical flight flutter testing was surveyed in late 1972 (ref. 2). At the time of this survey, United States industry relied almost exclusively on sinusoidal excitation provided by auxiliary aerodynamic vanes, inertia shakers, or the power control system. Random excitation techniques had not been used for flight flutter testing. For a number of years the staff of the TDT has used various subcritical response methods in wind-tunnel flutter model studies. In some cases external excitation of the model has been used, similar to full-scale flight flutter testing. However, the methods of excitation of models are usually more restricted. For instance, the model

control system is normally provided for trim and is not capable of high-frequency inputs. Space and weight are also usually too limited to allow internal shaker equipment. Consequently, most of the model subcritical damping work at Langley has been associated with methods that use natural wind-tunnel turbulence as the excitation force.

The purpose of this paper is to describe some experiences in the application of four subcritical response methods to predict model flutter characteristics in the Langley TDT. The four methods examined are co/quad, which requires sinusoidal forced excitation, randomdec and power spectral density (PSD), which require only random excitation, and the peak-hold spectrum method, which is applied to both a forced and random excitation system. The implementation of each method is described, and results from the application of all four methods to a cantilever, delta-wing model in the TDT are presented. Since this model was designed and built for active flutter suppression studies and was equipped with fast acting oscillating controls, it provided a unique opportunity for determining subcritical response data where sinusoidal forced excitation is required for comparison with damping data obtained using random excitation produced by turbulence. Also, co/quad and randomdec results obtained by using a complete, cable-mounted B-52 model are discussed.

FOUR PREDICTION METHODS

The four methods used to measure the subcritical (below the actual flutter speed) response characteristics are referred to herein as co/quad, randomdec, PSD, and peak-hold spectrum methods. These methods were used to measure the frequency and damping (or an inverse response amplitude proportional to the damping in the peak-hold spectrum case) in the predominant or critical vibration modes. By suitably plotting and extrapolating the subcritical damping in the vibration mode or modes of interest, the flutter point can usually be established. With each method, it was assumed that the response can be approximated by that of a single-degree-of-freedom system. The response data consisted of an accelerometer on the model under either a forced excitation or the random excitation from the tunnel turbulence. All of these methods can be used on-line, that is, used to translate the response time history samples into quantitative information for the test engineer while the test is in progress.

Briefly, the co/quad method measures the in-phase and out-of-phase components of the forced response generated by the sinusoidal frequency sweep technique. The randomdec method, a relatively new method described in reference 3, makes use of ensemble averaging of transient response to random excitation. The PSD method is a well-known procedure for the analysis of random response data. It is obtained directly from an ensemble average of the square of the magnitude of the Fourier transform of a number of segments of the time history. In the peak-hold spectrum method, Fourier components of a number of time history segments are determined and the envelope of the peak values of these components is obtained as a function of frequency.

DESCRIPTION AND IMPLEMENTATION

Co/quad Method

The co/quad method involved measuring the forced response of a model to an input force such as that generated by a trailing-edge control surface as illustrated schematically in figure 1. If a transfer function relating the response to the input force is determined as a function of frequency, then the damping in each mode can be obtained. For the model applications presented herein, the excitation force was provided by oscillating an aerodynamic control surface, and the model dynamic response $\ddot{h}$ was measured with an accelerometer. Since the measured actuator phase lag and amplitude variation over the frequency range of interest was small and the aerodynamic phase lags of the control surface were assumed to be small, the control surface actuator command signal δ_c was used as a measure of the excitation force. Cross spectrum between the control surface command signal and the model dynamic response was determined with a Spectral Dynamics SD109B co/quad analyzer. This analyzer presents two outputs in terms of in-phase (called co for coincident) and out-of-phase (called quad for quadrature) components between signals. Several means of calculating the damping are available directly from a co and quad type of presentation. As indicated in figure 1, the damping of a mode was estimated from the out-of-phase component by the frequencies labeled f_A and f_B. These are the frequencies at the half-power points and the structural damping g can be expressed in terms of these frequencies (fig. 1).

Randomdec Method

To obtain a randomdec signature, one simply collects a number of segments of the random response signal, each segment having the same initial amplitude, and ensemble averages them. If the system is linear and the excitation random, the ensemble average converges to the transient response of the system due to the selected set of initial conditions.

The implementation of randomdec as used in this paper is shown schematically in figure 2. The response time history shown in figure 2 contains many modes and is normally recorded on analog tape. For the on-line randomdec process, a band-pass analog filter was used for mode isolation and noise reduction. The starting point of each ensemble member was selected with the gating circuit (a standard laboratory oscilloscope triggering circuit was used). A Technical Measurement Corporation 400C computer of average transients was used for ensemble averaging. As the signature develops, it is monitored on an oscilloscope. An electronic counter records the number of segments averaged and a X-Y plotter provides a hard copy of the final signature. Structural damping ratio may be determined directly as indicated on figure 2.

With the implementation as described (fig. 2), the different time segments were averaged sequentially. That is, the computer processed all the results for one time segment before beginning to collect and average data for the next segment. Also, in the implementation as described, the averaging process for each time segment was obtained by taking only segments which cross the selected

trigger level with a positive slope. Thus, the randomdec signature represents the system transient response due to an initial amplitude and velocity.

PSD and Peak-Hold Spectrum Methods

The PSD and the peak-hold spectrum methods were implemented as shown in figure 3. Both methods were implemented using a Spectral Dynamics SD330A Spectrascope. This analyzer employs time compression techniques to achieve minimum analysis time for the frequency-tuned band-pass filter to convert the input signal from the time domain to the frequency domain. Following compression, the input signal is frequency analyzed using 250 synthesized filter locations that are tuned by a built-in sweep generator. With operator-selected modes of operation, this analyzer is highly flexible. When the averaging mode of operation is selected, the average spectrum characteristics of the random signal $\ddot{h}$ are obtained. The averager examines successive ensembles of spectrum functions and computes the averaged sum over a predetermined length of time. Shown on the left of figure 3 is a typical PSD obtained from the model dynamic response $\ddot{h}$. The resulting signature has a peak for each structural mode and, for well-separated peaks, the damping ratio may be obtained. As indicated in figure 3, the structural damping is equal to the frequency bandwidth, taken at the half-power point, and divided by the mode frequency.

An additional mode of operation of the Spectrascope allows for detection and storage of the peak values for each of 250 frequency windows. In this mode of operation, an ensemble spectrum composed of 250 frequency windows is obtained. Upon receipt of each subsequent spectrum, peak filter response at each location is updated in a positive direction. That is, only an increase in value causes an update to the new higher value. On the right of figure 3, a typical peak-hold spectrum is shown. With this method the damping parameter is not obtained. However, the reciprocal of the peak spectrum amplitude $1/P$ is proportional to the damping ratio and is used as a measure of system stability. The peak-hold method was applied using two forms of excitation, model response to tunnel turbulence and model response to sinusoidal force.

APPLICATIONS TO WIND-TUNNEL MODEL TESTING

The four subcritical response methods were applied to flutter test data of a delta-wing research model. Further application of the co/quad and randomdec methods were made using a B-52 flutter suppression model. Some results and comparisons are presented in figures 4 to 7.

Delta-Wing Flutter Model

A photograph of the delta-wing model is shown in figure 4. The trailing-edge control surface was used to provide the forced excitation. A detailed description of this wing is given in reference 4. The flutter motion of this model involves primarily the second natural vibration mode coupled with some primary bending.

The subcritical flutter characteristics of this model in the TDT at a Mach number of 0.90 is presented in figure 5. Two sets of the model data are shown. Figure 5(a) presents the variation of structural damping coefficient of the flutter mode with dynamic pressure. The damping results obtained with the co/quad, randomdec, and PSD methods are indicated with the open symbols. The model fluttered at a dynamic pressure of 5.89 kPa (123 lbf/ft^2) as indicated with the closed symbol. The solid line in the figure is faired through the randomdec data which, of the three methods shown, appears to give the most consistent forecast of the flutter point.

As a word of caution, it should be noted that frequency sweep methods, when used close to a flutter condition, may lead to dangerously large amplitude response as the forcing frequency sweeps through the flutter mode frequency.

A plot of the inverse amplitude of the peak spectrum (used as the stability criteria) is presented in figure 5(b) as a function of dynamic pressure. Shown are results from forced excitation (same excitation system as used in co/quad method) and results from random excitation (model response to tunnel turbulence). The best results were obtained with the forced excitation (faired data) while the response-only data showed some scatter. Although experience is limited in the use of this method, it is included since it appears promising as a flutter indicator.

Further illustration of the type of data generated with the use of the four subcritical methods is presented in figure 6. Shown are the data plots from which the damping levels presented in figure 5 were obtained. The wind-tunnel conditions were the same for each method (Mach number $M = 0.90$; dynamic pressure $q = 5.42$ kPa (113 lbf/ft^2)). In the implementation of the co/quad method, a 3.33-minute logarithmic sweep from 5 to 25 Hz was used. A damping level of 0.037 at a frequency of 10.8 Hz is indicated. Approximately 40 seconds of data were taken for the randomdec method giving a damping level of 0.048 for a frequency of 10.6 Hz. Forty seconds of data were used for the PSD and peak-hold spectrum methods (3.33 minutes for the peak-hold forced excitation procedure). A frequency of 10.7 Hz and a damping level of 0.037 is indicated for the PSD method. The flutter mode frequency for the peak-hold spectrum is 10.6 Hz.

B-52 Model

Further experience with the co/quad forced response method and the randomdec method were obtained using a 1/30-scale, dynamic model of a B-52. The model was equipped with fast acting control surfaces for flutter suppression studies which are described in reference 5. For this model, shown on the right of figure 7, the ailerons were used to generate the forcing function. Thus, for the co/quad method, the damping was estimated by determining the ratio of the outboard-accelerometer response to the aileron command for a frequency range of 4 to 24 Hz. The subcritical flutter characteristics of this model in the TDT are presented in figure 7. The damping results obtained with the co/quad and the randomdec methods are indicated with the open symbols. Both of these methods satisfactorily predict the measured flutter point at a dynamic pressure of 2.65 kPa (55.4 lbf/ft^2) as indicated by the closed symbol.

OBSERVATIONS

Although all four methods assumed that the response can be characterized by a single-degree-of-freedom system, they successfully provided a measure of the subcritical damping level. Each method can be implemented with commercially available instrumentation. The randomdec and PSD methods which depend on random unknown excitation, i.e., turbulence and buffeting, complement the forced sweep co/quad method. Both types of excitation inputs have their advantages. What is "noise" for co/quad is "input" for randomdec. Randomdec works best when there is large response to turbulence or buffet excitation — the region where co/quad data are least reliable. One limitation of the random excitation methods is when the flutter condition involves high frequency modes that may not be excited by random excitation such as turbulence and buffeting. In this instance the forced sweep method should be used.

Difficulties that may be encountered with the use of subcritical response methods include unwanted noise and closely spaced resonant frequencies. Methods (currently used in flight flutter testing) for eliminating or masking noise effects have been evaluated and several new techniques suggested in reference 6. Several system identification schemes were also developed in reference 6 to handle the situation where two or more frequencies of the system are close together.

As a result of experience gained during this early implementation of the randomdec method, further development of this method was undertaken. A current implementation (utilizing the new TDT data system) of the randomdec procedure is presented in reference 7. The feasibility of using the randomdec method in conjunction with a signature analysis procedure to determine the damping and frequency values of a two-mode aeroelastic system was established in reference 8. The signature analysis procedure was based on a least-squares curve fitting of the randomdec signature. The randomdec method was applied during the YF-16 flight flutter tests and for this application provided a satisfactory alternate to more costly conventional subcritical methods (ref. 9).

The reader is cautioned that for a case where a few knots increase in speed spells the difference between a well-damped response and violent flutter, subcritical damping techniques may not be applicable to predict the flutter condition. However, in this case, subcritical techniques will still be of value in correlation with subcritical analytical data and for use in parameter identification techniques to define the system mathematical model.

CONCLUDING REMARKS

Four subcritical response methods were applied to flutter test data for the same model, a cantilever delta wing. Excitation methods included forced excitation (co/quad and peak-hold spectrum) and random excitation (randomdec, PSD, and peak-hold spectrum). Further experience with the co/quad and the randomdec methods was obtained with flutter test data of a complete cable-mounted B-52

flutter model. With both flutter models, the subcritical methods tested in the paper satisfactorily predicted the measured flutter points.

REFERENCES

1. Reed, Wilmer H., III: Correlation With Flight of Some Aeroelastic Model Studies in the NASA Langley Transonic Dynamics Tunnel. NASA Symposium of Flutter Testing Techniques, Oct. 1975. (Paper No. 10 of this compilation.)

2. Rosenbaum, Robert: Survey of Aircraft Subcritical Flight Flutter Testing Methods. NASA CR-132479, 1974.

3. Cole, Henry A., Jr.: On-Line Failure Detection and Damping Measurement of Aerospace Structures by Random Decrement Signatures. NASA CR-2205, 1973.

4. Sandford, Maynard C.; Abel, Irving; and Gray, David L.: Transonic Study of Active Flutter Suppression Based on an Energy Concept. J. Aircr., vol. 12, no. 2, Feb. 1975, pp. 72-77.

5. Redd, L. T.; Gilman, J., Jr.; Cooley, D. E.; and Sevart, F. D.: Wind-Tunnel Investigation of a B-52 Model Flutter Suppression System. J. Aircr., vol. 11, no. 11, Nov. 1974, pp. 659-663.

6. Houbolt, John C.: Subcritical Flutter Testing and System Identification. NASA CR-132480, 1974.

7. Hammond, Charles E.; and Doggett, Robert V., Jr.: Determination of Subcritical Damping by Moving-Block/Randomdec Applications. NASA Symposium of Flutter Testing Techniques, Oct. 1975. (Paper No. 3 of this compilation.)

8. Chang, C. S.: Study of Dynamic Characteristics of Aeroelastic Systems Utilizing Randomdec Signatures. NASA CR-132563, 1975.

9. Brignac, W. J.; Ness, H. B.; and Smith, L. M.: The Random Decrement Technique Applied to the YF-16 Flight Flutter Tests. AIAA Paper No. 75-776, May 1975.

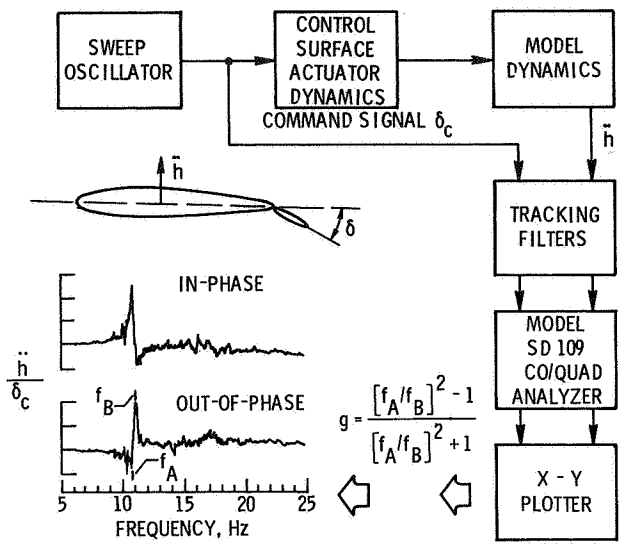

Figure 1.- Implementation of co/quad method.

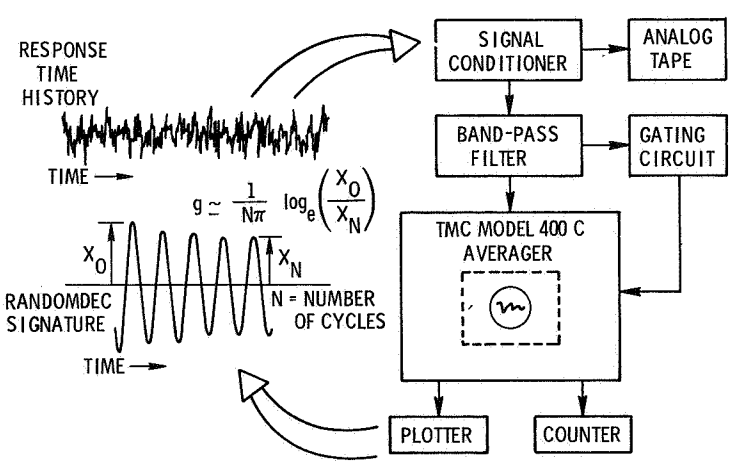

Figure 2.- Implementation of randomdec method.

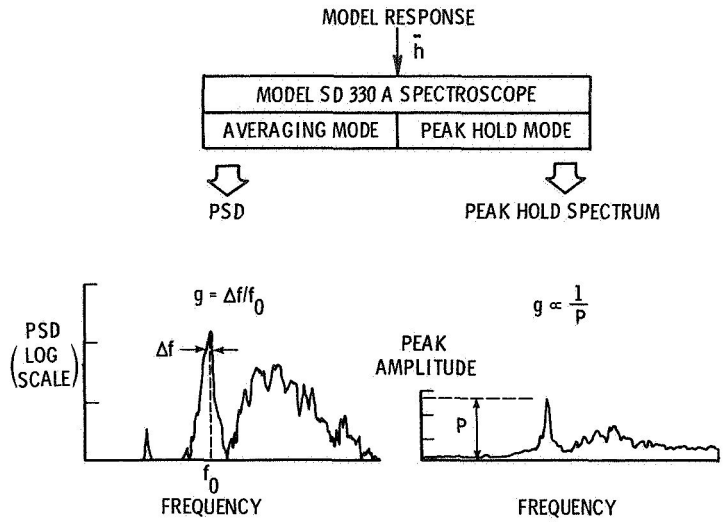

Figure 3.- Implementation of spectrum methods.

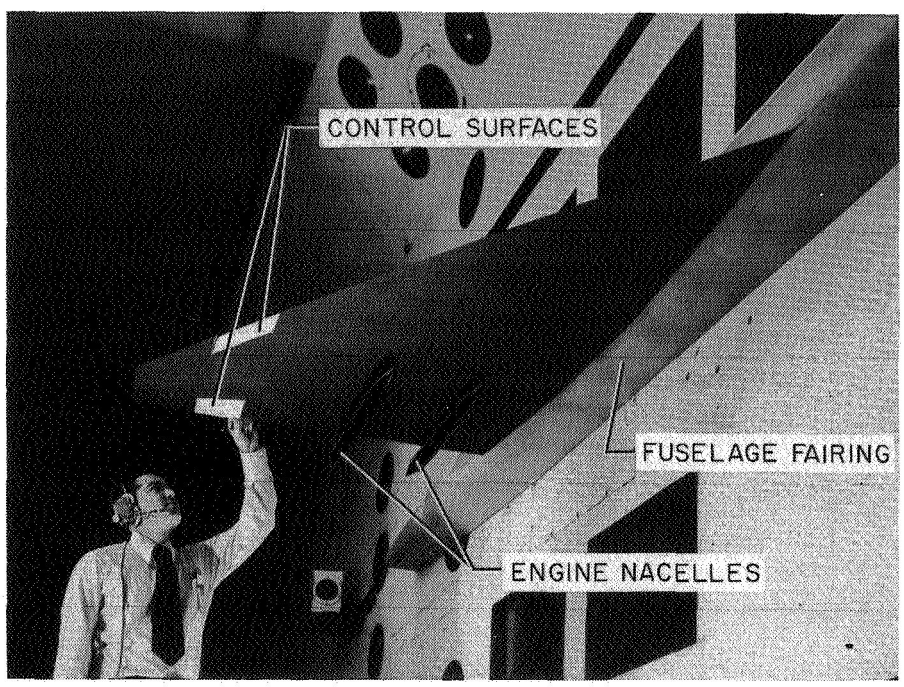

Figure 4.- Delta-wing model.

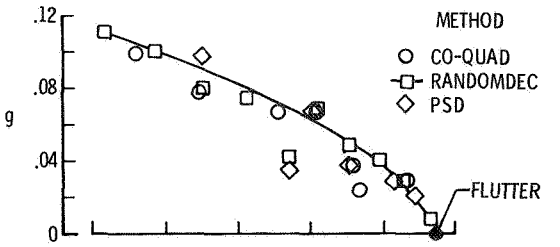

(a) Co/quad, randomdec, PSD results.

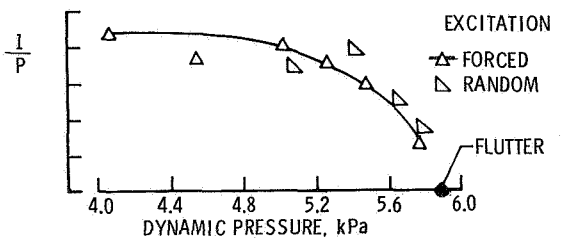

(b) Peak-hold spectrum results.

Figure 5.- Comparison of subcritical methods, delta-wing model (M = 0.90).

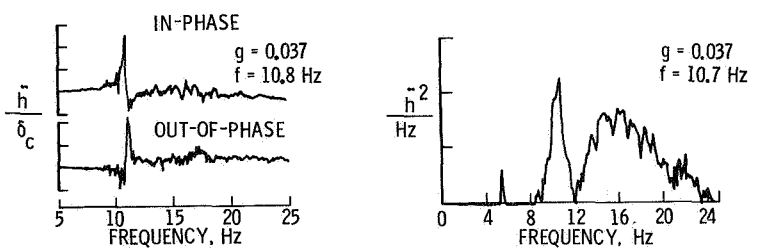

(a) Co/quad.

(c) PSD.

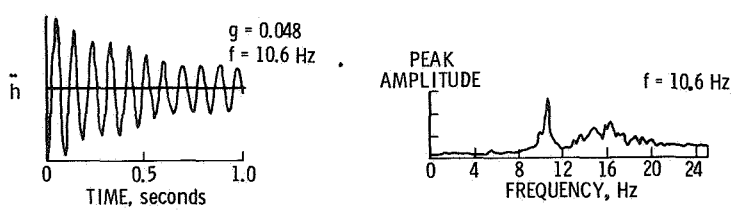

(b) Randomdec.

(d) Peak-hold spectrum.

Figure 6.- Illustration of subcritical methods. M = 0.90; q = 5.42 kPa (113 lbf/ft^2).

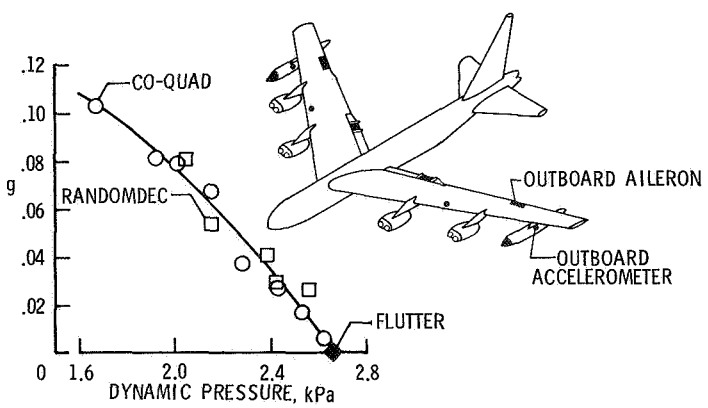

Figure 7.- Subcritical response of B-52 model.

WIND TUNNEL INVESTIGATION OF SUPERSONIC WING-TAIL FLUTTER

Lawrence J. Huttsell, Thomas E. Noll
and Donald E. Holsapple

Air Force Flight Dynamics Laboratory

SUMMARY

An experimental and analytical study was undertaken to establish the flutter trends of a highly swept wing-tail configuration in the low supersonic speed regime. Wind tunnel flutter data was also required for evaluating a new supersonic aerodynamic method for predicting wing-tail interference. A flutter model, consisting of a wing, horizontal tail, and splitter plate/fuselage mechanism, was tested in the Arnold Engineering Development Center (AEDC) Propulsion Wind Tunnel Facility (PWT) 4-Foot Transonic Tunnel in the Mach number range 1.1 to 1.3. Two types of flutter were encountered during the testing; a wing-tail flutter mode and a tail bending-torsion flutter mode. The wing-tail flutter speed was found to be a minimum at M = 1.2 for the configuration tested. Recorded model test data were digitized for a power spectral density (PSD) analysis and Random Decrement (Randomdec) analysis. Comparisons between the frequency and damping obtained from the PSD plots and the Randomdec signatures agreed very well. A limited flutter analysis was conducted using a Mach box unsteady aerodynamics method which accounted for interference and airfoil thickness. Analytical comparisons with experimental flutter speeds agreed very well. The analyses assuming zero thickness predicted flutter speeds higher than those measured, ranging from 1 percent at M = 1.12 to 8 percent at M = 1.28. With the airfoil thickness included, the correlation was improved such that predicted flutter speeds for all cases investigated were within 2 percent of experimental speeds. Flutter frequencies were not as well predicted, generally being somewhat higher than measured.

SYMBOLS

b	wing semichord measured streamwise and intersecting the elastic axis line at 75-percent wing span
f	frequency
g	structural damping coefficient
m	wing mass per unit span
M	freestream Mach number
P_T	total pressure

V freestream velocity at flutter

ρ air density

μ model to air mass ratio, $\frac{m}{\pi\rho b^2}$

ω flutter frequency

ω_h wing first coupled cantilever bending frequency

ω_θ uncoupled fuselage torsion frequency

INTRODUCTION

Today's advanced military aircraft must be capable of undertaking multi-mission roles. Variable sweep wings are used on some aircraft configurations for improving performance at different flight conditions. Low wing sweep angles are attractive during takeoff, landing, and long range cruise when higher aspect ratio is required; high wing sweep angles, which reduce drag, are desirable for high speed flight.

Initially it was thought that flutter speeds would increase at the high sweep angles thus complementing the use of the variable sweep wing. However, in 1966, Topp, Rowe, and Shattuck (Reference 1) conducted a theoretical and experimental program which determined that there are cases where this does not occur. Model tests indicated that for low sweep angles, the critical flutter mode involved the high frequency bending-torsion motion of the wing. As expected, the flutter speed increased as the wing was initially swept back. Near 58 degrees wing sweep, however, a new flutter mode involving the lower frequency modes of the wing, fuselage, and tail became evident. With further increases in wing sweep, the flutter speed dropped rapidly, and at 70 degrees, the flutter speed was lower than for the most forward swept case. The cause for the lower flutter speed and its rapid drop with increasing wing sweep was not fully understood at this time. Since this was a new unforeseen phenomenon, not predictable using available aerodynamic theories, further theoretical and experimental studies were conducted in the following years.

One of the first experimental programs in the area following the effort by Topp, et al., was sponsored by the Air Force Flight Dynamics Laboratory (AFFDL). In 1966, Balcerak (Reference 2) designed, constructed, and tested a series of constant chord 45 degree and 60 degree swept wing-horizontal tail flutter models. Wing and tail surfaces were identical in planform. Testing was accomplished at Mach numbers ranging from 0.4 to 1.24 and defined the effects of important wing-tail parameters on flutter. In some cases the flutter speed continued to decrease into the low supersonic speed regime.

In 1968, the AFFDL continued their investigation by conducting subsonic wind tunnel tests and analyses on a semispan model of a representative variable sweep wing aircraft configuration (Reference 3). Similar trends of flutter

speed versus sweep angle were found. The AFFDL paralleled the experimental investigation with a detailed theoretical study. Both a doublet-lattice method (Reference 4) and a kernal function method (References 5 and 6) were employed to predict the aerodynamic interaction between the wing and tail. Both methods predicted the flutter frequencies extremely well. Flutter speeds were conservatively predicted ranging up to 20 percent lower than the measured flutter velocities. Also, the theory predicted the flutter speed to decrease with increasing subsonic Mach number.

Since the transonic tests of Reference 2 showed that flutter speeds decreased as the Mach number increased, at least up to Mach 1.24, the development of a method to predict unsteady aerodynamic loads for interfering surfaces was required for the supersonic speed regime. Under AFFDL sponsorship, a Mach box method (References 7 and 8) was developed for supersonic interfering surfaces. This paper describes supersonic flutter tests of a half-span flutter model which was dynamically scaled from the model used in the earlier subsonic effort (Reference 3), and the limited analyses which were conducted for verifying the Mach box aerodynamic method.

SUPERSONIC WING-TAIL FLUTTER MODEL

The Air Force Flight Dynamics Laboratory defined the general design of a half-span flutter model consisting of a wing, horizontal tail, and splitter plate/fuselage mechanism. The detail design and construction of the model was performed by Atkins and Merrill, Inc., Ashland, Massachusetts.

The supersonic model was designed to flutter within the Arnold Engineering Development Center (AEDC) PWT 4-Foot Transonic Wind Tunnel by dynamically scaling the 60 degree sweep subsonic model of Reference 3, with the exception of the horizontal tail. The design fundamental frequency for the supersonic tail model was twice that of the wing. Higher tail frequencies were not obtained because the high stiffness characteristics of the subsonic tail could not practically be scaled due to the very low mass requirements for the supersonic model.

Figure 1 provides a photograph of the model showing the wing and tail surfaces, the splitter plate/fuselage mechanism, and the tunnel mounting system. The fuselage mechanism and the wing and tail attachments were enclosed within the fairing between the splitter plate and tunnel ceiling. The model was mounted from the tunnel ceiling in such a manner as to simulate antisymmetric vibration modes. This was achieved by attaching the models to a shaft assembly which was supported by bearings, thereby providing a roll degree of freedom. A roll stiffness was provided by a small spring mounted between the shaft assembly and the splitter plate. Variation in the fuselage torsional stiffness was obtained by changing the effective length of a constant cross-sectional bar which connected the fore and aft shaft assemblies. The wing and tail could either roll together or differentially since the shaft assemblies for the wing and tail surfaces were interconnected only through the torsion bar. Variations in the torsion bar length could be accomplished without affecting the separation

between the wing and tail. Two tail attachment points were also provided to allow a variation in horizontal separation between the wing and tail.

The wing and tail models were constructed using a stressed skin fabrication technique. This composite construction consisted of laminated fiberglass/epoxy skins which were high-temperature cured under pressure and stabilized with a honeycomb core. Strips of graphite were added along the span of the wing and tail to obtain the required bending stiffness. The wing was attached to the forward fuselage roll bar by means of a flexible carry-through structure with scaled torsion and bending stiffnesses. The tail was attached to the aft fuselage roll assembly by means of a carry-through structure with high stiffness.

Natural mode shapes and frequencies were computed using classical lumped mass methods. Figure 2 shows typical results for four elastic modes used in the flutter analysis. In general, agreement between the wing measured and predicted node lines and frequencies was good. The first mode (not shown in the figure) involves roll motion about the model roll axis with a measured frequency of 17.8 Hz; the second mode involves primarily wing carry-through torsion coupled with wing bending; the third mode involves tail bending and wing bending; the fourth mode involves primarily wing second bending and carry-through torsion; and the fifth mode is primarily tail torsion.

WIND TUNNEL TESTS

The tests were conducted in the AEDC PWT 4-Foot Transonic Wind Tunnel. A schematic of the data monitoring and recording system used during the flutter tests is shown in Figure 3. During testing, strain gage bridges were used to monitor and record the response of the model. Strain gage bridges were mounted just outboard of the wing and tail roots to measure the bending and torsion strains. Others were mounted on springs to measure wing carry-through torsion and bending, the fuselage torsion, and the model roll motions. The eight strain gage channels and a time code were displayed on a Varian strip recorder and copied on tape together with a voice track. Two X-Y oscilloscopes were used to monitor the coupling of the critical wing-tail modes; one of the oscilloscopes displayed fuselage torsion (FT) and wing carry-through torsion (CT) responses; the second oscilloscope displayed wing carry-through bending (CB) and wing carry-through torsion (CT) responses. An on-line Time/Data analyzer was used to display the frequency response (0-100 Hz) for either the wing carry-through torsion, the wing carry-through bending, or the fuselage torsion motion. The approximate frequency range of high model response was determined from such a display. Modes of interest were selected and processed through a 5 Hz bandwidth tracking filter to define the critical frequency.

The test Mach number was approached from a low total pressure (low dynamic pressure). The total pressure was increased at an essentially constant Mach number until flutter occurred. At selected test conditions, the response data was recorded and the frequencies measured using the tracking filter. Figure 4 presents the AEDC 4T wind tunnel standard operating envelope of total pressure

and dynamic pressure versus Mach number, and shows the flutter points obtained for each configuration tested. The first test configuration, wing bending to fuselage torsion frequency ratio (ω_h/ω_θ) of 0.62, was tested at M = 1.2 up to a total pressure of 129.3 kPa (2700 psf). No flutter was encountered. However, there was significant wing and tail motion, indicating the proximity to flutter. The structural damping coefficient (g) was estimated to be approximately 0.01. Tunnel limitations prevented further testing of this configuration. The fuselage torsional stiffness was then adjusted to give ω_h/ω_θ = 0.32, and the model was again tested. Wing-tail flutter was obtained at M = 1.12, 1.2, and 1.28. The flutter frequency varied from 85 Hz at M = 1.12 to 88 Hz at M = 1.28. Figure 5 presents a strip chart recording for the M = 1.28 test configuration. Both wing and tail responses are shown to be diverging, indicating that the test condition was slightly into an unstable region. The flutter mode resulted in catastropic damage to both surfaces as shown in Figure 6.

A tail bending-torsion flutter mode was encountered at M = 1.08 while reducing Mach number at a constant total pressure from the M = 1.12 wing-tail flutter point. The frequency of the tail flutter mode was 176 Hz which is slightly above the tail torsion mode shown in Figure 2. The time history response record for the wing and tail strain gages are shown in Figure 7 for this mode of flutter. The tail bending and torsion gages diverged very rapidly. The motion on the wing is very small in comparison to the tail motions for this predominantly tail bending-torsion coupling. The tail surface was rapidly destroyed following flutter onset.

DATA REDUCTION

Following the wind tunnel tests, selected flutter model response data were played back from analog tapes and digitized using an ITI 4900-Preston A/D system. Low pass analog filters (48 dB per octave roll-off) were used to band limit the digitized response data to a frequency range of 0-200 Hz. Both Power Spectral Density (PSD) and Random Decrement (Randomdec) analyses methods were used to reduce the test data.

PSD Method

Narrow band (0.46 Hz bandwidth) PSD analyses were performed using a Raytheon 704 Fast Fourier Analyzer system. Thirteen transforms with sample size of 2048 were averaged to provide a spectrum which was plotted on the Raytheon/Gould 4800 plotter. Figures 8 and 9 present the results of the PSD analysis of the random response data for the model with ω_h/ω_θ = 0.32 and M = 1.2 at two subcritical test conditions (total pressures of 95.8 kPa (2000 psf) and 105.3 kPa (2200 psf)). The response in the 84-86 Hz mode (the critical wing-tail mode) increased with total pressure as flutter was approached. At a total pressure of 105.3 kPa (2200 psf), the response in a 176 Hz mode became more evident. The frequency and damping were estimated from the PSD plots using standard techniques, and the results are presented in Table I for the critical wing-tail mode at the two test conditions discussed above and at two additional points.

Randomdec Method

The Randomdec method, invented by H. A. Cole, Jr. (References 9 and 10) was applied in this study to analyze the response generated by random excitation for determining the frequency and damping of the modes of interest. The Randomdec program used ensemble averaging of up to 300 digital samples of response data (.07 seconds in length). The program extracted the characteristic response signature, and the frequency and damping ratio from the random response data (0-200 Hz). A typical Randomdec signature for $\omega_h/\omega_\theta = 0.32$ is shown in Figure 10 for M = 1.2 and P_T = 2000 psf. This corresponds to the PSD plot shown in Figure 8. The Randomdec signature is very clean, and the structural damping can be easily determined.

Comparison of Results Using PSD and Randomdec Methods

The structural damping coefficient and frequency for the critical wing-tail mode which were obtained using PSD and Randomdec methods are presented in Table I. All frequency comparisons are within 2 percent. Structural damping comparisons between the two methods are within 0.012. At a total pressure of 110.1 kPa (2300 psf), flutter onset has been slightly exceeded as shown by a small negative damping whereas the PSD method is not capable of providing negative damping.

ANALYSIS AND CORRELATION

Limited flutter analyses were conducted using the supersonic Mach box program described in References 7 and 8. This method was developed to analyze lifting surfaces in close proximity in supersonic flow including aerodynamic interference. The analyses were conducted for the flight conditions at which wing-tail flutter occurred for $\omega_h/\omega_\theta = 0.32$. These analyses were conducted both with and without airfoil thickness included. The Mach box method includes an option for thickness corrections to the pressure distribution based on second order piston theory.

Table II presents comparisons of calculated flutter speeds and frequencies with corresponding measured values at Mach numbers 1.12, 1.2 and 1.28. Without airfoil thickness included, the analyses predicted flutter speeds ranging from approximately 1 percent at M = 1.12 to 8 percent higher than the measured speeds at M = 1.28. With the airfoil thickness included in the analyses, flutter speed predictions were improved. At M = 1.2, the calculated flutter speed was within 1.5 percent of the measured flutter speed, a 5 percent improvement over the analyses without airfoil thickness. At M = 1.28, the analyses with airfoil thickness included was within 1 percent of the measured flutter speed, an improvement of approximately 7 percent. Flutter frequencies were not as well predicted. The calculated flutter frequencies were 8 to 18 percent higher than the measured values.

Both measured and calculated flutter data are presented in Figures 11 and 12 in the form of flutter parameters $V/b\omega_\theta \sqrt{\mu}$ and ω/ω_θ versus Mach number.

The subsonic data from Reference 3 are also shown for comparison. In Figure 11, the predicted subsonic trend of $V/b\omega_\theta \sqrt{\mu}$ is decreasing with Mach number as shown for $\omega_h/\omega_\theta = 0.62$. The trend for $\omega_h/\omega_\theta = 0.32$ is shown dashed, since analyses were not conducted for the configuration but were estimated based on other similar trends. These subsonic analyses indicate that $V/b\omega_\theta \sqrt{\mu}$ continues to drop at least up to transonic speeds. The supersonic test results for $\omega_h/\omega_\theta = 0.32$ indicate that a minimum flutter speed was obtained at M = 1.2. This was significantly lower than the M = 0 subsonic test results. A further increase in Mach number to M = 1.28 provided some alleviation; however, the flutter parameter still remains below the M = 0 test results. The supersonic analyses, with or without airfoil thickness included, show increasing flutter speeds with increasing Mach number.

Figure 12 presents ω/ω_θ versus Mach number. Test results indicate an increasing value of ω/ω_θ as the Mach number increases, while the analyses predict a minimum flutter frequency ratio at approximately M = 1.2 followed by an increase at the higher Mach number tested (M = 1.28).

CONCLUDING REMARKS

In conclusion, the results of this wind tunnel investigation of a wing-tail flutter phenomena in the Mach number range 1.12 to 1.28 show less stability (lower flutter speed parameter) than earlier corresponding subsonic data. However, the results indicate some increase in flutter stability at M = 1.28 as compared with M = 1.2 data. Also, the Mach box analysis procedure with aerodynamic interference and airfoil thickness effects included was found to adequately predict the wing-tail flutter speeds of this phenomena.

REFERENCES

1. Topp, L.J., Rowe, W.S., and Shattuck, A.W.: Aeroelastic Considerations in the Design of Variable Sweep Airplanes. ICAS Paper 66-12, Fifth International Congress of the Aeronautical Sciences, London, England, September 1966.

2. Balcerak, J.C.: Flutter Tests of Variable Sweep Configurations. AFFDL-TR-68-101, September 1968.

3. Mykytow, W.J., Noll, T.E., Huttsell, L.J., and Shirk, M.H.: Subsonic Flutter Characteristics of a Variable Sweep Wing and Horizontal Tail Combination. AFFDL-TR-69-59, November 1970.

4. Albano, E. and Rodden, W.P.: A Doublet Lattice Method for Calculating Lift Distributions on Oscillating Surfaces in Subsonic Flows. AIAA Journal, Vol. 7, No. 2, February 1969, pages 279-285.

5. Laschka, B. and Schmid, H.: Unsteady Aerodynamic Forces on Coplanar Lifting Surfaces in Subsonic Flow (Wing-Horizontal Tail Interference). Presented at AGARD Structures and Materials Panel Meeting, Ottawa, Canada, September 1967.

6. Albano, E., Perkinson, F., and Rodden, W.P.: Subsonic Lifting Surface Theory Aerodynamics and Flutter Analysis of Interfering Wing/Horizontal Tail Configurations. AFFDL-TR-70-59, September 1970.

7. Ii, J.M., Borland, C.J., and Hogley, J.R.: Prediction of Unsteady Aerodynamic Loadings of Non-Planar Wings and Wing-Tail Configurations in Supersonic Flow, Part I, "Theoretical Development, Program Usage, and Application". AFFDL-TR-71-108, March 1972.

8. Kramer, G.D. and Keylon, G.E.: Prediction of Unsteady Aerodynamic Loadings of Non-Planar Wings and Wing-Tail Configurations in Supersonic Flow, Part II, "Computer Program Description". AFFDL-TR-71-108, March 1972.

9. Cole, H.A., Jr.: Method and Apparatus for Measuring Damping Characteristics of a Structure. United States Patent No. 3, 620, 069, 16 November 1971.

10. Cole, H.A., Jr.: On-Line Failure Detection and Damping Measurement of Aerospace Structures by Random Decrement Signatures. NASA CR-2205, March 1973.

Table I. - Damping Comparison for the Critical Wing-Tail Mode at M = 1.2, $\omega_h/\omega_\theta = 0.32$.

P_T (kPa)	PSD f (Hz)	PSD g	RANDOMDEC f (Hz)	RANDOMDEC g
95.76	84.0	0.100	85.2	0.096
100.55	86.0	0.070	85.6	0.058
105.34	86.5	0.020	87.0	0.009
110.12	86.1	-	87.0	-0.009

Table II. - Airfoil Thickness Effects on Flutter Trends, $\omega_h/\omega_\theta = 0.32$.

MACH NUMBER	ANALYSIS ZERO THICKNESS V_{CAL}/V_{EXP}	ANALYSIS ZERO THICKNESS $\omega_{CAL}/\omega_{EXP}$	ANALYSIS THICKNESS (NACA 64-006) V_{CAL}/V_{EXP}	ANALYSIS THICKNESS (NACA 64-006) $\omega_{CAL}/\omega_{EXP}$
1.12	1.013	1.167	-	-
1.20	1.064	1.081	1.015	1.128
1.28	1.077	1.182	0.993	1.136

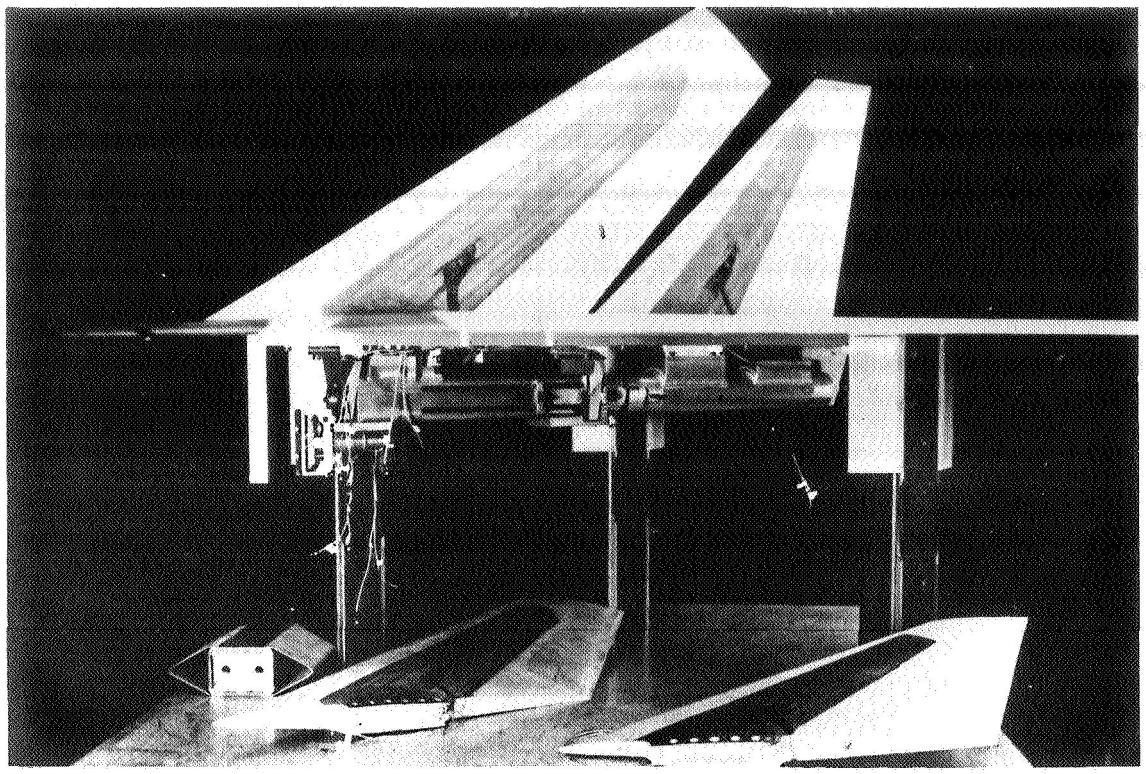

Figure 1. - Supersonic Wing-Tail Flutter Model.

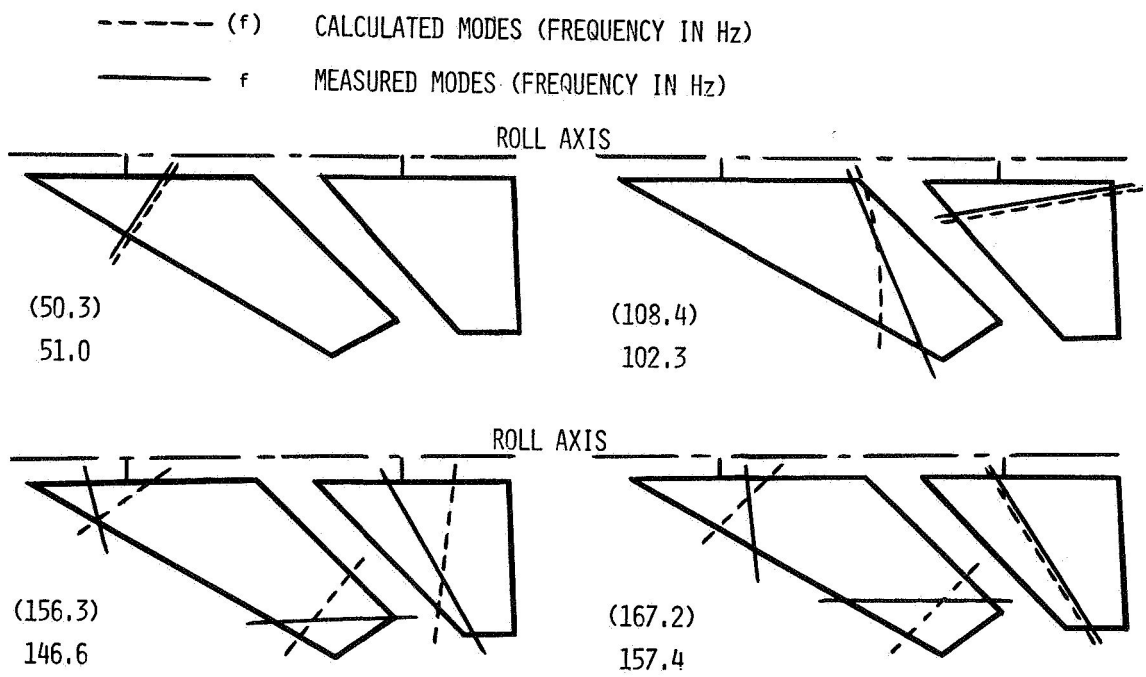

Figure 2. - Calculated and Measured Vibration Node Lines and Frequencies, $\omega_h/\omega_\theta = 0.32$.

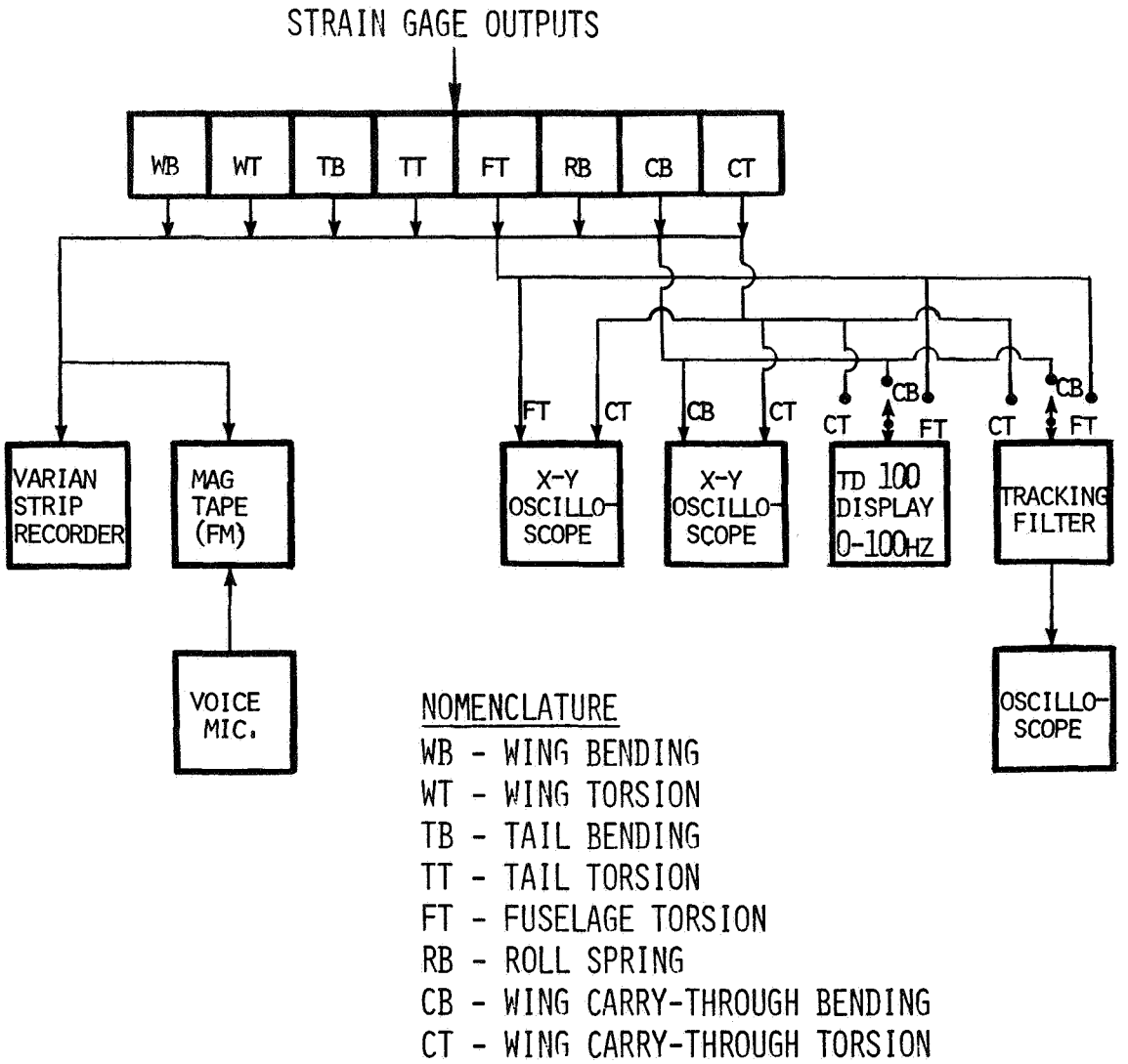

Figure 3. - Wind Tunnel Test Data Monitoring and Recording System.

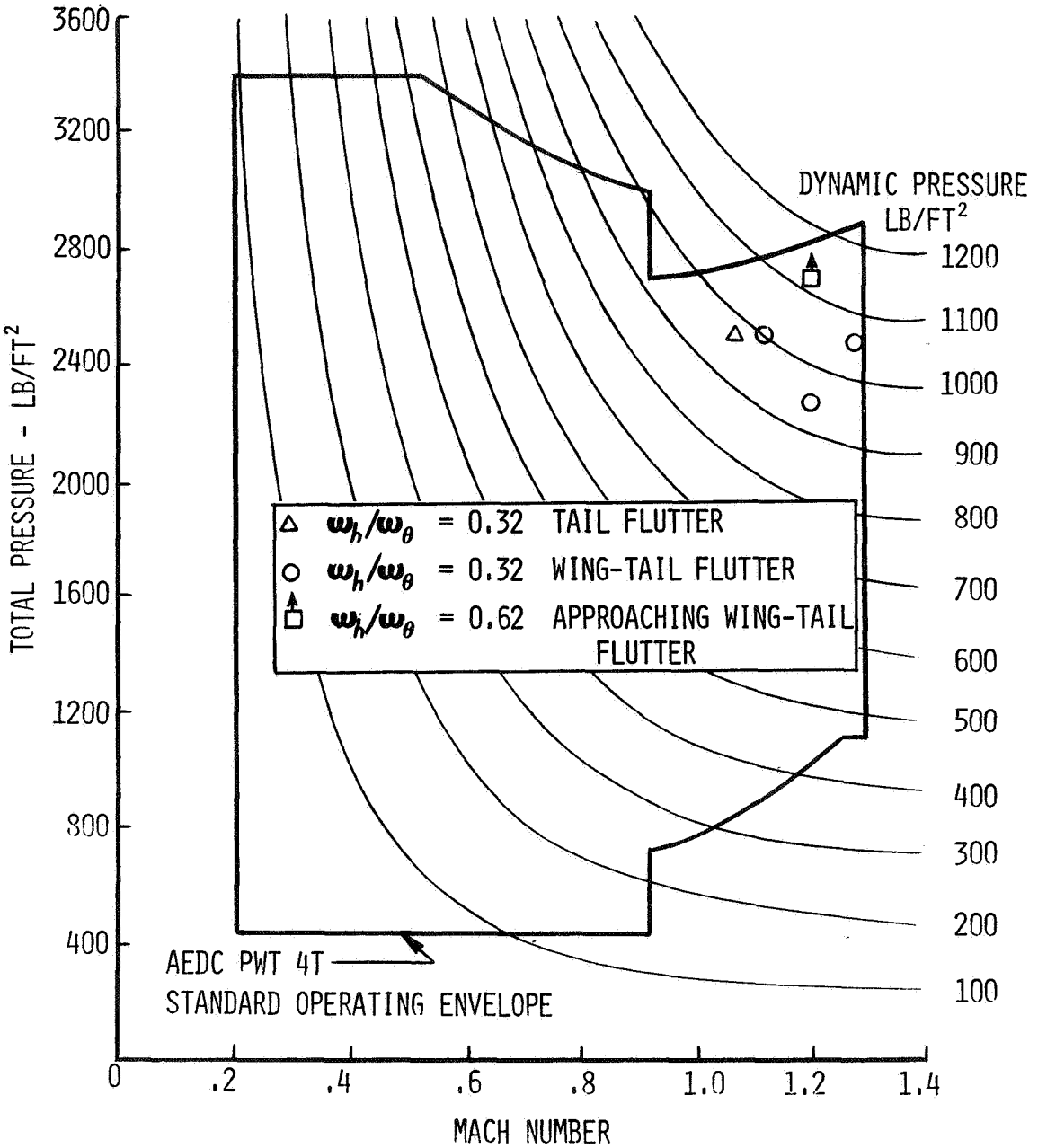

Figure 4. Wind Tunnel Operating Envelope with Experimental Flutter Data. (1 lb/ft^2 = 47.88 Pa.)

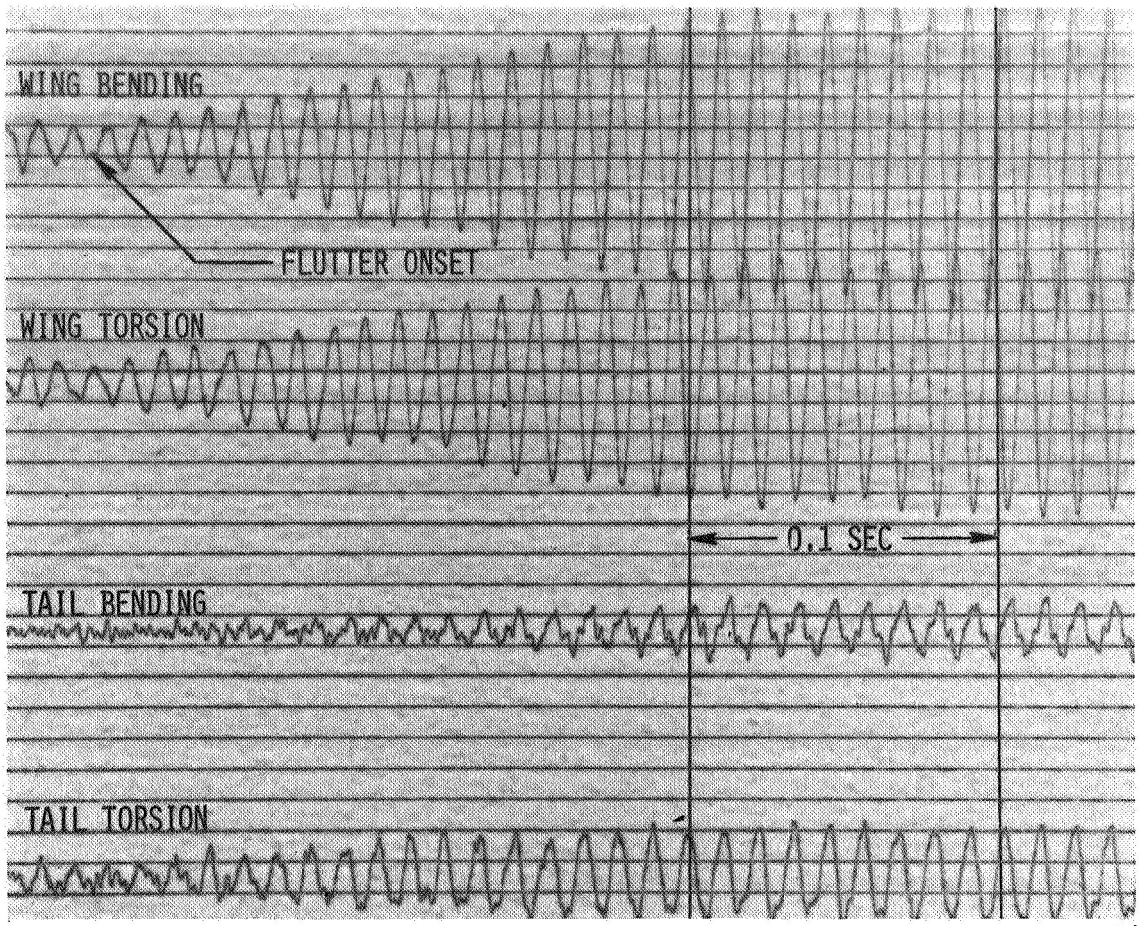

Figure 5. - Model Response at M = 1.28 and P_T = 118.5 kPa (2475 lb/ft^2), ω_h/ω_θ = 0.32.

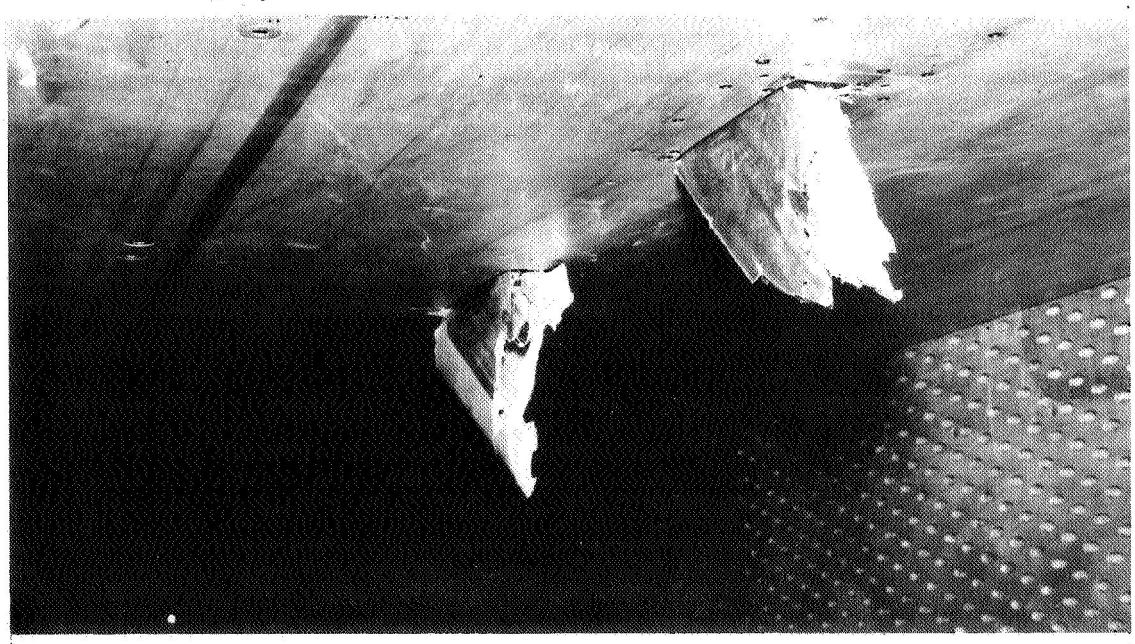

Figure 6. - Model Damage from Wing-Tail Flutter at M = 1.28, ω_h/ω_θ = 0.32.

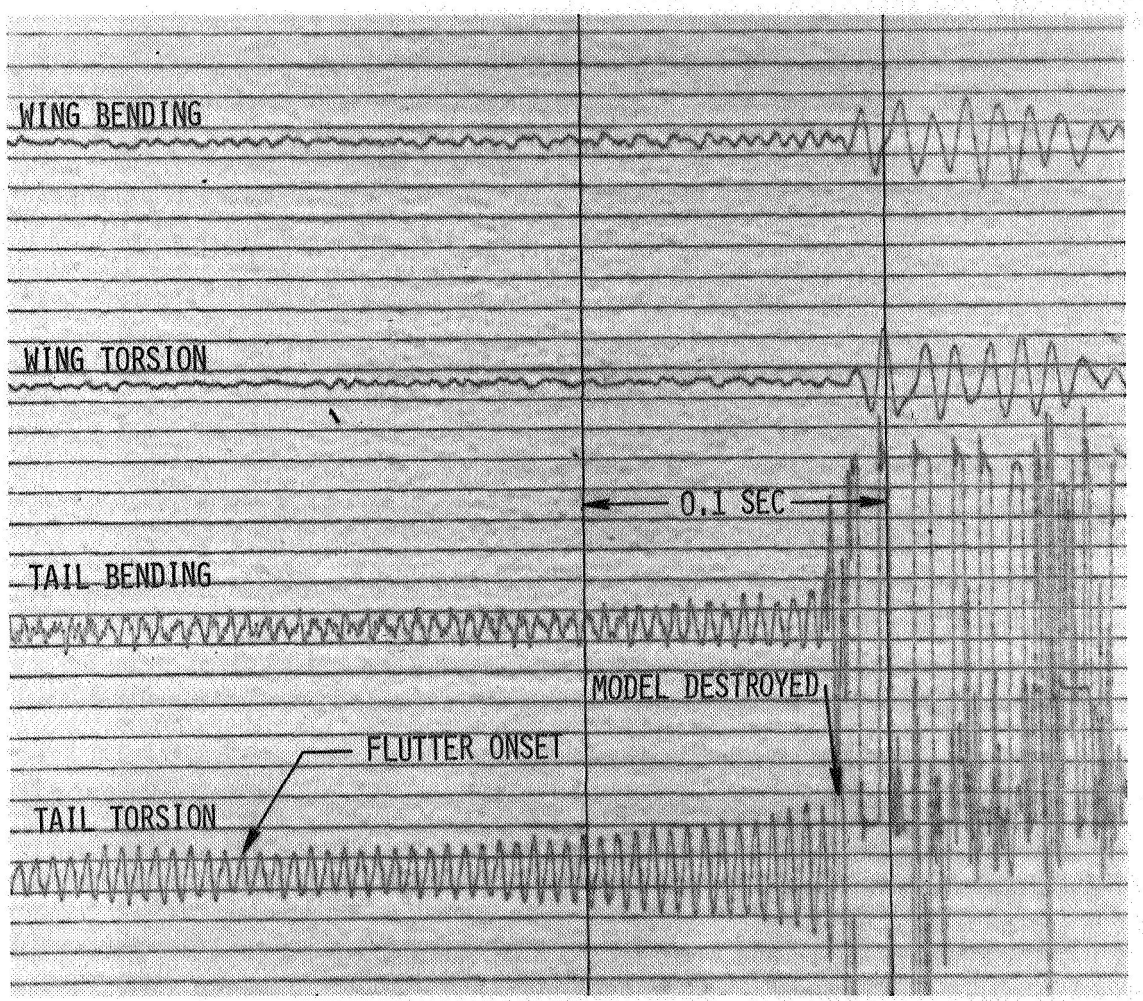

Figure 7. - Model Response at M = 1.08 and P_T = 119.7 kPa (2500 lb/ft^2), ω_h/ω_θ = 0.32.

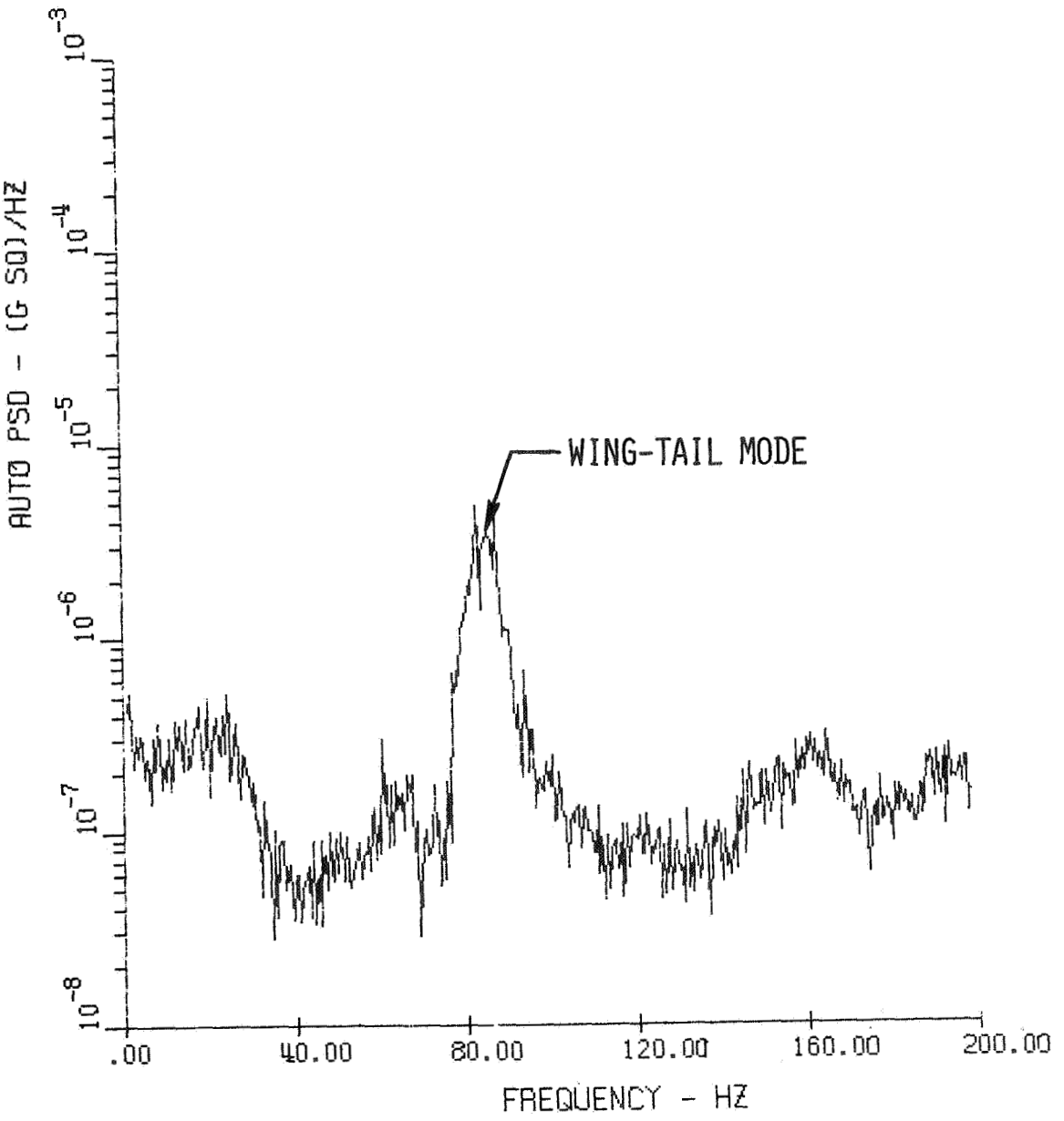

Figure 8. - PSD Plot for M = 1.2 and P_T = 95.8 kPa (2000 lb/ft^2), ω_h/ω_θ = 0.32.

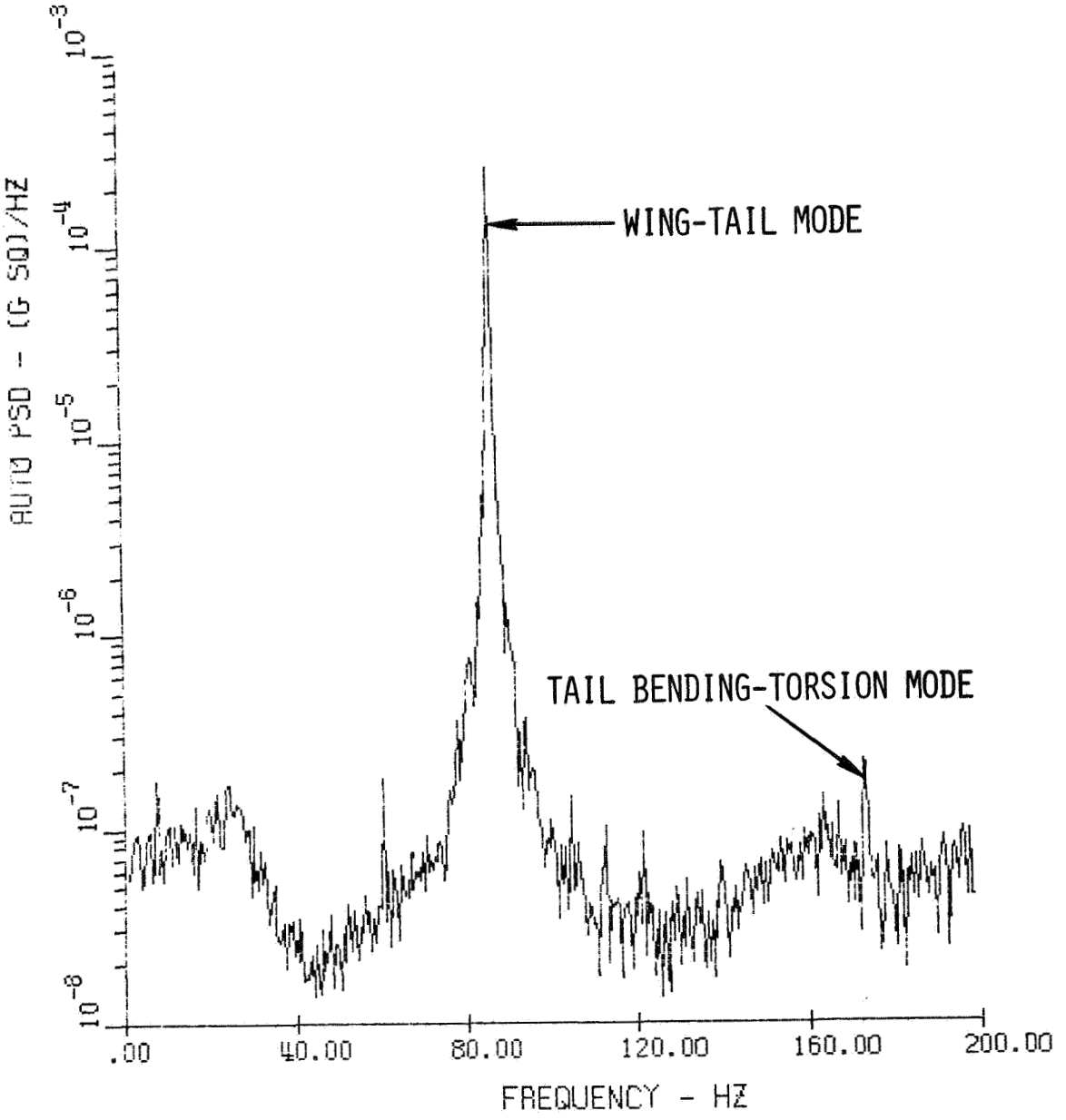

Figure 9. - PSD Plot for M = 1.2 and P_T = 105.3 kPa (2200 lb/ft^2), ω_h/ω_θ = 0.32.

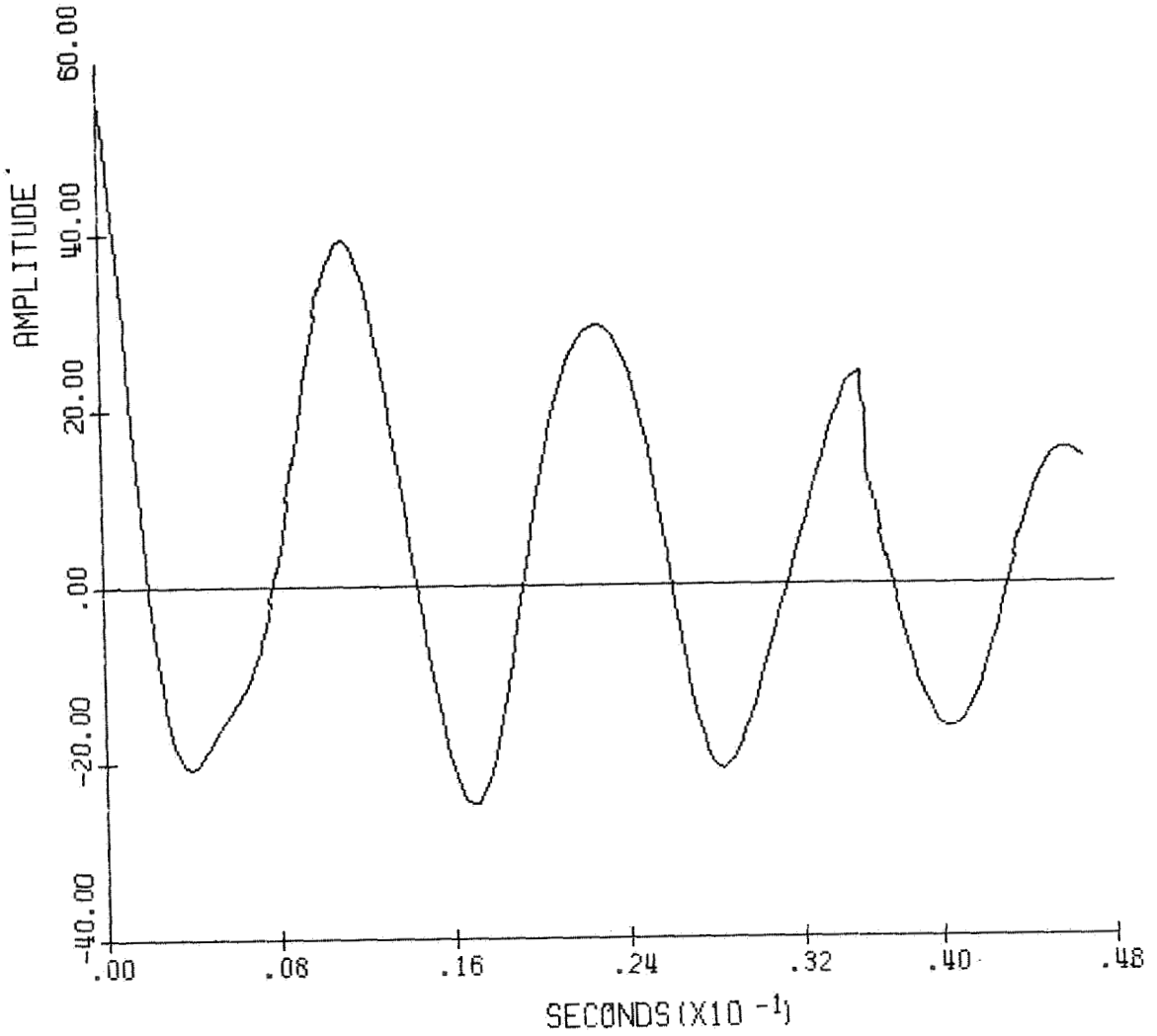

Figure 10. - Randomdec Signature for M = 1.2 and P_T = 95.8 kPa (2000 lb/ft^2), ω_h/ω_θ = 0.32.

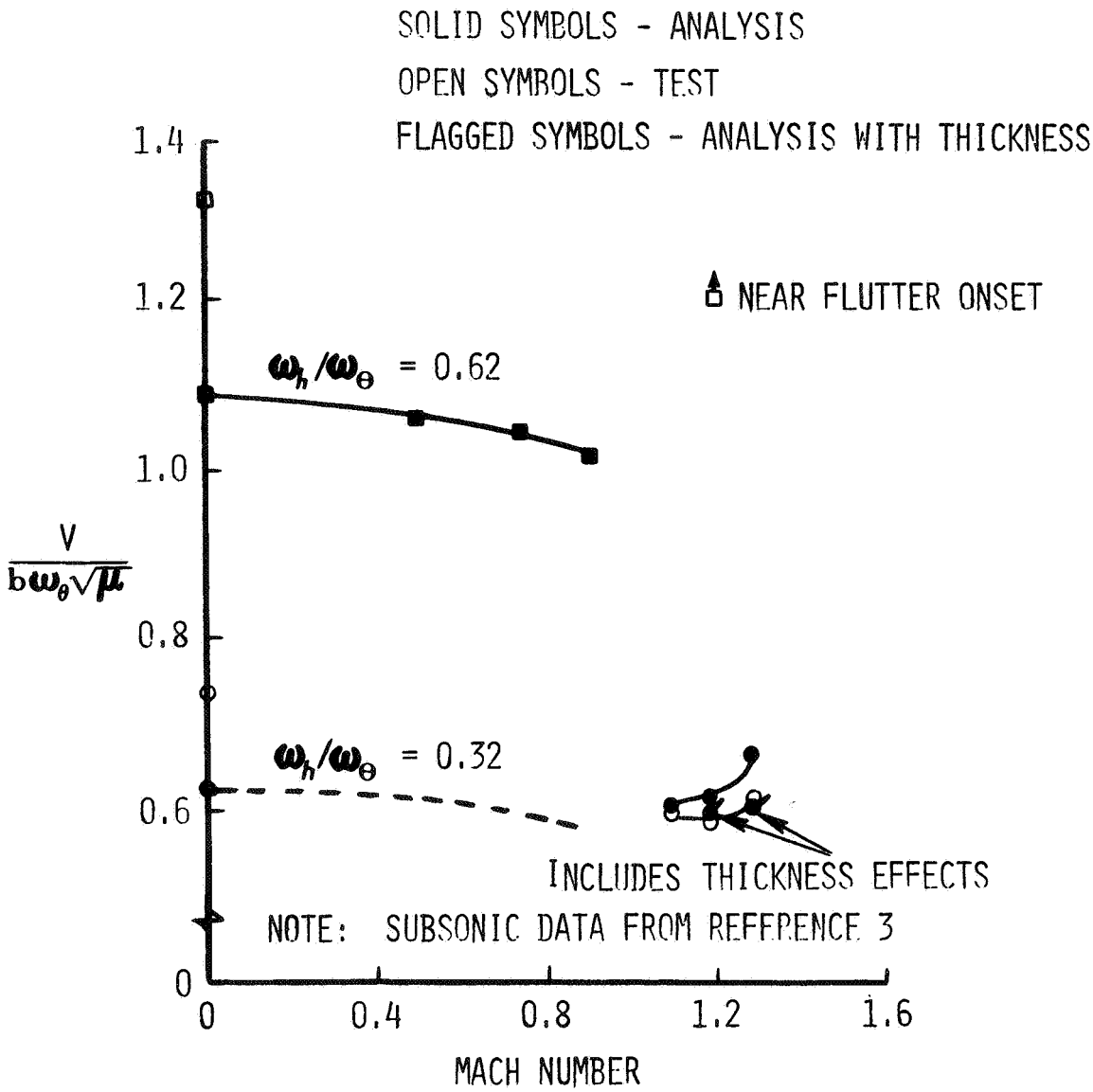

Figure 11. - $V/b\omega_\theta\sqrt{\mu}$ Versus Mach Number.

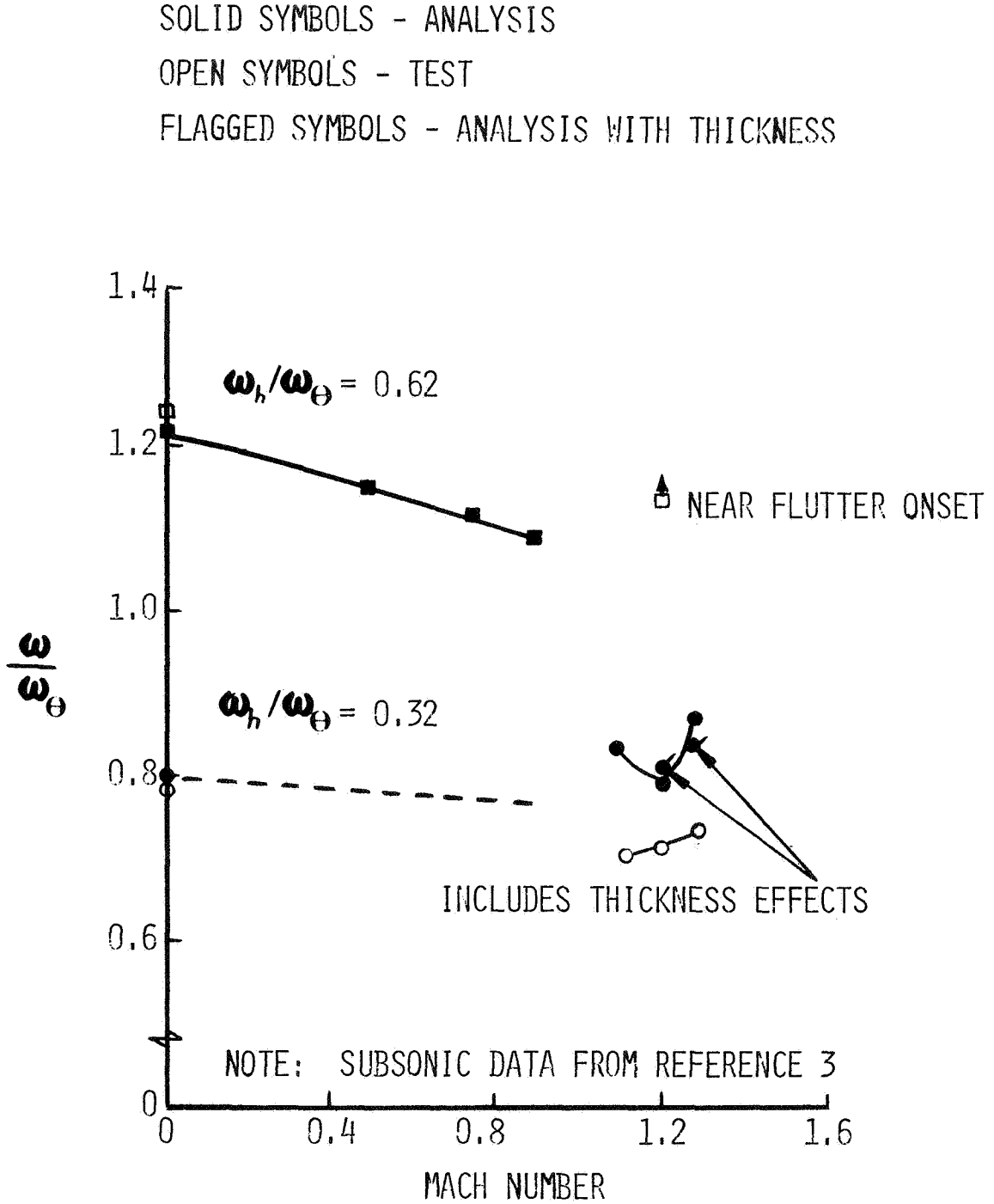

Figure 12. - ω/ω_θ Versus Mach Number.

THE DESIGN, ANALYSIS, AND TESTING OF A LOW-BUDGET WIND-TUNNEL FLUTTER MODEL WITH ACTIVE AERODYNAMIC CONTROLS*

R. Bolding

Fort Worth Division, General Dynamics Corporation

R. Stearman

The University of Texas at Austin

SUMMARY

Active control technology is playing a more significant role in aerospace and aircraft vehicle design and gives rise to the need to introduce the basic technology into the educational activities within the profession. The present paper describes a low-budget flutter model incorporating active aerodynamic controls for flutter suppression studies, designed as both an educational and a research tool. The study concentrates on the interfering lifting surface flutter phenomenon in the form of a swept wing-tail configuration. A flutter suppression mechanism was first demonstrated on a simple semirigid three-degree-of-freedom flutter model of this configuration employing an active stabilator control. This was then verified analytically using a doublet lattice lifting surface code and the model's measured mass, mode shapes, and frequencies in a flutter analysis. These preliminary studies were significantly encouraging to extend the analysis to the larger degree of freedom AFFDL wing-tail flutter model where additional analytical flutter suppression studies indicated significant gains in flutter margins could be achieved. The analytical and experimental design of a flutter suppression system for the AFFDL model is presented along with the results of a preliminary passive flutter test.

INTRODUCTION

The increased importance that active control technology plays in aircraft and aerospace vehicle design necessitates the introduction of the basic concept into the educational activities within our profession. While the basic technology evolved within the aerospace industries and the government laboratories, certain problem areas appear suitable for pursuit in an academic institution having a combined educational and research objective. The present paper describes one such attempt at a low-budget program carried out at the graduate

*This research was supported by the Air Force Office of Scientific Research, Office of Aerospace Research, United States Air Force.

level. This involved the design, construction, and wind-tunnel testing of an actively controlled wind-tunnel research flutter model. It focused on the development of a flutter suppression system for aerodynamically interfering lifting surfaces in the configuration of a closely spaced wing-tail geometry where the flutter mechanism is fairly well understood.

In early experiments, Topp, Rowe, and Shattuck observed the phenomenon of wing-tail interference flutter for the variable-sweep configuration and indicated in reference 1 that it was the result of aerodynamic interaction and elastic coupling between the wing and tail. For some sweep angles this can significantly reduce the flutter speed for the wing and tail below that for the isolated wing alone as illustrated in figure 1 taken from reference 1. A systematic and extensive study of this phenomenon was carried out by Mykytow, Noll, Huttsell, and Shirk in reference 2 and the wing-tail interference flutter mechanism was fairly well clarified. A small, interesting semirigid flutter model demonstrating this flutter phenomenon was also developed within the industry, as illustrated in reference 3. We later built and adapted this to the classroom demonstration model illustrated in figure 2. As the control configured vehicle and active control concepts further developed, a decision was made to extend the capabilities of this classroom model to demonstrate flutter suppression via active controls. This was undertaken with the hope that the objective could be accomplished, i.e., flutter suppressed over a significant velocity range, and that some insight could also be obtained as to the flutter suppression mechanism. The results of this study proved to be more encouraging than originally anticipated and further analytical studies were carried out on the AFFDL wing-tail flutter model of reference 2 which had several additional flexible degrees of freedom. Here again, parameter optimization techniques yielded control laws which demonstrated significant gains in flutter margin when an active stabilator or aileron control was employed. Flutter margins could be increased to that of the isolated wing. As a result of these analytical findings, it appeared desirable to evaluate the results in the wind tunnel and establish a level of confidence for the math modeling. The present study was undertaken with this objective in mind subject to the constraints of a low budget for model construction and wind-tunnel test time. This necessitated testing at a Mach zero condition in a subsonic wind-tunnel facility. In addition, to cut costs, the existing AFFDL Wind-Tunnel Flutter Model design was selected where minor modifications to the design could be made to yield an active stabilator control. The scope of the experiment was to evaluate control laws derived by parameter optimization techniques employing standard V-g, Vector Nyquist, and aerodynamic energy techniques. The experimental flutter data are to be correlated with analytical flutter calculations based upon lifting surface doublet lattice aerodynamics and experimentally determined mode shapes, generalized masses, and natural frequencies for the first five mode shapes of the system. The flutter suppression system analytical design studies are presented here along with a review of the model design and passive wind-tunnel flutter studies.

The cooperation of the Air Force Flight Dynamics Laboratory (AFFDL) in providing us with the basic model design details is appreciated. In addition, our visits with the Flight Controls staff of the Boeing Company, Wichita Division, were very helpful. Appreciation is also expressed to Emil Cwach,

General Dynamics, Forth Worth, and Lt. Kenneth Griffin, Air Force Flight Dynamics Laboratory, for their contributions to the program.

PRELIMINARY DESIGN STUDIES ON SEMIRIGID MODEL

The actively controlled flutter model, developed in the following program, evolved from preliminary design studies of flutter suppression systems applied to the small semirigid model illustrated in figure 2. At the time the study was initiated it appeared as though a flutter suppression system might be more easily developed for this type of model, that is, it seemed plausible that flutter suppression systems might significantly benefit the performance of variable-geometry aircraft with aerodynamic interference effects while possibly providing less impressive gains on more conventional aircraft. In view of this, exploratory wind-tunnel studies were initiated in the University of Texas 3 ft by 4 ft low-speed wind tunnel with this three-degree-of-freedom model. The degrees of freedom include a rigid body roll mode, one wing bending mode, and one fuselage torsion mode. For the actively controlled model an additional control degree of freedom was incorporated as a stabilator pitch mode. This finite degree of freedom or semirigid feature was achieved by concentrating elastic springs on the model at the wing root and at one position along the fuselage as illustrated by the component breakdown in figure 2.

Trial and error low-speed wind-tunnel tests indicated that a 40% increase in flutter margin could be easily achieved on this model employing a simple feedback coupled to a stabilator control. This was accomplished by taking the output from an accelerometer mounted on the stabilator or fuselage and feeding it through a phase and gain network (or variable phase oscillator) to a small shaker with a force output of 8.9 newtons (2 lb) which activated the stabilator control by means of a flexible mechanical linkage. Interpretation of high-speed movies of the study indicated that the more effective phase and gain selections were those which essentially rotated the stabilator control to eliminate the induced downwash as illustrated in figure 3. This figure represents a view of a typical section cutting through both wing and tail at a given spanwise station. The typical washout appearance of an upward bending swept wing is demonstrated here inducing a downwash over the stabilator forcing it to deform approximately 180° out-of-phase with the wing. The actual phasing will depend upon the wing-tail separation distance. As indicated, the most effective control command for suppressing this interference flutter was that which pitched the stabilator approximately in-phase with the main wing, thus eliminating the induced downwash.

To check the above hypothesis, an analytical study of the model was carried out employing the doublet lattice lifting surface theory and the model's measured mass, mode shapes, and frequencies in a V-g type flutter analysis. The results of this study are illustrated in figures 4 and 5 for the control loop open (passive flutter studies). The experimentally measured flutter speed is superimposed on the V-g data to illustrate the degree of correlation between theory and experiment. A polar plot of the open loop flutter mode in terms of the three generalized coordinates and the motion of a point on the wing and tail are illustrated in figure 5. The actual phasing between the wing and tail

motion is seen to be a little less than the 180° that was suggested. A similar polar plot of the closed loop configuration that suppressed flutter is illustrated in figure 6. This is again based on the doublet lattice aerodynamic modeling now including an active stabilator control and measured modes, frequencies, and model mass. The control deflection, that is, the stabilator pitch, is nearly in-phase with the wing motion which, according to figure 3, eliminates the induced downwash. The wing displacement slightly leads that of the control due to the wing-tail separation distance. An illustration of the gain in flutter margin obtained from both the analytical and experimental models is illustrated in figure 7. For the relatively high damping values (g = 0.05) found for the model structural modes, this represents over a 40% increase in flutter speed. Figure 8 illustrates that the flutter speed could be easily increased by another 50% if the sensor or accelerometer had been placed in a more optimal position such as on the wing instead of the tail.

All these preliminary studies employed an assumed form of control law, originally introduced by Nissim in reference 4, and utilized a parameter optimization procedure to select the control law coefficients which maximized the flutter speed. Details on this analysis can be found in reference 5.

One additional comment is in order concerning the aerodynamic modeling employed in this and the following studies. Both the semirigid and AFFDL model are half-span models; this considerably reduces the model cost and complexity of wind-tunnel installation and testing. These simplifying gains, however, result in the assumption that the model fuselage (in the semirigid case) and the wind-tunnel wall in the AFFDL configuration represents a reflecting plane through which no flow penetrates. In the lifting surface codes employed for the flutter analysis, this requires a symmetric mode input option into the study since the image system is performing a symmetric motion to satisfy the flow boundary condition. This should not lead to any serious problems since no attempt is made here to model a specific configuration where the actual wing-tail flutter mode is found to be antisymmetric.

ANALYTICAL DESIGN STUDIES ON AN ACTIVELY CONTROLLED AFFDL WING-TAIL FLUTTER MODEL

On the basis of the preliminary findings from the semirigid wing-tail model, further analysis seemed justified on a more complex flutter model of similar configuration. The AFFDL wing-tail flutter model had been extensively studied in the wind tunnel and its passive flutter characteristics well documented in reference 2. It was therefore chosen as the best candidate for further investigation. A flutter suppression design based upon optimal control principles and an approximate transient aerodynamic analysis was rejected as being too complex for the present study. Instead a frequency domain design analysis was carried out where the coefficients in an assumed form of control law were determined by parameter optimization procedures. The design study employed the standard V-g method of flutter analysis as well as the aerodynamic energy and Vector Nyquist concepts. Following the work of Nissim in reference 4, an assumed feedback control law was taken of the form

$$\{\delta\} = [C_R + iC_I]\ \{q\} = [C]\ \{q\} \tag{1}$$

where $\{\delta\}$ is a vector representing the displacements of the active aerodynamic control surfaces; $\{q\}$, the complex vector of generalized coordinates defining the motion of the main lifting surfaces; and $[C_R + iC_I]$, a complex matrix relating the motion of the main lifting surfaces to that of the control surfaces. The [C] matrix is the assumed form of feedback control law and its elements may be a function of the frequency or reduced frequency of motion as well as other parameters defining the flight envelope. This assumed feedback control law also implies that all the system generalized coordinates must be observed. This is not practical or even necessary in most cases. Consequently the outputs from a discrete set of motion sensors are related to the generalized coordinates defining the system motion by

$$\{Z\} = [F]\ \{q\} \tag{2}$$

where $\{Z\}$ is a complex vector representing the sensor outputs and [F] is a matrix representing the displacement of the sensors for unit values of the generalized coordinates. The matrix [F] defines the sensor locations and ideally selects or isolates out only those generalized coordinates in the flutter analysis that are important to the flutter suppression system design. Since the number of sensors required in the flutter suppression system are in practice much less than the number of generalized coordinates, the matrix [F] will be singular and the more practical control law expressible in the form

$$\{\delta\} = [\bar{C}_R + i\bar{C}_I]\ \{Z\} \tag{3}$$

or

$$\{\delta\} = [\bar{C}_R + i\bar{C}_I]\ [F]\ \{q\} = [C'_R + iC'_I]\ \{q\} \tag{4}$$

This may be incorporated into the standard flutter equation as

$$[K]^{-1}\ \{[M] + [Q] + [Q_c]\ [C'_R + iC'_I]\}\ \{q\} = \frac{(1+ig)}{\omega^2}\ \{q\} \tag{5}$$

where [K] and [M] are the generalized stiffness and mass, respectively, of the structure; [Q], the generalized aerodynamic force matrix excluding the contribution of the active controls; and $[Q_c]$, the sum of the generalized aerodynamic forces and inertias due to the active control input. The flutter damping parameter g and flutter frequency ω make up the flutter eigenvalue. In the analytical design study, only M = 0, sea-level conditions were investigated since they represented the anticipated wind-tunnel conditions. Equation (5) was, therefore, solved initially by the standard V-g method employing a parameter optimization technique to determine the control coefficients that maximized the flutter speed for selected configurations of the AFFDL flutter model.

This procedure employed only one active aerodynamic control in the form of a stabilator or aileron control. In addition, the study investigated control

feedback systems employing feedback from all the generalized coordinates as well as from those that could be measured by employing only two and three motion sensors. These sensors were placed in an optimal manner over the model planform to sense the most significant modes contributing to the flutter instability of the model. Details on this analysis can also be found in reference 5.

The accuracy of the analytical modeling on the AFFDL flutter model is illustrated in figure 9 where the experimentally determined flutter speed from reference 2 is superimposed on this figure. The present analysis differs slightly from the computed AFFDL flutter results. This is thought to be due to the different input mode shape procedures followed in the present study. This study utilized basically an external localized least-squares fit to the modal data and input slopes and deflections directly at the one-quarter-chord and three-quarter-chord points of the aerodynamic boxes. This essentially bypassed the global least-squares fit routine in the standard program input format. A slight gain in computational accuracy is anticipated by this procedure. This is further confirmed in figure 10 for a slightly different sweep configuration. The math model is thought to accurately represent the flutter characteristics of the AFFDL wind-tunnel flutter model described in reference 2.

By employing a Nissim form of control law and parameter optimization techniques, a flutter suppression system evolved employing an active stabilator control that increased the system flutter speed above that of the isolated wing. This is illustrated in figures 11 and 12. As indicated in figure 11, this could be accomplished by employing only two motion sensors, one on the wing tip and a second on the tip of the stabilator. It is further indicated here that no significant difference would be obtained even if all the generalized coordinates were measured. Figure 13 illustrates that further gains in flutter margin could be achieved for this configuration if an active aileron control were employed in place of a stabilator. This aileron configuration is illustrated in figure 14. Flutter margins were again improved beyond that of the isolated wing even when employing the same aileron for active control of the isolated wing to gain additional flutter margin. Similar features were found for the 45° sweep configuration. All these preliminary studies were felt to be positive enough to warrant the design of an experimental wind-tunnel flutter program that would check the accuracy of the flutter suppression system design and lend a degree of confidence to the math modeling.

FINALIZED WIND-TUNNEL MODEL DESIGN

As mentioned earlier, the basic model employed in this study is a variation on the AFFDL wing-tail flutter model designed by the Air Force Flight Dynamics Laboratory and discussed in reference 2. Some of the model design details were modified by personnel at The University of Texas at Austin to include an active stabilator control in pitch and a remote control of the wing sweep angle. This model and its installation in the 7 ft by 10 ft wind tunnel at Wichita State University is illustrated in figure 15. The model degrees of freedom include a rigid body roll mode, wing root bending and torsional flexibilities, fuselage torsional flexibility, and fully flexible wing and stabilator modes. In addition, the stabilator could be remotely pitched by means of a

hydraulic actuator to provide a stiff control degree of freedom. The wing could also be remotely swept with a hydraulic actuator to simulate various geometries as well as rapidly convert the flutter model to a stable configuration by quickly sweeping the wing forward, raising the system's flutter speed. This latter feature was added with the hope that in some cases it could suppress undesirable model responses that may occur during critical flutter conditions.

A schematic of the model's hydraulic control supply system, employed to activate both wing sweep and stabilator motions, is illustrated in figure 16. This control system is comprised of three major assemblies: the hydraulic power supply module, the servo control module, and the model hydraulic actuator system designated respectively as (a), (b), and (c) in the schematic. These components are also illustrated in figure 17. The hydraulic power supply module is built around an Everpac Model PA-101 air driven hydraulic pump obtained without charge from government surplus. The pump provides a flow of 7.647 cm^3/sec (0.467 in^3/sec) at 690 N/cm^2 (1000 psi) which is the normal working pressure of the system. Due to the relatively small capacity of the self-contained reservoir within the pump, an additional reservoir was installed in the hydraulic return line. The hydraulic power supply module also provides, to both the wing sweep system and the stabilator sweep system, backup accumulators charged to 345 N/cm^2 (500 psi) with nitrogen. These accumulators further serve to attenuate fluctuations in line pressure caused by pulsations of the pump or head pressure.

The servo control modules are mounted atop and outside the wind tunnel next to the model to minimize line lag effects to the model control actuators. This module provides terminal points for the servovalve electronics and houses two surplus Moog Model 971A servovalves rated at 18.03 cm^3/sec (1.1 in^3/sec) at 8 mA. These servovalves are employed to activate two Clippard Minimatic 7DD-1 double-acting actuators driving the wing sweep and stabilator motions. One end of the actuator rods is attached to a linear variable differential transformer (LVDT) which provides for precise control of the stabilator pitch and wing sweep angle while the other end drives the linkage motion. Signals to the wing sweep servoamplifier include the wing sweep control signal, position feedback from the wing sweep LVDT, and a dither signal to keep the valve free of sediment and improve transient response. Signals to the stabilator pitch servoamplifier include the conditioned transducer signals, position feedback from the stabilator pitch LVDT, and the dither signal.

The control feedback avionics, developed as a part of the flutter suppression system, are illustrated in figure 18. An analog control was developed due to the expense and complexity of digital systems. The avionics for the stabilator pitch control include printed circuit modules for input control and amplification, integration, and phase shifting. It allows for up to three channels of output which can command up to three separate aerodynamic surfaces. The unit can monitor signals from accelerometers, velocity pickups, and/or strain gages mounted at select positions on the model and blend these according to a preselected control law. The modular grouping of the different circuits in this manner permits the programing of a variety of control laws.

Chains of inexpensive high-input impedance operational amplifiers, which

constitute the basic elements of analog computers, were put together to perform the required control functions. EGC 941 M op amps were first breadboarded into functional blocks and tested to determine component values for best performance. Continuing the concept of functional blocks, modular construction was adopted in the layout of the model control panel thus enabling quick replacement of defective circuits and testing on a modular basis. Other benefits of modular construction were realized including ease in circuit modification and construction, as well as circuit substitution if desired. This system's approach to circuit design is discussed in reference 6 and greatly extends the capabilities of the design engineer who is faced with problems in the active control technology area.

VIBRATION AND FLUTTER STUDIES

In an attempt to obtain the most accurate math modeling for the study, experimental inputs were utilized in the analysis whenever practical. This included measurements of vibration modes, frequencies, and generalized masses for the first five modes of the system. Table I illustrates a comparison of the first five modal frequencies measured on the present model at a 60° sweep configuration with one of the models described in reference 2. Attempts were also made to measure the model's first five generalized masses following the procedures outlined in reference 7. The results of this study are illustrated in figure 19. An alternate study is currently in progress to make direct mass measurements that can hopefully be correlated with these data. The generalized mass data appear reasonable except possibly for the third mode which was difficult to excite in a clean responsive manner. Further studies are in progress to completely define the structural dynamic characteristics of the model as accurately as practical for several sweep configurations.

By mid-December 1974 the basic model design and fabrication had been completed to the point that an uncontrolled two-day flutter test was possible. These initial tests were conducted at the Walter H. Beech Memorial Wind Tunnel on the campus of Wichita State University, Wichita, Kansas. The test program provided basically a checkout of the model instrumentation and structural integrity in addition to a flutter data point that could be correlated with the computed flutter point provided by our math model. The uncontrolled model fluttered spontaneously at 70 meters per second (230 ft/sec) at a frequency of 8 Hz in the classical wing-tail flutter mode, whereas the model of reference 2 had a flutter speed of approximately 39 meters per second (230 ft/sec). Flutter was suppressed without damage to the model by a reduction of dynamic pressure in the wind tunnel. These results confirmed that the frequency range of unstable model responses lies well within the 0 to 15 Hz levels for which satisfactory preliminary checkouts have been made on the model control system. Finalized checkouts are currently being made on the model's overall control response characteristics to define completely the control transfer function.

CONCLUDING REMARKS

The preliminary findings obtained from the current study indicate that an active aerodynamic control in the form of a stabilator or aileron can be highly effective in suppressing subsonic wing-tail interference flutter. Flutter margins can be restored to at least that of the isolated wing by employing control gains and phasings utilizing parameter optimization techniques. The doublet lattice lifting surface theory was found to be adequate for predicting this flutter phenomenon as observed in the wind tunnel. Additional wind-tunnel studies are needed on the modified AFFDL wing-tail flutter model, however, to accurately assess the math modeling techniques employed in the present study for designing flutter suppression systems. One such test program is planned for the near future. Preliminary wind-tunnel studies have been carried out on the uncontrolled flutter model developed in the present study. The results verified the structural integrity of the model for the more advanced testing programs and provided a checkout of the instrumentation and a data point for correlation with our math model. Recent electronic developments in the form of both analog and digital modular devices at extremely low costs have brought many of the problem solutions in the active control technology area to within both the technical and economical grasp of the academic researcher as well as the alert designer.

REFERENCES

1. Topp, L.J., Rowe, W.S., and Shattuck, A.W.: Aeroelastic Considerations in the Design of Variable Sweep Wing Airplanes. ICAS/RAES, Sept. 1966, pp.1-25.

2. Mykytow, W.J., Noll, T.E., Huttsell, L.J., and Shirk, M.H.: Investigations Concerning the Coupled Wing-Fuselage-Tail Flutter Phenomenon. Journal of Aircraft, Vol. 9, No. 1, Jan. 1972, pp. 48-54.

3. Shelton, J.D., Tucker, P.D., and Davis, J.C.: Wing-Tail Interaction Flutter of Moderately Spaced Tandem Airfoils. AIAA Paper No. 69-57, AIAA 7th Aerospace Sciences Meeting, New York, Jan. 20, 1969.

4. Nissim, E.: Flutter Suppression Using Active Controls Based on the Concept of Aerodynamic Energy. NASA TN D-6199, 1971.

5. Cwach, E., and Stearman, R.: Suppression of Flutter on Interfering Lifting Surfaces by the Use of Active Controls. AIAA Paper No. 74-404, AIAA/ASME/SAE 15th Structures, Structural Dynamics and Materials Conference, April 17-19, 1974.

6. Sheingold, D.H.: Nonlinear Circuits Handbook. Analogue Devices Inc., Norwood, Massachusetts, 1974.

7. Able, I.: A Wind Tunnel Evaluation of Analytical Techniques for Predicting Static Stability and Control Characteristics of Flexible Aircraft. NASA TN D-6656, 1972.

TABLE I

MODAL FREQUENCIES
60° SWEEP CONFIGURATIONS

MODE NUMBER	AFFDL MODEL REF. 2 Hz	MODIFIED AFFDL MODEL PRESENT STUDY Hz
1	0.90	1.46
2	3.9	3.82
3	8.1	7.89
4	13.9	16.93
5	17.1	21.90

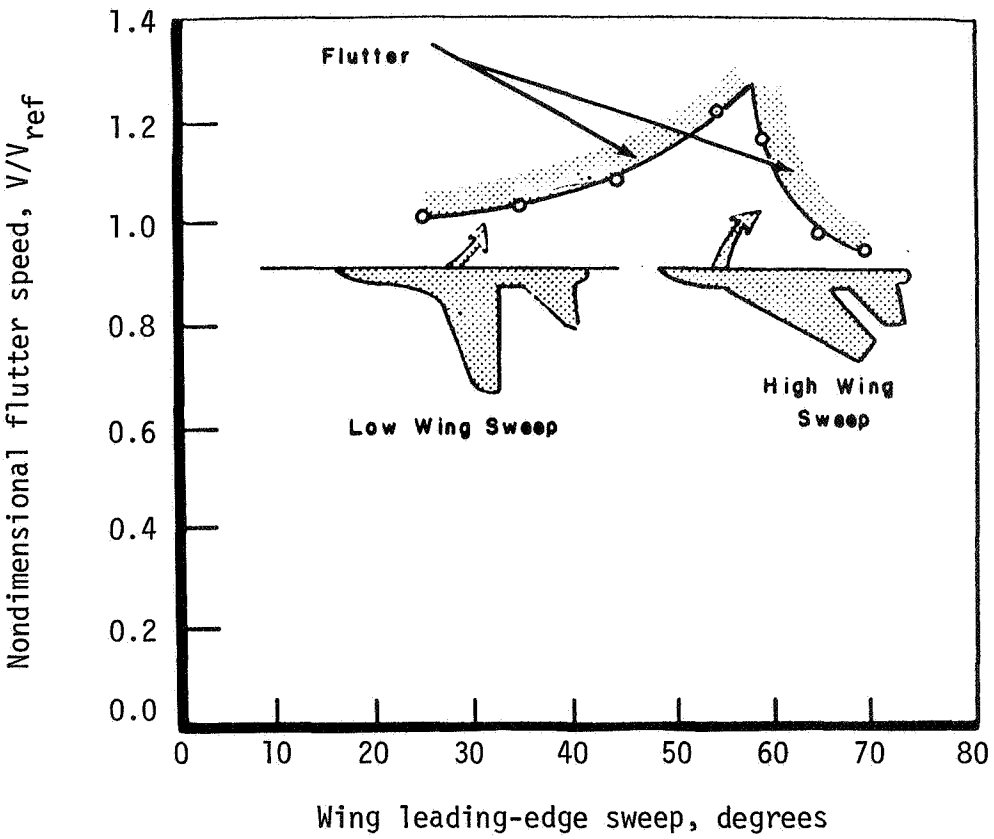

Figure 1.- Composite flutter boundary illustrating critical interference flutter condition for large sweep angles. (From reference 1.)

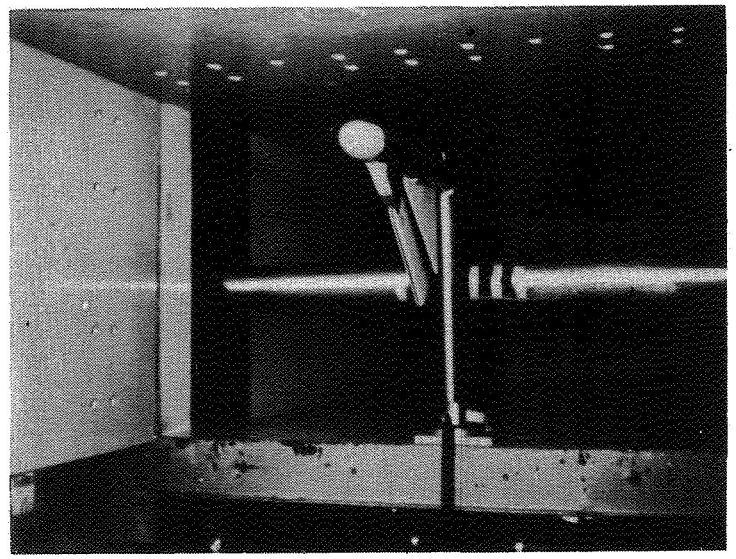

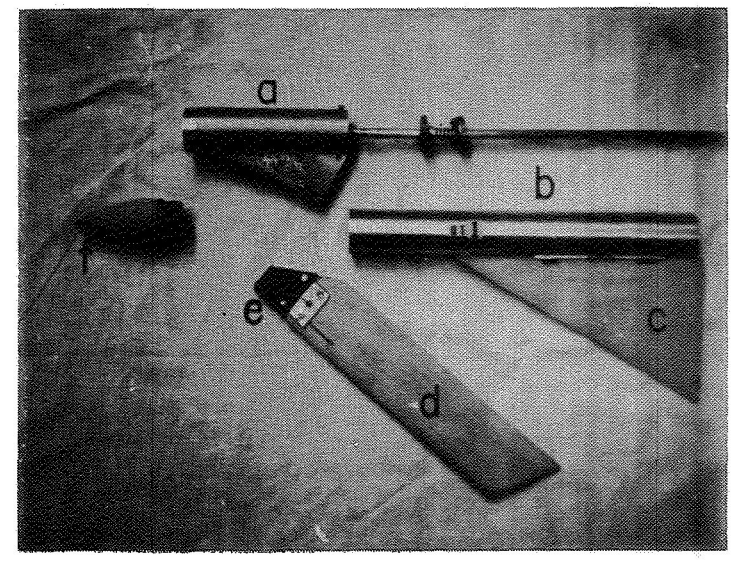

Figure 2.- Semirigid wing-tail flutter model. Construction details and installation in 3 ft by 4 ft wind tunnel.

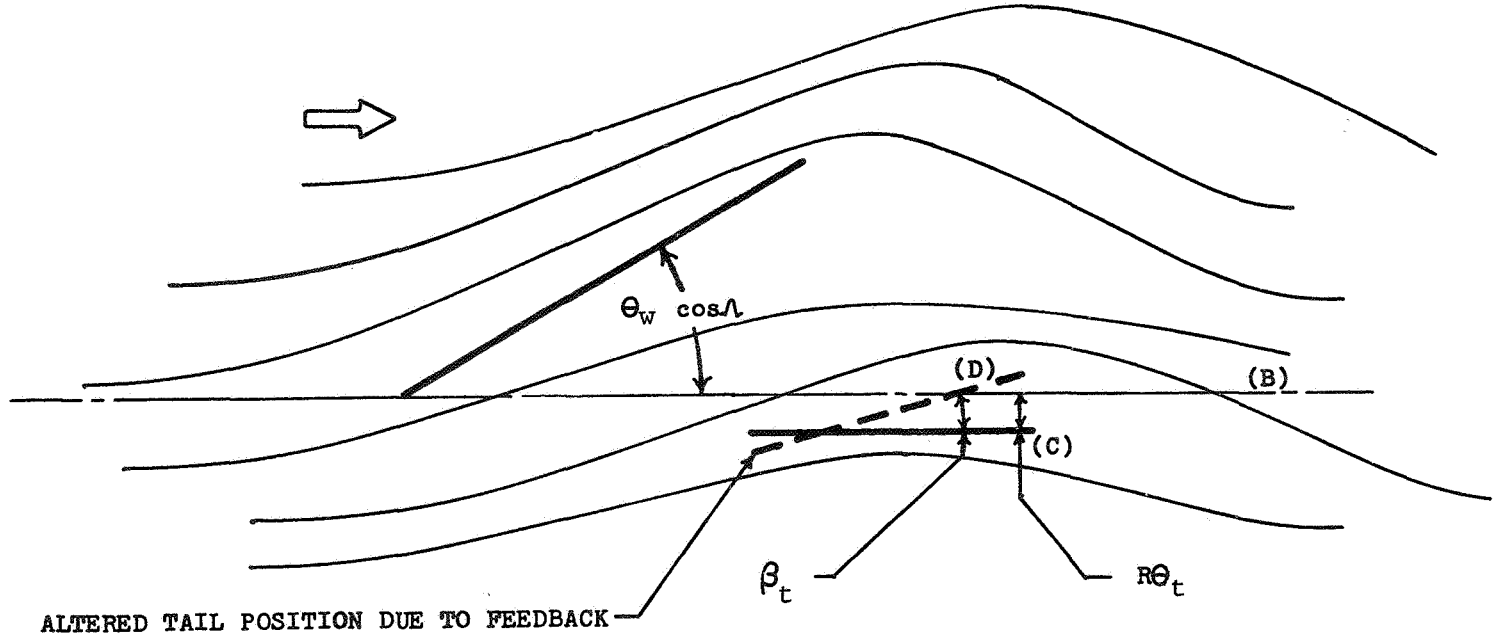

Λ = Wing sweep angle
R = Distance from central axis to typical section
θ_w = Wing flap angle
θ_t = Tail flap angle
β_t = Stabilator pitch angle

Figure 3.- Typical section flow field for wing-tail flutter model.

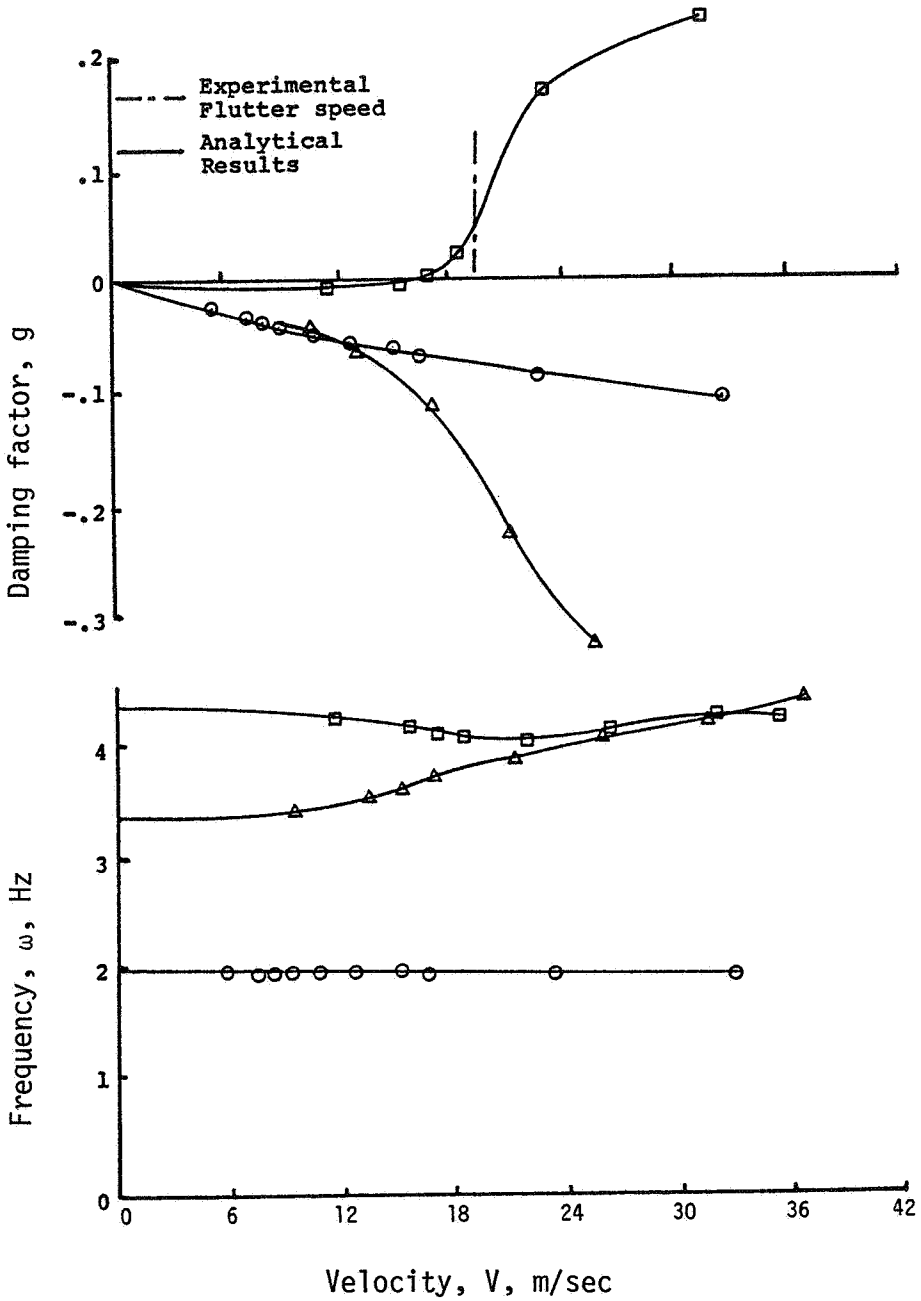

Figure 4.- Semirigid wing-tail model. Uncontrolled flutter speeds (open loop). 60° sweep configuration and approximately 1/4 wing chord separation distance between wing and tail; M = 0; sea-level conditions.

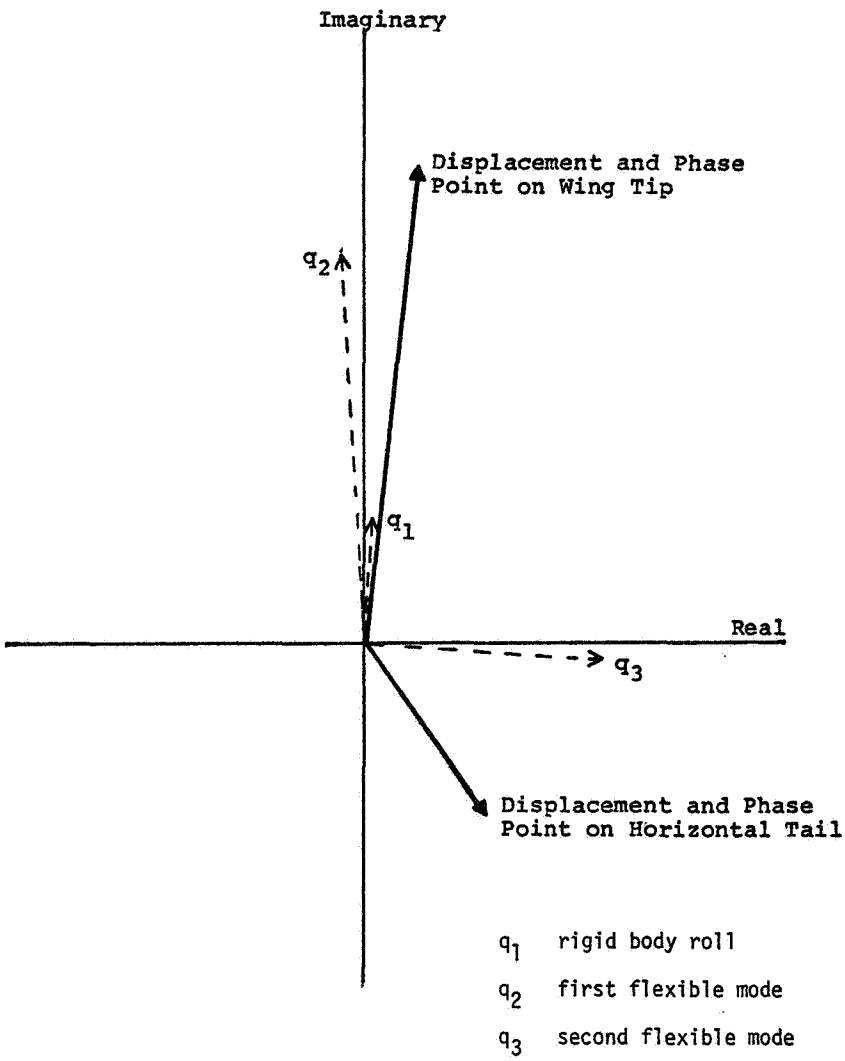

Figure 5.- Computed displacement and phase relationships in open loop flutter mode of semirigid wing-tail model. 60° sweep configuration and approximately a 1/4 wing chord separation distance between wing and tail; M = 0; sea-level conditions.

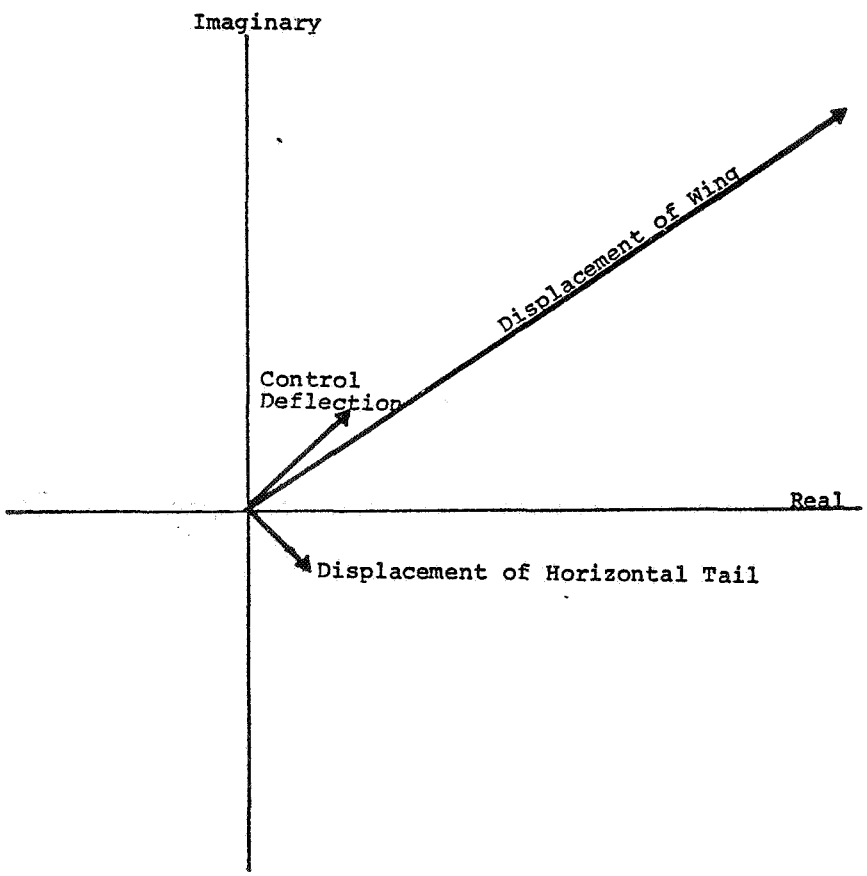

Figure 6.- Computed phase relationships between wing, tail, and control surface for controlled semirigid wing-tail model (sensor located on horizontal tail). 60° sweep configuration and approximately a 1/4 wing chord separation distance between wing and tail; M = 0; sea-level conditions.

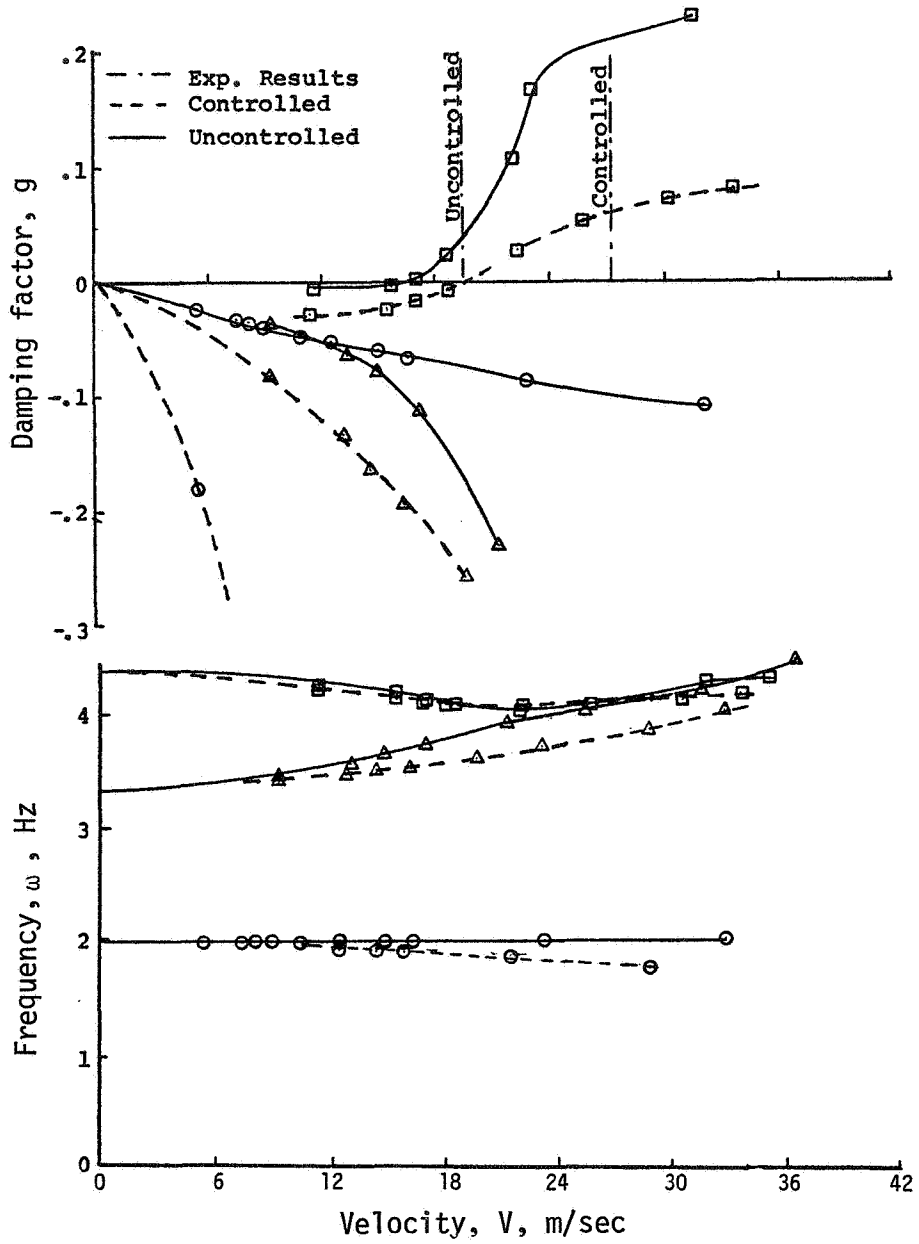

Figure 7.- Semirigid wing-tail model controlled and uncontrolled flutter speeds (experimental and computed). 60° sweep configuration and approximately a 1/4 wing chord separation distance between wing and tail; M = 0; sea-level conditions.

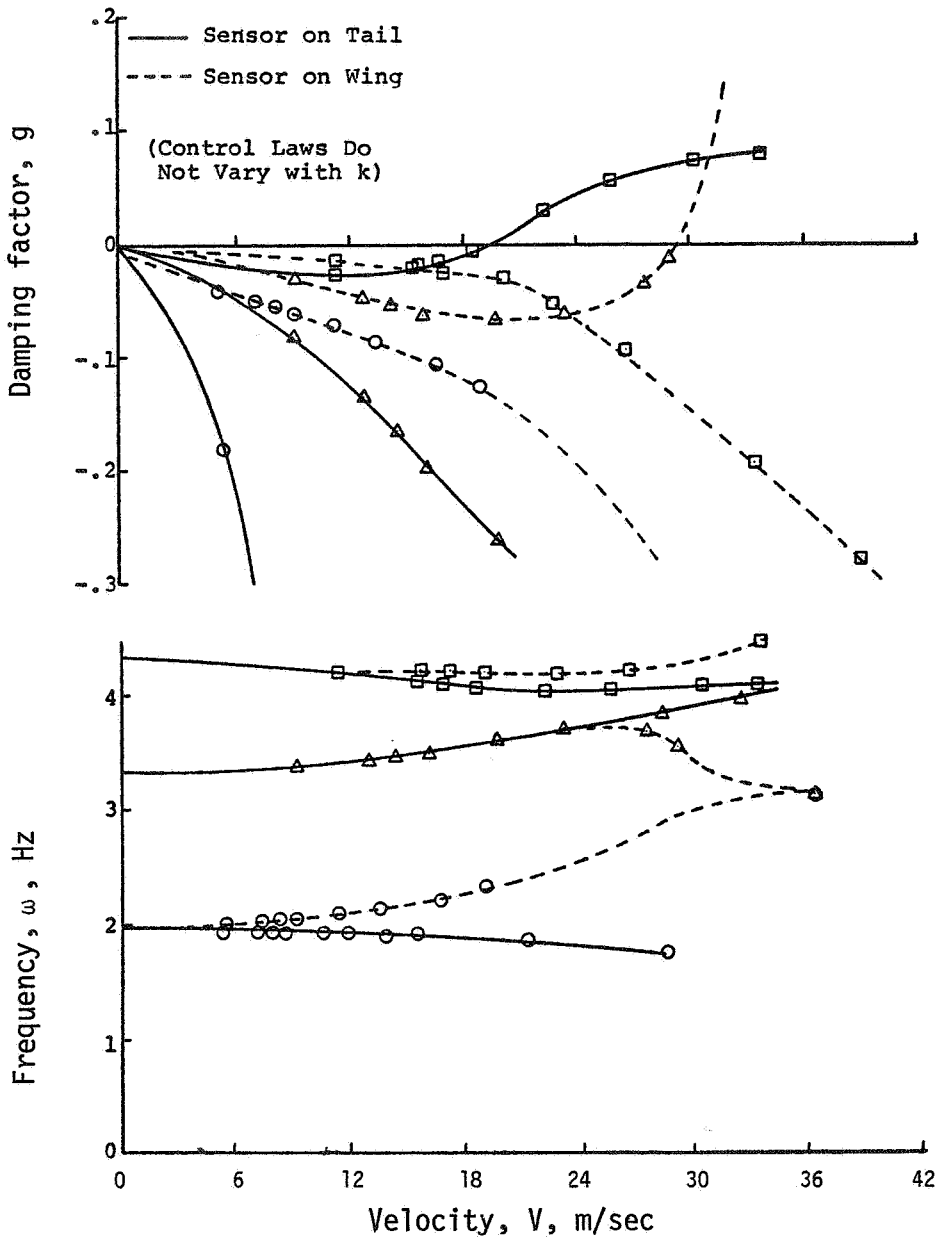

Figure 8.- Comparison of semirigid controlled model flutter results with sensor mounted on tail and wing.
M = 0; sea-level conditions.

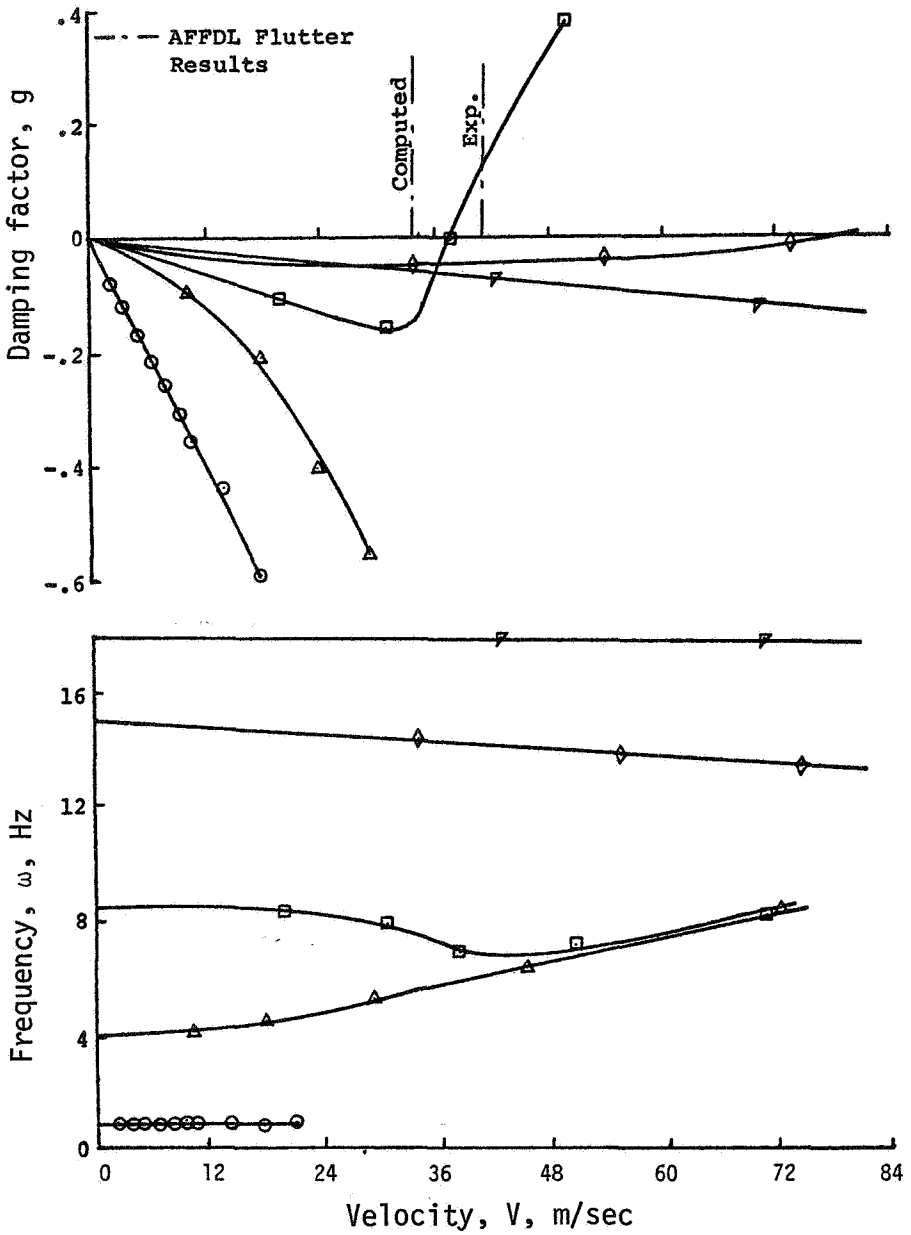

Figure 9. AFFDL model. Uncontrolled flutter speed; 60° wing sweep; M = 0; sea-level conditions.

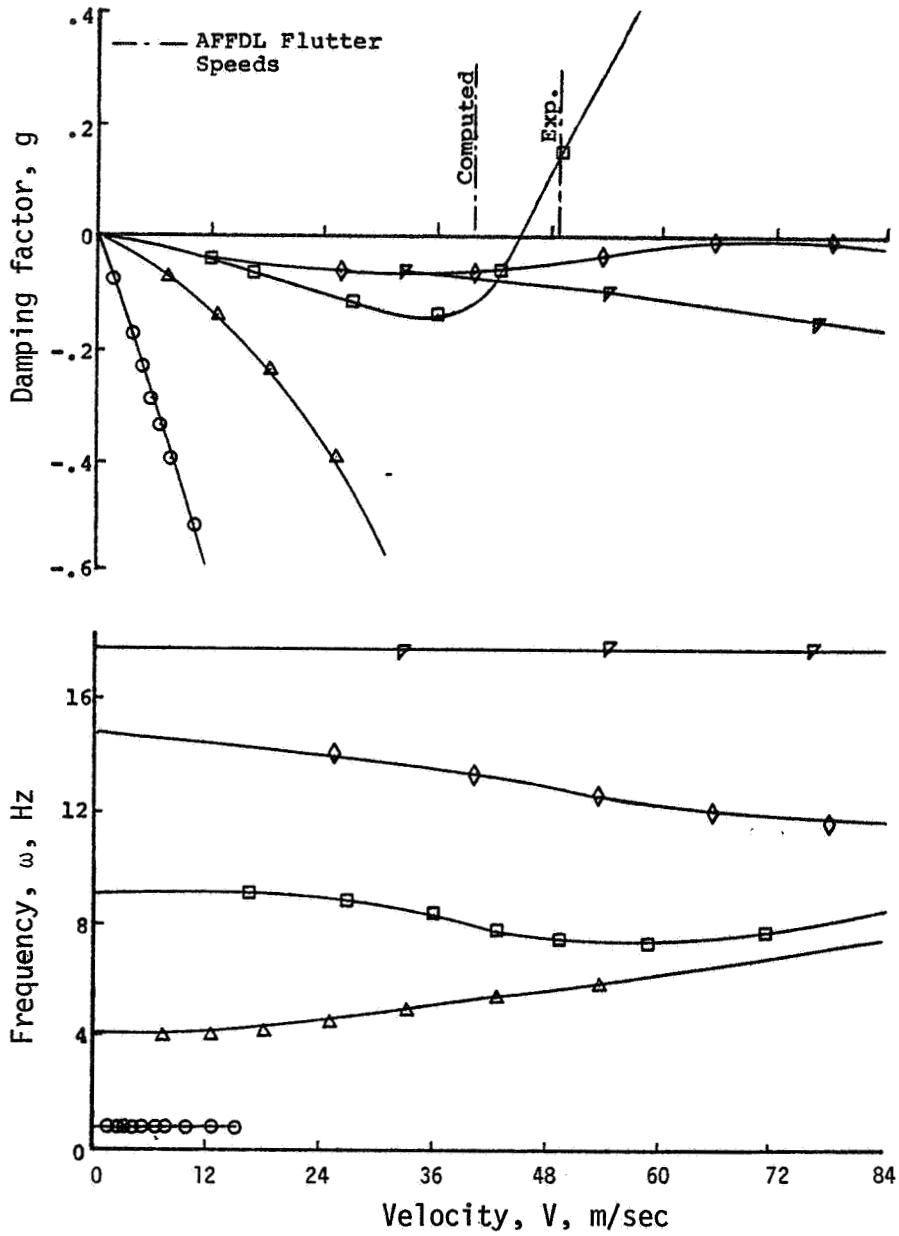

Figure 10. AFFDL model. Uncontrolled flutter speed; 45° wing sweep; M = 0; sea-level conditions.

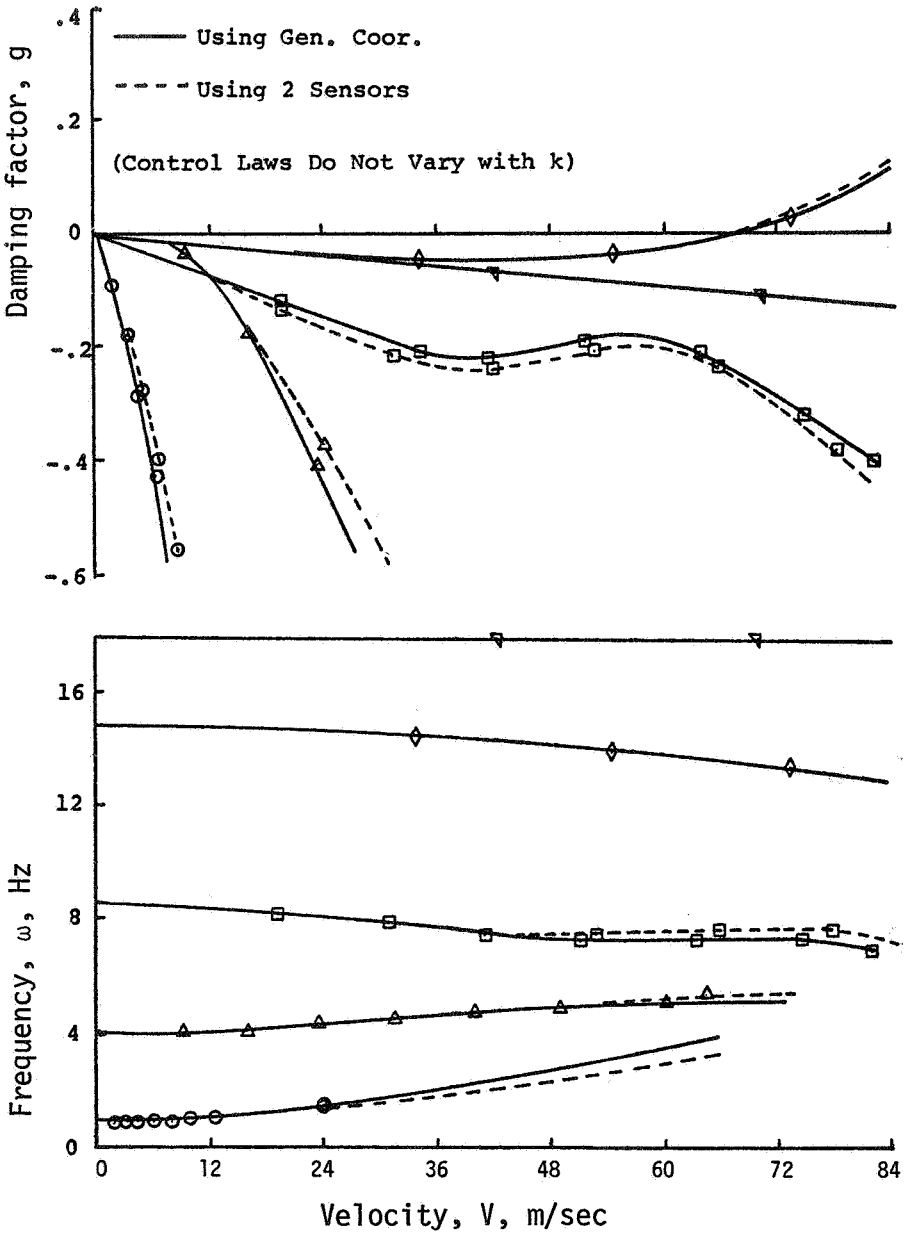

Figure 11. Comparison of flutter speeds on AFFDL model when using generalized coordinates and two sensors in control law (one sensor located near the outer wing tip trailing edge and one near the stabilator tip leading edge). 60° sweep configuration; active stabilator control; M = 0; sea-level conditions.

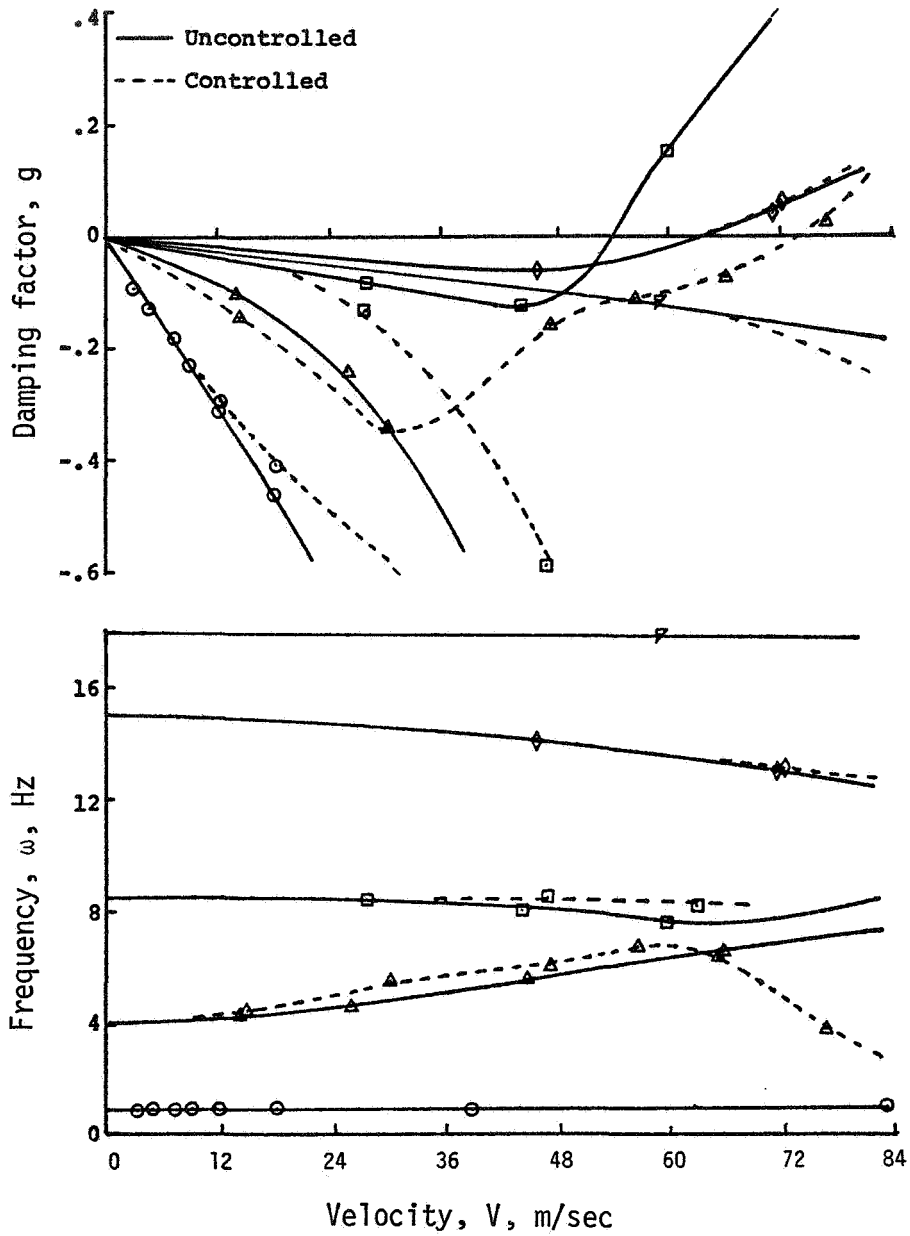

Figure 12.- Increase in flutter speed of isolated wing of AFFDL model. 60° sweep configuration; aileron is active control using generalized coordinates in control law; M = 0; sea-level conditions.

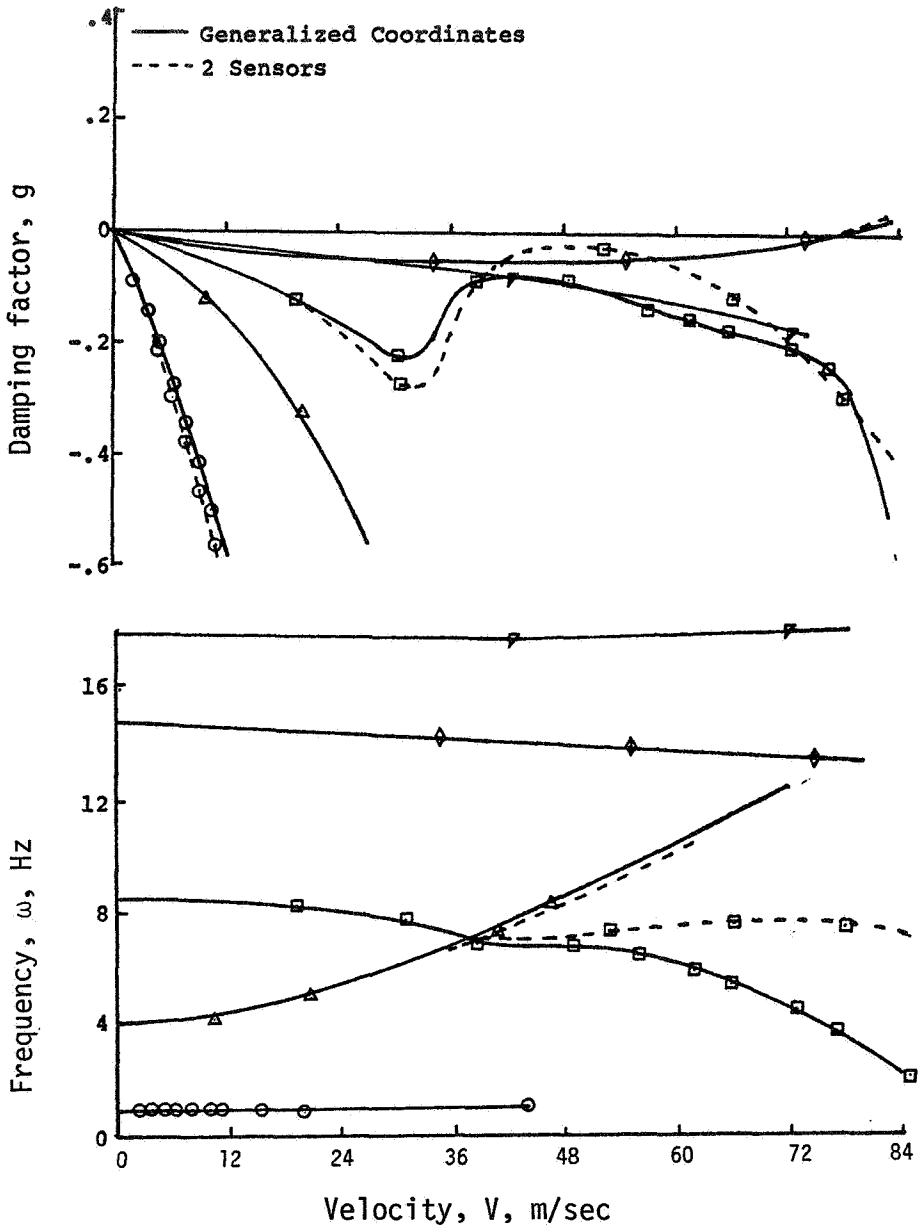

Figure 13.- Comparison of flutter speeds of AFFDL model using generalized coordinates and two sensors in control law (both sensors located on wing at 35% of local wing chord, one near the tio and one at the root chord). 60° sweep configuration; active aileron control; M = 0; sea-level conditions.

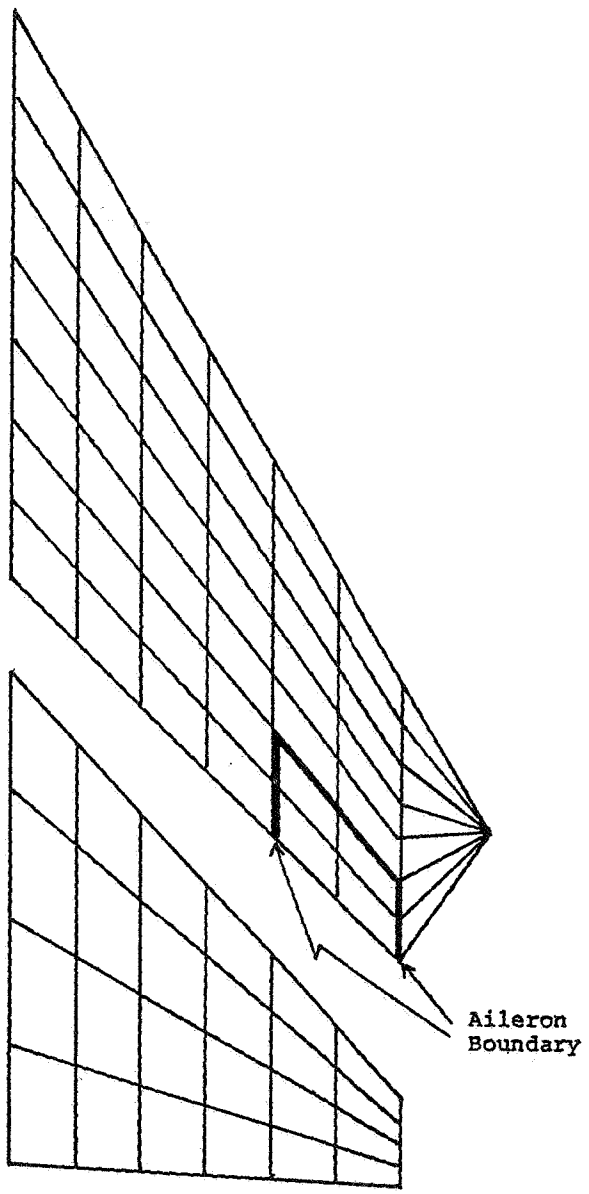

Figure 14.- Aerodynamic modeling for aileron on AFFDL model with 60° sweep.

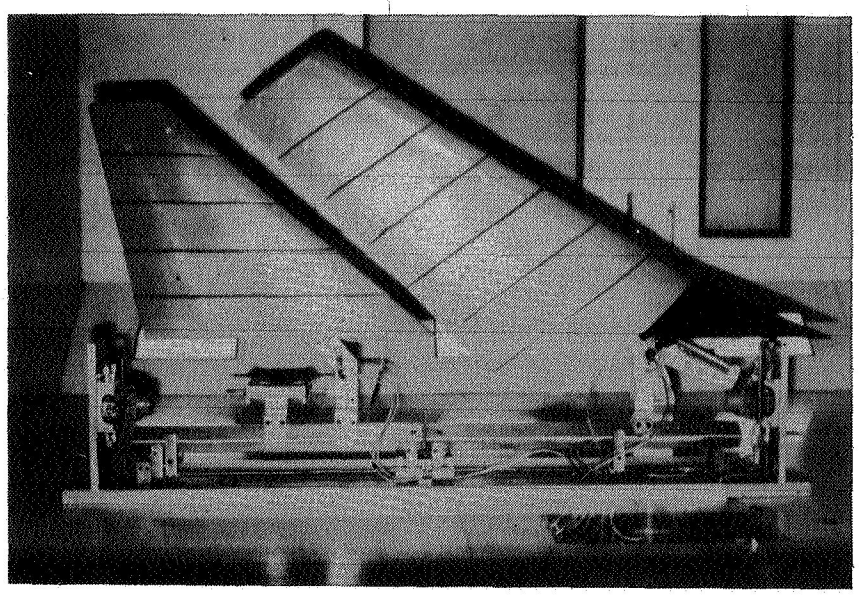

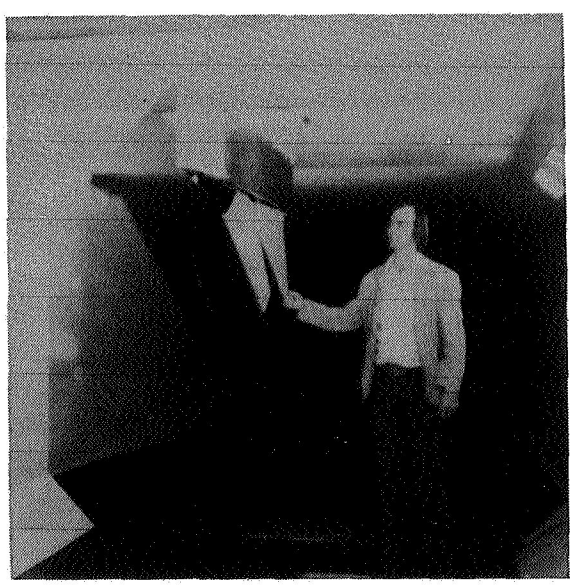

Figure 15.- Installation of modified AFFDL wing-tail flutter model in 7 ft by 10 ft subsonic wind tunnel.

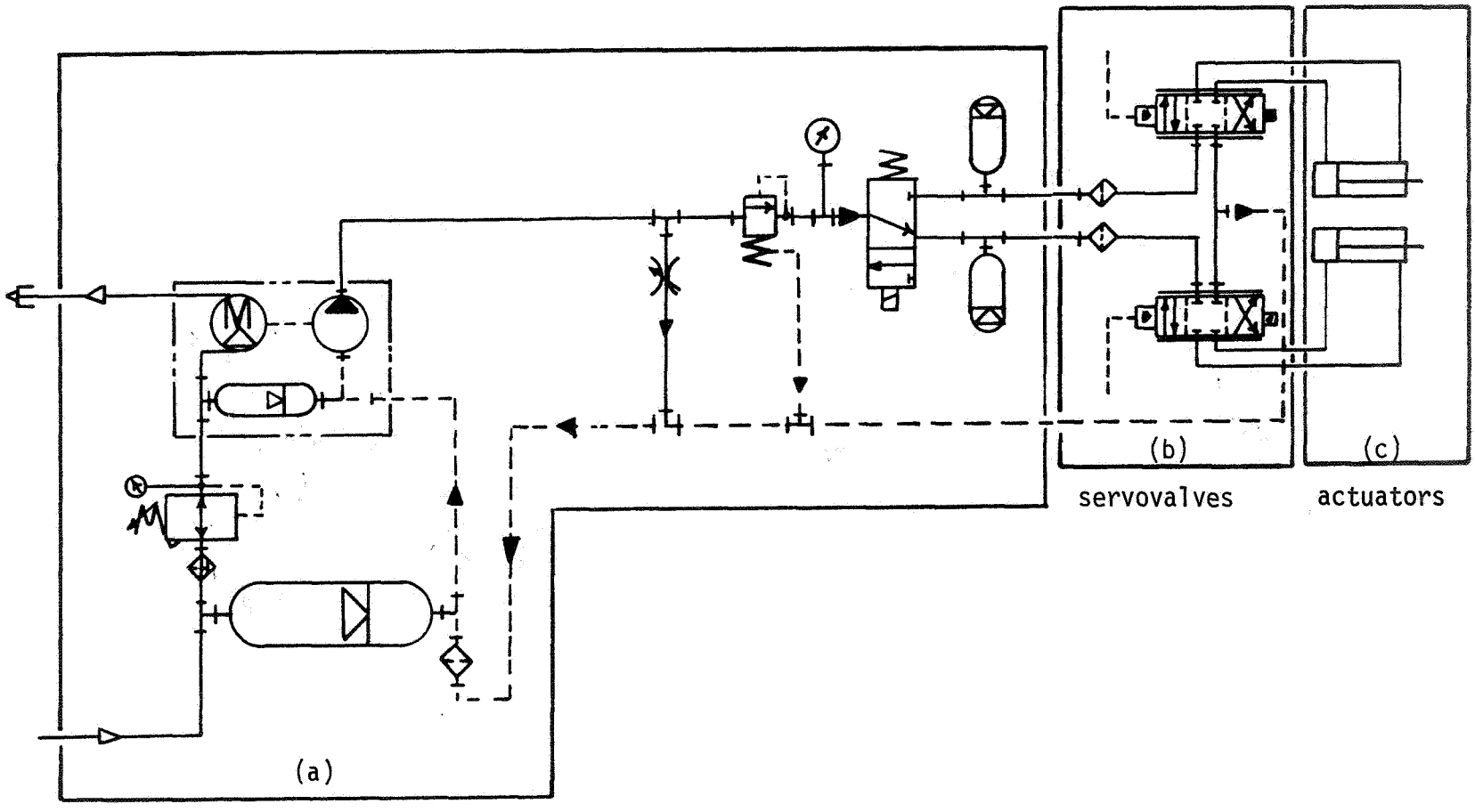

Figure 16. Schematic of hydraulic control systems for modified AFFDL wing-tail flutter model.

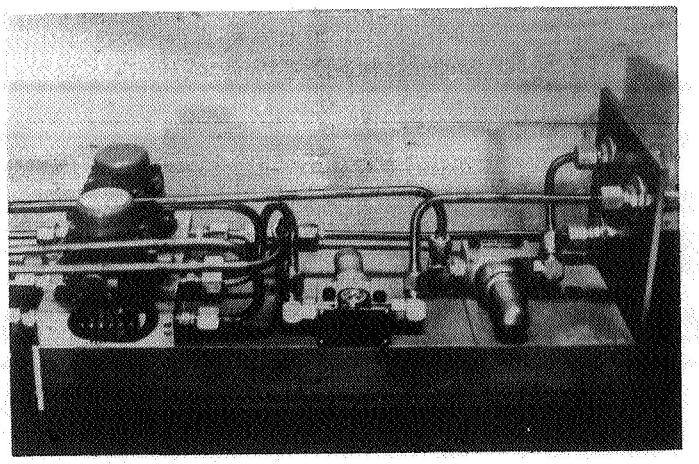

Servovalves

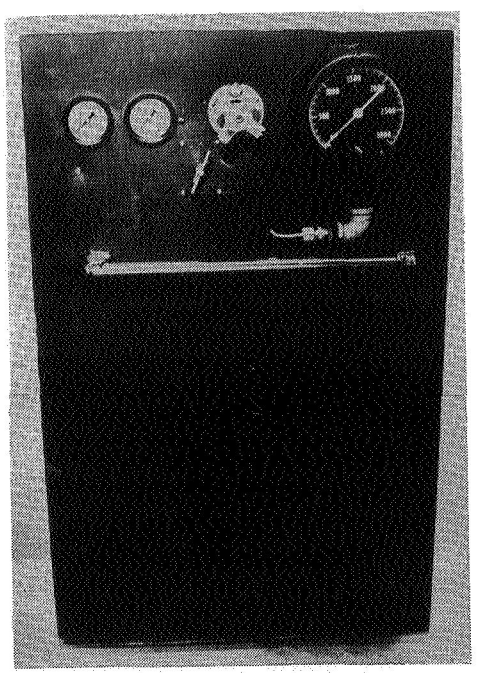

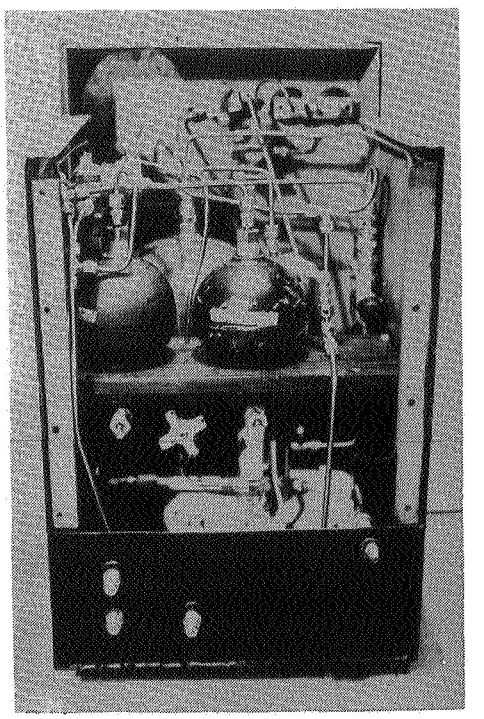

Hydraulic power supply

Figure 17.- Hydraulic power supply and servovalves for modified AFFDL wing-tail model.

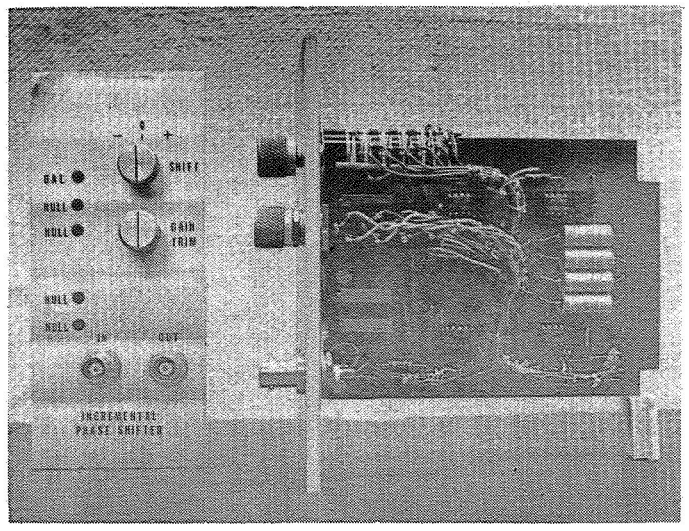

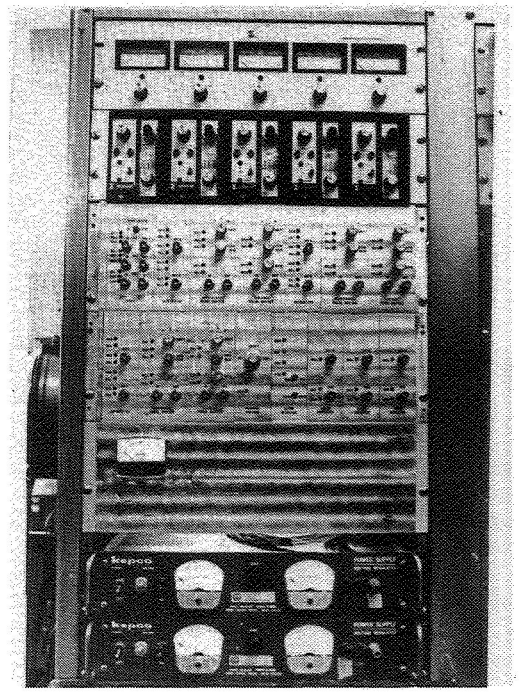

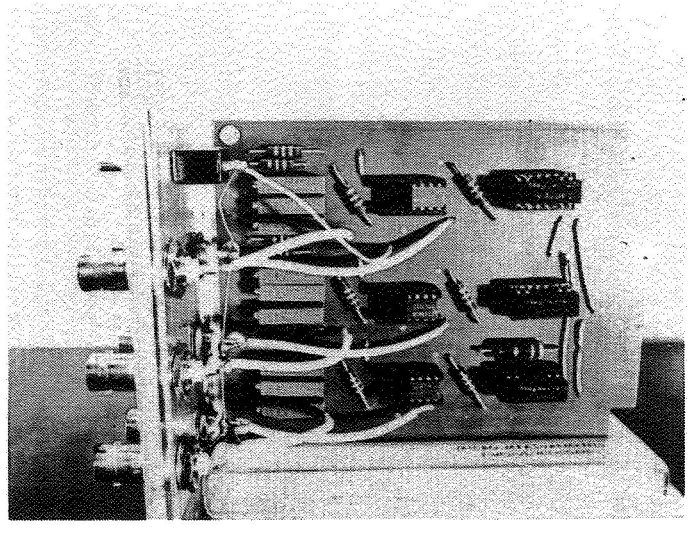

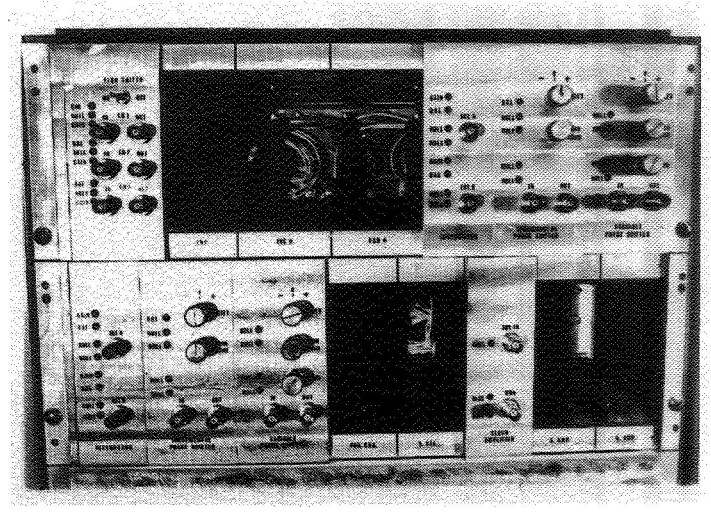

Figure 18.- Control feedback avionics for modified AFFDL wing-tail model. Small operational amplifiers illustrated along with modular units for performing various required control functions.

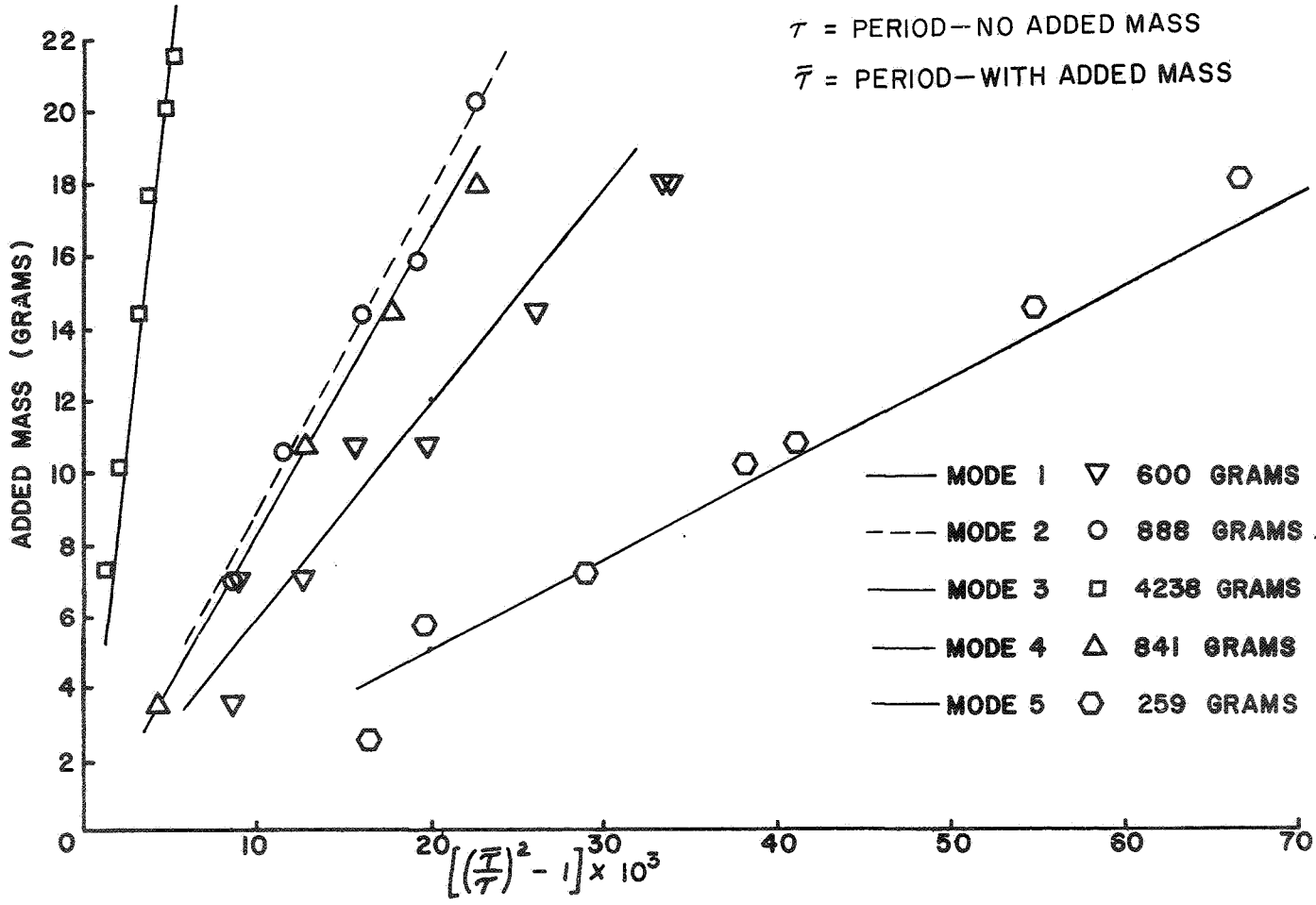

Figure 19.- Generalized mass measurements.

CORRELATION WITH FLIGHT OF SOME AEROELASTIC MODEL STUDIES IN THE NASA LANGLEY TRANSONIC DYNAMICS TUNNEL*

Wilmer H. Reed III

NASA Langley Research Center

SUMMARY

The NASA Langley transonic dynamics tunnel, which has a variable density Freon-12 (or air) test medium, was designed specifically for the study of dynamics and aeroelastic problems of aerospace vehicles. During the 15 years of operation of this facility, there have been various opportunities to compare wind-tunnel and flight-test results. Some of these opportunities arise from routine flight checks of the prototype; others, from carefully designed comparative wind-tunnel and flight experiments. This paper brings together in one place a collection of such data obtained from various published and unpublished sources. The topics covered are: gust and buffet response, control surface effectiveness, flutter, and active control of aeroelastic effects. Some benefits and shortcomings of Freon-12 as a test medium are also discussed. Although areas of uncertainty are evident and there is a continuing need for improvements in model simulation and testing techniques, the results presented herein indicate that predictions from aeroelastic model tests are, in general, substantiated by full-scale flight tests.

INTRODUCTION

At the time the forerunner of this symposium (Symposium on Flight Flutter Testing held in Washington, D.C., May 1958) was held 17 years ago, a new transonic wind tunnel was nearing completion at NASA Langley Research Center. Designated the Langley transonic dynamics tunnel (TDT), it has served, since becoming operational in 1960, as a National facility devoted exclusively to work on dynamics and aeroelasticity problems of aircraft and space vehicles in the transonic speed range.

An essential difference between the TDT and wind tunnels employed primarily in steady-state aerodynamic investigations stems from the scaling requirements which must be satisfied in aeroelastic model studies. For example, in addition to the need for adequate simulation of the aerodynamic flow field about the model, it is also necessary that the model stiffness, mass, and inertia properties simulate those of the full-scale structure and that the ratio of structural

*This paper is essentially the same as a presentation entitled "Comparison of Flight Measurements With Predictions From Aeroelastic Models in the NASA Langley Transonic Dynamics Tunnel," by Wilmer H. Reed III, presented at the 46th AGARD Flight Mechanics Panel Symposium on Flight/Ground Facility Correlation, Valloire, France, June 9-12, 1975.

density to test-medium density be the same for model and full scale. To aid in satisfying these requirements, the TDT uses a variable-density test medium of either air or Freon-12. The primary test medium, Freon-12, is four times as dense as air and has a speed of sound about one-half that of air; thus heavier and less expensive models may be used and the tunnel power requirements reduced. Some main features of the facility are indicated in figure 1.

Experimental aeroelastic research also imposes demanding requirements for specialized testing techniques. A review of such testing techniques developed by the staff of the Langley transonic dynamics tunnel for use in studies of various stability, control, and response characteristics of elastic aircraft is given in reference 1.

From time to time during the 15-year period of operation of this facility, there have been various opportunities to compare the results from wind-tunnel and flight tests. Some of these opportunities arise from routine flight checks of the prototype, others from carefully designed comparative wind-tunnel and flight experiments. This paper brings together in one place a collection of such data, gleaned from various published and unpublished sources, for the purpose of addressing the question: How well can dynamically scaled aeroelastic models, tested in a Freon-12 wind-tunnel environment, predict the behavior of their full-scale counterparts in flight? To this end, some advantages and shortcomings of Freon-12 as a wind-tunnel test medium are considered and then selected comparisons between wind-tunnel and flight tests in areas relating to dynamic response, static aeroelasticity, flutter, and active-controls research are presented.

AIR-FREON COMPARISONS

Before comparing test results obtained in the Langley transonic dynamics tunnel with flight data, a few comments are in order on air-Freon data comparisons since, by far, most of the tests conducted in this facility make use of a Freon-12 test medium. (Air can also be used as a test medium.) Freon-12 has several characteristics which make it a very attractive test medium for scaled dynamic model studies. Some of the more important properties at atmospheric pressure and temperature are compared with those of air in table I. The most advantageous characteristics are the high density and low speed of sound of Freon-12 relative to air at the same pressure and temperature. The relatively low speed of sound is significant for several reasons. For dynamic model tests in which the reduced-frequency scaling parameter $\omega b/V$ must be satisfied, the lower tunnel speed for a given Mach number reduces directly all pertinent frequencies and, consequently, simplifies instrumentation problems and reduces inertia loads. For tests involving rotating helicopter blades where model and full-scale tip Mach numbers must be the same, the stresses and hence the difficulties of fabrication are reduced. For flutter and other dynamic tests, where the ratio of structural-density to test-medium density must be the same for the model as the airplane, the more dense Freon-12 permits heavier models to be constructed. This is a distinct advantage when the difficulty of fabricating models light enough to simulate the mass characteristics of aircraft designs with composite structures and active controls operating at high speeds

and low altitudes is considered. The use of Freon-12 as a test medium allows the simultaneous satisfaction of both Mach number and Froude number for those instances where both compressibility and gravitational effects must be scaled. For Froude number similarity, an approximately 1/5-scale model is required. An additional benefit is that, for a given model size, test conditions of equal Mach number and stagnation pressure produce a Reynolds number in Freon-12 approximately three times that in air. Finally, since the power required to operate a wind tunnel at a given Mach number varies directly as the cube of the velocity, the use of Freon-12 offers a considerable savings in power.

The principal uncertainty associated with the use of Freon-12 as a test medium is the fact that its specific heat ratio γ is not the same as that for air (1.13 as compared with 1.4), so that quantitative differences exist between the compressibility relations for air and Freon. There have been numerous studies of the degree to which data obtained from tests in Freon-12 can be utilized to predict flow characteristics, structural response, or stability in air (refs. 2 to 5). For example, in references 2 and 3, the significance of this difference in gas characteristics on static aerodynamic coefficients was studied extensively, and means for converting Freon-12 data to equivalent air values were evaluated. These studies indicated that at subsonic and low supersonic Mach numbers the required corrections were small and that the difference between the converted results by two correction methods, the "transonic similarity rule" and the "streamline similarity rule," were very small. Reference 5 reports the results of an experimental subsonic and transonic flutter investigation of a 45° sweptback wing planform that was tested in air and in Freon-12 in the TDT. Comparisons of data in air and in Freon-12 indicated that for subsonic and transonic Mach numbers, the flutter speed obtained in Freon-12 may be interpreted directly as flutter speed in air at the same mass ratio and Mach number. Without the Freon-12 and air corrections, the Freon-12 data would result in a slightly conservative estimate of the flutter speed.

Although one might infer from these flutter data comparisons that the effect of different ratios of specific heat for air and Freon-12 are insignificant for unsteady aerodynamic forces up to low supersonic speeds, the effect on detailed unsteady pressure distributions has only recently been demonstrated analytically. Figure 2 presents some results of a finite-difference calculation of the pressure distribution on an NACA 64A006 airfoil in air and in Freon-12. The airfoil is oscillating in pitch about the midchord at a low reduced frequency ($k = 0.06$); the Mach number is 0.9. Small oscillations about a nonuniform mean flow field were considered in the calculation which yields a linear potential flow equation with variable coefficients that depend on the steady flow field. (See ref. 6.) The static pressure coefficient C_p and the amplitude and phase angle of the oscillating pressure, $|\Delta C_p|$ and ϕ, respectively, are shown in figure 2 as a function of chordwise location. The rapid change in the steady pressure coefficient C_p near the 65-percent chord location indicates a shock. The principal difference between the Freon-12 and air data is seen to be the locations of the peak unsteady pressures $|\Delta C_p|$ and the values of the phase angle ϕ in the vicinity of the shock. Inasmuch as shock waves and related transonic effects tend to be less severe for three-dimensional than for two-dimensional flow, the effects of γ on three-dimensional configurations may be correspondingly milder than those indicated here. Additional study is needed to further evaluate these effects in unsteady flow.

An experimental study that will partially fulfill this need is planned for the near future. The study will involve the measurement of unsteady pressure distributions on a cropped-tip delta wing oscillating in a pitching and a flapping mode in air and in Freon-12 at comparable Reynolds numbers through the transonic speed range. The model will also have oscillating leading- and trailing-edge control surfaces. This study should provide needed experimental data for evaluating advanced transonic unsteady aerodynamic theories and for evaluating the unsteady flow characteristics of air and Freon-12.

WIND-TUNNEL AND FLIGHT COMPARISONS

This section of the paper presents selected examples showing comparisons of results obtained in the TDT and in flight tests. In all cases Freon-12 was used as a test medium, and the models were dynamically and aeroelastically scaled to suitably match full-scale conditions. The following topics are covered herein:

(1) Gust response
(2) Buffet response
(3) Stability derivative extraction
(4) Flutter
(5) Active control of aeroelastic effects

Gust Response

The response of an aircraft to atmospheric turbulence is an important design consideration from the standpoint of loads, structural fatigue, and ride quality. The need for an experimental capability for the study of airplane response to gust loads led to the development of a technique for generating sinusoidal gusts in the test section of the TDT. This technique, described in reference 7, involves measuring the response of an aeroelastically scaled model in simulated free flight to a sinusoidal vertical gust field generated by oscillating vanes located upstream of the test section.

Some key features of the system are illustrated in figure 3. The model is suspended in the wind-tunnel test section by a two-cable mount system, which allows lateral and vertical translation of the model as well as angular rotation about all three axes. (See ref. 8.)

The airstream oscillator consists of two sets of biplane vanes mounted on each side of the test-section entrance. The vanes are oscillated sinusoidally in pitch about a zero mean angle of attack at frequencies up to 20 hertz. Trailing vortices from the vane tips, passing downstream near the sidewalls of the test section, induce a vertical-velocity component in the flow field near the center of the test section.

A typical variation of the vertical gust flow angle with frequency and lateral distance from the center of the test section is shown in figure 4 in

the form of a three-dimensional plot. Note that the gust angle decreases rapidly with increasing frequency, and there are variations in the flow angle across the tunnel.

Initial analytical and experimental studies in references 1 and 7 indicated the feasibility of the airstream oscillator technique. On the basis of these encouraging signs, a comparative wind-tunnel, flight, and analysis study was undertaken in late 1960 that used the B-52E aircraft as the test article.

The wind-tunnel program involved a 1/30-size dynamically scaled aeroelastic model of the B-52E. (See fig. 5.) In order to achieve reasonable simulation of the short-period mode on the model, it was necessary to use a variation of the two-cable mount system shown in figure 3. In this case, the cables were pinned to the model at a point near the center of gravity and the pulleys were mounted at the tunnel wall rather than within the contours of the model fuselage. This mount configuration has a very low rotational stiffness in pitch and provides adequate simulation of the short-period free-flight mode.

Figure 6 shows a sample of some unpublished results obtained by L. T. Redd and J. Gilman, Jr., of NASA Langley Research Center. Frequency response plots of a nondimensional coefficient of bending moment at the midwing span per degree of sinusoidal vertical gust angle are shown for three cases: (1) wind-tunnel-model tests using the airstream oscillator, (2) analytical predictions for the cable-mounted model, and (3) flight tests using spectral measurements of atmospheric turbulence and the associated response of the airplane. These data were produced with the aid of The Boeing Company, Wichita Division, under contract in a cooperative program by NASA Langley Research Center and the U.S. Air Force Flight Dynamics Laboratory.

With reference to figure 6, it should be noted that at very low reduced frequencies ($k = 0.01$, where k is the reduced frequency based on the mean aerodynamic semichord), the model response is affected by a mount system mode and the airplane response by spurious pilot-induced motions; at higher reduced frequencies ($k = 0.14$), the low gust input level produced by the airstream oscillator (see fig. 4) leads to measurement inaccuracies. The overall correlations between wind-tunnel, flight, and analytical predictions appear to be good, however, and indicate the airstream oscillator to be a useful and valid wind-tunnel technique for airplane gust loads research. (In the oral version of the paper a movie clip was used to illustrate gust response of the model and the airplane.)

Buffet Response

When buffet response and load predictions of complete aircraft are required, a dynamically scaled aeroelastic model test would seem to offer the best hopes of obtaining suitable data. Since viscous flow phenomena, including boundary-layer separation, are influenced in varying degrees by the value of the Reynolds number, this parameter would appear to be somewhat more significant for buffet studies than for flutter tests. Although the locations of local shocks and commencement of local separated flow may be Reynolds number dependent in varying degrees, depending on the particular aerodynamic configuration, there is some

experimental evidence to suggest that the integrated effects on the structural response and even on total lift may be small relative to other factors affecting the accuracy of buffet loads. The aeroelastic model approach for predicting buffet loads has been evaluated in reference 9 by comparing the normal-force coefficients and the scaled buffet bending moments and accelerations measured on a 1/8-scale flutter model of a variable-sweep fighter airplane with those measured in a flight-buffet-research program. (See ref. 10.) The model was "flown" on the basic cable-mount system described earlier with a lift balancing device (see fig. 3 and ref. 9) which counteracted the lift in excess of the model weight and thus allowed the model to be flown under conditions simulating high load factors (inertia and pitch-rate effects being neglected, of course).

Figure 7 compares the model and full-scale variation of normal-force coefficient C_N with angle of attack well beyond the buffet boundary for three angles of sweep. The model C_N was obtained from a load cell on the lift balancing cable, whereas the airplane C_N was obtained from an accelerometer located near the center of gravity. The model Reynolds number range was from 0.87×10^6 to 1.33×10^6 compared with flight values of 20×10^6 to 28×10^6. The Mach numbers indicated are model values. The airplane Mach number varied from slightly above the model value of the start of the maneuver to slightly below the model value at the end of the maneuver (high angle of attack). The variance was larger at the higher sweep angles. The model and airplane values of C_N are seen to agree reasonably well.

Figure 8 compares the airplane buffet response with model-predicted values of wing and horizontal-tail root-mean-square (rms) bending moments and rms accelerations at the center of gravity. The data are typical in that the full-scale-buffet bending moments on the wing and horizontal tails and the center-of-gravity buffet accelerations predicted from the model data agreed well with airplane values at all Mach numbers at a wing sweep angle of 26°. Although not shown here, at a wing sweep angle of 50° the agreement was reasonably good at all Mach numbers tested for the wing bending moments, but the correlation of the model and airplane center-of-gravity accelerations and horizontal-tail bending moments was not so good at the higher Mach numbers. At 72° sweep, both the airplane and model response were low and made evaluation of the technique difficult.

Stability Derivative Extraction From Cable-Mounted Wind-Tunnel Model Tests

Procedures for determining airplane stability and control derivatives from flight-test measurements have been under development since the early days of aviation. In recent years, however, a widespread surge of interest in this area has been triggered by the availability of highly automated data acquisition systems and advances in optimal estimation theory. The current status and prospects for the future of this technology were topics of a recent specialist meeting on methods of parameter identification in aircraft flight testing. (See ref. 11.)

Paralleling this focus on flight-testing techniques is an interest in applying similar procedures for the extraction of stability and control

derivatives from "free-flying" aeroelastically scaled wind-tunnel models. Preliminary indications from theoretical studies and companion wind-tunnel experiments are encouraging. The proposed procedure involves measuring the response of a cable-mounted model to known input disturbances such as control-surface deflections or external forces applied through the suspension cables. The stability derivatives are then extracted from equations of motion for the model and the suspension system using a maximum-likelihood parameter-estimation algorithm (based on ref. 12) which is being developed under contract by NASA Langley Research Center. The equations of motion represent five degrees of freedom (pitch, roll, yaw, vertical translation, and lateral translation) wherein the model is treated as an equivalent rigid body. The derived aerodynamic derivatives therefore represent quasi-static elastic derivatives. Deformation effects associated with gravity forces are neglected. However, by use of the lift balance mentioned earlier, high-angle-of-attack nonlinear aerodynamic coefficients may be determined.

The procedures described above are, in theory, capable of deducing the aerodynamic coefficients associated with whatever motions of the model are excited by the known external disturbances. Numerical experiments using simulated "noisy" wind-tunnel data show promise that most aerodynamic derivatives can be determined with acceptable accuracy. Further assessment of the method will be made in upcoming wind-tunnel model tests. In a previous study a simplified version of such a technique was applied to determine roll-control effectiveness for a cable-mounted aeroelastic model (refs. 1 and 13). The technique and some comparisons between wind-tunnel and flight results are summarized below.

The approach is based on the assumption that the dynamic response of a cable-mounted model to sinusoidal aileron deflection can be represented by a single-degree-of-freedom system in roll. The roll inertia of the model, the spring restraint of the mount system, and the wind-tunnel test conditions are assumed to be known; the roll damping coefficient C_{l_p} and aileron effectiveness coefficient C_{l_δ} are the unknowns to be determined. The amplitude and phase of the model-roll response to a sinusoidal aileron deflection are measured over a range of discrete frequencies. These measurements, when substituted into the equation of motion, produce a set of redundant algebraic equations which are solved by a least-squares procedure to give the unknown aerodynamics derivatives C_{l_p} and C_{l_δ}. The ratio of these coefficients is proportional to the free-flight control effectiveness which is normally expressed in terms of the wing-tip helix angle, pb/2V; where p is roll rate; b, wing span; and V, airspeed.

A comparison of the aileron effectiveness measured in flight with wind-tunnel model prediction is shown in figure 9. These results are for a large cargo transport aircraft at a Mach number of 0.75. The model data were obtained on a Mach scaled aeroelastic model used previously in flutter studies. Since the ailerons become ineffective as the aileron reversal point is approached, roll trim of the model was provided mechanically by differential deflection of the horizontal rear cables as shown in figure 3. The model and flight comparisons shown in figure 9 indicate that this relatively simple test technique can

provide satisfactory estimates of not only the reversal boundaries, but also the aileron effectiveness of the airplane as a function of Mach number and dynamic pressure.

Flutter

During high-altitude flight tests of a large cargo transport airplane, a flutter-type instability was encountered on the horizontal-tail surface of the T-tail empennage. The instability occurred at a Mach number near 0.8 but only during maneuvering flight when the elevator was deflected more than about 8° in either direction. The problem was characterized by a limited amplitude oscillation involving coupling between elevator rotation and stabilizer torsion at a frequency of about 24 hertz. (Since the phenomenon had the earmarks of two types of control surface instabilities, flutter and buzz, it has been referred to as "fluzz.") Prior to the incident, flight flutter tests and analyses, which were for small elevator deflections, indicated no flutter problems within the airplane's operating envelope. Subsequent flight investigations of various proposed solutions, such as vortex generators, dampers, and elevator mass balance, led to the selection of increased elevator mass balance as the most promising solution. (See ref. 14.)

Because there was little or no information available in the literature at the time on instabilities initiated by large control surface deflections, an experimental study was undertaken in the TDT to explore the phenomenon further. (See ref. 15.) Results from the study are summarized in figure 10. It was found that the basic instability phenomenon encountered on the airplane in flight tests was reproduced in the wind tunnel although at higher predicted speeds. Whereas in flight, the instability occurred when the elevator deflection exceeded 8° in either direction, it occurred in the wind tunnel only when the deflection exceeded 8° in one direction, that is, trailing edge down. The reason for this behavior may have been due to increased bearing friction in the model elevator associated with bending of the tail under static loads. Finally, it should be noted that the elevator mass balancing used as a solution to the airplane flutter problem also eliminated flutter on the model.

Active Control of Aeroelastic Effects

Active control system technology today is adding a new dimension to airplane design. Through application of active control concepts, or what has become known as CCV (Control Configured Vehicles), the designer can reap such benefits as weight savings, performance improvements, and better ride quality. Four such applications and associated potential benefits are (1) reduced static stability leading to decreased drag and smaller tail size, (2) gust and maneuver load alleviation leading to increased fatigue life and/or structural weight savings, (3) ride quality control leading to improved crew and passenger comfort, and (4) flutter suppression leading to weight savings or increased flutter placard speeds. All the above have been demonstrated by analysis, wind-tunnel tests, and flight tests. (See refs. 16 and 17.) Wind-tunnel and flight comparisons for two such applications — flutter suppression and load alleviation — are discussed in the remaining sections of the paper.

Active flutter suppression.- To demonstrate the feasibility of various active control concepts, the U.S. Air Force Flight Dynamics Laboratory initiated a flight program with The Boeing Company, Wichita Division, to study Control Configured Vehicle concepts using the B-52E airplane. (See ref. 18.) Included in the concepts studied by analyses and flight tests was active flutter suppression or, in other words, flutter mode control. In parallel with the CCV flight program, a companion wind-tunnel-model research program was undertaken jointly by NASA and the USAF with contract support by Boeing (Wichita). (See ref. 19.) The 1/30-size dynamically scaled aeroelastic model of the B-52E, used previously in gust research (fig. 5), was modified to simulate the active control systems of the CCV research airplane. Because of the increased weight associated with the miniature electromechanical control system added to the model, the model could not simulate the mass scaling factor for the nominal-weight CCV airplane. Therefore, for the purpose of comparing wind-tunnel and flight results special heavyweight airplane conditions were flown which required in-flight refueling. Thus, the airplane was altered to match the wind-tunnel model.

The wing-flutter mode control on the model, like the airplane, involved flaperons and outboard ailerons. Vibratory motions of the wing were sensed by accelerometers. These signals were sent from the model to a remotely located, general-purpose analog computer on which the control laws were simulated and then back again to the model as control surface command signals. Some sample results from this study (taken from ref. 19) are presented in figure 11 which shows the effect of the flutter mode control system on the subcritical damping measured in the wind tunnel and in flight. Note that the flutter speed of the model is within 8 percent of the flutter speed of the airplane; damping trends below the flutter speed are similar but the damping of the model is higher than for the airplane. In view of the high degree of complexity involved in the wind-tunnel model simulation, this agreement is considered to be very good. In fact, the wind-tunnel model results agree more closely with flight-test data than calculations do (not shown).

This flight validation of wind-tunnel modeling of active control systems thus tends to establish the technique as an economical, timely means of verifying the performance of Control Configured Vehicles of the future.

Active load alleviation.- Another application of active controls has been developed for the C-5A airplane as a means of reducing wing fatigue damage due to incremental maneuver and gust-load sources. This system, designated the active lift distribution control system (ALDCS), is described in detail in reference 20. Basically, the ALDCS uses accelerometers located in the outer wing to provide control surface command signals, through the airplane stability augmentation system, to servo actuators on the ailerons and elevators. The ailerons are deflected to redistribute the air loads on the wing so as to reduce inboard-wing stresses whereas the elevators are deflected to maintain trim. Specific design goals for the system are to reduce the incremental wing root bending moment by 30 percent without significantly affecting the performance, flutter margins, or handling qualities of the C-5A.

As part of the ALDCS development program, a wind-tunnel study of a 1/22-size dynamically scaled aeroelastic model equipped with proposed active control system was undertaken in the Langley transonic dynamics tunnel. The purpose of

this program, which was a joint effort of the U.S. Air Force, Lockheed Georgia Company, and the Langley Research Center was to gain added confidence in the ALDCS and to evaluate its possible effect on flutter before undergoing flight tests. The model is shown in figure 12. Unlike the active control system on the B-52 model described earlier, the C-5A model control system was powered by an onboard hydraulic system. The dynamic response characteristics (gain and phase lag) of this system matched those of the airplane up to frequencies of 35 hertz on the model.

The wind-tunnel model program included a number of facets, one being to evaluate the effectiveness of the ALDCS by measuring the wing bending-moment response to sinusoidal aileron frequency sweeps. Similar measurements were obtained in flight for comparable conditions. Some typical results from wind-tunnel and flight tests are presented in figure 13. This figure shows the variation with aileron frequency of the wing-root bending moment normalized to the maximum bending moment with ALDCS off which occurs at about 1 hertz, the wing fundamental bending frequency. The overall trends for the airplane and the model are similar; however, the airplane system is apparently more effective than was predicted by the model. The cause of this difference could be associated with the fact that the aileron control effectiveness measured statically on the model was only about two-thirds of that measured on the airplane. (The ailerons were sealed on the airplane but not on the model.)

A second difference to be noted is the peak on the model response at approximately 1/2 hertz (scaled to airplane) with the ALDCS on. This is believed to be due to coupling between the active control system and the model mount system. Similar coupling effects have been observed in test of the B-52 model with a simulated active-ride-control system. Here, the feedback gains of the ride-control system had to be reduced in order to avoid an instability arising from the control system coupling with mount system modes. Thus, improvements in model mount systems are needed to permit more accurate simulation of the active control systems designed to modify the airplane rigid-body dynamics.

(In the oral version of the paper a movie clip was used to show some effects of active controls on aeroelastic response of the B-52 and C-5A in flight and of models in the wind tunnel.)

CONCLUDING REMARKS

This paper has attempted to assess the validity of predictions obtained from dynamically scaled aeroelastic models in the Langley transonic dynamics tunnel that uses Freon-12 as a test medium. To this end wind-tunnel and flight-test results pertaining to various aeroelastic problem areas were brought together in one place for comparative evaluations. These areas include gust and buffet response, control surface effectiveness, flutter and active control of aeroelastic effects. Some benefits and shortcomings of Freon-12 as a test medium were also discussed.

Although some uncertainties remain, and there is the continuing need for improvements in simulation and testing techniques, the results presented herein indicate that the predictions from wind-tunnel studies are, in general, substantiated by full-scale flight measurements. During the 15-year period since the Langley transonic dynamics tunnel was put into operation, aeroelastic studies in this facility have provided a highly effective means of gaining insight into new phenomena, verifying analytical methods, and establishing flight safety — especially in the important transonic range where present analytical methods are usually inadequate.

Finally, it should be noted that with the existing capabilities of the Langley transonic dynamics tunnel, it is often difficult to fabricate models light enough to satisfy mass-scaling requirements for current aircraft designs. For future designs, embodying composite structures and active control systems, this difficulty is likely to be compounded many fold. To alleviate these emerging problems, planning is underway to increase, by 50 percent, the maximum power and thus the maximum stagnation pressure of the Langley transonic dynamics tunnel.

REFERENCES

1. Rainey, A. Gerald; and Abel, Irving: Wind-Tunnel Techniques for the Study of Aeroelastic Effects on Aircraft Stability, Control, and Loads. Aeroelastic Effects From a Flight Mechanics Standpoint, AGARD CP No. 46, Apr. 1969.

2. Von Doenhoff, Albert E.; Braslow, Albert L.; and Schwartzberg, Milton A.: Studies of the Use of Freon-12 as a Wind-Tunnel Testing Medium. NACA TN 3000, 1953.

3. Pozniak, O. M.: Investigation Into the Use of Freon 12 as a Working Medium in a High-Speed Wind-Tunnel. Note No. 72, Coll. Aeronaut., Cransfield (Engl.), Nov. 1957.

4. Treon, Stuart L.; Hofstetter, William R.; and Abbott, Frank T., Jr.: On the Use of Freon-12 for Increasing Reynolds Number in Wind-Tunnel Testing of Three-Dimensional Aircraft Models at Subcritical and Supercritical Mach Numbers. Facilities and Techniques for Aerodynamic Testing at Transonic Speeds and High Reynolds Number, AGARD CP No. 83, Aug. 1971, pp. 27-1 - 27-8.

5. Yates, E. Carson, Jr.; Land, Norman S.; and Foughner, Jerome T.: Measured and Calculated Subsonic and Transonic Flutter Characteristics of a 45° Sweptback Wing Planform in Air and in Freon-12 in the Langley Transonic Dynamics Tunnel. NASA TN D-1616, 1963.

6. Ehlers, F. Edward: A Finite Difference Method for the Solution of the Transonic Flow Around Harmonically Oscillating Wings. NASA CR-2257, 1974.

7. Gilman, Jean, Jr.; and Bennett, Robert M.: A Wind-Tunnel Technique for Measuring Frequency-Response Functions for Gust Load Analyses. J. Aircraft, vol. 3, no. 6, Nov.-Dec. 1966, pp. 535-540.

8. Reed, Wilmer H., III; and Abbott, Frank T., Jr.: A New "Free-Flight" Mount System for High-Speed Wind-Tunnel Flutter Models. Proceedings of Symposium on Aeroelastic & Dynamic Modeling Technology, RTD-TDR-63-4197, Pt. 1, U.S. Air Force, Mar. 1964, pp. 169-206.

9. Hanson, Perry W.: The Prediction of Structural Response to Buffet Flow: A State-of-the-Art Review. 39th AGARD Structural and Materials Meeting (Munich, Germany), Oct. 1974. (Available as NASA TM X-72627.)

10. Friend, Edward L.; and Monaghan, Richard C.: Flight Measurements of Buffet Characteristics of the F-111A Variable-Sweep Airplane. NASA TM X-1876, 1969.

11. Methods for Aircraft State and Parameter Identification. AGARD CP-172, Nov. 1974.

12. Mehra, Raman K.; Stepner, David E.; and Tyler, James S.: Maximum Likelihood Identification of Aircraft Stability and Control Derivatives. J. Aircraft, vol. 11, no. 2, Feb. 1974, pp. 81-89.

13. Abel, Irving: Evaluation of a Technique for Determining Airplane Aileron Effectiveness and Roll Rate by Using an Aeroelastically Scaled Model. NASA TN D-5538, 1969.

14. McAvoy, J. M.: C-141A Empennage Flutter Substantiation With Revised Elevator Balance Weights. Rep. No. ER-8471, Lockheed Georgia Co., June 15, 1966.

15. Sandford, Maynard C.; and Ruhlin, Charles L.: Wind-Tunnel Study of Deflected-Elevator Flutter Encountered on a T-Tail Airplane. NASA TN D-5024, 1969.

16. Holloway, R. B.: Introduction of CCV Technology Into Airplane Design. Aircraft Design Integration and Optimization, AGARD CP-147, vol. 1, Oct. 1973.

17. Doggett, Robert V., Jr.; Abel, Irving; and Ruhlin, Charles L.: Some Experiences Using Wind-Tunnel Models in Active Control Studies. Advanced Control Technology and Its Potential for Future Transport Aircraft, NASA TM X-70240, 1974.

18. Thompson, Glenn O.; and Arnold, James I.: B-52 Controls Configured Vehicle System Design. AIAA Paper No. 72-869, Aug. 1972.

19. Redd, L. T.; Gilman, J., Jr.; Cooley, D. E.; and Sevart, F. D.: Wind-Tunnel Investigation of a B-52 Model Flutter Suppression System. J. Aircraft, vol. 11, no. 11, Nov. 1974, pp. 659-663.

20. Grosser, W. F.; Hollenbeck, W. W.; and Eckholdt, D. C.: The C-5A Active Lift Distribution Control System. Impact of Active Control Technology on Airplane Design, AGARD CP-157, Oct. 1974.

TABLE I. COMPARISON OF SELECTED AIR AND FREON-12 PROPERTIES

AT ATMOSPHERIC PRESSURE AND TEMPERATURE

Property	Freon-12	Air	Freon-12/air
Specific heat, γ	1.13	1.4	0.807
Density, ρ, kg/m^3	4.896	1.226	3.99
Speed of sound, a, m/sec	152	341	0.446
Viscosity, μ, $N\text{-}sec/m^2$	12.81×10^{-6}	18.1×10^{-6}	0.708

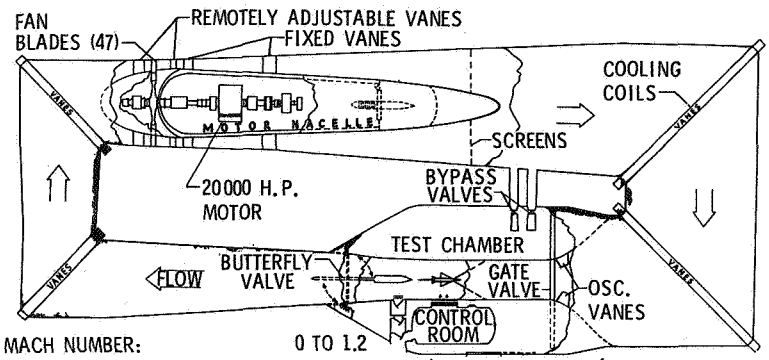

Figure 1.- NASA Langley transonic dynamics tunnel.

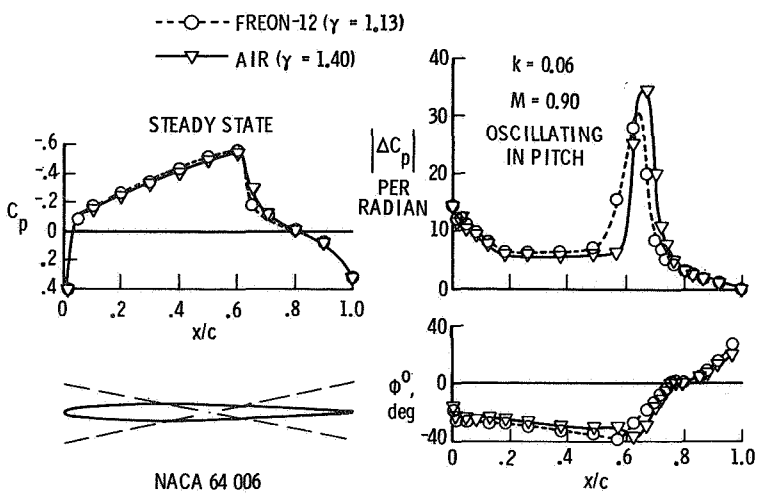

Figure 2.- Calculated pressure distributions for oscillating airfoil in air and in Freon-12.

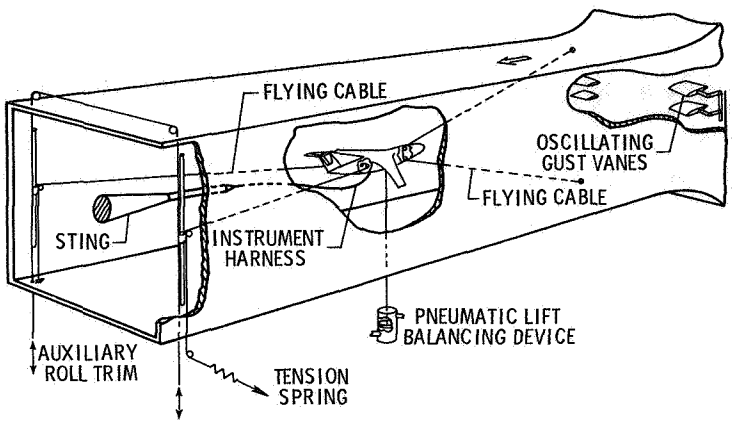

Figure 3.- Some aeroelastic model testing features in the Langley transonic dynamics tunnel.

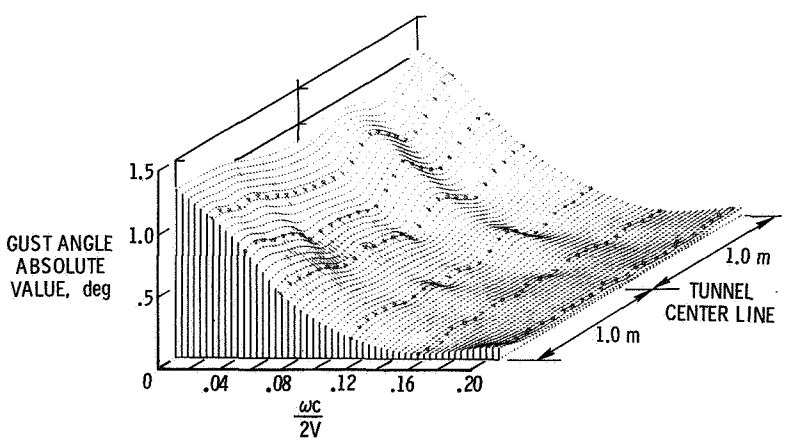

Figure 4.- Typical variation of gust flow angle with reduced frequency and lateral position for ±6° oscillating vane angle. (V = 35.4 m/sec and c = 0.233 m.)

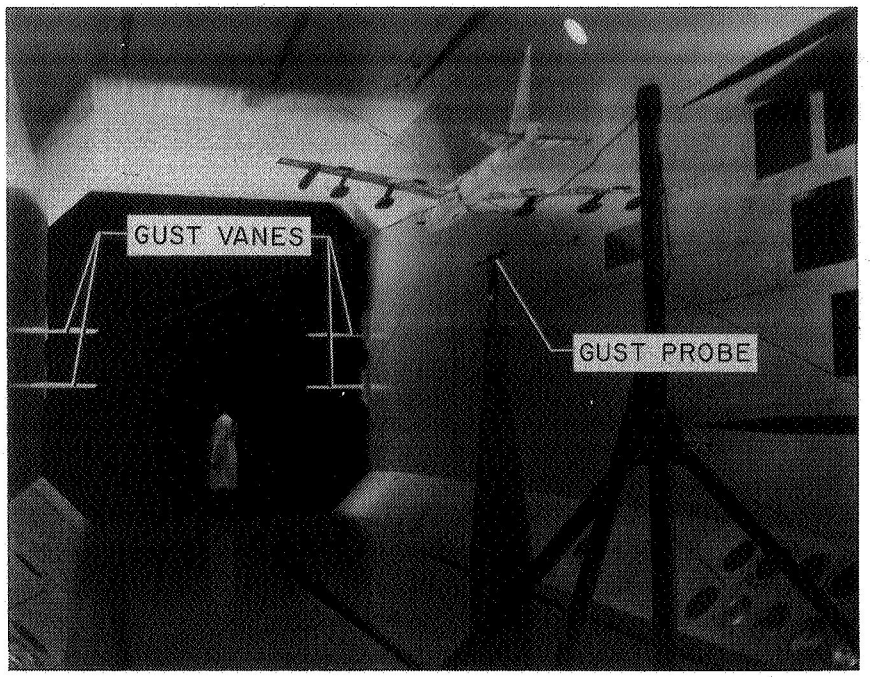

Figure 5.- View of B-52 aeroelastic model showing gust-generating vanes.

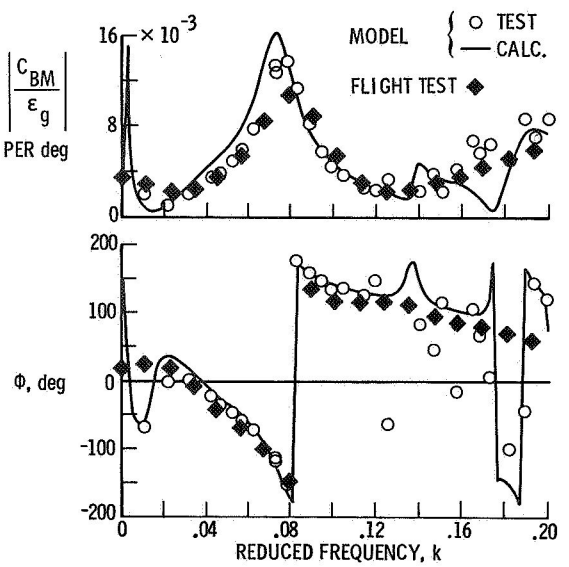

Figure 6.- Frequency response of B-52 from flight tests and wind-tunnel model tests using gust-generating vanes.

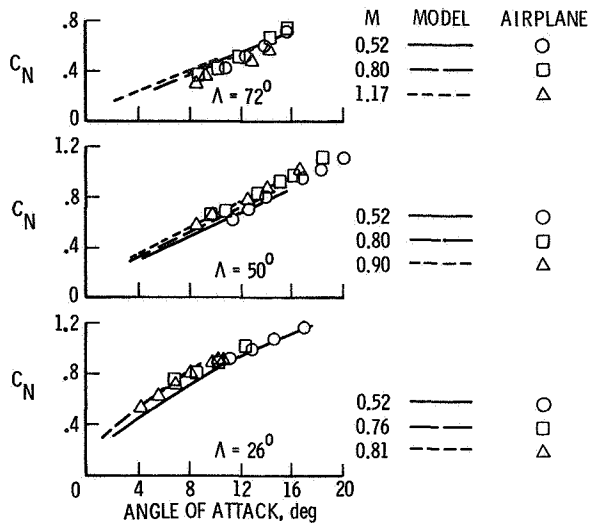

Figure 7.- Comparison of model and airplane C_N variation with angle of attack (ref. 9).

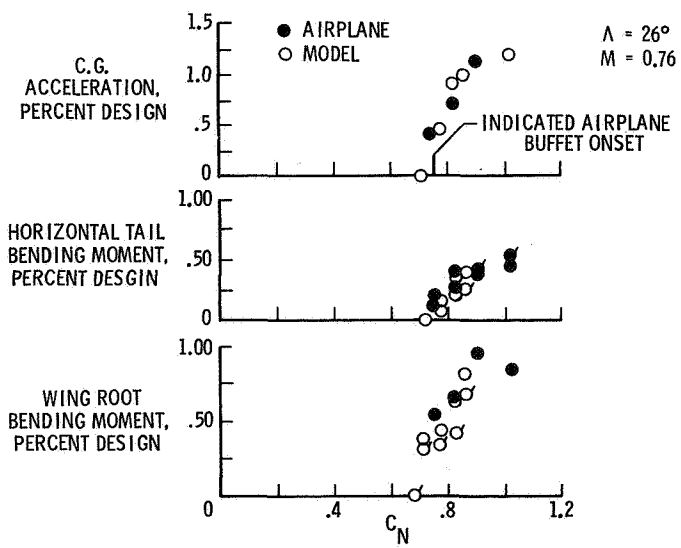

Figure 8.- Comparison of buffet response from airplane and model tests normalized to airplane design loads. M = 0.76; 26° wing sweep (ref. 9).

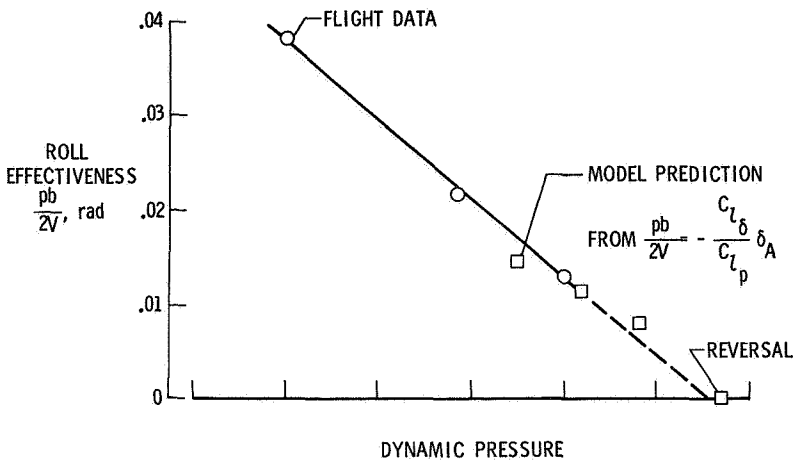

Figure 9.- Comparison of flight measurements and model-predicted aileron effectiveness (ref. 1).

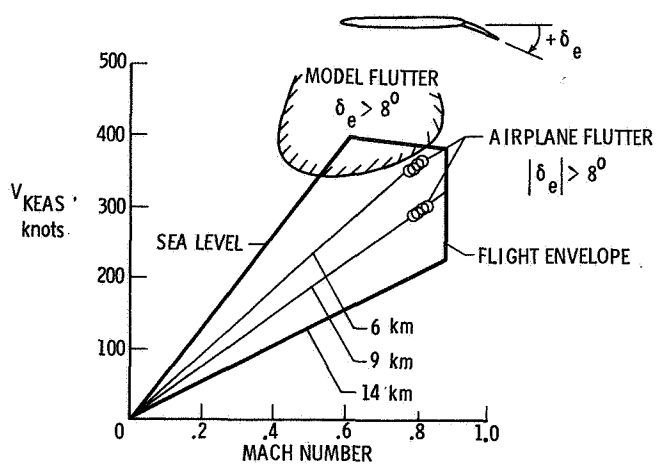

Figure 10.- Comparison of flight measurements and model-predicted flutter of T-tail with deflected elevator (ref. 15).

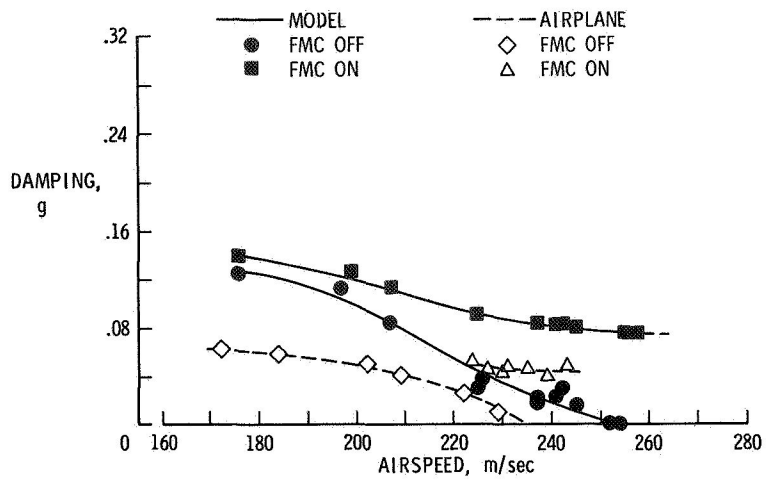

Figure 11.- Effect of flutter mode control system on damping of B-52 CCV model and airplane (ref. 19).

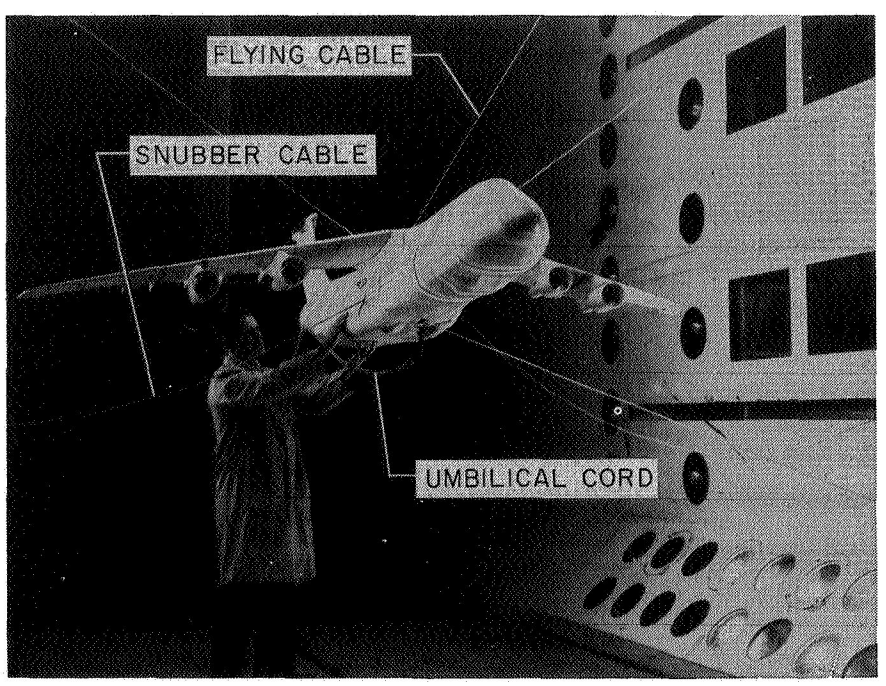

Figure 12.- Model of C-5A with active lift distribution control system in Langley transonic dynamics tunnel.

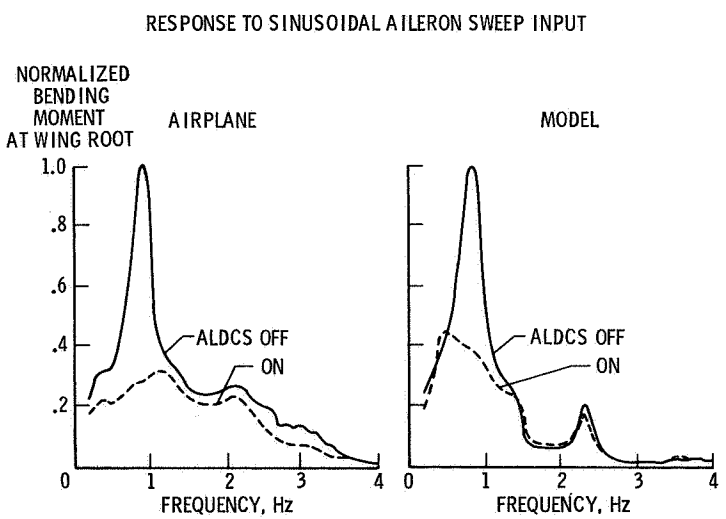

Figure 13.- Characteristics of C-5A active lift distribution control system determined in wind-tunnel and in flight tests.

PANEL DISCUSSION

THEORETICAL ANALYSIS VERSUS TESTING - A TRADE-OFF

Holt Ashley, Stanford University, Moderator:

Good evening. Let me welcome this knowledgeable and experienced audience to our panel discussion. If you have read the program, the title is Theoretical Analysis Versus Testing - A Trade-Off. Now in view of the title that was assigned to those who serve in this panel, I think it is probably a good thing that the event occurred at this time and this place on the program, after everyone has had a big dinner and a couple of drinks. At least it might give some of us, above and beyond my friend John Houbolt, the courage to take the extreme positions that will be required for success on our part and entertainment for you. I do want to make a semiserious remark before I go on, and that is, I would like to add my congratulations to the other remarks that have been made informally and today's various speakers. I really have to say that I've been to several hundred AIAA meetings of various kinds, and I have not heard a more interesting and informative group of papers than were presented this afternoon. Furthermore — and this you do not all know — there was somehow arranged for a small group of us, at the end of our lunch hour, the most dramatic flight test demonstration that has ever been my pleasure to see. Standing out in front of the hangar we first saw the B-1 flying overhead, in all its glory on its way to some low-level flight test. Perhaps Harold Sweet will say something on that later this evening. Shortly thereafter, we watched the X-24B drop off a B-52 and perform one of its final dead-stick approach and landing flights. The weather was so great that we watched it all the way from release to touchdown. It was quite a thrill. I don't know what it has to do with flutter, but we appreciate it.

Now let me begin to introduce the panel members. Starting from your right at the end of the table:

Gene Baird - Grumman Aerospace Corporation

M. Jonathan Turner - Boeing Commercial Airplane Co.

Professor Ed Garrick - The most unretired "retired" NASA scientist at Langley Research Center; he also worked at MIT for a year in the 1950's.

Harold Sweet - B-1 Division, Rockwell International

David E. Brandt - Vice President, Engineering, of Enstrom Helicopter Corporation; by the way, he got out of MIT in 1960 and made Vice President in just 15 years; he went there just two months ago from Boeing Vertol Company.

We welcome you all, gentlemen, and we are looking forward to hear what you have to say.

Let me briefly describe to you what a criminal investigator would call the M.O. of this panel. After I relieve myself of a few words and remarks, I plan to call on the panelist in alphabetical order. There is no other fair way to do it except reverse alphabetical order. Now, hopefully, the letter that I wrote to each panelist will have the following effect. That the expected value of the time used for their talks will be five minutes, with a sigma of not to exceed two minutes. Then I shall try to stimulate them to interact with one another in the way of questions and comments for however long that takes, perhaps 15 to 20 minutes. Afterwards — this I believe is always the best time of a ceremony of this kind — is for questions and comments from the audience. So let me say two things about that:

1. Please start thinking up your tough questions now

2. When you finally have the opportunity, please wait for the microphone and identify yourself, so that your name and company may be recorded on the tape

We are recording all of these comments and questions. Hopefully, we can break up by 9:00 p.m. because your moderator has to catch a 12:00 flight from L.A. tonight.

Now something about the subject which we've been asked to address. As someone whose contributions have been largely theoretical, you might expect me to take the theoretical side of the issue that we are talking about, but actually I am not going to do that. I hope perhaps Ed Garrick will come and be the Devil's Advocate and talk about the wonders of theory that we all believe in.

I would like to point out to you that the topic we have been given is identified with a trade-off. We have not been presented with an inexorable choice between two extreme alternatives. As you all know, the flutter validation of any new design, by Mil. Specs. or FAR's or whatever, consists of a closely coordinated succession of theoretical analyses of various degrees of complexity with wind-tunnel test on models of reasonable sophistication and finally a flight test program. I think that what we should be addressing tonight, as a function of the type of aircraft, its size and intention, is what is the proper balance among those various classes of activities that contribute to this activity of flutter validation. We heard today a lot about the cost of model testing and flight testing. In fact, I don't think that the argument was settled on which is more expensive: to do a flight flutter testing program on an airplane or to build a model and test it in the TDT.

At the same time, I think you will agree with me that our analytical tools are improving steadily and that computer costs (per cycle or per operation) are decreasing very rapidly. It may well be that, either today or some time in the future which we might attempt to determine, we are relying more than is necessary on the experimental part of the spectrum I described

and not enough on the analytical part. I should mention to those of you that are not aware of it that Clarence Perisho had a sort of lesson-of-the-day in mind when he picked our topic. It happens that I brought this along in case anybody wants to look at it. It is an article by Dean Chapman, Hans Mark and Mel Pirtle, entitled "Computer vs. Wind Tunnels for Aerodynamic Flow Simulations," published in the April 1975, issue of Astronautics and Aeronautics (a magazine sent out by an obscure aeronautical society). That article makes some very controversial statements. They start out by pointing to the historical examples from ballistics, orbital mechanics, and thermal neutron flux in moderated reactors, as being places where the computer essentially took over from experiment or test as the definitive way of designing and validating the design of these devices. They then make a massive leap to fluid mechanics generally, as a solution to the Navier-Stokes equations including, God help them, turbulent flow and separation. They state the conviction that the same process will take place in that area. Let me read just three quotations from this article:

> "As computers have improved, aerodynamicists progressively improved approximations to the full governing equations of motion. This historical process should continue, in general, until computers yield detailed solution of the Navier-Stokes equation in practical time and cost." [implied at any Reynolds number.]
>
> "Two developments will be necessary:
>
> a. Accurate turbulence models applicable to separated and attached flows.
>
> b. Computer capabilities two orders of magnitude greater than ILIAC IV." [This is their requirement for just getting to the point where there is a chance of duplicating the wind tunnel.]

And finally, they say that to displace wind tunnels as the principal source of flow calculation for aircraft design, computers must reach the speeds of 10^4 times that of ILIAC IV. They make the argument that it is possible that in the 1980's or the 1990's we may indeed see computers of this type. The rest of their conclusions you can draw for yourself.

Let me make the point that, when it has to do with what we call "classical flutter," their argument may be more valid for our area than it is for the one they are talking about. I will give you three reasons:

1. We are reasonably sure about Newton's laws of motions, even when they are expressed in terms of an adequate number of modes of free vibration and the generalized coordinates for calculation.

2. The structures specialists, particularly in the area of finite elements, have been working longer with computer representations than the fluid mechanics ever have. I would claim we are a lot closer to a very effective description. For example, small perturbation analyses are based on the fact that the structure has yield strains in the order of 2/10 of 1 per cent. Where are you going to see perturbations that small in fluid mechanics?

3. I believe we are often justified in using small-perturbation gas dynamics, perhaps even in the case Bill Rodden called attention to this afternoon. When we can do that, surely we are in better shape than Chapman and company will be with the Navier-Stokes equation in the prediction of turbulence.

So perhaps the question is not whether this theory will be playing a much larger role in flutter, but rather when.

Eugene F. Baird, Grumman Aerospace Corporation:

The subject for the panel discussion this evening is forcing us to look into the crystal ball. However, looking into the future is a necessary first step in planning the future resources that will be required by the Aerospace Industry for flutter prevention.

In response to the question as to whether there is potential for trade-offs between analysis and test for flutter prevention, the answer is obviously yes. But as to whether these trade-offs can be realized in the future, all I can do is make certain observations which might help to identify the prerequisites for these trade-offs. The particular trade-off which I wish to consider is a reduction in the cost of flutter prevention procedures through an increased emphasis on analyses and a consequent reduction in tests while maintaining the same degree of assurance of the effectiveness of the flutter prevention procedures. The fact that analysis is less costly than test, using current state-of-the-art techniques in both disciplines, is not difficult to show. We realize, however, that the analysis techniques currently being used are not sufficiently accurate to permit a reduction in the amount of testing and its associated costs. The use of more sophisticated computer programs which yield accurate flutter results throughout the speed regime will obviously involve an associated increase in computational requirements and an increase in the number of computer analyses. If we extrapolate the trend of computer development and associated cost of performing a given mathematical problem versus time, it is apparent that the costs are reducing quite significantly. The question that we have to address, however, is whether the significant increase in size of computer programs required to perform these more sophisticated flutter analyses as a substitute for test will still result in a viable trade-off.

At this point, in order to put my discussion into perspective, I would like to indicate the overall flutter prevention costs incurred in the development of the F-14 fighter airplane (table 1). Two important facts are

apparent in this table.

TABLE 1.- FLUTTER PREVENTION COSTS FOR F-14

ANALYSIS	29%	
WIND TUNNEL	27%	71%
GVT	19%	
FLIGHT TEST	25%	

R&D COSTS ≈ 0.48%

One is that the cost of testing, without considering a large investment in test equipment and data acquisition systems, accounted for 71 percent of the total cost. The other fact is that flutter prevention accounted for only 0.48 percent of the total research and development costs. One might consider half a percent of the R&D costs to be almost "in the noise level". However, one must recognize the larger number of disciplines involved in aerospace vehicle development. The repercussions of each discipline deciding its own costs are also "in the noise level". There is obviously a need for all of us to consider how we can cut down the costs associated with our own particular discipline.

There is one other facet of the analysis versus test trade-off which I haven't discussed to this point, but which I consider to be very important. Traditionally in my company, and I'm sure in most other companies, most testing occurs at a point when the design is well defined. In fact, proof model flutter testing must necessarily occur at a time when most of the structural characteristics of the airplane have been "immortalized" in detailed design drawings. Consequently, if a problem is uncovered at that point, there can be large cost repercussions. The fact that analyses of the detailed design configuration inevitably precede the test phase is an important factor. If we could analyze the configuration with a greater degree of confidence, the potential for design changes at a late stage in development could be significantly reduced.

Most of what I have said to this point is somewhat on the philosophical level, but let us now get down to engineering facts. An obvious prerequisite to increased reliance on analytical techniques is the development of more complex mathematical models which address the various disciplines associated with flutter (that is, aerodynamic, structural, and control system analyses) and which yield results that are considerably more accurate than have hitherto been achieved. In the field of aerodynamics, Chapman's recent paper has given us a projected requirement of computer resources versus aerodynamic analysis capability which indicates that the transition from inviscid nonlinear transonic aerodynamic analyses to viscous analyses, including separation effects, will require an increase in computer capability of two

orders of magnitude over ILLIAC IV. However, the role of viscous effects in oscillatory flow associated with flutter is an area which has not been well investigated or quantified. In view of the significant differences in required computer resources, a valuable initial step in minimizing the cost of development of reliable mathematical techniques for prediction of unsteady aerodynamic forces would be to perform planned series of tests to ascertain the types of configuration and the flight conditions for which evolving inviscid transonic aerodynamic analyses are applicable and also to identify the regimes where viscous effects are important. Such subject areas would include buzz, transonic flutter, and panel flutter.

In the structural analysis discipline, finite-element methods are now routinely used with a high confidence level for linear systems; however, there have been many examples in recent years of discrepancies between structural analysis and test. This obviously, from a flutter viewpoint, includes the prediction of vibration mode shapes and frequencies. In many instances, reconciliation between the two has been demonstrated by more detailed study of some aspects of the structure. This is particularly true of complex joints, nonlinear elements (such as thin panels close to buckling), or areas with different load paths in tension and compression. However, after-the-fact explanation of discrepancies are not sufficient. If a real trade-off between analysis and test is to exist, the analysis must be correct the first time. In the structural analysis discipline, perhaps we must investigate the need for more complex, that is to say higher order, structural elements or even nonlinear elements.

The third discipline to address in terms of improved mathematical modeling is control system analysis, which is playing an increasingly important role in flutter prevention because of the increased emphasis on active control systems to enhance airplane performance. Current problems include the prediction of hydraulic actuator impedance characteristics and the prediction of active control system feedback signals. This latter problem is obviously very much interrelated with the accuracy of prediction of vibration modes. This is a highly interactive subject area in which recent airplanes have experienced problems which could conceivably be very costly in their resolution unless we can be assured that we have good aerodynamic, structural, and control system modeling.

In summary, whether significant trade-offs between analyses and test will exist in the future remains to be seen. The fact is that the earlier we can identify a problem through enhanced analysis capabilities, the less costly the overall airplane procurement program will be. There is no question that we should continue to direct our efforts toward more accurate analysis techniques. But, it appears that these techniques will not be available until some time in the future. Until they are actually in hand, we must obviously continue to concentrate on increasing the efficiency of testing, which I believe will maintain its vital role in flutter prevention.

David E. Brandt, Enstrom Helicopter Corporation:

I'm probably the only one in this panel who will address the rotary wing field. I had really hoped to be last on the agenda, at the "bottom of the barrel" so to speak, where of course rotor R & D has always been.

The topic of this panel-discussion, "Theoretical Analysis Versus Testing - A Trade-Off" almost leaves me speechless because in the technical world of the lifting rotor, helicopter, tilt rotor, and machines of this type, the debate of theory versus testing for theoretical verification almost cannot begin without addressing the question, "Where is the theory?"

Now this is a relative statement, of course. I have to compare myself to the fixed wing technologists who abound here this evening and, to draw on an analogy appropriate for an after dinner speech, who select their analytical tools from a smorgasbord of the most delectable gourmet dishes. A rotor technologist, on the other hand, selects his dishes from a skid row garbage dump. My twenty years on skid row, watching the fat cat of the classical flutter field filing points on "T's" in the word "flutter" to make it look a little sharper, certainly have taught me the internal fury in the word "discrimination" and, by the same token, the bittersweet satisfaction of knowing who's really having the fun.

The serious aspect of this untenable situation is that the customer of a rotary wing vehicle, who has a job to do and who wants progress, continues to reach forward without ever having done his homework. He blows millions of dollars, if not hundreds of millions of dollars, on hardware programs, whereas one percent of these dollars applied to fundamental analysis to understand what he is dealing with would have put him money ahead. We end up with a three hundred million dollar fiasco, such as the Cheyenne program, which unquestionably has had a long-range impact inhibiting the development of today's so badly needed lifting rotary, short-haul vehicles. No wonder the industry is scared to death to change more than one little screw per decade in a rotor system, when the only thing they know about it is what they learn by experience. The fundamentals are not understood; the analytical base to support him is, for the most part, unverified.

The lack in leadership and vision, that pushed members of my part of the aerospace industry into this situation, certainly has to be shared by both industry and government agencies alike. It is my opinion, in particular, that the blame has to fall heaviest on the government agencies.

It is one thing to rationalize that today's industry leaders grew up in the helicopter industry, in the bicycle shop days, where they built hardware and tested it. Then they would put every crutch they could jam into the shotgun to try to fix it, never really knowing where the successes came from. We can blame it on them if we want to. But today, when we find the best technologists in the industry who have grown up and have become program managers doing the thing and spending millions of dollars for experimental development and not one nickel for fundamental analysis, you start looking for the source of the problem.

Money constraints, schedule constraints, and competitive constraints--we've faced these things through all of our careers. There is nothing new there.

My question is, "Where is the government leadership?" Who is sponsoring research so that the industry manager has a tool to lean on that he can trust and have confidence in? Where is the guy who asked the questions that put us all to the test in protecting the public interest and challenged what is going on?

Everyone who is in this room well knows the team effort that goes on between the guy in government and the guy in industry and how we get along to get a professional job done. A classic scenario will illustrate the many facets of this teamwork. You have been struggling for a year trying to fix the horizontal stabilizer. It's the one thing that is in your mind the day you're sent off to the customer on another issue, but, of course, the first thing your boss tells you is, "Handle the problem but don't talk about the horizontal stabilizer." You walk into your counterpart's office and he greets you with "Hi Dave, how is your wife?"

"The problems with the horizontal stabilizer aren't as bad as you probably hear, Harry." "Yea, I know; if you don't understand the fundamentals, you don't know you've really fixed it throughout the whole flight envelope, and you are concerned about fail-safe implications to what you have done." "I guess you are going to insist we go back and use some fundamental analysis, aren't you?" "Unhuh" is Harry's reply.

You grit your teeth and at home you report, "Boy, that Harry is really sharp. I didn't even get a chance to sit before he said, 'Oh Dave, how is your old piece of tail doing?' Then he bore right down on me." You go on to explain what the requirements are that must be met and the questions that must be answered. Then you proceed to do the fundamental analysis that we've been trying to do the last year.

It sounds easy? It used to be, but for at least five years I haven't been able to find anybody to ask me any questions or write a letter of challenge with some teeth in it which gets the management's attention.

I believe the hingeless rotor is to the short-haul transportation of this country what the swept-wing jet was to commercial aviation. Lockheed tried to make it work (as well as several others) and with providence smiling had some success with XH-51. The Army, frustrated and hungry for progress, took the bait and the result was almost the death of the hingeless rotor.

How can you scale up a successful aircraft into something different when you don't understand the fundamental parameters that affect the aeroelastic stability? How can you build an aeroelastically scaled wind-tunnel model if you don't know even simple facts like whether the control system's stiffness is an important parameter?

When the Army got burned $300 million worth, they responded by creating the Air Mobility Research & Development Laboratory system. There are approximately 650 people doing research in AMRDL which is probably more than the entire helicopter industry by a significant amount. NASA was seduced to bed by the Army (or vice versa),and for the first time in decades, NASA began to give the appearance of waking up to its responsibilities in the rotor wing field.

By now you say, since this has all happened five years ago, the state-of-the-art should really be moving along, we ought to be doing great. The fact is that the helicopter industry efforts directed at fundamentals are practically at a standstill. The industry is being starved to death. Some of the most competent people in this business are now working for the Army. They are interested in the advancing of the state-of-the-art, but only as long as they can do it themselves. "Yes," they say, "those are really good ideas, and the work needs to be done. We can't give you any support because we don't want to burden ourselves monitoring your contracts. Get somebody else." And that's the way it's been for a long time.

You know that you are not going to use an analysis somebody else developed unless you have used it for enough years to have some confidence in it. If you don't trust it, you don't use it, and you sure won't commit to a hardware program unless your management is prepared to fund a brute force experimental effort to make it work.

Five years ago, the Boeing Vertol Company thought they had learned a little bit about hingeless rotors, having had a close association with the "by dumb luck" successful BO-105. To satisfy the Army's UTTAS program, they stuck their necks out with not one but two hingeless rotors (main and tail) which were of distinctively different types. (Philosophical Note: If you think the customer won't believe you when you say you can "leap tall buildings with a single bound," tell him you can leap <u>two</u> tall buildings with a single bound - backwards and blindfolded.)

Today, I am happy to report that the Vertol UTTAS is, in fact, a truly superb machine, and I believe that it will set the industry standard for the next two decades. Using the unverified analysis drawn from the "garbage pit" for guidance, with a lot of wind-tunnel testing on dynamic models, we managed to make the main rotor stable as predicted. Even the tail rotor, after solving only seven distinct different modes of aeroelastic instability, is stable as a rock today. Three years in the wind tunnel, and I can't tell you how many millions of dollars, but not two cents for fundamental analysis to give us some guidance of how to go. Don't change a screw, don't change the weight of paint on the rotor, don't use a different manufacturing process, and everything will be all right. About midyear, before I left this program, they wanted to change the manufacturing process for this tail rotor. "How much will it cost to build it, Dave?" I looked him in the eye and said, "How about a million bucks, Harry?" and he didn't blink, so I said, "This year," and eventually got him to blink.

Well, what's the summary of the story? I never did find anyone to ask me a question at least after the proposal stage, not one question, no one to write a letter - a letter with teeth in it so that we could both put the hooks to the management and get on the "fundamental" job that needed to be done. I despair that the research that provides the basis for tomorrow's developments will continue at the slow, uncoordinated pace that the internal government engineers will find comfortable. And here I sit before you today, now I am one of the management in my own little bicycle shop, and all I can say is, "Oh, WOW! Where is the leadership?"

I. E. Garrick, NASA Langley Research Center:

I remember visiting a museum ship near Stockholm - an old sailing vessel that had been recovered from the sea bottom and restored; it had capsized on its launching with much loss of life - in particular, that of the marine engineer who had designed it. He was summarily executed! So also the real test of an aircraft, regardless of a mountain of ground work, is its flight-worthiness, and we would prefer not to extend the analogy of the marine engineer to the flutter engineer. Some of you may recall Leon Tolve's account of the history of flight flutter testing in the 1958 forerunner symposium, where pilots in early flutter tests were reassured when the flutter engineer went along on the flight (and Tolve, who did accompany many such flights, implied that the pilot had more faith in him than he had in himself).

I am pleased to have had a role in suggesting the republication of the proceedings of the 1958 symposium - the document was declassified only in 1971. It is a valuable document both by itself and against which to measure 17-1/2 years of change; and perhaps, facetiously, this panel provides a unique chance to eat or to repeat our previous words.

Flight flutter testing is the search for exposing possible low damping regions of flight; it is without doubt the most sophisticated type of flight test; and often it provides a shakedown of other trouble areas as well. It is obvious that we would like to reduce the amount of flight flutter testing required to a minimum. But consider, for example, the space shuttle and its orbiter where flight testing in the traditional sense is not feasible. The first flight test of the orbiter is scheduled to take place in 1977 by releasing it from its carrier B-747 airplane. From a few such proof flights, which need to be at low dynamic pressure relative to those of either the shuttle launch or the orbiter reentry, inferences must be drawn on its complete flight safety. Comparisons must be made with many calculations and with model, component, and full vehicle ground tests. Clearly, great reliance is being placed on the "math models" used in design and development. By math model we now mean really a mathematical engineering model composed of finite elements rather than the physicist's model of mathematical equations.

The complete shuttle vehicle, with its liquid fuel tank, twin solid boosters, and orbiter, presents numerous stability, loads, and dynamics problems in its ascent configuration and, similarly, many control and

stability problems on its orbiter reentry. Analysis involving substructuring methods will play a central role here, too, in the identification and solution of these problems, as will also the use of simulators and model and component ground tests.

The uses of finite element methods in structures and of similar methods in aerodynamics are two of the major changes that have taken place in the past 17 years. But perhaps some of the greatest changes that have come about in flutter test methods may be traced to the space program. Advanced computers have, of course, been essential to the space program with the real-time calculation of orbits and control of spacecraft; and, in turn, by feedback, the space program has led to greatly improved computer hardware and software. Continuous improvements in both flightborne micro-computers and ground-based computers have profoundly altered the outlook on the balance of test and analysis. Consider that real-time test and data analysis permit the time duration and the number of flights in flutter testing to be greatly reduced and that the latest generation of computers are capable of more number operations (such as a 64-bit number addition) in a second than there are seconds in a year! Purely numerical methods are rapidly multiplying throughout aerodynamics and structures. In March of this year at the NASA Conference on Aerodynamic Analyses Requiring Advanced Computers at Langley, solutions to difficult problems of flows with shock waves, separated flows, transonic flows, and of Navier-Stokes equations were exhibited; though, of course, solutions of the turbulent flows problems are still "around the corner."

Another change that has come about mainly through the influence of the space program and which is bringing an entirely new dimension to aeronautics and to flutter testing is the use of active controls in control configured vehicles (CCV). Much has been written on this in the recent and burgeoning literature. Use of active controls for stability or load alleviation must not degrade flutter characteristics. Active control of flutter itself was pioneered in flight by a modified B-52 airplane. As the airplane used a ballasted tip tank, these tests represented really active control of wing-store flutter. Comparison, in this case, of flight, wind-tunnel model tests, and analysis shows common trends; but numerical differences in flutter speed of the order of 10 percent indicate some room for improvement.

Active control places new emphasis on the analysis of nonlinear domains, distinctions between mild and violent flutter, and analysis of subcritical response and its correlation with effective damping concepts. Special interest attaches to the behavior of the gradients of the eigenvalues of the aeroelastic equations of motion taken with respect to various parameters.

The documented record of obtaining flutter in flight is quite sparse. Hence, it may be useful, I feel, to include in the proceedings of this meeting mention of two such cases.

Information for the first of these for the B-57F airplane is by courtesy of R. P. Peloubet and described in General Dynamics - Fort Worth document FZP-680, April 1965. The subsonic airplane having a moderately tapered unswept wing of aspect ratio 7.5 experienced flutter outside its normal operating

envelope, and a subsequent flight investigation gave results indicated in figure 1. Also shown are calculated flutter speeds by the kernel function method.

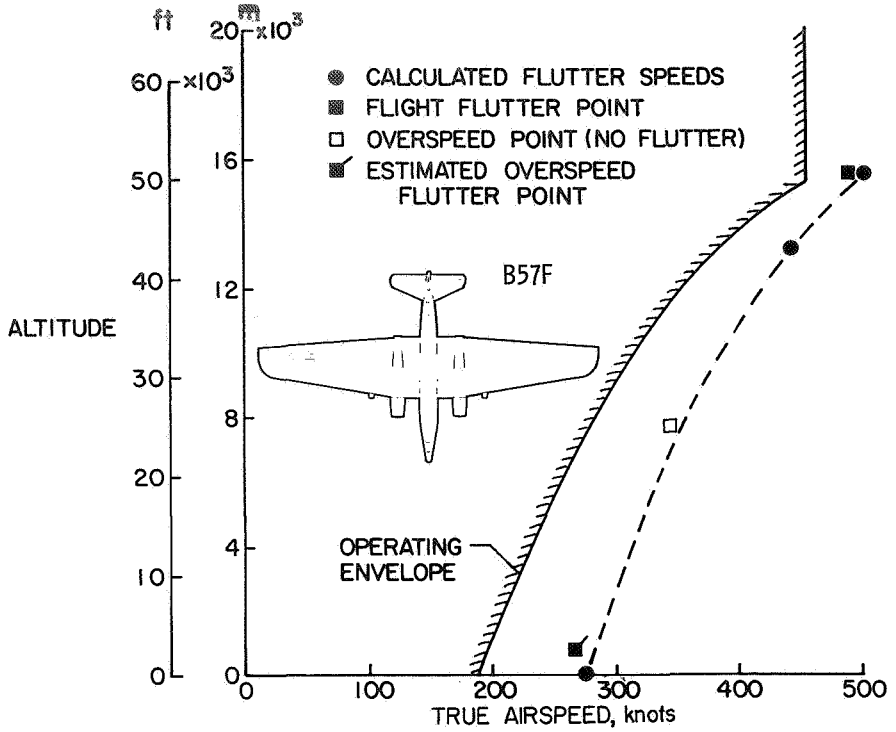

Figure 1.- Measured flutter results and calculated values by kernel method.

The second case (fig. 2) is for a missile whose canard wings came off at M = 1.7 within the operating flight boundary. Calculations by R. V. Doggett, Jr.,

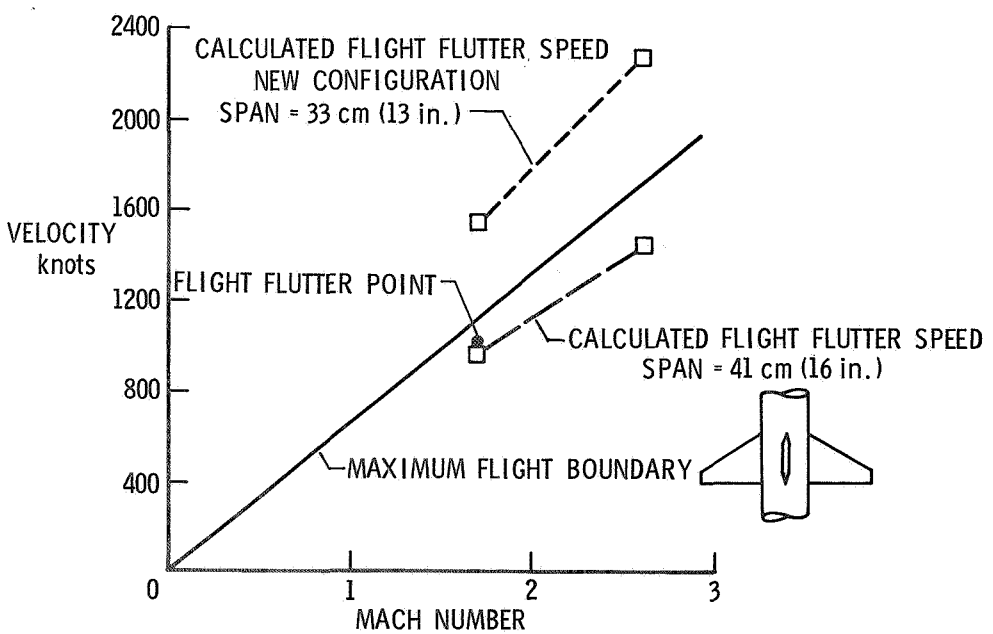

Figure 2.- Flutter of missile wings at M = 1.7.

and R. W. Hess using piston theory agreed well with the flight test results. A redesigned wing of shorter span performed satisfactorily.

Before closing these remarks, I wish to remind us all that doing calculations faster does not make them more reliable and that there may always be a residue of uncertainty in flutter calculations and a degree of hazard in flight flutter testing. Our job is to reduce these to a minimum.

And to close I repeat my closure of 17 years ago: "Thus, 'flutter' itself should take on a broader meaning combining cybernetics, dynamic stability, and aeroelasticity. For flutter is a process of pumping energy from the external flow into the structure, and feedback control instabilities are similar processes with internal energy sources. Along with all of this there must come also better physical insight into the mechanism and phenomena of instability whether through damping, or energy, or analog simulation, or mathematical tracing of roots and modes, or whatnot. Finally, it is not only necessary to understand but to understand well and clearly enough so that those in research or engineering management who make decisions can also see the problems in their proper light."

Harold Sweet, B-1 Division, Rockwell International Corporation:

Let me start by saying that analyses have no legitimate role in flutter safety demonstration and verification. Analyses can predict a probable flutter speed, but they cannot demonstrate flutter safety. Only flight can do that. Now, having rejected analyses, then I also reject flight flutter testing. My wife, when I told her I was coming to a flight Flutter Test Symposium, said, "Well, if you get flutter in flight, isn't it too late?" In all due respect to the pilot that Wilmer Reed reported on, I hope we are not looking for flutter in flight. We should be looking for flutter safety. Just as we test for performance and for inlet compatibility, we should be testing for the positive element of flutter safety, not for the negative element flutter.

I like to think that there is a similarity between the flutter clearance of an airplane and the sport of mountaineering. To start with, it takes a certain peculiar type of individual to have a desire to engage in either activity. The summit, or peak, represents the goal of flutter safety demonstration for a particular aircraft. There are usually several routes of varying difficulty with differing exposure or risk for reaching the goal.

My correlation function is a Sierra peak, Mt. Conness. At over 4120 meters it has an easy route up the east ridge. There are approaches from the northeast face and southwest face. My analogy says that to the north and northeast of the ridge is the chasm of analysis and to the south and southwest is the abyss of experiment.

The climb to the northeast face from the analysis side goes to the class 5 climb. Now the numerical rating of climbs means the higher the rating, the more difficult the climb. The class 5 climb is a piton protected climb of considerable skill. This is not a direct route to summit. You are obstructed by an overhand requiring a traverse to get around. The overhang obstructs the view of the summit and requires a deviation from a direct path to the summit in exactly the same manner that you cannot get directly to the goal of flutter safety from an analysis. Only a predicted flutter speed is possible from which safe restricted flight envelopes (the traverse from the overhang) can be specified.

The climb from the experiment side to this peak goal is not only class 5 but class 5a, or class 6, if you're of the old school of units. It requires direct aids where your weight is being supported by artificial climbing aids. I rate the direct approach to the summit from the experiment side, and unlike the analysis approach, it goes up a chimney directly to the summit as a more difficult approach than from the analysis. Now the analysis will, at least, have a safe margin prediction that you can move off from. Going directly by the experiment route is a real sporty course.

Going up the easy east ridge the climb start is a scree slope. A scree slope is one that's covered with loose rock where for every step you take up the slope, the slope slides backwards on you two steps. This is sort of symbolic of the thrashing around that is usually done in the early design stages of an aircraft. Recently we all have been working with optimization programs. This is where analysis will become supreme. Normal flutter analyses can show a flutter deficiency, but they cannot give an efficient lightweight solution. The pathfinding capability being provided by the optimization programs we are rapidly assimilating can aid the climb up that scree slope.

This east ridge, as it approaches the summit narrows to a spine a few meters wide and 100 meters long. Way down to the right is the analysis chasm; way down to the left is the experiment abyss. As one crosses the spine, he is guided by the analysis exposure on one side and experiment exposure on the other. Analyses are used to design the experiment such that the greatest probability of experiment success is obtained. The real role of analysis is to guide the exposure required in the experimental assault. The experiments are recycled into the analyses to gain analytical improvement and improve the test condition matching; thus, the exposure and limitations of the analysis assault are reduced. As far as climbing the east ridge is concerned, it goes as a class 2 climb. This is a little more than a trail hike with some boulder-hopping on the spine and summit. Interfacing experiment and analysis is represented by the choice of going around the boulder on the analysis side or on the experiment side.

Normally, cost and physical constraints can be expected to modify the design. To me this is somewhat like having planned to climb on solid granite in the Sierra and suddenly be on Glacier Park's quartzite. Glacier's rock tends to be rotten, that is it crumbles and doesn't consistently provide the solid hand/foot holds and piton anchors that are inherent with granite. The summit goal is attainable providing the changed climbing conditions are recognized immediately.

In the final analysis, tradeoffs between analysis and experiment are those which give the leader of the climb, the flutter engineer, the highest confidence in the flutter safety of the aircraft.

M. J. Turner, Boeing Commercial Airplane Company:

From my initial discussion with the program chairman I gathered that he wanted me to serve here as a member of the large aircraft fraternity, and from that viewpoint to present a few comments on the outlook for cost reduction in achieving flutter clearance of new aircraft. Even if we limit our attention to large transport aircraft, the range of future possibilities from long haul supersonic aircraft to medium range subsonic transports is rather staggering. For that reason I shall not attempt to make any quantitative overall assessment of cost reduction possibilities but limit my remarks to a brief review of current capability and research needs to check the escalation of flight test costs. (The contrast in scope of the flutter clearance problem for supersonic and subsonic transport aircraft is indicated in figure 1.) Undoubtedly my thinking has been colored to a large extent by my association with the not-so-recent National SST Program, related follow-on activities under DOT contract, and a current NASA Contract (NAS1-12287) covering structural design studies of an arrow-wing supersonic transport.

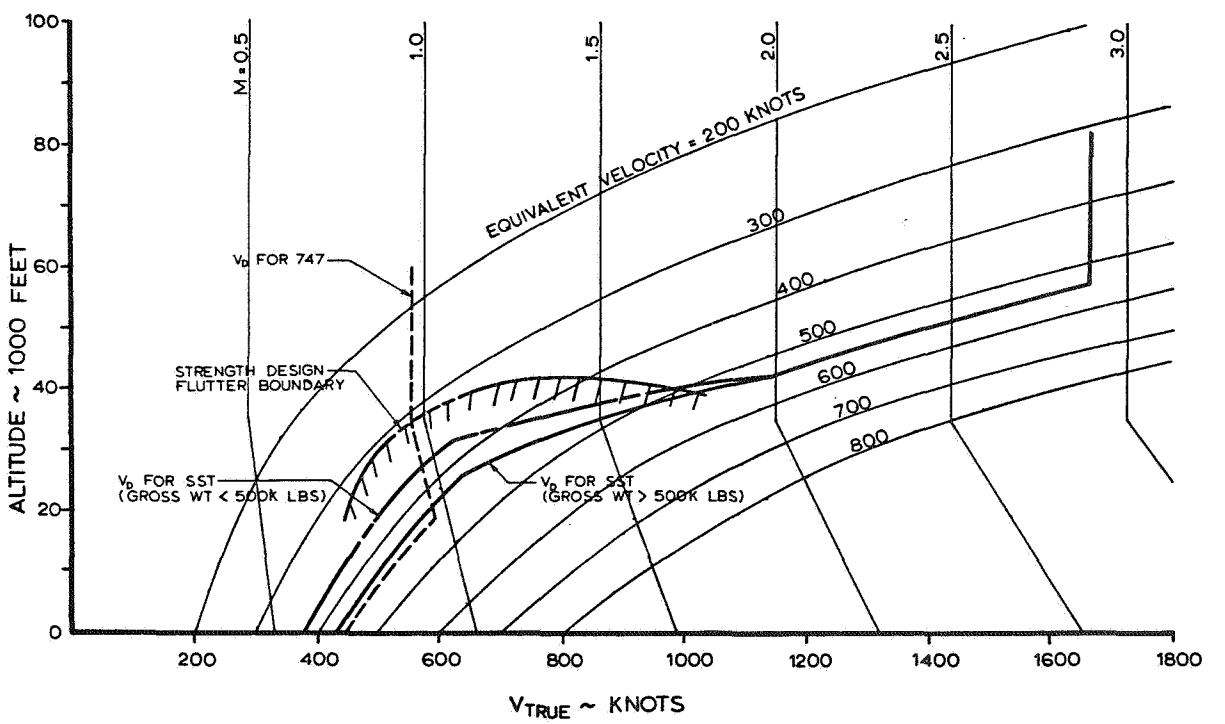

Figure 1.- Flight envelopes. V_D is design dive speed. M is Mach number. 1 ft = 0.3048 m.

Although dynamic behavior is very configuration sensitive, large transport aircraft are generally characterized by relatively low frequencies of the revelant modes of primary structure often with very close spacing of natural frequencies. About 20 natural modes of primary structure may be required to achieve a reasonably adequate flutter analysis, and a wide range of mass distributions (fuel and payload) must be considered. These characteristics tend to complicate the modeling problems--both for theoretical analysis and wind tunnel testing. Flutter prevention is likely to be an important structural design consideration, as illustrated in figure 2, emphasizing the need for efficient and accurate multidiscipline analytical design tools for both preliminary design and detail design applications.

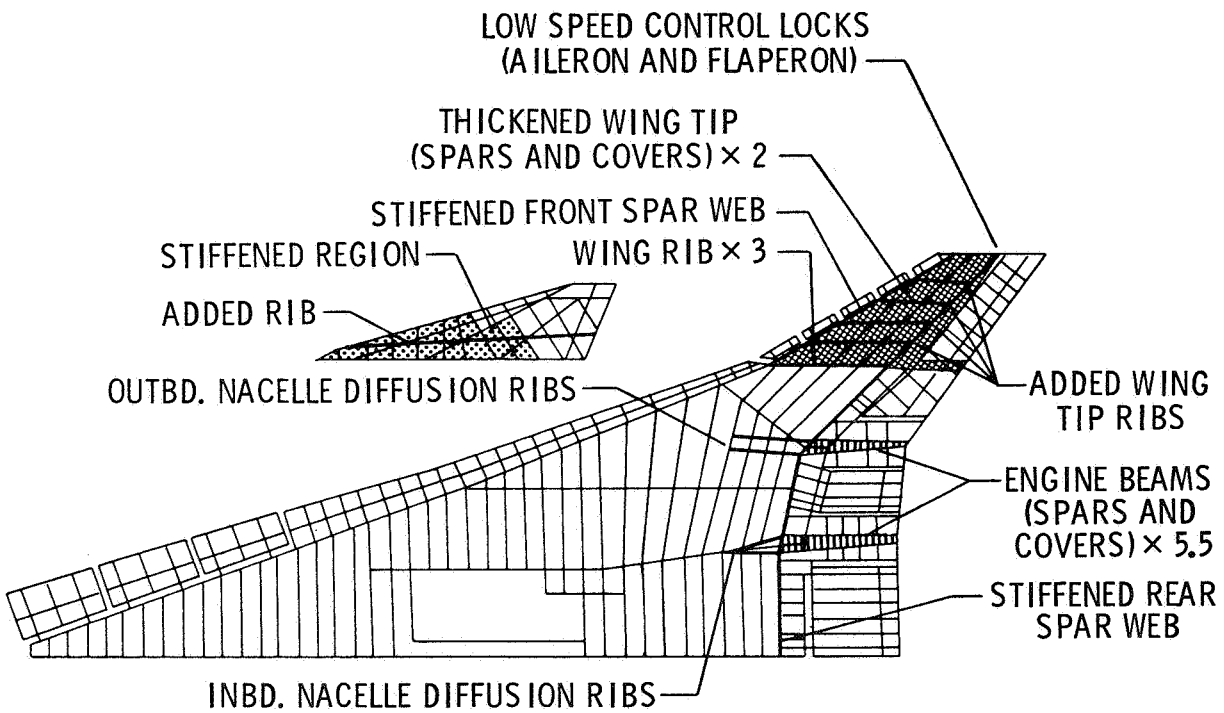

Figure 2.- Arrow-wing structural design study.
Contract NAS1-12287.

The scheduled costs reflected in the flight test plan are primarily derived from a risk assessment. This is a rather subjective process, influenced by calculated margins, multiplicity of potentially critical flutter modes, parametric sensitivity studies, correlation between wind tunnel model tests and analysis, and experience from previous flight tests. Results of a typical model test/analysis correlation study from the National SST Program are shown in figure 3. These data were derived from a component study of a semispan wing model; only flutter speeds (dynamic pressures) and flutter frequencies are compared. The gap in analytical capability indicated

near Mach 1 is still with us; this is a source of major concern in test planning for high performance aircraft. If the program had survived, similar data for a complete model would have been available to support final flight test planning.

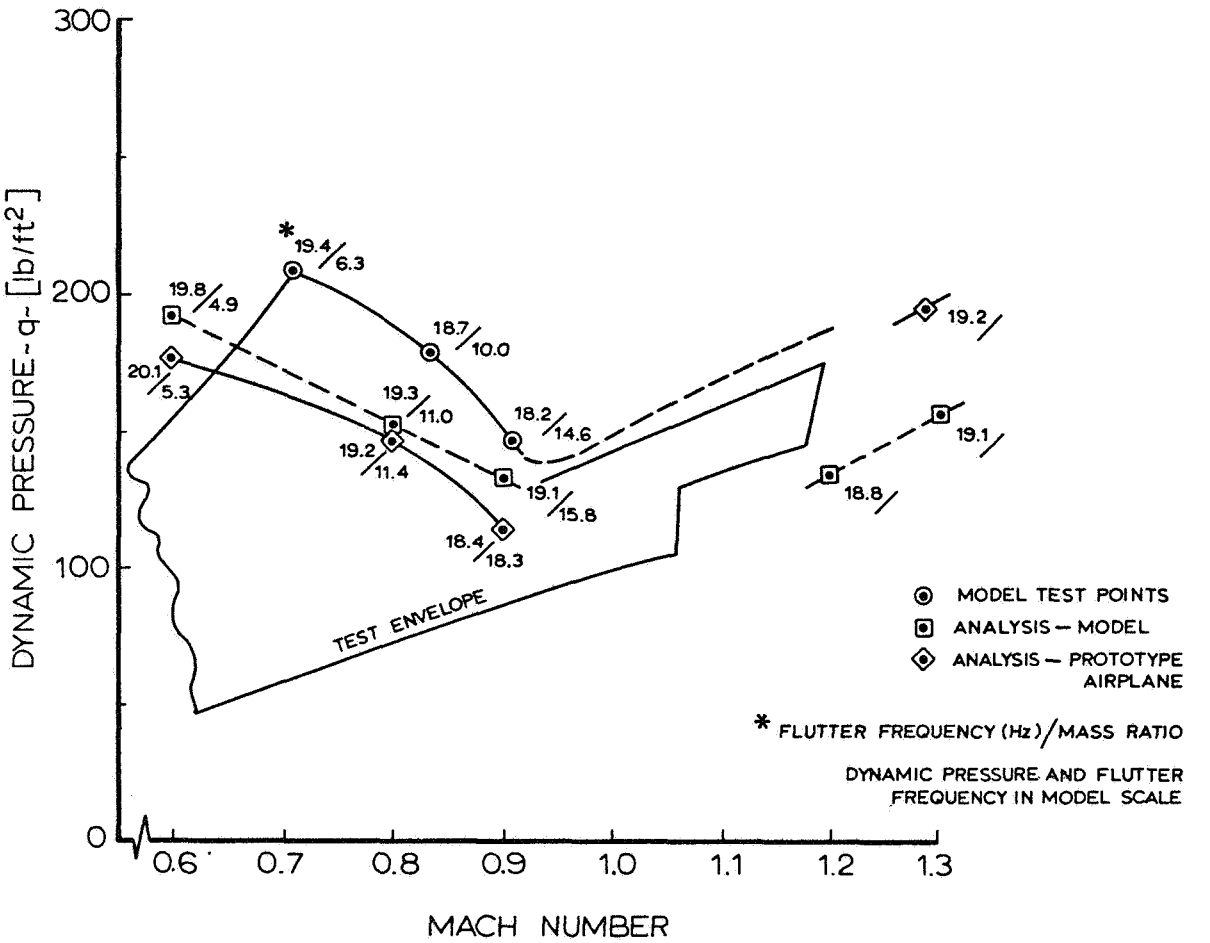

Figure 3.- Analysis/test comparison; transonic wing model.
1 lb/ft^2 = 47.9 N/m^2.

Significant escalation of flight test costs sometimes occurs when unexpected trends appear during the test. Improvement in accuracy of the flutter prediction process is obviously the only remedy for that kind of experience, and this capability must provide for future design innovations. Some of the obvious areas of concern for the future are:

- Unsteady transonic aerodynamics--theoretical, experimental, and empirical correction procedures
- Structural modeling criteria

- Active controls
- Supercritical airfoils
- Wing mounted engines with large, high bypass ratio nacelles

As indicated by the papers presented at this symposium, significant progress has been made in recent years toward better integration of analysis, wind tunnel model testing, ground vibration testing, and flight flutter testing. During the next decade I believe it is reasonable to expect substantial advances in the following areas:

(1) Integrated analytical design tools

(2) Three-dimensional, unsteady, nonlinear inviscid aerodynamic theory

(3) Experimental unsteady aerodynamics

(4) Subcritical analysis and subcritical testing techniques

(5) Active modal control technology

Progress in these areas should improve flutter prediction capability, reduce risk, and thereby help to control the cost of flight flutter testing. However, it is also reasonably certain that new design innovations will contribute a sufficient element of uncertainty to justify some flight flutter testing of any new high performance aircraft.

Holt Ashley:

I will allow five minutes to see if any of the panel members have brief questions and comments.

Harold Sweet:

Regarding the grandiose analytical approaches, thank God I will be retiring, I hope, before those computers are built.

I. E. Garrick:

Regarding the rotor, which was brought up earlier, I want to call attention to the fact that the April 1975 issue, I believe the Journal of Aircraft had a very fine review of the problem of propulsion systems. These are not helicopter rotors, but in a way I think they were all interesting, the theoretical, semiempirical procedures that were outlined in the various papers.

David Brandt:

I've been waiting for someone to suggest that the proponents for analysis should make the first flight.

Bill Bousman, Ames Directorate, U. S. Army Air Mobility R&D Laboratory:

It has been a bad night for us at Ames. There have been all sorts of nasty things said about Hans Mark. I would like to defend his position, but I had a note from the computer center a month ago saying that our time slot in the computer was cut by one third because they were increasing wind-tunnel support time.

All of us heard about being a combined mountain climber, aeroelastician, and flutter freak; at least now I understand why two weeks ago when I tried to climb by Mt. Conness on the east side I had so much trouble. I'm an experimentalist, and that's the analytical side.

I also found out that I'm in bed with 2000 NASA employees by working for the Army. I have a great deal of sympathy with what Dave has said this evening. I have sat in his office and he talked about his problems, and I sat there and mumbled all those good words that he has mentioned. But when it comes for a solution for the problem, I am pretty much a skeptic. It would be very nice if we were all much smarter so we could fix these things as they come up, but that will never happen. I also doubt that pouring the government's money into these problem areas will get us much in terms of fundamental understanding. I just don't have any answer for Dave's problem.

Chris Borland, Rockwell International Corporation:

Comments to Holt: The initial remarks by Dr. Ashley brought out comments from just about everybody on the Chapman-Mark article. I had the privilege of attending the second AIAA Computational Fluid Dynamics Conference in Hartford, Conn., this year, and the article was an object of extreme controversy. I would like to report to this gathering that the view that the computer is going to displace and/or replace the wind tunnel is by no means universal among the people who are involved in the area or field of computational fluid dynamics. Some remarks by Pat Roache, who is one of the biggies in this business, address the point that numerical methods under development are probably the area where the biggest action is. This was completely ignored by the article, which said that bigger computer turbulence models were needed to solve everything once and for all. I think the consensus of feeling was that both the wind tunnel and the computer will be around for a long time, so the experimentalist need not look into his retirement plan to figure out how soon he can get out of the business, because he's going to be there for quite a while.

Also, I would like to address some remarks to Mr. Sweet — who happens to be my boss. He increased my computer budget, so I know that I heard what he has to say is that what we really have to do is tread the narrow path between analysis and experiment. Anybody who falls off either side of the mountain, they are sadly mistaken.

Holt Ashley:

Thank you Chris. I think we should all say a word about that Chapman-Mark article. This is not the only forum from which they have taken something of a beating on what they said; they are all big boys you know, and they are quite capable of defending themselves in this environment. I still suspect, although I can't prove it, that they all had their tongues displaced perhaps a few microinches in the direction of one or the other cheek when they wrote this.

Harold Sweet:

Chris is doing some finite element flow field work, particularly with respect to oscillation in cavities, which I have some great hope for, except that I can't afford his computer bill and I am not sure the Bank of America can either.

Bruce McKeever, Time/Data Corporation:

I have a comment to Jon Turner: I would like to suggest you modify your stand a little bit on getting your algorithm thoroughly developed before you bring on the real test. My own experience indicates that people who are smart enough to come up with a new technique which could be useful aren't wise enough to devise any kind of artificial test that is equal to one real physical experiment.

M. J. Turner:

What I meant to say is that, in developing confidence in analysis, one must first of all verify the adequacy of the basic technologies involved - in our case unsteady aerodynamics, structural behavior, and active control dynamics. Finally, I think there are in the past numerous instances where we overlooked the extremely important additional requirement of verifying the integrated analytical capability for complex systems having thousands of degrees of freedom. Before a newly developed analysis program is applied to

a design project it is essential to run some test cases on representative systems, with sufficient detail to identify the obstacles that result from shear complexity.

Bill Rodden, MacNeal-Schruendler Corporation:

I have written elsewhere that government is spending much of its money in supporting the wrong people to solve problems that we don't have. The forthcoming Proceedings of 1500 pages from the NASA Conference on Computational Fluid Dynamics makes me say "WOW!" When the government wants to solve real research problems instead of imaginary ones, then we can begin to think about reducing testing costs, but not until then.

I. E. Garrick:

I happened to be present at the March Conference at Langley, and I was truly impressed with the real understanding and approaches to numerical methods that those people are making. I think they are making a darn good beginning. I think Bill Rodden is getting too impatient. I really think it's a good beginning in this area of work, and we can really expect some great improvements in the direction which Bill Rodden is talking about, but I don't think it will go all the way.

Holt Ashley:

I want to add something to the theoretician's defense. I've heard too many cracks here about how we can do things only after the facts, so let me just remind you of one little story, which is completely out of the area of aeroelasticity so it is not self serving. You have an airplane that you call the F4H, and you wanted to get to high altitude fast. There are all sorts of ways of doing it. Not all are as successful as it was thought they should be. Certainly the static-performance approach of keeping the maximum distance between the thrust and drag curves with respect to altitude will do the job. Now Art Bryson and a student of his did a simplified equation approach and an optimum trajectory calculation, and they showed how to do it right. They demonstrated the importance of putting the nose down while going through the transonic range. They gave the Navy a recipe for making this flight and said it would take 334 seconds to go from low speed and altitude to level flight at Mach 1 and 65000 feet. It was 2 minutes faster than the Navy had ever been able to do it, but they went out and did it in 332 seconds. There are a few stories like that we should remind ourselves of.

Clarence Perisho, McDonnell Douglas Corporation:

I think you touched on something I have been thinking of in the course of listening to the panel, and that is that nothing is going to replace flutter testing for the flight vehicle. Certainly, a very important place for analysis is in design, but I keep hearing the word correlation. The question is, do you think that analysis will replace the discovery on models of configuration-sensitive interaction flutter today? Is there any possibility that analysis will be any better than what we have seen in the experiment?

M. J. Turner:

I think that there has been a change in the last two or three decades in the role of model testing, now commonly regarded as a procedure for verification of the analytical tools that are being used, while analysis is being used as the principal design tool. Analysis is certainly not going to replace testing completely, but with more extensive application of active controls I believe that the flutter verification will be more readily absorbed into the flight test program, with some reduction of time and costs. Furthermore, with new data processing techniques there is an opportunity to use an on-line computer to improve our diagnostic capability. If surprises do occur, we should then have a better capability of understanding the situation.

Charlie Coe, NASA Ames Research Center:

I can't resist the comment that it almost seems as if the theme of the whole discussion implies that there is some threat to a lot of people because of some development of analytical procedures or methods that eventually will come down the line and threaten the experimental, or vice versa. First, I like Harold Sweet's analogy not necessarily so much for the mountain climbing approach, but I can't help but think that, to a great extent, if you want to get from here to there you would like to have a road map of some sort to study the best approach to get there. The fact that you have been able to study by some analytical procedure the best route — the best method and possibly the lowest-cost method — to get to your destination, that still doesn't eliminate the need to get there. So you still, as Harold says, have to conduct your experimental test and flight test or whatever to demonstrate that you are there. Perhaps the cost of actually making the demonstration can be reduced, but the need is still there. It's my personal opinion that the balance is between analytical procedures and wind-tunnel testing techniques; the wind tunnel is just an analog computer. So there is a strong similarity between the analytical approach by the wind tunnel versus numerical techniques or whatever, and again it's the cost breakdown

that really makes the difference. I think that, in the end, the balance of which way it will go, of course, depends on cost factors but also on brains. That's the other thing, if we have the knowledge, granted the developing knowledge for reaching our goals by analytical procedures, experimental procedures, or whatever, I think that the balance is going to come in proportion to the brain power. I sort of feel that it is really the best of all these factors.

TIME SERIES ANALYSIS IN FLIGHT FLUTTER TESTING AT THE AIR FORCE FLIGHT TEST CENTER: CONCEPTS AND RESULTS

12

Russell W. Lenz
Air Force Flight Test Center

and

Bruce McKeever
Time/Data Corporation

SUMMARY

Concepts of using digital time series analysis for flight flutter testing at the Air Force Flight Test Center (AFFTC) are discussed. The AFFTC Flight Flutter Facility is described. Use of a minicomputer-based time series analyzer and a modal analysis software package is described, as are the results of several evaluations of the software package. The reasons for employing a minimum phase concept in analyzing response only signals are discussed. The use of a Laplace algorithm is shown to be effective for the modal analysis of time histories in flutter testing. Sample results from models and flight tests are provided. The limitations inherent in time series analysis methods are discussed, and the need for effective noise reduction techniques is noted. The use of digital time series analysis techniques in flutter testing is shown to be fast, accurate, and cost effective at AFFTC.

INTRODUCTION

A basic mission of the Air Force Flight Test Center (AFFTC) is the flight testing of new or modified aircraft. The testing of these aircraft and their external store configurations has produced the need for a support capability in the area of flight flutter clearance. Because of the nature of the AFFTC mission, the flutter testing method must meet the following requirements and be effective under the following circumstances:

(1) The analysis capability must be usable during the testing of all types of aircraft, and it must be general enough to cover contractor testing requirements.

(2) The test engineer may not have complete knowledge of the expected flutter characteristics. Flutter prediction analyses,

wind tunnel testing, or ground vibration testing may not have been accomplished on the configuration under test.

(3) Onboard excitation systems may or may not be installed. The input forcing function might not be measurable.

(4) An entire flutter program could consist of a single flight, limiting the time available for in-flight experiments with analysis techniques.

(5) The use of both traditional and newly developed techniques must be possible.

(6) The analysis capability must minimize program cost and flight test time yet insure flight safety.

Flutter test engineers have been analyzing time histories of data for many years by using analog techniques during postflight analysis sessions. In-flight analysis was often limited to strip chart recorder observations. Often the aircraft was equipped with an excitation system, and frequency sweeps were conducted to identify modal frequencies. The sweeps were followed by multiple frequency dwell/quick stop points to obtain damping. This method was often time consuming. If pilot-induced control surface impulses were used, it was not uncommon for the engineer to observe a record in which closely spaced modes made it impossible to determine the modal characteristics of the single modes in real time.

The potential for a nearly real-time analysis capability resulted from the development of the fast Fourier transform (FFT) in 1965. Spectral analyzers which used minicomputer technology to perform FFT's became available shortly thereafter, and the first commercial modal analysis package designed for a minicomputer analyzer was developed in the early 1970's. For the first time, flight test engineers had access to an inexpensive dedicated system which could be used to make accurate real-time modal analyses.

In 1972, AFFTC acquired, and has subsequently developed, an analysis system which meets the requirements mentioned above. The AFFTC flutter test capability was originally developed by two AFFTC structural dynamicists, Captain James A. Long, Jr., and Sergeant Robert L. Berry, and their contributions are gratefully acknowledged. A minicomputer-based time series analyzer and the associated modal analysis software are the heart of the system, which is used to apply digital time series analysis techniques to structural response data. This paper briefly describes the AFFTC Flight Flutter Facility, presents some mathematical background for the analysis techniques being used, gives examples of data obtained

during 3 years of evaluating these methods, and discusses the advantages and limitations of these nearly real-time analysis techniques.

SYMBOLS

A	amplitude of the complex frequency response function
a =	$\omega\zeta$, per sec
b =	$\omega\sqrt{1-\zeta^2}$, per sec
C	autocorrelation, V^2
$\dot{C}$	derivative of the autocorrelation with respect to time
c	constant
f	frequency, Hz
g	structural damping
H	complex frequency response function
h	impulse response function, V
j =	$\sqrt{-1}$
k	resolution element number
m	mass, kg (slugs)
P	real component of the frequency response function
Q	imaginary component of the frequency response function
R	magnitude of the residue, V
r	complex residue
S	power spectrum, V^2
s	Laplace variable
T	arbitrary time in a sample data frame, sec
t	time, sec

u	dummy variable
X	Fourier transform of input signal
x	input signal, V
Y	Fourier transform of response
Y'	minimum phase power spectrum, V^2
α	attenuation or absolute damping, per sec
Δf	frequency resolution, Hz
Δt	time in data frame prior to taking an FFT, sec
ζ	viscous damping ratio
θ	phase of the residue, deg
σ	absolute damping, $2\pi\alpha$, per sec
τ	autocorrelation time lag, sec
ϕ	phase of the impulse response, rad
ω	frequency, rad/sec
$*$	complex conjugate

Subscripts:

i	index
x	input
y	response

FLIGHT FLUTTER FACILITY

The AFFTC Flight Flutter Facility was designed to permit test engineers to use traditional strip chart analysis techniques in conjunction with advanced digital time series analysis methods. Pulse code modulation (PCM) or frequency modulation (FM/FM) flight data are converted to analog signals which can be analyzed by either technique (fig. 1). The analog filters improve the strip chart analyses by reducing noise and isolating modes. They also prevent aliasing (frequency foldback) in the digital analyses.

The hardware and software of the AFFTC system were updated several times to meet changing requirements and to increase analysis speed. The current system configuration (fig. 2) uses a 28,000-word minicomputer. The panel control unit is used during the operation of the two-channel spectrum analyzer and the small cathode ray tube (CRT) display unit. The X-Y plotter is used to produce copies of the unit's displays. A paper tape reader/punch device is used to input or save system software. The alphanumeric/graphics display terminal is the primary input/output device. It is operated in conjunction with a hard copy unit which generates a reproducible copy in 9 seconds. A multiplexer permits the simultaneous sampling of up to 16 channels of data. Antialiasing filters (low pass filters set at 30 hertz or 60 hertz) prevent higher frequencies from aliasing or folding back to lower frequencies during the digital analysis. The sampled digital time histories and the analyzer setup information are stored on two 1.2-million-word disk units. One disk unit permits the time history data used in the nearly real-time analysis of selected data channels to be stored prior to analysis. Multiple analysis approaches may be applied to the stored data. The data disk also enables an engineer to recall additional channels of data while the aircraft is turning or refueling or when strip charts indicate that a particular channel is of interest. The second disk unit is reserved for storing the program software. The six tunable bandpass (12 low pass or high pass) filters improve strip chart analyses, permit more flexibility in the selection of antialiasing filter cutoffs, and allow bandpass-filtered signals to be analyzed digitally without having to use digital filters. A patch panel links the various system components. Not shown in the photograph are the three strip chart recorders and a programmable calculator with its associated terminal.

A reduced system can and has been used at AFFTC during flutter testing. The panel-operated, two-channel spectrum analyzer can be used in conjunction with strip chart analyses, but this approach requires more flight time and results in less overall accuracy than can be obtained by using the entire capability. The current AFFTC configuration is considered to be a minimum facility for efficient operation.

The primary mode of system operation uses the alphanumeric/graphics display terminal and selected AFFTC- or contractor-written software. The engineer uses one or more of the available analysis techniques (described later in the paper) to generate trends of modal frequency, damping, or amplitude. During AFFTC tests in which control surface impulse excitation is used, at least two response channels are analyzed before the pilot is cleared for the next test condition. For test planning purposes, approximately 4 minutes are allowed per test point, although this estimate increases if the aircraft is to be power limited during

the test. The use of the multiple analysis techniques available in the system permits the AFFTC engineers or contractors to adapt quickly to the characteristics of a particular aircraft or to changing flight conditions.

TIME SERIES/LAPLACE ANALYSIS

The digital time series analysis techniques used at AFFTC utilize the FFT to linearly transform a structural response time history into a complex frequency domain function which is comprised of sinusoids with specific amplitude and phase characteristics. The squared magnitude of a response as a function of frequency (auto power spectrum) can be obtained as follows:

$$S_{yy}(j\omega) = Y^*(j\omega) \cdot Y(j\omega) \tag{1}$$

where $Y(j\omega)$ is the Fourier transform of a response time history and $Y^*(j\omega)$ is the complex conjugate of $Y(j\omega)$. If the input force time history ($x(t)$) is also measured, a cross power spectrum can be computed:

$$S_{xy}(j\omega) = X^*(j\omega) \cdot Y(j\omega) \tag{2}$$

The amplitude and phase relationship between the response and a given input is used to define a system transfer function (complex frequency response function) as follows:

$$H(j\omega) = \frac{Y(j\omega)}{X(j\omega)} = \frac{X^*(j\omega) \cdot Y(j\omega)}{X^*(j\omega) \cdot X(j\omega)} = \frac{S_{xy}(j\omega)}{S_{xx}(j\omega)} \tag{3}$$

The use of the cross spectrum and input auto spectrum removes the need for complex division, and, more importantly, the cross spectrum tends to improve transfer function estimates by removing the effects of noise that is not correlated with the input force.

The Fourier transform of the transfer function is the impulse response function, which is a time history comprised of damped sinusoids that indicate structural response to an impulse type of input. The frequency, damping, amplitude, and phase of the sinusoids that make up the impulse response function (or complex frequency response function) define the modal characteristics of the structure at the measured location for a specific flight condition.

Modal analyses of these tranfer functions or impulse response functions are being made in the technical community in many different ways. Some methods use minicomputers, some larger computers. Much of the AFFTC analysis capability is based on a Time/Data 1923/50 Time Series Analyzer and the associated Modal Analysis (Laplace) Package software. Some of the techniques discussed in this paper are specific to this software package. The overall AFFTC analysis capability attempts to capitalize on the strengths and compensate for the limitations of each software component so that the final flutter clearance is as rapid and accurate as possible.

The determination of the system transfer function is of fundamental concern. The software subroutine package used permits modal analysis when the input and output time histories are measured and when the structural response alone is measured. Aircraft responses excited by pilot-induced control surface impulses have been analyzed without knowing the true forcing input.

It is assumed that the response in the response only case is characteristic of a minimum phase system. This implies that the system is physically realizable, that damping is stable for all modes, and that of all the impulse responses with the same autocorrelation, the one selected has the most rapid initial buildup of energy. When these conditions are met, a form of the Hilbert transform can be used to calculate the minimum phase of the system given only its amplitude characteristics. (The minimum phase calculations are described and compared with the more common autocorrelation technique in the appendix.) To calculate the transfer function accurately directly from the derived minimum phase spectrum, $Y'(j\omega)$, an additional assumption is made as follows:

$$H(j\omega) = \frac{Y'(j\omega)}{X(j\omega)} \tag{4}$$

where $X(j\omega)$ is a constant. The input forcing function has a constant amplitude frequency power spectrum in the frequency band of interest. This is characteristic of impulse, random noise, and swept sine wave inputs. In reality, the input spectrum is not perfectly flat, but the assumption still produces reasonable accuracy, and the merit of the technique has been proven in flight test. If the input is not flat, the response may indicate high energy at a location that corresponds to a pole of the drive function. This possibility must be considered by the engineer because it occurs in all techniques of response only analysis.

If the input forcing function can be measured, it is better to use the transfer function estimate obtained from equation (3). The transfer function estimate, whether calculated directly or by using the minimum phase concept, contains the modal information which is extracted during the Laplace analysis.

The Laplace analysis uses the concept of a partial fraction expansion of the complex frequency response function to define modal parameters for each pole, $s = s_i$, in the Laplace plane, as follows:

$$H(j\omega) = H(s) = \sum_i \left\{\frac{r_i^*}{s + s_i^*} + \frac{r_i}{s + s_i}\right\}$$

$$= \sum_i \left\{\frac{R_i e^{j\theta_i(\pi/180)}}{s + (2\pi\alpha_i - j2\pi k_i)} + \frac{R_i e^{-j\theta_i(\pi/180)}}{s + (2\pi\alpha_i + j2\pi k_i)}\right\} \qquad (5)$$

A graphical description of the poles and the related modal parameters is given in figure 3. The pole location, s_i, defines the absolute damping, α_i, and the frequency line number, k_i, of the mode. The numerator in equation (5), r_i, is a complex residue composed of a magnitude, R_i, and a phase, θ_i. This residue defines the modal eigenvector when measurements are made over an entire structure. For structures with nonproportional damping, the residue defines a complex mode; but for modes with proportional damping, the phase relationships of the eigenvector points only differ by approximately 0° or 180°. The impulse response function in the form derived by the Laplace software demonstrates the physical meaning of the modal parameters:

$$h(t) = \sum_i \left\{2R_i e^{(-2\pi\alpha_i)t} \cos\left[2\pi k_i t + \theta_i(\pi/180)\right]\right\} \qquad (6)$$

The absolute damping and the frequency line number can be related to the more familiar damping ratio, ζ, or structural damping, g, and frequency, f, as follows:

$$\zeta = \frac{1}{2} g = \alpha \frac{1}{\sqrt{k^2 + \alpha^2}} \qquad (7)$$

$$\approx \frac{\alpha}{k} \text{ for lowly damped modes}$$

$$f = \frac{(k)\ (\text{sample rate})}{(\text{frame size})} \text{ Hz} \qquad (8)$$

A description of the theory of defining modal parameters in terms of the Laplace plane and an explanation of the validity of the partial fraction expansion of the transfer function in terms of poles and residues is to be found in reference 1. Reference 1 also discusses the concept of nonproportional damping. The algorithm that is actually used to transfer mathematically from the Fourier representation of a system to the Laplace plane (fig. 3) is currently proprietary information. An intuitive verification of the technique can be made, however, by observing that the impulse response in equation (6) can be defined by using the superposition of the Laplace parameters. The use of such a mode generation approach has made it possible for engineers to generate known functions digitally and to perform circle checks on the modal results calculated from the transfer function.

The Laplace software contains procedures that attempt to identify the modes which have the highest spectral energy and the lowest damping. A modal energy value is calculated for each pole as a percentage of total energy in the frequency band being analyzed. Only the modes with a percentage energy greater than a selected cutoff value and with an attenuation (absolute damping) less than a specified cutoff are included in the mode list printout. This procedure eliminates long mode list printouts and makes it much easier for the analyst to identify and track the modes that are of interest to him.

The accuracy of the Laplace algorithm and its ability to separate closely spaced modes has been investigated at AFFTC by using digitally generated transfer functions. Single or bipolar modal parameter lists were input, a complex transfer function was derived, the Laplace routines calculated the modal parameters, and a comparison was made between input data and the extracted data in order to assess program limitations. The single mode study verified that frequency was derived accurately and that damping was calculated to within 10 percent of the correct value for the modes with viscous damping ratios less than 0.10, except for modes near the upper cutoff frequency. A typical error envelope showing the maximum values of damping which resulted in a 10-percent error in damping is shown in figure 4. The attenuation curve demonstrates that the interference effect of the ends of the data frame can be significant. Knowledge of this effect and the relationship between damping ratio and absolute damping (eq. (7)) is used by the analyst to insure that appropriate frame sizes and sampling rates are selected in order to extract the modes of interest accurately.

The bipolar digital complex frequency function study used a parametric variation of damping ratio and frequency resolution

element separation. The separation in hertz, Δf, between resolution elements k_i and k_{i+1} is

$$\Delta f = \frac{1}{\Delta t}, \tag{9}$$

where Δt is the time in seconds contained in the data frame prior to performing the Fourier transform. Damping ratio was varied from 0.005 to 0.10 and frequency separation was in the range of 1 to 160 elements in a complex frequency domain frame of 256 lines. The following results were obtained:

(1) Accuracy of the frequency and damping ratio estimates increased as the separation between the two modes increased.

(2) The error in the calculation of the characteristics of modes with low damping ($\zeta \leq 0.035$) was less than 10 percent. A five-resolution-element separation between modes was the minimum necessary to consistently maintain this accuracy.

(3) As two modes converged in frequency, the accuracy of the estimates was degraded. Lightly damped modes ($\zeta \leq 0.035$) were evaluated accurately regardless of the presence of other modes. Estimates of closely spaced modes which had higher damping were in error, but the accuracy of the estimate improved if both modes were highly damped.

The digital studies verified that all significant modes (sufficient energy and low damping) would be accurately identified by the Laplace software from a given transfer function. (The highly damped modes were of minor concern to AFFTC engineers during a real-time flight test clearance program. When desired, these modes were analyzed separately by using more appropriate techniques.)

The Laplace package software was also evaluated by using analog computer models. Table 1 shows the results of a four-mode case in which a pulse excitation was used. These response only cases were analyzed by using the minimum phase algorithm before performing the Laplace analysis. The frequency was generally accurately determined for well excited modes when damping ratios were less than 0.20. The analyst used the frequency response magnitude plots to verify the estimates visually. The frequency and damping values were determined accurately for modes that were well within the design envelope of the Laplace software ($\zeta < 0.10$). The highly damped modes often exhibited low calculated damping values (on the order of 0.001), although this error was readily apparent to the engineer by observing the transfer function magnitude plots. The false modes were also identified by observing their low energies and/or low residues on the mode list printout.

Analog models were also used to verify the system's accuracy for swept sine wave results. A unique approach reported in reference 2 has been employed to reduce truncation errors encountered when the sweep time is too long (core is too restricted) to be included in one frame of data. The traditional approach in averaging has been to ensemble average data in the frequency domain. (If multiple frames of data are required, take the FFT of each frame and frequency average the multiple frequency domain results.) As shown in figure 5, a mode's response may be truncated by a frame. This results in erroneous modal parameter estimates. The new approach, which is called time averaging at AFFTC, uses the fact that the frequency content is continually changing so that multiple time histories can be superimposed without distorting the earlier portions of the time history. The periodic nature of the FFT (fig. 6) permits the entire swept sine wave response to be averaged without truncation errors because all the time segments are still represented in the time history that is Fourier transformed. The repeating signal at the top of figure 6 can be added to the repeating signal in the middle of figure 6 (the second frame in the sweep in fig. 5), and the result (at the bottom of fig. 6) appears to be two segments of data of length 2T which are superimposed after being shifted with respect to each other by 1T. The total frame length being transformed is T, and this is the value that determines the frequency resolution. This procedure would not be accurate if the same frequency content occurred in multiple frames - if, for example, noise significantly excited the modes. A good procedure in this instance is to include the entire mode response within one data frame so that there is no response truncation and minimal noise interference. Typical Laplace results for a swept sine wave model are provided in figure 7 for the two types of averaging.

The digital and analog simulations demonstrated to AFFTC engineers that the Laplace package software was well suited to the evaluation of critical modes in flutter testing. A multimode response could be analyzed without knowing where the modes were in advance, and all nonhighly damped modes would be extracted simultaneously with good accuracy. The pulse type of response only data was evaluated well by using the minimum phase concept to generate the phase of the transfer function.

FLIGHT FLUTTER TEST APPLICATIONS AND RESULTS

The use of digital time series analysis techniques in flight tests verified the advantages of the AFFTC system and

reminded the engineers of the limitations inherent in all time series analysis methods. The system was used in the testing of a number of different aircraft types with different excitation systems. Tests of the F-111 transonic aircraft technology (TACT) vehicle and a B-52D aircraft configured with various external stores used pilot-induced control surface pulses, tests of the A-10 airplane used aerodynamic vane exciters, and the tests of the B-1 air vehicle used dynamic mass exciters. The actual analysis techniques used in these programs varied somewhat depending on the modes of interest and the testing conditions.

Typical hard copy output for a test in which control surface pulses were used is shown in figures 8 and 9 and table 2. The AFFTC software was written to utilize the Laplace software package subroutines efficiently during a real-time flutter analysis. Figure 8 contains a time history of sampled response data for an elevator pulse during a B-52D aircraft/store certification program. The dashed lines indicate the 6.25 seconds of data which were analyzed by using the minimum phase assumption. The maximum response peak was used as a starting location because it resulted in more consistent data trends. (The pilot input did not result in a true spike input because the dynamics of the control system caused small overshoot oscillations.) The magnitude of the transfer function is shown in figure 9. The engineer could also view the coincident, quadrature, or phase spectrums or phase plane plots. The vertical lines in figure 9 were drawn automatically at frequencies selected for analysis by the Laplace software. The analyst then had the opportunity to change the frequency analysis band, damping (alpha) cutoff, and energy threshold; or he could have the mode list (table 2) displayed and copied. If the input was known, the time history would not normally be displayed and the minimum phase assumption would not be needed to derive the transfer function; but the rest of the analysis would be the same.

In table 2, the damping levels of the 4.16-hertz and 5.76-hertz modes would be questioned by the analyst because of low energies and residues (poor excitation). It is significant that two high energy, high residue, closely spaced modes were identified. The frequency and damping of these modes could not be determined easily by using traditional strip chart logarithmic decrement analyses. The total time required to perform the analysis and obtain the hard copy results shown was 1.1 minutes. Additional time histories were analyzed from disk data as desired. Multiple data trends were plotted by hand during the flight, but mode results stored on the disk were plotted during postflight sessions using the graphics display unit and its hard copy device. These hard copy outputs permitted efficient

postflight data review and reduced the number of man-hours required to generate an accurate final report.

Resolution and Record Length

A limitation encountered in the time series analysis of structural response data whether digital or analog methods are used is the relation between frequency resolution and record length (eq. (9)). In the stick rap response data above, the resolution, Δf, was 0.16 hertz because only a 6.25-second time frame was filled with data before the signal decayed to the noise level. The response signature for modes with higher damping or higher frequencies may be considerably shorter than in the example, and the resolution would end up by being lower. (If the frame size is not shortened appropriately, the data appear to have lower damping because of the continuously excited data in the noise level and statistical variability.)

As demonstrated in figure 10, the reduction in resolution has several effects on the data: (1) the data curves are smoothed and less noise is evident; (2) the ability to separate closely spaced modes decreases; and (3) the minimum damping level which can be defined increases. The last effect could be catastrophic in flutter testing.

Signal To Noise Ratio

The resolution problem intensifies when the signal to noise ratio in flight testing is degraded. When this happens some smoothing of the data is necessary. However, the effective frequency resolution then decreases. Both higher force levels and longer sweep times are used to improve the signal to noise ratio. The calculation of the transfer function depends on the correct measurement of input and output. If the aircraft is excited significantly by turbulence or buffet, the measured input is wrong; therefore, the estimate of the transfer function is wrong, and this distorts the modal parameter calculations.

In figure 11, the signal to noise ratio in the response is poor. The aircraft was power limited at its high speed flutter points, so the linear sweep times were restricted to 7 seconds. The transfer function for this time history is shown in figure 12. Most of the energy in figure 12 is in a symmetric mode (between the dashed lines), but the structure was being excited antisymmetrically by aerodynamic vanes. The poor transfer function estimate prevented the antisymmetric mode of interest from being analyzed accurately by the software. The engineers used the

bandpass filters and the reliable frequency dwell/quick stop methods to track the mode of interest. Better estimates of the true transfer functions were obtained when the signal to noise ratio improved, and the Laplace technique then generally gave reasonable results. Dwell/quick stop methods were also used to obtain damping estimates for modes of interest which exhibited energy levels which were too low for accurate digital analysis.

The technique of adding or subtracting channels of data to emphasize symmetric or antisymmetric modes has been used with some success on data similar to those shown in figures 12 and 13. The resulting signal to noise ratio improved in that only the modes of interest were included, but the buffet response in the mode of interest also increased. The process was useful while a minimum phase analysis was used to identify modes, but the direct calculation of the transfer function was still in error because of the multiple inputs.

Random Noise Excitation

The flexibility of the minicomputer-based analyzer permits the engineer to select alternative analysis techniques if required. During the F-111 TACT program, transonic buffet excited modes with frequencies which were higher than the frequencies being excited by the stick raps. The Laplace software, working with a 5-second sample of data which followed the stick rap, would identify the higher modal frequencies, but the calculated damping level would be low because of the continuous excitation during the sampling. These modes were analyzed during postflight sessions by using the waveform-averaging capability of the analyzer to generate a randomdec signature.

The randomdec analysis, a technique developed by Henry Cole, Jr. (ref. 3) uses 30 to 45 seconds of buffet response to generate a pseudo impulse response function. As figure 13 shows, the impulse response characteristics of the 16.7-hertz mode could readily be identified. When a minimum phase analysis was applied to the response spectrum generated over the same time period as was used to calculate the randomdec signature (fig. 13), the calculated damping was low. The frequency-ensemble-averaged auto-spectrum did not have enough averages to reduce the statistical variability. The noise spikes in the power spectra would be identified as lightly damped modes by the software. Smoothing the data reduced the effective resolution of the data to unacceptable levels. The analog randomdec technique was not used in real time because the analyst would have been limited to one response channel and one frequency. The stick raps excited the modes of interest from a flutter standpoint (approximately 5 hertz and

7 hertz) and the analyses were done on multiple channels in nearly real time.

A digital version of the randomdec process has been written recently, so multiple channels and frequencies can be analyzed from the time histories stored on disk. The technique will be used in selected analyses, but it still has difficulty in separating closely space modes and it is sensitive to bandpass filter bandwidth.

CONCLUDING REMARKS

The use of digital time series analysis techniques at the Air Force Flight Test Center (AFFTC) has been beneficial in terms of time and accuracy. The Modal Analysis (Laplace) Package software proved to be a valuable tool for analyzing transfer functions which had been calculated either from known inputs or from minimum phase response spectra. Of particular value was the ability of the Laplace method to analyze significant, lightly damped modes even when the modes were closely coupled. The engineer needed a working knowledge of both aeroelasticity and time series analysis to analyze flutter test data, but he did not need to know the location or the number of the significant modes before the analysis. (Prior knowledge does make things easier, however.) The AFFTC minicomputer-based system is a tool that is flexible and low in cost (in terms of initial investment and reduced test time), and it can easily be reprogramed as new algorithms are developed.

The limitations of the analysis are related to record length, signal to noise ratio, and measurement of frequency response functions. New techniques of noise reduction and transfer function enhancement are being studied at AFFTC as well as at many other places. The effective use of turbulence- or buffet-excited response data is also being pursued.

The mission of AFFTC and the requirements this mission sets for a real-time flutter test analysis system mean that the approach taken must be general and that the technique must be cost effective. The use of digital time series analysis techniques at AFFTC during the last 3 years has been helpful in clearing aircraft quickly and safely and has also been very instructive in the proper use of these methods. The engineers at AFFTC expect the implementation of improved digital techniques to result in even greater benefits during future flutter testing.

APPENDIX

COMPARISON OF MINIMUM PHASE CRITERIA WITH THE AUTOCORRELATION APPROACH

For certain conditions, there is a definite one-to-one relationship between the frequency response characteristics P and Q where

$$H(j\omega) = P(\omega) + jQ(\omega) = A(\omega)e^{j\phi(\omega)} \tag{A1}$$

The amplitude, $A(\omega)$, and the phase, $\phi(\omega)$, are uniquely related to the real and imaginary components of the transfer function:

$$A(\omega) = \sqrt{P^2(\omega) + Q^2(\omega)} \tag{A2}$$

$$\phi(\omega) = \arctan\left(\frac{Q(\omega)}{P(\omega)}\right) \tag{A3}$$

It can be noted that the logarithm of the transfer function is related to the log amplitude characteristic and the phase characteristic in the same manner that $H(j\omega)$ is related to P and Q in equation (A1).

$$\ln H(j\omega) = \ln (A(\omega)) + j\phi(\omega) \tag{A4}$$

If the system is both stable and causal, Hilbert transforms can be derived which relate P and Q (ref. 4):

$$P(\omega) = -\frac{1}{\pi}\int_{-\infty}^{\infty} \frac{Q(u)}{u - \omega}\, du \tag{A5}$$

$$Q(\omega) = \frac{1}{\pi}\int_{-\infty}^{\infty} \frac{P(u)}{u - \omega}\, du \tag{A6}$$

The similarity of equations (A1) and (A4) makes it possible to calculate either the amplitude or phase given the other. In this case, the logarithm of $H(j\omega)$ must have neither unstable poles nor zeroes.

$$\ln A(\omega) = -\frac{1}{\pi}\int_{-\infty}^{\infty} \frac{\phi(u)}{u - \omega}\, du \tag{A7}$$

$$\phi(\omega) = \frac{1}{\pi} \int_{-\infty}^{\infty} \frac{\ln A(u)}{u - \omega} \, du \qquad \text{(A8)}$$

Of more practical interest in calculating the phase in digital studies is the following equation, which utilizes the Fourier transform (ref. 5).

$$\phi(\omega) = \text{DFT} \left\{ \left\{ \frac{1}{2} - U\left(t - \frac{T}{2}\right) \right\} \cdot \{\text{IFT}(\ln S_{yy}(\omega))\} \right\} \qquad \text{(A9)}$$

where

DFT — direct Fourier transform,

IFT — inverse Fourier transform, and

T — arbitrary time in the data frame with the fundamental Fourier period going from 0 to T

$$\frac{1}{2} - U\left(t - \frac{T}{2}\right) = \begin{cases} +\frac{1}{2} & 0 < t < \frac{T}{2} \\ 0 & t = 0, \frac{T}{2}, T \\ -\frac{1}{2} & \frac{T}{2} < t < T \end{cases}$$

The $\phi(\omega)$ which is calculated is known as a minimum phase, and the system is a minimum phase system. The complete frequency response function is estimated by combining the minimum phase with the square root of the autospectrum. The frequency response may then be inverse Fourier transformed to give the true impulse response function for the minimum phase system.

Three assumptions must be made about the data for the minimum phase procedure to be used. First, it is assumed that all modes have stable damping. Second, the system is assumed to be causal; that is, the impulse response is considered to be zero for negative time and it is assumed that the system cannot respond to an input before it occurs. Third, of all frequency responses with the same autospectrum, the one selected is assumed to have the smallest total change in phase angle from zero to maximum frequency. This implies that, of all impulse responses with the same autocorrelation, the one selected has the most rapid initial buildup of energy.

The first two criteria would almost certainly be true in an aircraft response. The third criterion is more difficult to verify for a particular structural response, but the minimum phase

usually approximates the true impulse response better than the zero phase imposed during an autocorrelation. If the structural response builds up to its maximum amplitude quickly (an estimate is less than 1 cycle) when subjected to an impulse, the minimum phase assumption should be valid. If the buildup is slow (several cycles), the results of the minimum phase procedure are probably invalid. The frequency and damping obtained from the impulse response would still be correct, but the amplitude would be incorrect.

If the system does comply with the previous criteria, the autocorrelation and the autospectrum of the minimum-phase-estimated complete frequency response are exactly the same as the autocorrelation and autospectrum of the true frequency response. The results of the minimum phase procedure can be compared with the results of the autocorrelation technique. The autocorrelation of an impulse response is not always equal to the impulse response, and the derivative of the autocorrelation of an impulse response is not always equal to the impulse response. An explanation of the autocorrelation and the derivative of the autocorrelation can be found in reference 6.

As shown in reference 6, a simple damped mass system with sine phase will have the following impulse response:

$$h_1(t) = \frac{1}{mb} e^{-at} \sin bt \tag{A10}$$

where m is mass, $b = \omega\sqrt{1 - \zeta^2}$, and $a = \omega\zeta$.

If a cosine phase function is defined, a second impulse response can be determined as follows

$$h_2(t) = \frac{1}{mb} e^{-at} \cos bt \tag{A11}$$

and the autocorrelation of these two functions can be calculated:

$$C_1(\tau) = \frac{e^{-a\tau}}{4m^2a\omega^2} \left[\cos (b\tau) + \frac{a}{b} \sin (b\tau)\right]$$

$$= \frac{1}{4m\omega^2} h_1(\tau) + \left(\frac{b/a}{4m\omega^2}\right) h_2(\tau) \tag{A12}$$

$$C_2(\tau) = \frac{e^{-a\tau}}{4m^2a\omega^2}\left[\left(1 + 2\frac{a^2}{b^2}\right)\cos(b\tau) - \frac{a}{b}\sin(b\tau)\right]$$

$$= \frac{\left(1 + 2\frac{a^2}{b^2}\right)\frac{b}{a}}{4m\omega^2} h_2(\tau) - \frac{1}{4m\omega^2} h_1(\tau) \qquad \text{(A13)}$$

The derivative of these autocorrelations can also be written as follows:

$$\dot{C}_1(\tau) = -\frac{1}{4ma} h_1(\tau) \qquad \text{(A14)}$$

$$\dot{C}_2(\tau) = \frac{-1}{2mb} h_2(\tau) - \frac{1}{4ma} h_1(\tau) \qquad \text{(A15)}$$

As noted in reference 6, $\dot{C}_1(\tau)$ is equal to, within a constant, $h_1(t)$. If a new function is now defined such that c_1 and c_2 are the following constants

$$h_3(t) = c_1 h_1(t) + c_2 h_2(t) \qquad \text{(A16)}$$

the following autocorrelation and autocorrelation derivative equations can be obtained:

$$C_3(\tau) = c_1^2 C_1(\tau) + 2c_1c_2\frac{a}{b}C_1(\tau) + c_2^2 C_2(\tau) \qquad \text{(A17)}$$

$$\dot{C}_3(\tau) = c_1^2 \dot{C}_1(\tau) + 2c_1c_2\frac{a}{b}\dot{C}_1(\tau) + c_2^2 \dot{C}_2(\tau) \qquad \text{(A18)}$$

It is evident from equations (A17) and (A18) that while the attenuation and oscillation rates of an unknown impulse response are uniquely determined without knowing the phase by calculating the autocorrelation or the derivative of the autocorrelation, the amplitude cannot be determined except for a very lightly damped impulse. It has also been found that the autocorrelation, or its derivative, of the particular impulse response is not always proportional to the impulse response.

The derivation of the system parameters from the response only cannot be expected to give as good an answer as can be obtained when the input and output are used. However, the autocorrelation method and the minimum phase approach often give reasonably accurate estimates of frequency and damping. An advantage of using the minimum phase assumption, when it is applicable, is that the mode shape (with the exception of a possible

180° phase shift) can be determined for modes with proportional damping. For complex modes, both the autocorrelation and the minimum phase mode shape estimates are distorted, but the latter estimate is better.

REFERENCES

1. Hurty, Walter C.; and Rubinstein, F.: Dynamics of Structures. Prentice-Hall, Inc., 1964.

2. Norin, R. S.; and Sloane, E. A.: A New Algorithm for Improving Digital Random Control System Speed and Accuracy. Proceedings of the 21st Annual Technical Meeting of the Institute of Environmental Sciencies, Volume 2, 1975, pp. 46-52.

3. Cole, Henry A., Jr.: On-Line Failure Detection and Damping Measurement of Aerospace Structures by Random Decrement Signatures. NASA CR-2205, Mar. 1973.

4. Solodovnikov, V. V. (W. Chrzczonowicz, transl.): Statistical Dynamics of Linear Automatic Control Systems. Second ed. Van Nostrand Reinhold Co., 1965.

5. Oppenheim, Alan V.; and Schafer, Ronald W.: Digital Signal Processing. Prentice-Hall, Inc., 1975.

6. Houbolt, John C.: Subcritical Flutter Testing and System Identification. NASA CR-132480, Aug. 1974.

TABLE 1.- MODEL COMPARISON FOR FOUR MODE CASES WITH EQUIVALENT PULSE EXCITATION.

CASE NO.	MODEL EXCITATION	MODE 1 f_1	MODE 1 ζ_1	MODE 2 f_2	MODE 2 ζ_2	MODE 3 f_3	MODE 3 ζ_3	MODE 4 f_4	MODE 4 ζ_4	TYPE OF SIGNAL
----	MODEL	3.0	.050	6.0	.020	8.0	.10	12.0	.200	----
17	$\dot{X}_1(0) = \dot{X}_2(0) = .5v$	3.0	.0526	6.0	.0222	7.40	.0362	-	-	DISPLACEMENT
	$\dot{X}_3(0) = \dot{X}_4(0) = 1.0v$	3.0	.0510	6.0	.0192	8.40	.0293	-	-	VELOCITY
18	$\dot{X}_1(0) = \dot{X}_2(0) = .25v$	3.0	.0510	6.0	.0206	7.79	.0600	-	-	DISPLACEMENT
	$\dot{X}_3(0) = \dot{X}_4(0) = .5v$	3.0	.0594	6.0	.0198	7.79	.0338	11.8	.0044	VELOCITY
19	$\dot{X}_1(0) = \dot{X}_2(0) = .125v$	3.0	.0505	6.0	0198	7.79	.0654	-	-	DISPLACEMENT
	$\dot{X}_3(0) = \dot{X}_4(0) = .25v$	3.0	.0578	6.0	.0197	7.79	.0364	11.6	.0092	VELOCITY
20	$\dot{X}_1(0) = \dot{X}_2(0) = .062v$	3.0	.0476	6.0	.0205	8.20	.0572	-	-	DISPLACEMENT
	$\dot{X}_3(0) = \dot{X}_4(0) = .125v$	3.0	.0636	6.0	.0193	7.99	.0304	-	-	/ELOCITY

TABLE 2.- AFFTC FLUTTER TEST RESULTS: MODE LIST PRINTOUT. (27,000 ft = 8239 m)

RUN NO. = 18
SPEED = 350.E
ALTITUDE = 27000
X-DUCER = 7.

SETUP NUMBER = 1
ENRG. THRES. = .01
ALPHA CUTOFF = 25.6
% TOT. ENERGY = .9789

MODE NO:	% ENERGY:	FREQ:	S-DAMP:	RESIDUE:	PHASE:
1.	28.73	2.24	.0967	1.511	-79.78
2.	69.15	3.04	.0536	1.756	-76.61
3.	1.038	4.16	.0507	.2792	-58.11
4.	1.072	5.76	.0447	.3597	-134.3

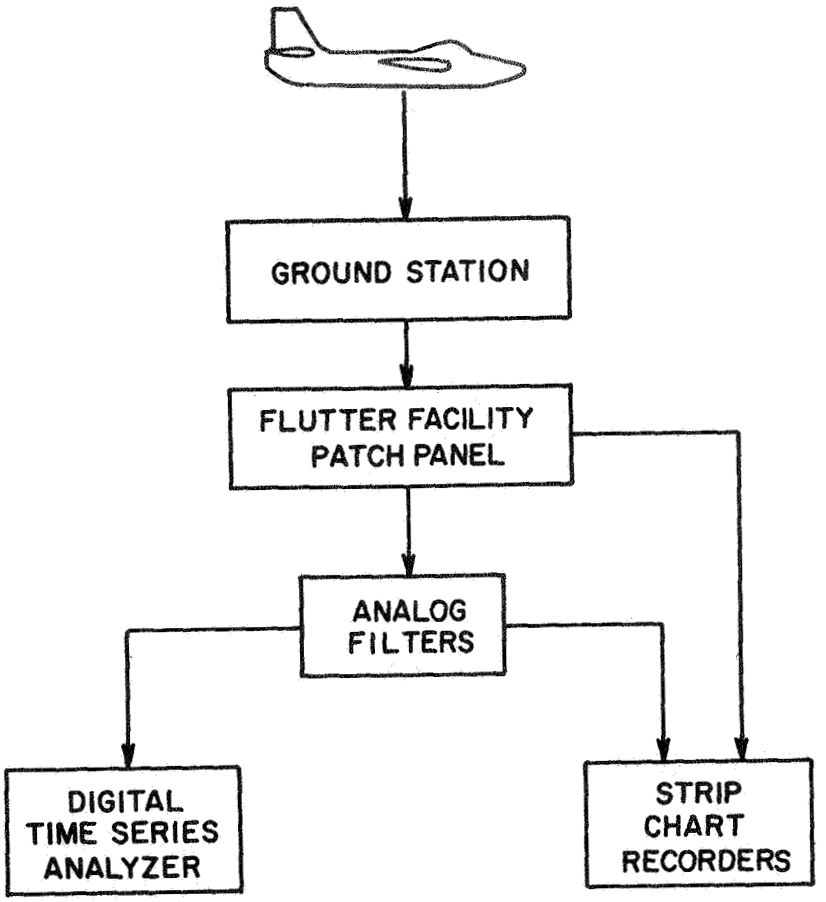

Figure 1.- Flutter test data flow.

Figure 2.- AFFTC flutter facility equipment.

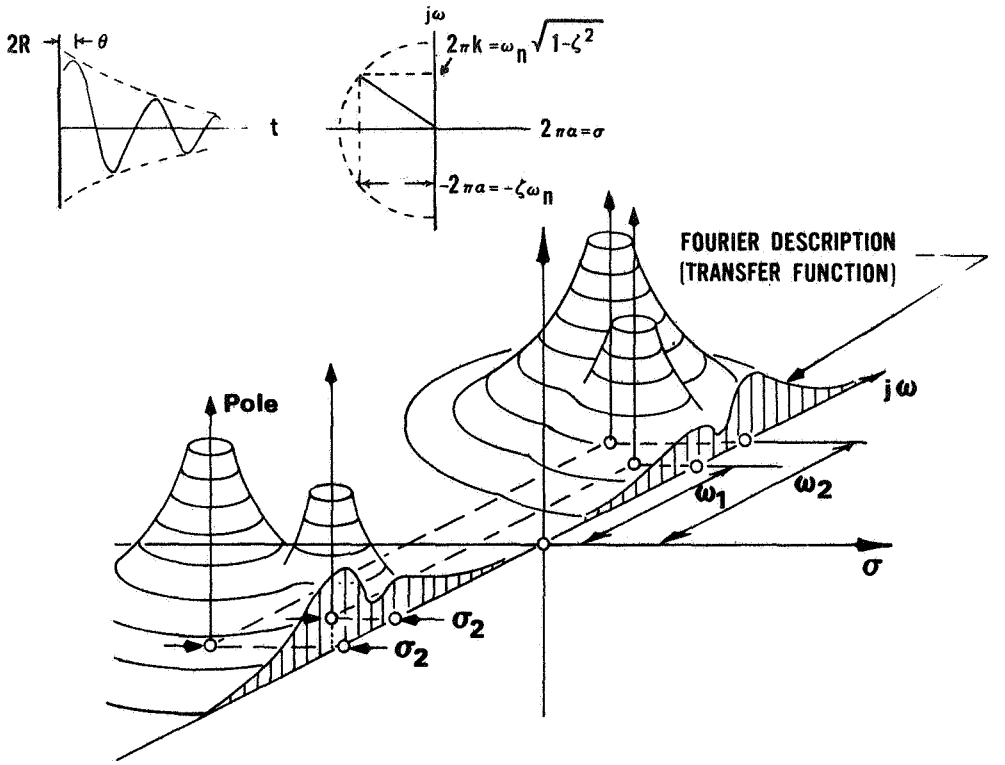

Figure 3.- Transfer function parameters.

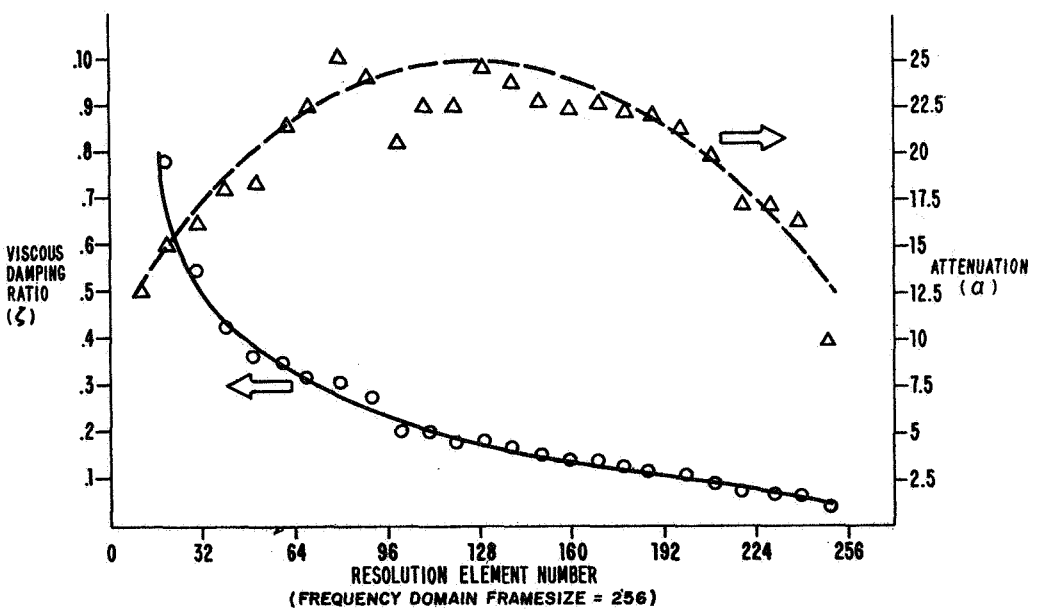

Figure 4.- Ten-percent error limitation plot.

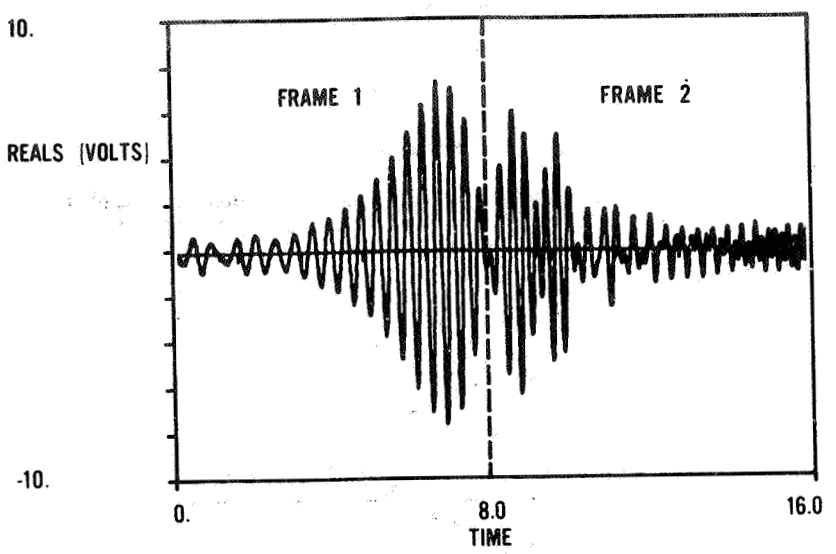

Figure 5.- Truncation of data frames.

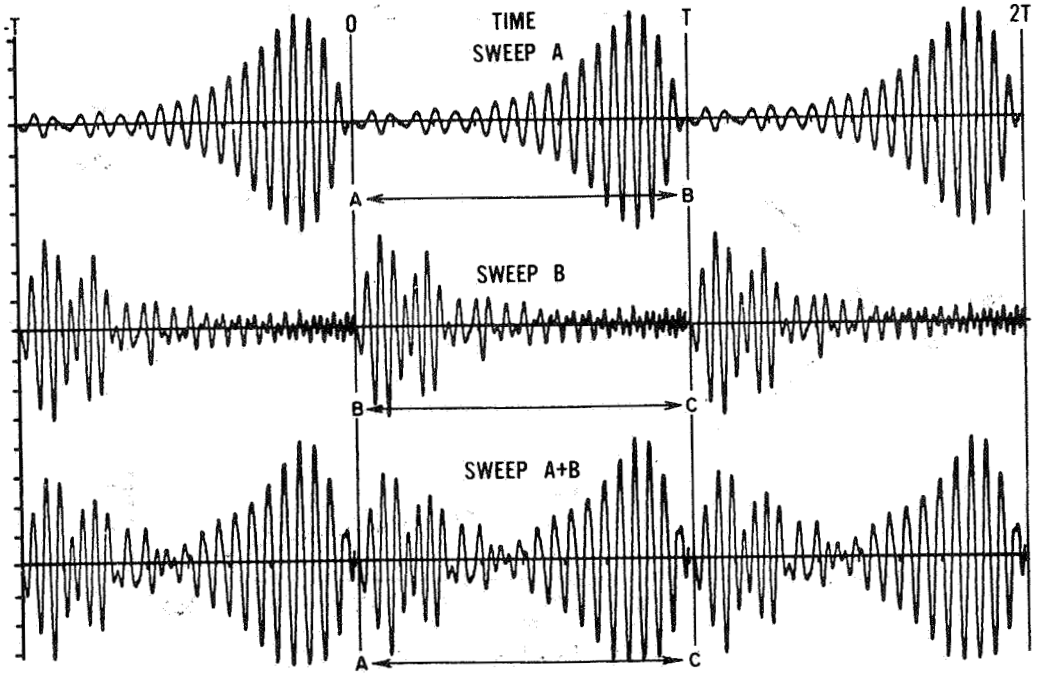

Figure 6.- Time averaging.

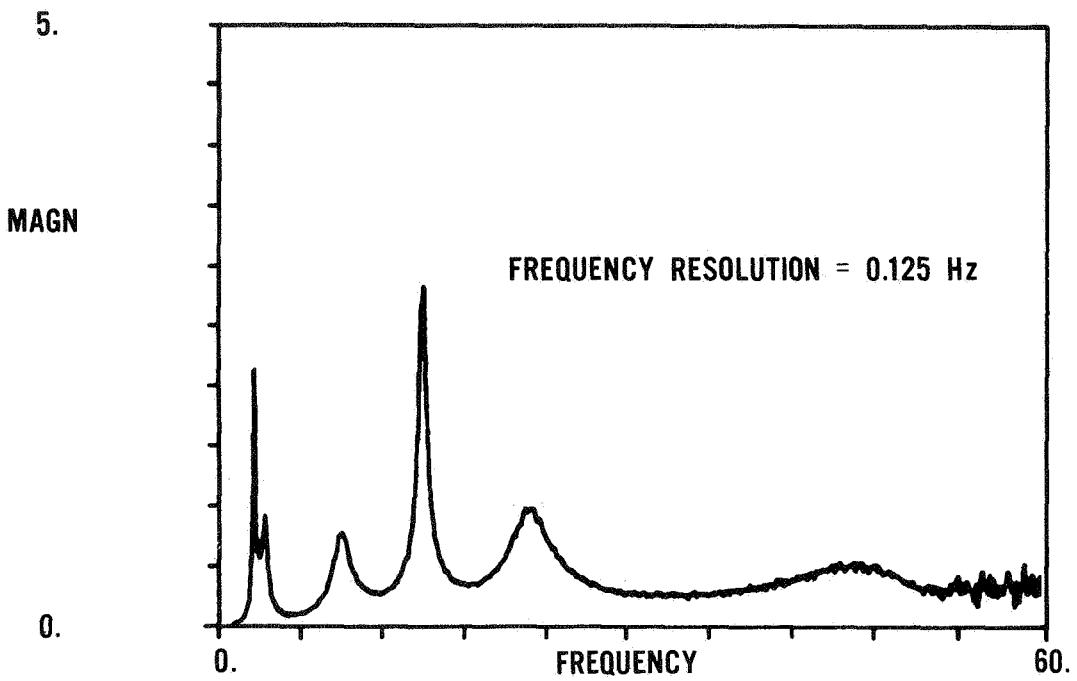

• MODEL PARAMETERS

FREQUENCY	STRUCTURAL DAMPING
2.56	.040
3.34	.103
8.79	.119
14.74	.032
22.27	.119
45.80	.204

• COMPUTED PARAMETERS

TIME AVERAGING		FREQUENCY AVERAGING	
FREQUENCY	S-DAMPING	FREQUENCY	S-DAMPING
2.62	.0423	2.62	.0915
3.37	.107	3.37	.0873
8.75	.072+	8.87	.03+
15.0	.0319	15.0	.0363
22.5	.03+	22.25	.018+
—	—	—	—

Figure 7.- Analysis of model data using swept sine input.

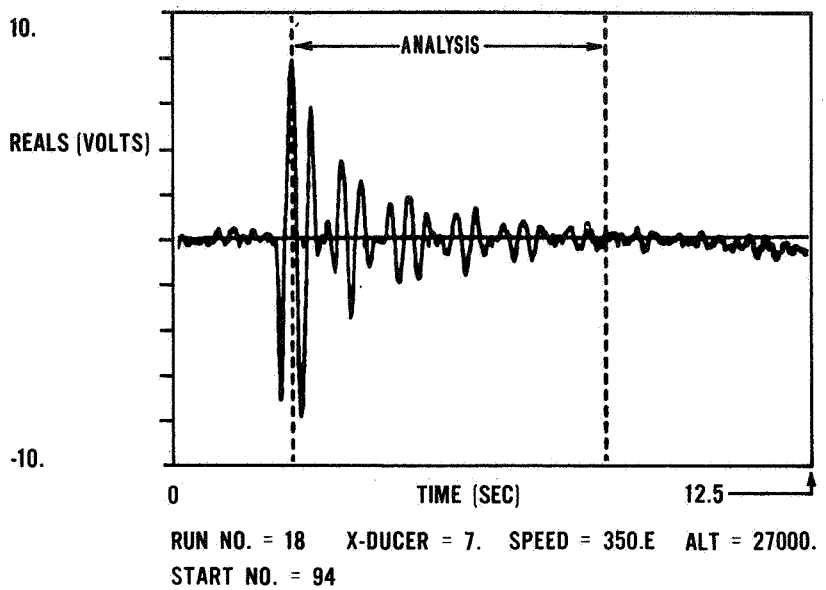

Figure 8.- AFFTC flutter test results: time history selection. (27,000 ft = 8230 m)

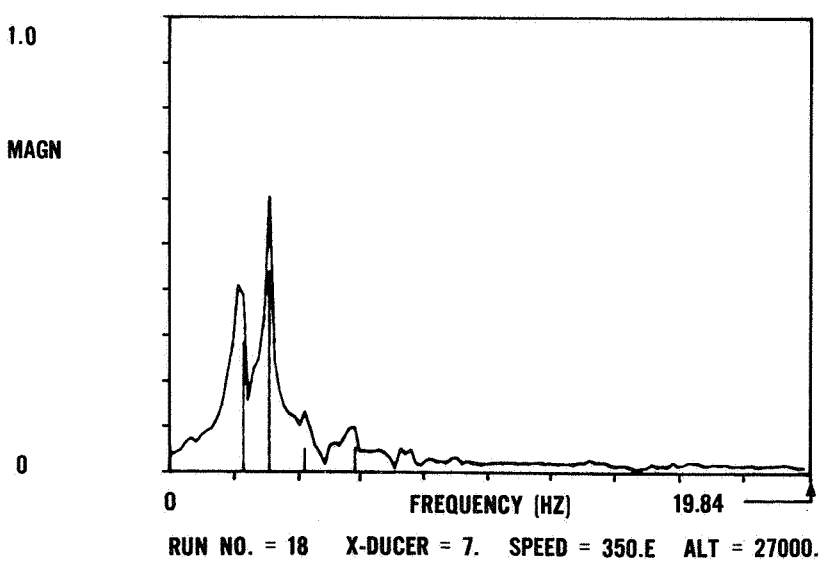

Figure 9.- AFFTC flutter test results: transfer function magnitude. (27,000 ft = 8230 m)

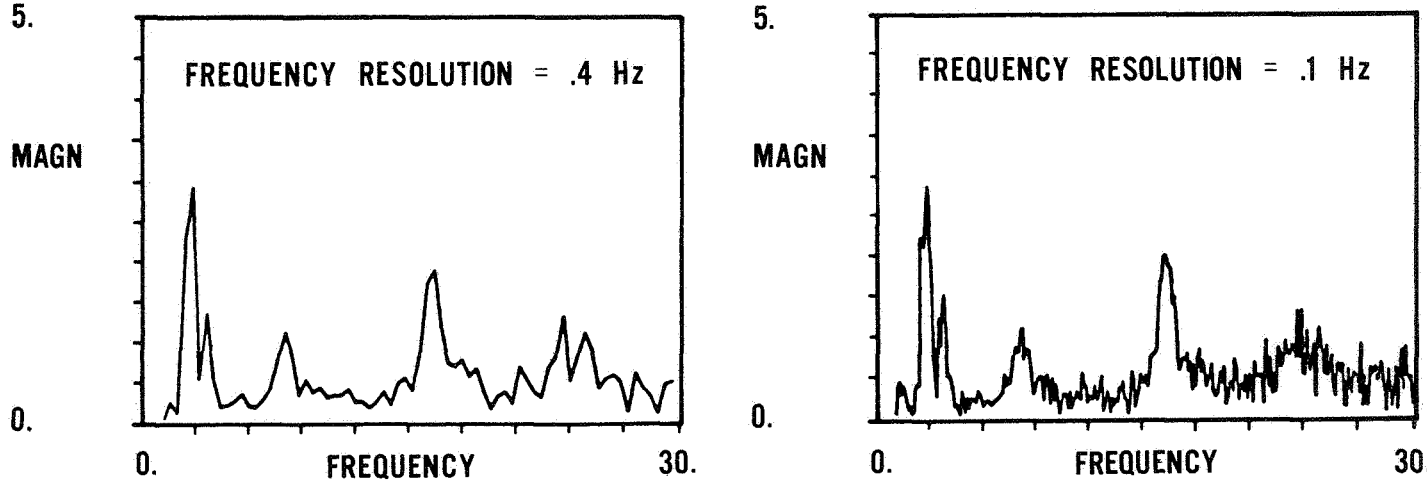

Figure 10.- Relationship between frequency resolution and data smoothing.

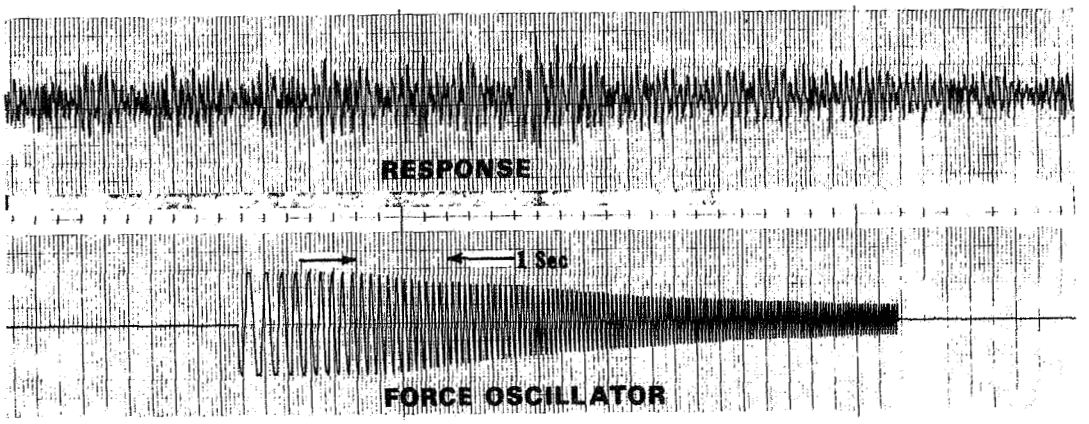

Figure 11.- Forced response in the presence of noise.

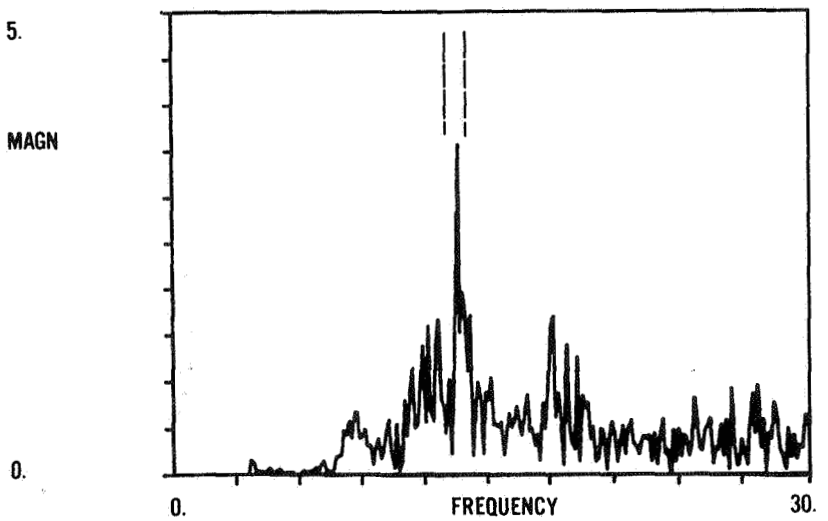

Figure 12.- Magnitude of the transfer function for a forced response in the presence of noise.

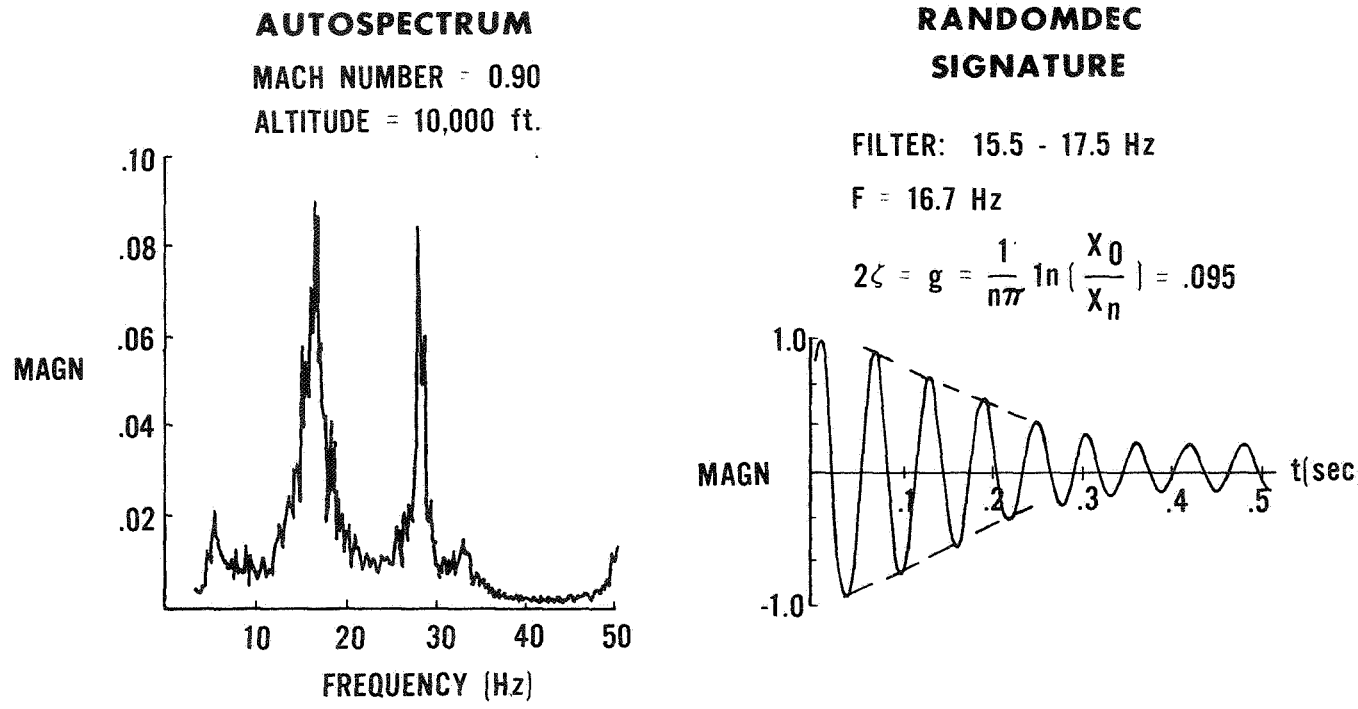

Figure 13.- AFFTC flutter test results:
random noise excitation.
(10,000 ft = 3048 m)

FLIGHT FLUTTER TESTING TECHNOLOGY AT GRUMMAN

H. J. Perangelo
Grumman Data Systems Corporation

F. W. Milordi
Grumman Aerospace Corporation

13

SUMMARY

The stringent requirements for flutter testing modern-day aircraft have led Grumman to develop new analysis techniques to be used in its Automated Telemetry Station for on-line data reduction. The initial technique developed by Grumman utilized a least-squares difference-equation linear-systems identification approach to extract resonant frequency and damping coefficient information from digitally filtered input and response data. This technique was successfully used on the F-14A flutter program starting in 1971, providing a quantum increase in capability relative to previously used techniques. The main advantages of the approach are

(1) Multimodal (highly coupled) analysis capability
(2) Quantitive answers for highly damped modes
(3) Ability to handle fast shaker sweeps (2 to 70 Hz in 15 sec)

These advantages, coupled with the computational and data storage capacity of the ATS, reduced test time, saved fuel, and significantly increased flight test efficiency.

Grumman has since expanded its flutter data reduction capability to encompass correlation, random decrement, and spectral techniques which are used in conjunction with its least-squares difference-equation identification approach to determine modal characteristics of response signals excited either by deterministic or random means. Cross-correlation data preconditioning techniques have exhibited superior noise rejection characteristics relative to the digital filtering approach initially employed; however, the proper utilization of these techniques generally requires an increase in data record length or sweep time. This is particularly evident when response signals are of a bimodal nature or contain low frequency modes (<10 Hz). Autocorrrelation functions and random decrement signatures analyzed via the Grumman identification approach show similar trends. From the standpoint of computational time, the random decrement method is preferred over the autocorrelation approach for the analysis of randomly excited data, while from an accuracy viewpoint both methods are equivalent.

The analysis of a nonlinear resonant system via a simplified least-squares response-error modeling technique has been successfully demonstrated.

Grumman is currently evaluating the feasibility of employing more complex versions of this identification approach to expand its flight flutter testing capability.

INTRODUCTION

Since 1970, significant strides have been made in reducing flight test flutter response data. These strides have resulted from the marriage of modern digital computing capability with new analysis techniques. Grumman's contribution has been made through the effective application of its least-squares difference-equation (LSDE) identification approach. The successful utilization of this analysis technique required an on-line interactive computer system. This system was embodied in the Grumman Automated Telemetry Station (ATS) which played an instrumental role in the timely completion of the F-14A flutter program. Staying abreast of the rapidly changing technology in the area of flight flutter testing has resulted in the development of a broad range of software programs encompassing many of the latest techniques. The value of these new data processing techniques is enhanced when used in conjunction with the LSDE identification approach. The section "Analysis Software Description" outlines how these new techniques have been implemented in application programs for use in the ATS. Appendix A contains a detailed mathematical description of the concepts that form the basis for the software algorithms used (all equation references in the body of this paper refer to relationships defined in the appendixes).

The section "Software Interactive Capabilities" describes the control the user has in interfacing with the various on-line analysis programs. Both system and program options are discussed, with emphasis placed on the program options that directly influence the quality of results. Verification of the software's technical base is discussed in the section "Test Results From Simulated Data." An analog computer six-degrees-of-freedom structural model, containing closely coupled modes, was used to generate response data with known modal characteristics. These data provided an absolute reference for evaluating software accuracy. The various programs were used to assess the modal characteristics of signals from clean sweeps, noisy sweeps, and randomly excited response data. Numerous runs were statistically analyzed to give an indication of the consistency of these programs.

Analysis of flight data with the various programs is discussed in the section "Test Results From Flight Data." The data analyzed included unimodal and bimodal response signals excited via a swept frequency shaker and/or random aerodynamic forces. The frequencies of the various modes analyzed ranged from 5.0 to 60.0 Hz with damping coefficients ranging from 0.075 to 0.25.

A nonlinear response-error modeling analysis approach, currently under investigation by Grumman, is described in the section "Current Developmental Activity." Some preliminary results obtained in the analysis of a hard-spring nonlinear resonant system are also discussed. A mathematical description of the approach used is contained in Appendix B.

BACKGROUND

Prior to 1970 the flight flutter testing methods relied primarily upon manual and analog analysis techniques such as log decrement, vector plotting, and reciprocal amplitude for structural stability indications. These methods were adequate for the classical analysis of clean signals which contained modes that were relatively uncoupled. However, an aircraft's structural response does not always approach this classical mold, and such phenomena as buffet, multimodal response, high damping, and nonlinearities severely limit the accuracy of these techniques. This resulted in a minimum of reliable and quantified answers being obtained during a test program, putting great pressure on the flutter test team and making experience and intuition rather than concrete information the prime decision maker. At times, luck was not a small part of success. Inherent in this situation was a well-founded concern for safety of flight, which resulted in the use of small test increments and numerous test altitudes. The cost of a flutter program was high in terms of number of flights and length of calendar time. The trend toward more sophisticated aircraft attaining high Mach numbers and dynamic pressures, coupled with the change in design requirement toward more flexible light weight structures, minimized predicted flutter margins and put additional pressures on the flutter test team. It became obvious that experience and intuition were not enough, the need was for better quantitative data which demanded new analytical test tools.

In this time frame, an overall change in test requirements and philosophy were sparked by time constraints set on the Grumman F-14A test program. Not only did flight flutter testing have to be expedited but so did all other discipline testing. Maximum results in the shortest calendar time was the requirement; the solution was the application of a high-speed digital computer system, new analysis techniques, telemetry of data, multidiscipline testing, and inflight refueling. Digital computers would provide speedy calculation of results, telemetry and multidiscipline testing would maximize the answers obtained at a given test point, and inflight refueling would increase flight duration. The computer system would be on-line to accept user inputs to update analysis parameters during the actual test sequence or in intermaneuver processing conducted during refueling. The objective was to reduce the traditional day-to-day data turnaround time to that of the refueling duration while achieving a simultaneous improvement in accuracy and confidence. This concept of an interactive on-line computer system become a reality in 1968 when Grumman made a large capital investment to purchase hardware and to develop system and application software to satisfy flight test requirements. The hardware/software system developed is called the Automated Telemetry Station.

AUTOMATED TELEMETRY STATION

The ATS consists of 3 major hardware subsystems. These are the Telemetry Formatter, Preprocessor, and Central Computer/Display Subsystems. A short description of each now follows:

The Telemetry Formatter subsystem receives the transmission from the aircraft, simultaneously recording and decoding the data stream for transfer to the Preprocessor. Additional functions such as time-code translation/generation, filtering, and output to analog display devices are also accomplished here.

The Preprocessor subsystem accepts the data from the Telemetry Formatter and performs the following tasks:

(1) Syllabizes bit streams into appropriate word lengths
(2) Maintains synchronization between the bit streams and the Formatter
(3) Converts data to engineering units via fifth-order calibration polynomials and limit checks it
(4) Records converted data on magnetic tape in central computer compatible format (optional)
(5) Buffers data into 0.1 second blocks and transfers the blocks on demand to the central computer at a maximum word rate of 15 000 per second
(6) Controls and monitors the Telemetry Formatter for the central computer

The Central Computer/Display Subsystem initiates operation of the ATS, performs analysis of selected data received from the Preprocessor and responds to user requests from the Data Analysis Station (DAS), an interactive console and graphic display device. The central computer can display data or calculated answers to the analyst at the remote DAS display. From this location, the analyst can request the central computer to configure the ATS, initialize real-time programs, change analysis parameters through interactive displays, process real-time data and display results, display test data on the display console screen or brush recorders, and record console displays (containing answers, data, or parametric information) on either hardcopy or microfilm.

Data flow management (figure 1) begins when the telemetry signal, containing frequency modulated (FM) and pulse-code modulated (PCM) components, is transmitted from the test aircraft. The data are received by a remote tracking antenna and relayed via a microwave link to the ATS. Data flows to a radio-frequency (RF) section which demodulates the data stream into 3 tracks, one carrying 26 500 words per second of PCM data and two carrying 14 channels each of FM flutter response data on proportional bandwidth subcarriers. The demodulated FM information then flows to the Analog to Digital Converter (ADC) which samples each parameter at 500 samples per second.

The data from the ADC is then transferred to the preprocessor. The serial PCM data flows to the Bit Synchronizer, which shapes the PCM pulse(s) and transfers them to the preprocessor for conversion to parallel format. The preprocessor collects, converts, and blocks the data for shipment to the central computer. Data transferred to the central computer is directly passed to the disk memory unit, a portion of which is allocated to the storage of 9 million words (i.e., 10 minutes of data at Grumman's normal flutter

test data rate of 15 000 words per second - which is ample capacity for thirty 15-second shaker sweeps). Data flows from the disk to the central processor unit (CPU) where it is analyzed by the specified program. Results in the form of plots and tabulations are displayed on the cathode ray tube (CRT) of the DAS. Copies of these displays are produced by the hardcopy and/or microfilm units. In parallel with the digital data flow, the outputs of the FM discriminators are displayed on Brush Tables in proximity to the DAS console.

FLUTTER TEST PHILOSOPHY

Every aircraft manufacturer performs flutter testing in order to verify predicted aeroelastic characteristics and comply with customer specifications. Paramount in the flight flutter test program is the assurance of crew safety while quantitatively identifying the structural stability of an expensive prototype aircraft.

Flight flutter testing would be trivial if flutter analyses were able to conclusively predict all flutter mechanisms, modal frequency and damping trends, and flutter speeds. Realistically, the flutter analyses are used as a baseline guide by the flutter test team as indicators of critical mechanisms and associated flutter speeds. Although predictions that agree with test results increase everyone's confidence, the decision for envelope expansion must be based on actual data and the answers derived from that data.

The potential destructive nature of flutter demands a cautious, systematic buildup in both airspeed and Mach number initiated at subcritical speeds. Aircraft structural responses are carefully monitored during accelerations to the planned test points. Data acquired at each point are completely analyzed, plotted, and extrapolated to the next test point prior to continued envelope expansion. The planned test points are continually altered based on the existing trends - too steep a trend will decrease test increments whereas a shallow trend will increase the increment. Inherent in this situation is the assumption that accurate, quantitative answers are being acquired from the analysis techniques. The objective during flight flutter testing is to acquire the best available decision base. Every effort is made to supply high quality response and driving function data to the analysis software. For example, if data acquired during a shaker sweep are noisy due to buffet response, the sweep will be repeated at a higher shaker gain setting in order to increase the signal-to-noise ratio. However, there will be times when increasing the shaker gain will not significantly improve the signal-to-noise ratio; then, techniques which precondition the data via correlation methods will be utilized to improve answer accuracy. These superior noise rejection techniques generally require a larger data sample and increased analysis time, but this may be necessary to insure accurate and consistent results.

The Grumman flutter flight test engineer has several different software programs, containing various analysis techniques, to choose from. Depending on the type of test program, one or more of these analysis programs will be utilized. They range from the TLEFAD program, which is used when information relative to the aircraft modal frequencies at the given test condition are

known, to the RESIDO program, which assumes that frequency information is not known and first calculates a frequency response function. Provisions for analyzing clean and noisy swept frequency responses, transients, and purely random excitation are contained within these programs. The ability to select different analysis techniques gives the flight test team complete flexibility to handle the flutter testing of a new aircraft design, the modification of an existing aircraft, or a nonscheduled evaluation requiring quick response. In all cases, the emphasis is on the best answers with minimum test costs.

ANALYSIS SOFTWARE DESCRIPTION

Software Overview

The ATS provides the test analyst with a powerful and flexible means of performing the on-line analysis of test data. This facility allows individual, FORTRAN coded, application programs with specific analysis capabilities to be quickly called upon to analyze or re-analyze telemetered test data as the need arises. Grumman has developed a number of different application programs, to be used in the ATS, for the purpose of reducing flutter response data to determine its modal characteristics.

The application programs were designed to provide sufficient analytical flexibility to handle adequately all expected test requirements. As such, the analytical methods employed had to be capable of analyzing flutter response data with or without a measured driving function signal and are compatible with any one of the following means of structural excitation:

(1) Swept frequency excitation
(2) Random excitation
(3) Abrupt control surface inputs
(4) Shake and stop excitation
(5) Impulsive input excitation

The LSDE identification algorithm provides the primary means of extracting resonant frequency and damping coefficient information. This identification technique is capable of handling complex multimodal response signals and is well suited to the analysis of data containing those highly coupled modes encountered as the flutter speed is approached.

The dominant assumption underlying this identification approach is that the response data is generated by a linear dynamic system. Initially, the technique was applied to the analysis of digitally filtered swept frequency test data in support of the F-14A flutter program. (See references 1 and 2.) The linearity assumption allows the identification approach to also be applied to signals that have been preprocessed by the following methods:

(1) Cross-correlation of system input and response with another function
(2) Autocorrelation of system response when system excitation is random or has a broadband-flat spectrum

(3) Random decrement signature of system response when excitation is random

The mathematical theory underlying the utilization of the above methods, in conjunction with the LSDE identification algorithm, to analytically determine system resonant frequency and damping coefficient information is explained in Appendix A.

Grumman currently has, at its disposal, three primary and two supporting applications programs to assist in reducing flutter response data at its ATS facility. The primary programs all use the LSDE identification algorithm, in conjunction with one or more of the previously mentioned data preprocessing techniques, to extract modal information. Program selection is predicated on the user's knowledge of the response data being analyzed rather than the analytical methods to be used.

If knowledge about the modal content of the test signals is available, data reduction is usually accomplished through the utilization of the TLEFAD program. Conversely, if little is known about the data or if it is desired to obtain an overall view of the modal content, either the RESIDO or ENERGY programs would be used. These programs determine the modal characteristics of the data from calculated frequency response functions. The COQUAD and APSD programs also compute frequency domain information that is sometimes helpful in establishing the modal content of response data. These latter two programs do not use the LSDE identification approach to establish modal characteristics and are normally used only in a supporting role. A utilization-oriented description of these five applications programs is given in the following discussion.

Tracking Known Modes

The TLEFAD analysis program was specifically designed to track the migration of modal resonant frequencies and damping coefficients as the flight envelope of an aircraft is expanded. The application of this program requires that the user have some knowledge of the modal composition of the flutter response data, this information being provided from previous engineering flutter analysis, ground vibration surveys, earlier test results, etc. The ability of the TLEFAD program to handle rapid shaker sweeps, simultaneously analyzing data from a number of different response transducers (up to 14 per sweep), allows this program to be particularly productive. This program plays an important role whenever timely decisions on aircraft flight test envelope expansion must be made since inherent speed of computation, flexibility, and noise rejection are improved by use of known modal information. In addition, cross checking by analysis of data from independent response transducers enhances user confidence in the resonant frequency and damping results obtained.

TLEFAD estimates modal characteristics via the LSDE identification approach. Analysis options in the program allow the user to select the preprocessing method to be used in the reduction of various types of response

data. For example, if the test data consisted of forced system response and input signals embedded in a moderate amount of noise, the data could simply be digitally band-pass filtered to highlight the mode or modes of interest in each frequency range. This filtered data would then be used in conjunction with the difference-equation model defined by equation (25) to determine resonant frequency and damping coefficient information. If, on the other hand, similar type data were to be analyzed in a highly noisy environment, increased noise rejection could be obtained by selecting the cross-correlation analysis preprocessing option. Here the driving function signal (or some function related to it such as a shaker tuning signal) would be digitally band-pass filtered over the frequency range of interest, and cross-correlated with the unfiltered response and driving function signals. The resulting cross-correlation functions would then be used in the difference-equation model defined by equation (26) for parameter identification purposes.

If the test data represents response signals driven by random excitation or by an input signal whose spectrum is broadband-flat, the response data can be preprocessed by autocorrelation methods. A calculated autocorrelation function can be used in conjunction with equation (27) to establish modal frequency and damping results. However, the difference-equation model defined by equation (28) is actually used when the autocorrelation preprocessing option is selected. This equation uses the cross-correlation function between digitally band-pass filtered response and unfiltered response signals, instead of the true autocorrelation function, and yields better results because it emphasizes the modal response in the frequency range of interest.

From this discussion, it is evident that in order to effectively use the TLEFAD program the user should have some approximate knowledge of the significant modal frequencies expected in the test data. This information provides the basis for specifying difference-equation model order, as defined by the constant N in equation (24), and for establishing the pass-band to be used in the digital filtering of the raw test data. In addition, the user selects the segment of data to be analyzed by either specifying an elapsed time duration or a frequency range in the case of swept frequency excitation. In this latter case, the program computes the instantaneous frequency of the shaker signal and processes data, for the indicated transducers, over the specified frequency range of interest using the selected preprocessing option and difference equation model order. Generally, the critical item is the selection of the filter pass-band and not the analysis data segment which can have a wide frequency range.

The primary output of the program consists of a tabulation of the resonant frequency and damping coefficient results obtained for each specified mode in every data segment. These results are augmented by diagnostic information (denoted by numerical flags such as -1.0 or -1.5 in the damping coefficient column) if the real poles are detected or if difficulties are encounted in extracting all the roots of the specified difference-equation model. Auxiliary information defining aircraft altitude, airspeed, and Mach number are also included in this tabular CRT output. Secondary CRT outputs of the program include a tabulation of backup (validation) data used in assessing the accuracy of results, a plot of calculated shaker frequency versus time

when swept frequency data are analyzed, and plots of any computed correlation functions. Examples of typical program outputs, in response to the cross-correlation analysis of the noisy swept frequency response data shown in figure 2, are set forth in figures 3 to 7.

Identifying Unknown Modes

Several different on-line programs are used to aid in the determination of the modal composition of flutter response data. These programs vary in the complexity of their analytical manipulations but are similar in that they all provide frequency domain information that forms the basis for ascertaining the modal content of the data. For example, the APSD program is often called upon to provide a power spectral density plot of a given response signal. The primary purpose of this program is to provide a quick look at the overall vibrational energy distribution as a function of frequency. Although this program is not normally used to establish modal damping coefficient information, it follows from equation (13) that this information might be deduced from a power spectral density function, using the one-half power method, if the input spectrum is broadband-flat. A typical power spectral density plot, obtained from the APSD program in analyzing the randomly excited response data contained in figure 2, is shown in figure 8.

The ENERGY, RESIDO, and COQUAD programs were primarily designed to evaluate swept frequency or random response data to detect whether any significant modes of vibration have been excited. If modes have been excited, these programs attempt to identify their number and to establish the damped natural frequency and damping coefficient of each detected mode. These programs are similar in that they all use a fast Fourier transform algorithm to compute a frequency response function. They differ in the way in which they manipulate this function to determine modal information.

If the test data contain a system driving function measurement, these programs can be directed to compute the cross-correlation function between system input/response quantities and the autocorrelation function of the system input. Transforming the resulting correlation information into the frequency domain and dividing the resulting cross-spectrum by the auto-spectrum results in a frequency response function representing the transfer function characteristics of the system under test. On the other hand, if the nature of the test data is consistent with the requirements of autocorrelation or random decrement signature analysis, the programs can compute frequency response information through the transformation of either one of these two functions. Although the frequency response functions computed from an autocorrelation function or a random decrement signature are somewhat different in form, they both can be considered representative of a transfer function characteristic possessing poles identical to the actual system under test.

System resonant frequency and damping coefficient information is determined in the COQUAD program by means of the frequency response component analysis method. Figures 9 and 10 show the amplitude and phase characteristics of a frequency response function computed by the COQUAD program in

analyzing simulated swept frequency velocity response data containing three modes (with damped natural frequencies of 3.0, 8.0, and 12.0 Hz and corresponding damping coefficients of 0.1, 0.1, and 0.2). Figures 11 and 12 show the in-phase and quadrature spectra of the calculated frequency response function. These figures are annotated to illustrate the component analysis computations implemented in the COQUAD program to determine the resonant frequency and damping coefficient information shown in the final program output tabulation. (See figure 13.) The ability of the COQUAD program to accurately determine system resonant frequency and damping coefficient information generally degrades as the modal frequency separation in the response data becomes small. For this reason, the program is primarily used to provide a supporting or alternate form of analysis in the actual reduction of flight test data. The COQUAD program is useful in applications where sufficient modal frequency separation exists.

The ENERGY and RESIDO programs provide the primary means of reducing frequency response information to determine the overall modal characteristics of the data. The modal identification process used by these two programs is similar. They both rectangularly window the calculated frequency response function and invert the windowed frequency domain information into the time domain. The windowed frequency response information reflects the response of a system having the calculated frequency response characteristic to an input signal having a rectangular frequency domain amplitude function with zero phase angle. The time domain form of this artifically created input signal is analytically computed and used along with the inverted response signal to determine system resonant frequencies and damping coefficients for those modes within the windowed frequency range using the LSDE algorithm. Digital band-pass filtering of the raw time domain signals is employed to minimize the effects of neighboring modes whose resonant frequencies are close to the windowed frequency range.

The differences between the ENERGY and RESIDO programs lie in the manner in which frequency response information is windowed and in the way the number of modes in a given window is established. The ENERGY program essentially scribes one or more lines across the calculated frequency response function at appropriate level(s) specified by the user. Generally, the intersection of the calculated frequency response function with these lines establishes the frequency windows to be used. The number of modes in each windowed section can be either automatically calculated or manually inserted after an examination of the frequency response function or its in-phase and quadrature spectrum. The number of modes in each window establishes the difference-equation model order to be used in the identification process. Conversely, the RESIDO program allows the user to segment the frequency response function into slightly overlapping windows spanning the entire frequency range of interest. These segments are individually inverted into the time domain where one or more user-specified models are used to determine the difference-equation coefficients corresponding to each window.

In both programs, the analytically determined difference-equation models essentially define Z-transfer function models (see equation (21)) pertaining

to various sections of the overall system frequency response function. These transfer function models are used to compute the energy of each mode calculated in each frequency window via a residue computation. Those modes whose resonant frequencies are within the windowed frequency range of the model and which, in addition, exceed some user selected level of significance are displayed on the primary output tabulation of the program. All computed modes, some of which can be mathematical fictions due to over-specified difference-equation model order, are output on a secondary program output tabulation. The final computation carried out by these programs is that of reconstructing the frequency response information from the mathematically determined Z-transfer functions. This reconstructed function can be compared to that previously calculated from the test data in order to ascertain the quality of the analytical fit. Examples of the excellent results, obtained in applying the ENERGY program to analysis of the clean swept frequency response data shown in figure 2, are set forth in figures 14 to 17. Results for the 42 Hz mode do not appear on the primary output tabulation because the energy of this mode was below the user selected level of significance for the test run. It should be noted that the correct answers were obtained for this mode, as indicated on the annotated secondary output tabulation in figure 16.

SOFTWARE INTERACTIVE CAPABILITIES

The on-line applications software used in the ATS is executed under control of the real-time TeleSCOPE 340 operating system. This system collects and stores data on a disk recall file over a total interval of time defined as a maneuver. Data analysis is implemented over maneuver sub-intervals called events. The flutter analysis programs selected by the user process event data from the disk. The operating system transfers data to the central computer on the request of the application program. In this manner, the analysis program is able to process data at a rate that is consistent with the requirements of its algorithm. Data can be processed in near-real-time, with the duration of analysis being a function of the complexity of the analysis technique.

At maneuver "initialization", the user has the ability to change or correct previously stored initialization information from the DAS console through the use of option displays which have been built into the various programs. The on-line flutter analysis programs require this interactive initialization capability in order to optimize analysis algorithms to suit the course of events occurring in a given flight. Before the flight, the analysis options are set to values which are considered adequate. In the case of the TLEFAD program this information is based on prior knowledge of the vehicle under test. Some analysis parameters are redefined after each maneuver, with less and less changes occurring as the flight progresses. For the RESIDO, ENERGY, and COQUAD programs, analysis options are initially set to much wider tolerances because of the broad overview analysis that is performed by these programs.

The most significant interactive capabilities associated with the use of the various flutter analysis programs are set forth in tables 1 and 2. Table

1 defines the system command options controlling the overall execution and displaying of program outputs from the DAS. An overview of the analysis options under the interactive control of the analyst are contained in table 2. Through the manipulation of these options, the analyst can generate a large volume of results. This can be a pitfall if not used prudently. For example, within the structure of the TLEFAD program a single frequency sweep can be analyzed for 14 different transducers using 2nd, 4th, and 6th ordered analysis, yielding a total of 84 separate frequency and damping answers to be evaluated. This is where experience is important, requiring judicious utilization of programs and options to avoid a deluge of results. However, from an overall flutter analysis point of view, the built-in ability to select different analysis program options enables the analyst to establish a high degree of confidence in the results obtained and increases the probability of a safe flutter buildup.

TEST RESULTS FROM SIMULATED DATA

The software on-line ability to accurately analyze flutter response data is best assessed by considering the results obtained in analyzing known test data simulating actual flight response characteristics. The results discussed herein were obtained by analyzing data from a highly coupled analog computer six-degree-of-freedom structural model. Clean and noisy swept frequency, as well as randomly excited response data generated by this model, was analyzed by the software in a normal flight-test configuration. This essentially consisted of feeding the analog test signals through the ATS facility where they were digitized and subsequently analyzed by various on-line programs. The results of this analysis were displayed on a CRT, at the Data Analysis Station, where they could be either copied to microfilm or hardcopy for record purposes. Analyzing the data in this manner reflects the normal processing errors associated with digitizing the data as well as the operational constraints of processing the data in a near-real-time environment.

Representative samples of the test data are shown in figure 2. The actual damped natural frequencies and structural damping coefficients of the six modes contained in these data are defined on figure 2. The random excitation used to drive the simulated system dynamics was generated by passing a broadband-flat noise source through a 3-Hz low-pass filter having a 6-dB per octave roll-off. In the noisy swept frequency configuration, the rms value of the model response to the noise input was approximately 6 volts. The rms value of the clean swept frequency response signal varied from 15 to 35 volts in the vicinity of the various resonances of the model. For the randomly excited test runs, the model was configured to achieve a reasonable contribution from all modes as indicated by the representative power spectral density plot of these data shown in figure 8.

Test results obtained by analyzing the clean and noisy swept frequency response data with the TLEFAD program, using the various preprocessing options available, are shown in table 3. These preprocessing options are denoted as direct analysis, cross-correlation analysis, and autocorrelation analysis and

reflect the respective utilization of the difference-equation models defined by equations (25), (26) and (28) for identification of modal resonant frequencies and damping coefficients. Data analysis for the various modes was initiated and terminated as a function of the frequency of the excitation signal. The frequency range over which data were analyzed for each mode or pair of modes is indicated in table 3 along with the filtering characteristics and difference-equation model order used in extracting the results. Overspecified difference-equation model orders were used to accommodate the presence of neighboring modes. The results quoted reflect the answers obtained for the known mode or modes within the pass-band of the digital filter used.

The results shown for the clean swept frequency are nearly perfect and reflect the answers obtained in a single run since there was little variability in the answers from run to run. Results quoted from the analysis of noisy data consist of the mean value plus and minus the one sigma standard deviation for system damped natural frequencies and damping coefficients that were obtained in analyzing data from ten independent shaker sweeps. These results indicate the superior noise rejection characteristics of the correlation methods, which tended to obtain results whose mean values were closer to the true modal values and which had less dispersion than those obtained via the direct analysis method, if a sufficient amount of data was available for averaging. The effect is seen in the test results by noting that the accuracy of the correlation results generally improved as modal frequency increased. This is a consequence of the exponential sweep function which increases the density of response data cycles as the frequency of the mode(s) increases. A confirmation of this was obtained by increasing the duration of the sweep and contrasting the significant improvement in the quality of the correlation results in the low frequency range with the minor changes in the upper frequency range where the amount of data previously analyzed was already sufficient for good results.

The randomly excited response data were analyzed via the RESIDO and TLEFAD programs. The TLEFAD program was set up to analyze the data via the autocorrelation preprocessing option, using the same filtering and modeling selections previously defined in the analysis of the swept frequency data. The only exception was that the data were analyzed over a specific time duration rather than a frequency range. These random data were also analyzed by the RESIDO program, using both the autocorrelation and random decrement signature methods over a frequency range of 1.6 to 57.0 Hz. The overall frequency range was uniformly segmented into four frequency intervals covering the approximate frequency ranges of 1.6 to 3.9, 3.9 to 9.5, 9.5 to 23.3, and 23.3 to 57.0 Hz. Fourth and sixth ordered difference-equation models were used to fit the overall frequency response function in each frequency segment. The results quoted herein reflect the utilization of the fourth ordered model in the lower two frequency ranges and the sixth ordered model in the upper two frequency ranges since the mathematically reconstructed frequency response information generally indicated that these models had achieved the best fit to the data.

Table 4 contains a summary of the results obtained in analyzing the randomly excited response data. Here again, a statistical summary of the results is presented, representing the mean value plus and minus the one

sigma standard deviation, for each set of runs. The number and duration of the runs for each set of results is appropriately indicated. In general, runs of equal duration were made over identical data sets, the only exception being that two less runs were made with the TLEFAD programs. Although only slightly evident in this set of runs, the results obtained by the TLEFAD program are generally better or equivalent to those obtained from the RESIDO program. This general trend is attributed to the fact that in operating the TLEFAD program the user takes advantage of his knowledge of the data modal composition to establish a more optimum selection of digital filtering characteristics and difference-equation model order. It should be noted that the 90-second duration results obtained from RESIDO indicate little difference between the autocorrelation and the random decrement signature methods and that the 180-second random decrement results show an improvement in overall accuracy due to increased time averaging. The random decrement signature level in all runs was set to the rms value of the first 4 seconds of data collected in each run.

TEST RESULTS FROM FLIGHT DATA

Typical time histories of the actual flight data analyzed are shown in figure 18. These data are grouped into the following frequency ranges and data types:

TYPE / RANGE	Clean	Noisy	Random	Bimodal
Less than 10 Hz (low)	Figure 18(a) Figure 18(b)	Figure 18(c)	Figure 18(d)	Figure 18(h) Figure 18(d)
10 Hz to 25 Hz (mid)	Figure 18(e)		-	-
Greater than 25 Hz (high)	Figure 18(f)	-	Figure 18(g)	-

A summary of the results is shown in table 5. The results shown are from the analysis of clean and noisy exponential sweeps (from 2 Hz to 70 Hz in 24 seconds) and from 90- to 180-second random excitations. The modes analyzed are characterized by the notation

(1) AW1B - antisymmetric wing first bending
(2) SW1B - symmetric wing first bending
(3) SW2B - symmetric wing second bending
(4) FLAPR - flap rotation
(5) W1B/STRP - wing first bending/store pitch

Before a detailed discussion of these results is presented, a few general comments are in order. The concept used in determining a tabulated number was the same as that used in the F-14A flutter program and is a result of the large capacity of the computer system and the program options available to the analyst. Specifically, these numbers are an average of the modal information obtained when the following program options (when

appropriate for the analysis method) were employed:

(1) Overspecification of analysis order
(2) Data analysis window variation
(3) Correlation lag range variation

In most cases 2nd, 4th and 6th ordered analysis was performed. If the number of results for a particular mode are less than six (which is considered a minimum for a statistical analysis), only the average result (without indication of the standard deviation) is tabulated.

Included are results from the TLEFAD program using the direct option which (see references 1 and 2 for additional discussion of results obtained using this analysis method) was the technique used during the F-14A flutter program. It is therefore considered to be the reference against which all other techniques are compared.

Considerable effort was spent on the analysis of the low frequency range, because realistic noise inputs such as buffet or gusts exhibit their highest spectral content in this range making it the most difficult frequency range to analyze.

Sweeps that are classified as clean do possess a certain minimal noise level but this is considered negligible compared to the other sweeps analyzed. The AW1B, SW1B, and FLAPR clean sweep, noisy sweep, and random noise data were obtained in level 1g flight at .85 Mach/25000 ft (1 ft = 0.3048 m). The noisy sweep and random data were obtained by holding the aircraft at 10° angle of attack at the given test condition, causing partial airflow separation and random excitation. Random flap excitation resulted from vorticies of the F-14A overwing fairing impinging on the flap. The SW2B sweep was obtained at .70 Mach/15000 ft, with the W1B/STRP sweep obtained at 1.05 Mach/6000 ft.

AW1B/SW1B Results

Analysis of the clean sweep AW1B results shows excellent agreement between the various techniques. The smallest standard deviation is with the TLEFAD cross-correlation option. The RESIDO cross-correlation scatter is higher because, in normal use, tight analysis control is not utilized with this program. As expected, all corresponding noisy sweep results had more scatter as exhibited by the greater standard deviations. However, the TLEFAD cross-correlation mean result is excellent, and the smaller scatter indicates the greater consistency that is achieved by utilizing the TLEFAD windowing philosophy in presence of noise relative to the wide windowing (overview) philosophy of RESIDO.

During random excitation both the AW1B and SW1B modes are excited, requiring TLEFAD direct results from both modes for reference purposes. The complete set of results shown for the AW1B mode reflects the consistency obtained using the different analysis techniques in the low frequency range.

Analysis of the SW1B mode was limited to clean sweep reference runs (using the direct and cross-correlation options in TLEFAD) for comparison with results obtained from randomly excited response data.

Because of the multimodal nature of the random response data only 4th and 6th ordered analysis results were considered. The TLEFAD autocorrelation 90- and 180-second results for the SW1B mode are good with slight improvement in results shown for the longer duration time slice. The AW1B results are not as good. However the trend again is favorable, the absolute error decreasing from 26% to 19% when the data duration time is doubled. The RESIDO autocorrelation and random decrement results are considered good for both modes with the exception of the SW1B frequency results.

SW2B Results

Data for the SW2B mode, which were acquired during 1g level flight, are classified as clean, but the response level is very low and it does possess a noise level which is greater than that of other clean sweeps. This is due to the location of the wing shaker near a SW2B node line which results in a low excitation level. Therefore it is felt that the true classification of this sweep lies between clean and noisy. Results for all the techniques utilizing the LSDE identification algorithm are consistent, establishing confidence in the utilization of all these techniques for flight data of such a low response level. The discrepancy between these results and those obtained from COQUAD is attributed to the decreased signal-to-noise ratio which had an adverse effect on this program.

FLAPR Results

The FLAPR results are sectioned into three distinct blocks each one associated with the clean sweep, noisy sweep, and random noise input. On the surface, it would appear that the programs are not capable of analyzing this mode because the frequency and damping results of each block are completely different. However examination of transfer function plots from the clean and noisy sweeps and power spectial density plots from the random excitation showed that the flap frequency and damping does change. It is believed that the different flap modal characteristics result because angle of attack changes increase static loading causing an increase in hinge moment. However, each block's results are consistent and it can be concluded that accurate identification for highly damped modes is a reality. This cannot be overlooked when explosive flutter mechanisms are being considered.

W1B/STRP Results

The final flight data discussed is a highly coupled bimodal response involving a classical W1B/STRP. Even though the data were acquired in a highly transonic region, the highly swept wing and sleek F-14A fuselage minimized transonic buffet effect, enabling it to be classified as clean.

These bimodal response data were analyzed with the TLEFAD program via the direct and cross-correlation methods and the RESIDO program using the cross-correlation method. The results for the three analysis techniques used are very consistent and varied little with changes in program options. No attempt was made to use COQUAD due to the inaccurate results normally obtained by the use of this program on bimodal response data. In all cases results for 6th ordered analysis models are presented because in this frequency range there is a 7-Hz fuselage vertical bending mode that is lightly reflected in the response data.

Experience gained in the analysis of simulated data indicates that accurate results are usually obtained when there is consistency between the different analysis methods. Extrapolating this trend to the results obtained here further confirms the fact that the LSDE identification algorithm is capable of successfully analyzing bimodal flight test data.

CURRENT DEVELOPMENTAL ACTIVITY

The Grumman LSDE identification approach is implemented in a manner that is predicated on linear systems theory. Occasionally, situations are encounted (most often due to mechanical effects) where response data manifest nonlinear behavior. The reduction of these data by linear techniques is difficult, if not impossible. Thus, it was decided to review existing analytical techniques that could provide a "nonlinear" analysis capability.

In recent years, various organizations have expended a considerable amount of effort in evaluating response-error modeling techniques for the purposes of extracting information on aircraft stability derivatives. (See references 3 and 4.) These techniques presume knowledge of the form for system dynamics, which is also a basic assumption of the LSDE identification approach used in reducing flutter response data. Grumman's current technique establishes system parameters by minimizing the mean-square equation-error resulting from the substitution of preprocessed data into an assumed difference-equation model. Response-error modeling techniques differ in that they determine system parameters by matching the response signal generated by an assumed dynamic model to actual response signal measurements so as to either minimize the error between them or increase the probability of obtaining good parameter estimates.

Since response-error modeling techniques can be implemented to analyze data from either linear or nonlinear systems, it was decided to direct an initial evaluation of the approach toward the more general problem of nonlinear system identification. In particular, the investigation was directed toward the evaluation of data from a nonlinear (hard-spring) resonant system. A detailed discussion of the technique, from the perspective of the example problem under investigation, is contained in Appendix B.

The basic approach consisted of implementing the technique so as to minimize the mean-square error between the actual and modeled systems. The

actual system was considered to have a nonlinear spring effect proportional to the square of displacement amplitude; the coefficient of the nonlinear spring was set at one-tenth of the value of the linear spring coefficient. Swept frequency runs were made for several different values of system damping coefficient. A discussion of the convergence problems encountered and how they were circumvented, by using algorithm constraints and initialization information inherent in the test data, is also contained in Appendix B.

The fundamental conclusions reached in this investigation indicated that the approach could be effectively used in the analysis of nonlinear response data. Plots showing the convergence of model parameters from their initially assumed values towards their true values are shown in figure 19. In general, it should be noted that the number of runs required to achieve convergence increased as the damping of the system decreased. This undesirable characteristic of the approach can probably be minimized through the utilization of second-order sensitivity coefficient terms and this will be pursued in subsequent investigations.

APPENDIX A

BASIC LINEAR SYSTEM CONCEPTS

This appendix contains a mathematical summary of the linear system concepts that form the basis for the algorithms used in the reduction of flight test flutter response data. The material is broken down into four sections. The first two deal with the underlying dynamic assumptions and linear system relationships that characterize system behavior. A derivation of the dynamic difference-equation modeling approximation that forms the basis for determining system resonant frequency and damping coefficient information is contained in the third section. The fourth section describes the least-squares identification algorithm used to determine difference-equation model coefficients and how these coefficients are processed to establish system resonant frequency and damping information.

Fundamental Stability Criteria

The ultimate objective of flutter test analysis is to measure or establish the relative margin of stability for the aeroelastic dynamics of an aircraft over its specified flight envelope. A basic assumption underlying Grumman's current on-line software analytics is that aircraft flutter dynamics are governed by a linear ordinary differential equation of the following form:

$$\sum_{n=0}^{N} d_n \frac{d^n y(t)}{dt^n} = \sum_{m=0}^{M} c_m \frac{d^m x(t)}{dt^m} \qquad (1)$$

where

$y(t)$ = displacement response (at some structural location)
$x(t)$ = structural driving function
d_n, c_m = constant coefficients (with $d_N = 1.0$)
N, M = positive integer constants ($M<N$)

If $Y(s)$ and $X(s)$ are used to denote the Laplace transforms of $y(t)$ and $x(t)$ it follows from equation (1), assuming the dynamic system is initially at rest, that

$$\frac{Y(s)}{X(s)} = H(s) = \frac{\sum_{m=0}^{M} c_m s^m}{\sum_{n=0}^{N} d_n s^n} = \frac{c_M \prod_{m=1}^{M} (s-z_m)}{\prod_{n=1}^{N} (s-p_n)} \tag{2}$$

where

$H(s)$ = dynamic system transfer function
z_m = zeros of H(s), roots of numerator polynomial
p_n = poles of H(s), roots of denominator polynomial

From the theory of linear systems, it is known that the dynamics equivalently defined by equation (1) or (2) are inherently stable if the characteristic roots of equation (1) or the poles of equation (2) lie in the left half of the complex plane. The aeroelastic dynamics of an aircraft structure represent a multi-degree-of-freedom system having resonant modes that can generally be related to those poles of H(s) which appear in complex conjugate pairs, such as

$$P_{2k} = -\alpha_k + i\beta_k \tag{3a}$$

$$P_{2k-1} = -\alpha_k - i\beta_k \tag{3b}$$

An aircraft encounters "flutter" or aeroelastic instability when α_k in equations (3a) and (3b) becomes negative. In practice it is common to refer to the damped natural frequency and structural damping coefficient of a given resonant mode. These particular variables are related to corresponding poles of H(s) by

$$g_k = \text{Structural damping coefficient of kth mode} = \frac{2\alpha_k}{(\alpha_k^2 + \beta_k^2)^{1/2}} \tag{4}$$

$$f_{dk} = \text{Damped natural frequency of the kth mode in Hz} = \frac{\beta_k}{2\pi} \tag{5}$$

As shown in equation (4), the structural damping coefficient of a mode is directly related to the real part of the modal pole and thus represents a measure of the stability of the corresponding mode under a given flight condition.

Underlying Background Relationships

Any analytical formulation of the solution to the problem of determining the natural frequencies and associated damping coefficient information from a response record implies a system model of the form defined in equation (1). Mathematical relationships used for the extraction of frequency and damping information can be implemented in a variety of ways. The actual method to be selected for a given application is strongly dependent on the nature of the test data to be analyzed. Several basic relationships pertaining to the system defined by equation (1) play an important role in either the implementation or understanding of analytical reduction algorithms applicable to different types of test data. Fundamentally the output of the linear system defined by equation (1) is uniquely determined from the knowledge of its impulse response function h(t) in accordance with the following time domain convolution integral:

$$y(t) = \int_{-\infty}^{+\infty} x(t-\sigma)h(\sigma)d\sigma \qquad (6)$$

where

$h(t)$ = the inverse Laplace transform of H(s), defined in equation (2)

If desired, the lower limit of integration in equation (6) can be changed from $-\infty$ to 0, since the subject system is causal (i.e., $h(t) = 0$ for $t<0$). This equation is possibly the most fundamental (least constrained) relationship characterizing linear system behavior. If x(t) and h(t) belong to the class of functions that are transformable, a useful frequency domain relationship can be obtained from equation (6) by taking its Fourier transform. The resulting equation is

$$Y(i\omega) = H(i\omega)X(i\omega) \qquad (7)$$

where

$Y(i\omega)$, $X(i\omega)$ = Fourier transforms of y(t) and x(t)
$H(i\omega)$ = System transfer function = $H(s)\big|_{s = i\omega}$

Equations (1), (2), (6), and (7) are all fundamental relationships that in themselves completely define system dynamic behavior.

Some interesting insights into test data analysis can be obtained by manipulation of equations (6) and (7). First if one filters the system response signal with a linear filter having a transfer function $F(i\omega)$ it follows that the filtered response signal is defined by

$$Y_f(i\omega) = Y(i\omega)F(i\omega)$$

which from equation (7) is seen to equal

$$Y_f(i\omega) = H(i\omega)X(i\omega)F(i\omega) = H(i\omega)X_f(i\omega) \tag{8}$$

where

$Y_f(i\omega)$, $X_f(i\omega)$ = Fourier transforms of filtered signals $y(t)$ and $x(t)$

Equation (8) states that the filtered response and driving function signals are dynamically related to each other through the same system transfer function as the unfiltered signals. Thus, in the analysis of system response to a known driving function, identically filtered measurements of system input and output data can be used without masking dynamic behavior. This filtering plays an important role in minimizing noise effects.

Certain well-known cross-correlation and cross-spectral relationships can be easily established along classical lines starting with either equation (6) or (7). The development here will emphasize those items considered significant in the computation of these functions for systems identification purposes. First consider the calculation of the cross-correlation of some arbitrary signal $w(t)$ with $y(t)$ and $x(t)$ over the finite interval of time ranging from t_1 to t_2 seconds as denoted by

$$\phi_{wy}(\tau) = \frac{1}{t_2 - t_1} \int_{t_1}^{t_2} w(t)y(t + \tau)dt \tag{9}$$

$$\phi_{wx}(\tau) = \frac{1}{t_2 - t_1} \int_{t_1}^{t_2} w(t)x(t + \tau)dt \tag{10}$$

Substituting y(t) from equation (6) into equation (9) results in the following cross-correlation convolution integral:

$$\phi_{wy}(\tau) = \frac{1}{t_2-t_1}\int_{t_1}^{t_2} w(t)\left[\int_{-\infty}^{+\infty} x(t+\tau-\sigma)h(\sigma)d\sigma\right]dt$$

$$= \int_{-\infty}^{+\infty} h(\sigma)\left[\frac{1}{t_2-t_1}\int_{t_1}^{t_2} w(t)x(t+\tau-\sigma)dt\right]d\sigma$$

$$= \int_{-\infty}^{+\infty} h(\sigma)\phi_{wx}(\tau-\sigma)d\sigma \qquad (11)$$

If the system is assumed to be initially at rest, it follows that both $\phi_{wy}(\tau)$ and $\phi_{wx}(\tau)$ are zero for $\tau<-t_2$ and that the upper limit of integration in equation (11) can be changed from $+\infty$ to $t_2+\tau$. Because the lower limit of integration can be set to zero, due to system causality, the resultant computation is finite. The majority of test situations involve the analysis of data from a stable system excited by a finite duration input signal. Under such conditions the correlation functions computed via equations (9) and (10) will tend to zero as τ increases in magnitude and thus represent functions whose Fourier transforms exist. Taking the Fourier transform of equation (11) results in the following cross-spectral relationship:

$$\Phi_{wy}(i\omega) = H(i\omega)\Phi_{wx}(i\omega) \qquad (12)$$

where

$\Phi_{wy}(i\omega)$, $\Phi_{wx}(i\omega)$ = Fourier transforms of $\phi_{wy}(\tau)$ and $\phi_{wx}(\tau)$

Comparing equation (11) with (6) and equation (12) with (7) reveals that the cross-correlation and spectral functions involved are mathematically related in the same manner as actual system input and output variables. Thus, an algorithm attempting to identify system resonant frequencies and damping coefficients from measured response and driving function signals can use cross-correlation or cross-spectral techniques to reduce the data without

disguising system characteristics. It should be noted that the above mentioned relationships hold regardless of the interval between t_1 and t_2. Obviously as this time interval increases, noise rejection improves and the calculated functions $\Phi_{wx}(\tau)$ and $\Phi_{wy}(\tau)$ become better approximations to their classical cross-correlation functions. Although cross-correlation and spectral techniques are slower from a computational point of view, they are more powerful in suppressing noise effects than simple filtering.

Autocorrelation and autospectral calculations, requiring only response signal measurements, can prove of value in analyzing flutter response data obtained from an aircraft excited by a driving function possessing an impulsive autocorrelation function. Random excitation having either a spectrum which is broadband-flat or one which can be considered as the output of a linear system which is driven by a broadband-flat random input satisfy this requirement. This random excitation can be obtained either naturally from a source such as atmospheric turbulence or artifically via random shakers. Deterministic signals such as a broadband sine wave sweep, a narrow spike, or function such as sine $(\omega t)/(\omega t)$, where ω is somewhat larger than the highest significant frequency in the response data, also satisfy the impulsive autocorrelation function requirements.

The mathematical significance underlying the autocorrelation approach can be evolved from either equation (6) or (7). Starting from equation (7), multiplying both sides of this equation by its complex conjugate results in

$$Y(-i\omega)Y(i\omega) = H(-i\omega)H(i\omega)X(-i\omega)X(i\omega)$$

or (13)

$$\Phi_{yy}(i\omega) = |H(i\omega)|^2 \Phi_{xx}(i\omega)$$

If $\Phi_{xx}(i\omega)$ is broadband-flat then

$$\Phi_{yy}(i\omega) \simeq |H(i\omega)|^2 = H(-i\omega)H(i\omega) \qquad (14)$$

Taking the inverse Fourier transform of equation (14) results in

$$\Phi_{yy}(t) = \int_{-\infty}^{+\infty} h(\tau)h(t + \tau)d\tau \qquad (15)$$

$$= \int_{-\infty}^{+\infty} h(-\tau)h(t - \tau)d\tau$$

Equation (15) indicates that the function $\phi_{yy}(t)$, which is essentially equivalent to the autocorrelation function of $y(t)$, is equal to a similar relationship representative of the autocorrelation function of $h(t)$. This equation also indicates that $\phi_{yy}(t)$ is equivalent to the system output response resulting from the input driving function equal to the impulse response function folded about the $t=0$ axis. For values of $t>0$ it follows that $\phi_{yy}(t)$ is actually the free decay of the system to the aforementioned input.

Another method for analyzing randomly excited response data, that has emerged in recent years, is the random decrement signature method. (See reference 5.) This method essentially averages fixed-duration segments of a random response record to obtain what is termed a random decrement signature. The particular segments to be selected and averaged from a given random response record are determined on the basis of signal level. Essentially, a predetermined level is established. Every time the amplitude of the response signal rises past or sinks below this level a fixed-duration segment of data, starting at the time the level is crossed, is averaged with previously accumulated segments. It can be reasoned that as the number of averaged segments increase the resultant random decrement signature will approach the free decay of the system from an initial displacement equal to the predetermined signature level. In some respects the random decrement signature is similar to an autocorrelation function in that both relationships represent free decay information. However these relationships are not equivalent since they represent different free decay problems.

Difference-Equation/Z-Transform Modeling Approximation

Grumman flutter analysis software uses what has been termed a model-matching method as a primary means of extracting resonant frequency and damping coefficient information from test data. Actually, the process is a least-squares equation-error parameter identification technique. In essence, coefficients or parameters of a dynamic model are analytically manipulated to obtain the best fit, in a least-squares sense, to the test data. The dynamic model used in the identification process takes the form of a finite-difference equation. This difference-equation model is a discrete version of equation (1) which is well suited for use in a digital computer where sampled values of test data must be dealt with. A detailed

derivation of this difference-equation model, accomplished through the use of Z-transform mathematics and sample-data system theory, is contained in reference 1. A somewhat abbreviated derivation is set forth below for the convenience of the reader.

The essence of the derivational approach is to model the continuous system with an open-loop sample-data system so that the synchronously sampled input and output signals of the modeled system approximately agree with their corresponding continuous system counterparts at the sampling instants. This is accomplished by assuming a sampled system model containing the continuous system transfer function H(s), as defined in equation (2), preceeded by a data reconstruction element possessing a polygonal hold characteristic.(See chapter 11, reference 6.) In the operational "s" notation of the Laplace transform, the transfer function for a polygonal hold reconstruction element is defined by

$$D(s) = \frac{e^{Ts}}{Ts^2}(1 - e^{-Ts})^2 \tag{16}$$

where

T = time increment between sampled data points

This data reconstruction element converts the sampled input to the model into a continuous signal constructed by connecting the sampled input points with straight lines. Driving the continuous system dynamics with this approximation to the actual input signal generally results in an output signal that agrees well with the actual system response signal, provided the sampling frequency is at least 5 times the upper pass-band limit of the continuous system and of a sufficient rate to insure a relatively smooth reconstructed input signal. The resultant transfer function for the modeled plant dynamics is

$$P(s) = D(s)H(s) \tag{17}$$

$$= \frac{(1-e^{-Ts})^2}{e^{-Ts}} H_1(s)$$

where

$$H_1(s) = \frac{1}{Ts^2} H(s)$$

The analysis of sample-data systems is generally accomplished through the use of the Z-transform in much the same manner as continuous systems analysis is tied together through the use of either the Laplace or Fourier transforms. The Z-transform represents a convenient means for handling sampled time functions. The Z-transfer function of a sample data system relates the Z-transforms of sampled system output to sampled system input and is simply converted to a time domain difference equation between sampled system input and output quantities. The Z-transfer function relationship for the modeled sample-data system is defined by

$$\frac{R(Z)}{X(Z)} = P(Z) \tag{18}$$

where

$R(Z)$ = Z-transform of sampled model output
$X(Z)$ = Z-transform of sampled input signal
$P(Z)$ = Z-transfer function of sampled data model
$Z = e^{Ts}$

Using the time shifting theorem, it follows from equation (17) that

$$P(Z) = \frac{(1 - Z^{-1})^2}{Z^{-1}} H_1(Z) \tag{19}$$

Now since $H_1(s)$ is expressible as a finite ratio of polynomials in s, whose denominator polynomial is of higher order than that of its numerator, it is possible to compute $H_1(Z)$ from $H_1(s)$ in accordance with the following integral definition of the Z-transform:

$$H_1(Z) = \sum_{\substack{\text{poles of} \\ H_1(s)}} \text{Res.} \left[H_1(s) \frac{1}{1-e^{Ts}Z^{-1}} \right] \tag{20}$$

Equation (20) expresses $H_1(Z)$ in terms of a sum of residues for the bracketed expression over the poles of $H_1(s)$. The result is that $H_1(Z)$ is expressible as a finite ratio of polynomials in Z. Substituting equation (20) into (19) and carrying out the indicated analytical manipulations, for the given form of $H_1(s)$, results in the following expression for P(Z):

$$P(Z) = \frac{\sum_{n=0}^{N} b_n Z^{-n}}{\prod_{n=1}^{N} (1-e^{p_n T} Z^{-1})} = \frac{\sum_{n=0}^{N} b_n Z^{-n}}{\sum_{n=0}^{N} a_n Z^{-n}} \tag{21}$$

Equation (21) shows that the Z-transfer function of the modeled sampled-data system is a finite ratio of polynomials in Z. The order of the numerator and denominator are both equal to N, which corresponds to the order of the denominator polynomial of H(s). This is a consequence of the data reconstruction device used and the assumed form of H(s). From equation (18) and (21) it follows that

$$R(Z) = -\sum_{n=1}^{N} a_n Z^{-n} R(Z) + \sum_{n=0}^{N} b_n Z^{-n} X(Z) \tag{22}$$

Taking the inverse Z-transform of equation (22) results in the following difference equation relationship:

$$r(t) = -\sum_{n=1}^{N} a_n r(t-nT) + \sum_{n=0}^{N} b_n x(t-nT) \tag{23}$$

where

r(t) = the inverse Z-transform of R(Z)

Equation (23) represents the dynamic difference-equation relationship between the modeled sample-data systems response r(t) and sampled values of the actual system input x(t). Since it is assumed that the modeled system response is approximately equal to the actual response of the continuous system at discrete sampling increments, this difference equation relationship is more appropriately written as

$$y(kT) = -\sum_{n=1}^{N} a_n y(kT-nT) + \sum_{n=0}^{N} b_n x(kT-nT) \tag{24}$$

where

k = a positive integer constant
y(kT), x(kT) = values of y(t) and x(t) at t=kT
a_n, b_n = constant difference equation coefficients corresponding to demonimator and numerator Z-transfer function polynomial coefficients

The a_n difference-equation coefficients in equation (24) are related to the poles p_n of the system transfer function H(s) as indicated in equation (21). System resonant frequencies and damping coefficients are determined from the poles of H(s) through the relationships defined in equations (3a) and (3b).

It follows from equation (8) that filtered system response and driving function data, $y_f(t)$ and $x_f(t)$, are related by the same general difference-equation relationship. Thus,

$$y_f(kT) = -\sum_{n=1}^{N} a_n y_f(kT - nT) + \sum_{n=0}^{N} b_n x_f(kT - nT) \qquad (25)$$

From equations (9) to (12), it obviously follows that the cross-correlation functions $\phi_{wy}(t)$ and $\phi_{wx}(t)$ are related in a similar fashion, resulting in

$$\phi_{wy}(kT) = -\sum_{n=1}^{N} a_n \phi_{wy}(kT - nT) + \sum_{n=0}^{N} b_n \phi_{wx}(kT - nT) \qquad (26)$$

If the system is excited by an input signal having a broadband-flat spectrum, the autocorrelation function of system response $\phi_{yy}(t)$ will be representative of the free decay of the system for values of t greater than zero. In this case, the following difference-equation relationship is implied:

$$\phi_{yy}(kT) = -\sum_{n=1}^{N} a_n \phi_{yy}(kT - nT) \qquad (27)$$

When dealing with response signals representing the free decay of the system, it follows from equation (24) that

$$y(kT) = \sum_{n=1}^{N} -a_n y(kT - nT)$$

It also follows that

$$w(jT)y(jT + kT) = \sum_{n=1}^{N} -a_n w(jT)y(jT + kT - nT)$$

where

j = a positive integer constant
w(t) = an arbitrary function of time

and, therefore,

$$\sum_{j=0}^{J} w(jT)y(kT + jT) = \sum_{j=0}^{J} \sum_{n=1}^{N} -a_n w(jT)y(jT + kT - nT)$$

or that, for the free decay problem, the following cross-correlation difference equation applies:

$$\phi_{wy}(kT) = \sum_{n=1}^{N} -a_n \phi_{wy}(kT - nT) \qquad (28)$$

Equations (25) to (28) represent those fundamental difference-equation relationships utilized by Grumman's on-line software for the purpose of identifying system resonant frequency and damping coefficient information.

Resonant Frequency/Damping Coefficient Identification

Equation (24) defines the basic difference-equation relationship used by Grumman's least-squares equation-error parameter identification algorithm. This equation will be used in the following analytical description of the technique although it should be understood that any of the difference equations represented by equations (25) to (28) could be used, as dictated by the manner in which the measured test data are initially processed.

Analytically, the least-squares equation-error identification technique minimizes the value of the function J shown below:

$$J = \sum_{k=k_1}^{k_2} (y_k - \bar{y}_k)^2 \tag{29}$$

where

k_1, k_2 = integer constants defining the data set over which J is to be minimized

y_k = y(kT) = the system response quantity at time kT

$\bar{y}_k$ = $\bar{y}$(kT) = the system response quantity estimated by the difference equation at time kT

In particular

$$\bar{y}_k = -\sum_{n=1}^{N} \bar{a}_n y_{k-n} + \sum_{n=0}^{N} \bar{b}_n x_{k-n} \tag{30}$$

where

$\bar{a}_n$, $\bar{b}_n$ = estimates of the a_n and b_n coefficients contained in equation (24) which minimize the function J

x(kT) = x_k = the system input quantity at time kT

If the system response signal is the only quantity required in data analysis, the second summation on the right-hand side of equation (30) is dropped.

The procedure for minimizing J consists of substituting equation (30) into equation (29) and taking the partial derivatives of the resulting expression with respect to the $\bar{a}_n$ and $\bar{b}_n$ coefficients, setting the expressions thus obtained to zero. This results in 2N+1 equations in 2N+1 unknowns which are to be solved for the desired coefficient information over the entire data set. The solution of these simultaneous linear equations, to obtain the desired estimates for difference-equation coefficients, can be expressed in the following matrix form:

$$\bar{K} = \{[B]^T[B]\}^{-1}\{[B]^T C\} \tag{31}$$

where

$$\overline{K} = \begin{bmatrix} -\overline{a}_1 \\ \vdots \\ -\overline{a}_N \\ \overline{b}_0 \\ \vdots \\ \overline{b}_N \end{bmatrix} \tag{32}$$

$$C = \begin{bmatrix} y_{k_1} \\ y_{k_1+1} \\ \cdot \\ \cdot \\ y_{k_2} \end{bmatrix} \tag{33}$$

$$[B] = \begin{bmatrix} y_{k_1-1} & \cdots & y_{k_1-N} & x_{k_1} & \cdots & x_{k_1-N} \\ y_{k_1} & \cdots & y_{k_1+1-N} & x_{k_1+1} & \cdots & x_{k_1+1-N} \\ \cdot & & \cdot & \cdot & & \cdot \\ \cdot & & \cdot & \cdot & & \cdot \\ \cdot & & \cdot & \cdot & & \cdot \\ y_{k_2-1} & \cdots & y_{k_2-N} & x_{k_2} & \cdots & x_{k_2-N} \end{bmatrix} \tag{34}$$

Equation (31) mathematically defines the identification process used in determining difference-equation coefficients. In this equation the superscripts T and -1 denote the respective matrix transpose and inverse operations.

Once the identification algorithm determines the $\overline{a}_n$ coefficients, as elements of the $\overline{K}$ vector, the roots of the denominator polynomial of the estimated Z-transfer function $P(Z)$ are computed. It follows from equation (21) that the roots of this polynomial are related to the estimated poles of H(s) by

$$\bar{\gamma} = e^{\bar{p}_n T} \tag{35}$$

where

$\bar{\gamma}$ = the nth root of the estimated Z-transfer function denominator polynomial
$\bar{p}_n$ = the estimated nth pole of H(s)

It can be seen from equation (35) that estimates for the real poles of H(s) are defined by

$$\bar{p}_n = \frac{1}{T} \ln (\bar{\gamma}_n) \tag{36}$$

From equations (3) and (35) it follows that estimates for the complex conjugate poles of H(s) are defined by

$$\bar{\gamma}_{2k} = e^{(-\bar{\alpha}_k T + i\bar{\beta}_k T)} = u_k + iv_k \tag{37a}$$

$$\bar{\gamma}_{2k-1} = u_k - iv_k \tag{37b}$$

and it follows that

$$-\bar{\alpha}_k = \frac{1}{T} \ln \sqrt{u_k^2 + v_k^2} \tag{38}$$

$$\bar{\beta}_k = \frac{1}{T} \left[\arctan \left(\frac{v_k}{u_k}\right) \right] \tag{39}$$

The real and imaginary parts of the complex conjugate poles of H(s) are computed in accordance with equations (38) and (39). The real poles of H(s) are computed from (36). System damped natural frequencies and damping coefficients are calculated from the real and imaginary parts of the complex conjugate poles of H(s) using the relationships shown in equations (4) and (5).

APPENDIX B

EXAMPLE NONLINEAR RESONANT SYSTEM IDENTIFICATION PROBLEM

The example problem described in this appendix depicts the application of the response-error modeling technique to the identification of a simplified nonlinear resonant system problem. The technique can be applied to the analysis of linear as well as nonlinear systems although it generally requires more computation time than the difference equation-error technique currently used by Grumman in the analysis of linear data. The utilization of response-error modeling techniques to linear and nonlinear system identification problems is currently undergoing extensive investigation, covering a broad range of scientific and engineering applications. Specific algorithms vary in complexity, generally depending on the manner in which model parameters are determined from response error.

The intent of the example described herein is to apply the concept, in its simplest form, to the analysis of resonant system phenomena typical of that which might be encountered in the analysis of flutter response data. The discussion set forth below is broken down into three sections. These sections respectively cover a statement of the example problem, a description of the analytical approach to be used in its solution and a discussion of some preliminary results obtained.

Problem Statement

The problem addressed here concerns itself with the identification of a nonlinear (hard-spring) resonant system defined by the following differential equation:

$$\ddot{Y}(t)+C_o\dot{Y}(t)+K_oY(t)+K_1\,\mathrm{sgn}[Y(t)]Y^2(t) = F(t) \qquad (40)$$

where

C_o, K_o, K_1 = constant parameters
$Y(t)$ = system displacement response
$F(t)$ = system forcing function
$\mathrm{sgn}[Y(t)]$ = +1 if $Y(t)$ is positive or
-1 if $Y(t)$ is negative

The constant parameters C_o, K_o, and K_1 determine the dynamic behavior of the system. Therefore, the identification process consists of defining the value of these parameters from measured data. It is assumed that relatively

clean measurements of system velocity response and forcing function are available. It is further assumed that the system is initially at rest and that the forcing function is a swept frequency sine wave whose frequency is varied from some point below to some other point above the apparent resonant frequency of the system.

The least-squares response-error modeling technique is to be used as the method for achieving system identification. This technique essentially assumes that the form of the dynamics are known, thus allowing the establishment of a dynamic system model. The identification process is implemented by varying the coefficients in the model so as to minimize the mean-square-error between the measured velocity response of the actual system and the corresponding velocity response of the assumed model.

Underlying Analytical Approach

Since knowledge of the actual system's form is assumed, the following equation defines the system model:

$$\ddot{y}(t)+c_o\dot{y}(t)+k_o y(t)+k_1 \operatorname{sgn}[y(t)]y^2(t) = F(t) \tag{41}$$

The lower-case nomenclature used in equation (41) distinguishes modeled system quantities from those of the actual system, as defined by equation (40). Starting with initial estimates for c_o, k_o, and k_1, along with measured values of system driving function, equation (41) is solved to obtain its velocity response over some interval of interest. Model parameters are incremented, from run to run, so as to minimize the following mean square error function:

$$J = \int_0^T E^2(t)\, dt \tag{42}$$

where

T = time duration of analysis

$E(t) = \dot{Y}(t)-\dot{y}(t)$

In order to analytically compute the parameter changes required to minimize J it is necessary to express $\dot{y}(t)$ as a function of these quantities. For a given forcing function, $\dot{y}(t)$ can be considered to be a function of its current parameter values (i.e., c_o, k_o, and k_1) and time. The form of $\dot{y}(t)$ for some other set of parameter values (i.e., $c_o + \Delta c_o$, $k_o + \Delta k_o$ and $k_1 + \Delta k_1$) can be simply approximated from the first order terms of the Taylor series expansion for $\dot{y}(t)$ as indicated in the following equation:

$$\dot{y}_\Delta \approx \dot{y}_o + \frac{\partial \dot{y}_o}{\partial c_o} \Delta c_o + \frac{\partial \dot{y}_o}{\partial k_o} \Delta k_o + \frac{\partial \dot{y}_o}{\partial k_1} \Delta k_1 \tag{43}$$

where

$$\dot{y}_o = \dot{y}(c_o, k_o, k_1, t)$$
$$\dot{y}_\Delta = \dot{y}(c_o + \Delta c_o, k_o + \Delta k_o, k_1 + \Delta k_1, t)$$

The partial derivatives of the right-hand side of equation (43) are time varying sensitivity coefficients which are solutions to sensitivity differential equations. These differential equations are easily derived from equation (41) by taking the partial derivative of this latter equation with respect to each parameter as indicated below:

$$\frac{\partial \ddot{y}_o}{\partial c_o} = \frac{d^2}{dt^2} \frac{\partial y_o}{\partial c_o} = \frac{\partial}{\partial c_o} [-c_o \dot{y}_o - k_o y_o - k_1 \operatorname{sgn}(y_o) y_o^2 + F(t)]$$

$$= -c_o \frac{d}{dt} \frac{\partial y_o}{\partial c_o} - k_o \frac{\partial y_o}{\partial c_o} - 2k_1 \operatorname{sgn}(y_o) y_o \frac{\partial y_o}{\partial c_o} + \cancelto{0}{\frac{\partial F(t)}{\partial c_o}} - \dot{y}_o$$

which can be written as

$$\ddot{S}_1 + c_o \dot{S}_1 + [k_o + 2k_1 \operatorname{sgn}(y_o) y_o] S_1 = -\dot{y}_o \tag{44}$$

where

$$S_1 = \frac{\partial y_o}{\partial c_o}$$

In a like manner the sensitivity equations for k_o and k_1 are defined by

$$\ddot{S}_2 + c_o\dot{S}_2 + [k_o + 2k_1 \text{sgn}(y_o)y_o]S_2 = -y_o \tag{45}$$

$$\ddot{S}_3 + c_o\dot{S}_3 + [k_o + 2k_1 \text{sgn}(y_o)y_o]S_3 = -\text{sgn}(y_o)y_o^2 \tag{46}$$

where

$$S_2 = \frac{\partial y_o}{\partial k_o}$$

$$S_3 = \frac{\partial y_o}{\partial k_1}$$

Equations (44), (45), and (46) are linear, second-order, differential equations with time varying stiffness coefficients that are a function of the modeled system's displacement signal. The excitation signals driving the sensitivity differential equations are a function of the velocity or displacement response of the modeled system. The time varying sensitivity coefficients required in equation (43) are obtained by solving equations (44) to (46) along with equation (41).

Now that all the elements in equation (43) are defined, it can be substituted into equation (42) resulting in

$$J = \int_0^T [\dot{Y} - \dot{y}_o - \dot{S}_1\Delta c_o - \dot{S}_2\Delta k_o - \dot{S}_3\Delta k_1]^2 dt \tag{47}$$

The function J is minimized by taking its partial derivative with respect to each of the incremental parameter changes and setting the resulting expressions to zero. The solution of the three simultaneous linear equations,

to obtain the three incremental parameter changes, can be expressed in the following matrix form:

$$P = [S]^{-1}V \tag{48}$$

where

$$P = \begin{bmatrix} \Delta c_o \\ \Delta k_o \\ \Delta k_1 \end{bmatrix} \tag{49}$$

$$V = \int_0^T \begin{bmatrix} \dot{S}_1(Y-y_o) \\ \dot{S}_2(Y-y_o) \\ \dot{S}_3(Y-y_o) \end{bmatrix} dt \tag{50}$$

$$[S] = \int_0^T \begin{bmatrix} \dot{S}_1^2 & \dot{S}_1 S_2 & \dot{S}_1 S_3 \\ \dot{S}_2 S_1 & \dot{S}_2^2 & \dot{S}_2 S_3 \\ \dot{S}_3 S_1 & \dot{S}_3 S_2 & \dot{S}_3^2 \end{bmatrix} dt \tag{51}$$

The elements of the P vector, computed by multiplying the inverse S matrix by the V vector, express the parameter changes resulting from a given pass through the data. The process is generally repeated until the parameter changes become small or the calculated value of J falls below some prescribed level.

Example Problem Results

A digital-computer algorithm using the defined analytical approach was designed for the purposes of making a preliminary evaluation of the technique. In this evaluation the K_o and K_1 system parameters were set at numerical values of 3948 and 394.8, with the value of C_o being varied

between 3.142 and 12.57. A linear system with these values for C_o and K_o would have a resonant natural frequency of 10 Hz and structural damping coefficients ranging from 0.05 to 0.2. The apparent resonant frequency of the actual nonlinear (hard-spring) system is generally higher than 10 Hz increasing with the magnitude of system displacement. This, in turn, is a function of the system's inherent damping and the magnitude of the driving function. The assumed form of the driving function was an exponential swept frequency sine wave covering the 6 to 20 Hz frequency range in approximately 6 seconds. The amplitude of the driving function was held at a constant amplitude which was numerically equivalent to K_o.

Initial runs indicated that convergence of the algorithm was dependent on having reasonable initial estimates for system parameters. In practice good estimates are not always available. Rather than increasing the analytical complexity of the coefficient updating technique, which was considered outside the scope of this preliminary investigation, it was decided to adopt a strategy that could be applied in practice, with suitable constraints, to generally insure convergence. The strategy adopted was based on the inherent information contained in the test data and the user's presumed knowledge for the form of the system's dynamics. In accordance with this strategy, the initial value of k_1 was set to zero, with the initial value of k_o taken as the squared value of the apparent resonant frequency of the response data. This frequency is simply determined by measuring the period of the response signal in the vicinity of its peak value. The initial value for c_o was selected at a tenth of the square root of k_o. This would correspond to a nominal structural damping coefficient of 0.1 if the system were linear.

Algorithm parameter updating was constrained so that k_1 would be set back to zero if its value went negative or became greater than the current value of k_o. The value of k_o was prevented from falling below a tenth of its initial value. Finally, the parameter changes from run to run were constrained so that the change in k_o could not exceed the initial value of k_o and that the change in k_1 could not exceed a tenth of the initial value of k_o. If either or both of these parameter changes exceed their corresponding limits all parameter changes were uniformly attenuated by a factor (not to be less than a tenth) in an attempt to prevent any parameter change from exceeding its limit. For the problem at hand, the above constraints are considered loose and were determined empirically with no attempt being made to refine them in an optimal sense.

Using this strategy, results were obtained in analyzing data from systems having C_o damping terms of 12.57, 6.283, and 3.141. The stiffness

coefficients K_o and K_1 were held at constant values of 3948 and 394.8. The results listed below reflect the ability of the approach to converge on the true coefficient values with the inherent characteristic of requiring more iterations as damping decreases.

	Analysis Pass	Model Parameter c_o	k_o	k_1
For C_o = 12.57	0	6.911	4777.	0.0
	1	11.70	4724.	35.56
	2	14.32	4411.	217.4
	3	12.87	3843.	439.6
	4	12.67	3977.	386.2
	5	12.57	3947.	395.2
	6	12.57	3948.	394.8
For C_o = 6.283	0	7.540	5685.	0.0
	1	10.51	4644.	323.6
	2	6.423	4618.	391.0
	3	8.113	4914.	387.5
	4	8.337	5136.	262.5
	5	6.139	4151.	394.0
	6	6.832	4482.	343.3
	7	6.458	4157.	368.3
	8	6.294	3943.	397.5
	9	6.282	3948.	394.7
	10	6.283	3948.	394.8
For C_o = 3.141	0	8.796	7738.	0.0
	1	5.727	5803.	474.2
	2	5.960	4981.	605.8
	3	4.738	6064.	260.7
	4	2.967	5557.	235.6
	5	3.244	5630.	234.8
	6	3.280	5359.	263.3
	7	3.284	5066.	293.7
	8	3.306	4745.	328.0
	9	3.281	4300.	372.9
	10	3.171	3979.	396.1
	11	3.137	3954.	394.1
	12	3.140	3949.	394.6
	13	3.141	3948.	394.8

REFERENCES

1. Waisanen, P.R., and Perangelo, H.J.: Real Time Flight Flutter Testing via Z-Transform Analysis Technique. AIAA Paper No. 72-784, 1972.

2. Baird, E.F., and Clark, W.B.: Recent Developments in Flight Flutter Testing in the United States. Paper presented at 34th meeting of AGARD Structures and Materials Panel, Lyngby, Denmark, April 1972.

3. Taylor, Lawrence W.,Jr., and Iliff, Kenneth W.: Systems Identification using a Modified Newton-Raphson Method - A FORTRAN Program. NASA TN D-6734, May 1972.

4. Grove, Randell D., Bowles, Roland L., and Maybew, Stanley C.: A Procedure for Estimating Stability and Control Parameters from Flight Test Data by using Maximum Likelihood Methods Employing a Real-Time Digital System. NASA TN D-6735, May 1972.

5. Cole, Henry A., Jr.: On-Line Failure Detection and Damping Measurement of Aerospace Structures by Random Decrement Signatures. NASA CR-2205, March 1973.

6. Ragazzini, J.F., and Franklin, G.F.: Sampled-Data Control Systems. McGraw-Hill Book Company, Inc., New York, 1958.

Table 1.- System command options

Item	Input*	Function
Maneuver mode	KB	Application program selection
Plot menu	LK, LP	Selects plots and/or tabs for display
Start maneuver	LK	Initiates real time data transfer to disk
Start event	LK	Initiates processing and tagging of data
Stop event	LK	Tags end of data slice to be processed
Stop maneuver	LK	Ends disk recording and processing
Recall mode	KB, LK	Allows intermaneuver disk data processing
Plot recall	KB, LP	Allows display of previous analysis results
Utility option	KB, LP	Enables access to files for purposes of changing plot scales, data scaling and certain program analysis variables

* Input types: KB - Keyboard type-ins
LK - Latchkey push button selection
LP - Display light pen selection

Table 2.- Overview of major analysis program options

Item	Analysis options
Model analysis order	Model order can be varied from 2 up to 14 for each response transducer
Multiple analysis order	Multiple ordered analysis models can be specified for use on response data yielding separate results
Data preprocessing	Recusive digital filtering, cross-correlation analysis, autocorrelation analysis, or random decrement signature processing
Filtering control	Specification of pass-band and roll-off characteristics (up to 36 dB per octave)
Correlation lag range	Selection of correlation function positive and negative lag range
Transform size	Fast Fourier transform size up to 2048 points
Data window	Specification of time duration or frequency range
Transducer selection	Analysis of 1 to 28 measurements at 500 samples per second
Data sample rate	500, 250,or 100 samples per second

Table 3. - Summary of TLEFAD results on simulated swept frequency response data

TLEFAD pre-processing option	Analysis results*				Data analysis window	Filter pass-band	Model order
	Clean		Noisy				
	f_d	g	$f_d \pm 1\sigma$	$g \pm 1\sigma$			
Direct	2.00 3.00	.100 .050	2.01±.026 3.06±.050	.092±.018 .038±.013	1.6 to 3.6 Hz	1.5 to 3.9 Hz	6
	8.01	.075	7.95±.055	.078±.022	7.0 to 9.0 Hz	6.0 to 10.5 Hz	4
	16.0	.031	16.0±.032	.033±.007	14.0 to 18.0 Hz	12.0 to 19.0 Hz	4
	42.6 52.2	.189 .053	37.4±1.10 51.6±.404	.100±.023 .083±.007	33.6 to 54.6 Hz	33.0 to 67.0 Hz	6
Cross-correlation	2.00 3.00	.100 .050	2.00±.023 3.01±.018	.093±.019 .048±.011	1.5 to 4.5 Hz	0.0 to 3.9 Hz	6
	8.01	.075	7.99±.043	.073±.012	6.0 to 10.0 Hz	6.0 to 10.5 Hz	4
	16.0	.030	16.0±.000	.030±.002	12.0 to 20.0 Hz	12.0 to 19.0 Hz	4
	41.8 52.0	.198 .050	41.0±.468 52.0±.052	.220±.024 .050±.001	35.0 to 59.0 Hz	33.0 to 67.0 Hz	6
Auto-correlation	1.99 3.00	.104 .050	2.00±.025 3.01±.023	.077±.024 .037±.008	1.5 to 12.0 Hz	1.5 to 3.9 Hz	6
	8.00	.075	8.01±.139	.072±.030	4.0 to 12.0 Hz	6.0 to 10.5 Hz	6
	16.0	.031	16.0±.032	.028±.003	10.0 to 22.0 Hz	10.0 to 19.0 Hz	4
	41.8 52.1	.198 .050	41.5±.239 52.1±.048	.203±.011 .050±.002	26.0 to 62.0 Hz	33.0 to 67.0 Hz	6

* f_d = damped natural frequency of mode

g = structural damping coefficient of mode

σ = standard deviation

Table 4. - Summary of results on simulated randomly excited response data

Program	Option	Time duration (seconds)	Number of runs	True results		Analysis results	
				f_d	g	$f_d \pm 1\sigma$	g $\pm 1\sigma$
TLEFAD	Auto-correlation	90	11	2.00	.100	2.00±.042	.084±.019
				3.00	.050	3.00±.024	.041±.011
				8.00	.075	8.01±.055	.063±.017
				16.0	.030	16.0±.060	.031±.006
				42.0	.200	41.6±1.03	.182±.029
				52.0	.050	52.1±.149	.051±.004
RESIDO	Auto-correlation	90	13	2.00	.100	2.01±.034	.068±.015
				3.00	.050	3.01±.017	.041±.012
				8.00	.075	8.01±.052	.067±.016
				16.0	.030	16.0±.055	.025±.004
				42.0	.200	42.1±.380	.186±.024
				52.0	.050	52.2±.168	.052±.006
	Random decrement	90	13	2.00	.100	2.00±.037	.068±.023
				3.00	.050	3.00±.029	.041±.015
				8.00	.075	8.02±.060	.059±.017
				16.0	.030	16.0±.073	.027±.005
				42.0	.200	42.6±.526	.194±.044
				52.0	.050	53.4±.307	.055±.007
		180	6	2.00	.100	2.00±.021	.076±.009
				3.00	.050	3.01±.018	.045±.010
				8.00	.075	8.03±.051	.058±.011
				16.0	.030	16.0±.049	.027±.002
				42.0	.200	42.5±.407	.185±.026
				52.0	.050	52.3±.157	.053±.006

Table 5. - Summary of flight test data results

	Mode / Analysis	AW1B		SW1B		SW2B		FLAPR		W1B/STRP	
		f_d σ	g σ	f_d σ	g σ	f_d σ	g σ	f_d σ	g σ	f_d W1B f_d STRP	g W1B g STRP
clean sweep	TLEFAD	6.15	.089	5.26	.134	15.2	.097	48.1	.251	6.46	.107
	direct	.097	.011	.080	.022	.197	.008	2.44	.028	7.74	.080
	TLEFAD	6.15	.095	5.24	.139	15.2	.103	49.3	.252	6.44	.101
	cross-corr	.035	.007	.055	.014	.155	.009	.652	.007	7.76	.079
	RESIDO	6.14	.086	-	-	15.1	.082	49.8	.238	6.45	.104
	cross-corr	.143	.036	-	-	.358	-	1.84	.028	7.67	.071
	COQUAD	6.10	.117	-	-	14.8	.124	49.5	.227	-	-
		-	-	-	-	-	-	-	-	-	-
noisy sweep	TLEFAD	5.91	.100	-	-	-	-	-	-	-	-
	direct	.308	.035	-	-	-	-	-	-	-	-
	TLEFAD	6.12	.103	-	-	-	-	54.2	.063	-	-
	cross-corr	.230	.027	-	-	-	-	-	-	-	-
	RESIDO	6.17	.093	-	-	-	-	54.4	.073	-	-
	cross-corr	.320	.040	-	-	-	-	-	-	-	-
90 sec. random	TLEFAD	6.04	.066	5.20	.117	-	-	-	-	-	-
	autocorr	-	-	-	-	-	-	-	-	-	-
	RESIDO	6.02	.109	5.76	.107	-	-	59.5	.215	-	-
	autocorr	-	-	-	-	-	-	-	-	-	-
	RESIDO	6.03	.102	5.69	.094	-	-	58.7	.197	-	-
	random-dec	-	-	-	-	-	-	-	-	-	-
180 sec. rand.	TLEFAD	6.15	.106	5.19	.124	-	-	-	-	-	-
	autocorr	-	-	-	-	-	-	-	-	-	-
	RESIDO	6.07	.076	5.67	.161	-	-	-	-	-	-
	autocorr	-	-	-	-	-	-	-	-	-	-

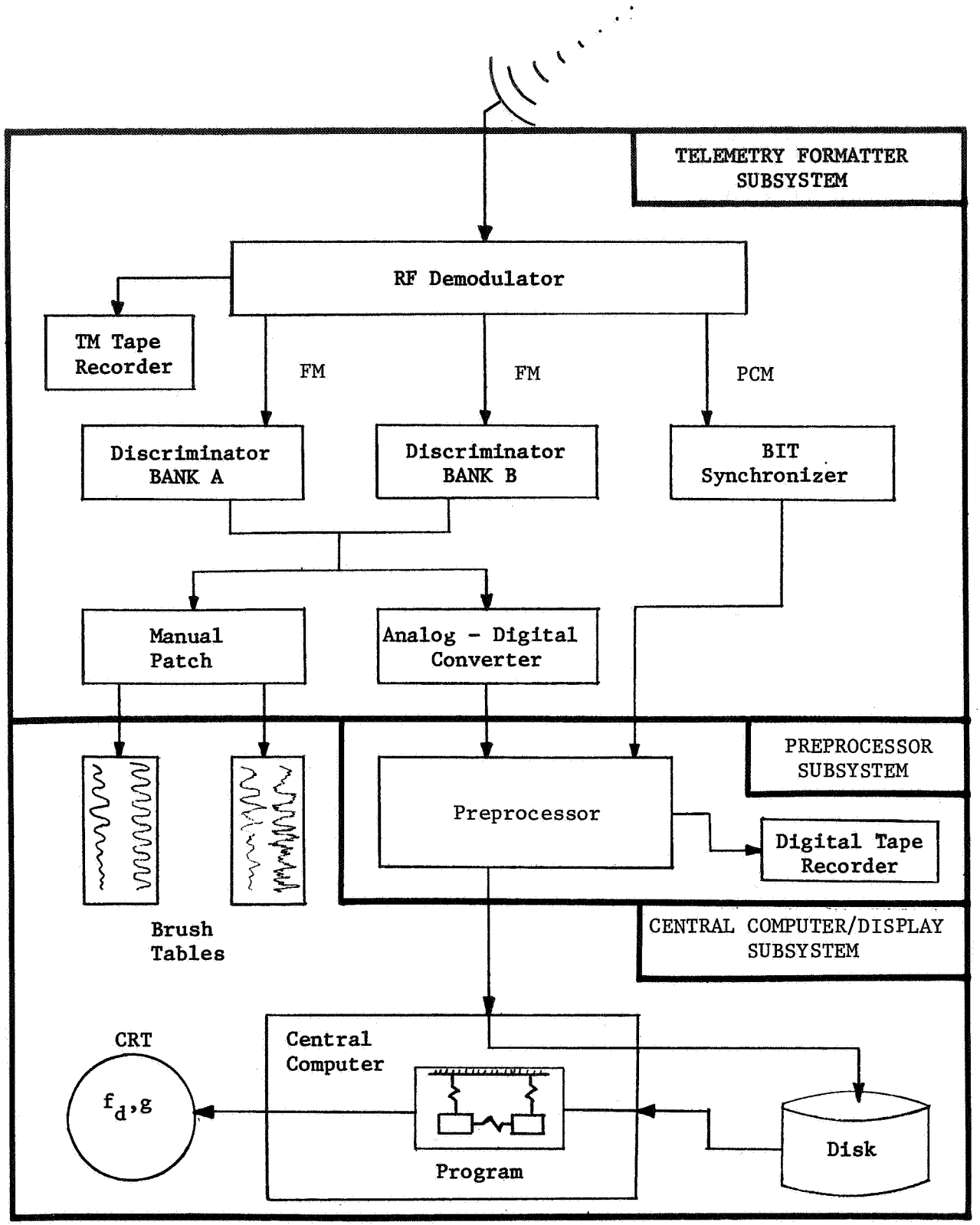

Figure 1. - Block diagram of Automated Telemetry Station.

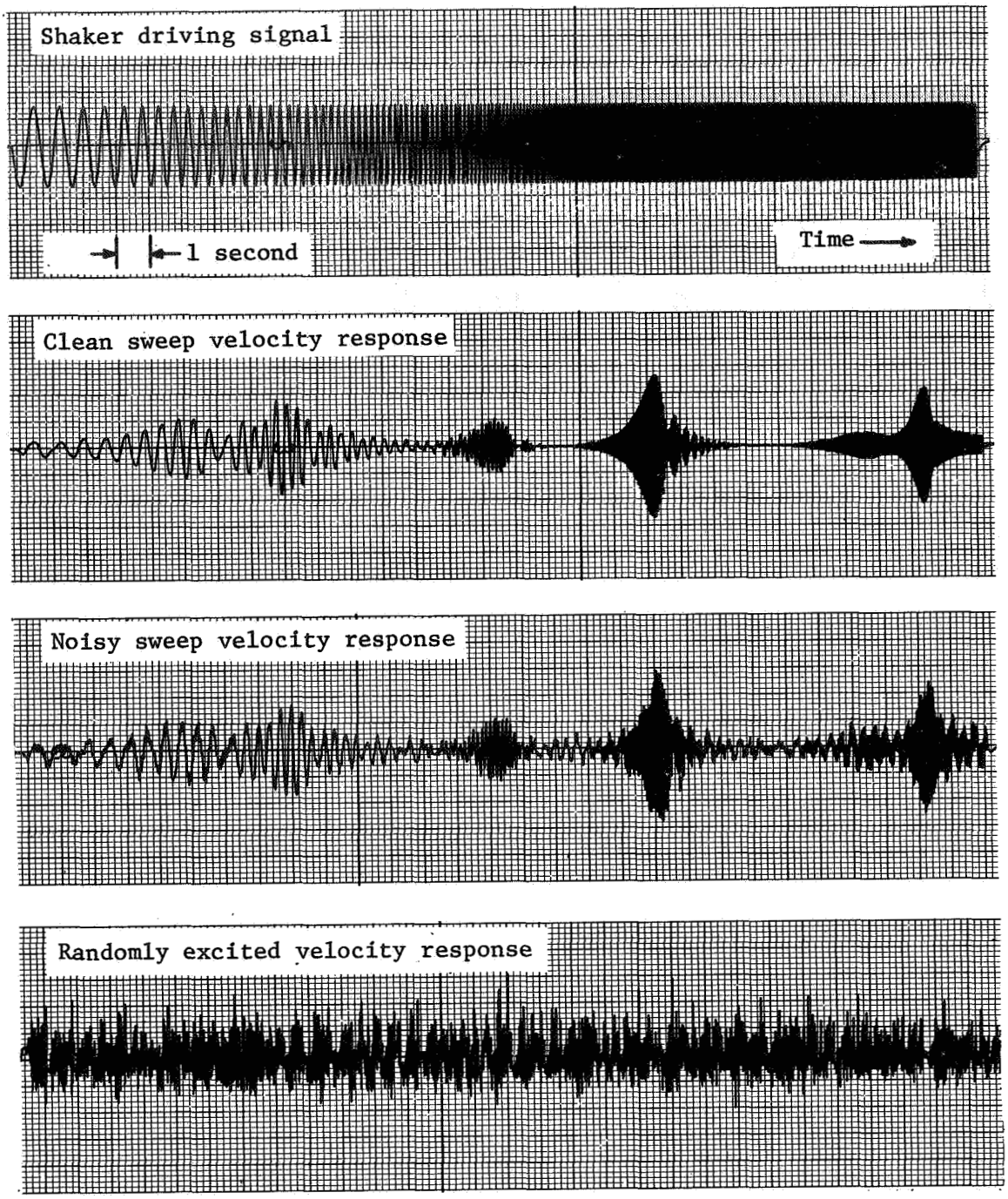

Modal characteristics: freq.= 2.00 - 3.00 - 8.00 - 16.0 - 42.0 - 52.0
damp.= .100 - .050 - .075 - .030 - .200 - .050

Figure 2.- Simulated flutter response data.

MODE - IDENTITY			PRIMARY XDUCER F-1	PRIMARY XDUCER G-1	SECONDARY XDUCER F-2	SECONDARY XDUCER G-2	KEAS	MT	MPT	EVENT TIME
M0210	0	1	2.00	0.083						9.6040
M0305	0	1	2.97	0.058						9.6040
M0011		1	-1.5	-1.50						9.6040
?	?	1	0.06	-1.00						9.6040
M0807	5	2	4.94	1.264						15.172
M08DU	M	2	8.00	0.070						15.172
M1603	0	3	12.2	0.561						20.096
M16DU	M	3	15.9	0.029						20.096
M4220	0	4	0.02	-1.00	0.000	590.5	0.93	1515.2		27.908
M5205	0	4	0.00	-1.00	0.000	590.5	0.93	1515.2		27.908
M0014		4	40.8	0.188	0.000	590.5	0.93	1515.2		27.908
?	?	4	51.9	0.052	0.000	590.5	0.93	1515.2		27.908

Resonant frequency - damping coefficient results obtained from noisy sweep in figure 2.

Figure 3. - Annotated primary output tabulation from TLEFAD program.

MODE -- ID			PRI CHAN	SEC CHAN	PRI ERROR FACTOR	SEC ERROR FACTOR	ACTUAL DATA--LOAD	ACTUAL FA	ACTUAL FB
M0210	0	1	15	99	1.598-4	00000	0059	1.49	4.50
M0807	5	2	15	10	2.566-4	1.630-6	0032	5.99	10.0
M1603	0	3	15	19	1.650-6	5.617-8	0120	11.9	20.0
M4220	0	4	15	99	1.108-6	00000	0001	54.9	59.0

Figure 4. - Validation output tabulation from TLEFAD program.

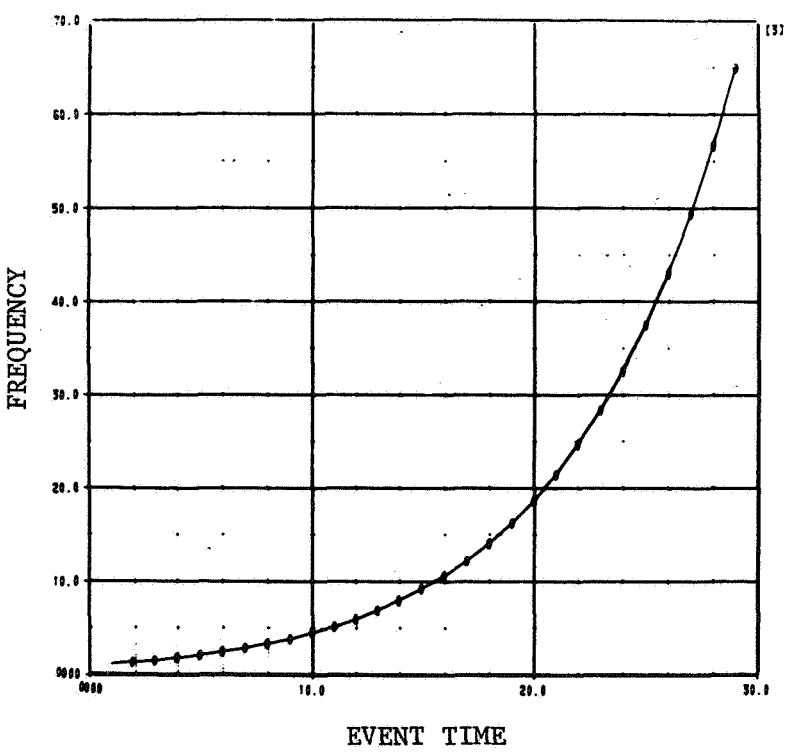

Figure 5. - Shaker frequency plot from TLEFAD program.

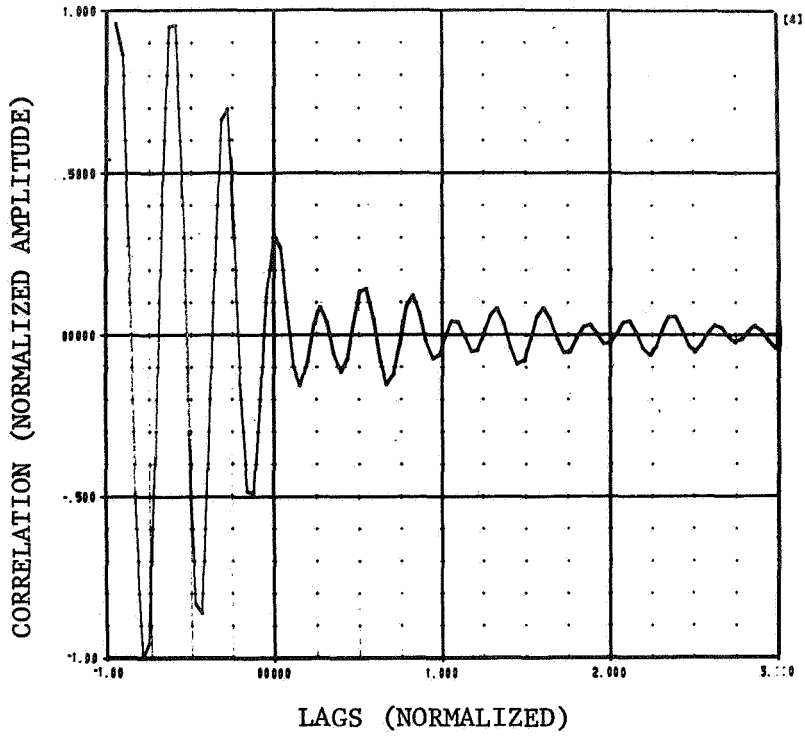

Figure 6. - Input signal cross-correlation function from TLEFAD program.

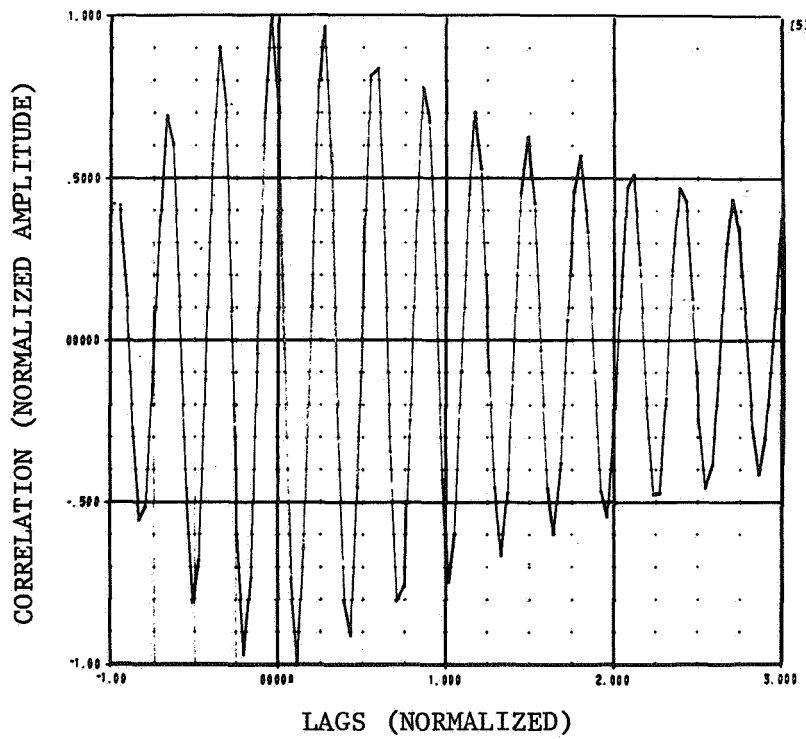

Figure 7. - Response signal cross-correlation function from TLEFAD program.

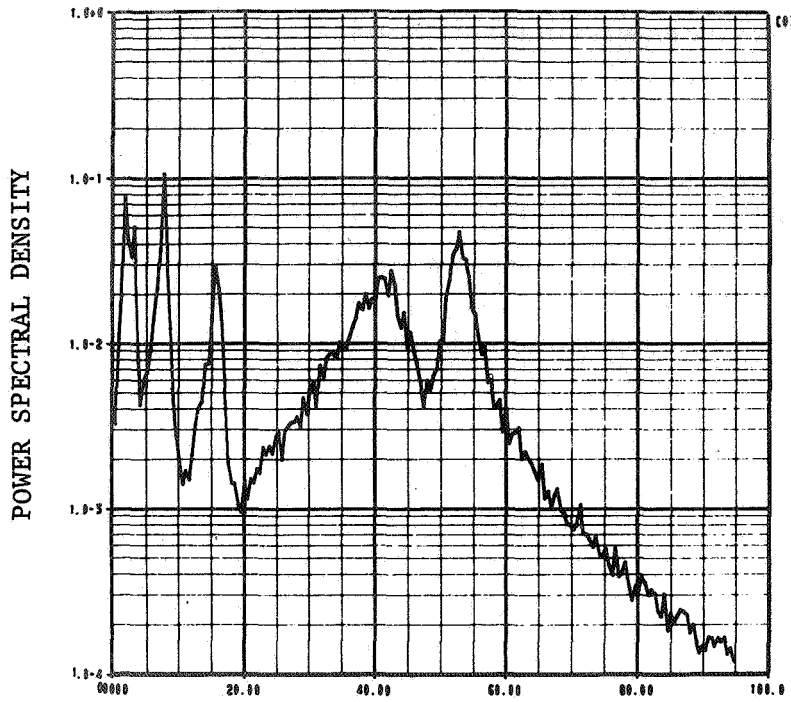

Figure 8. - Power spectral density plot from APSD program.

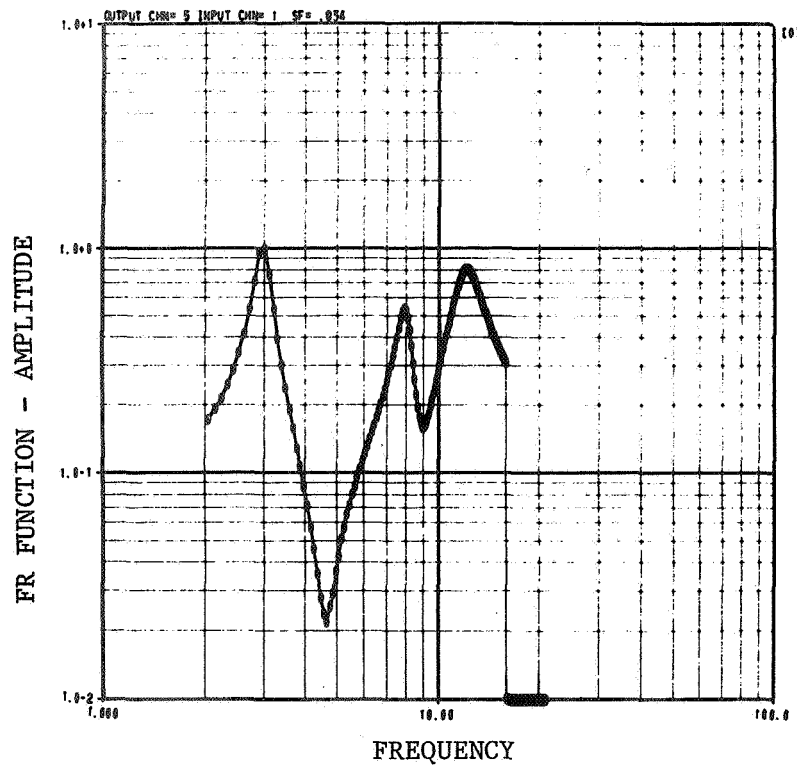

Figure 9. - Frequency response function amplitude from COQUAD program.

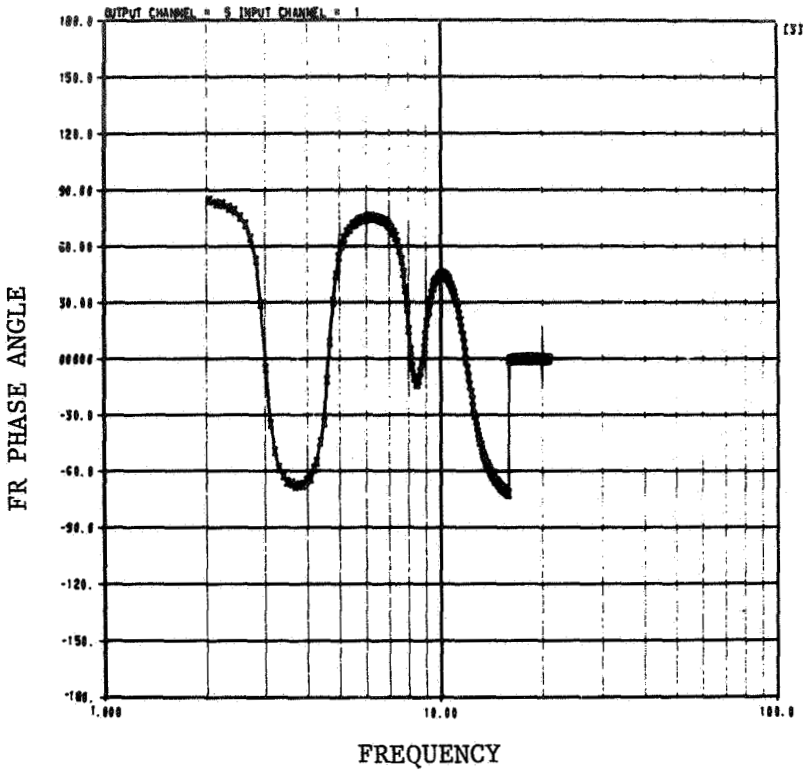

Figure 10. - Frequency response phase angle from COQUAD program.

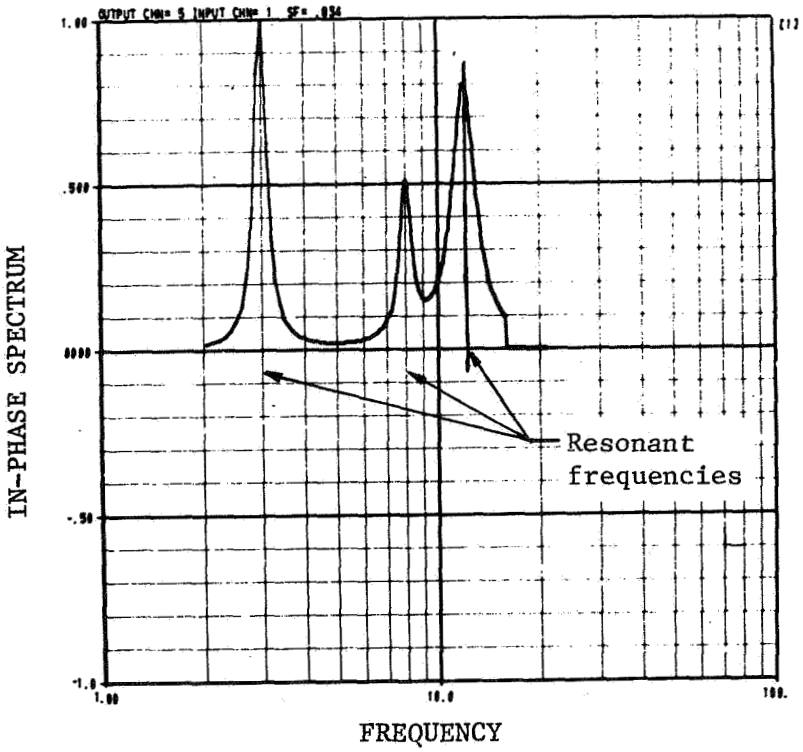

Figure 11. - Annotated in-phase spectrum from COQUAD program.

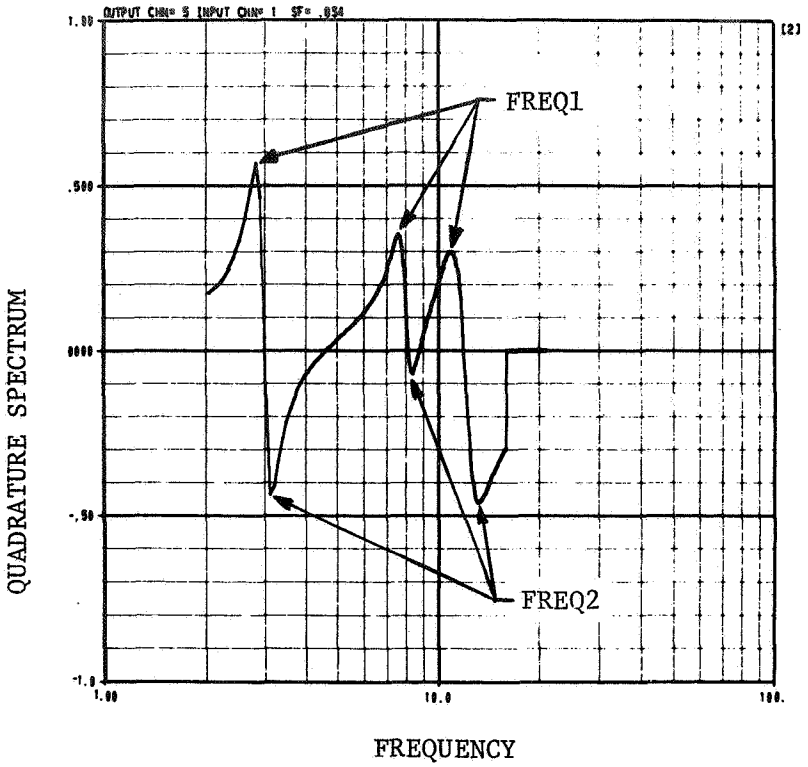

Figure 12. - Annotated quadrature spectrum from COQUAD program.

$$\text{DAMP. COEF.} = \frac{(\text{FREQ2}/\text{FREQ1})^2 - 1}{(\text{FREQ2}/\text{FREQ1})^2 + 1}$$

[3]

XDUCER-CHNL	RES. FREQ.	DAMPING COEF.	FREQ1	FREQ2 [4]
05	3.027	.098	2.852	3.125
05	8.007	.097	7.617	8.398
05	12.01	.104	10.93	13.18

Figure 13. - Annotated output tabulation from COQUAD program.

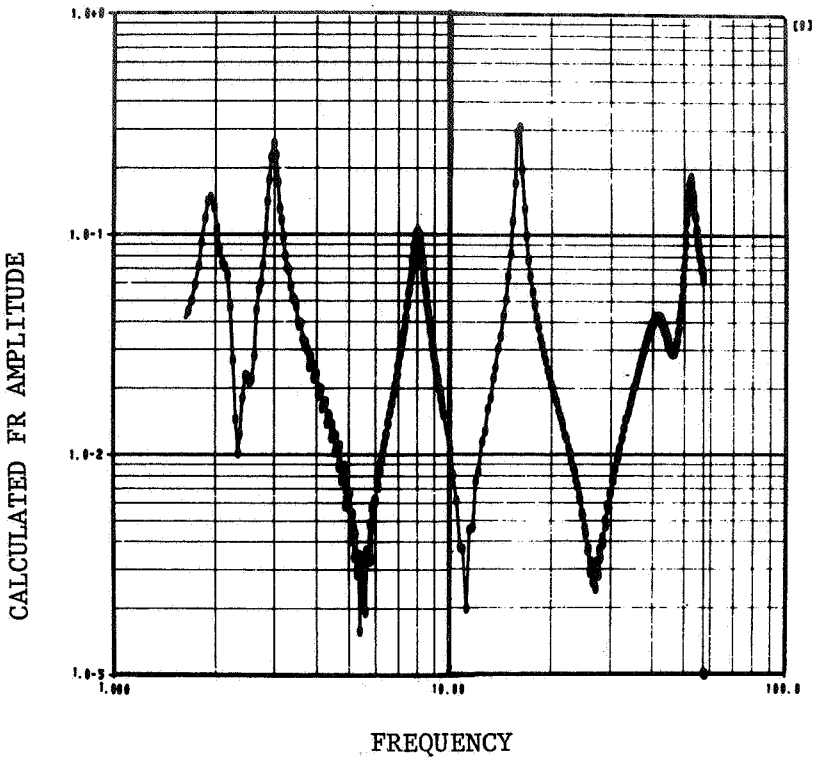

Figure 14. - Calculated frequency response function amplitude from ENERGY program.

ANALYSIS PASS	OUTPUT CHANNEL	RESONANT FREQUENCY	DAMPING COEFFICIENT	MODAL ENERGY	WINDOWING LEVEL	DEGREES OF FREEDOM	XFORM FREQ INCREMENT	ACTUAL FREQ LOWER	WINDOW UPPER
01	09	16.02	.0304	1.657+0	.020	01	.2441	13.2	20.5
01	09	52.11	.0525	4.319-1	.020	02	.2441	35.1	57.0
02	09	16.00	.0202	1.579+0	.010	02	.2441	12.4	22.9
02	09	52.04	.0490	4.357-1	.010	03	.2441	31.7	57.0
01	09	1.970	.1043	2.681-1	.020	01	.0406	1.58	2.21
01	09	3.001	.0501	9.585-1	.020	03	.0406	2.25	4.68
01	09	7.998	.0740	1.388-1	.020	01	.0406	6.64	9.66
02	09	1.999	.0975	2.995-1	.010	03	.0406	1.58	5.56
02	09	3.001	.0498	9.915-1	.010	03	.0406	1.58	5.56
02	09	7.998	.0752	1.476-1	.010	02	.0406	6.30	10.0

Figure 15. - Primary output tabulation from ENERGY program.

ANALYSIS PASS	OUTPUT CHANNEL	RESONANT FREQUENCY	DAMPING COEFFICIENT	MODAL ENERGY	WINDOWING LEVEL	DEGREES OF FREEDOM	POINTS LOADED	ACTUAL FREQ WINDOW LOWER	UPPER
01	09	16.02	.0304	1.657+0	.020	01	00155	13.2	20.5
01	09	43.15	.1920	1.791-2	.020	02	00107	35.1	57.0
01	09	52.11	.0525	4.519-1	020	02	00107	35.1	57.0
02	09	17.56	.1414	2.741-4	.010	02	00154	12.4	22.9
02	09	16.00	.0282	1.579+0	.010	02	00154	12.4	22.9
02	09	41.74	.2027	1.765-2	.010	03	00105	31.7	57.0
02	09	52.04	.0490	4.357-1	.010	03	00105	31.7	57.0
02	09	-.047	-1.00	00000	.010	03	00105	31.7	57.0
02	09	.0029	-1.00	00000	.010	03	00105	31.7	57.0
01	09	1.970	.1043	2.681-1	.020	01	00113	1.58	2.21
01	09	3.001	.0581	9.585-1	.020	03	00273	2.25	4.60
01	09	2.153	.1606	3.354-2	.020	03	00273	2.25	4.60
01	09	5.056	.4000	1.255-3	.020	03	00273	2.25	4.60
01	09	7.990	.0740	1.388-1	.020	01	00105	6.64	9.66
02	09	8.215	.7963	1.052-2	.010	03	00254	1.58	5.56
02	09	1.999	.0975	2.995-1	.010	03	00254	1.58	5.56
02	09	3.001	.0498	9.915-1	.010	03	00254	1.58	5.56
02	09	7.990	.0752	1.476-1	.010	02	00098	6.30	10.0
02	09	.0446	-1.00	00000	.010	02	00098	6.30	10.0

Diagnostic for real difference equation root.

Figure 16. - Annotated secondary output tabulation from ENERGY program.

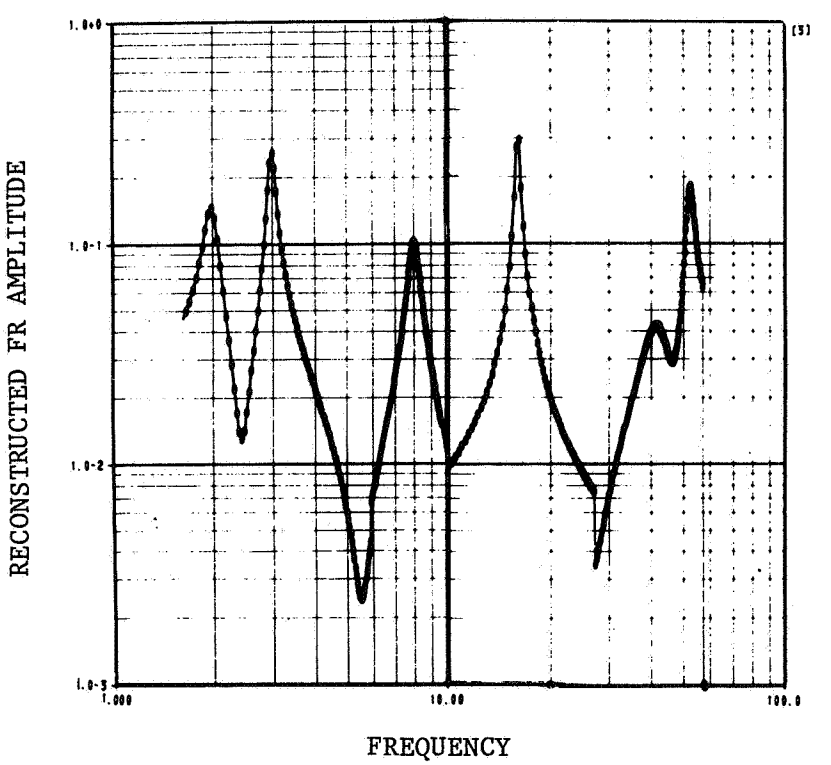

Figure 17. - Reconstructed frequency response function amplitude from ENERGY program.

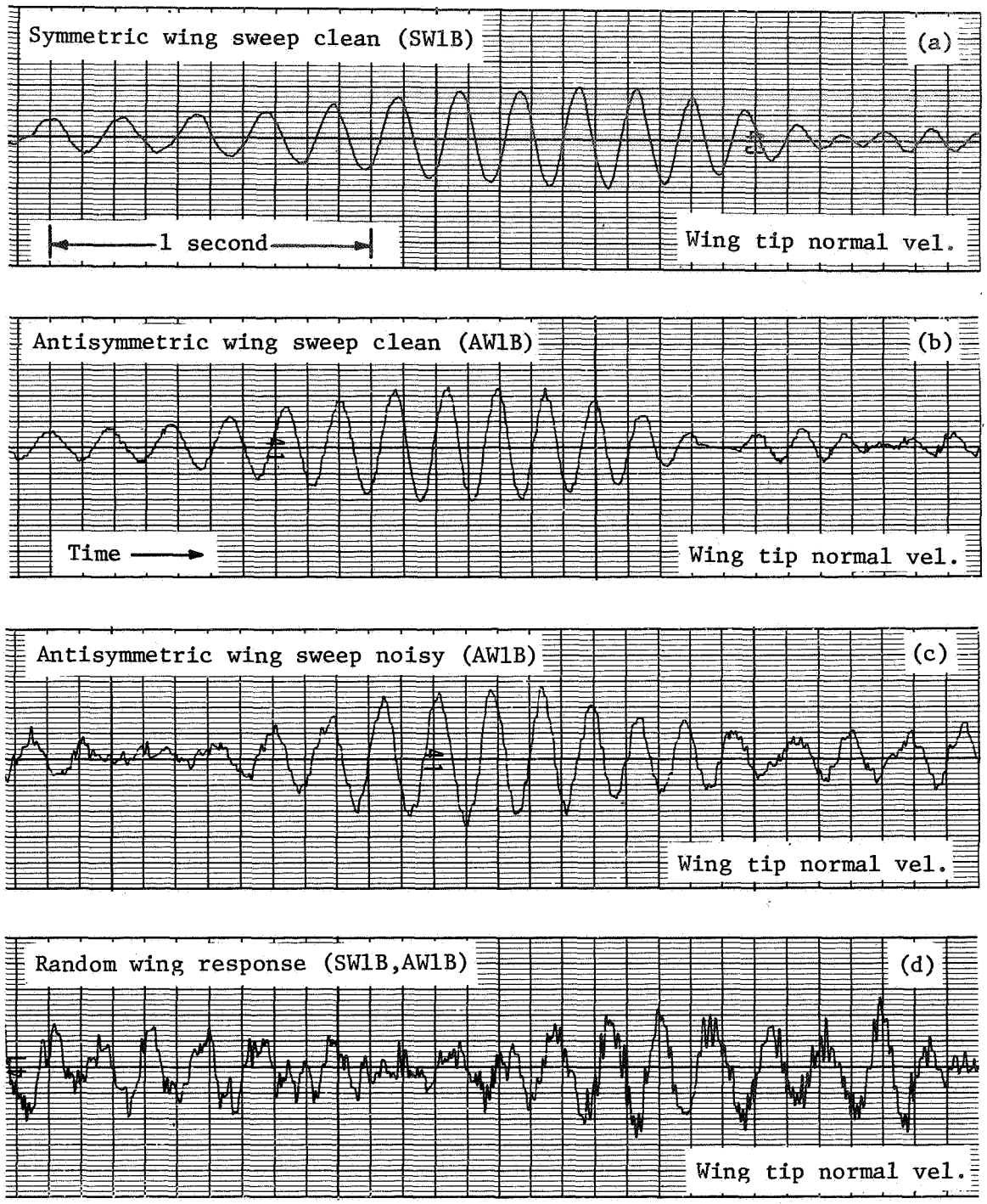

Figure 18.- Flight test flutter response data.

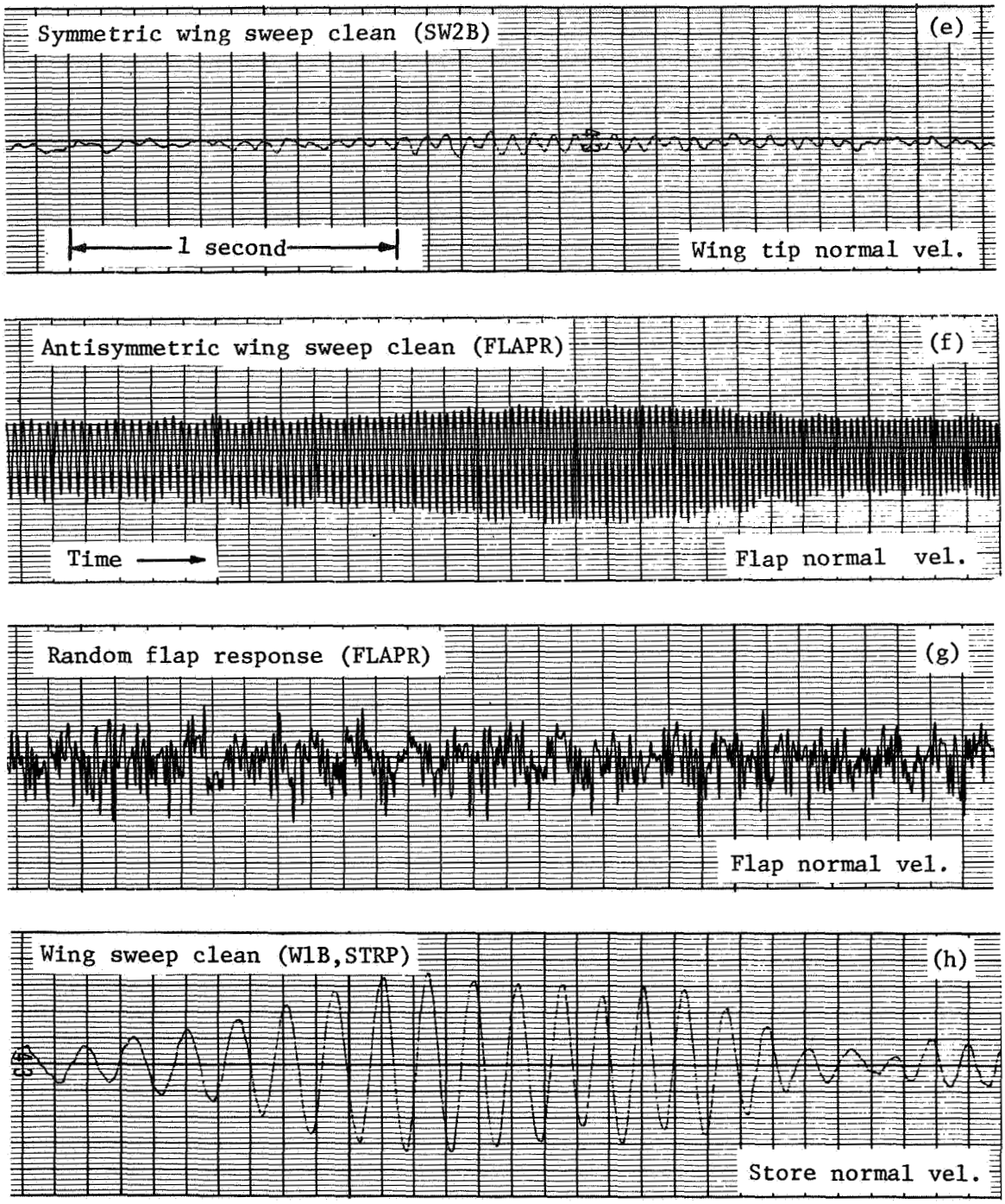

Figure 18. - Concluded.

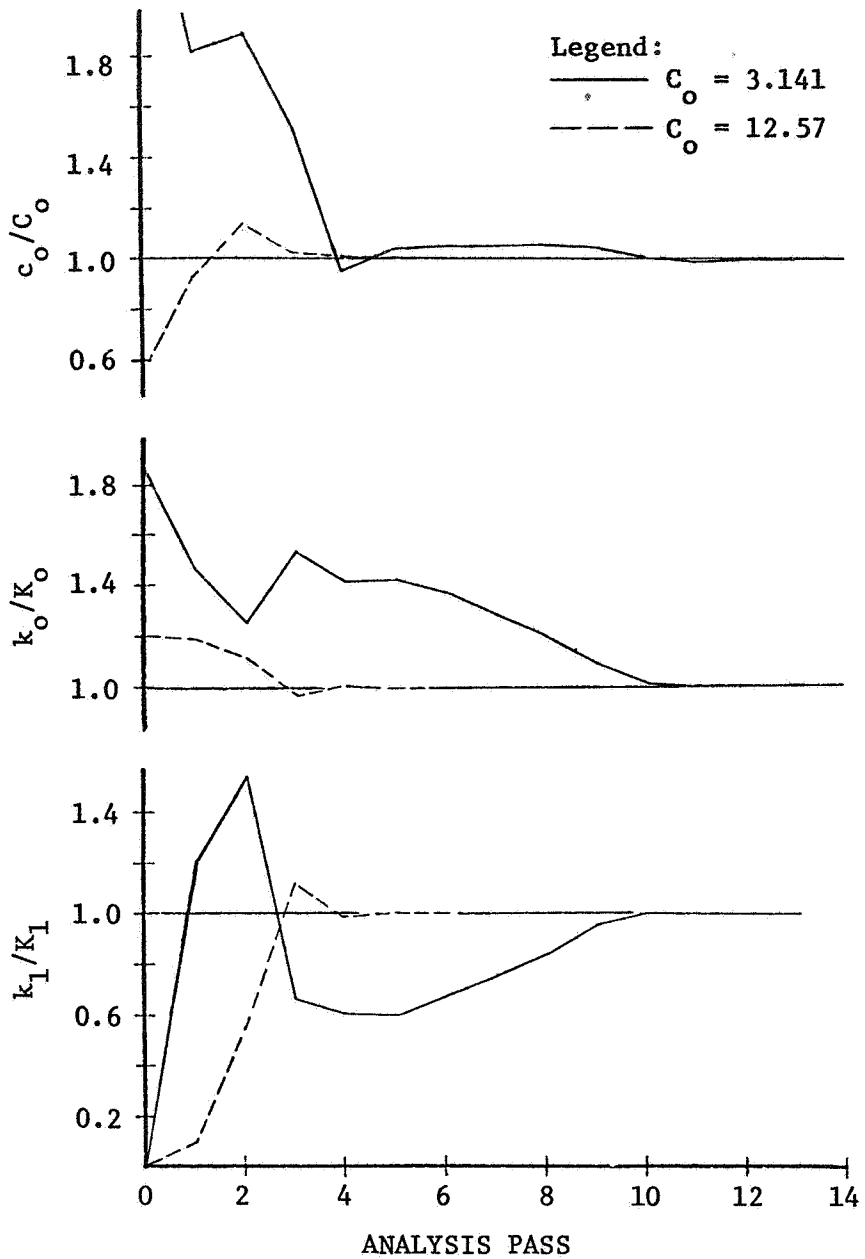

Figure 19. - Parameter convergence for nonlinear model.

THE APPLICATION OF DIGITAL COMPUTERS TO NEAR-REAL-TIME PROCESSING OF FLUTTER TEST DATA

S. R. Hurley

Lockheed-California Company

SUMMARY

A description of procedures used in monitoring, analyzing, and displaying flight and ground flutter test data is presented. These procedures include three digital computer programs developed to process structural response data in near real time. Qualitative and quantitative modal stability data are derived from time history response data resulting from rapid sinusoidal frequency sweep forcing functions, tuned-mode quick stops, and pilot-induced control pulses. The techniques have been applied to both fixed- and rotary-wing aircraft, during flight, whirl tower rotor systems tests, and wind tunnel flutter model tests.

An hydraulically driven oscillatory aerodynamic vane excitation system is described. This system was recently utilized during the flight flutter test programs accomplished during Lockheed L-1011 and S-3A development.

INTRODUCTION

The present day costs of prototype/development flight vehicles and overall demands on flight testing time require the flutter engineer to minimize both flight and calendar time associated with flutter substantiation and flight envelope clearance. This objective must be accomplished while maximum safety of flight to the flight crew and vehicle is maintained. Test and data analysis procedures must also be developed to minimize the risk of structural damage and/or loss of the high cost, dynamically scaled wind tunnel flutter models normally used during the pre-prototype phase of a flight vehicle development program. These objectives can be attained only by a well-coordinated test program which utilizes reliable procedures of instrumentation, signal conditioning, excitation technique, and data transmittal/storage/retrieval/display, properly integrated and compatible with the particular characteristics of the test vehicle.

The installation of special sinusoidal excitation devices, although desirable, can be justified only for those cases where the stability of a number of flutter-significant modes must be monitored, or for those cases where alternate or more economical excitation techniques, such as control pulses, do not adequately excite the modes of interest. In investigating the effect of

relatively minor design changes which arise during the operational phase of an aircraft, such as control system changes, external store additions, and significant mass or stiffness variations, alternate excitation methods which do not demand special purpose hardware installations may be used. These methods include the well-known control pulse (manual or electrical) for low frequency modes generally less than 10 Hz, as well as recent developments in computerized data analysis techniques applied to turbulence-induced structural response data. The latter methods rely primarily on various Fourier transforms and spectral analysis procedures to determine modal frequency and damping characteristics. Examples of such techniques are described in references 1, 2, and 3.

This paper briefly describes the various flutter testing techniques utilized at the Lockheed-California Company in recent years as applied to several major flight vehicle programs. Primary emphasis is placed upon the online data monitoring capabilities made possible by the availability of modern computerized data handling systems.

Proper acknowledgement should be given to several associates at the Lockheed-California Company who were instrumental in developing, and making operationally practical, the techniques described in this paper.

Edmund A. Bartsch and Darrow Richardson developed the real-time decay program and the real-time response program. Bill Kobayashi developed the peak plot analysis with contributions made by Joe Buttitto, Burt McCorkle, Bridget Shycoff, and Erick Sturcke.

MODAL EXCITATION

So that the flutter-significant modes of the Lockheed L-1011 aircraft could be properly evaluated, an hydraulically driven oscillatory aerodynamic vane excitation system was developed and installed on the wingtips and stabilizer tips. The same system was later used during the S-3A flutter tests, being mounted on the aft fuselage. The vane actuators were developed by Royal Industries, Santa Ana, California. The aerodynamic vanes were designed and fabricated at Lockheed by using helicopter rotor blade design and fabrication techniques, which provided the required structural capability to withstand the extreme inertial and aerodynamic loadings imposed on the vanes at the required frequencies. Photographs of the vane installation and control units are shown in figures 1 and 2.

Salient features of the excitation system are:

A. It provides constant and selectable sinusoidal force over the frequency range of from 0.5 to 25 Hz for L-1011 application and 2.5 to 50 Hz for S-3A application.

B. It utilizes an automatic linear period frequency sweep function. Sweep time/rate is selectable. The sweep rate utilized during the L-1011 program optimized modal response, minimized sweep time, and optimized frequency shift due to sweep rate. The S-3A sweep rate optimized response amplitude/test time.

C. The installed unit weight is approximately 46 kilograms.

D. The airfoil used was symmetrical with 53-cm span and 46-cm chord. The vane was mass balanced with center of gravity at the axis of rotation (20% chord). The aerodynamic center, as determined by wind tunnel tests, was approximately 1.25 cm aft of the axis of rotation, minimizing actuator force requirements. Blunt trailing edges were added to the vanes to ensure a zero lift trail stability when unpowered.

E. The vane force capability was ±1000 newtons at 200 KEAS with proportionally higher forces available at higher speeds. The maximum vane oscillatory angle of attack was $\pm 15^{\circ}$. The force on each vane was individually selectable.

F. Automatic fail-safe features were designed into the actuator control system to limit vane force, vane amplitude, and/or aircraft structural response.

G. There were provisions for manually tuning particular modes of interest and stop vanes at zero lift position within less than 1 cycle.

H. The vanes can be driven either in phase or 180° out of phase as required to excite symmetric or antisymmetric airplane modes.

In addition to the use of the oscillatory vanes to provide modal excitation, certain modes were investigated by using control pulses or electrically commanded symmetric aileron impulses. In the case of certain wind tunnel flutter model tests, modal damping characteristics have been determined by applying the peak plot data analysis method to model response time histories excited by existing wind tunnel turbulence.

The choice of excitation is based on the specific modes of interest, cost considerations, and data analysis procedure to be used.

DATA ANALYSIS METHODS

Real-Time Decay Analysis

The real-time decay analysis program was developed to analyze telemetered flight flutter test data by use of an online computer and to help make a rapid determination of the damping of structural modes excited either by control pulses or by tuning with sinusoidal forcing devices and quick-stopping the excitation input.

The decay analysis program is based on the well-known assumption that the decay time history of the free oscillation following a pulse or quick stop is an exponential function. A plot of the log magnitude of the decay versus time is, therefore, a straight line. The output of the real-time decay program is a plot of the log of the successive half-cycle amplitudes versus number of half cycles, which is proportional to time if constant frequency of decay is assumed. The compute mode of the program is triggered by a pilot- or ground-initiated flag signal just prior to the control pulse input or by a flag signal automatically generated just prior to the oscillatory vane stop electrical command. When the compute mode is triggered, the computer processes the time history data as follows:

It searches for extreme values, maxima and minima, in such a way that each successive extreme value Y_i is determined and stored (fig. 3).

It calculates the double amplitude D_i for each half cycle, by the equation:

$$D_i = \left| \frac{1}{2} (Y_{i-1} + Y_{i+1}) - Y_i \right|$$

where $i = 1,2,\ldots. N-1$, with $N \leq 40$, a practical maximum number of half cycles.

The logarithm of the double amplitude D_i is calculated and normalized to 1.0 for the maximum value as follows:

$$LD_i = \log_{10} D_i - \log_{10} D_{i_{max}} + 1.0$$

A high-speed line printer is utilized to rapidly plot the normalized logarithm LD_i versus i, the number of half cycles. A typical example of the printed output is shown in figure 4. In previous applications, up to nine response parameters have been simultaneously analyzed and plotted within 30 to 40 seconds after the control pulse or quick stop.

Using engineering judgment, the engineer can fair a straight line through the plotted data and rapidly determine a quantitative damping value using a transparent overlay.

As noted in figure 4, the printout format serves as a convenient data-keeping device by identifying the following:

(1) test number
(2) flight number
(3) date
(4) run code number
(5) response parameter number/identification
(6) equivalent airspeed, Mach number, and pressure altitude at the time of pulse calculated from telemetered pressure measurements
(7) type of signal conditioning (filtering) utilized

(8) a printout of least-squares linear curve fit of the function LD_i versus i between the first maximum LD_i, identified as S, and a number of consecutive half cycles (M). The calculated value of structural damping (g), percent error (E%), and the average frequency (FM) over the computer-selected decay region are also printed

If the computer-selected decay region agrees with the flutter engineer's judgment, the damping and frequency can be taken directly from the printout. In addition, these computer-calculated values of g and FM can be digitally displayed in the data-monitoring area during flight.

Before the response time history signals are used as input to the real-time decay analysis program, the telemetered data are filtered through analog filters selected to isolate the anticipated modes of interest, depending on proximity and response amplitude of adjacent modes. The units used are selectable as low pass, high pass, or band pass filters, and they reliably condition exponentially decaying signals having structural damping rates of up to 25%. The analog signals, after proper filtering, are digitized in computer-compatible format at a rate of 500 samples per second prior to processing. A typical flow chart of a PCM data acquisition and monitoring configuration is shown in figure 5.

This analysis method is applicable for modal response cases where the mode is excited to an initial level of approximately three times the average level of response to random and atmospheric turbulence forcing levels. In addition, the technique relies heavily on engineering judgment in selecting the proper time slices. The computer program does, however, minimize the time and manual plotting effort previously required in analyzing free decay response data.

Real-Time Response Analysis

The real-time response program was developed primarily to provide rapid evaluation of the stability trends relative to a large number of modes as a function of airspeed. This technique is utilized when sinusoidal frequency sweep forcing devices are available on the test aircraft. Again, computer-processed data are available within approximately 30 seconds after the end of the sweep excitation. Typical sweep times are 40 to 60 seconds for a frequency range of 3.0 to 50 Hz. The sweep function used, though not a requirement, was a linear period sweep defined by the relationship

$$F(t) = \frac{F_o}{1 + a F_o t}$$

where

$F(t)$ = frequency at time t - Hz

F_o = frequency at time t = 0 - Hz

t = time = sec

a = dimensionless sweep rate

This function was selected as the best compromise between response amplitude, frequency shift, and time required to sweep through the desired frequency range. The response characteristics resulting from a linear period sweep were based on a study conducted by Edmund A. Bartsch and contained in Lockheed Report LR 16484, "Flight Flutter Testing Method."

Typically, nine response parameters are processed simultaneously. The response analysis is based on the assumption that the response ratio varies inversely as the modal damping rate. Plots are maintained to track relative response versus equivalent airspeed (see figure 6 as a typical example).

The response time history signals of each parameter are preconditioned, prior to being used as input to the computer program, through constant bandwidth (±2.5 Hz) tracking filters to minimize extraneous responses and high frequency noise. The tracking filter center frequency is controlled by the telemetered function generator signal which drives the oscillatory aerodynamic exciter vanes. The analog outputs of the tracking filters are then digitized at a rate of 500 samples per second and converted to engineering units for processing. Flag signals are used to trigger sweep-start and sweep-stop time in the computer. The sweep-stop signal causes the computer to stop receiving data, complete calculations, and start printing results. A typical real-time response analysis printout is shown in figure 7.

The computer program processes the time history data as follows:

It determines input and response amplitudes. The input function is the output of a strain gage bridge on the oscillating vane which is calibrated to measure vane normal force.

Input frequency at time of maximum response is calculated from the average period of the three previous and the three subsequent cycles of the input function.

It determines the time at which maximum and minimum response amplitudes occur, eliminating minor or transient fluctuations by a minima criteria identified as a "window," retaining and printing out only the significant response maxima and minima.

The results of the real-time program are presented in tabular form (figure 7). A separate sheet is printed for each response parameter of interest. As noted in figure 7, the following data are printed out versus elapsed time from sweep-start for all response maxima and minima which satisfy the "window" criteria specified within the swept frequency range.

Time of input peak in seconds (time of max. and min. response)

Input period in seconds

Input frequency in Hz

Vane input amplitude in pounds

Response amplitude in engineering units (i.e., lb, in-lb, acceleration (g))

Response ratio in engineering units

In addition to the response ratio, and general test identification, the following information is also printed:

Start and stop time of sweep

Indicated airspeed

Equivalent airspeed

Altitude

Mach number

The identification of modal maxima is made by the flutter engineer, based on frequency and relationship to response data at previous airspeeds. Both symmetric and antisymmetric sweeps are normally made to evaluate all pertinent modes.

Peak Plot Data Analysis Program

The peak plot data analysis program was developed at the Lockheed-California Company and is described in detail in Lockheed Report 25111, "Fourier Transform Analysis," dated March 31, 1972. This technique has been used at Lockheed to obtain modal frequency and damping data from time history data obtained from rotor system whirl tower tests, wind tunnel flutter model tests, and L-1011 and S-3A flight flutter tests. This method is utilized for those particular modes where the modal data of interest have a high level of signal contamination or extraneous response of adjacent modes. The peak plot program is available to the flutter engineer as an interactive computer graphics program which allows nearly instantaneous iterative solutions to be obtained. Simple light pen commands can be used to optimize data plotting and solution displays. Hard copies of desired data plots are easily obtained.

The peak plot method may be briefly described as follows:

The Cooley-Tukey fast Fourier transform (FFT) algorithm is applied to the digitized time history test data sample in order to generate a plot of the log of the Fourier transform, log $F(\omega)$, as a function of the log of the frequency, log (ω). The frequency of the mode or modes of interest is "coarsely" displayed by the light pen detecting the indicated frequency peak(s) on the screen displayed plot. Figure 8 illustrates an example of such a plot.

After selecting the mode and frequency of interest, the program then uses a direct computation of the discrete Fourier transform given by

$$F(\omega_k) = \Delta t \sum_{i=0}^{N-1} f(t_i) \left[\text{Cos}\,\omega_k t_i - j\,\text{Sin}\,\omega_k t_i\right]$$

where ω_k is the frequency of the mode to be analyzed, Δt is the data sampling interval, N is the number of data points in the block being transformed, t_i is the i^{th} time point, and j is $\sqrt{-1}$.

Since ω_k is an approximate frequency, procedures have been programmed to iterate to a nearly true ω by adjusting the harmonic number, k, and number of data points, N, used in the transform.

The next step in the method generates a time history of the function

$$G(\tau) = \ln \left| F(\omega_k) \right| , \quad t_1 \leqslant \tau \leqslant t_2$$

The time dependence of the function $G(\tau)$ is obtained by computing the function $\ln \left|F(\omega_k)\right|$ for a sequence of data blocks where $G(\tau)$ is computed by using the test data f(t) for the time interval

$$\tau \leqslant t \leqslant \tau + (N-1)\,\Delta t \quad ; \quad \tau \text{ is the time of first data point in the block being transformed.}$$

A running Fourier transform is used for computing efficiency. The data for each block is efficiently transformed by a recursive formula which uses the results from the previous block. After the first block, the result for subsequent blocks is obtained by a single deletion of a term, and the addition of a new term to the result of the previous block.

The basis for the peak plot method is that the transient response is closely approximated by an exponentially damped sinusoid. The actual peak plot is a plot of $\ln \left|F(\omega_k)\right|$ versus the time corresponding to the first data

point for the sequence of data blocks. A measure of the damping is obtained by dividing the slope approximation of the plot by the frequency, ω_k.

Figure 9 presents a peak plot/time history display of a data sample representing a relatively highly damped control pulse response in the presence of noise and random excitation. The peak plot method has been used as an online procedure in some applications, but primarily as a postflight or posttest data analysis tool.

CONCLUDING REMARKS

Each of the flutter testing methods described has certain advantages and disadvantages such as cost, ease of use, specific excitation requirements, and applicability to specific test objectives and is used individually or in combination as judged necessary. None of the methods described provides conclusive stability data under certain flight conditions such as heavy Mach or transonic buffet conditions for higher damped modes. All methods described rely heavily on the engineer-in-the-loop approach for final judgement.

The availability of high-speed/capacity computers has provided the necessary tool for developing advanced data analysis methods which more fully satisfy the desired objectives of flutter testing at economically feasible levels. Current development studies within the aerospace industry and government agencies are contributing to more satisfactory solutions of the problem.

REFERENCES

1. Newman, K. W.; Skingle, C. W.; and Gaukroger, D. R.: The Development of Rapid - Testing Techniques for Flutter Experiments. C. P. No. 1274, 1974.

2. Soovere, Jaak; Turbulence Excited Frequency Domain Damping Measurement and Truncation Effects. NASA Symposium of Flutter Testing Techniques, Oct. 1975. (Paper No. 5 of this compilation.)

3. Mackenzie, Alexander: Application of the Fast Fourier Transform to Ground Vibration Testing, and Flight Flutter Testing. Proceedings of the Fifth Annual Symposium of The Society of Flight Test Engineers, Anaheim, California, August 7-9, 1974.

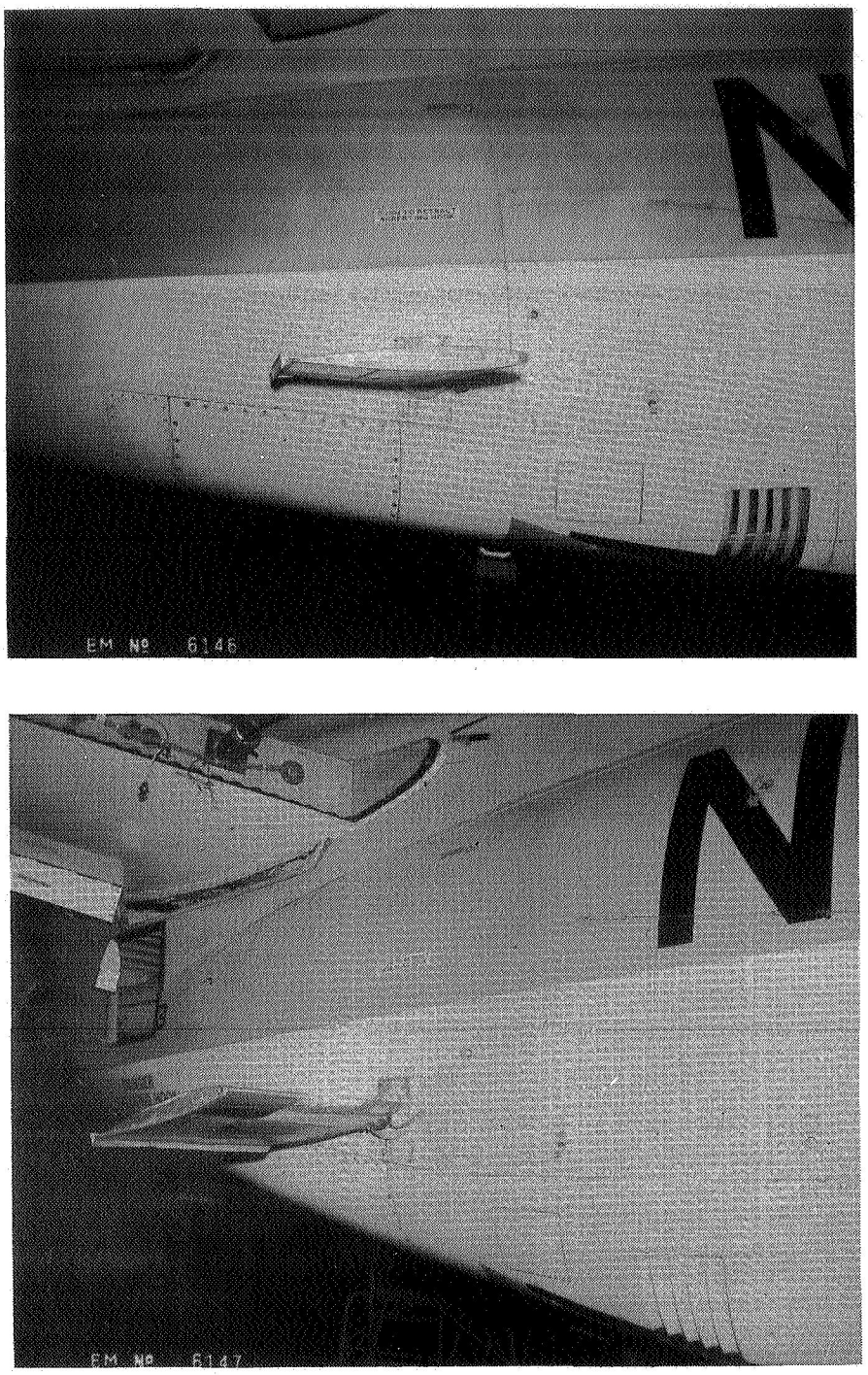

Figure 1. Photographs of flutter vane installed on aft fuselage.

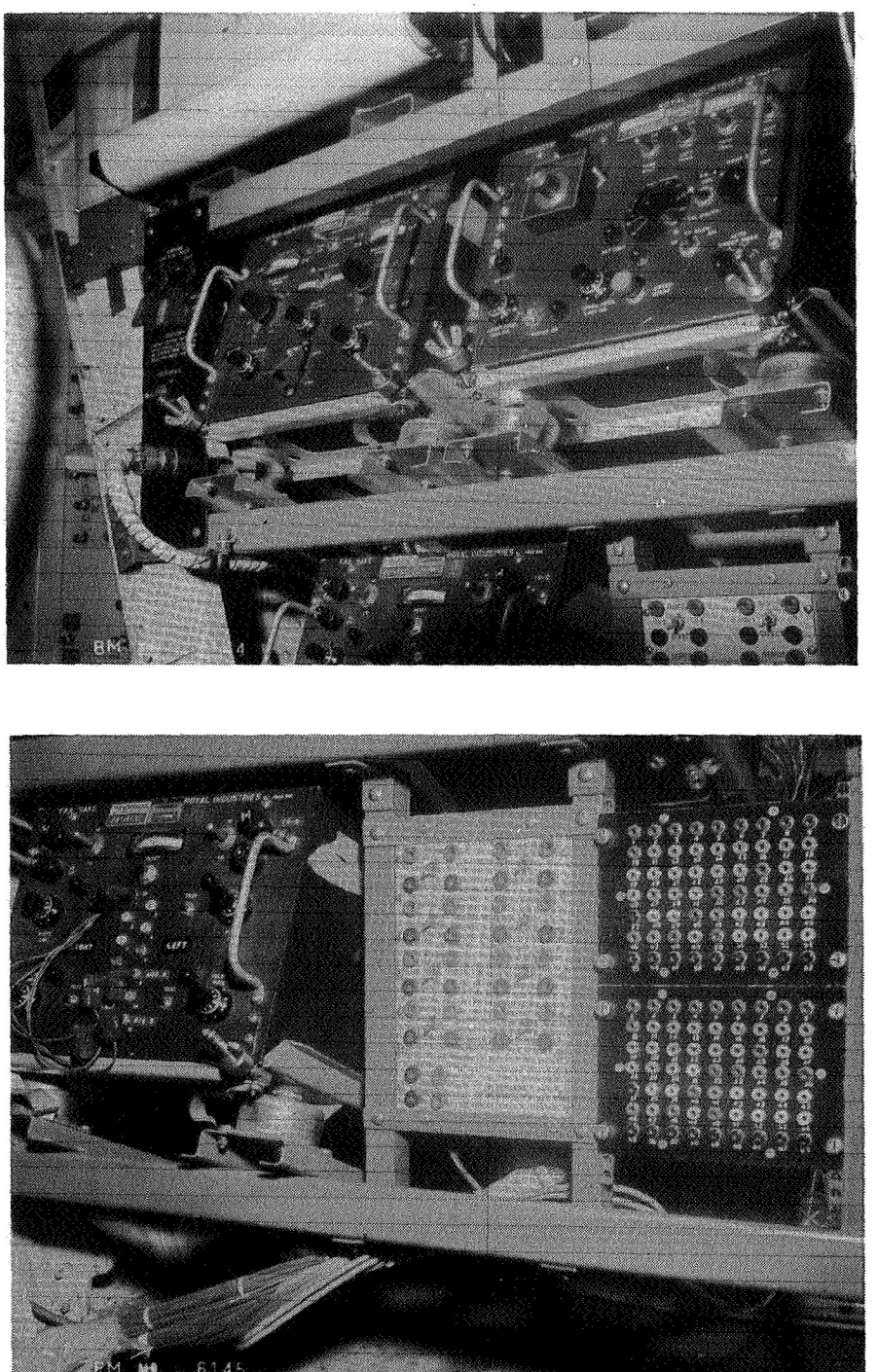

Figure 2. Photographs of the flight flutter test vane excitation control units.

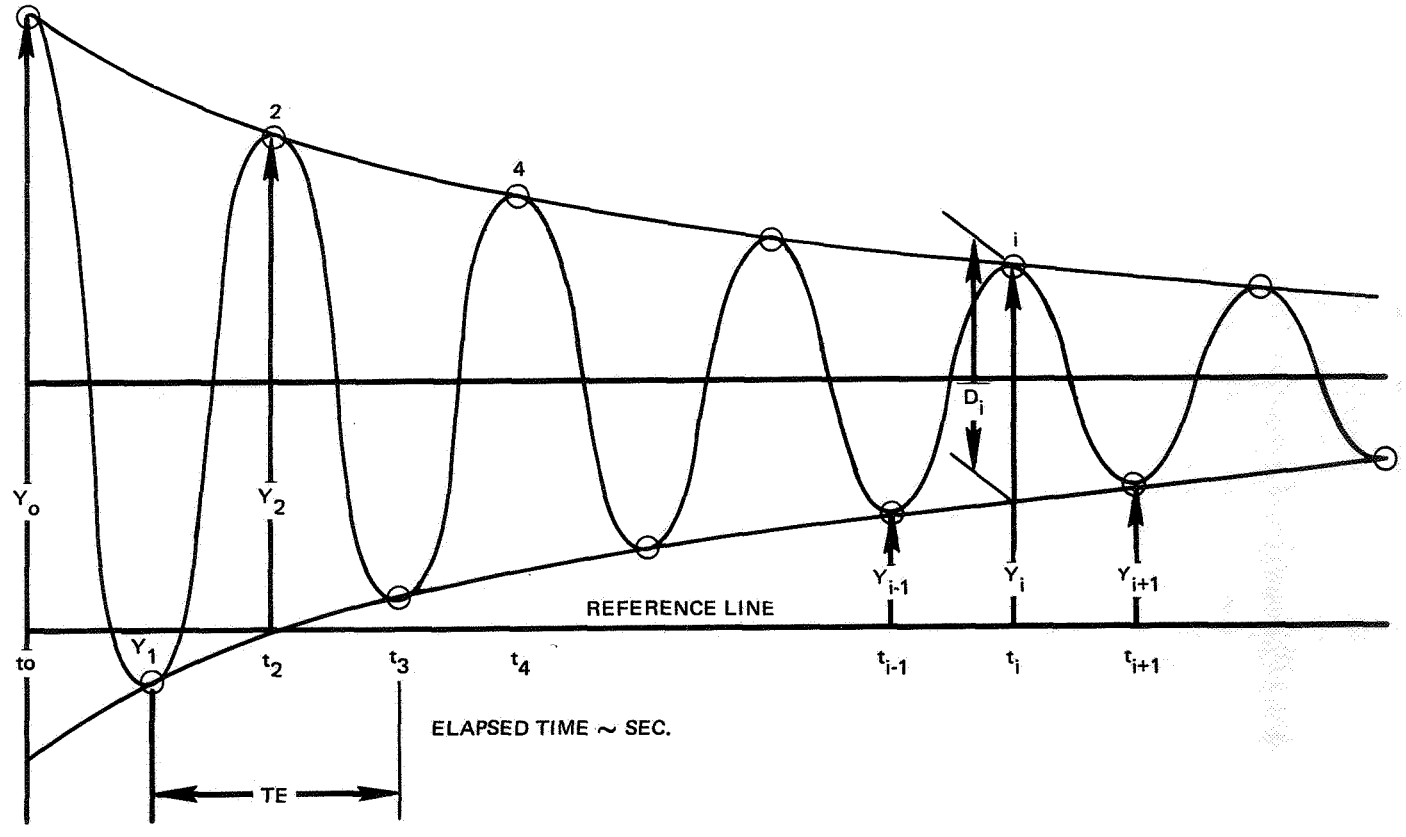

Figure 3. Real-time decay analysis time history assumed.

TEST 71 F 77 RUN 16 DATE 11-18-72 MODE 8

MEASUREMENT A3014 RT STAB T LON AC

START 12 HR 58 MIN 20.287 SEC IAS 369 KIAS HP 15100 FT MACH .7420 EAS 367

NO	TIME	FREQ	PEAK AMPL
0	.158		2352
1	.222	8.3	1731
2	.278	8.5	2335
3	.340	8.1	1747
4	.402	8.8	2360
5	.454	8.9	1722
6	.514	8.5	2331
7	.572	8.5	1800
8	.632	8.5	2232
9	.690	8.3	1865
10	.752	8.3	2209
11	.810	8.5	1892
12	.870	7.7	2155
13	.940	8.6	1921
14	.986	8.3	2154
15	1.060	7.8	1942
16	1.114	9.4	2143
17	1.166	9.4	1945
18	1.220	8.9	2121
19	1.278	8.6	1970
20	1.336	6.7	2086
21	1.428	6.7	1961
22	1.486	10.0	2156
23	1.528	10.0	1937
24	1.586	10.0	2138
25	1.628	6.7	1991
26	1.736	6.7	2087
27	1.778	11.4	1968
28	1.824	10.6	2118
29	1.872	10.4	1953
30	1.920	10.0	2115
31	1.972	10.0	1970
32	2.020	10.0	2105
33	2.072	9.6	1974
34	2.124	10.0	2093
35	2.172	8.9	1995
36	2.236	10.0	2085
37	2.272	11.4	2004
38	2.324	10.0	2083
39	2.372	12.5	2010
40	2.404	16.1	2070

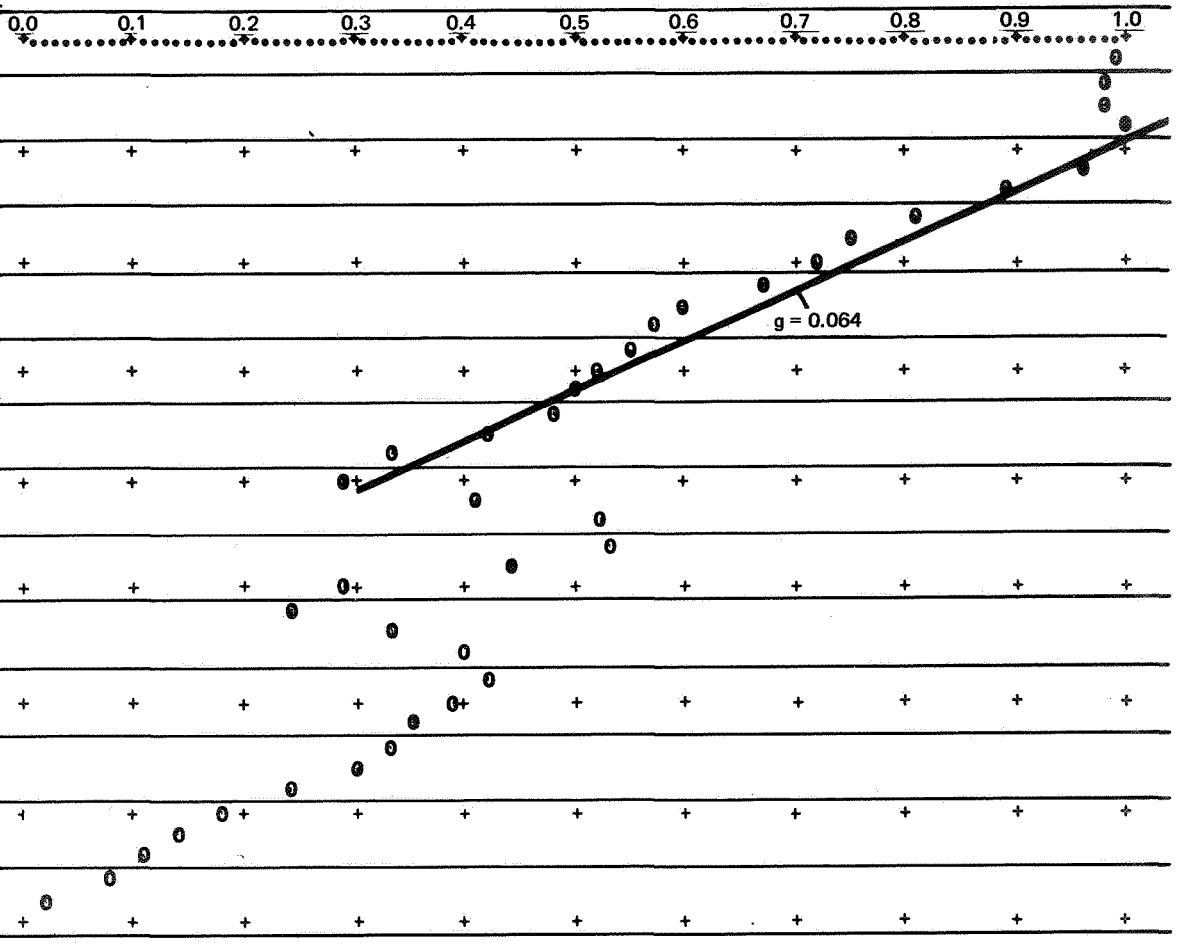

M	S	g	E%	FM
17	4	.064	7.06	8.57

FE 08.0

1 FOOT = 0.3048 METER

LP 12 HP

TEST 71 F 77 RUN 16 DATE 11-18-72

Figure 4. Typical computer printout for real-time decay analysis.

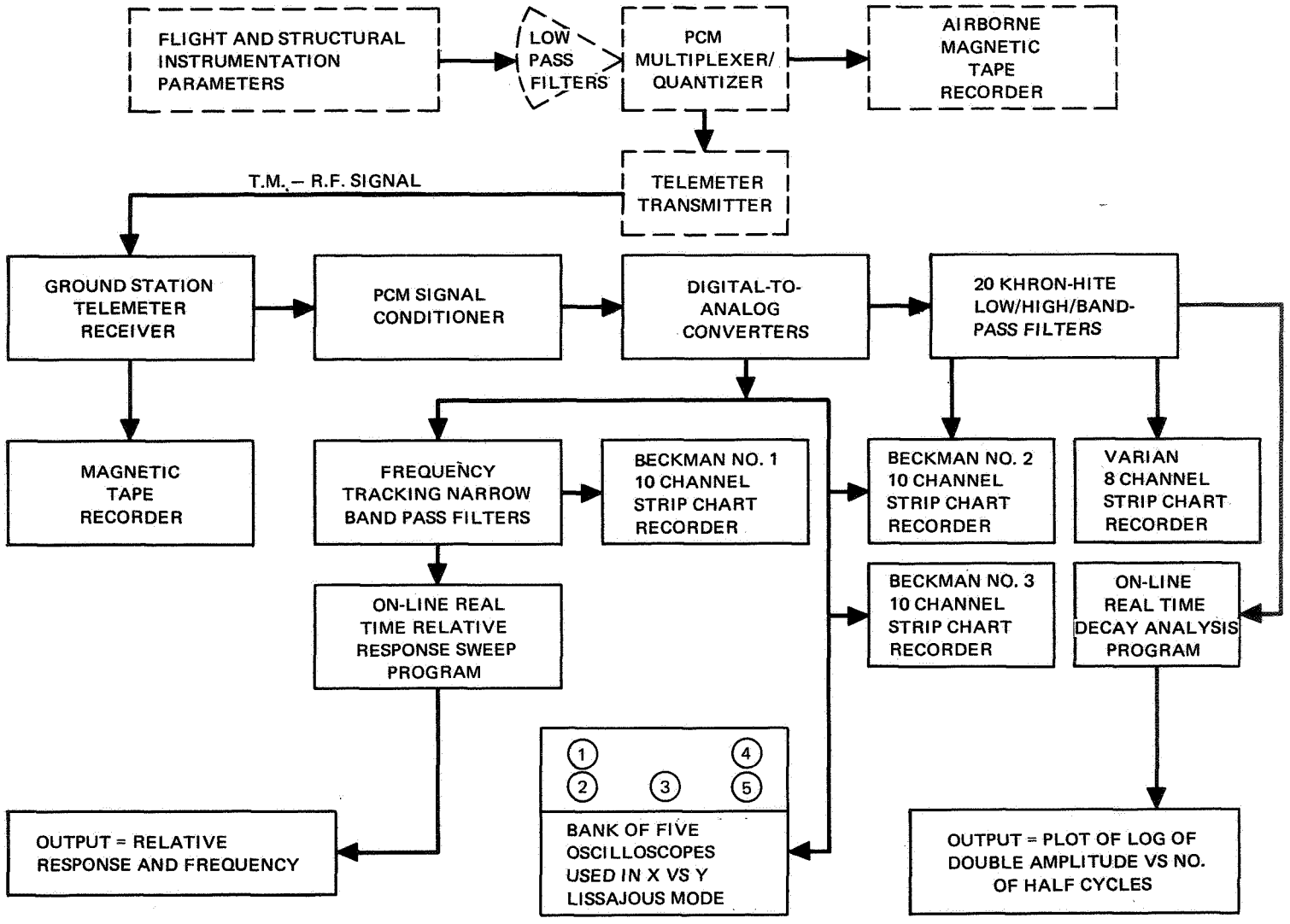

Figure 5. Typical flow chart of a PCM data acquisition/analysis/monitoring system.

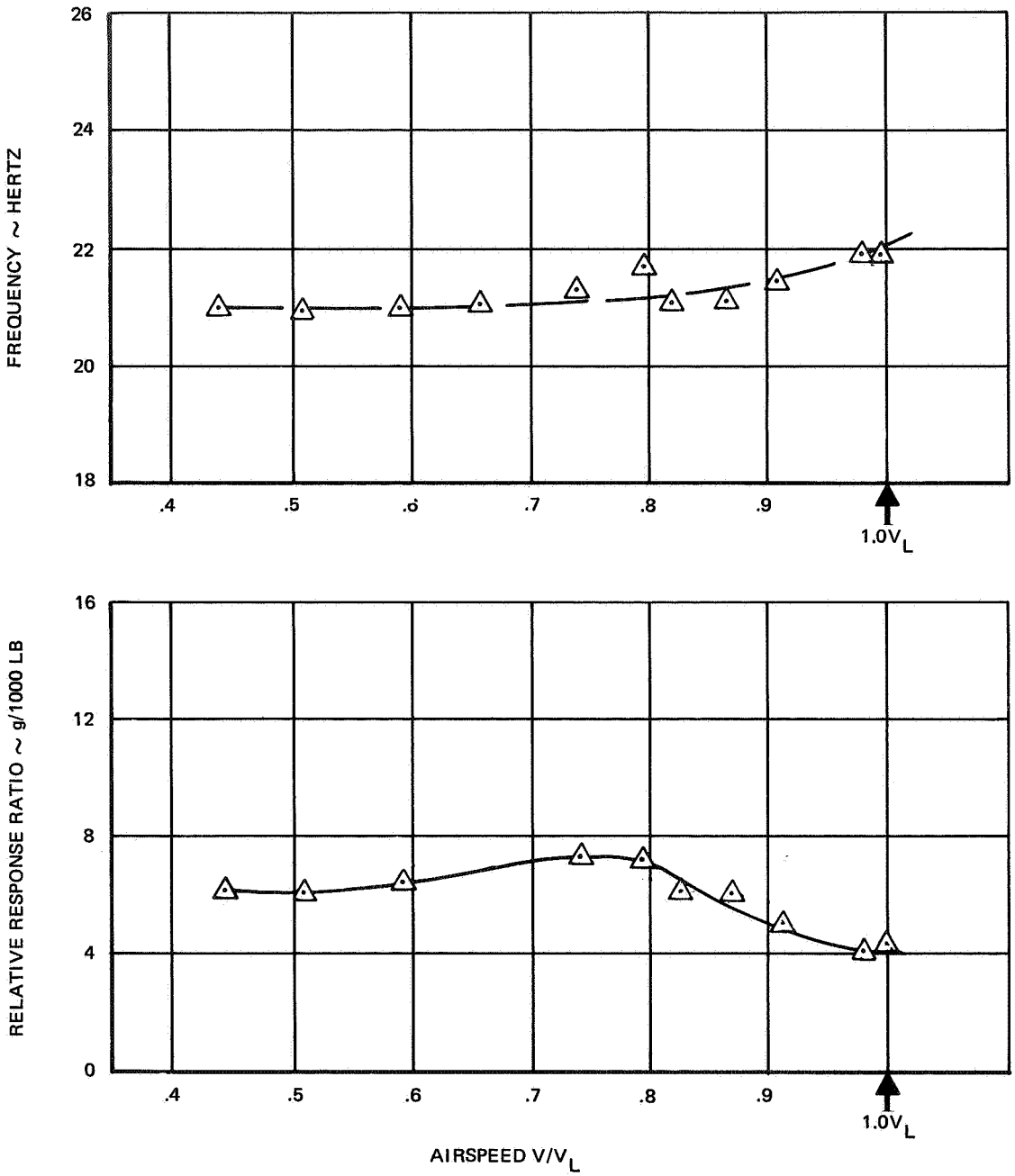

1 POUND = 4.448 NEWTONS

Figure 6. Typical frequency and response ratio vs. equivalent airspeed from real-time response analysis.

TEST 73 F 82 RUN 6 DATE 321 ALT 8K KEAS. 420 M.74

FLIGHT FLUTTER TEST REAL TIME ANALYSIS
WINDOW = 20 EXCITATION WS+
MEASUREMENT A3013 RT STAB T VER AC

	HRS	MIN	SEC	KIAS	HP	MACH	KEAS
START	14	19	19.711	422	6170	.7220	426
STOP	14	19	41.122	424	5370	.7170	429

TIME AT INP PEAK SEC.	INPUT PERIOD SEC.	INPUT FREQ HZ	INPUT AMPLITUDE LB	RESPONSE AMPLITUDE G	RESPONSE RATIO g/LB X 10^{-3}
4.024	0.129	7.73	221.0	.20	.9
6.350	0.115	8.69	214.0	.54	2.5
7.302	0.109	9.14	208.0	.29	1.3
7.518	0.107	9.28	212.0	.51	2.4
7.840	0.105	9.46	211.0	.35	1.6
7.994	0.104	9.55	211.0	.67	3.1
8.204	0.103	9.67	210.0	.25	1.2
11.194	0.084	11.85	203.0	1.46	7.2
11.934	0.079	12.55	208.0	.12	.6
12.170	0.078	12.76	199.0	.62	3.1
12.518	0.075	13.21	200.0	.26	1.3
13.286	0.071	14.08	207.0	.93	4.5
13.672	0.068	14.63	205.0	.37	1.8
14.236	0.064	15.46	205.0	.54	2.6
14.366	0.064	15.54	206.0	.22	1.1
14.746	0.061	16.21	197.0	.33	1.7
18.912	0.035	28.30	224.0	.94	4.2
19.388	0.032	30.61	229.0	1.79	7.8
19.690	0.030	32.60	230.0	1.24	5.4
20.914	0.023	43.47	176.0	3.32	18.8

1 FOOT = 0.3048 METER
1 POUND = 4.448 NEWTONS

Figure 7. Typical computer printout for real-time response analysis.

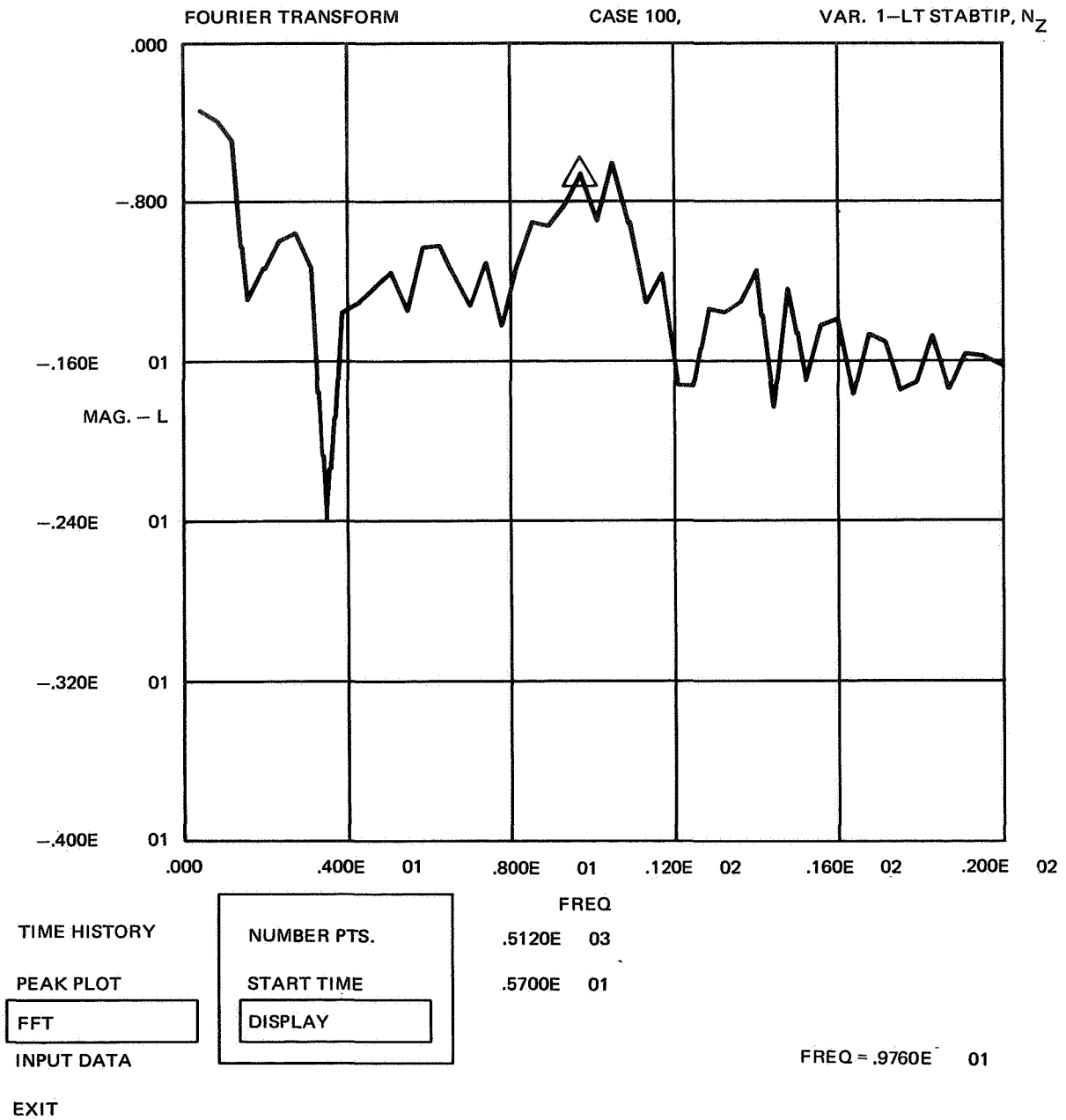

Figure 8. Typical Fourier transform display plot.

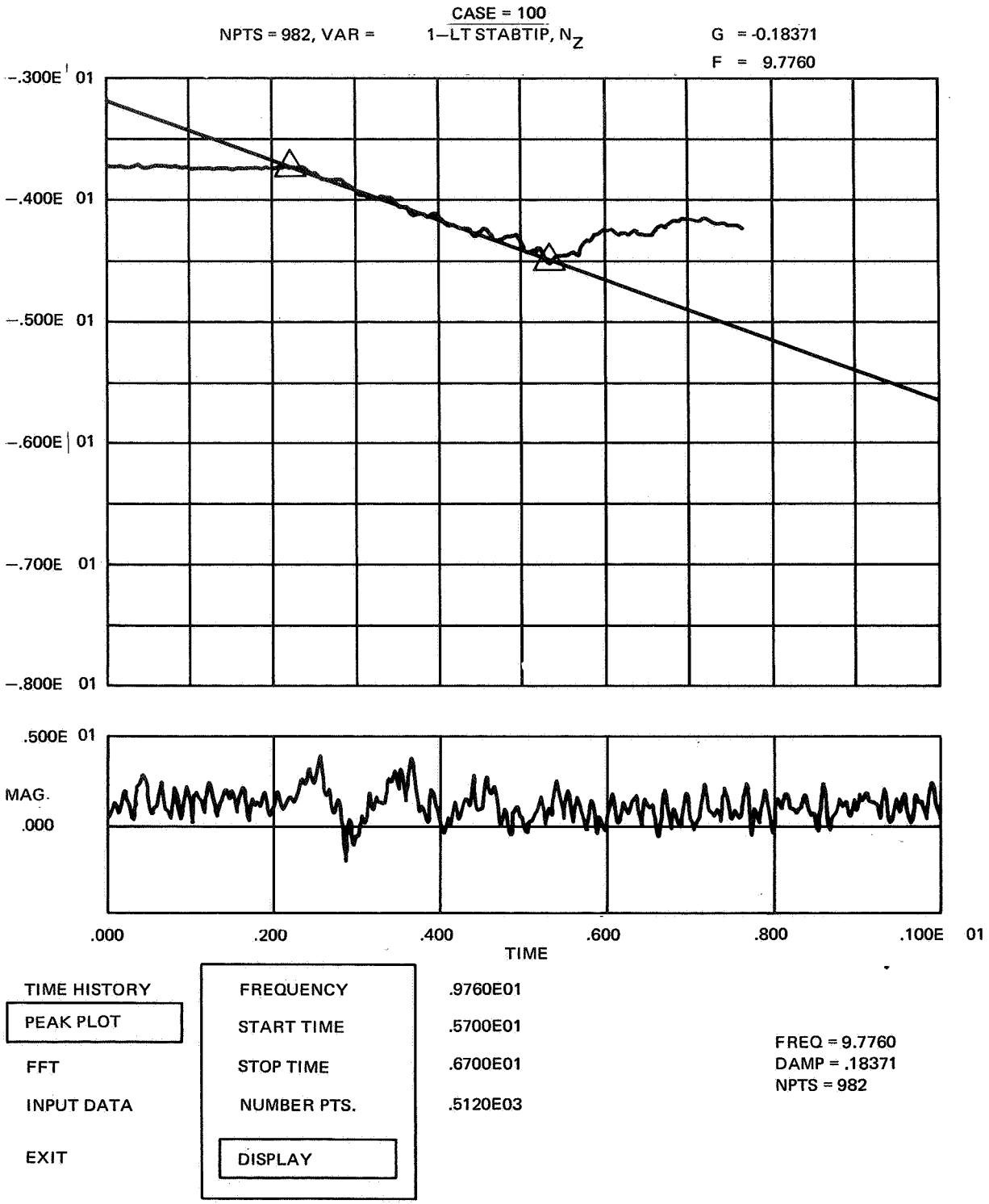

Figure 9. Typical peak plot display.

THE APPLICATION OF RECENT TECHNIQUES IN FLIGHT FLUTTER TESTING

M. A. Abla

Gates Learjet Corporation

SUMMARY

A flight test program is instituted in order to evaluate the applicability of two recent flight flutter testing methods. These methods are the random decrement (randomdec) and autocorrelation techniques. The relative merits of each method are based on analyzing response data obtained by sinusoidal and random excitation. A parameter identification digital program, using least squares approach, is developed to determine the aeroelastic characteristics of a two mode system. To date, the final results of the two types of excitation have been obtained primarily by the randomdec method. Therefore, this paper is limited to discussions and recommendations based on these results.

INTRODUCTION

The Gates Learjet Corporation (GLC), a relative newcomer to the general aviation field, has consistently upgraded the flight flutter testing techniques used during aircraft certification. For instance, sinusoidal excitation of the control surfaces has replaced the pilot impulse technique; application of the shake and stop approach has produced decay responses of better quality; and additional stability criteria, such as the amplitude response and flutter margin (ref. 1), have become possible. Further improvements have recently been made feasible by the acquisition of new computer equipment. It is anticipated that the facility improvement will facilitate implementation of recent data reduction techniques resulting in reduced program costs and time delays.

A survey of the available literature was made in order to classify the various approaches which have been used or proposed. The autocorrelation and randomdec methods showed the greatest promise for possible implementation. As a result, a program was initiated to investigate the relative merits of these two methods. This comparative investigation was to be based on actual random and sinusoidal flight response data obtained on a Learjet Model 25; the ultimate objective being to recommend a particular technique for use in future flight flutter testings.

Most of the analysis has been done using the randomdec approach. Therefore, the major portion of this paper is devoted to discussions, evaluations, and recommendations based on these results. This paper presents these discussions along with the problems encountered.

PROGRAM DESCRIPTION

This section of the paper presents an overall description of the flight test program, computer program, and data reduction procedure.

Flight Test Program

Flight testing was planned with two objectives in mind. The first objective was to obtain actual flight test data for this program. The second objective was to gain insight regarding the relative merits of sinusoidal excitation versus random atmospheric turbulence.

The test airplane was a Learjet Model 25B (figure 1). Briefly, this model is a small, high performance business jet with a speed envelope of 350 knots and Mach .86. Main exterior features include a T-tail, two jet engines installed on the aft fuselage, and two large fuel tanks permanently mounted on the wing tips.

For test purposes, the airplane was fitted with two accelerometers on each tip tank and a potentiometer on each aileron, calibrated to measure aileron position. Aileron sinusoidal excitation was provided by input of a voltage signal of variable frequency into the autopilot roll servos.

An airborne recording system was used to record structural response data. Accelerometer outputs were processed through a GLC 1250 signal conditioner, converted to pulse duration modulation with a Vector 527 encoder, and recorded on magnetic tape by a Honeywell 5600 tape recorder.

The flight test procedure consisted of recording response data for three types of excitation. At each test speed, the plan called for obtaining two-minute recordings of random response data due to atmospheric turbulence, sinusoidal response data for a frequency range of 1.5 to 10 cycles per second and transient response data due to aileron pulses by the pilot. The test speeds ranged from 250 to 350 knots at an altitude of 4.57 km (15,000 ft) with full fuel in the wing and tip tanks.

Computer Program

This section describes briefly the computer program developed in order to analyze response data from a single channel transducer. The computer system (figure 2) is a Varian 620L with accessories such as ASR-33 Teletype, Tektronix 4010 Cathode Ray Tube (CRT), Pertec 6X40 Tape Drive and Statos 31 Printer/Plotter. The program includes subroutines capable of generating three kinds of randomdec signatures and a system identification parameter routine using a least squares approach.

The randomdec methods are based on Cole's and Houbolt's techniques described in refs. 2 and 3, respectively. These methods are as follows:

Option 1: Cole's approach of triggering each time the response crosses a preselected level, regardless of the sign of the slope (figure 3a).

Option 2: Cole's approach of triggering each time the response crosses zero with a positive slope (figure 3b).

Option 3: Houbolt's approach of triggering each time the response crosses zero with a positive slope, and triggering and inverting each time the response crosses with a negative slope (figure 3c).

The least squares approach follows the technique given in ref. 4. The program is capable of deducing the aeroelastic properties of both a one- and two-degree-of-freedom system, buried in a randomdec signature or an autocorrelation function. The latter is not a part of the computer program, and is obtained using an autocorrelation analyzer.

Data Reduction Procedure

The data reduction procedure was established based on both an extensive checkout of the program and the guidelines suggested by Chang (ref. 5). The data used for the checkout was obtained from a typical flight flutter test having two closely spaced modes.

Initially, the engineer monitors the response data displayed on the CRT, and then exercises an option to use all or part of the time history record. The next step is to choose one of the three randomdec options and to initiate the analysis using the selected response data. At the same time the randomdec averaging process is progressing, the program is conveniently displaying the signature generation on the CRT. Once convergence is achieved, the user may discontinue the averaging process and then proceed to curve fit a preselected length of the randomdec signature.

The proper signature length to be curve fitted is usually chosen based on a detailed analysis of the data obtained at the initial test speed. The recommended procedure is to curve fit different segments of the converged randomdec signature, and to plot damping and frequency values of the simulated modes versus signature length. Based on the constant behavior of these parameters and on a computed normalized standard deviation of the curve fit, the engineer can adequately select a signature length which assures him of reliable results.

To use this program, the engineer is required to input initial estimates of the unknown parameters to be determined. These parameters are frequency, damping ratio, amplitude, phase angle, and zero offset. Through an iterative process, the program solves for the final parameters which best match the experimental data. The closer the assumed parameters are to the actual values, the more likely convergence will occur.

RESULTS AND DISCUSSIONS

The procedure outlined in the previous section has been applied to response data obtained at one wing location using sinusoidal and random excitation. The sinusoidal and random results are first discussed separately and then compared with those obtained by the pilot pulse for final evaluation.

In line with the recommended data reduction procedure, the sinusoidal response data obtained at 250 knots was analyzed first in order to select the proper length of the randomdec signature. The randomdec signature was determined using Houbolt's technique (option 3) and was curve fitted for signature lengths of .45, .9, 1.35, 1.8 and 2.2 seconds. The curve fit analysis was performed to deduce the modal properties of the first and second wing antisymmetric modes. The results are shown in figure 4.

A study of figure 4 reveals that the two natural frequencies and the damping coefficient of the second mode are fairly constant with signature length. The damping coefficient of the first mode, on the other hand, shows inconsistent behavior at first, but then tends to stabilize for signature lengths between 1.6 and 2.2 seconds. Results from a similar analysis at 350 knots tend to confirm these observations (figure 5). Consequently, a signature length of 1.8 was selected.

The above analysis was repeated at 250 knots using Cole's zero crossing method (figure 6). This figure indicates that both options 2 and 3 yield roughly equivalent values.

Having established the proper signature, a complete analysis was conducted on the sinusoidal response data obtained at each test speed. Figure 7 shows the results of the analysis at 250 knots using option 3. As shown, figure 7a is the measured response due to sinusoidal aileron oscillation and figure 7b shows the converged randomdec signature. Figure 7c is a plot of the selected length of this signature (symbolized by X) and of the simulated signature shown as a solid line. The SD in figure 7c indicates the percent of the normalized standard deviation. This parameter is a measure of how well the theoretical curve fits the experimental data. The curves presented in figures 7d and 7e are the simulated decay responses of the two modes extracted by this analysis. The results of a similar analysis at 350 knots are shown in figure 8.

Some difficulties, due to flight testing problems, were experienced in the analysis of the random response data. Lack of atmospheric turbulence during this flight test necessitated a long search for an area with adequate turbulence, and as a result, this part of the test was conducted under very rough air conditions. Thus, the desired two minutes of random response records were difficult to obtain. The flight records obtained were so short that they were almost inadequate for the purpose of this study. However, in spite of these problems, an attempt was made to analyze the longest response record. This record consisted of 15 seconds of data at 350 knots.

Figure 9 presents the results of this analysis. Convergence of the randomdec was never achieved. As shown, only the second mode was predicted. All attempts to deduce the first mode failed. This was possibly due to the predominance of the second mode, as might be seen in the random response data (figure 9a). The natural frequency predicted seems to be reasonable but the damping is on the low side. In any case, the poor quality of the signal analysis, as indicated by the poor curve fit and the high SD (figure 9c), needs to be improved before any confidence is placed in the results. Such improvement might be achieved by incorporating a band-pass filter in the system, as described in reference 6.

As a final check on the results determined by the randomdec method, the 350 knot transient response data obtained using pilot pulse was analyzed. The method of analysis was the peak amplitude method. Basically, an envelope of the peaks and troughs of the free decay was sketched. The height between the envelope lines was then measured at each peak or trough. The logarithm of the height was plotted against the number of the wave (figure 10) and the best straight line was then drawn through the first part of the curve. The slope of this line was used to determine the damping ratio.

The results obtained at 350 knots by the peak amplitude method and the randomdec technique, using the random and sinusoidal response data, are summarized in Table 1. Also, the frequencies obtained by ground vibration testing are included in this table. A review of this information reveals that all methods compare well on frequencies. The randomdec method, using sinusoidal excitation, gives damping values for the second mode that agree well with those obtained from the peak amplitude analysis. With regard to the first mode, only the randomdec with sinusoidal excitation yielded damping values. However, on the basis of the small SD parameters and the reasonable results of the second mode, one cannot help but assume that the results obtained by the randomdec method, using sinusoidal excitation, are correct.

This same conclusion cannot be drawn from the results of the randomdec using random excitation. This is due to the fact that the randomdec signature had never converged nor was a good curve fit ever obtained.

CONCLUSIONS

The following conclusions can be stated on the basis of the discussions and results presented in this paper.

1. The application of the randomdec method using sinusoidal excitation appears to be a reasonable technique for use in flight flutter testing.

2. Although air turbulence is present in isolation, the problem of finding it during a flight flutter test makes its feasibility, as a source of excitation, questionable.

3. The use of the randomdec method using random excitation might be improved by utilizing a band-pass filter.

4. A least squares curve fit routine seems to be an efficient and accurate method for determining modal properties of a two mode system.

REFERENCES

1. Zimmerman, N.H.: Weissenburger, J.T.: Prediction of Flutter Onset Speed Based on Flight Testing at Subcritical Speeds. Journal of Aircraft, July - August 1964.

2. Cole, H.A., Jr.: On-line Failure Detection and Damping Measurements of Aerospace Structures by Random Decrement Signatures. NASA CR-2205, March 1973.

3. Houbolt, J.C.: Subcritical Flutter Testing and System Identification. NASA CR-132480, August 1974.

4. Wilcox, Philip R. and Crawford, William L.: A Least Squares Method for Reduction of Free Oscillation Data. NASA TN D-4503, 1968.

5. Chang, C.S.: Study of Dynamic Characteristics of Aeroelastic Systems Utilizing Randomdec Signatures. NASA CR-132563, 1975.

6. Brignac, W.J.; Ness, H.B.; Smith, L.M.: The Random Decrement Technique Applied to the YF-16 Flight Flutter Tests. AIAA Paper No. 75-776, presented at the AIAA/ASME/SAE 16th Structures, Structural Dynamics, and Materials Conference, Denver, Colorado, May 1975.

VELOCITY-KNOTS	METHOD	RESPONSE DATA	FREQUENCY--HZ		DAMPING RATIO	
			MODE 1	MODE 2	MODE 1	MODE 2
0	GROUND VIBRATION TEST	CO-QUAD	5.7	6.56	-	-
350	PEAK AMPLITUDE	FREE DECAY	-	6.34	-	.047
	RANDOMDEC	SINUSOIDAL	5.3	6.27	.037	.0488
	RANDOMDEC	RANDOM	-	6.2	-	.034

Table 1 Comparison of Results at 350 Knots

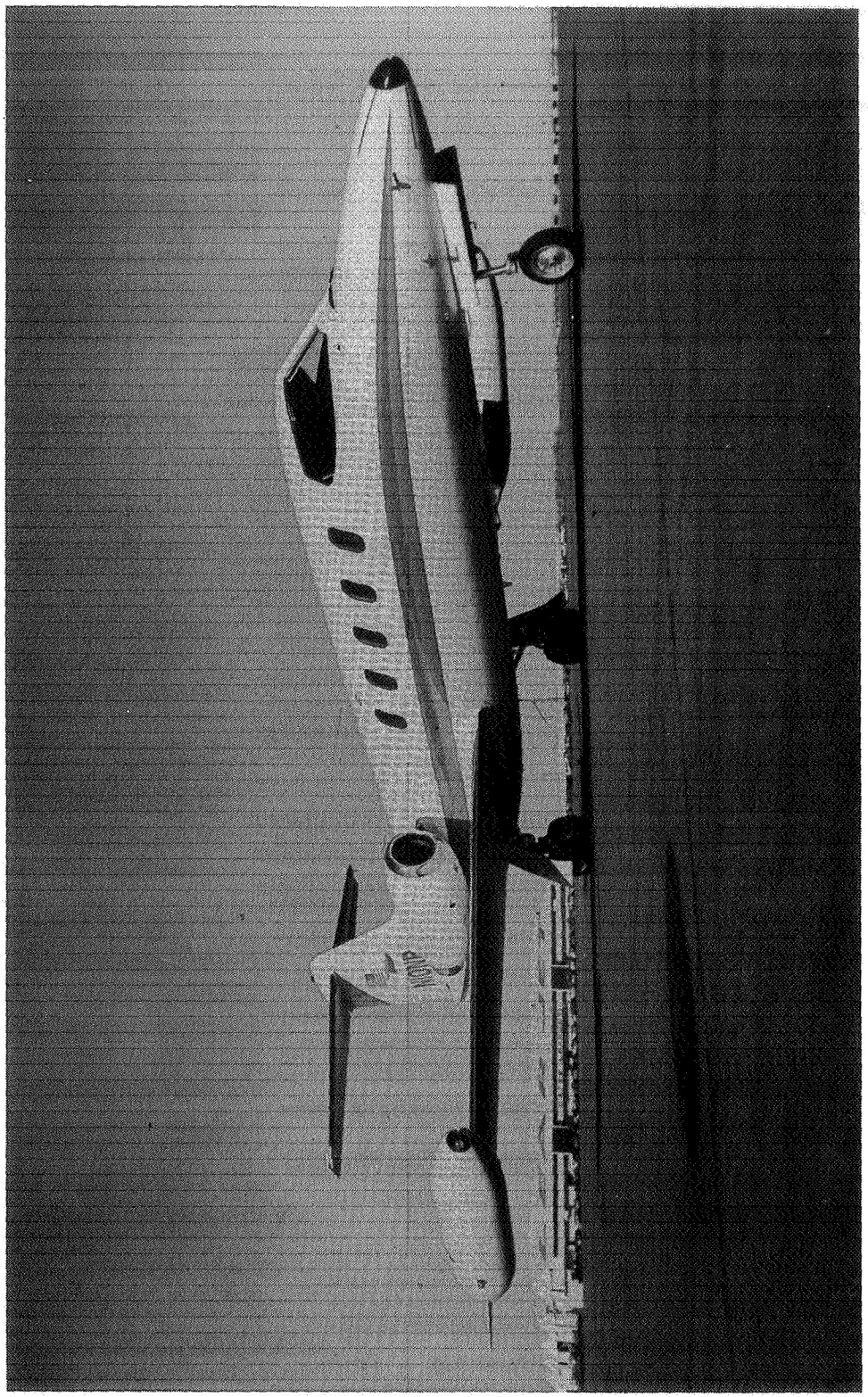

Figure 1.- Learjet model 25B.

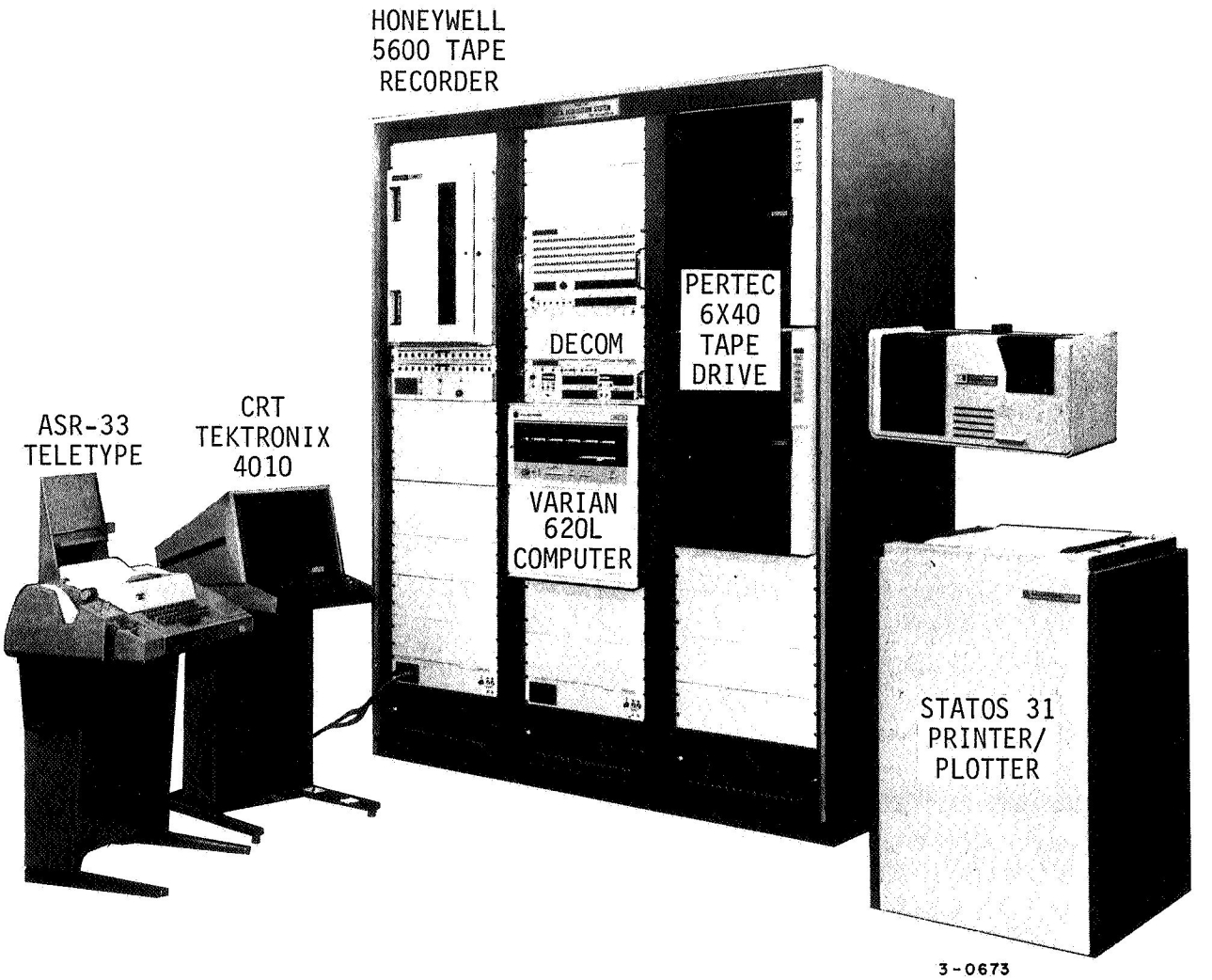

Figure 2.- Varian 620L computer system.

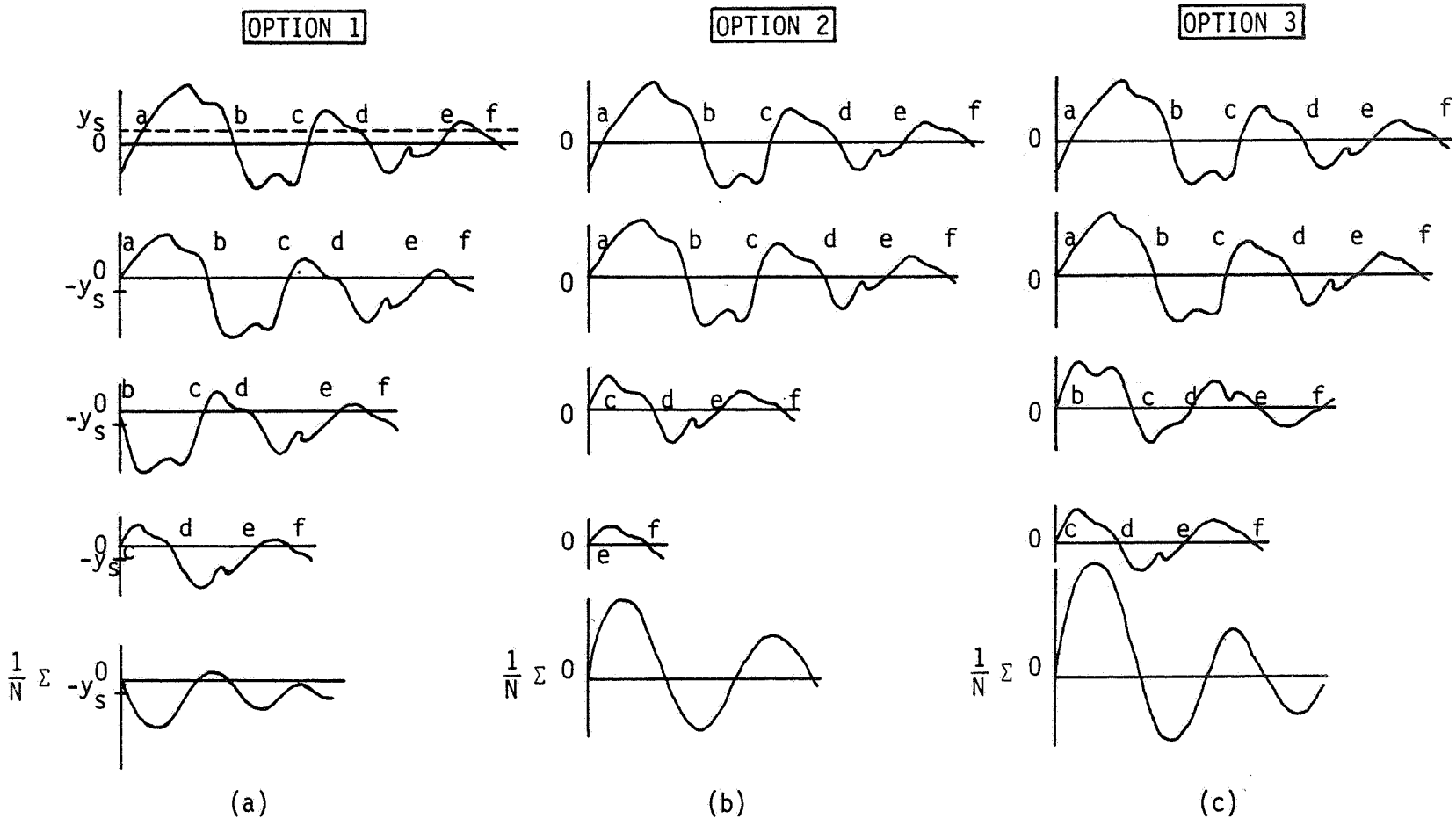

Figure 3.- Randomdec methods.

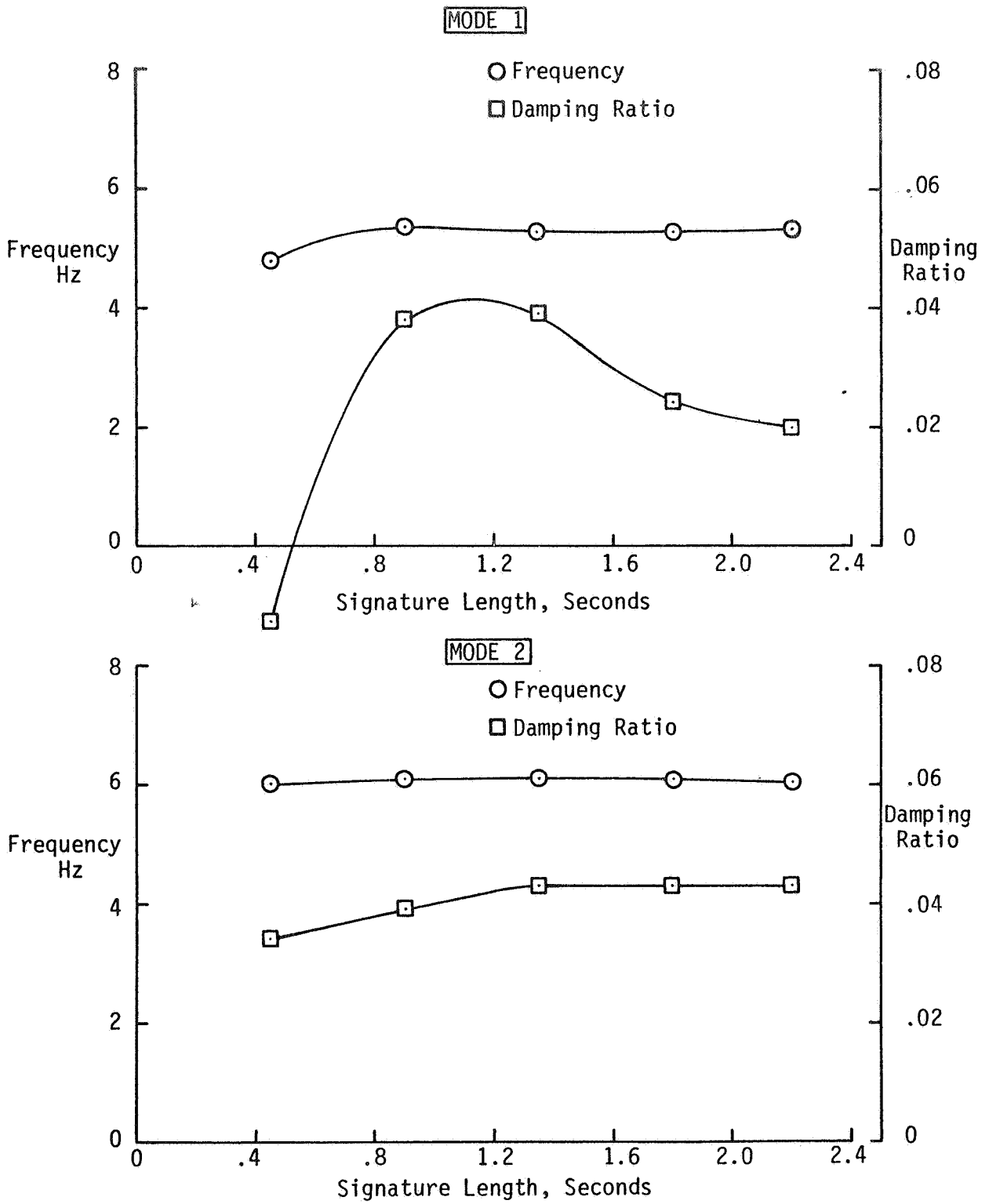

Figure 4.- Modal characteristics versus signature length using sinusoidal excitation at 250 knots.

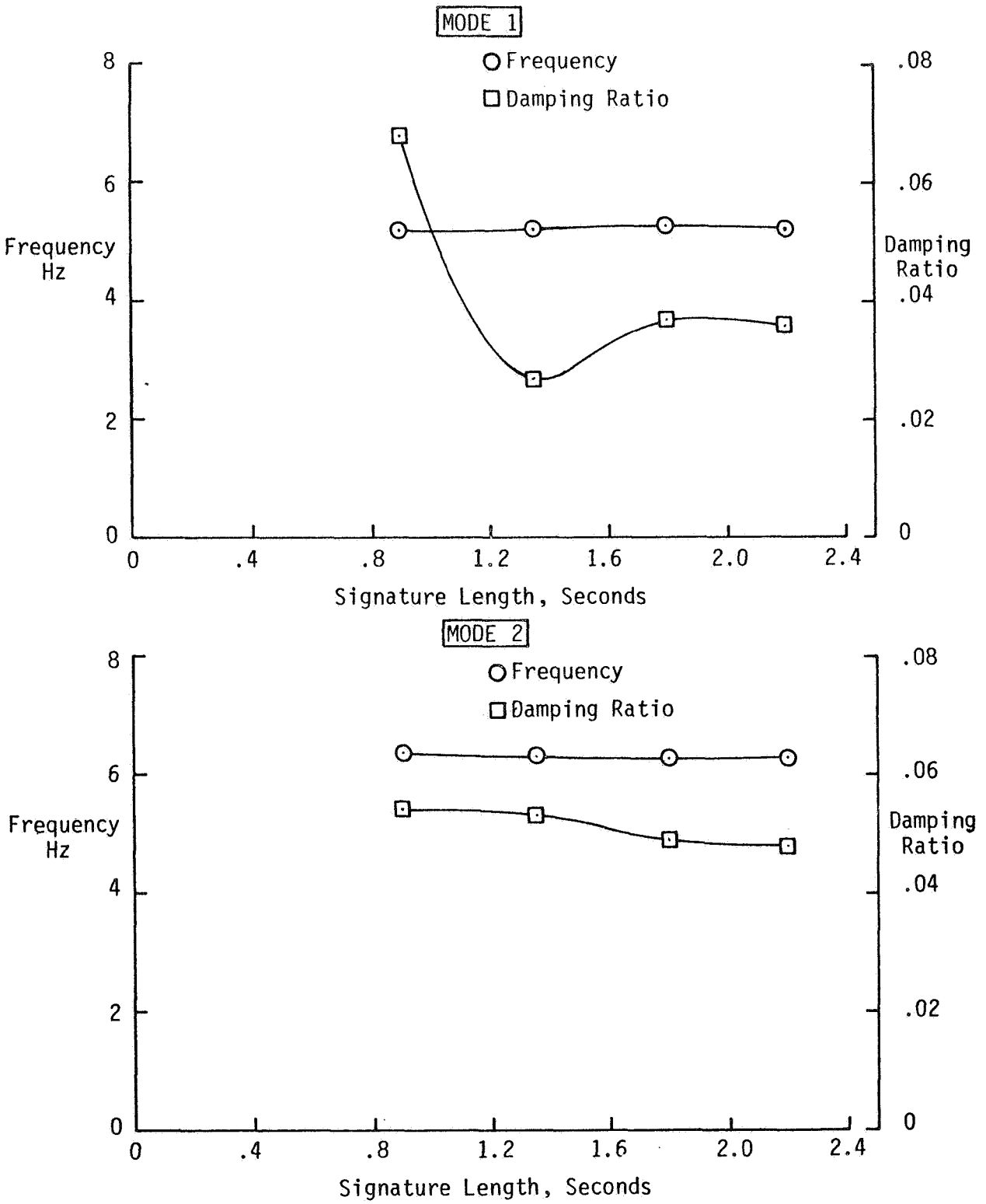

Figure 5.- Modal characteristics versus signature length using sinusoidal excitation at 350 knots.

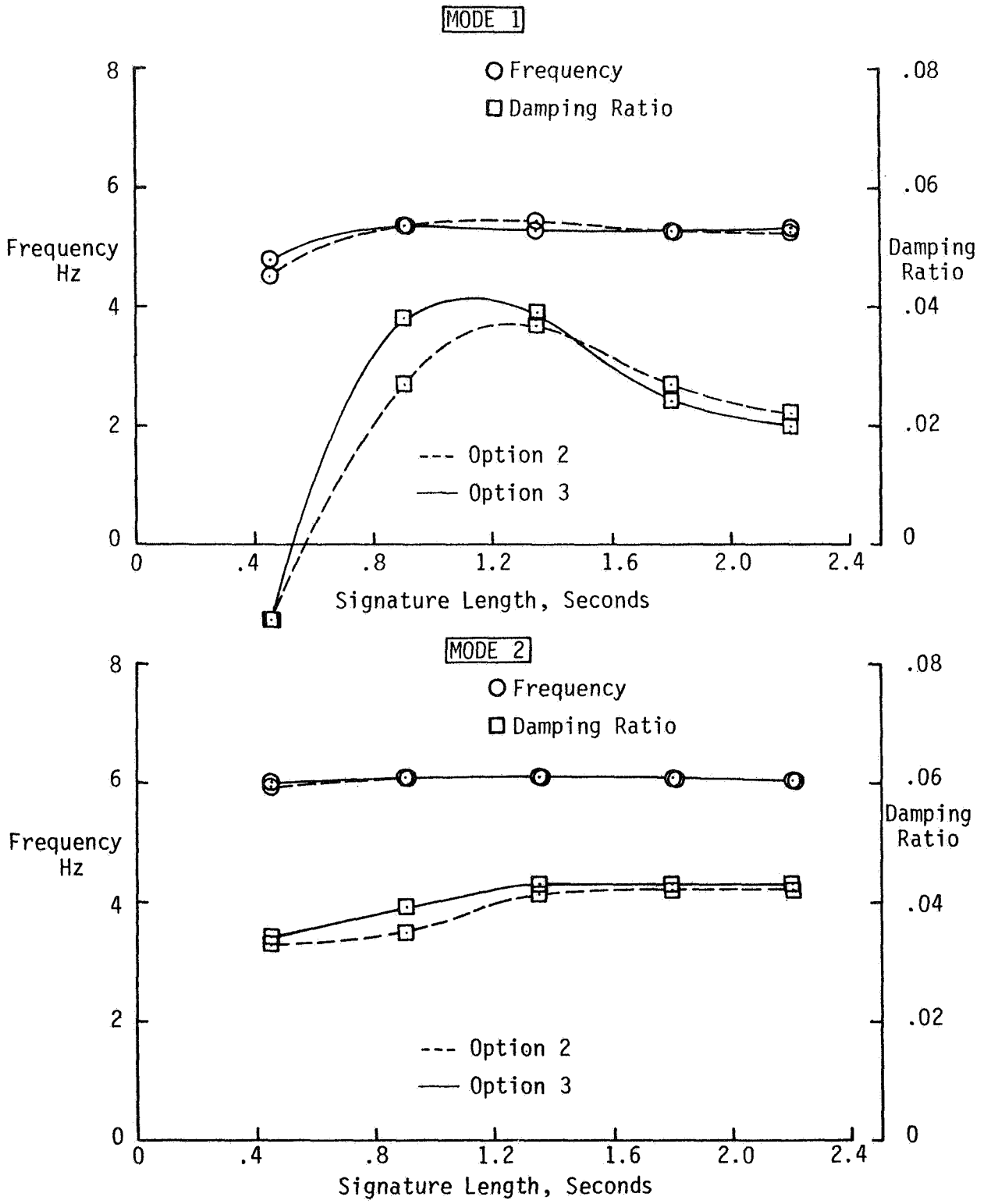

Figure 6.- Randomdec analysis using options 2 and 3 at 250 knots.

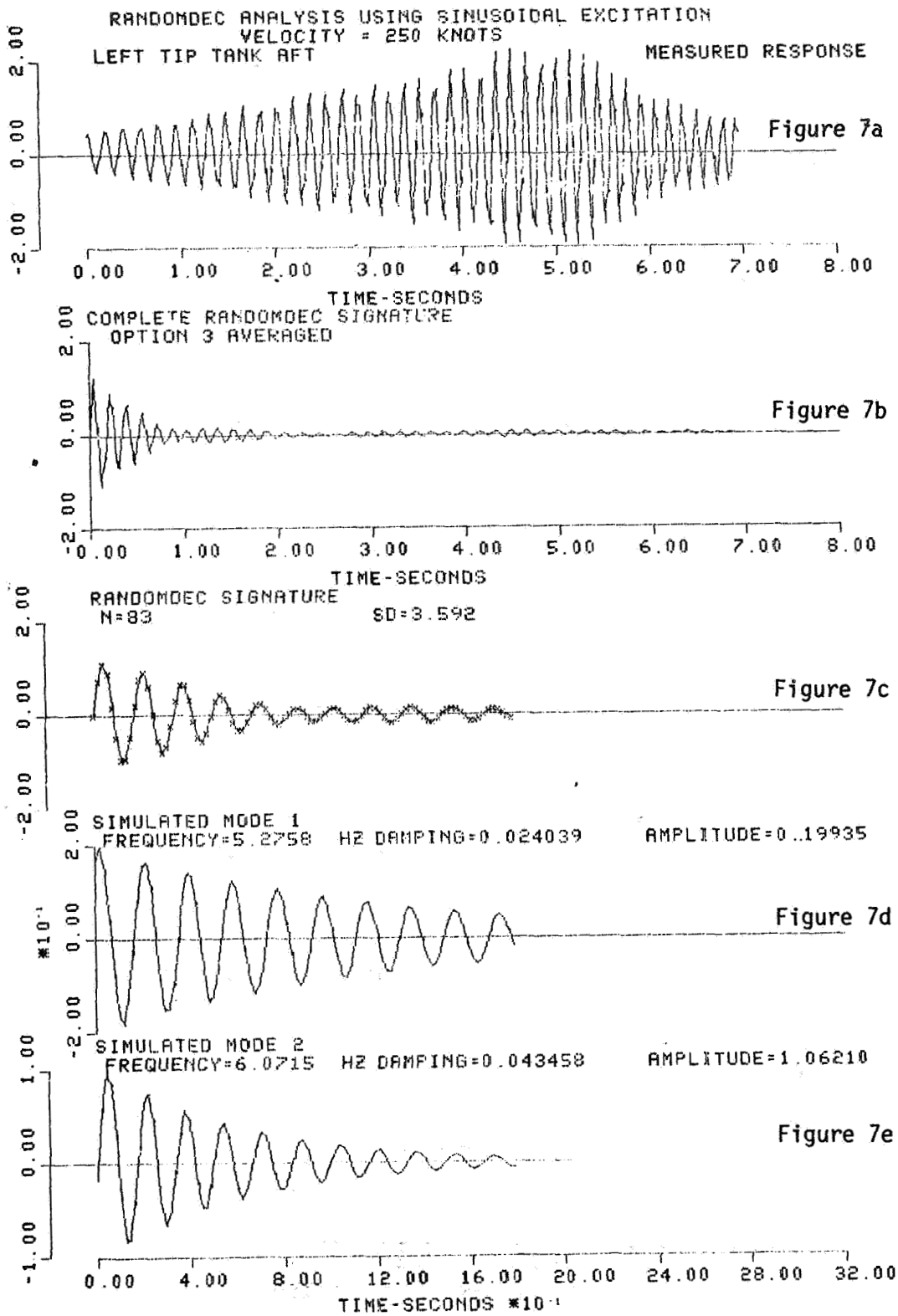

Figure 7.- Randomdec analysis using sinusoidal excitation at 250 knots.

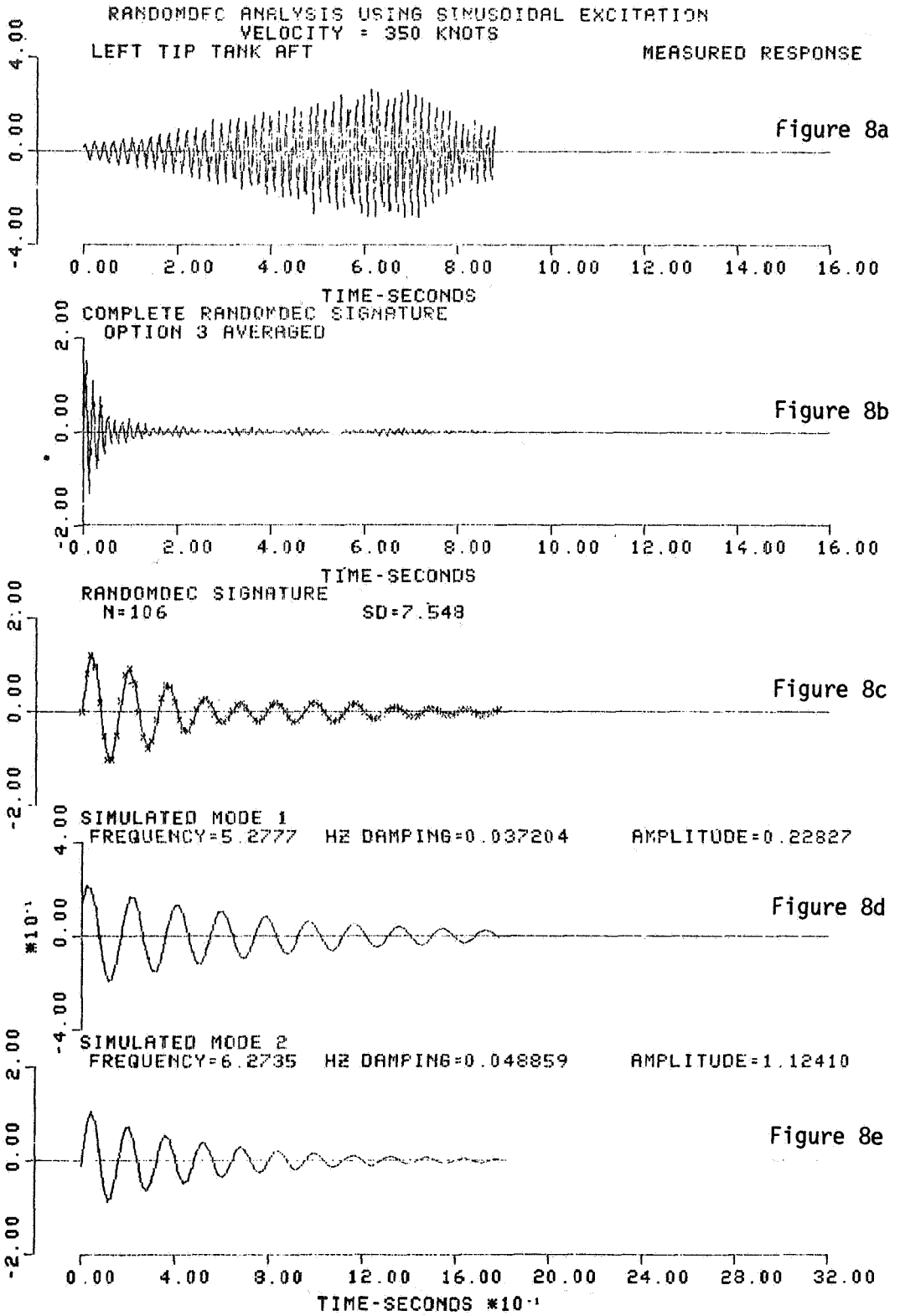

Figure 8a

Figure 8b

Figure 8c

Figure 8d

Figure 8e

Figure 8.- Randomdec analysis using sinusoidal excitation at 350 knots.

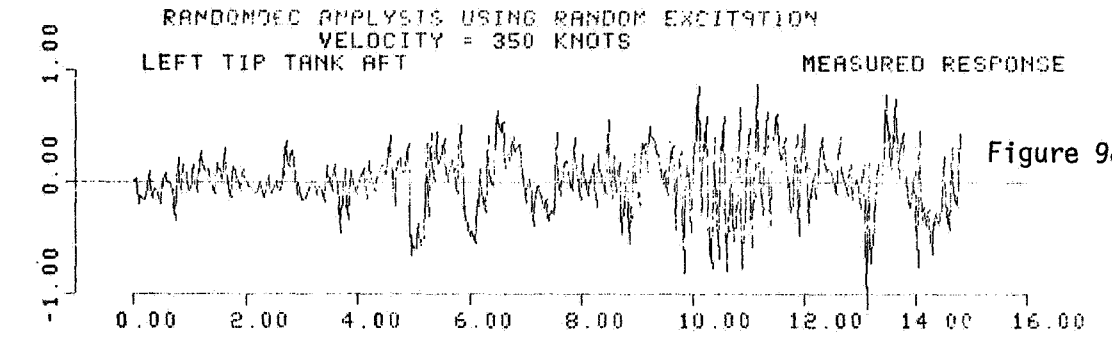

Figure 9a

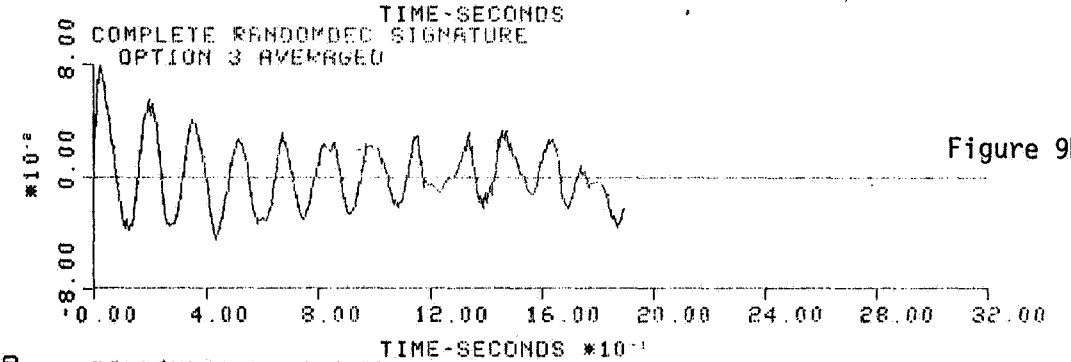

Figure 9b

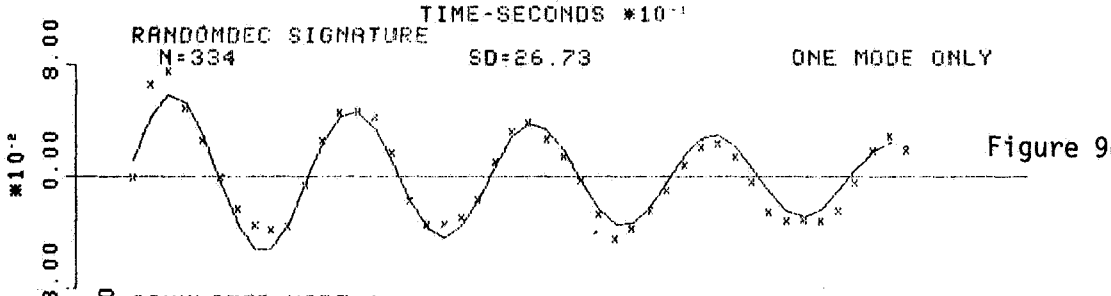

Figure 9c

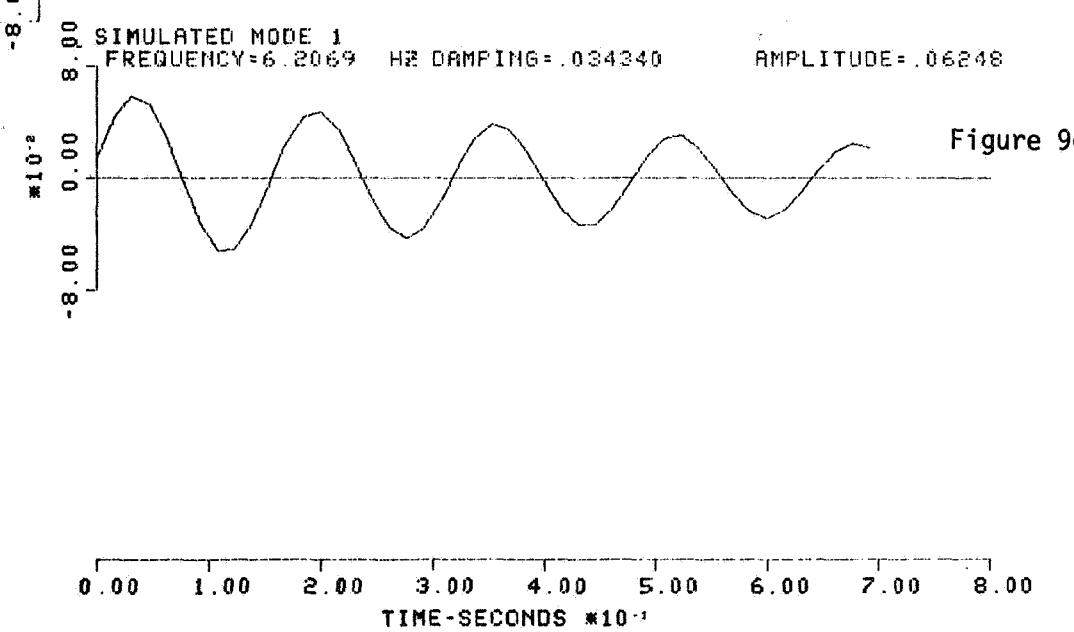

Figure 9d

Figure 9.- Randomdec analysis using random excitation at 350 knots.

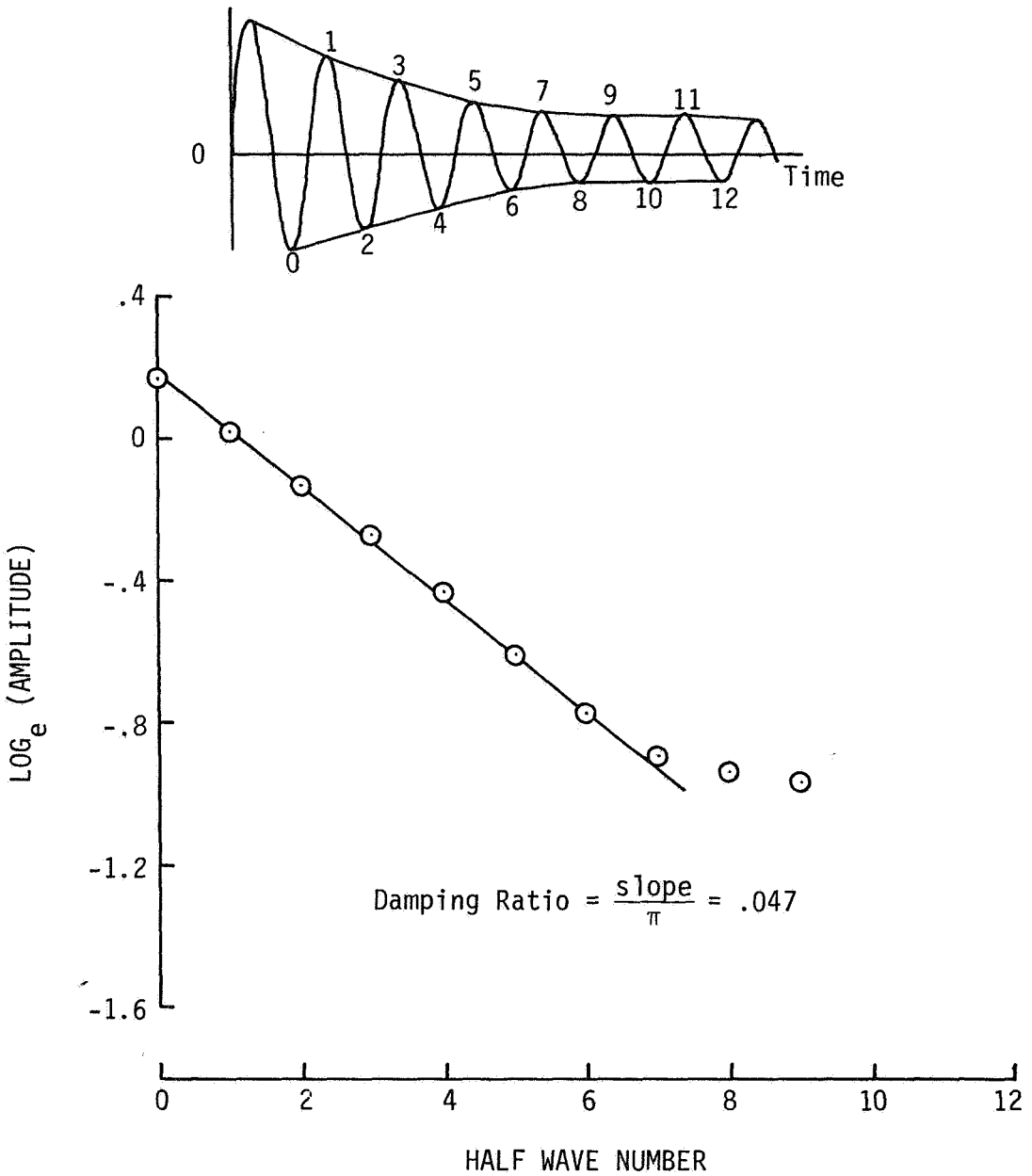

Figure 10.- Logarithmic amplitude at 350 knots.

F-15 FLIGHT FLUTTER TEST PROGRAM

Henry Katz, Francis G. Foppe,
and Daniel T. Grossman

McDonnell Aircraft Company

ABSTRACT

The F-15 flight flutter test program is described. Special emphasis is given to test philosophy, data reduction techniques, and test results. The approach utilized for this program not only provided the data necessary to establish a measure of stability for all important flutter mechanisms at each test point, but also allowed extrapolation of the data to actually define all critical flutter boundaries. Such quantitative information was not only useful to definitively establish the flutter status of the aircraft as it was flown, but also provided a solid foundation for assessing the impact of any future design changes.

INTRODUCTION

With very few exceptions, flight flutter testing has historically been conducted on a rather qualitative basis; that is, the only data obtained were the damping available at the test point being flown, with a possible extrapolation of damping trends of the lower damped modes. There generally was no quantitative indication as to the amount of stability remaining at any given point.

The goal set for the F-15 flight flutter test program was to provide a system which would - accurately, quickly, and with a high degree of visibility - allow extrapolation of the data to actually define critical flutter boundaries, in addition to providing a measure of stability for all the important mechanisms at each test point. This was accomplished by designing the aircraft excitation and instrumentation systems to provide high-quality response data which could be speedily and accurately converted to complete (i.e., concerning all modes of interest) damping and frequency information which - in turn - could be utilized for reliable flutter margin predictions by the methods of Reference 1. The accuracy and reliability of these flight flutter test system data not only permitted the pursuit of a minimum flutter margin design concept (and with it optimum weight - see Reference 2) through inflight verification of actual flutter margins of safety, but also provided a quantitative basis on which to quickly assess the impact of future design changes.

This paper concerns itself primarily with test philosophy, data reduction techniques and systems, and test results. Aircraft systems and test operations are covered in Reference 3.

ABBREVIATIONS AND SYMBOLS

CRT	cathode ray tube
g	structural damping coefficient
H_{pc}	pressure altitude, calibrated
Im	imaginary part of transfer function at frequency ω
KEAS	knots equivalent airspeed
L/H	left-hand side
M	Mach number
NBFM	narrow band frequency modulation
PCM	pulse code modulation
Q	dynamic pressure
Re	real part of transfer function at frequency ω
R/H	right-hand side
T_{AF}	temperature at altitude
T-plot	transmissibility plot
V_E	equivalent airspeed
V_T	true airspeed
μ	ratio of structural mass to aerodynamic mass
ρ_A	density at altitude
ω	frequency
ω_n	natural frequency

APPROACH

The quantitative definition of F-15 flutter boundaries from flight test data was accomplished by means of the Flutter Margin technique of Reference 1. This technique permits reliable prediction of flutter speeds on the basis of subcritical test data. Its application requires knowledge - at every test

point - of damping and frequency of every mode involved in potentially critical flutter mechanisms. This complete damping and frequency information was obtained from a unique data reduction facility operating on the aircraft data provided by the exciter and instrumentation systems described in detail in Reference 3.

The method of Reference 1 assumes that data is obtained at different velocities while maintaining the same aerodynamic center and lift curve slopes. Strictly speaking, it is therefore valid only when Mach number is kept constant. The emphasis in this program was, therefore, to obtain constant Mach number cross sections which could be utilized for extrapolation of the data to projected flutter boundaries. M = 0.80 was selected as one of the primary Mach number cross sections to obtain a high subsonic extrapolation point for reference and for correlation with subsonic analyses and wind tunnel tests. Another primary cross section was taken at M = 1.2, the F-15 sea-level design Mach number. Additional Mach numbers at which cross sections were taken were selected on the basis of analyses, wind tunnel tests, and the early portion of the test program, which was dedicated to determining critical Mach numbers by obtaining test data from 0.73 to 1.5 Mach numbers while maintaining a constant dynamic pressure (442 KEAS). The data obtained at this constant dynamic pressure were then reduced in terms of the Flutter Margin parameter to aid in selecting critical Mach numbers for the various critical flutter mechanisms.

Figure 1 shows Flutter Margin as a function of Mach number for one of the critical flutter mechanisms: antisymmetric boom torsion versus stabilator rotation. Basically, a subsonic and a supersonic level can be observed - with some secondary altitude (or μ) effects. The highest Mach number at which the lower subsonic level occurs is just slightly above M = 0.9. Based on such data, and similar results for other modes, M = .93 and M = 1.1 were selected as additional primary Mach numbers and a cross section with three or more flight test points was taken at these points. Secondary Mach numbers of 0.98, 1.04, and 1.15 (with only two flight test points) were selected to provide intermediate checks at a minimum cost in terms of flights required.

A typical flutter prediction at a critical Mach number is shown in Figure 2. It should be noted that the extrapolation is made on the basis of a parabola through the flight test points and the zero airspeed point. Wind tunnel test data have shown that the actual flutter speed will be offset slightly from the parabolic extrapolation toward a point obtained by a straight-line extrapolation through the inflight test points alone. Thus, when the parabola is convex (curving toward the abcissa), the results will be slightly conservative, and the parabola will be used to establish the flutter boundary. In the case of a concave parabola, the straight-line extrapolation will be more conservative and should therefore receive more consideration.

Although, in its strictest sense, the prediction method is invalid for constant altitude data, secondary extrapolations were made at constant altitudes of 1525 and 10 400 m (5000 and 34 000 ft) by taking advantage of the fact that, once supersonic flow is established, the aerodynamic center and lift curve slope are again quite well behaved. An example of a constant altitude extrapolation is shown in Figure 3.

Figure 4 shows the points at which flight flutter data were taken and also indicates the direction of the extrapolations.

EXCITER SYSTEM

The aircraft exciter system, described in detail in Reference 3, furnishes the known forcing function to which aircraft response can be measured. It has the capability to oscillate either the stabilators or the ailerons. Either set of control surfaces can be excited symmetrically (in-phase) or antisymmetrically (out-of-phase). Excitation can be provided either in the form of sweeps (slowly varying frequency through a given range) or dwells/decays (excitation at a given frequency for a certain short time, followed by an abrupt exciter shut-off).

INSTRUMENTATION SYSTEM

As described in Reference 3, the aircraft instrumentation system consists primarily of strain gages, which provide not only the desired response characteristics but also permit relatively independent measurement of the modes of interest. This is important, since it is desired to separate the response in the various modes, especially when these modes are close to each other in frequency. Figure 5 shows the sensor locations on the aircraft and also denotes the primary degree of freedom to be measured by each.

DATA SYSTEM

The heart of the F-15 flight flutter test system is the data handling system. It reduces the information provided by aircraft instrumentation in response to the forcing function furnished by the aircraft exciter system to several forms useful to the flutter engineer.

The F-15 data system can be divided into two parts:

a. The on-line system, which aids in the assessment of stability at the test point being flown at the time; and

b. The post-flight system, which provides a complete evaluation of all the data available to aid in arriving at damping and Flutter Margin trends so as to establish the flutter safety of the next point(s) to be flown and also to extrapolate to predicted flutter boundaries.

On-Line Data System

This portion of the data system provides real-time information as to the stability of the aircraft at the point(s) being flown. It is schematically represented in Figure 6. As can be seen, it involves a mixture of conventional

displays (strip recorders and Lissajous figures) and less conventional information in the form of digitally computed transmissibility plots.

Strip chart recorders

Thirty-two channels of narrow band frequency modulated (NBFM) data are displayed on four strip chart recorders. These channels present the output of strain gages to describe aircraft response and forcing functions. The channels are arranged so that components of critical flutter mechanisms (for example, boom lateral bending and fin bending) are side-by-side to enable close monitoring for the development of any correlation between these degrees of freedom.

The data displayed on the recorders perform the following functions:

a. Allow observation of any correlation between any two degrees of freedom during acceleration into an unexplored flight regime. Such correlation could indicate the approach to an instability.

b. Permit real-time determination of critical modal frequencies during turbulence excitation.

c. Obtain the damping of modes of interest whenever dwell/decay excitation is utilized.

d. Indicate the frequencies of maximum response during a frequency sweep.

e. Monitor the quality of the forcing function during sweeps.

f. Allow observation of the level of turbulence, to determine if acquisition of excitation response data is feasible.

Lissajous displays

Four Lissajous figures each are displayed on four oscilloscopes. The pairs are chosen to provide maximum information on the stability of potential flutter mechanisms. This is accomplished by "beating" the signals from two gages, e.g. from boom lateral bending and fin bending, against each other. The signal from any of the thirty-two NBFM channels can be selected for either axis of any of the sixteen Lissajous figures. These figures are used to observe the phase and frequency relationship between important modal pairs during acceleration into an unexplored flight regime, and are also used to observe the frequency dependence of amplitude and phase during sweeps.

Transmissibility plots

Transmissibility plots are obtained by normalizing response parameters to a parameter which is a measure of the forcing function, e.g. stabilator hinge moment when the stabilators are oscillated. These plots are computed from digitized aircraft response data and present amplitude and phase information as a function of frequency. Figure 7 shows a typical transmissibility plot.

One real-time transmissibility plot (T-plot) for a selected data channel is displayed on a cathode ray tube (CRT) during a sweep. This plot is used to obtain response information for the critical mode of interest. The information is more accurate than can be obtained from the strip recorders in a real-time environment. A side benefit of the real-time T-plot is the immediate acquisition of corrected flight parameters (equivalent airspeed, Mach number, altitude, etc.), which are also displayed on the CRT.

Hard-copy transmissibility plots for six selected data channels are produced on a Gould plotter within 90 seconds after a sweep. The information from these plots, in conjunction with that already obtained from the real-time T-plot, affords the opportunity to obtain a check on frequency and damping values for most of the modes of interest. The ability to determine resonant frequencies almost immediately permits the selection of accurate dwell frequencies during the flight, thus providing good-quality decay data.

Post Flight Data System

This system involves a complete evaluation of all the data available to arrive at damping and Flutter Margin trends so as to establish the flutter safety of the next test point(s), and also to extrapolate to predicted flutter boundaries. A digital computer is used to extract frequency and damping information by the methods of Reference 4 and to provide the data storage and computational capabilities required for the Flutter Margin calculations and predictions. Figure 8 shows the data flow in this system. As can be seen, there is considerable man/machine interaction.

Extraction of frequency and damping data

After the completion of each test flight, transmissibility plots are generated from the onboard tape for all parameters of interest, nominally 12 per sweep, 6 for each side of the aircraft. Frequency and damping are obtained manually from these transmissibility plots by observing resonant peaks and calculating damping on the basis of bandwidth and/or the slope of the phase shift. This information is combined with frequency and damping data obtained from the dwell/decays and the output generated by the automatic modal extraction technique. (The latter is performed in St. Louis because of the larger computer capacity there.)

In the automatic technique, based on Reference 4, the resonant frequencies are considered to occur when the derivatives of the Argand arc-length reaches a maximum with respect to frequency. These maxima are extracted using a least-squares straight-line-slope testing technique. Plots of the derivative are provided to the flutter engineer by the computer (see Figure 9). It was found that a Hanning smoothing technique, applied to both the transfer function and to the derivative data, substantially reduces the error induced by experimental scatter (turbulence, etc.).

To automatically obtain the damping values from the transfer function, the multi-degree of freedom function is initially separated into single degree of freedom segments. The bandwidth of these segments depends on the frequency

separation of the modes and is not the same for all modes. Damping values are extracted for each of the segments by first fitting a least-squares circle to the transfer function data in the complex plane. Damping values are then calculated for each data point used to define the circle, utilizing the equation $g = -\frac{Im}{Re}\frac{\omega_n^2 - \omega^2}{\omega_n \omega}$. The damping values obtained on the basis of the points farthest from the natural frequency are considered to be the most accurate, since they are least sensitive to any error in the frequency term. Therefore, emphasis is placed on the four points which are farthest from the resonant peak (two on each side). The four damping values are presented, along with the average, in a table included with the derivative plot, Figure 9.

Generally, the automatically extracted modes will fall into three categories: good modes, other physical modes, and fictitious modes. In a "good" mode the four damping values will be very close to each other and the same resonant frequency will be shown in the tabulation, the derivative plot and the original transmissibility plot. For example, on Figure 9 the 18.6 Hz boom lateral bending mode and the 33.8 Hz fin tip roll mode are the only good modes to be extracted from this particular gage.

The second category of modes has the following characteristics:

a. Similarity in damping of the two "lower" points and the two "upper" points, but a difference between the "upper" and "lower" points.

b. Good phase-shift at the resonant frequency.

c. Different resonant frequencies indicated by the tabulation, the derivative plot, and the transmissibility plot.

Such modes are generally physical, i.e. real, modes of the airplane, but this particular gage is not the best to discern them; they are better picked off from some other sensor. The 9.9, 13.4, 23.5 and 26.7 Hz modes tabulated in Figure 9 fall into this category.

The 35.4, 37.3 and 39.8 Hz modes are fictitious and can be recognized as such by:

a. Unequal damping values within the "low" and "high" points,

b. Low or even negative damping indications not substantiated by derivative and transmissibility plots.

Utilization of frequency and damping data

Frequency and damping data obtained from the various sources are cross-plotted versus altitude and Mach number for each mode of interest to make sure that they are properly tracked. Figure 10 shows a sample plot of frequency and damping versus Mach number at a constant altitude of 1525 m (5000 ft). Two

modes, fin bending and boom lateral bending, are shown for one side of the aircraft, to demonstrate the range of data scatter that can be expected. As can be seen, the frequency and damping information obtained from the various sources is generally quite consistent. However, in some cases, especially for some of the higher damped modes (see the fin-bending mode in Figure 10), there may be some disagreement between the different bits of information. In such cases, the input data are reviewed regarding their relative merit, e.g. the quality of the decay data, the consistency of the automatically extracted data, and the adequacy of the manually obtained data. Based on a judgment of the relative quality of the different pieces of information, a determination is made on the "final" frequency and damping values to be used for this mode and its "reasonableness" is evaluated by reviewing cross-plots versus altitude and Mach number. This "final" information for each side of the aircraft is then entered into computer storage by means of a remote "Execuport" terminal located at the test site. These data can be retrieved either in tabular form or as Gould plots of frequency, damping, and Flutter Margin versus altitude and Mach number.

At this point, the following data are therefore available to the flutter engineer:

a. Plots of frequency and damping versus altitude for each mode of interest at each cross-section Mach number - Figure 11 is an example of such a plot.

b. Plots of frequency and damping versus Mach number for each mode of interest at each constant altitude cross section - see Figure 10 for sample data of this kind.

c. Plots of Flutter Margin versus equivalent airspeed for each modal combination of interest at each cross-section Mach number (this also includes a prediction of the flutter speed based on a parabolic extrapolation) - see Figure 12.

d. Plots of Flutter Margin versus Mach number for each modal pair of interest at each cross-section altitude - see Figure 13.

Constant altitude flutter velocity predictions are then obtained by manually selecting the Mach number from the constant altitude flutter margin plots at which supersonic flow characteristics appear to be established (e.g. M = 1.18 on the plot in Figure 13), and utilizing only test data above that Mach number for the supersonic extrapolation at this altitude.

A cross-plot of all the Flutter Margin predictions is then made for each modal pair of interest (see Figure 14 for an example) and evaluated in terms of minimum flutter margin. It should be noted that, although modes as determined from left-hand and right-hand data were tracked independently, on the F-15 they were close enough to each other that one flutter boundary could be used to represent them both.

RESULTS

The modes to be observed during the F-15 flight flutter test program were selected on the basis of the results of analytical studies, wind tunnel tests, and ground vibration tests. The modes (both symmetrical and antisymmetrical) tracked on this basis were: fin first bending, fin torsion, fin tip roll, stabilator bending, stabilator pitch, boom lateral bending, boom torsion, boom vertical bending, wing first bending, wing second bending, wing first torsion, outer wing torsion, and aileron rotation.

Data obtained for these various modes were then evaluated in terms of damping versus airspeed at 1525 m (5000 ft), damping versus altitude at the cross-section Mach numbers (to extrapolate to the damping value to be expected at sea level), and flutter boundaries on the basis of Flutter Margin of various modal pairs representing potential flutter mechanisms.

Tables I and II summarize the results of these evaluations in terms of minimum predicted flutter margin for the various mechanisms. It can be noted that there are six flutter mechanisms (three symmetric and three antisymmetric) with predicted flutter margins between 15 and 20 percent, substantiating the success of the minimum weight design concept pursued on the F-15.

Based on our experience to date, we feel that predictions can reliably be carried only to a velocity which is no farther from the last test point than about 1.5 times the difference between the first and last inflight test points. On this basis, since our tests were between altitudes of 6100 and 1525 m (20 000 and 5000 ft), flutter velocity predictions showing greater than 25% flutter margin of safety have no specific quantitative values attached to them.

Shapes of flutter boundaries

Shapes of predicted flutter boundaries were generally either in the form of the boundary given in Figure 14, with Mach numbers between 0.9 and 1.1 being critical, or as shown in Figure 15, with the maximum sea-level Mach number being critical.

Application to design changes

The quantitative knowledge of actual flutter margins provides a firm basis on which to assess the impact of prospective design changes. For example, we may want to incorporate an aircraft modification which, according to analysis (which has been substantially verified by correlation with quantitative flight test data) and possibly also wind tunnel tests, lowers the flutter speed of a certain mechanism by 5%. If we have flight test data in hand that show that we now have 25% margin in this mechanism, we not only have considerable confidence that we can go ahead, but we also have no need to go into another involved flight flutter test program.

We have already had several such opportunities to apply the quantitative F-15 flight flutter test data to the evaluation of design changes.

CONCLUDING REMARKS

The flight flutter test procedure used on the F-15 provides not only a demonstration of adequate damping throughout the aircraft flight envelope, but also permits quantitative demonstration of margin of safety. Such quantitative information is not only useful to definitively establish the flutter status of the aircraft as it was flown, but also provides a solid foundation on which to assess the impact of any future design changes.

REFERENCES

1. Zimmerman, N.H., and Weissenburger, J.T.: Prediction of Flutter Onset Speed Based on Flight Flutter Testing at Subcritical Speeds. Journal of Aircraft, Vol. 1, No. 4, 1964.

2. Shelton, J.D., and Tucker, P.B.: Minimum Weight Design of the F-15 Empennage for Flutter. AIAA/ASME 16th Structures Meeting, May 1975.

3. Nash, D.E., Katz, H., and Moody, W.C.: F-15 Flight Flutter Testing: Aircraft Systems and Test Operations. AIAA 1975 Aircraft Systems and Technology Meeting, August 1975.

4. Kennedy, C.C. and Pancu, C.D.P.: Use of Vectors in Vibration Measurement and Analysis. Journal of Aeronautical Sciences, Vol. 14, 1947.

TABLE I
MINIMUM FLUTTER VELOCITY MARGINS FOR SYMMETRIC MECHANISMS

MECHANISM	MARGIN OF SAFETY
FIN BENDING vs BOOM LATERAL BENDING	15%
STABILATOR BENDING vs STABILATOR ROTATION	19%
WING FIRST BENDING vs OUTER WING TORSION	20%
BOOM VERTICAL BENDING vs STABILATOR ROTATION	25%
BOOM LATERAL BENDING vs BOOM TORSION	> 25%
STABILATOR BENDING vs BOOM TORSION	> 25%
STABILATOR ROTATION vs BOOM TORSION	> 25%
FIN BENDING vs FIN TORSION	> 25%
STABILATOR BENDING vs BOOM VERTICAL BENDING	> 25%
BOOM TORSION vs BOOM VERTICAL BENDING	> 25%
FIN TORSION vs FIN TIP ROLL	> 25%
WING FIRST BENDING vs WING FIRST TORSION	> 25%
WING SECOND BENDING vs WING FIRST TORSION	> 25%
WING SECOND BENDING vs OUTER WING TORSION	> 25%

GP75-0710-2

TABLE II
MINIMUM FLUTTER VELOCITY MARGINS FOR ANTI SYMMETRIC MECHANISMS

MECHANISM	MARGIN OF SAFETY
FIN BENDING vs BOOM LATERAL BENDING	16%
STABILATOR ROTATION vs BOOM TORSION	17%
BOOM LATERAL BENDING vs BOOM TORSION	20%
WING FIRST BENDING vs OUTER WING TORSION	25%
STABILATOR BENDING vs BOOM TORSION	> 25%
BOOM VERTICAL BENDING vs STABILATOR ROTATION	> 25%
WING SECOND BENDING vs OUTER WING TORSION	> 25%
STABILATOR BENDING vs STABILATOR ROTATION	> 25%
FIN BENDING vs FIN TORSION	> 25%
STABILATOR BENDING vs BOOM VERTICAL BENDING	> 25%
BOOM TORSION vs BOOM VERTICAL BENDING	> 25%
FIN TORSION vs FIN TIP ROLL	> 25%
WING FIRST BENDING vs WING FIRST TORSION	> 25%
WING SECOND BENDING vs WING FIRST TORSION	> 25%

GP75-0710-1

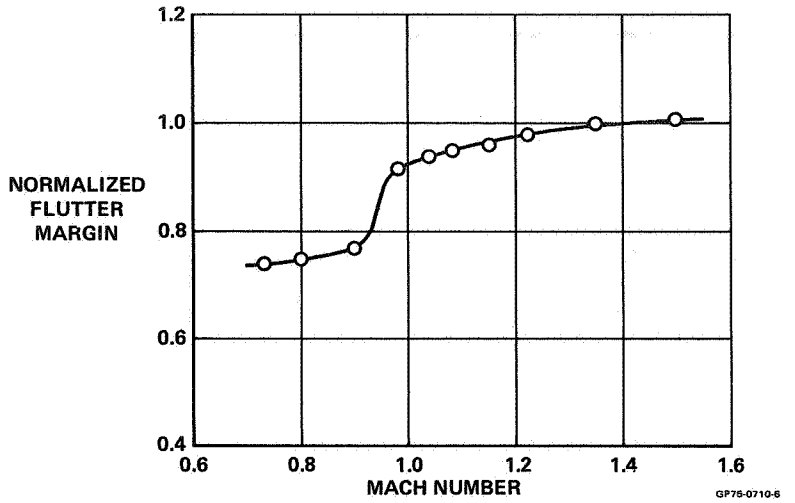

Figure 1.- Flutter margin at constant dynamic pressure. Antisymmetric boom torsion versus stabilator rotation at 442 KEAS.

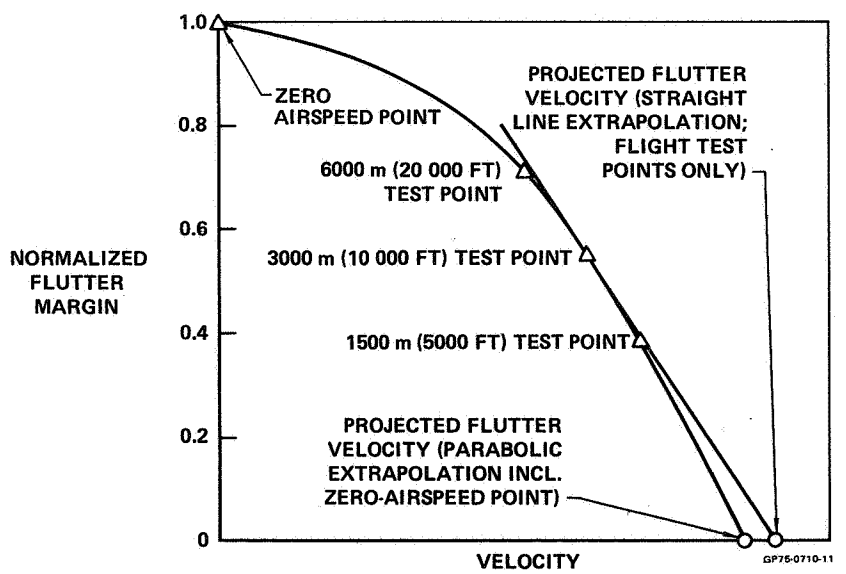

Figure 2.- Flutter prediction at constant Mach number.

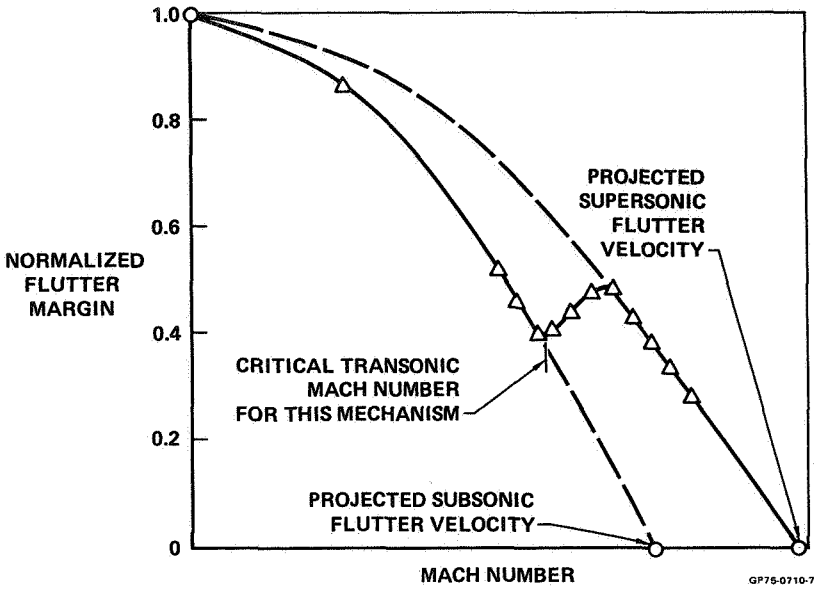

Figure 3.- Flutter prediction at constant altitude.

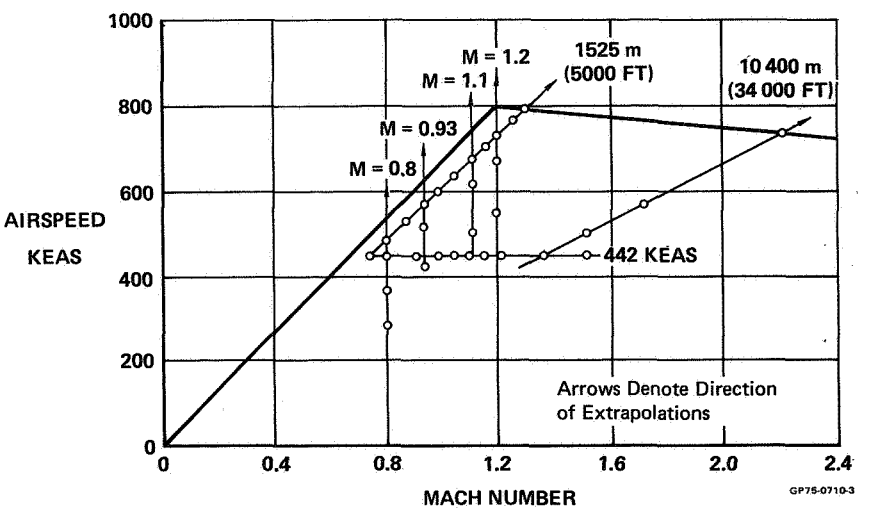

Figure 4.- F-15 flight flutter test points.

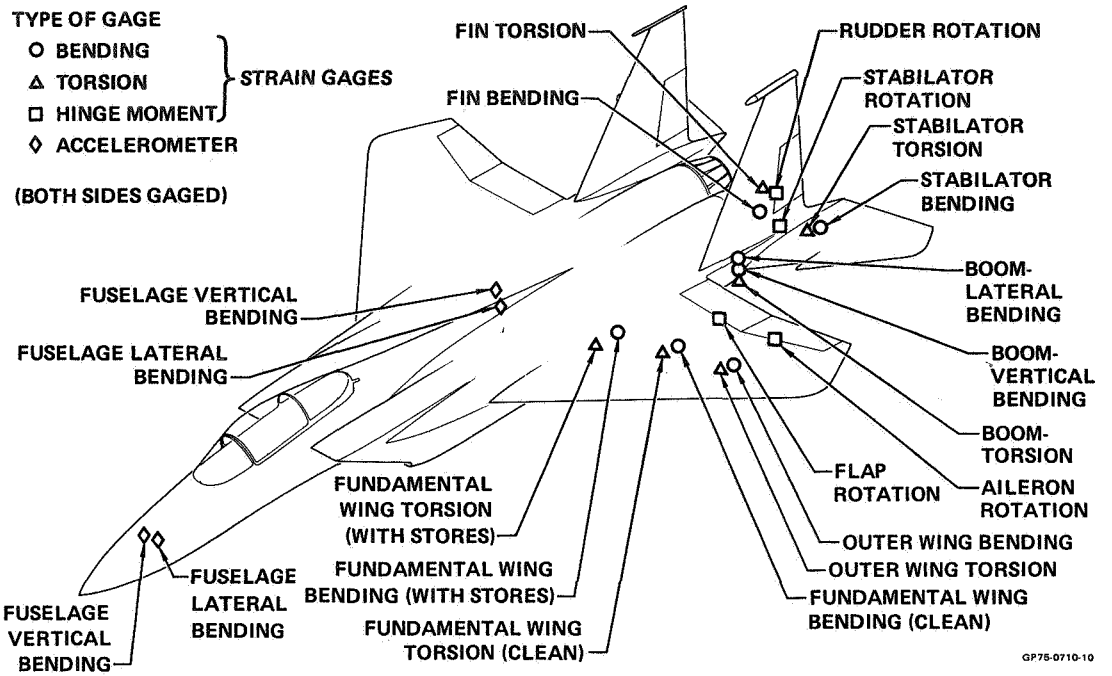

Figure 5.- Location of instrumentation.

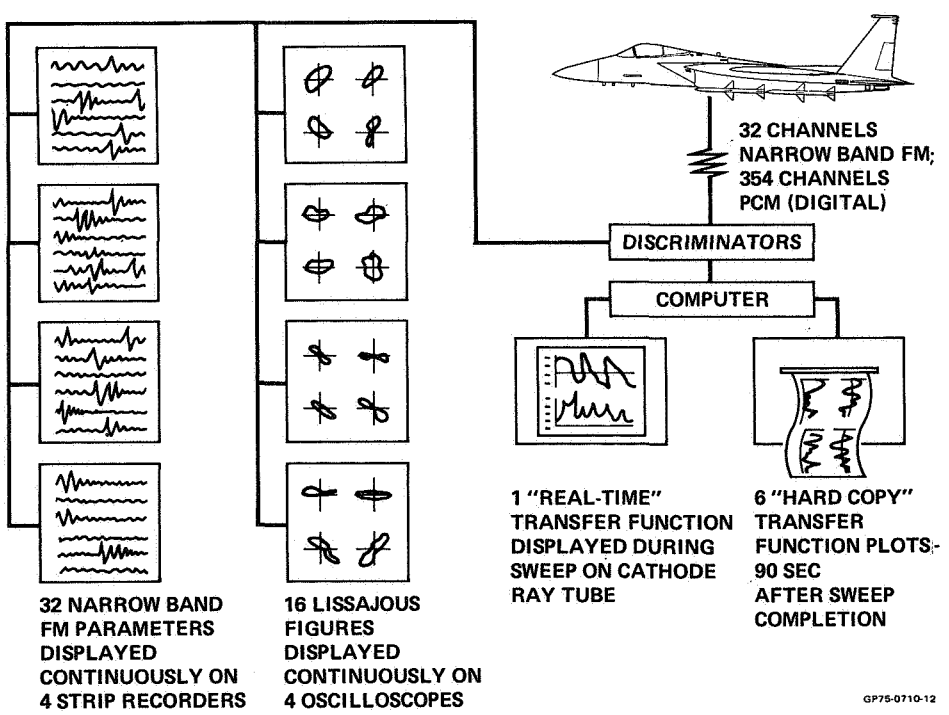

Figure 6.- On-line data reduction of telemetered signals.

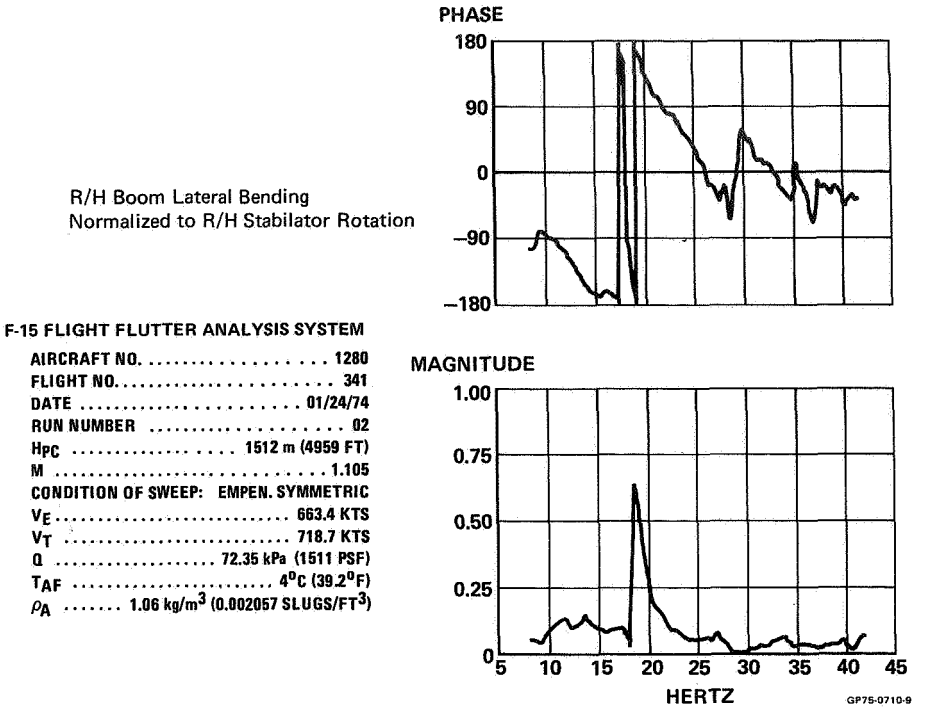

Figure 7.- St. Louis transmissibility plot.

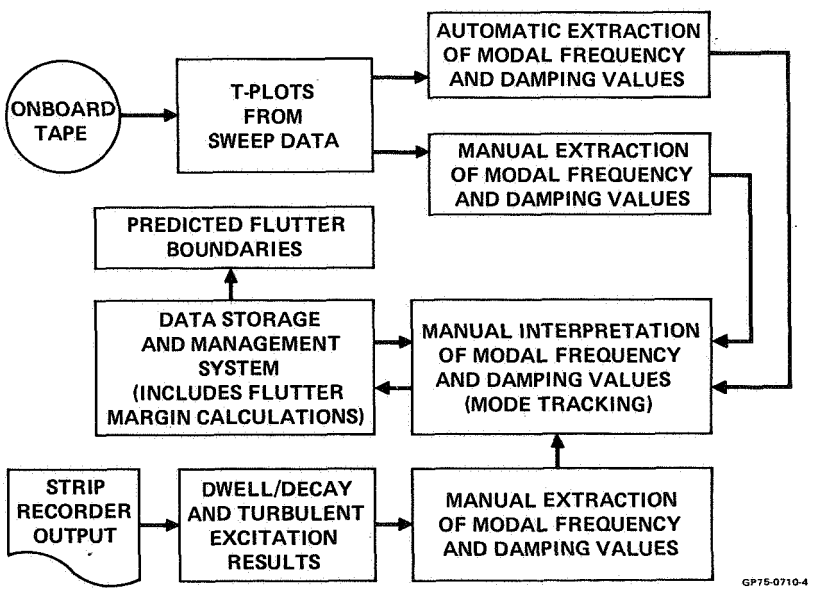

Figure 8.- Post-flight data system schematic.

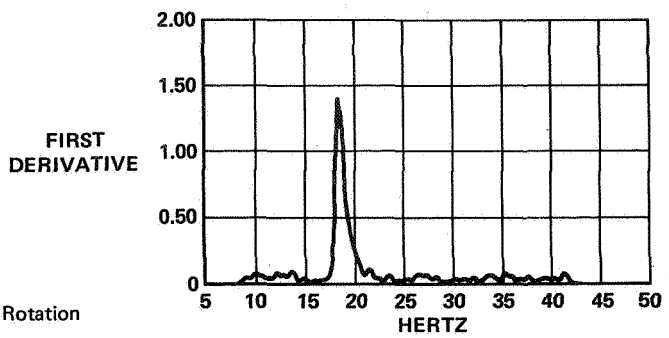

R/H Boom Lateral Bending
Normalized to R/H Stabilator Rotation

F-15 FLIGHT FLUTTER ANALYSIS SYSTEM

AIRCRAFT NO. 1280
FLIGHT NO. 341
DATE 01/24/74
RUN NUMBER 02
H_{PC} . . . . . 1512 m (4959 FT)
M 1.105
CONDITION OF SWEEP: EMPEN. SYMMETRIC
V_E . . . . . 663.4 KTS
V_T . . . . . 718.7 KTS
Q . . . . . 72.35 kPa (1511 PSF)
T_{AF} . . . . . 4°C (39.2°F)
ρ_A . . . . . 1.06 kg/m^3 (0.002057 SLUGS/FT^3)

FREQUENCY AND DAMPING DATA

NUM	FREQ	DAMP	DAMP	DAMP	DAMP	AVG DAMP
1	9.90	0.123	0.114	0.169	0.164	0.142
2	13.40	0.038	0.031	0.024	0.024	0.029
3	18.60	0.019	0.018	0.020	0.021	0.019
4	23.50	0.118	0.100	0.272	0.240	0.183
5	26.69	0.005	0.001	0.034	0.033	0.018
6	33.80	0.025	0.026	0.023	0.028	0.026
7	35.40	−0.002	−0.002	0.001	0.001	0.001
8	37.31	0.033	0.027	0.007	0.008	0.019
9	39.80	0.005	−0.008	−0.009	−0.014	0.005
10						
11						
12						

GP75-0710-8

Figure 9.- St. Louis Argand derivative plot and automatic frequency and damping extraction results.

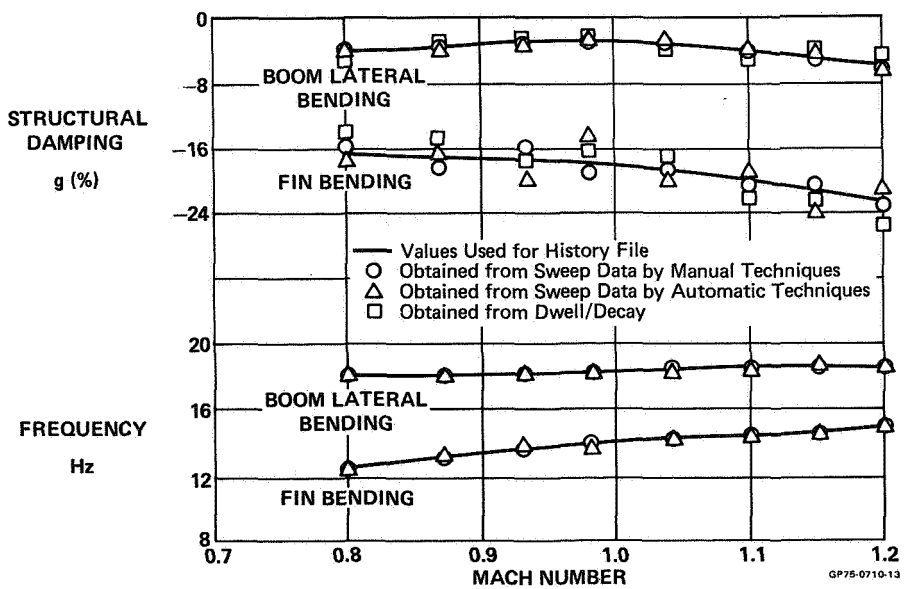

Figure 10.- Frequency and damping versus Mach number for symmetric fin bending and boom lateral bending modes. L/H data at 1525 m (5000 ft) altitude.

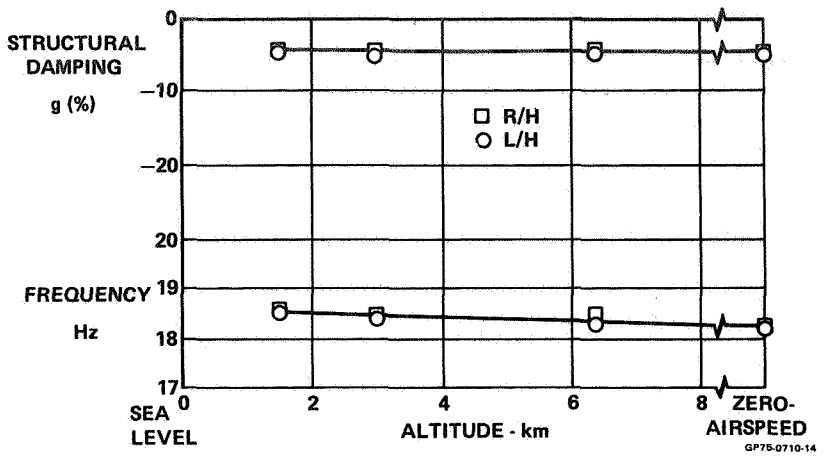

Figure 11.- Frequency and damping versus altitude for symmetric boom lateral bending at constant Mach number of 1.10.

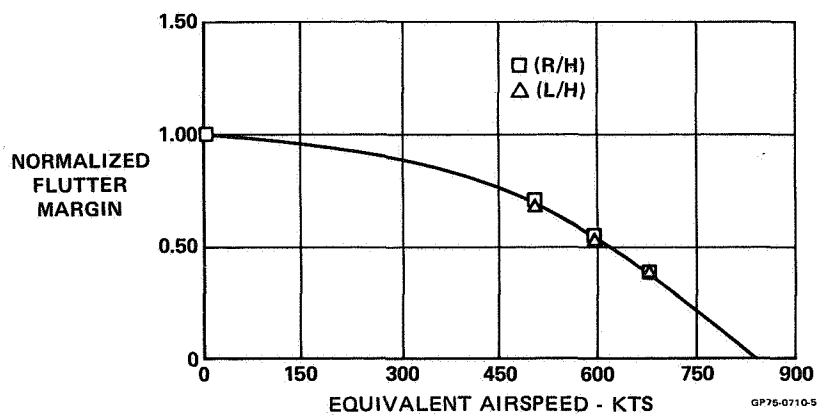

Figure 12.- Flutter margin versus equivalent airspeed. Symmetric boom lateral bending versus fin bending for constant Mach number of 1.10.

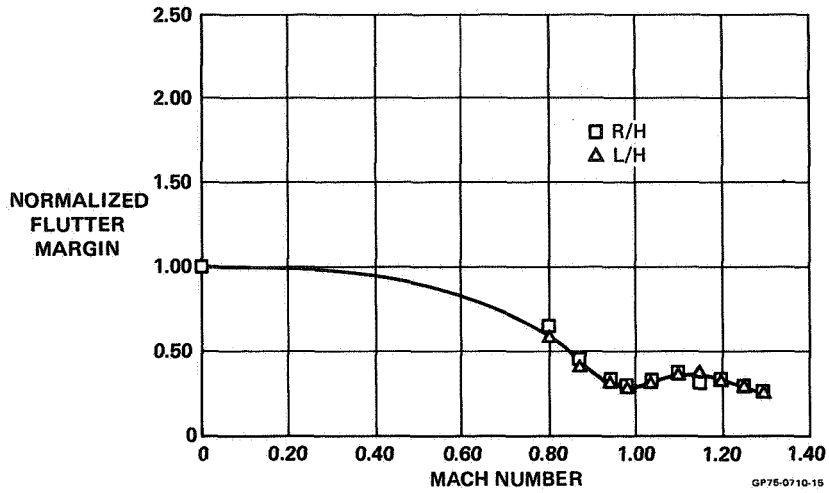

Figure 13.- Flutter margin versus Mach number. Symmetric boom lateral bending versus fin bending at constant altitude of 1525 m (5000 ft).

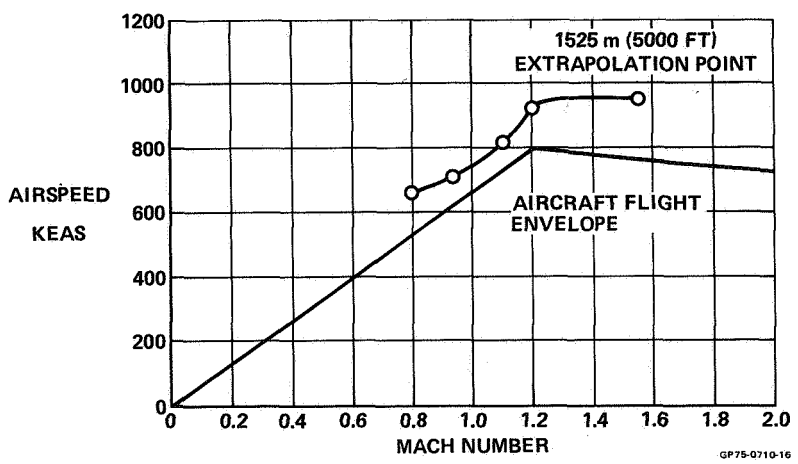

Figure 14.- Flutter boundary for fin bending versus boom lateral bending mechanism - symmetric.

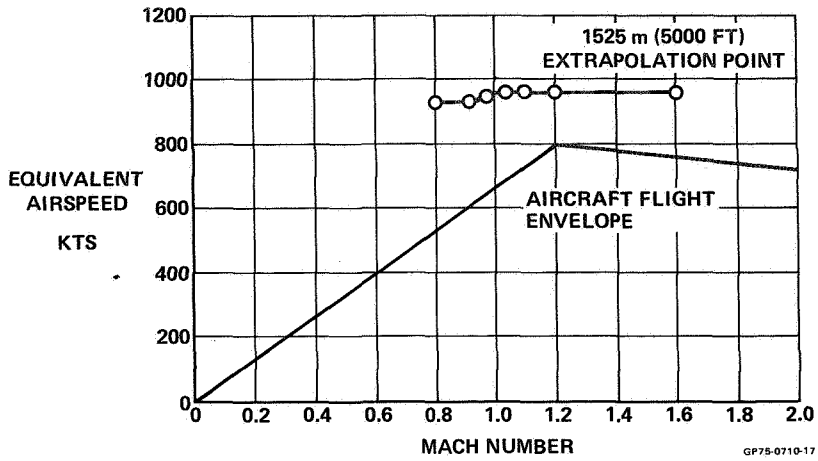

Figure 15.- Flutter boundary for wing first bending versus outer panel torsion mechanism - symmetric.

YF-16 FLIGHT FLUTTER TEST PROCEDURES

Warren J. Brignac, Halvor B. Ness,
Maynard K. Johnson, and Larz M. Smith

Fort Worth Division
General Dynamics Corporation

SUMMARY

The procedures used for flight flutter testing of the YF-16 lightweight fighter prototype are described. The Random Decrement technique was incorporated to augment the initial plan to use only the pilot pulse approach. With Random Decrement, subcritical damping of the structural modes is extracted from the turbulence-induced random vibrations of the structure. Hence, the method bypasses the requirement for an excitation system needed in the conventional approaches. Damping is obtained from the Randomdec Signature of each mode. The Randomdec Signature is analogous to the transient response to an initial displacement. To obtain a Randomdec Signature, one collects and averages a number of segments of the random response of the mode. Expeditious flutter clearance of the YF-16 was accomplished, marking the first known application of the technique to a full-scale test article. Although the Random Decrement apparatus used was lacking in completeness, it produced damping on check problems which were consistent with values from conventional methods. For the YF-16, it was possible to identify and track most of the modes of interest for each of the configurations tested. Good quantitative damping was obtained for the lower surface modes. Most of the higher modes were detectable and at least a qualitative evaluation of the damping was possible. Most of the testing was done at the more critical low altitudes where the random excitation is high. Due to equipment limitations, only one channel could be monitored on a real time basis. Therefore, most of the analysis was accomplished on a postflight basis. Damping values obtained substantiate the adequacy of the flutter margin of safety.

To confirm the structural modes which were being excited, a spectral analysis of each channel was performed using the AFFTC Time/Data 1923/50 Time Series Analyzer.

The inflight test procedure included the careful monitoring of strip charts, three axis pulses, rolls and pullups.

Conclusions are that, for the YF-16, the procedures used, including Random Decrement, were a satisfactory alternate to more costly conventional test procedures.

INTRODUCTION

A vital step in an aircraft development program is the substantiation of freedom from flutter by means of flight flutter tests. Since flutter clearance is a pacing item for expanding the speed envelope, the need for accurate, rapid and low cost means to forecast flutter is widely recognized. Because flight flutter tests have been costly and time consuming, there have been continuing efforts by industry (Reference 1) and government agencies (Reference 2) to upgrade their procedures. As indicated by a recent survey (Reference 3), most current methods require onboard forced excitation, usually sinusoidal, to excite the structural modes. Damping is then obtained by a variety of methods including from decay records from the well-known "shake and stop" technique. The incorporation of high speed digital computers into the data acquisition and reduction operations has resulted in some significant advances in the state of the art. The methods, however, still tend to be both expensive and time consuming. The excitation system itself is usually a costly item.

Alternatives to methods requiring forced excitation have been advanced. These methods utilize inflight or wind tunnel turbulence as the excitation source. In one approach, PSD analyses of the response signals are made and damping is obtained from the frequency and bandwidth associated with each peak in the PSD plot. The PSD approach is more widely used in Europe at this time.

The Random Decrement approach, the application of which is to be discussed herein, is a second alternate to forced excitation methods. The method was invented by H. A. Cole, Jr., and is

fully documented (Reference 4 and 5). The Random Decrement method is basically an ensemble averaging of the turbulence-induced random vibrations of the test article. As is illustrated in Figure 1, Cole advocates triggering each data sample at a constant level, Y_t. Assuming linear superposition, the time history of each sample can be regarded as the combined solution from (1) an initial step displacement, (2) an initial velocity and (3) a random forcing function. Note that the Figure 1(c) sample represents the response to the same initial displacement as Figure 1(b), a different initial velocity with the opposite sign, and a different random forcing function. It can be reasoned intuitively that when a large number of samples are averaged, only the response to the constant initial displacement will remain because the average of responses due to the alternating initial velocities and the random forcing functions will tend to zero. Thus, it is seen that the ensemble average converges toward the transient response to an initial step. For a constant trigger level, the ensemble average (Randomdec Signature) will be constant even if the amplitude of the forcing function varies. If the ensemble average is made up of samples with initial positive slopes only, then the resulting trace represents the transient response to a combined step and initial velocity. Under these conditions the Randomdec Signature would vary with the intensity of the forcing function, thus minimizing the use of the signature trace as a failure detector. However, the damping as determined from the decay rate of the signature trace would be valid. A rigorous mathematical derivation of Random Decrement is given in Reference 6. Included are descriptions of other triggering procedures and automated methods of analyzing the Randomdec Signature to obtain damping.

The main objective of this paper is to present the results of the application of a simplified flutter test technique to a flight article. It is hoped that these results will be of use to others who may be considering new methods and/or improvements for similar techniques.

BACKGROUND

The YF-16 is a lightweight fighter prototype whose high performance credits include supersonic sea-level capability. A top and side view of the airplane is shown in Figure 2. The design features a thin (4%) aluminum wing with leading-edge maneuver flaps and trailing-edge flaperons. The all-movable

horizontal tail and the conventional fin-rudder vertical tail have graphite composite skins. Although flutter and aeroelastic considerations had a considerable impact on the design, cost and schedule constraints on the prototype programs dictated a flutter prevention program which minimized flight flutter tests. In the initial planning, flight flutter tests were to be conducted with pilot pulses. The austere flight flutter test program was to be supported by comprehensive analyses and a complete 1/4 scale flexible model to be tested in the NASA Langley 16-Foot Transonic Tunnel. A twenty percent margin of safety was to be utilized for design.

It was during early tests of the YF-16 1/4-scale model components that General Dynamics was first exposed to the Random. Decrement concept. NASA LRC tunnel personnel had assembled a Random Decrement analyzer and were using it to monitor the tunnel tests. Although the single-channel instrument limited the extent of on-line monitoring, the capability to extract quantitative damping was demonstrated. An example of the damping of one mode at successive speed increments is shown in Figure 3. NASA LRC had also indicated (see Figure 4) satisfactory agreement between Random Decrement and PSD methods on predicting the flutter speed of an SST wing model.

Following the exposure to Random Decrement at the tunnel test, General Dynamics assembled a Random Decrement analyzer analogous to the NASA equipment and undertook a further evaluation of its capability. An investigation was made on an electric analog computer model of a simple two-degree of freedom system illustrated in Figure 5. The electric model is analogous to a model in a wind tunnel or an airplane in flight and subcritical damping can be determined by the "shake and stop" procedure. Using the Random Decrement analyzer, damping was also obtained with the model being excited by sea-level simulated atmospheric turbulence. As shown in Figure 5, consistent damping and flutter speeds were obtained by the two methods. The damping obtained by the Random Decrement analyzer did not vary significantly with excitation levels higher by a factor of two.

An additional limited evaluation was made using F-111 taped flight flutter test data. Wing tip vanes were used for excitation on the F-111 program; consequently, generally good wing damping records had been obtained. The general observation was that good damping agreement was observed for modes with high ambient response levels and, conversely, poor agreement was shown when the ambient excitation level was low. It was observed that,

in cases of low ambient excitation levels, the damping as evaluated by the Random Decrement analyzer was lower than that from the forced excitation.

Following the somewhat cursory evaluation described above, it was decided to implement Random Decrement for the YF-16 flight flutter test program. Some apparent basic limitations of the method were recognized. However, it was felt that realistic damping could be obtained for all modes that were excited by the ambient environment. Separation problems when mode frequencies are close were expected but this problem plagues all methods. In addition, the capability to analyze rapidly any unexpected vibratory phenomenon was highly desirable.

PROCEDURE

The four airplane configurations which were tested are shown in Figure 6. The 1400 liter (370 gallon) external tank loading was tested full, empty and at two intermediate fuel levels. The onboard flutter instrumentation is shown in Figure 7. Included are two accelerometers in each wing tip, one in each horizontal tail tip and one in the vertical tail tip. The output of each transducer was telemetered to the ground and also recorded on-board on magnetic tape. Each telemetered item was displayed on an analog recorder. Variable band-pass filters were used on the accelerometer signals to narrow the response to the frequency range of interest. Any six channels could also be patched to the Random Decrement analyzer for analysis individually.

The test procedure included a slow acceleration to the test point while the strip charts were carefully monitored. Speed was stabilized for 30 to 60 seconds to accumulate data for Random Decrement analysis. Then the pilot would pulse the controls about all three axes, roll 360^{o} in each direction and do a symmetric pullup.

The test procedure was augmented with Random Decrement as follows. The stabilized period at each test point was sufficient to obtain damping only of one selected mode. Since only one Random Decrement analyzer was available, analysis of additional modes could only be accomplished on a rotating basis at the expense of a longer stabilized period. In general, this was not done because the need was not apparent. Instead, all channels were carefully analyzed on a postflight basis.

The on-line and postflight Random Decrement analysis was carried out with the system illustrated in Figure 8. The random output signal was first run through a band-pass filter to isolate a mode before going through the analyzer. The heart of the system is the Hewlett-Packard Model 5480B Signal Analyzer which performed the function of acquiring each data sample and displaying an updated average continuously on an oscilloscope. Programming on this computer is hardwired to panel-mounted push-button controls which enable program START, STOP and MEMORY CLEAR commands. This feature proved to be of considerable operational utility since analysis could be rapidly updated to reflect a change in flight condition or to examine a different measurement location. The ability to switch in and display the random waveform on the scope was very valuable with regard to setting the trigger level for sampling. After triggering, the system reads each data sample at 1000 intervals. The analyzer may be somewhat less than optimum in that it is triggered by positive slope crossings only. As previously mentioned, the analysis time for each damping record usually varied from 30 seconds to a minute depending on the excitation level and the frequency of the mode. Generally, the damping trace was observed to converge after about 25 to 40 samples were acquired. An item which greatly facilitated the postflight data analysis was the conveniently located magnetic tape unit with start, stop and rewind controls operated by the Random Decrement analyzer operator. The reason is that setting optimum trigger levels and locating resonant frequencies can require many passes through the magnetic tape.

The procedure for setting up the analyzer was to first observe the random signal on the oscilloscope to determine existence of periodic motion. The time scale was varied on the CRT display to cover the desired range of frequencies. Obvious aides in detecting specific frequencies were the calculated vibration frequencies, the ground vibration test results, and a frequency spectral analysis described at the end of this section. The variable band-pass filters were adjusted to focus on a specific desired frequency. The trigger level was adjusted by observing the filtered signal on the oscilloscope and triggering at the maximum level possible that would still allow the accumulation of a satisfactory number of data samples within the test period.

The frequency detection portion of this process could be started while the airplane was in transit to the test area or otherwise preparing for the test run. The trigger setting was

done after the airplane reached the test speed. With a little experience this could be done fairly quickly. The only time difficulty was experienced was when the turbulence level varied greatly during the test period. Moderate to heavy turbulence was preferred because the setup was easier and a shorter time period was required to accumulate a sufficient number of data samples. In extremely smooth air, the low structural amplitude caused problems in obtaining sufficient data samples and led to some loss of confidence in the accuracy of the results.

A spectral analysis of each data channel was performed to confirm that all structural modes which were responsive to the random excitation were in fact being identified and tracked by the Random Decrement Analyzer. The analysis was performed using the AFFTC Time/Data 1923/50 Time Series Analyzer. This analysis produced the conventional power vs frequency chart and provided graphic confirmation of the frequency content of the response.

OVERALL RESULTS

The flutter free envelopes which were demonstrated are shown in Figure 9. It is noted that the cleared envelopes were those required for prototype evaluations and the design envelopes are somewhat larger. Although full envelope capability is indicated by analysis, model tests and flight flutter test results, the prototype program's tight schedule did not call for full clearance. All subsonic points for each configuration were accomplished on one flight. Generally, two points per flight were accomplished in the low supersonic region. Only one test point per flight was accomplished at the high supersonic speeds to allow a complete postflight evaluation before proceeding to the next test point. The flight flutter test program was planned as part of an integrated program in which considerable data in other disciplines was acquired before the envelope expansion was completed. The flutter test program was completed on schedule with the maximum test dynamic pressure of 103 000 N/m^2 (2150 psf) being reached approximately three months after the first flight.

As expected based on analysis and model test results, the flight flutter test program was accomplished expeditiously and without any major problems. One specific flight test incident occurred which had not been anticipated. Early in the flight test program, a gain sensitive oscillation of the nominal 6.5 Hz antisymmetric wing mode became apparent due to a coupling with

the flight control stability augmentation system. The instability is reviewed in detail in a separate paper (Reference 7) and only the highlights will be discussed here. The oscillation was first encountered at approximately .85M at 6096 m (20 000 feet) where insufficient control system interaction analyses had been accomplished. Most of the control system interaction analyses had been accomplished at 1.2M where flutter margins were a minimum and no problem was indicated. The actual problem occurred where the roll effectiveness of the flaperons was the highest. The problem was quickly identified and a fix worked out consisting of a notch filter in the roll feedback loop and realignment of gains in the command and feedback loops. It is worth mentioning that the YF-16's fly-by-wire control system made quick implementation of the fix possible.

Random Decrement was very useful in further defining the region of instability which is shown in Figure 10. The region was actually traversed with reduced roll gains before the final fix was incorporated. As will subsequently be shown, the Random Decrement results show a significant difference between the mode's characteristics with reduced gains and with the notch filter installed. The difference is due to the phase shift which the filter introduces.

Overall, Random Decrement demonstrated that most of the modes of interest were excited by the random environment and solid damping is indicated throughout the flight envelope. A review of the damping records obtained is presented in the following section.

DAMPING

The quality of the damping obtained is described in Table I for the basic configuration with and without tip missiles. The table indicates the modes of each surface that were most easily detected. In general, these are the first two wing modes and the fundamental tail modes. The higher modes, including some in addition to the ones in Table I, were usually detectable but the quality of the decay record was poor or erratic. The fundamental horizontal tail mode was detectable but highly damped. The higher horizontal tail modes were apparently very highly damped also. A complete set of decay records for a missiles-on test point is shown in Figures 11 and 12. Mode identification

corresponds to that given in Table I. Plots of damping versus Mach number for the missiles-on fundamental wing symmetric, wing antisymmetric, and vertical tail modes are shown in Figure 13. Corresponding decay records are shown in Figures 14 and 15. Note that the frequencies of the two wing modes are relatively close and some difficulty was experienced in separating the responses. The problem was overcome by adding the signals from corresponding transducers on opposite sides to emphasize the symmetric response and subtracting to emphasize the antisymmetric response. The process is illustrated in Figure 16. A simple network of isolation resistors was used to combine the output of two discriminators. The outputs were summed to get the symmetric response. The phase of one discriminator was reversed to obtain the antisymmetric response. No attempt was made to correct for the slight difference in sensitivity of the accelerometers involved.

The basic wing modes for the configurations with pylon-mounted external stores were detected at approximately the same frequencies listed above and exhibited similar damping characteristics. The carriage of the external stores well inboard (at 27 percent of the exposed semispan) accounts for the small effect on the basic wing frequencies. For the external store configurations, the fundamental store pitch and yaw frequencies were also detected and their decay records extracted. Typical examples of external store decay records are shown in Figure 17 for the airplane with empty 1400 liter (370 gallon) tanks.

Some further examples of the results obtained with Random Decrement are in connection with the oscillation of the antisymmetric mode. Shown in Figure 18 is a comparison of the damping at .9M and 1520 m (5000 feet), before and after the notch filter was added. Before the notch filter was added, the motion of the mode was sustained although of extremely low magnitude for the applicable gain setting. Shown in Figure 18(a) are the individual decay records from opposite wing tips and the decay records obtained after adding and subtracting the wing tip response. It is noted that even though the antisymmetric mode appears to dominate the individual responses, a good damping record was obtained for the symmetric mode. Shown in Figure 18(b) are the corresponding records after the filter was added. Note that even though the numerical value of the feedback loop gain was close to the "before filter" value, positive damping is shown for the antisymmetric mode. As previously mentioned, the difference is apparently due to the favorable phase shift from the filter.

All of the results hereto shown were for relatively low altitude levels where the ambient excitation levels were generally high and damping of each of the principal structural modes was obtained. Early in the test program, some horizontal tail and vertical tail data was obtained at higher altitudes. Although the ambient response levels were lower than at low altitude, no difficulty was encountered in obtaining consistent damping at 6096 m (20 000 feet) and 9144 m (30 000 feet). Damping records for the fundamental tail modes at 1520 m (5000 feet), 6096 m (20 000 feet), and 9144 m (30 000 feet) are shown in Figure 19. The damping at the higher altitude is noticeably lower. The question arises as to whether the damping is lower due to lower density or to inaccuracies associated with the lower excitation levels. In the case of the fundamental tail modes, it is believed that sufficient excitation was provided from wing downwash, etc., so that the high altitude damping is realistic. The high altitude damping for the higher modes is believed to be more questionable.

CONCLUSIONS

Application of Random Decrement to the flight flutter tests of the YF-16 has led to the following evaluation of the technique:

1. The frequency and damping of most of the predominant structural modes can be obtained.

2. The quality of the damping depends on the excitation level, the damping level, and the accumulation of a sufficient number of samples, usually 25-40.

3. The lower structural modes are more easily detected and good quality damping can be expected for these modes.

4. The higher structural modes can usually be detected but damping values tend to be more qualitative than quantitative.

5. Separation of symmetric and antisymmetric modes of nearly the same frequency was possible.

6. As used, the Random Decrement analysis relied heavily on postflight analysis because of the single analyzer available.

7. The method has the obvious limitation of not being able to detect a particular mode if it is not excited. Also, closely spaced modes cause analysis problems.

8. Some of the limitations mentioned here can be overcome with improved facilities and analysis techniques.

For the YF-16, the results from the Random Decrement analysis substantiate the predicted flutter margins of safety. Hence, Random Decrement was a meaningful addition to the flight flutter test procedure and served as a satisfactory alternate to more costly conventional techniques. The principal result was that quantitative damping was obtained which would not have been possible for this airplane with the pilot pulse technique.

FUTURE PLANS

Full scale development of the production F-16 is now in progress. The flutter prevention plan is the same as followed for the prototype YF-16 including a twenty percent margin of safety for design. Planned flight flutter tests will use procedures similar to those described in this paper. The flutter test equipment is being expanded to provide two-channel capability through acquisition of a second Hewlett-Packard Model 5480B Signal Analyzer.

All flutter test data on the YF-16 was both recorded on onboard tape and transmitted via telemetry to the ground receiving station using FM/FM techniques. The F-16 full scale development test aircraft will be equipped with the AFFTC Automatic Test Instrumentation System (ATIS). This is a high rate (up to 512K bits/sec) PCM system. The existing Random Decrement analysis system uses analog input; therefore, digital-to-analog conversion will be required. Experimental confirmation of the sampling rates necessary in order to produce an acceptable damping record has been accomplished. It has been determined that an absolute minimum of four samples per cycle of response is required.

SYMBOLS

A,B	points at which response crosses specified reference amplitude, Y_t
f	frequency, Hz
f_F	flutter frequency, Hz
f_o	frequency of selected response mode, Hz
Δf	band width of response mode at half-power point, Hz
g	damping coefficient
K_h	translational spring constant, dynes/cm
K_α	rotational spring constant, dyne cm/rad
M	Mach number
q	dynamic pressure, N/m^2
t	time, sec
V	airspeed, knots
V_F	flutter speed, knots
V_1, V_2	equivalent initial velocity at points A and B
x_n	half-amplitude of nth cycle of exponential decay curve
x_o	half-amplitude of initial cycle of exponential decay curve
Y_t	reference amplitude of response
γ	viscous damping ratio

REFERENCES

1. Baird, E. F., and Clark, W. B.: Recent Developments in Flight Flutter Testing in the United States. Presented at 34th Meeting of the AGARD Structures and Materials Panel, April 1972, AGARD Report 596

2. Houbolt, J. C.: Subcritical Flutter Testing and System Identification. NASA CR-132480, August 1974

3. Rosenbaum, Robert: Survey of Aircraft Subcritical Flight Flutter Testing Methods. NASA CR-132479, August 1974

4. Cole, Henry A., Jr.: Method and Apparatus for Measuring Damping Characteristics of a Structure. United States Patent No. 3,620,069, 16 November 1971

5. Cole, H. A., Jr.: On-Line Failure Detection and Damping Measurements of Aerospace Structures by Random Decrement Signatures. NASA CR-2205, March 1973

6. Chang, C.S.: Study of Dynamic Characteristics of Aeroelastic Systems Utilizing Randomdec Signatures. NASA CR-132563

7. Peloubet, R. P., Jr.: YF-16 Active-Control-System/ Structural Dynamics Interaction Instability. Presented at 16th AIAA/ASME/SAE Structures, Structures Dynamics and Materials Conference, May 1975

TABLE I PRIMARY STRUCTURAL FREQUENCIES

	SYMMETRIC		ANTISYMMETRIC	
A. MISSILES ON				
WING	FREQUENCY (Hz)		FREQUENCY (Hz)	
1ST BEND.	4.9	GOOD DECAY	8.0	GOOD DECAY
MISSILE PITCH	6.7	GOOD DECAY	6.4	GOOD DECAY
2ND BEND.	21.7	FAIR DECAY	22.0	FAIR DECAY
TORSION-FLAPERON ROT.	38.4	FAIR DECAY	36.6	FAIR DECAY
HORIZONTAL TAIL				
1ST BEND.	25.2	HIGH DAMPING	25.7	HIGH DAMPING
2ND BEND.	50.1	NOT DETECTED	51.2	NOT DETECTED
PITCH	95.6	HIGH DAMPING	97.1	HIGH DAMPING
VERTICAL TAIL				
1ST BEND.			15.2	GOOD DECAY
2ND BEND.			39.0	POOR DECAY
RUDDER ROTATION			56.5	NOT DETECTED
B. MISSILES OFF				
WING				
1ST BEND.	8.5	GOOD DECAY	10.9	FAIR DECAY
LAUNCHER PITCH	17.2	POOR DECAY	17.4	FAIR DECAY
2ND BEND.	29.7	GOOD DECAY	32.0	FAIR DECAY
TORSION-FLAPERON ROT.	39.6	POOR DECAY	40.8	POOR DECAY

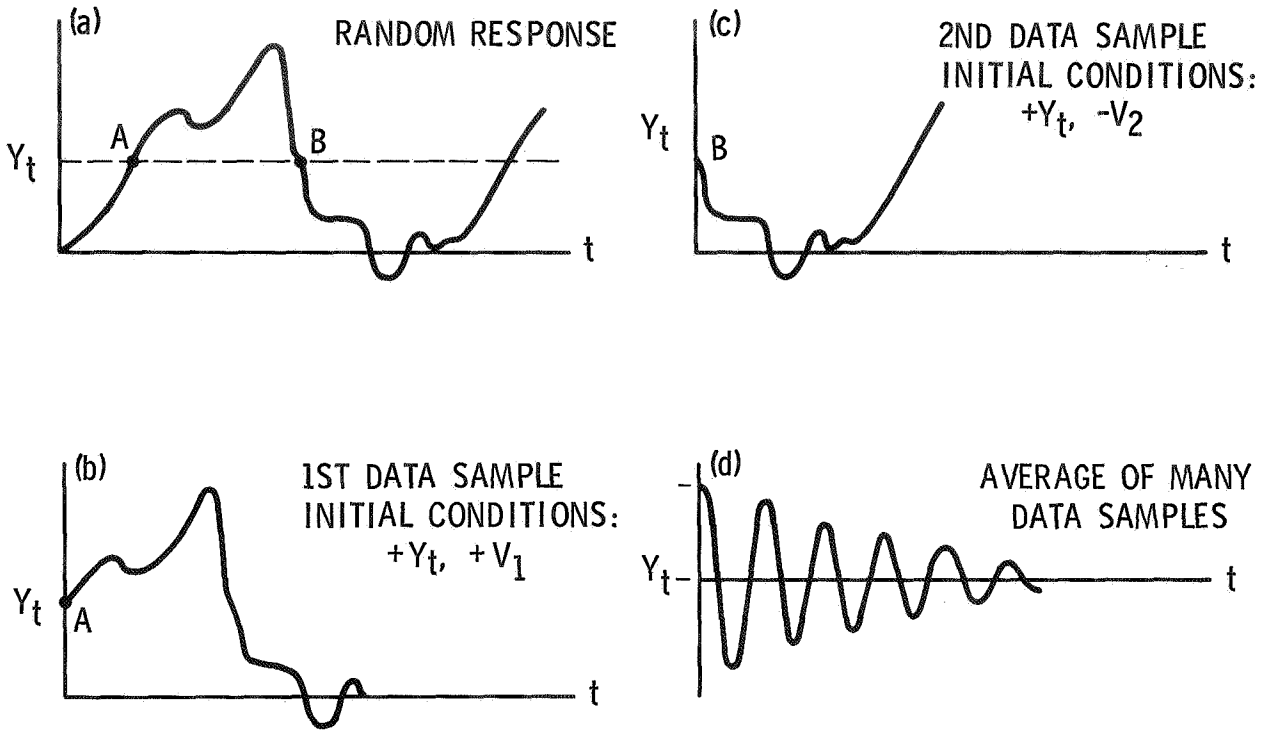

Figure 1 Random Decrement Concept

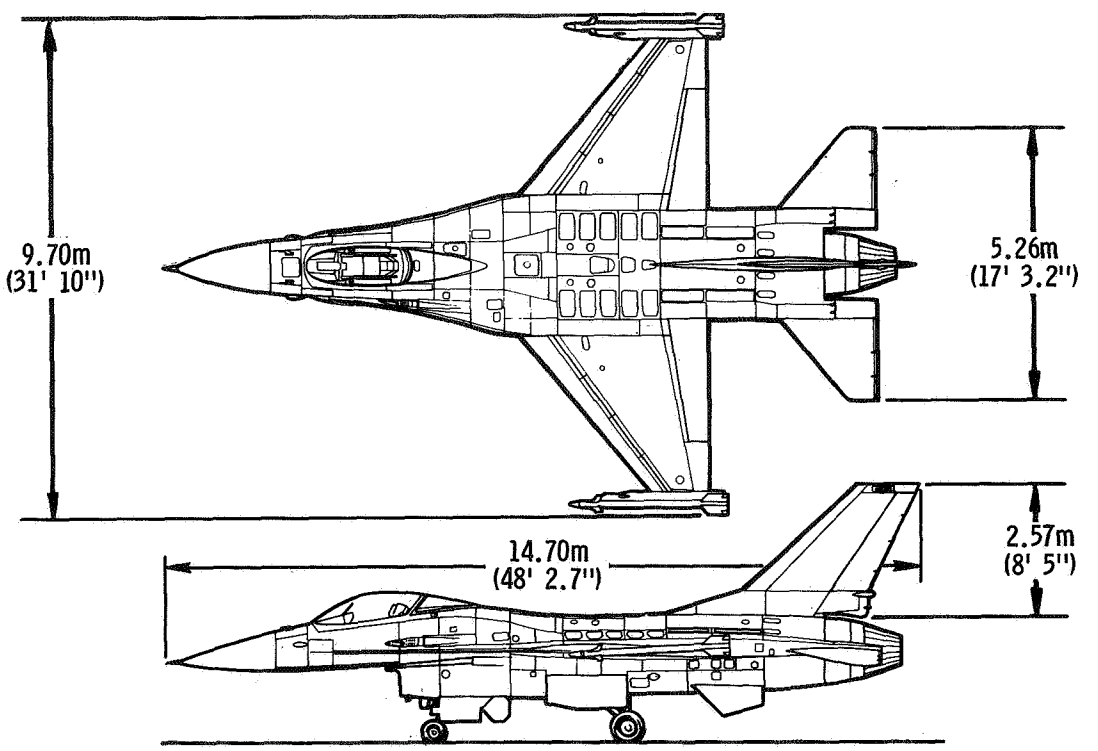

Figure 2 YF-16 Airplane

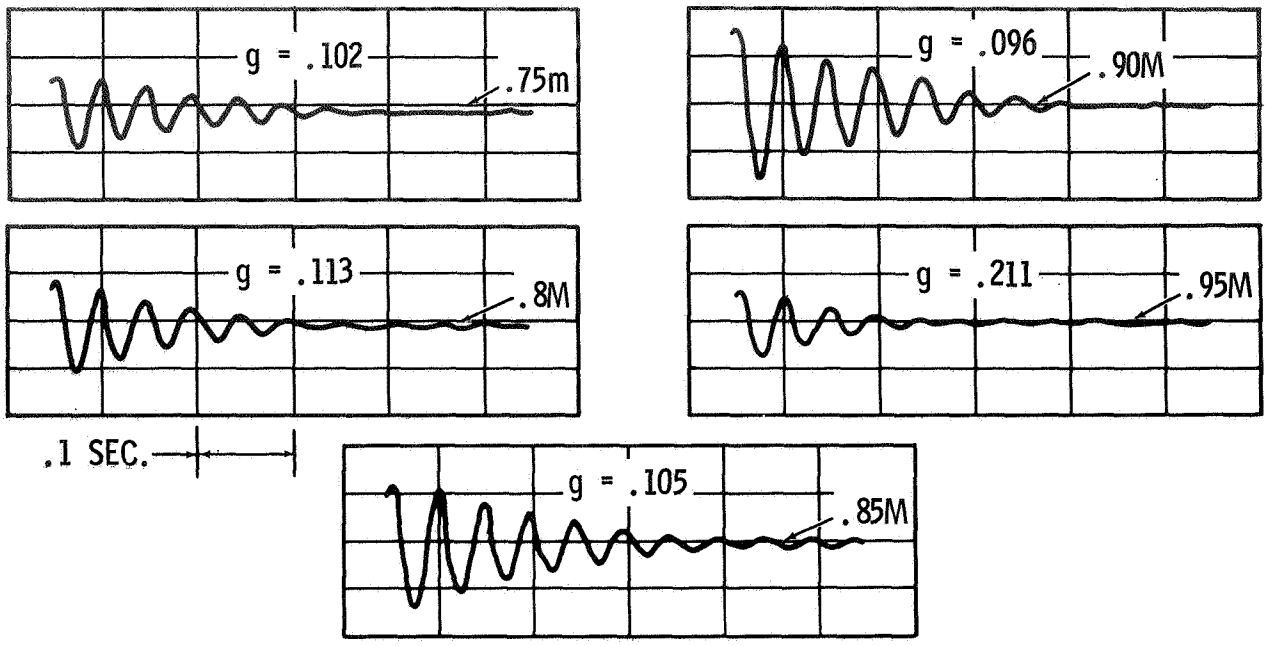

Figure 3 Model Pylon Damping

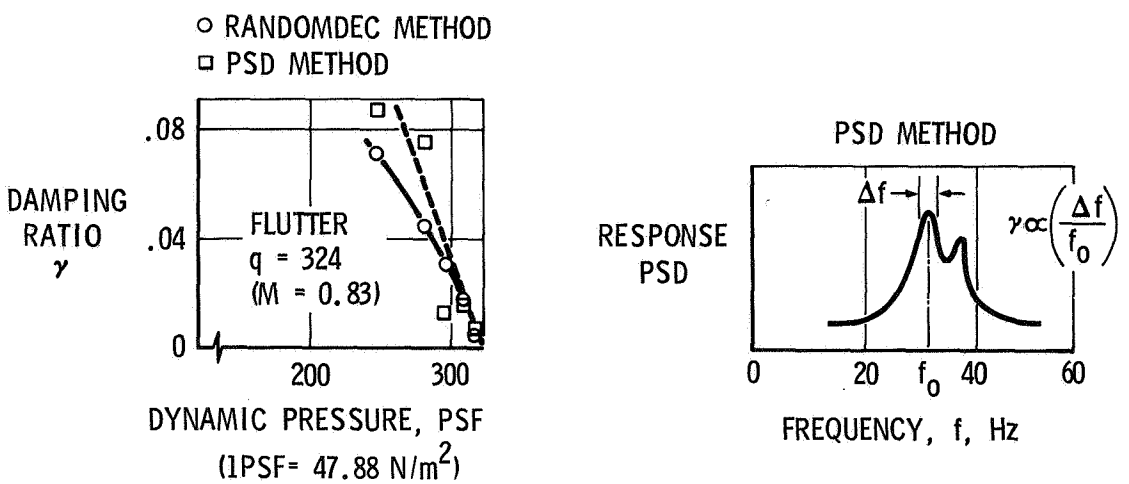

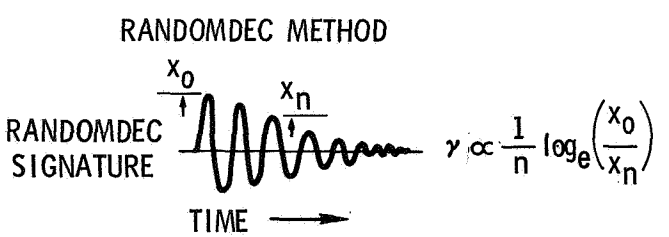

Figure 4 SST Model Damping

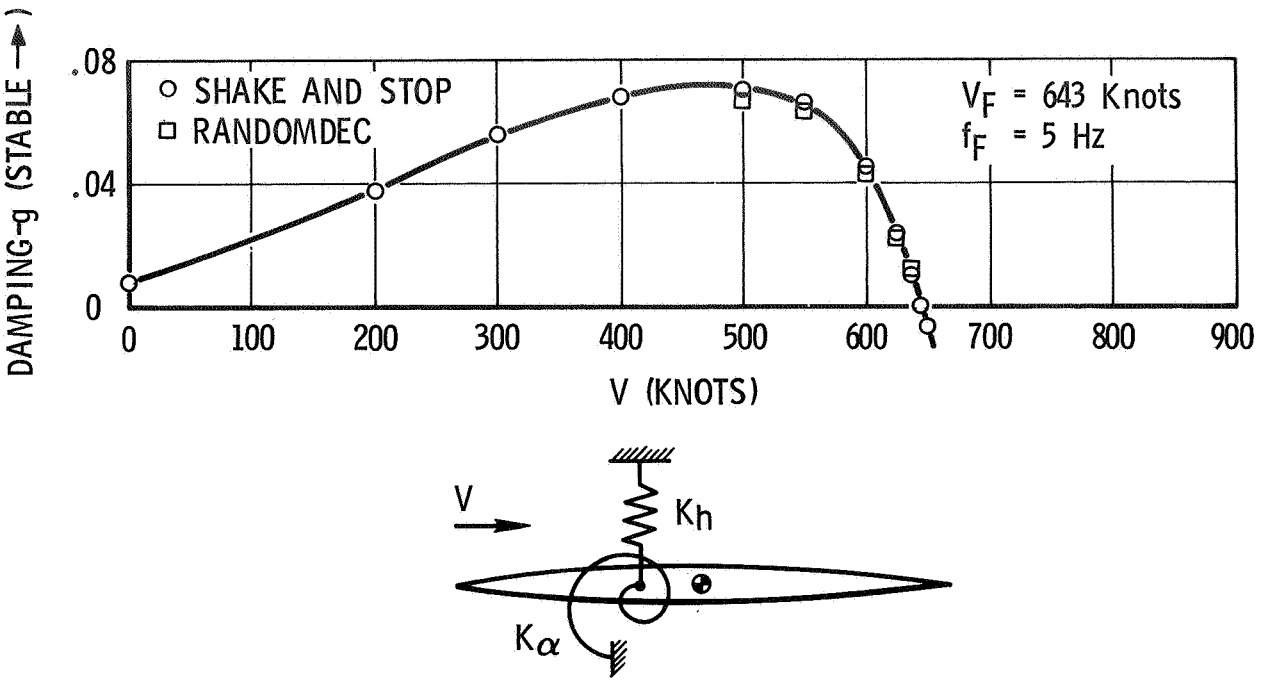

Figure 5 Analog Model Damping

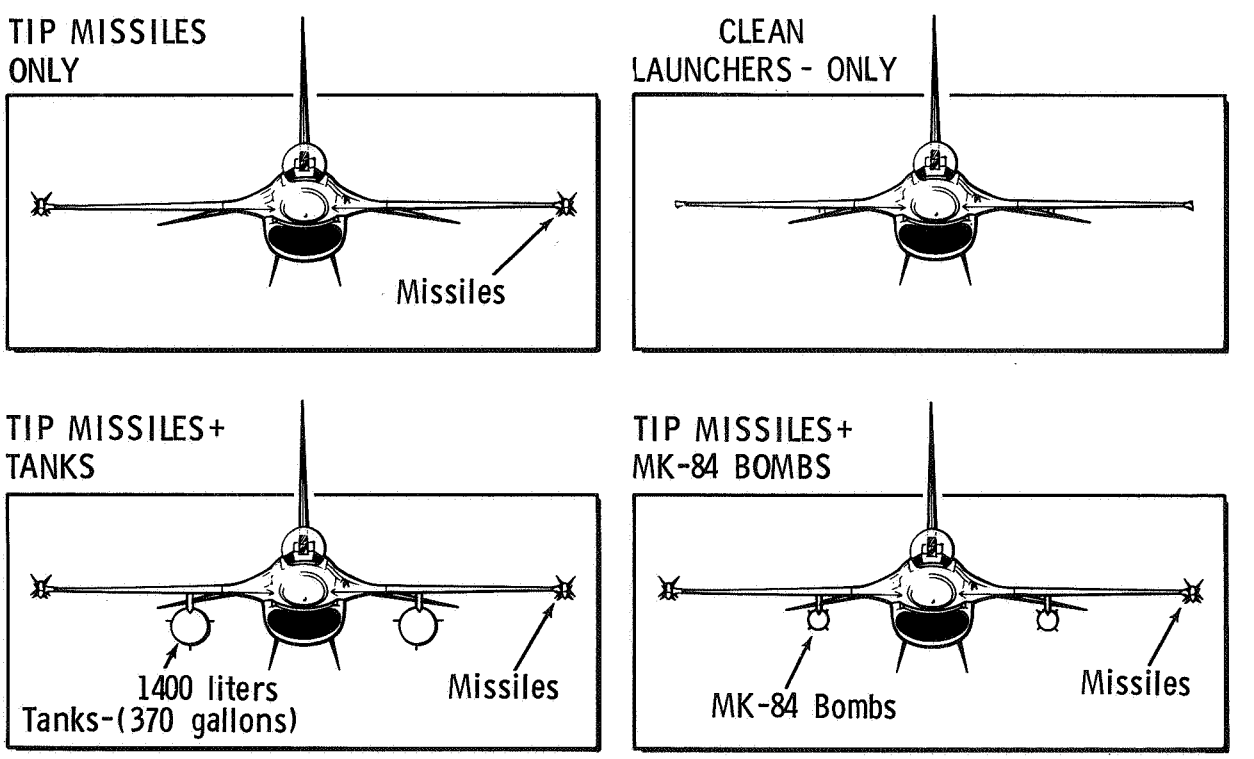

Figure 6 YF-16 Test Configurations

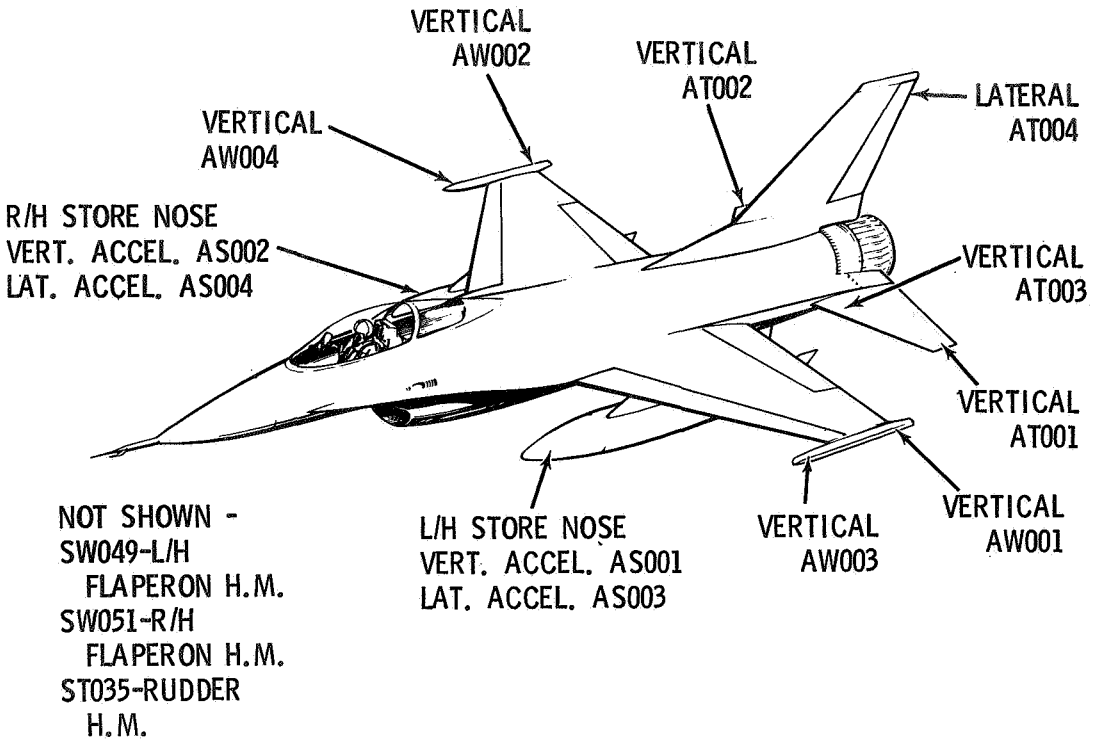

Figure 7 YF-16 Test Instrumentation

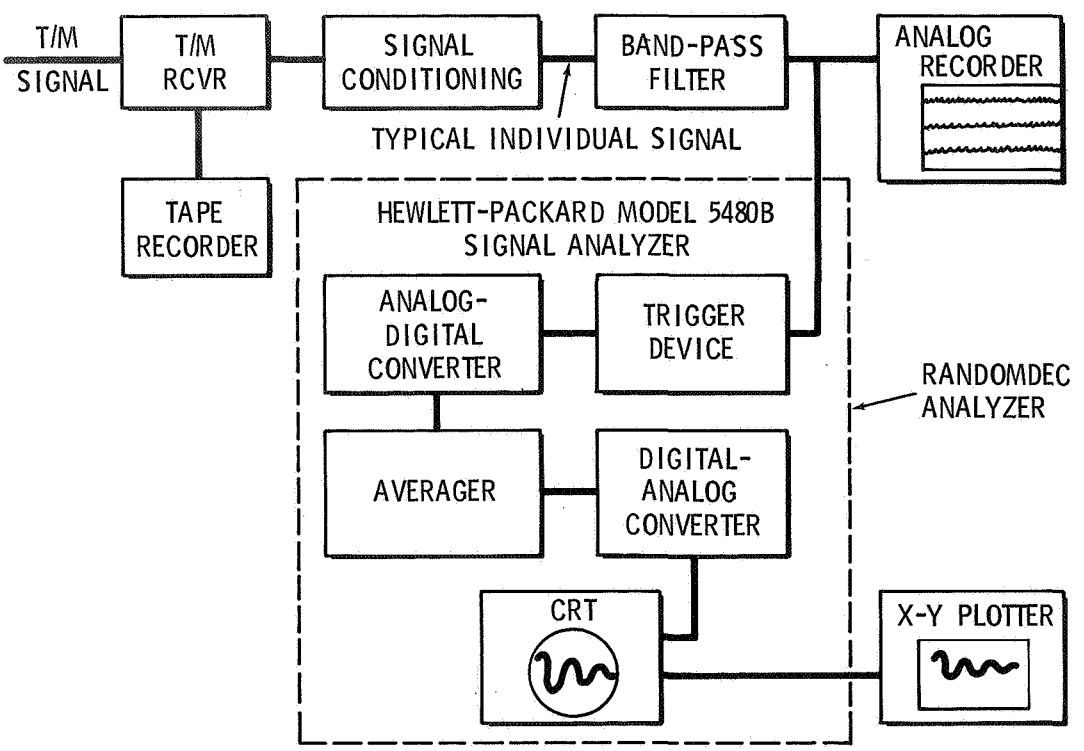

Figure 8 Random Decrement Analyzer

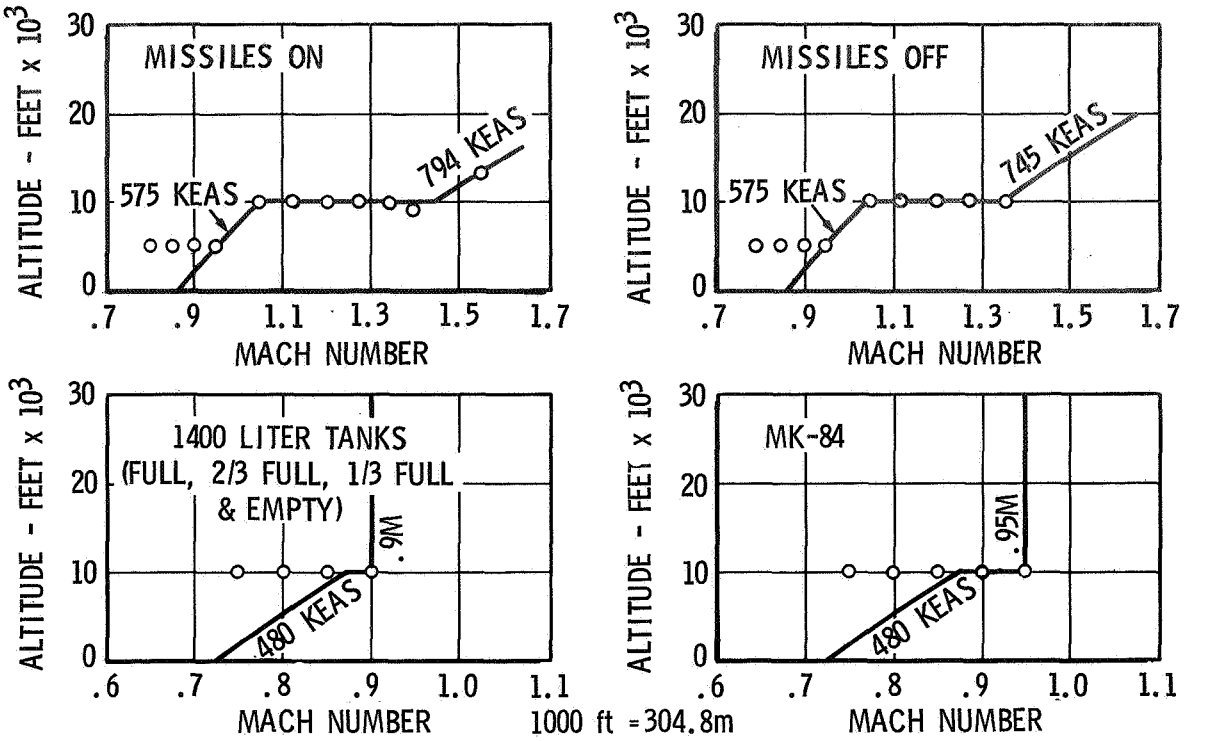

Figure 9 YF-16 Test Points

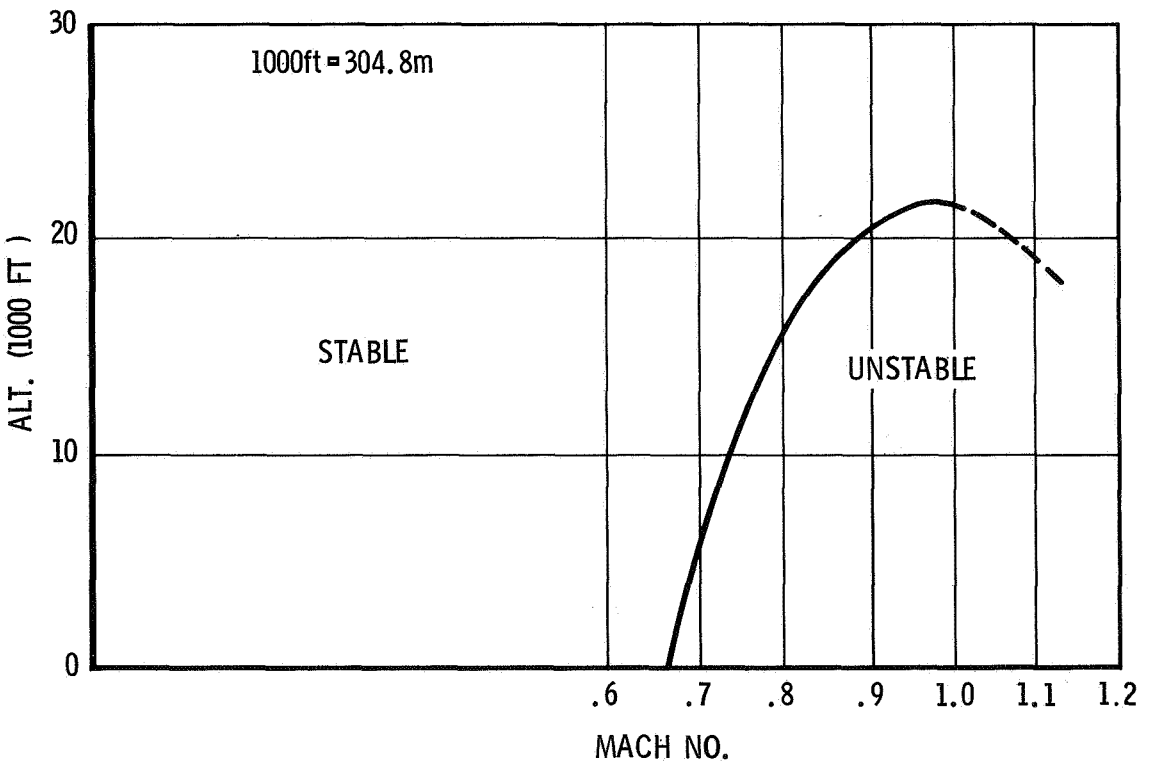

Figure 10 Control System Instability

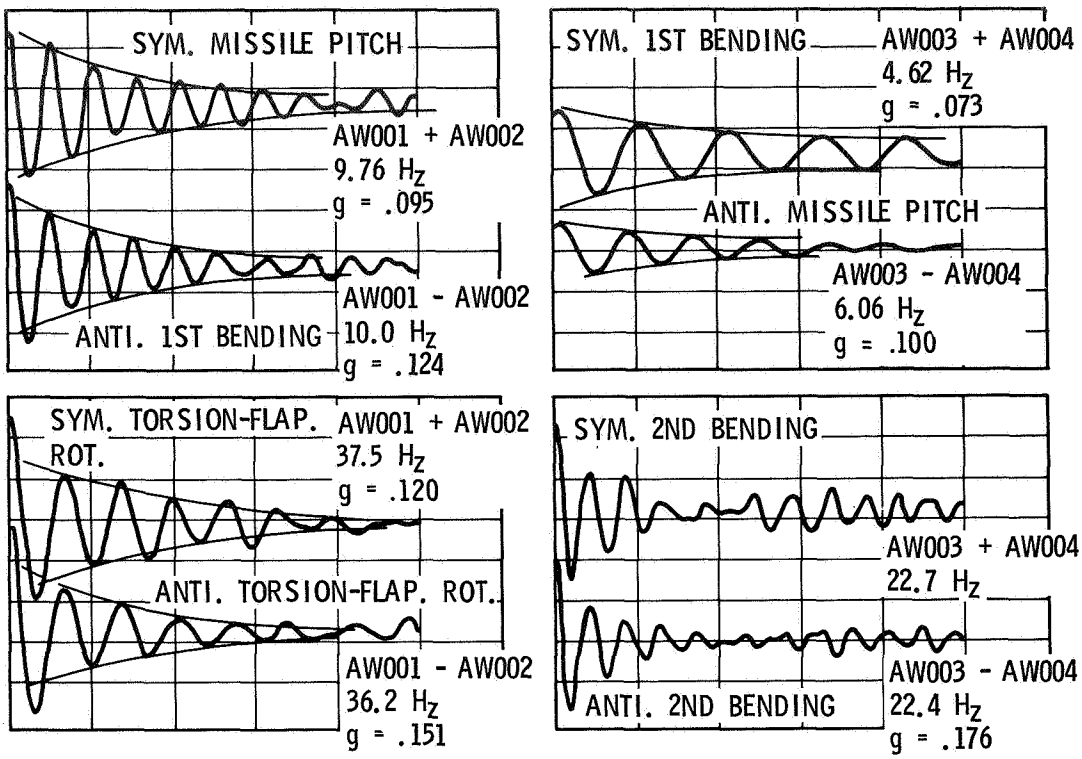

Figure 11 YF-16 Wing Decay Records - 1.34M, 3048m (10 000 Ft)

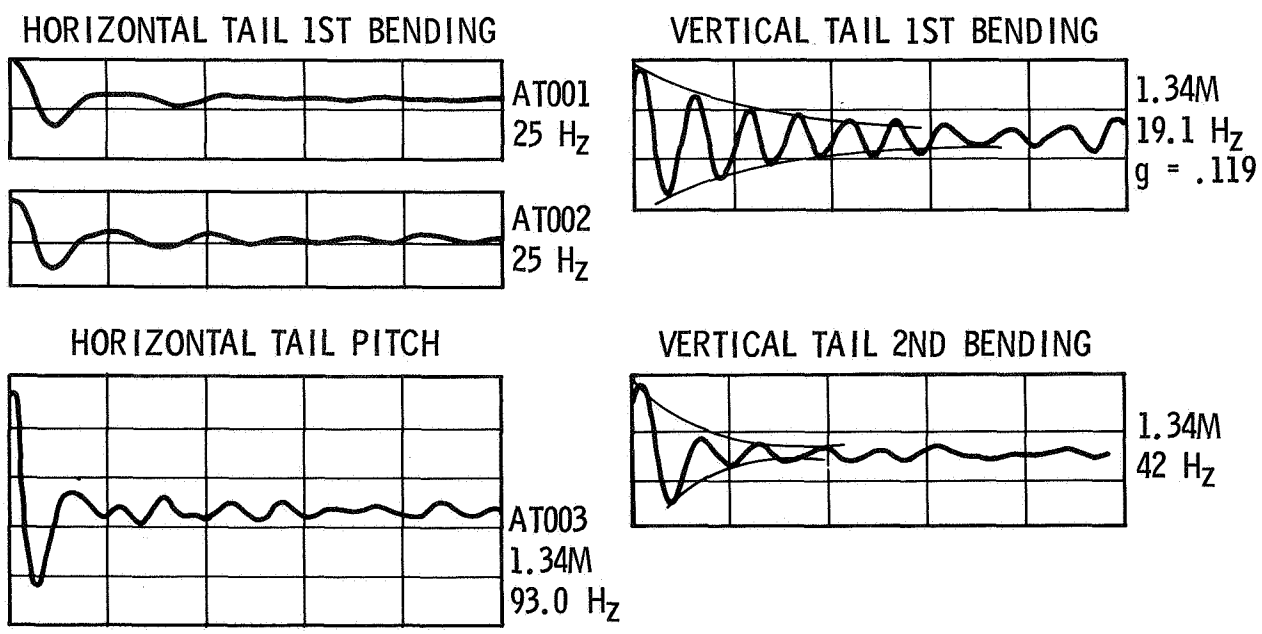

Figure 12 YF-16 Tail Decay Records - 1.34M, 3048m (10 000 Ft)

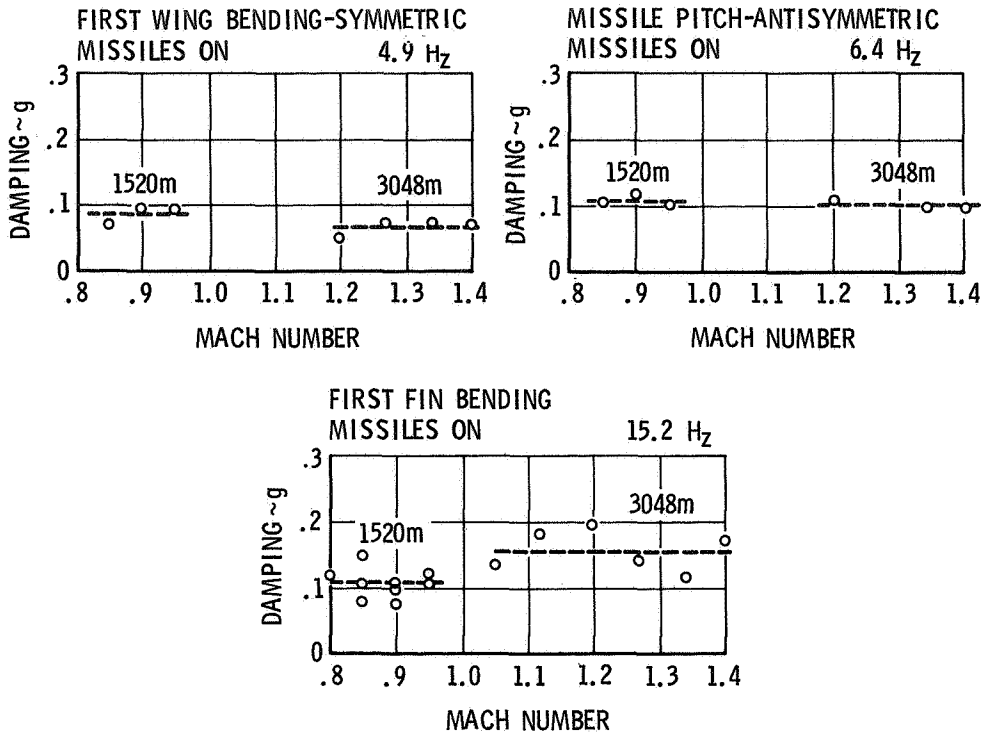

Figure 13 YF-16 Damping vs Mach Number

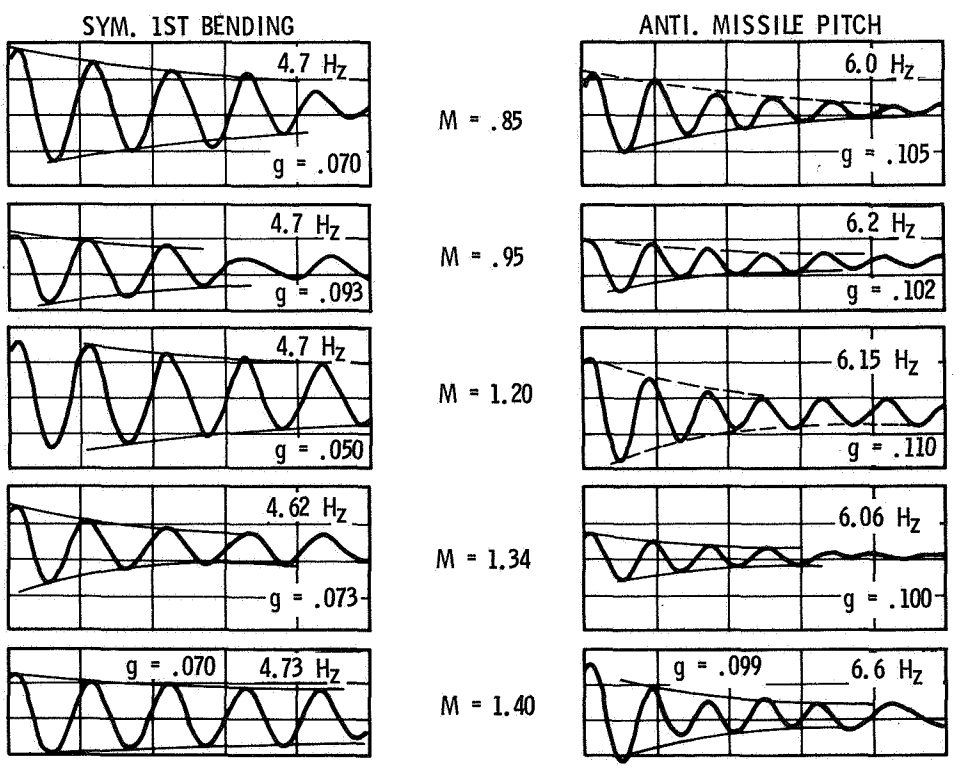

Figure 14 YF-16 Wing Decay Records

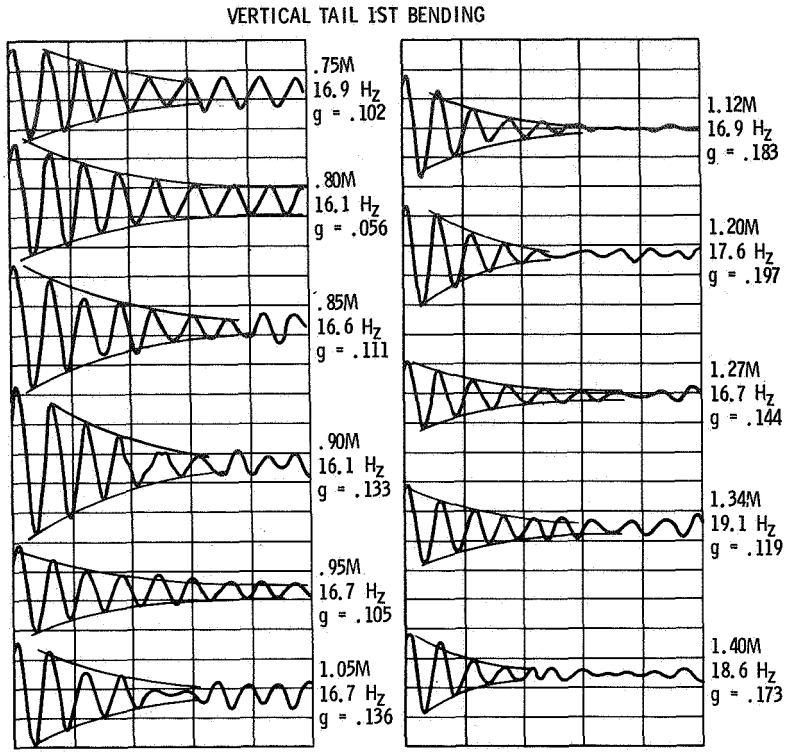

Figure 15 YF-16 Vertical Tail Decay Records

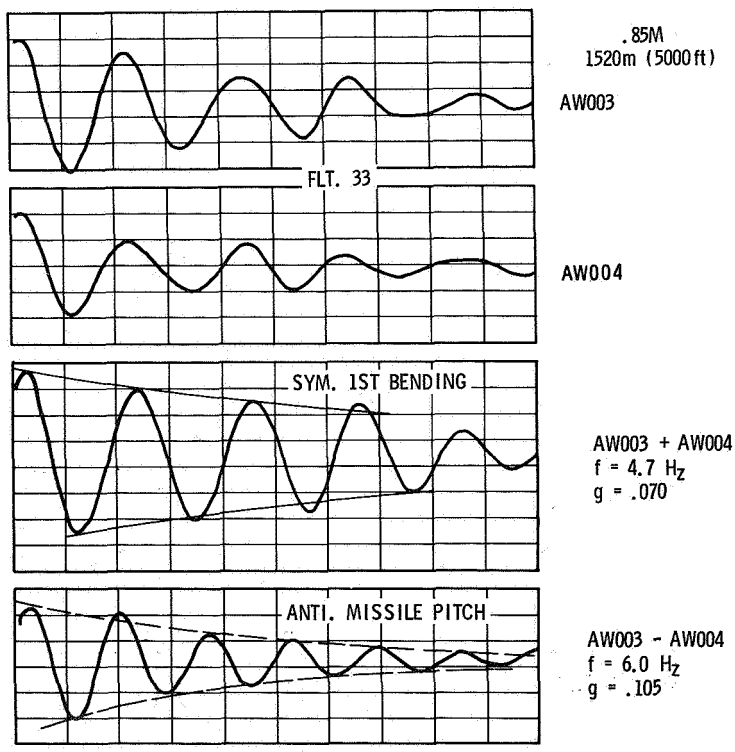

Figure 16 Symmetric and Antisymmetric Response

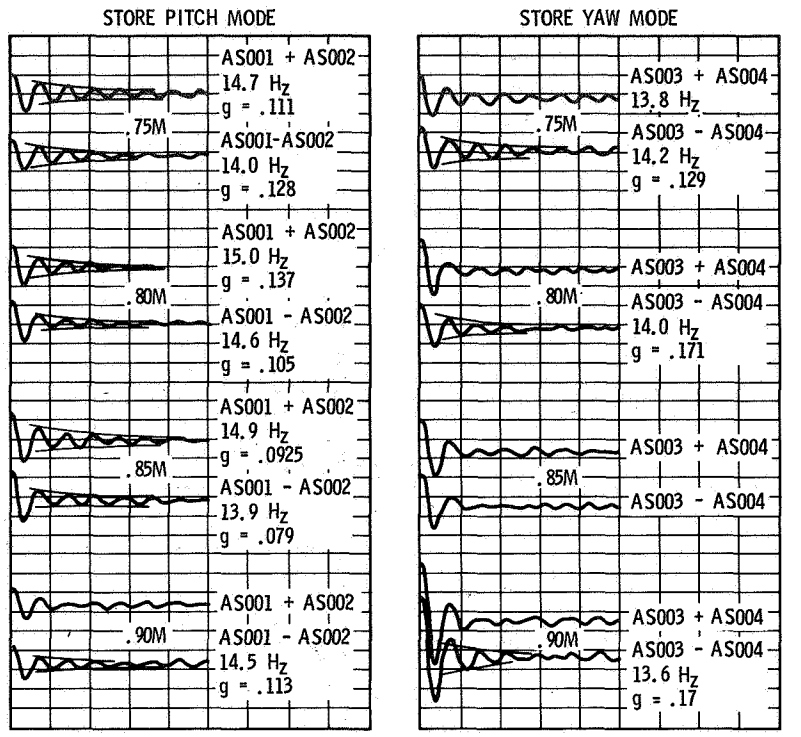

Figure 17 External Store Damping

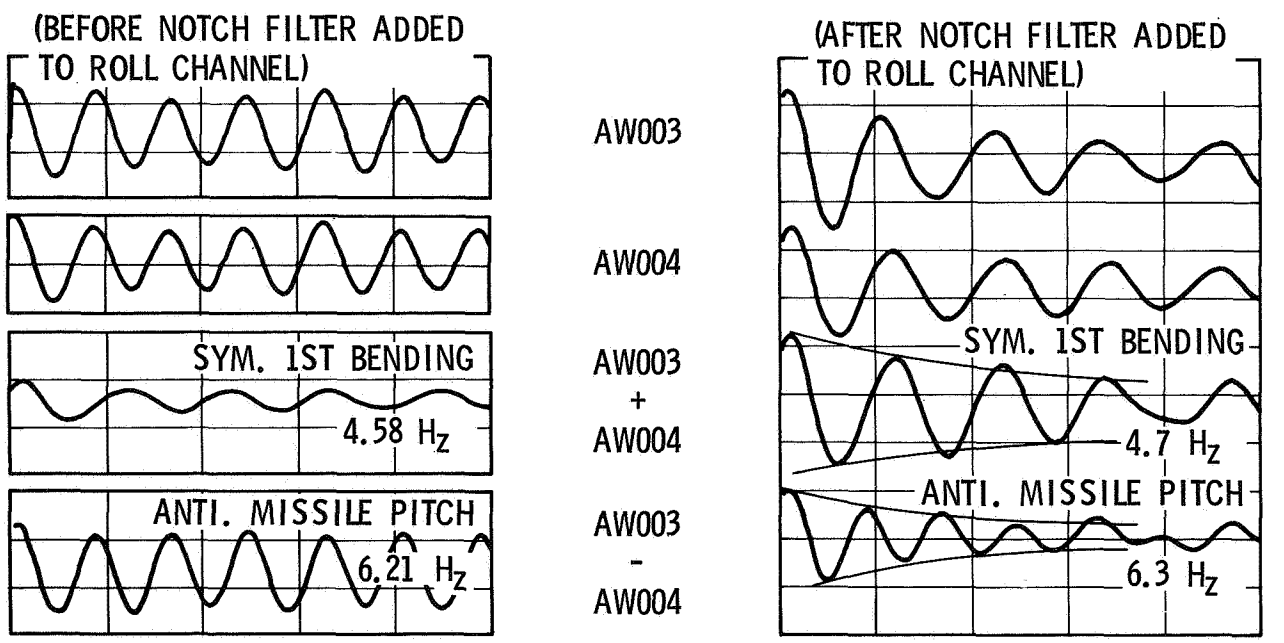

Figure 18 Effect of Notch Filter

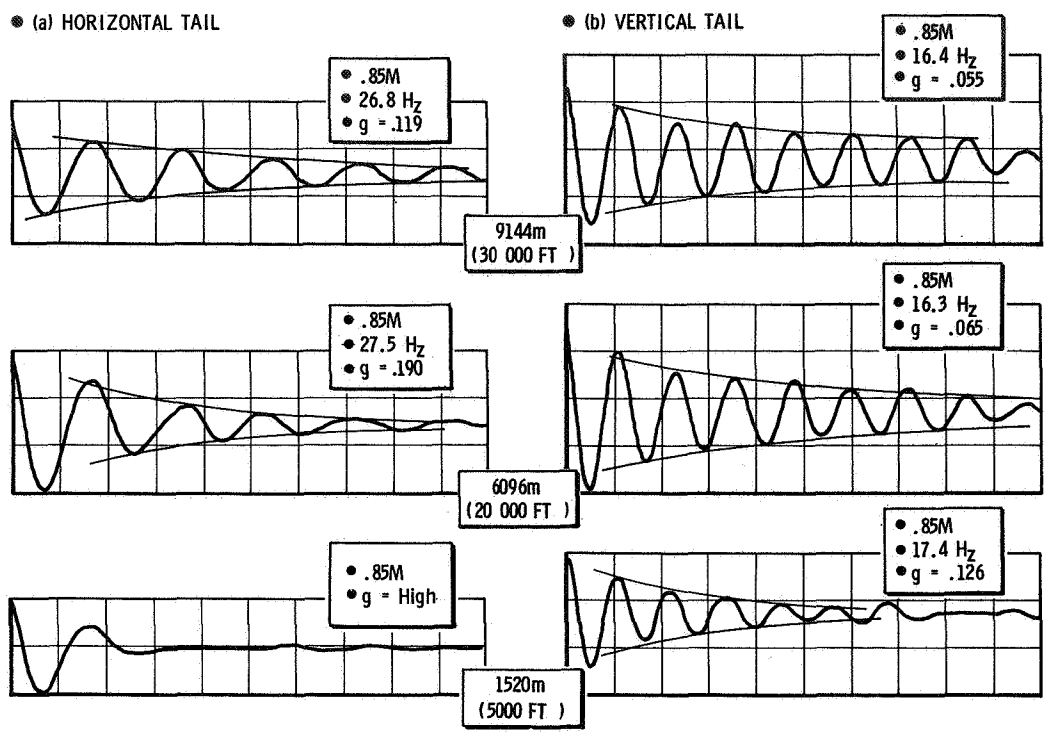

Figure 19 Tail Damping vs Altitude

INFLIGHT ROTOR STABILITY MONITOR

William A. Kuczynski
Sikorsky Aircraft Division
United Technologies Corporation

ABSTRACT

An inflight rotor stability monitor which has been developed at Sikorsky Aircraft to support stability testing of new rotorcraft is described. The monitor has as its core a damping estimation algorithm which embodies spectral analysis techniques. The interactive system is activated and controlled from a Cathode Ray Tube (CRT) and operates on-line in a flight test telemetry environment. Accurate estimates of the level of damping of critical system modes are generated within one minute of the completion of a prescribed test maneuver. The stability monitor has been used successfully during the past two years to support various Sikorsky research and development flight programs including the UTTAS, CH-53E, S-67 Fan-in-Fin, and ABC.

INTRODUCTION

One of the more difficult tasks the engineer is faced with is the identification and estimation of the level of damping of critical system modes from experimental data. His task is particularly formidable in the test environment where the pressure to make decisions quickly is high and the consequences of poor judgement may be severe. In the past, it was not uncommon for an engineer to be asked to bless the continued expansion of a test envelope with only time history oscillograph records from previous test conditions upon which to base his judgement. For well-behaved, lightly damped modes, which are sufficiently separated in frequency from other modes and forced response frequencies, real time filtering improved his capability of estimating damping levels. However, the effective use of filtering techniques required sinusoidal frequency sweep excitations or sufficient prior knowledge of the systems' characteristics to allow the use of bandpass filters. Sinusoidal sweep excitations are not always practical, particularly in flight. Also, filter rise times must be compatible with system time trends and sweeps rates in order to avoid overestimating damping because of spectrum averaging at critical frequencies. Of course, the overriding disadvantage of these techniques is that the engineer was still working with analog records which was very time consuming. Thus, most of his judgements were necessarily qualitative.

With the acquisition of the Real-Time Acquisition and Processing of Inflight Data (RAPID) system at Sikorsky Aircraft (see Reference 1) in the early 1970's, the avenue was paved for the development of improved inflight stability monitoring techniques. An inflight stability monitor was developed at Sikorsky in 1973 and has been used extensively for the past two years. It has as its core a

modal damping estimation algorithm which is based on well-known spectral analysis techniques. The advantage of spectral analysis is that a time signal is transferred to the frequency domain where modal responses are separated from each other and from steady state responses. This permits easy identification of lightly damped system modes.

There is no one task in the stability monitor procedure which was particularily difficult to develop. On the contrary, each step is quite straightforward and easily achieved by standard methods. Even the damping estimation technique is now thought to be ubiquitous in the industry (see Reference 2) though a description of it is not known to be published in the literature. The real challenge in the development of the system was to make it work in the flight test telemetry environment. This involved providing adequate flexibility and accuracy while minimizing total time required to estimate system stability.

DESCRIPTION OF INFLIGHT STABILITY MONITOR SYSTEM

The Inflight Rotor Stability Monitor is an interactive system designed to provide an on-line stability estimation capability during the envelope expansion of new rotorcraft. The core of the system is the Sikorsky Aircraft ground station, RAPID, which consists of a SYSTEMS 86 computer with a full complement of standard and special peripheral devices (see Reference 1). The monitor involves two activities, the real-time acquisition, conditioning and calibration of measurements telemetered from an aircraft and the estimation of lightly damped modes of the test article from these data. The first of these steps is a standard function of the RAPID system. The damping estimates are made with a special purpose program designed to operate in telemetry environment during the short interval of time between test conditions. The stability monitor is shown schematically in Figure 1. During a flight, data are continuously transmitted to RAPID via telemetry. When a stability test is conducted, say for example the rotorcraft is excited by a control pulse, the engineer captures a "burst" of data by activating the Telemetry program from the CRT. The entire track of data (10 measurements) are digitized and calibrated (changed from volts to engineering units) in real time and stored on a disc. The Stability Estimation Program is then activated from the CRT. The program, which will be described in detail later, is highly interactive and consists of 3 steps: (1) review of the time data, (2) identification of critical system modes, and (3) calculation of the damping of these modes. The program is very flexible and very fast with the speed largely dependent upon the user's reaction time. Plots and printouts of pertinent data are program options. Upon the completion of the data processing, the user returns control of the system to the telemetry program for acquisition of another data burst.

The attributes which were considered important during the development of the Inflight Stability Monitor were speed, flexibility, and accuracy. The time required to estimate the damping of the critical system modes was the most important consideration. Since the program is an interburst processor, if the elapsed time required to complete the analysis is appreciably greater than the

time required by the pilot to set up for the next test point, total test time is increased resulting in increased risk and cost. One minute was targeted as the maximum allowable time for the computation of a damping estimate of a single critical mode. Minimum elapsed time actually achieved is approximately 30 seconds and depends largely upon the time share demands of the computer from the other sources when the On-line Stability Monitor is in use. One minute elapsed time is generally achievable regardless of the demands on the computer.

Since the times associated with computer calculations and data transfer are measured in micro- and milli-seconds and human response times are measured in seconds and minutes, effort was focused on speeding up the time required to make decisions by the users. The most important feature of the RAPID System which allowed the achievement of a one minute elapsed time for a damping estimate is the lightpen on the CRT.

Nearly all the decisions which have to be made interactively are done so with the lightpen. Options are preprogrammed and the user simply selects the options which fulfills his requirements with the lightpen. Sufficient latitude in the options is preprogrammed to handle most situations. Selecting an option is much faster than deciding what a value should be. Also activating the computer with the lightpen is faster than activation through a keyboard input.

Flexibility was also considered important during the development of the program. The ability to select from a number of different measurements and to choose a arbitrary section of the time data from the total record were requirements. It was reasoned that one would not always know, apriori, the measurement which responds the most in a mode so the ability to choose interactively was desirable. Also definition of mode shape and sensor reliability were factors which were considered.

The accuracy of the frequency and damping estimates were of course, of great importance. Desired accuracy was achieved by specific features in the actual algorithm developed to calculate modal damping.

DESCRIPTION OF STABILITY ESTIMATION PROGRAM

The stability estimation program involves three basic tasks:

Selection of time data for analysis
Identification of lightly damped modes
Calculation of damping

Each task has a CRT display associated with it and options which are exercised interactively to accomplish the task. The program can be best described by discussing each CRT display. The displays are from a typical rotorcraft application. The rotor is excited in flight with a longitudinal stick pulse. This control impulse generates a transient response of the rotor and airframe.

The first CRT display, Figure 2, is used to scan the time data and select an appropriate section of a measurement for further processing. The display is comprised of plotted time histories, a column of options to facilitate selection of specific data for further processing and print and plot options. Time histories of four parameters are displayed at a time. The program is sized to accomodate up to twenty signals with the NEW CURVES + - option, the vehicle by which different sets of curves are brought to the screen. The section of the burst of data which is displayed can be changed with the PAGE option, + to move forward in time and - to move backward. The length of the section of data displayed is arbitrary (within limits) and prescribed in the input data. The frequencies in the data and the sample rate are important considerations in sizing these initial time history displays. Generally, these time history curves are only used to find the transient response which is necessary for the damping calculation, so good signature is not required. The user prescribes the time at which he wants to start the analysis by keying in a value TO. The start time is usually when the system transient response to the excitation is a maximum. For the example shown TO = 2.65 sec is selected. The length of the data sample which is processed is prescribed by the number of points (2^N, N is an integer) and the SAMPLE RATE FOR ANALYSIS options. The total length of the data sample is:

$$T = (\text{SAMPLE RATE})(2^N)(\Delta t)$$

where Δt is the digitizing rate. The length of data determines the fundamental frequency $\omega_f = 1/T$ Hz and the achievable resolution in the spectral analysis which is performed next. 2^N data points are used because the FFT algorithm used for the spectral analysis is computationally most efficient with this constraint. The highest frequency in the spectral analysis is

$$\omega_{max} = 1/(\text{SAMPLE RATE})(\Delta t) \quad \text{Hz}$$

and must be selected to prevent aliasing of the data. In that respect, ω_{max} must be kept conveniently higher than the preprocessing filter bandwidth.

The measurement which is to be analyzed is selected with the CHOOSE CURVE option. A zero phase shaft digital band-pass filter can be applied to the data by prescribing a positive center frequency in the FILTER option. The filter roll off and bandwidth are prescribed in the input data. In general, the filter is not needed for accurate damping estimates except for those situations where the transient response signal to noise ratio is very poor.

It is worthwhile to note that default values for all options are specified in the program imput. Thus, if the user is familiar with his system's characteristics, his only actions are to select a start time (TO) and lightpen the CONTINUE option to proceed to the next step in the analysis.

The identification of lightly damped modes is performed in the frequency domain. A Fast Fourier Transform is used to calculate the discrete Fourier Transform of the time data sample selected. The magnitude of the transform is normalized to yield Fourier coefficients and plotted versus frequency in the second CRT display (Figure 3). A simple search routine is built into the

program to select peaks in the spectrum within a predetermined frequency range (input). These frequencies are ordered by their magnitude and displayed at the right of the plot.

For rotary wing applications, the system normally responds at harmonics of the rotor rotational frequency (forced response) and at natural modal frequencies if properly excited.* Prior knowledge of the system being tested makes identification of forced responses trivial and thus permits the easy recognition of significant transient modal responses. The user selects (light-pen) the frequency of the mode for which he wants a damping estimate with the PICK FREQUENCY option. He then can proceed to the damping estimation task by exercising the CONTINUE option. Should it be obvious to the user from the Fourier Transform plot that a significant transient modal response is not present in the signal, he may return to display 1 by activating the RETURN to A option. Records of the spectral data may be obtained with the PLOT & PRINT options.

It is worthwhile to note at this juncture the value of the Fourier Transform itself in dynamic testing. There are many situations when the test engineers task is to monitor for a transient modal response caused by random excitations during test envelope expansion. The Fourier Transform is an excellent tool for detecting such responses. Of course, the shape of the resonance peaks in the Fourier Transform can also be used directly to estimate modal damping if the system modes are sufficiently separated in frequency so that a single degree of freedom is approximated.

In the example shown in Figure 3, there are two modal responses, one at 7.0 Hz and the other at 6.0 Hz. The former is primarily a SAS/flapping mode and the latter a blade edgewise mode. The peaks at 4.9 H_z and 9.8 H_z are forced responses at one and two per rotor rev.

Before continuing to the description of the third CRT display it is timely to discuss the actual damping estimation procedure. Knowledge of the technique is a prerequisite to a meaningful discussion of the data on the third display.

Damping Estimation Procedure

Assume that there exists a time history of a signal which contains the transient response of one or more natural modes of a system. Assume further that the system is approximately linear. The damping of a mode (as defined by its frequency ω_o), can be estimated as follows. A percentage of the total data sample which comprises an integer number of cycles of the frequency of interest is first selected. The discrete Fourier coefficient $F(\omega_o)$ of this data sample is then calculated. Repeating this computation for similar blocks of data which are successively displaced in time generates the function $F(\omega_o)$

*An exception is when the system stability is governed by periodic coefficients in which case the modal frequencies can be at integer multiples of 1/2 the rotor frequency.

versus time. An estimate of the damping (ζ) of the mode is the slope of the curve ln $F(\omega_o)$ vs time divided by the frequency ω_o.

If one accepts less than rigorous mathematics, the appropriateness of this procedure can be illustrated. Consider the damped sinusoidal function

$$f(t)=Ae^{-\zeta\omega_o t}\sin(\omega_o t+\phi)$$

The Fourier sine and cosine coefficients for N cycles of data starting at an arbitrary time t_o are defined as

$$a_1 = \frac{\omega_o}{\pi N}\int_{t_o}^{t_o+\frac{2\pi N}{\omega_o}} f(t)\cos(\omega_o t)dt$$

$$b_1 = \frac{\omega_o}{\pi N}\int_{t_o}^{t_o+\frac{2\pi N}{\omega_o}} f(t)\sin(\omega_o t)dt$$

Expanding these integrals and manipulating intensively, we arrive at two relatively simple expressions for a_1 and b_1:

$$a_1 = \frac{Ae^{-\zeta\omega_o t_o}}{2\pi N}(1-e^{-\zeta 2\pi N})\left\{\frac{\sin\phi}{\zeta} + \frac{[\zeta\sin(2\omega_o t_o+\phi)+2\cos(2\omega_o t_o+\phi)]}{\zeta^2+4}\right\}$$

$$b_1 = \frac{Ae^{-\zeta\omega_o t_o}}{2\pi N}(1-e^{-\zeta 2\pi N})\left\{\frac{\cos\phi}{\zeta} + \frac{[-\zeta\cos(2\omega_o t_o+\phi)+2\sin(2\omega_o t_o+\phi)]}{\zeta^2+4}\right\}$$

These can be combined to compute the magnitude of the Fourier coefficient

$$c_1 = \frac{Ae^{-\zeta\omega_o t_o}}{2\pi N}(1-e^{-\zeta 2\pi N})\left[\frac{1}{\zeta^2} + \frac{1}{\zeta^2+4} - \frac{2}{\zeta^2+4}\cos(2\omega_o t_o+2\phi)\right.$$

$$\left. + \frac{4}{\zeta(\zeta^2+4)}\sin(2\omega_o t_o+2\phi)\right]^{\frac{1}{2}}$$

Rearranging, we see that c_1 has the same form as the original function f(t); i.e.,

$$c_1 = Ke^{-\zeta\omega_o t_o}\sin(2\omega_o t_o+\Phi)$$

where K is a constant and Φ a phase angle which is of no concern. Thus, the envelope of decay of the Fourier coefficient c_1 is exactly the same as that of f(t). In the stability estimation program, the curve ln c_1 vs t_o is developed and the linear slope divided by the modal frequency to obtain an estimation of f.

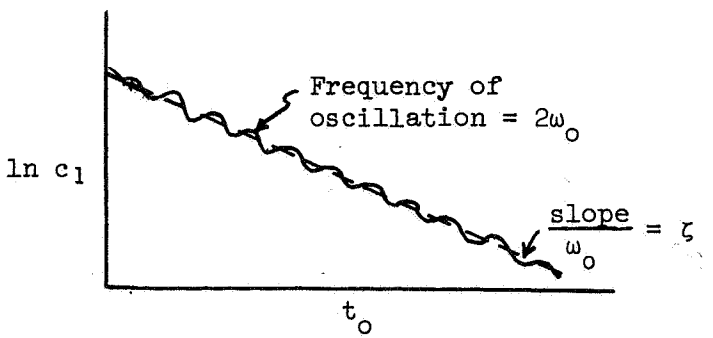

Inaccuracies in the Damping Estimate

The major problem which is encountered in the damping estimation procedure arises because a typical time history response is composed of responses at several frequencies. Since finite length data samples are processed, frequency interaction occurs when the Fourier coefficients are calculated. The interaction is commonly called leakage and can be illustrated quite easily. If you calculate the Fourier transform of a simple sine function f(t) = sin $\omega_o t$ for a data sample of finite length, it will have the following form:

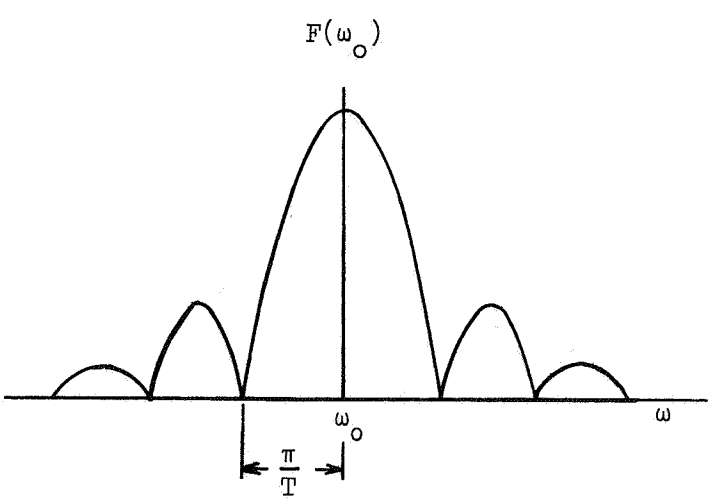

The maximum value of the transform will occur when $\omega = \omega_o$ and the sidelobes will be zero when

$$\omega - \omega_o = \frac{n\pi}{T} \quad (n = 1, 2, 3, \ldots)$$

If a signal contains two or more frequencies, the Fourier Transform is the summation of the transforms at each frequency. For example, the transforms of two sine waves having frequencies ω_o and ω_1 are sketched below.

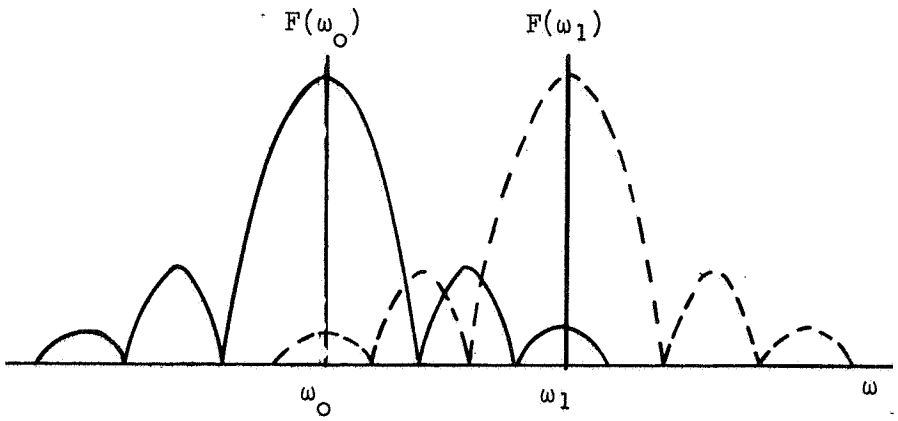

It can be seen that when summed, the sidelobs from one transform will affect the transform at the other frequency. This is exactly the phenomenon that occurs when the damping of a mode is computed when other frequencies are present in the time history. For many cases, the leakage has minimal effect; the frequencies are well separated, the magnitude of the response at the frequency of interest is large compared to other responses or the data sample is of sufficient length to minimize the magnitudes of the sidelobes. Difficulties arise when two or more frequencies are very close to each other or the magnitude of the modal response is small compared to other system responses. For the case of two frequencies which are close, the length of the data system can be adjusted so that the sidelobe from one frequency is zero at the other frequency, viz,

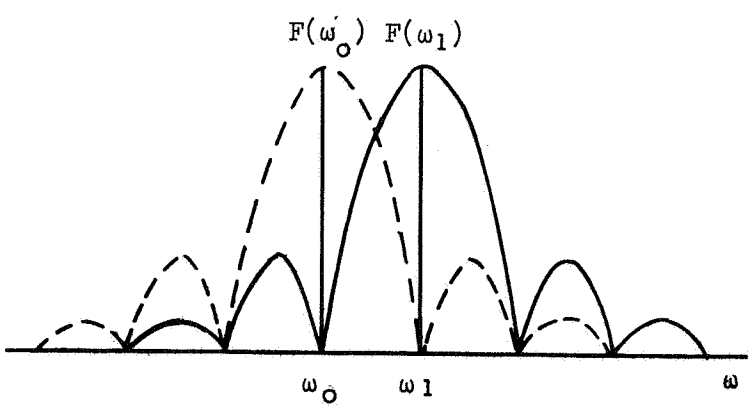

For this example, the Fourier analysis at ω_o is unaffected by the response at ω_1 and vice versa. For three or more frequencies which are close, the length of the data sample required to achieve similar decoupling may be impractical. For these cases, prefiltering of the data with low, high or bandpass digital filters may be required. Since filters have associated rise times, the damping estimates may have to be corrected accordingly. Another technique is to pass the data through a time window such as a Hanning window as a part of the damping estimation procedure. The effect of the window is to increase the rate of roll-off of the sidelobes at the expense of broading the main lobe.

Though all of these treatments of the data are possible, our experience has shown the satisfactory results are almost always achieved utilizing only the simple adjustment of sample length to decouple the frequency of interest from its major competing frequency.

With a general knowledge of the procedure used to estimate the damping of a mode, we are in a position to discuss the steps leading to the actual calculation. After a frequency has been selected from the second CRT display, an initial percentage (program input data) of the time signal is selected to form the data sample for the damping calculation. The frequency of the mode is then corrected. This is necessary because the FFT produces only 2^{N-1} spectral lines and the actual frequency of the mode can be expected to be between two lines. The adjustment of the frequency is accomplished by maximizing the magnitude of the Fourier coefficient as a function of frequency in the vicinity of the transform frequency. Very fine frequency changes are made by adjusting the length of the data sample by one point at a time. Thus, a curve of amplitude versus frequency is developed; i.e.,

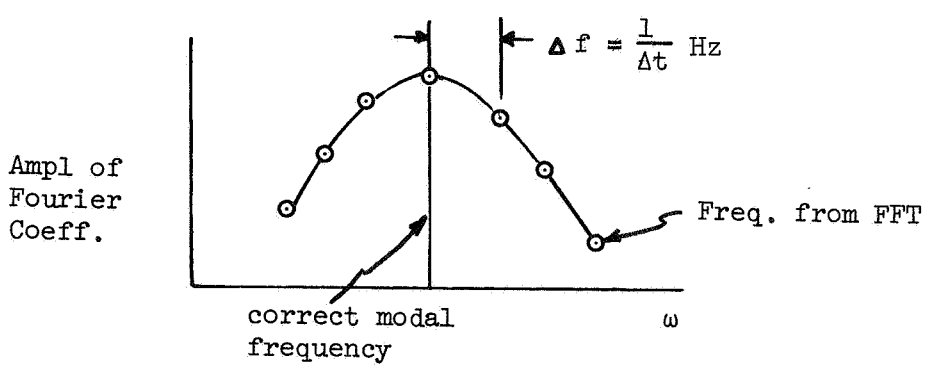

and the corrected modal frequency determined. This same procedure is then applied to the frequency of the largest response in the signal within the designated frequency range and the sample length further adjusted to minimize the interaction of the two frequencies.

After these preparations are complete, the damping of the mode is calculated. The final CRT display (Figures 4 & 5) presents the estimated modal damping and data with which to judge its accuracy. Two figures are shown, one for each of the modes identified from the Fourier Transform. The display consists of a time history plot of the time data and a plot of the natural log of the Fourier coefficient versus time. Backtracking momentarily, it is recalled that the LOG_e (FC) curve is developed by performing repetative Fourier analyses of a fixed percentage of the total data sample which moves with time. For the examples shown approximately 70% of the record length formed the data sample which moved from t = 2.65 to t = 3.19, or 0.54 seconds.

As discussed earlier, the linear slope of the LOG_e (F.C.) vs time curve divided by the modal frequency is the modal damping. As a general rule, the more linear this curve, the better the damping estimate. In the right hand column of the display are printed the corrected modal frequency, the modal damping in decimal form and the standard deviation of the least squares linear curve fit through the Fourier analysis curve. The deviation is used as a measure of the accuracy of the damping estimate. There are occasions when it is obvious from the Fourier coefficient plot that the entire curve should not have been used for the damping estimate. Typical examples are starting the analysis before the transient response has built up to its maximum value or continuing the analysis beyond a time when the signal to noise ratio is acceptable. For such conditions, the EDIT feature can be used to prescribe the beginning (T0) and end (T1) of the Fourier coefficient curve for the damping estimate. When either T0 and/or T1 are changed, the damping and standard deviation are automatically updated.

Several options are available to the user after he has completed his review of the damping estimate. There are the standard plot and print options which provide hard copy of pertinent data. The user may return to the Fourier Transform display (CHOOSE NEW W) to select another frequency for a damping estimate, or he may return to display 1 (CHOOSE NEW CURVES) to process another measurement or he may return to the telemetry program (RETURN TO T/M) to record another burst of data.

CONCLUDING REMARKS

During the past two years, the applications of the Inflight Stability Monitor at Sikorsky have been many. The first on-line application was the expansion of the CH-53E tail rotor stability envelope on a whirl stand. The estimated saving in test time on that program was 80% over the then accepted stability test techniques. Since that beginning, the system has been used to support the S-67 Blackhawk Fan-in-Fin, the UTTAS, the CH-53E, and ABC flight test programs. Confidence in the technique has grown and the system is fast becoming a standard tool for stability testing during aircraft development.

The stability estimation program has also received extensive use as an off-line diagnostic and data processing tool. It is operated off-line in RAPID in exactly the same way as it is on-line, with the source of time data an analog tape rather than telemetry. Off-line applications are typically modal damping calculations, mode shape definition and harmonic and spectral analyses. The program also receives extensive use as a post processor of time history data from analytical rotor simulation programs. For these applications at Sikorsky, a UNIVAC 1110 computer version of the program is available which is coupled with the simulation program. The total system is also a natural application for wind tunnel tests, especially if the facility has a dedicated digital computer.

REFERENCES

1. RAPID--A Data Acquisition and Processing System for Flight Test Cost and Schedule Improvement, Victor G. Berecz, Presented at the 30th Annual National Forum of the American Helicopter Society, Washington, D.C., May, 1974.

2. Integrated Rotor/Body Loads Prediction, R. M. Carlson, A. W. Kerr, Presented at the AGARD Specialists Meeting on Helicopter Rotor Loads and Prediction Methods, Milan, Italy, March 30-31, 1973.

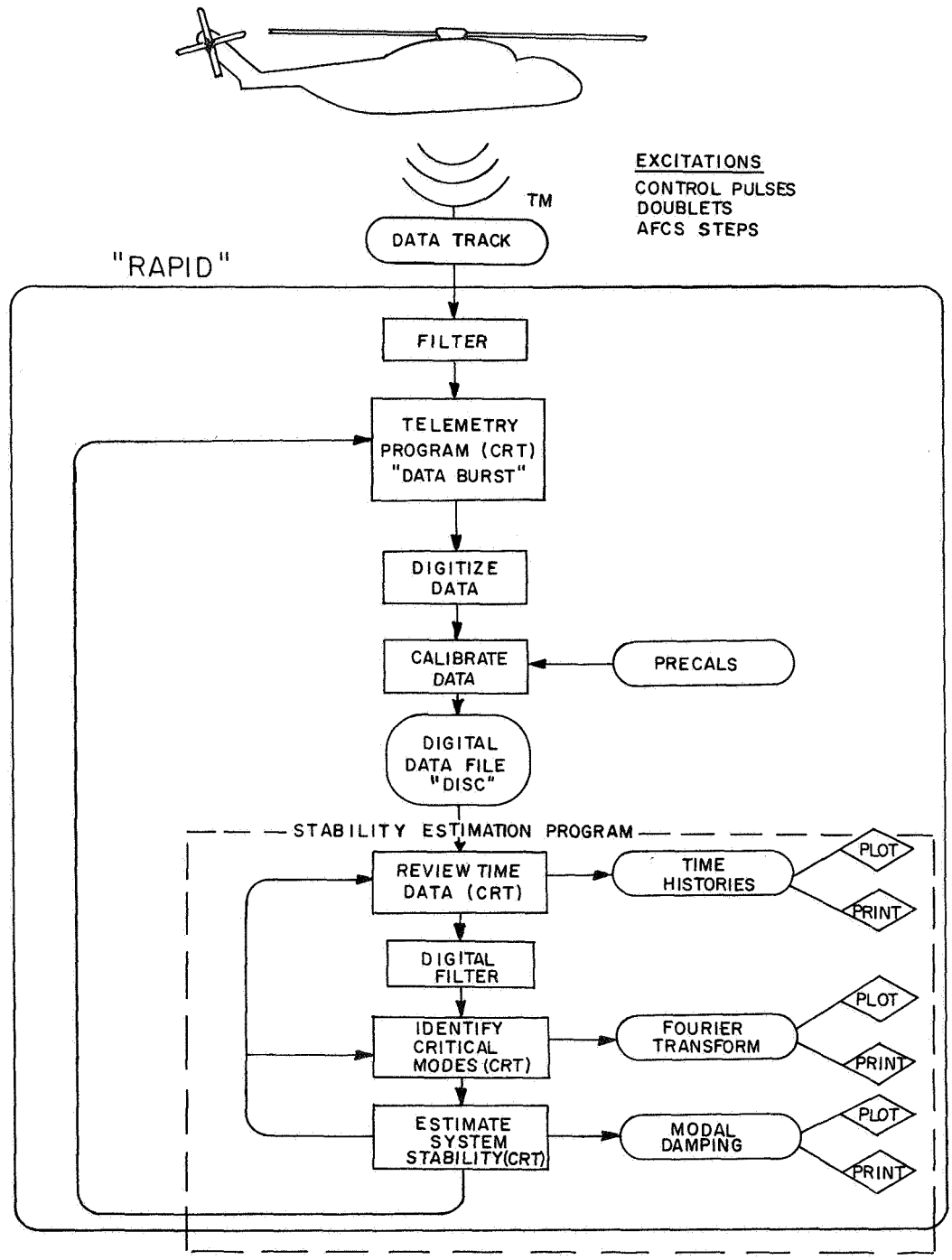

Figure 1 Inflight Rotor Stability Monitor Flow Chart.

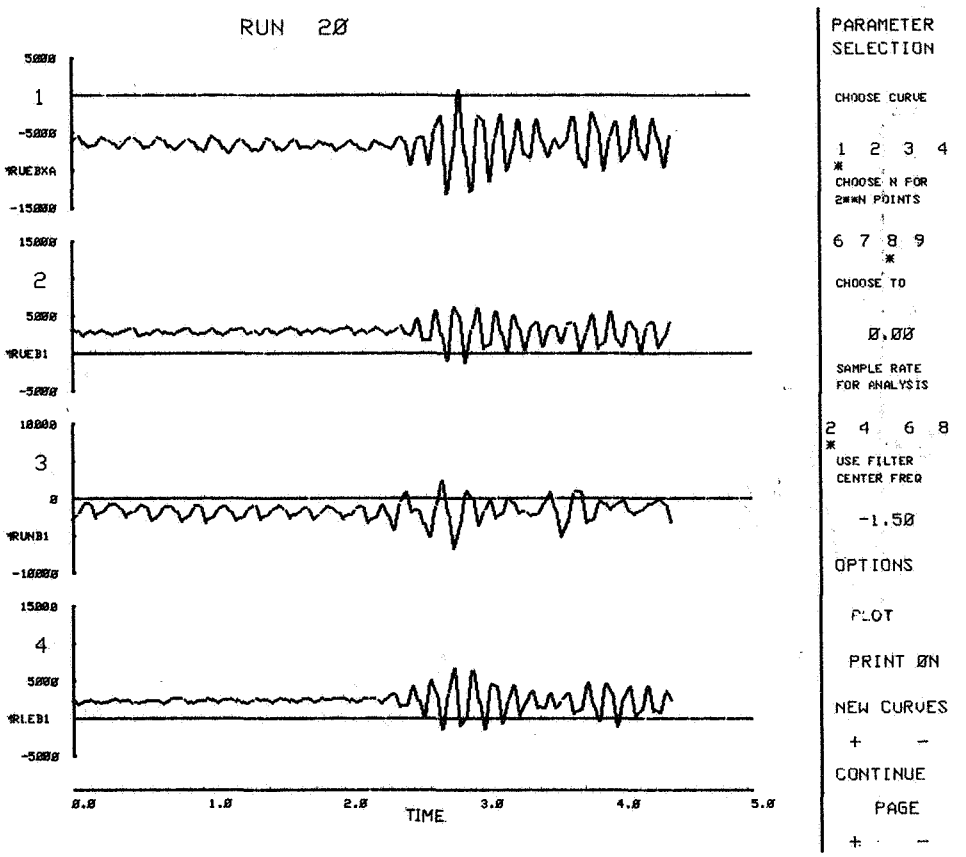

Figure 2 CRT Display 1, Time History Data.

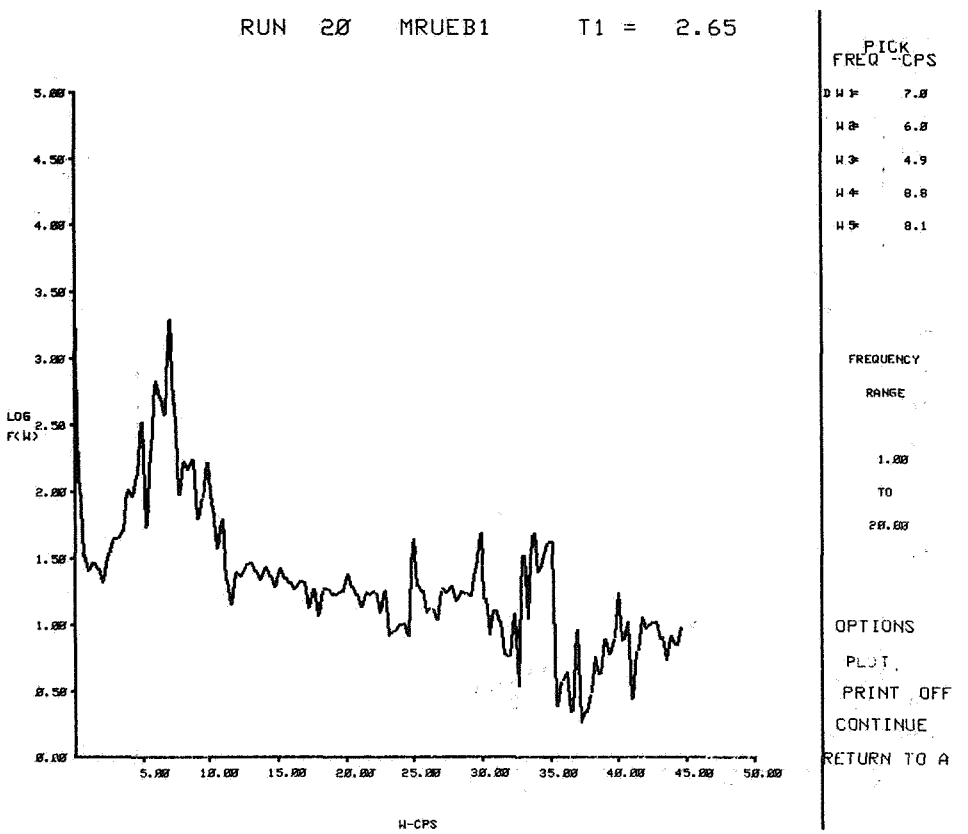

Figure 3 CRT Display 2, Magnitude of Fourier Transform. (1 cps = 1 Hz.)

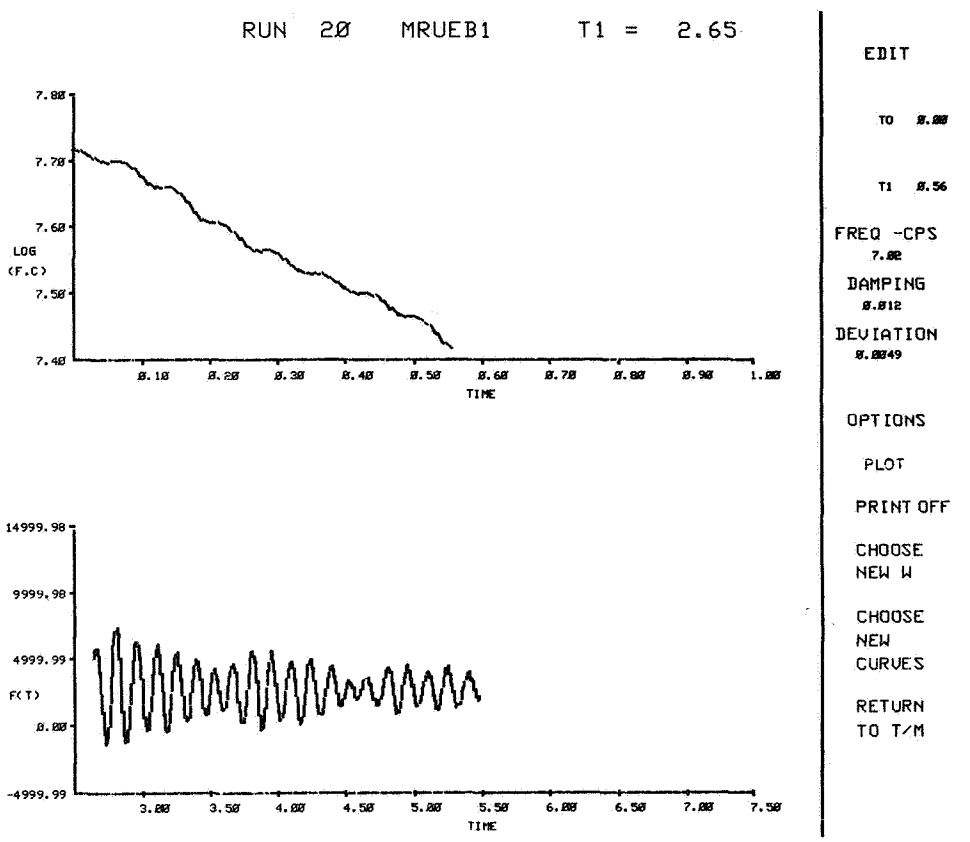

Figure 4 CRT Display 3. Modal Damping Estimate, ω = 7.02 Hz.

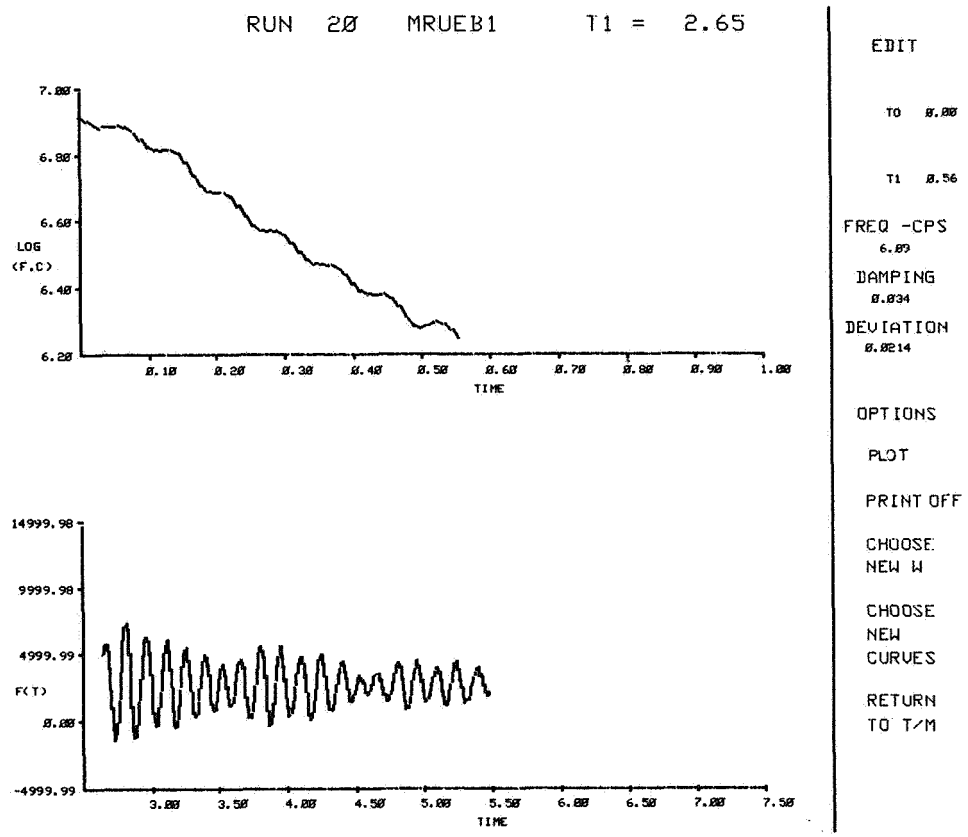

Figure 5 Modal Damping Estimate, ω = 6.09 Hz.

INVESTIGATION OF AEROELASTIC STABILITY PHENOMENA OF A HELICOPTER BY IN-FLIGHT SHAKE TEST

Wen-Liu Miao, W. Thomas Edwards, and David E. Brandt
Boeing Vertol Company

ABSTRACT

The aeroelastically stable Boeing YUH-61A helicopter was developed through a systematic program of configuration analysis and model testing which has resulted in a successful flight test program. The analytical capability of the helicopter stability program, C-56, is discussed. The parameters which are found to be critical to the air resonance characteristics of the soft in-plane hingeless rotor systems are detailed.

A summary of two model test programs, a 1/13.8 Froude-scaled BO-105 model and a 1.67 meter (5.5 foot) diameter Froude-scaled YUH-61A model, are presented. Emphasis is placed on the selection of the final parameters which were incorporated in the full scale YUH-61A helicopter, and model test data for this configuration are shown.

The actual test results of the YUH-61A air resonance in-flight shake test stability are then presented. This includes a concise description of the test setup, which employs the Grumman Automated Telemetry System (ATS), the test technique for recording in-flight stability, and the test procedure used to demonstrate favorable stability characteristics with no in-plane damping augmentation (lag damper removed). The data illustrating the stability trend of air resonance with forward speed and the stability trend of ground resonance for percent airborne are presented.

INTRODUCTION

The successful development of a helicopter with a soft in-plane hingeless rotor system requires that certain potential aeroelastic stability problems be examined, in particular the air and ground resonance phenomena. Both air and ground resonance are coupled rotor/airframe instabilities which may occur when the natural aircraft body pitch or roll frequency, involving hub motion, is equal to or close to the difference between rotor speed and the in-plane natural frequency. However, with the proper choice of certain critical rotor parameters, such as, blade precone, pitch-flap coupling, pitch-lag coupling, control system stiffness, and blade in-plane natural frequency, the stability of the coupled rotor/airframe can be controlled. This has already been demonstrated with the Boeing Messerschmitt-Boelkow-Blohm BO-105 helicopter.

For the development of the Boeing Vertol YUH-61A helicopter, a systematic approach was made to the aeroelastic design of the aircraft which results in the optimization of the critical parameters. The approach entails:

Computer analysis of stability characteristics

Preliminary model testing, to correlate analysis and determine the most influential stability parameters

Detailed model testing of the proposed configuration

Flight envelope expansion of the full scale helicopter by determining degree of stability through in-flight shake test

The YUH-61A stability testing was performed at the Grumman Aerospace Corporation facility at Calverton, Long Island. To expedite this work and to promote minimum risk, the Grumman Automated Telemetry System (ATS) was used to provide on-line real-time analysis of the data.

Many of the model test data were presented in previous papers. For the sake of completeness, portions of those works are summarized herein.

The authors express their appreciation to W. F. White and C. E. Hammond of the U. S. Army Air Mobility Research and Development Laboratory at Langley for their help with processing and verifying the YUH-61A flight test data with the moving block/Randomdec computer program.

ANALYSIS

A method for determining the ground resonance characteristics of a helicopter with an articulated rotor (Reference 1) has existed for over thirty years. Analyses of this type considered only the resonance of the forces generated by blade cyclic in-plane motions with a single effective hub mass restrained to move in two translational directions without aerodynamic effects. This translating, effective hub mass attempted to represent a modal combination of hub and airframe translations and pitching and rolling motions. These pitching and rolling motions are of little consequence in the analysis of a rotor with small flap hinge offsets. However, if there is a sizeable effective flap hinge offset, as in the case of a hingeless rotor system, these motions produce large aerodynamic flapping moments which can damp the ground resonance or related air resonance modes (Reference 2). Therefore, the pitching and rolling motion as well as the aerodynamic consideration become indispensable for the hingeless rotor system. The C-56 program was developed to provide this more exact representation.

Analytical Capability (C-56 Program)

The C-56 analysis retains the degrees of freedom of the helicopter rotor and airframe which influence the air and ground resonance characteristics. This relatively simple but adequate analytical representation includes these pertinent freedoms:

Three rigid-body fuselage translations

Two rigid-body fuselage rotations (pitch and roll)

Four mast or pylon motions (lateral and longitudinal translations, pitch, and roll) defined at the softest pylon-to-fuselage junction

Two tail boom flexibilities

Nine rotor freedoms (one collective and two cyclic modes for blade pitching, flapping, and in-plane motions) (excludes reactionless modes)

A drawing of the 20 degrees of freedom is shown in Figure 1.

The equations of motion for this entire multidimensional system are derived from Lagrange's equations. A brief discussion of this derivation was presented in Reference 3.

This representation permits the investigation of a wide range of parameters affecting rotor/airframe stability. In addition to making it possible to study the effects of basic characteristics, such as rotor speed, rotor thrust, aircraft gross weight, forward speed (in an extended version of the program), and Lock number, the representation makes it possible to examine the following parameters: precone, control system stiffness, lag frequency, and pitch-lag and pitch-flap coupling terms. Although other parameters may also be investigated, these in particular have a strong influence on stability.

Parameter Sensitivity

The mechanism of the air and ground resonance of the hingeless rotor helicopter and its attendant source of damping were discussed elsewhere, e.g., Reference 2. It suffices to say that since the prime source of damping in the air and ground resonance mode is the blade flap response, any parameter which affects the coupled blade feather, flap, and lag motions has the potential for stabilizing or destabilizing the mode. A sensitivity study revealed that the favorable couplings were nose-up pitch and upward flap, both of which caused blade lag, and upward flap, which caused nose-down pitch. Any hub geometry and blade design which result in these three types of coupling in a soft in-plane rotor system will beneficially affect the air resonance stability. Let us now examine some of the most common design parameters.

Precone. Precone here means the precone of the blade feathering axis. Figure 2 shows the precone effect on the YUH-61A air resonance mode stability. As the blade feathering axis precones up towards the equilibrium position, the modal damping decreases.

As discussed in Reference 2, with the blade feathering bearing inboard of the blade flexure, precone of the blade feathering axis directly controls the magnitude of the flap-pitch coupling caused by the Coriolis force. The perturbation Coriolis force due to flapping up velocity acts toward the leading edge of the blade. With the blade equilibrium position above the feathering axis producing a moment arm, there results a nose-down perturbation pitching moment, which is favorable. Figure 3 shows schematically the reduction of the moment arm with increasing precone; hence the reduction of the favorable flap-pitch coupling.

Control system flexibility. Figure 4 shows the effect of the control system flexibility on the air resonance mode stability of the YUH-61A. Comparing the stiff control system to the nominal control system, we see that the former degrades the stability for collective pitch from 25 to 240 percent of hover 1g collective (θ_{NOR}) and enhances the stability from then on up.

Since the stability is influenced by the blade flap-pitch and pitch-lag coupling, its dependence on the control system flexibility is expected. As discussed in Reference 2, there exists favorable flap-pitch coupling for the low collective pitch region, in this case from 25 to 200 percent θ_{NOR}, and unfavorable coupling at high collective pitch, in this case from 200 percent on up. The stiff control system minimizes the coupling effect and therefore produces the trend shown in Figure 4. The choice of the control system stiffness therefore depends on the practical operational collective pitch range for which the rotor is designed.

Lag frequency. There are several factors which have a primary influence on the air and ground resonance characteristics of the helicopter. One of these is the placement of the lag frequency with respect to the coupled airframe pitch-dominant and roll-dominant modes. This has been discussed for an aircraft with a gross weight of about 2045 kg (4500 pounds) in Reference 4.

As stated in that reference, there are two potential resonance points which are, in general, detrimental to aircraft air resonance characteristics. These points, shown in Figure 5, should be avoided for all flight conditions of the particular aircraft. However, there are two possible stable regions of rotor operation which are available for a given helicopter design. Both of these regions now have been shown to provide satisfactory stability margins, with the Boeing YUH-61A designed for region 1 and the MBB BO-105 designed for region 2.

The choice of the optimum operating region for these helicopters indirectly results from the aircraft mission. The mission profile sizes the rotor system, aircraft gross weight, and pitch and roll inertias. The roll predominant and pitch-predominant modes are strongly coupled with the rotor

cyclic flapping, which provides the stiffness for those directions in flight. Therefore, with the aircraft pitch- and roll-predominant modes fixed by the above considerations, the in-plane blade stiffness, and therefore lag frequency and Ω-ω_ζ, is then chosen to meet rotor load requirements and to place the rotor speed in the center of one of the operating regions.

YUH-61A Analytical Results

For the final YUH-61A configuration, the various beneficial parameters are combined to produce a stable configuration. A summary of the key rotor and fuselage parameters is shown in Table 1.

Table 1 Summary of YUH-61A Parameters

Parameter	Value
In-plane Frequency (ω_ζ)	0.70 per N_R (Normal Rotor Speed)
Pitch-Flap Coupling (δ_3)	-22.5° (Flap Up-Pitch Nose Down)
Precone	0°
Droop	3.25° Up
Blade Torsion Frequency (ω_θ)	3.76 per N_R
Rigid Airframe Roll Frequency	0.366 per N_R
Rigid Airframe Pitch Frequency	0.095 per N_R
In-plane Damping Augmentation	0% (In-plane Structural Damping ≈ 1.0%)
Landing Gear Damping Augmentation	0%

These parameters were modeled for the C-56 program, and air resonance and ground resonance characteristics were determined. A plot of the predicted air resonance stability as a function of thrust and rotor speed is shown in Figure 6. The low RPM boundary in this plot corresponds to the resonance of Ω-$\omega\zeta$ with the pitch-dominant mode, and the high RPM boundary corresponds to the resonance of the Ω-$\omega\zeta$ mode and the roll-predominant mode. The reduction in stability at high thrust (or collective pitch) levels is due to detrimental flap-pitch coupling in this region, as explained in Reference 2.

The results of the ground resonance analysis as a function of percent airborne is shown in Figure 7. This plot displays the Ω-ω_ζ mode modal damping for three different rotor speeds ranging from the aircraft's minimum value (N_{min}) to the maximum design limit speed (N_{DL}). This completely covers the range explored later on the first test vehicle.

MODEL TESTS

The model tests performed in conjunction with the development of an aeroelastically stable YUH-61A configuration were conducted in two parts.

1/13.8 Froude-scaled BO-105 model

1.67 meter (5.5 foot) diameter Froude-scaled YUH-61A model

Froude-Scaled BO-105 Model

This 1/13.8 Froude-scaled BO-105 model (Reference 2) was developed to provide a direct means of validating the analytical methods detailed above and to demonstrate the power of the several rotor parameters to influence aircraft air resonance characteristics. The model has the same blade first flap, lag, and torsion frequencies as full scale, with provisions to vary hub precone, blade sweep, and blade lag damping to observe their effects on rotor stability. The model parameters are summarized in the following table.

Table 2 1/13.8 Scale BO-105 Model Parameters

Parameter	Value
Rotor Diameter	71 cm (28 in.)
Chord	1.94 cm (0.762 in.)
Gross Weight	0.85 kg (1.87 lb)
Precone	Variable
ω_β/Ω (Flap)	1.12
ω_ζ/Ω (Lag)	0.62
ω_θ/Ω (Pitch)	3.6
Roll Inertia	0.456×10^{-3} m-kg-sec^2 (0.0395 in-lb-sec^2)
Pitch Inertia	1.224×10^{-3} m-kg-sec^2 (0.106 in-lb-sec^2)

The air resonance characteristics for this model are determined primarily by the frequency placement as a function of rotor speed of the significant modes: (a) $\Omega-\omega_\zeta$, the air resonance mode; (b) aircraft pitch, rigid body pitch restrained by rotor flap; and (c) aircraft roll, rigid body roll restrained by rotor flap, as detailed in the previous section of the lag frequency sensitivity. The plot of these modal frequencies and the related modal damping versus rotor speed is shown in Figure 8.

At a given rotor speed the variation of rotor thrust, or collective pitch, produces changes in $\Omega-\omega_\zeta$ mode modal damping. A typical plot of this effect is shown in Figure 9. The modal damping plot of $\Omega-\omega_\zeta$ shows two possible regions of model instability. The first is at low collective, from 30 percent to 50 percent of hover 1g collective, and reflects the mild reduction in the stability of the isolated rotor lag mode. The second, high collective region displays a steep modal damping gradient which is created by detrimental flap-pitch coupling at the high thrust (Reference 2).

The importance of both rotor speed and maneuver thrust on air resonance characteristics was realized, so the model was tested through a wide range of rotor speeds and thrust conditions. The stability observed at these conditions was correlated with analytical stability boundaries. A typical map of this type is shown in Figure 10. In addition to lending confidence in the analytical methods, this test and analytic work confirmed the power of several rotor parameters to enhance and control air resonance stability characteristics (Reference 2). These parameters are as follows:

Precone of the blade feathering axis

Control system flexibility

Lag damping

1.67 Meter (5.5. Foot) Diameter Froude-Scaled YUH-61A Model

The next step in the development of the aeroelastically stable YUH-61A configuration is the testing of a 1.67 meter (5.5 foot) diameter model (Reference 5). This soft in-plane hingeless rotor system was tested on a gimbal which allowed the helicopter rigid-body pitch and roll motions. The rotating frequencies of this model are scaled to full scale and therefore are different from those of the BO-105 Froude-scaled model. A summary of the model parameters appear in Table 3.

Table 3 Summary of 1,67 Meter Diameter Model Parameters

Parameter	Value
Rotor Diameter	1,67 m (5,5 ft)
Chord	6,6 cm (2,6 in.)
Gross Weight	17,64 kg (38,8 lb)
Precone	Variable
ω_β/Ω (Flap)	1,09
ω_ζ/Ω (Lag)	0,67
ω_θ/Ω (Pitch)	4,30
Roll Inertia	0,01479 m-kg-sec^2 (1,281 in.-lb-sec^2)
Pitch Inertia	0,08844 m-kg-sec^2 (7,66 in.-lb-sec^2)

Figure 11 shows the nondimensional natural frequencies as a function of rotor speed for this model. Comparison of this figure and Figure 8 reveals that the basic difference between the two models is the placement of the roll-predominant mode. In the 1,67 meter (5.5 foot) diameter configuration, the coalescence of the roll-predominant mode and the Ω-ω_ζ mode occurs slightly beyond 120 percent normal rotor speed (N_R).

Tests of the model in hover determined that two unstable regions similar to those predicted by analysis were present (Figure 6). In a typical map of test points in hover, Figure 12 demonstrates the boundaries: one is at about 70 percent of normal rotor speed and 120 percent of normal collective pitch, corresponding to the resonance with the body-pitch-predominant mode, and one is at 135 percent RPM and 100 percent collective, corresponding to the resonance with the body-roll-predominant mode.

The stability of the air resonance mode was also explored with respect to forward speed using the 1,67 meter diameter model. A plot of the test data at level flight trim collective pitch is presented in Figure 13. Because of the instrumentation arrangement during this phase of testing, the damping values were recorded from the rate of decay exhibited in the chord bending gage. The time to half amplitude observed in this way is equal to that of the Ω-ω_ζ air resonance mode. However, the frequency in the rotating system is ω_ζ, and therefore the data must be multiplied by the ratio of $\omega_\zeta/(\Omega-\omega_\zeta)$ to represent the air resonance mode damping. This is demonstrated and is shown in Figure 17, a typical time history of the YUH-61A in-flight shake test results.

During this test program, the test technique employed to obtain these data was refined. It was determined at the time that by exciting the model with lateral stick deflections in a sinusoidal fashion at a frequency of Ω-ω_ζ, the mode of interest could be observed. A typical time history which

demonstrates this method of excitation and the measurement of damping is shown in Figure 14. As shown in this figure, the excitation produces a characteristic $\Omega-\omega_\zeta$ modal response characterized by the lead-lag motions of the blades at ω_ζ (observed in the rotating system) and by body roll and pitch motion at $\Omega-\omega_\zeta$ (observed in the fixed system).

In addition, the optimum values for the rotor and airframe parameters were determined for incorporation in the full scale design. These were presented in Table 1 in the previous section.

YUH-61A FLIGHT TEST

The YUH-61A stability testing was performed at the Grumman Aerospace Corporation facility at Calverton, Long Island (Figure 15). It was conducted during the envelope expansion phase of the flight test program. Because of the test technique adopted, which enables the determination of modal damping or degree of stability at every test point, in conjunction with the test setup and the test procedure employed, this in-flight stability shake test is truly a minimum risk program.

Test Setup

To expedite this work and to promote minimum risk, the Grumman Automated Telemetry System (ATS) was used to provide on-line real-time analysis of the data.

This data system has a wide range of operational capabilities (Reference 6), one of which is rotor system stability investigation. A schematic representation of the flow of information from the test aircraft to the data analyst is shown in Figure 16.

A frequency-modulated (FM) hybrid telemetry system is installed in the test aircraft. The transmitted signal includes flight-crew voice communications, a pulse-code-modulated (PCM) data set, an FM data set, and a time-code-generation signal. The primary data parameters which are observed and measured for the stability testing are as follows: chordwise bending moment from all four blades; flapwise bending moment; blade torsional moment; main transmission lateral and longitudinal accelerations; lateral and longitudinal stick positions; lateral and longitudinal stability and control augmentation system (SCAS) output; pitch, roll, and yaw of helicopter; pitch, roll, and yaw rates.

During a test flight, this raw signal is continuously recorded on magnetic tape in the ground station. In addition, a pilot-controlled on-board magnetic tape records these data plus additional data sets.

The ATS computers control the flow of information from the telemetry data stream to the analytical station. For a given test event, the analyst determined the level of inherent stability from two ATS output systems. The primary system is a real-time digital computer analysis of the rate of decay of the critical parameters from an initially excited state. The results of the analysis are displayed at the data analyst's station (DAS) on a cathode-ray tube (CRT) display.

As a backup to this system and to provide supplemental analytic capability, strip charts are utilized. The strip charts were found particularly useful in evaluating the quality of data being analyzed in terms of the contamination of the pure modal decay by random gusts. A more detailed explanation of DAS operation is presented in Reference 6.

Test Technique

The test technique employed to determine inherent stability levels for the YUH-61A was developed through model testing. This technique involves basically the following sequence:

Establish test condition

Turn on recording system

Turn on excitation

Turn off excitation

Record convergence of aircraft motions

Analyze data to obtain modal damping

Proceed to new test condition

The excitation for each test condition is supplied by a shaker system directly connected to the aircraft control system. The shaker is constructed with manual pilot-controlled selection of the shaker frequency, the axis of excitation, the shaker authority or gain, and the on-off controls. The output of the shaker is fed directly to the aircraft swashplate; therefore the required excitation frequency to the swashplate is $\Omega-\omega_\zeta$, which in turn excites the blade at ω_ζ, producing response in the air resonance mode.

During these tests the axis of excitation was limited to purely lateral or purely longitudinal. The tests of the 1.67 meter diameter model indicated that lateral excitation is the most responsive direction for the air resonance mode; for example, see Figure 14. Therefore, after this was confirmed on the flight test vehicle during the initial test conditions, the lateral excitation was used exclusively. A stick whirl excitation induced manually by pilot was used at the suggestion of C. E. Hammond of Langley. This resulted in quite satisfactory test results.

Figure 17 shows the time history of a typical test event. The time histories from the top down are blade chordwise bending, filtered chordwise bending, filtered main transmission lateral acceleration, SCAS (or shaker) input, and main rotor one per rev. The chord bending reflects the blade lead-lag motion in the rotating system, while the transmission lateral reflects the body lateral roll motion in the fixed system. Because of the closeness in frequency of the main rotor speed and the first in-plane natural frequency, even with a low pass filter, the one per rev forced response is still evident in the filtered chord bending trace. However, if this residual forced response is subtracted from the total chord bending response, the time for the chord motion to decay to half amplitude is the same as the time for the transmission lateral motion. This is expected, since the components of the physical system should decay at the same rate when a pure mode is excited. Modal damping can be obtained from either the chord bending or the transmission lateral, with the restraint that the reference frequency is $\Omega-\omega\zeta$, not $\omega\zeta$. Note also that the filtered traces have a time lag as compared to the excitation stop point, partly because of the low pass filters used.

Test Procedure

A maximum effort has been made throughout the entire YUH-61A development program to maintain minimum risk while providing and demonstrating adequate air resonance mode stability margins. During the actual flight test program, this was accomplished by the temporary addition of high in-plane damping (6 percent critical damping) to the rotor system by using lag dampers and by the temporary use of high damping landing gear shock struts.

The YUH-61A design configuration, because of the choice of the key rotor parameters, requires no lag dampers or landing gear damping. This was demonstrated by first obtaining the stability levels for the aircraft with installed lag dampers (adjusted to 6 percent critical in-plane damping) and high damping landing gear. Following stability checks of ground resonance characteristics and hover conditions, the high damping landing gear was replaced by the design gear, which has no damping for ground resonance purposes. The flight envelope for the YUH-61A was then expanded, demonstrating stability for climbs, descents, turns, forward speed, and various other conditions. From this work the critical flight conditions were determined. Finally, the damping of the lag damper was reduced by decrements of 2 percent critical damping until it was finally removed. The aircraft has now been flown to speeds beyond maximum level flight speed, V_H, at various gross weights, and under various maneuver conditions, and its stability has been demonatrated throughout.

YUH-61A Flight Test Stability Results

Ground resonance stability. Collective pitch sweeps were performed to investigate the ground resonance characteristics. These sweeps were made at three different rotor speeds, 94 percent N_R, 97 percent N_R, and 102 percent N_R. The test results performed at 97 percent N_R are shown in Figure 18. For this

work, the aircraft was configured to design gross weight, with the design landing gear and the lag dampers removed. At all three speeds there is a trend of increasing stability as the collective is increased from 0 percent to 100 percent airborne. This increase equals 5.0 to 7.5 percent modal damping at each of the rotor speeds. In general, this is in good agreement with the earlier C-56 analysis results (Figure 7).

Air resonance stability. The investigation of air resonance as a function of airspeed was conducted as part of the envelope expansion program of the YUH-61A. The measured Ω-ω_ζ mode modal damping values for the YUH-61A is shown in Figure 19. As with the ground resonance work, the aircraft is configured to design gross weight with the lag dampers removed. As shown in this figure, the test values of the stability of the aircraft varies from about 7 percent modal damping in hover, out-of-ground effect, to a peak damping value of 12 percent critical near 80 percent V_H. In general, the damping is about level with airspeed. The minimum value at 106.5 percent V_H with the lag dampers removed is 7 percent. Notice that the trend in damping with airspeed matches data taken during the test of the 1.67 meter diameter Froude-scaled model (Figure 13), except that the magnitude of the test data is different because of lower inherent structural damping in the model.

CONCLUSIONS

Several conclusions can be drawn from this systematic approach to the aeroelastic stability problem of a soft in-plane hingeless rotor helicopter.

1. The YUH-61A has a stable soft in-plane hingeless rotor system.

2. The stable characteristics of the YUH-61A helicopter are attributed to the proper choice of the blade frequencies relative to the normal operating rotor speed and the hub parameters incorporated into the final design, such as zero precone of the blade feathering axis, and equivalent hinge sequence of pitch-flap-lag from inboard to outboard.

3. The sensitivities of stability to these parameters were analyzed by a 20 degree-of-freedom analysis and verified by two model tests.

4. A shake and decay technique was developed during a second, 1.67 meter diameter model test. This enabled the measurement of modal damping ratios, or the degree of stability, at every test point.

5. The test technique developed and perfected during model testing is useful for the in-flight shake test of the full scale helicopter. This technique, combined with the Grumman Automated Telemetry System, provides an efficient way to conduct the flight test program.

6. The in-flight shake test is the final step in the systematic approach to develop a rotor system free of aeroelastic instability when coupled to the airframe.

7. With an analytical tool substantiated by model testing, and the analytical trend study also verified by test, confidence can be placed in the predicted stability characteristics of a new vehicle. A flight program can be laid out, then, with minimum risk.

REFERENCE

1. Coleman, R.P.: Theory of Self-Excited Mechanical Oscillations of Hinged Rotor Blades. NACA ARR-3G29, July 1943.

2. Burkam, J.E.; and Miao, W.: Exploration of Aeroelastic Stability Boundaries with a Soft-in-Plane Hingeless-Rotor Model. Preprint 610, 28th Annual National Forum of the American Helicopter Society, May 1972.

3. Hohenemser, K.H.: Hingeless Rotorcraft Flight Dynamics, AGARD Publication, AGARD-AG-197, September 1974, pp. 25-27.

4. Lytwyn, R.T.; and Miao, W.: Airborne and Ground Resonance of Hingeless Rotors. Preprint 414, 26th Annual National Forum of the American Helicopter Society, June 1970.

5. Miao, Wen-Liu; and Huber, Helmut B.: Rotor Aeroelastic Stability Coupled With Helicopter Body Motion. NASA SP-352, 1974, pp. 137-146.

6. Marshall, D.L.; and Steinmann, H.H.: UTTAS Flight Test: Real-Time Data Analysis. 30th Annual National Forum of the American Helicopter Society, May 1974.

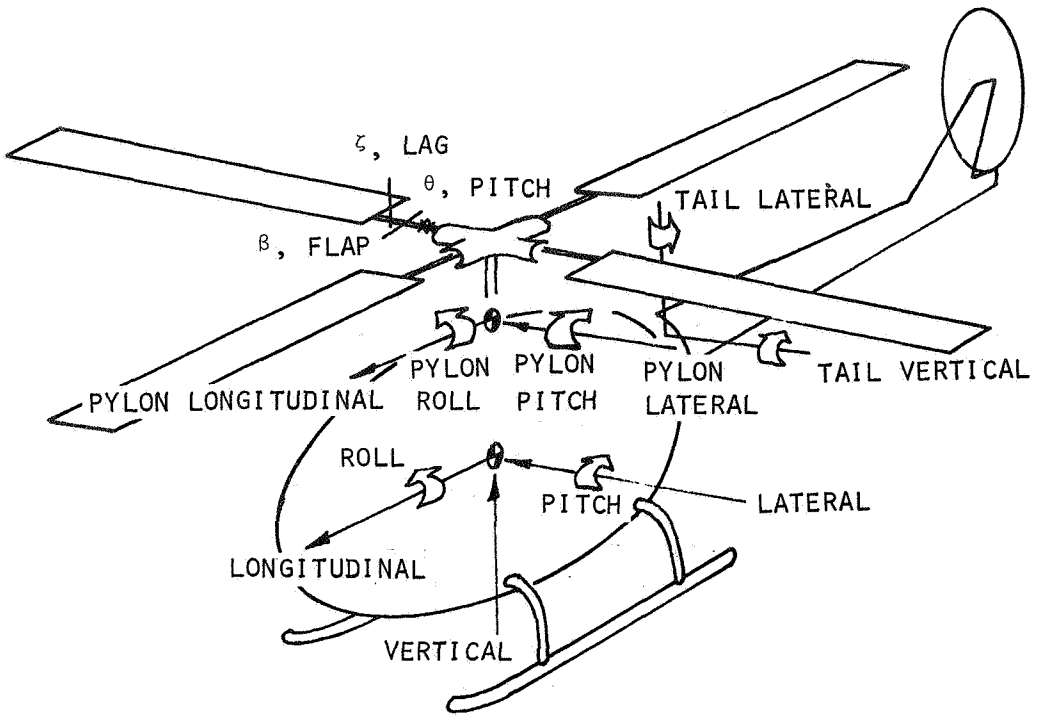

Figure 1. Coupled Rotor-Fuselage Analytical Model C-56.

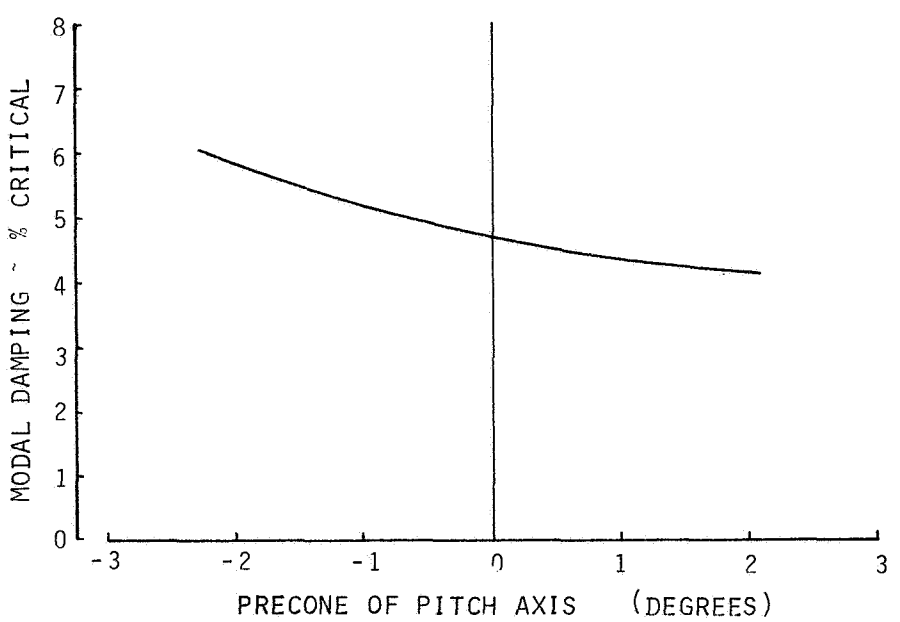

Figure 2. Effect of Precone on Air Resonance Stability.

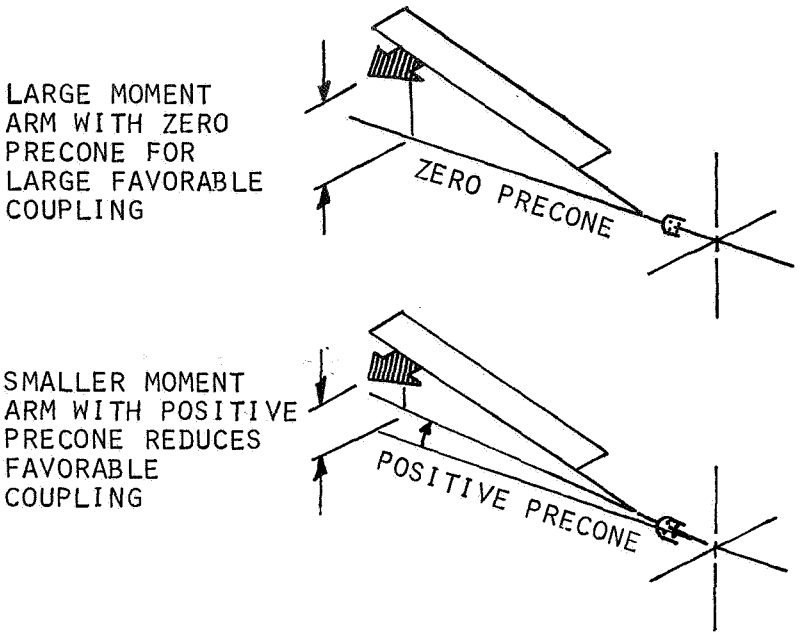

Figure 3. Effect of Precone in Reducing Favorable Flap-Pitch Coupling.

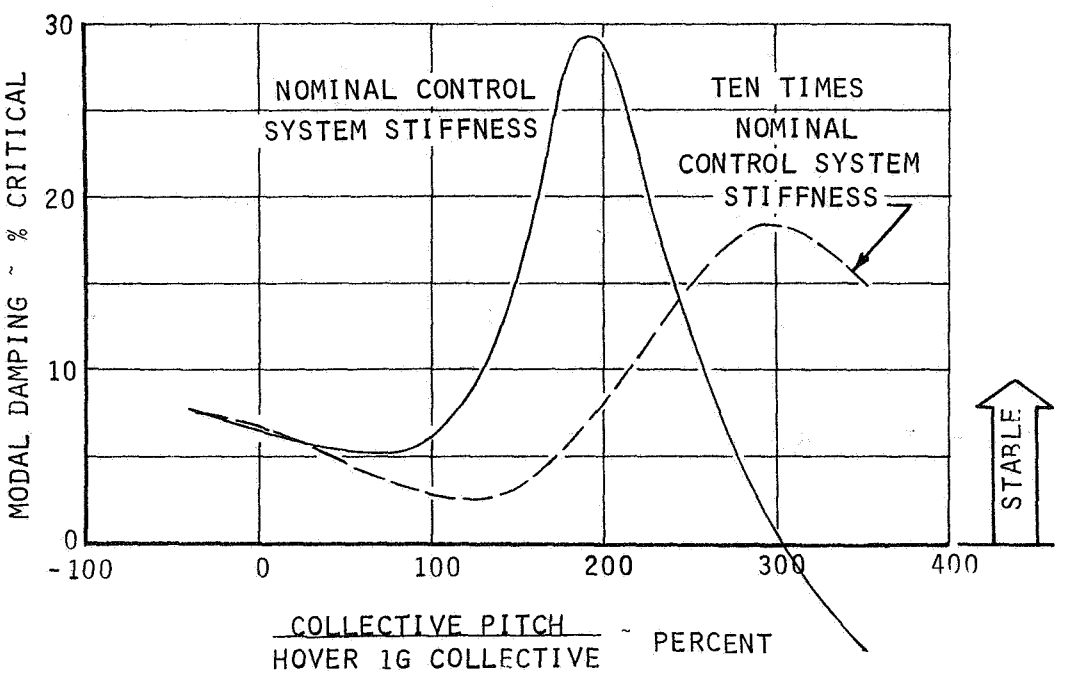

Figure 4. Effect of Control System Flexibility.

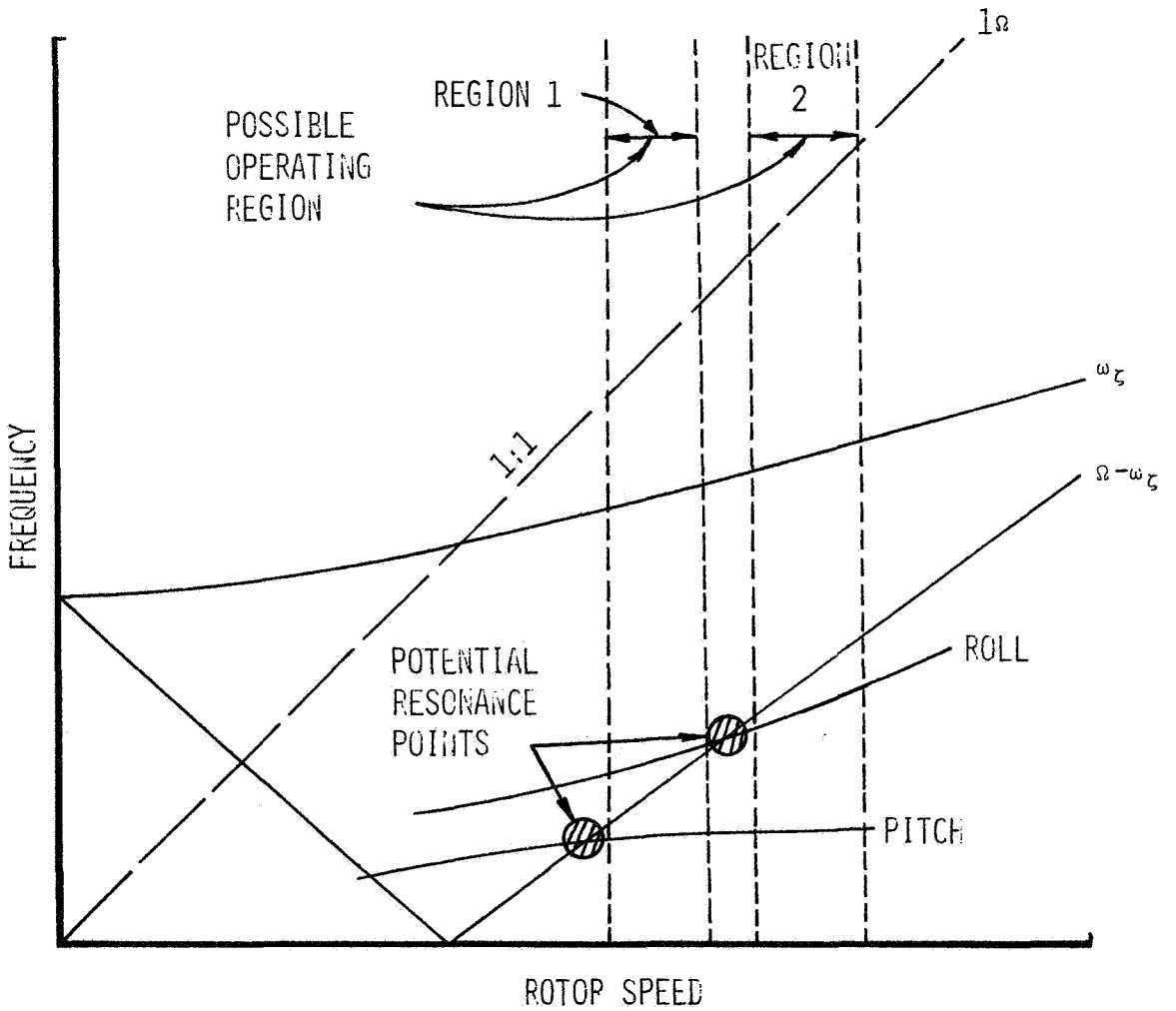

Figure 5. Potential Air Resonance Points and Operating Regions.

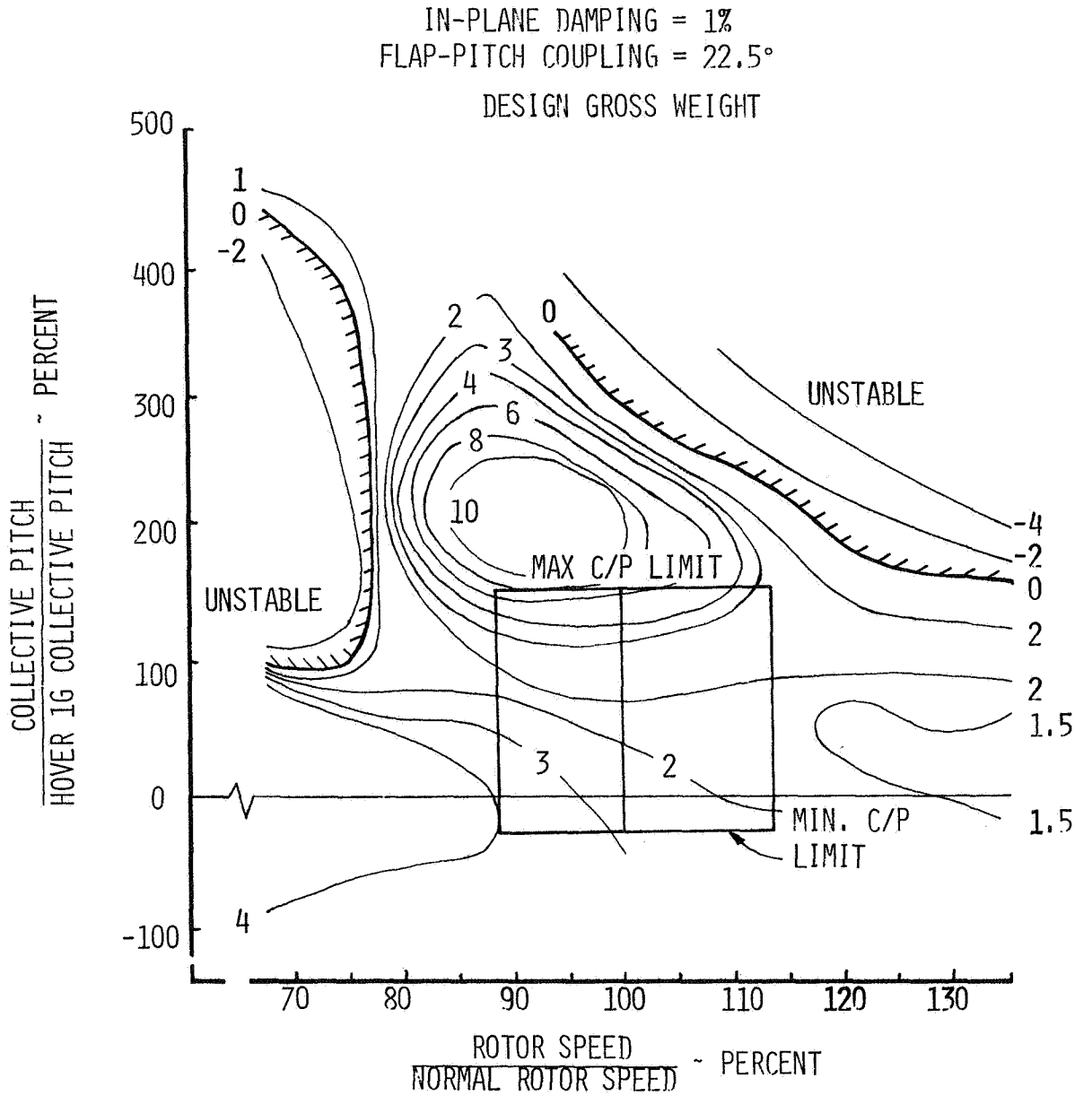

Figure 6. YUH-61A Air Resonance Characteristics.

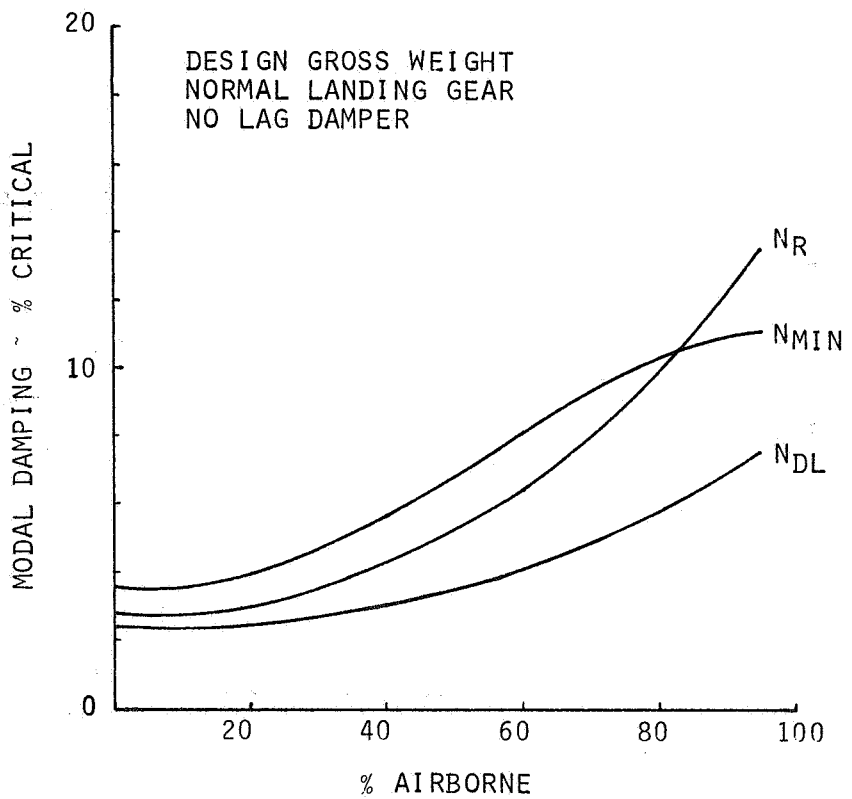

Figure 7. YUH-61A Ground Resonance Characteristics.

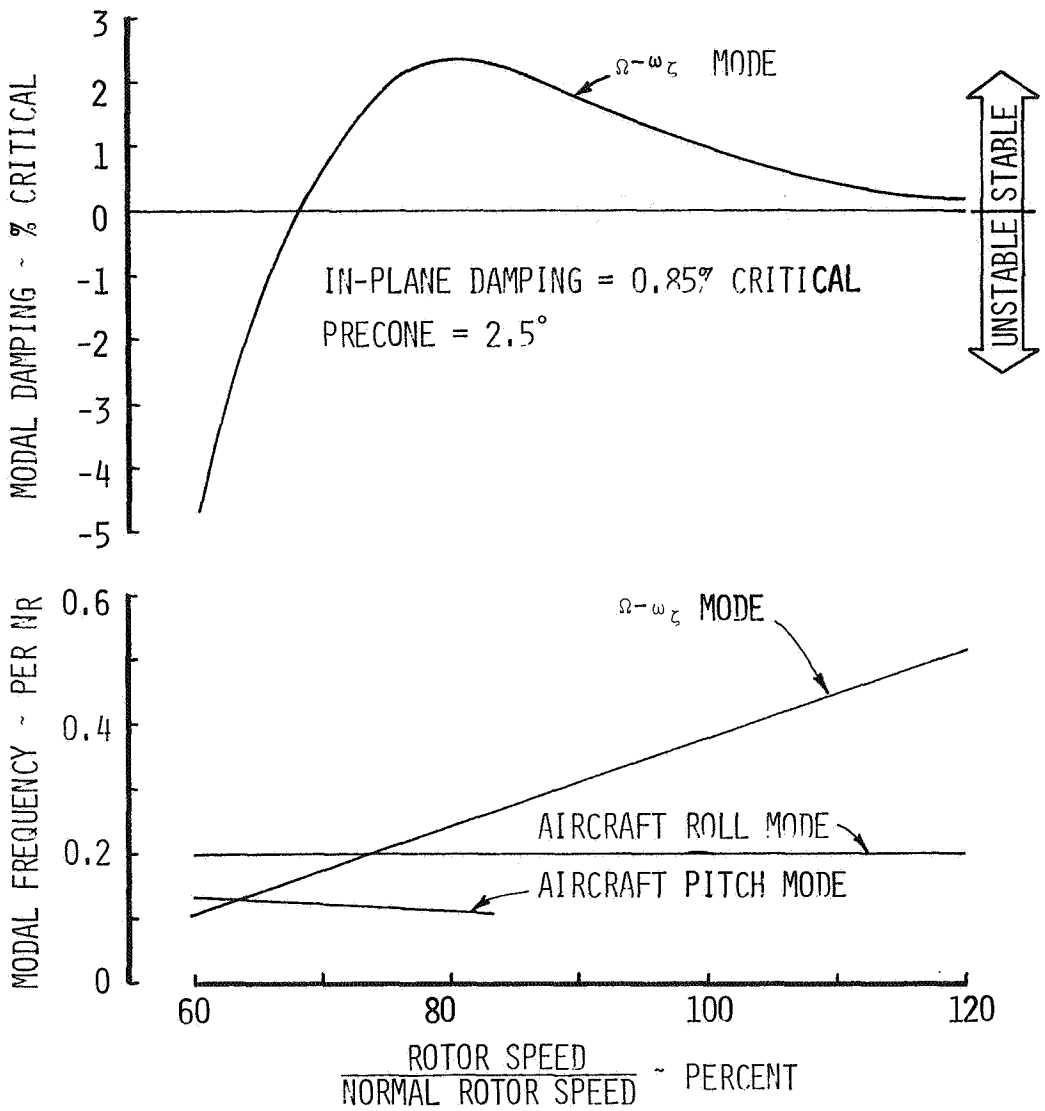

Figure 8. 1/13.8 Scaled BO-105 Model-Modal Frequencies and Damping.

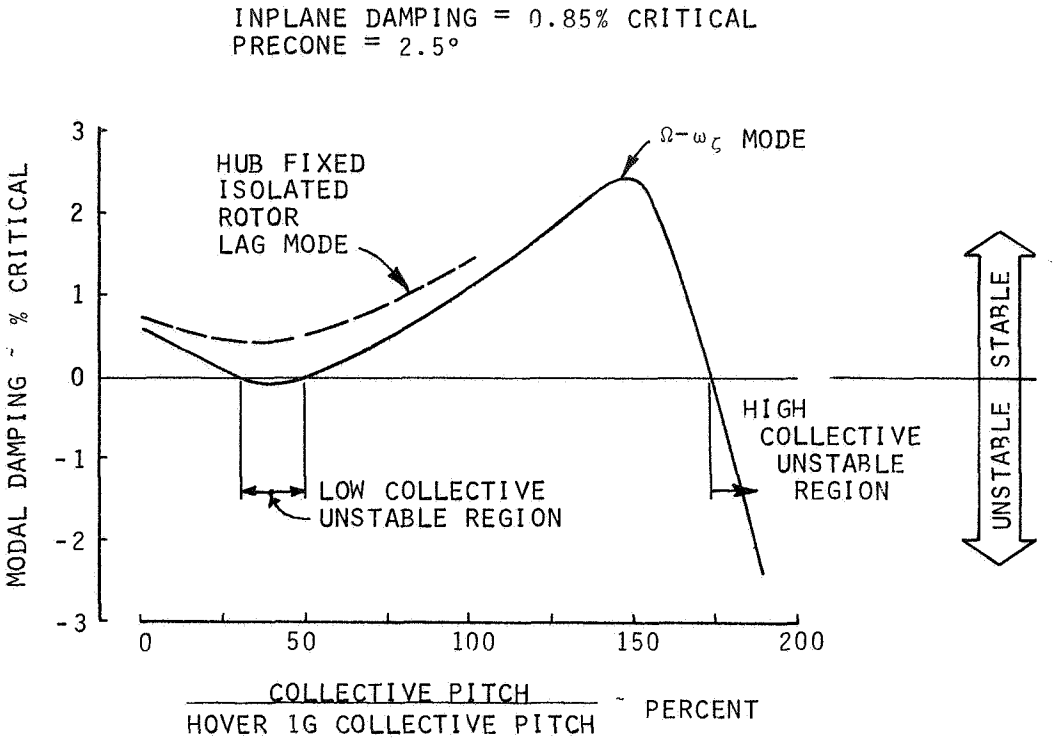

Figure 9. Thrust Effect on Stability.

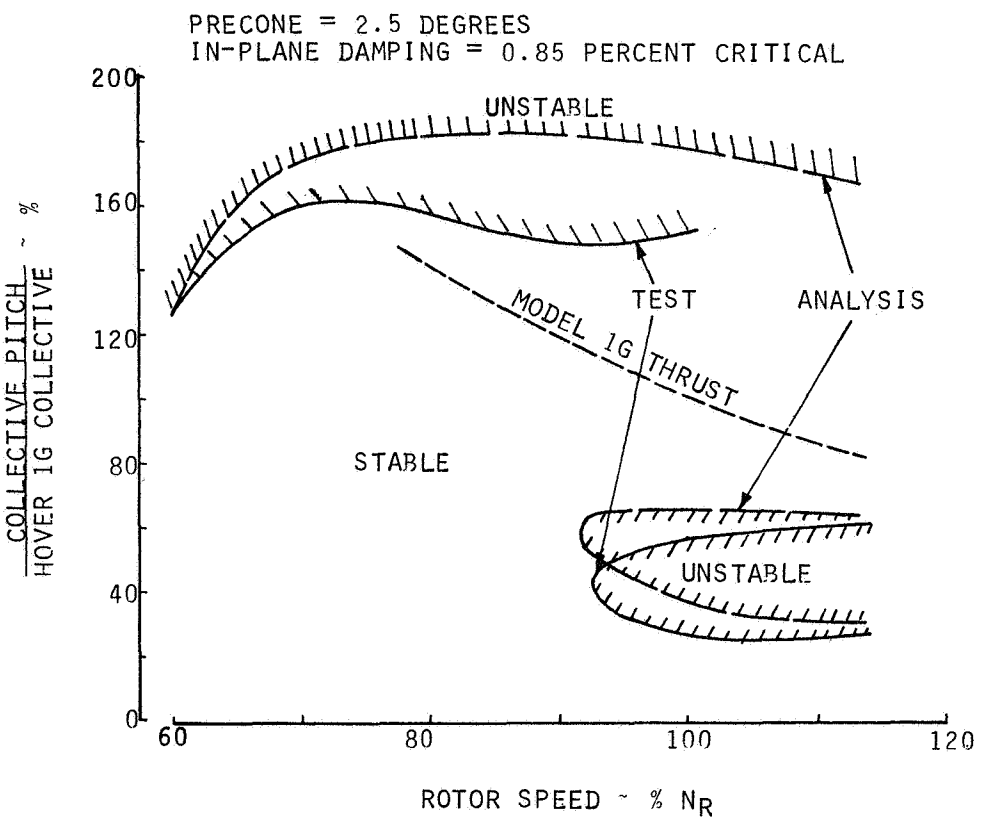

Figure 10. Stability Map of 1/13.8 Scaled BO-105 Model.

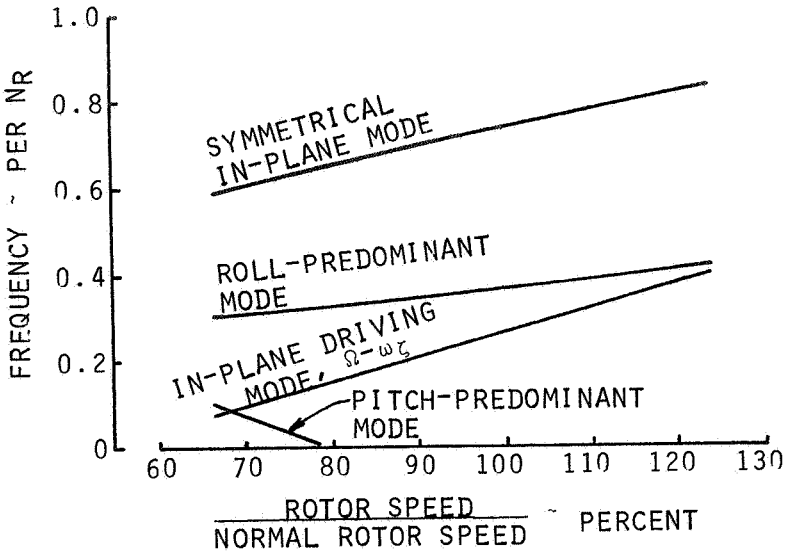

Figure 11. 1.67 Meter Diameter YUH-61A Model-Modal Frequencies.

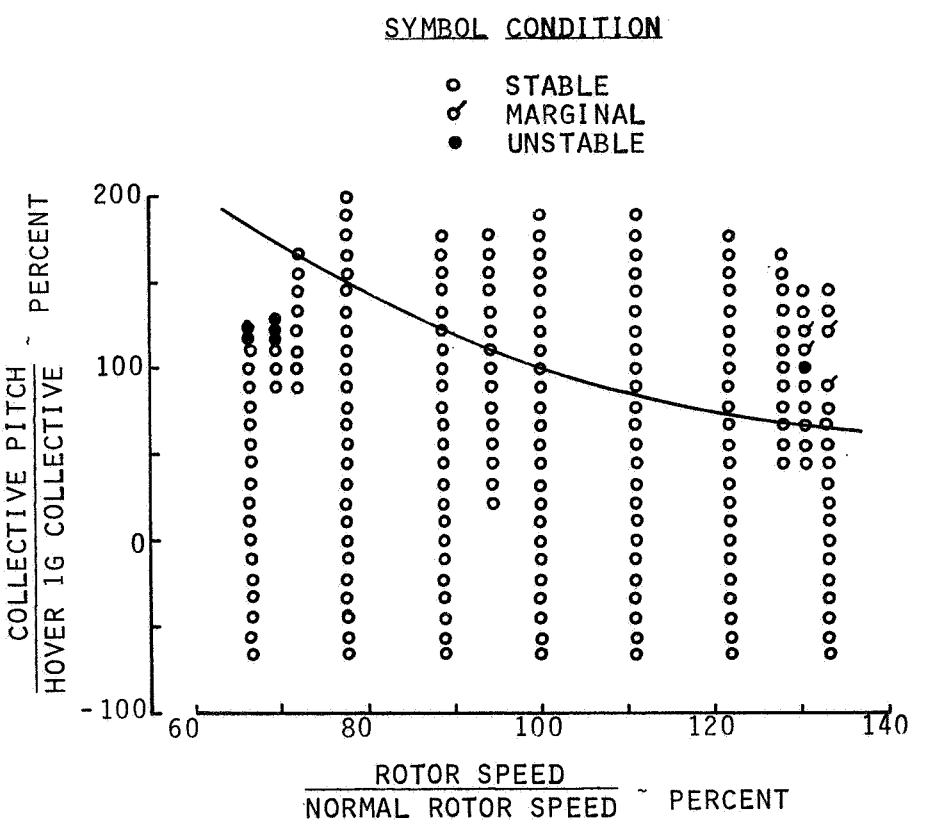

Figure 12. Map of Stability Test Points.

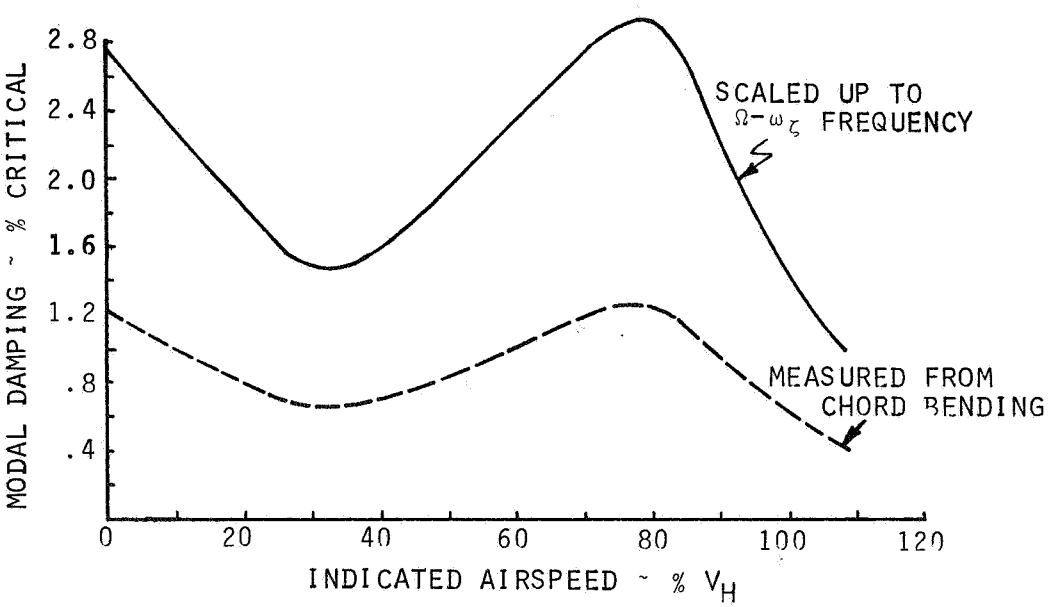

Figure 13. Stability in Forward Flight.

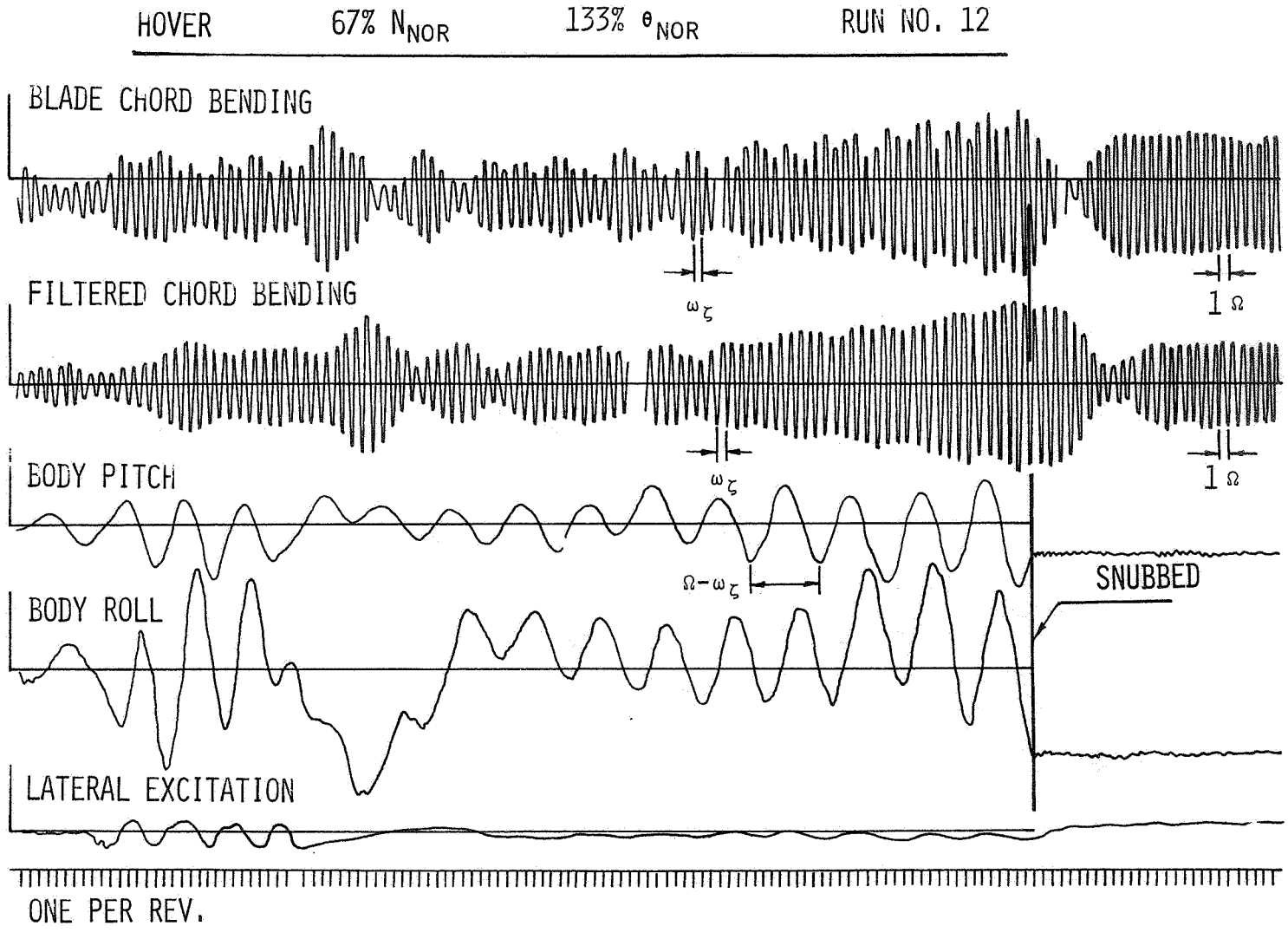

Figure 14. Typical Time History of 1.67 Meter Model.

Figure 15. YUH-61A Helicopter.

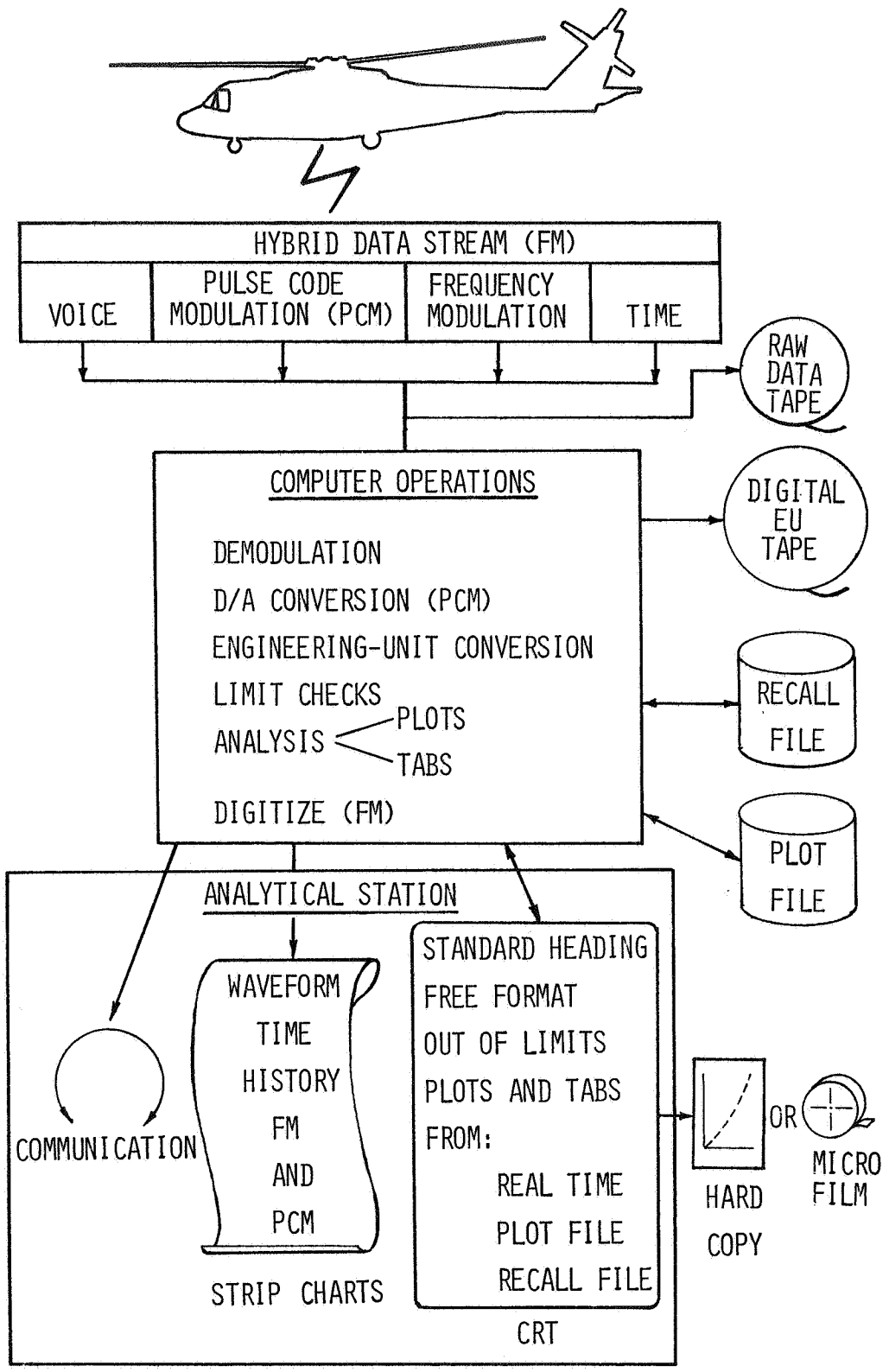

Figure 16. Schematic of Real-Time Data System.

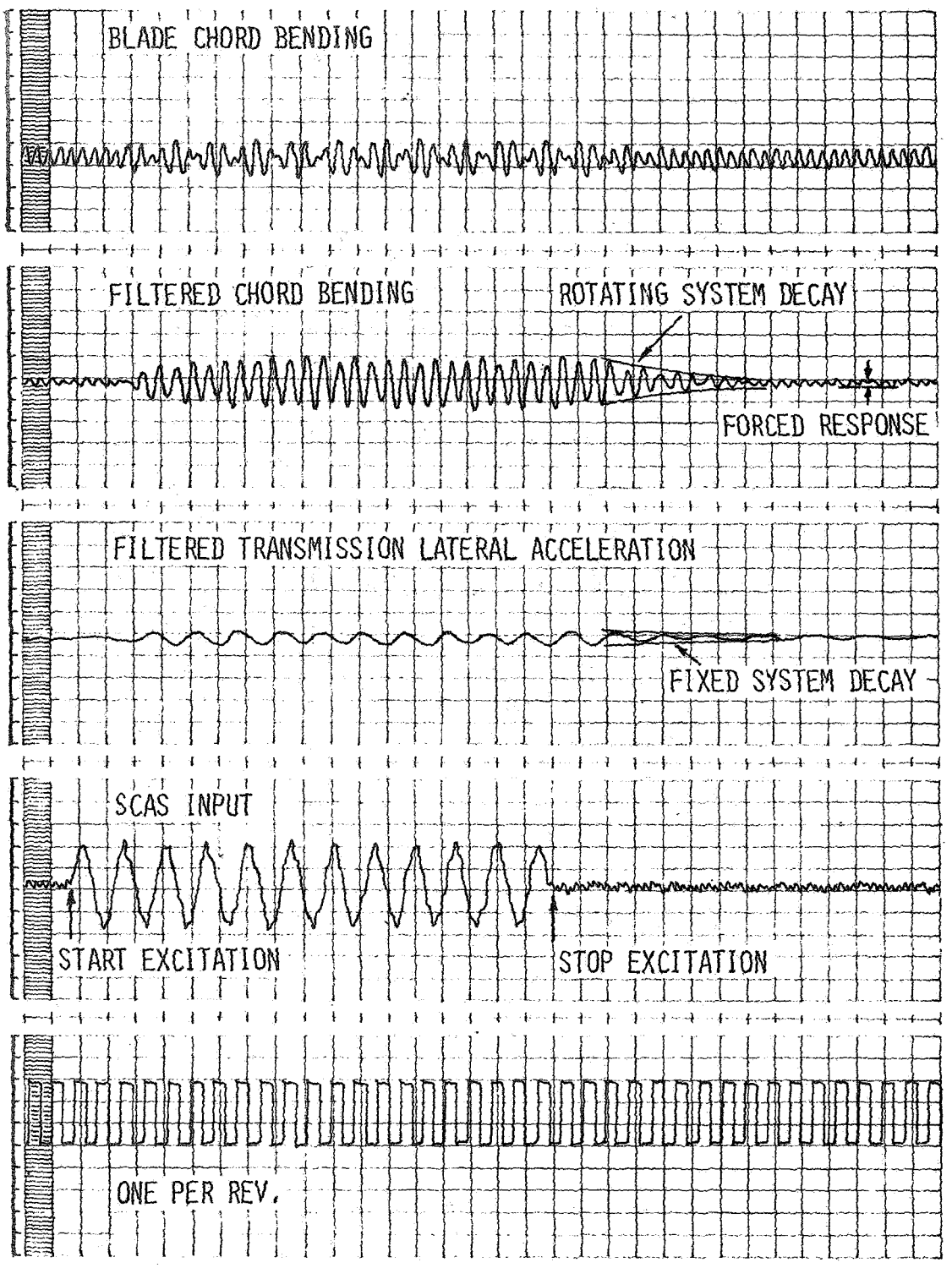

Figure 17. Typical Time History of YUH-61A.

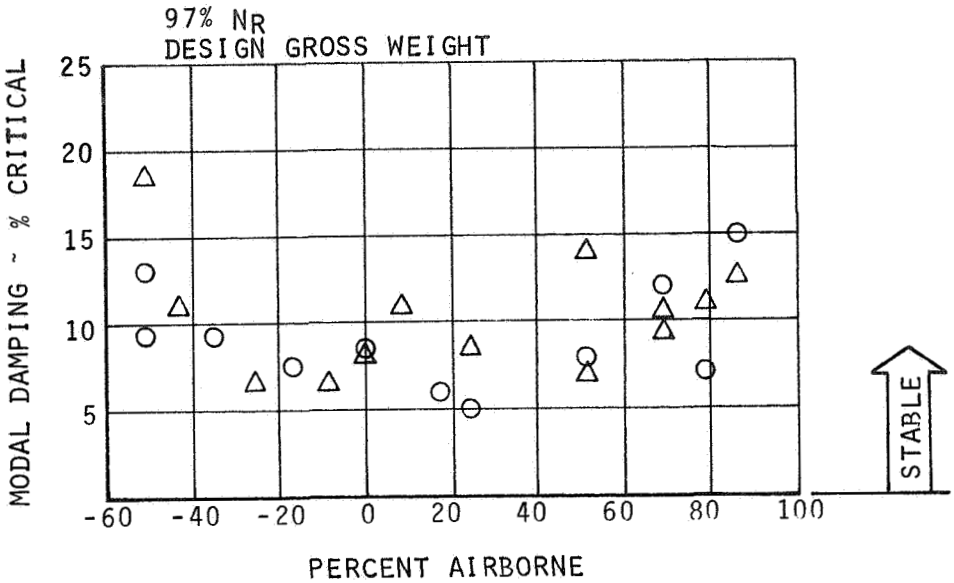

Figure 18. YUH-61A Ground Resonance Test Data.

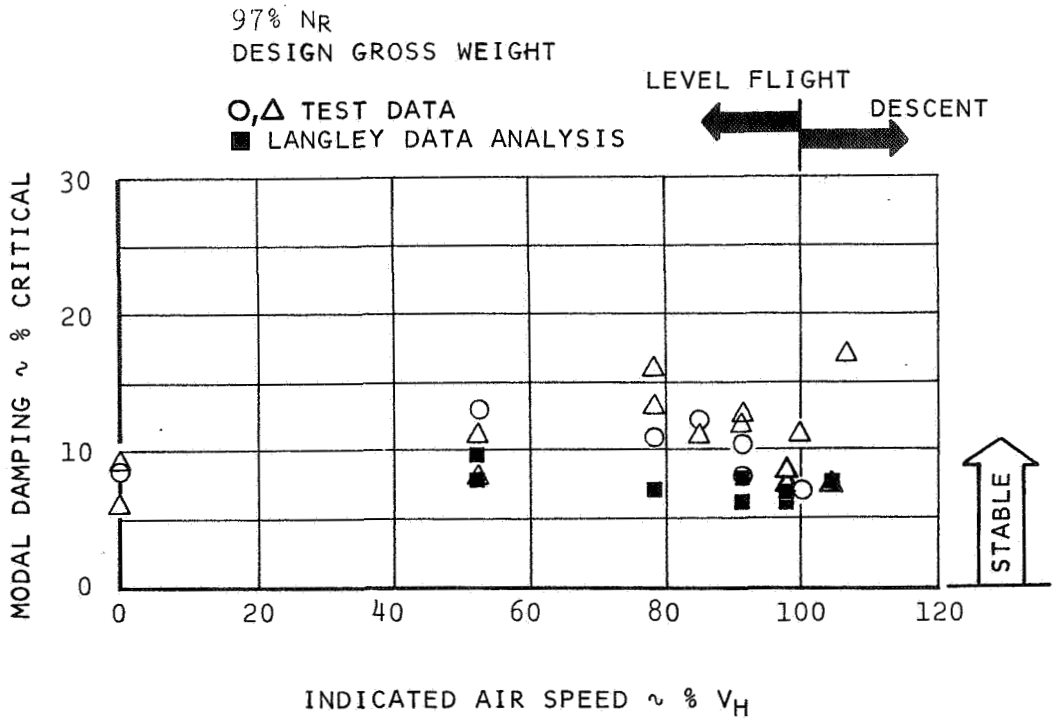

Figure 19. YUH-61A Air Resonance Test Data.

FLIGHT FLUTTER TESTING OF ROTARY WING AIRCRAFT USING A CONTROL SYSTEM OSCILLATION TECHNIQUE

Jing G. Yen, Sathy Viswanathan,
and Carl G. Matthys

Bell Helicopter Company

SUMMARY

This paper describes a flight flutter testing technique in which the rotor controls are oscillated by series actuators to excite the rotor and airframe modes of interest, which are then allowed to decay. The moving block technique (see ref. 1) is then used to determine the damped frequency and damping variation with rotor speed. The method has proved useful for tracking the stability of relatively well damped modes. The results of recently completed flight tests of an experimental soft-in-plane rotor are used to illustrate the technique. This technique will also be used for flight flutter tests of the NASA/Army XV-15 Tilt Rotor Research Aircraft, to investigate its propeller whirl flutter stability characteristics, and this application is also discussed briefly.

INTRODUCTION

A soft-in-plane rotor has recently been built and flight tested by Bell Helicopter Company. This type of rotor system has the potential for ground and air resonance instability. The potential mode of instability, the lead-lag motion of the blades coupled with the fuselage rigid body roll mode, has a frequency of 0.75 per rev (3.55 Hz) in the rotating system. The mode was predicted to be well damped, since sufficient elastomeric lead-lag damping was employed. However, since it was the first rotor of this type developed by Bell Helicopter Company, an extensive ground/air resonance test program was conducted to investigate the ground/air resonance phenomena.

The measurement of the stability characteristics of rotary wing aircraft is complicated by the need to excite modes in a rotating system and by the fact that both the rotor and the airframe are subject to steady state harmonic loading. This loading tends to mask the transient response of any relatively well damped mode. The development of an on-line flight flutter testing technique for helicopters or tilt-rotor aircraft hence becomes a formidable task, both to cause the proper excitation and to reduce the data. A flight flutter testing technique has been developed, as described in this paper, to oscillate the rotor controls by means of the series actuators in a sense and a magnitude prescribed by the user.

The authors acknowledge the assistance of Ken Builta of Electronics Development in the design of the rotor excitation system, and Al Eubanks of Scientific and Technical Computing in development of the analysis.

SYMBOLS

$F(\omega)$	Fourier transform of f(t)
SCAS	stability and control augmentation system
$X(\omega)$	Fourier transform of a response
f(t)	excitation signal
t	time
Ω	rotational speed of rotor
ω	frequency of a mode in a dynamics system
ω_1	frequency of the mode of interest in a dynamics system
ω_ζ	blade lead-lag natural frequency

ROTOR EXCITATION SYSTEM

For a soft-in-plane rotor test program, it is desirable to excite the rotor at a relatively low amplitude and at a prescribed frequency. The system developed to perform the excitation for flight flutter testing of the Bell Model 609 soft-in-plane rotor uses the SCAS actuators, driving them from an HP203A dual signal generator. This rotor exciter can supply either a continuous signal of a single frequency, or a pulse spectrum which can be selected to excite only one natural frequency of several which may be present. A functional diagram of the system is shown in figure 1. The upper portion shows the system which drives the rotor, and the lower part shows the nulling system. This nulling system is an option which allows the user to cancel the steady state one-per-rev and two-per-rev signals before the input spectrum is applied, thus isolating the response to the input signal only. Figure 2 shows a diagram of the rotor exciter. Point A has a pulse output to the computer to indicate when the input has been completed. Point B is the demodulated one-per-rev to the nulling system.

The underlying principle behind the single-mode excitation technique can be explained in terms of a linear system with many degrees of freedom. The Fourier transform of the response vector is obtained by post-multiplying the matrix of the frequency response function by the column of the Fourier transform of the forcing function. (See, for example, ref. 2) The frequency response functions exhibit peaks corresponding to natural frequencies of the system.

The shape of the Fourier transform of the forcing function is governed by the shape of the forcing function in the time domain. For example, the Fourier transform of the forcing function depicted in figure 3a is shown in figure 3b. $F(\omega)$ has a large magnitude corresponding to frequency ω_1, and a rather low magnitude elsewhere. Since the Fourier transform of the response, $X(\omega)$, is obtained as a matrix product of frequency response function and $F(\omega)$, the response motions will be motions predominately at the frequency ω_1. (This, however, does not mean that the mode of interest alone is excited and the other

modes are properly suppressed.) Various types of forcing function f(t) can be chosen to produce a desired spectrum $F(\omega)$.

ON-LINE STABILITY ANALYSIS

The Bell experimental Model 609 flex-hinge rotor, a four-bladed, soft-in-plane design, is mounted on a Bell 1501 fuselage. The elastomeric lead-lag hinge offset is 13.2 percent of the rotor radius which is 752 cm (296 in.). The blade first flapping frequency is 5.08 Hz (1.07 per rev). There are two potentially unstable modes for this experimental soft-in-plane rotor system. One, a coupled roll-yaw mode of the fuselage on the landing gear, has a frequency of 2.3 Hz. The other, the blade first lead-lag mode, has a frequency of 3.55 Hz at low strain conditions.

Ground Resonance Test

The roll mode stability was monitored by an accelerometer at the top of the mast. The test oscillated the SCAS actuators in a sense equivalent to moving the cyclic stick in a counter-clockwise direction at a frequency near 2.3 Hz. The aerodynamic hub moments and hub shears then excited the fuselage roll mode at its natural frequency. The high damping, the presence of high one-per-rev response, and some unknown noise made the data reduction difficult. Figure 4a shows the roll mode response at 260 rpm when a 7-Hz filter was used. The moving block analysis of this response indicated the modal damping to be at 19.7 percent critical. Figure 4b shows the result of filtering the same raw data through a 3-Hz analog filter. In this case, the moving block technique showed the modal damping to be at 20.8 percent critical. Since the 3-Hz filter brings out the highly damped roll mode more clearly, and since the calculated damping is approximately the same as in the other case, the decay plots of the roll mode in other ground run conditions were all filtered through 3-Hz filters before undergoing the moving block analysis.

The blade lead-lag motion was sensed by a strain gage on the grip damper arm. For the blade lead-lag stability test, the SCAS actuators were cycled as if the cyclic stick were being moved in a counter-clockwise direction at a frequency of one-per-rev minus the blade lead-lag frequency $(\Omega-\omega_\zeta)$. This is equivalent to exciting the lead-lag mode aerodynamically at its natural frequency in the blade rotating system. Figure 5a shows the response of the lead-lag mode to a SCAS input at high collective (immediately before lift-off) and a rotor speed of 280 rpm. The modal damping obtained from the moving block technique was 4.3 percent critical in the rotating system. The data were then passed through a 4-Hz filter with the results shown in figure 5b. The modal damping determined by the moving block analysis was 4.2 percent critical in the rotating system. The filtering process again highlighted the modal decay and did not affect the moving block result.

A summary of damping variations measured at various rotor speeds for the lead-lag mode and fuselage roll mode in the fixed reference system is shown in figure 6. The decrease in damping with increase in blade collective is attributed to the destabilizing Coriolis force and the characteristic of an elastomeric damper, a phenomenon predicted by the ground resonance analysis.

Air Resonance Analysis

The blade lead-lag mode in hover was also excited with the SCAS actuators. Figure 7 shows the lead-lag decay at the design rotor speed of 285 rpm filtered through a 4-Hz filter. The moving block technique determined the modal damping to be 5.4 percent critical.

XV-15 VTOL FLIGHT FLUTTER TEST PLANS

The NASA/Army XV-15 Tilt Rotor Research Aircraft will enter flight testing in September 1976. Bell Helicopter Company, the prime contractor, is building two of these aircraft which will have a design gross weight of 57.8 kN (13000 lb) and a maximum speed of 364 knots. Of primary interest from the standpoint of flutter are the stability of the coupled rotor/airframe system and flutter of the empennage.

Coupled Rotor/Airframe Stability

The XV-15 has a nacelle on each wingtip. Each nacelle houses a T-53 engine and a transmission, and each transmission drives a 25-foot, gimbaled, stiff-in-plane three-bladed rotor. The nacelles are oriented with their shafts vertical for takeoff, landing, and flight in the helicopter mode, and are mechanically tilted 90 degrees for flight in the airplane mode. To prevent aeroelastic instability of the coupled rotor/airframe system, the wing is designed to be very stiff in torsion and in bending (it is 23% thick with spars at 5% and 50% chord, fully monocoque) and the nacelle is attached to the wing at the front and rear spar to make the attachment stiff in pitch and yaw.

The calculated coupled rotor/airframe stability characteristics in the airplane mode of flight indicate that instability occurs first in the wing chordwise bending mode and, at higher speeds, in wing beamwise bending and in torsion These are shown in figure 8. The instability is similar in nature to propeller nacelle whirl flutter, but involves elastic bending of the blade and elastic deflections of the blade pitch control system in addition to the precession of the rotor disc. There is considerable confidence in the predicted stability characteristics, since the coupled rotor/airframe stability analysis has shown excellent agreement with flutter model tests and with tests of a full-scale semi span wing in the NASA Ames 40 x 80 foot wind tunnel (ref. 3).

Empennage Flutter

The XV-15 has an H-tail, a configuration that gives it good high-speed directional stability characteristics. Although flutter was of concern during the design, the empennage was designed to avoid resonance of the empennage modes with rotor excitation frequencies. For good frequency placement, the horizontal stabilizer is very stiff in bending and torsion. The elevator and rudder are powered by irreversible hydraulic actuators (dual for the elevator) with lock and load mechanisms to make them irreversible in the event of a hydraulic system failure. As a result, the empennage has a large flutter margin that has been confirmed by flutter model tests in the 16-foot transonic tunnel at NASA Langley (ref. 4).

Flight Flutter Testing Method

For tests to determine the frequency and damping of the coupled rotor/airframe modes, the research XV-15 will have series actuators in the wing flaperon and rotor blade collective pitch control linkages. The copilot or flight test engineer will control the amplitude and frequency of the actuators, which have limited authority so that a hardover cannot cause excessive stresses or aircraft responses that the pilot cannot easily control. The actuator frequency response is flat to well above the frequency of the highest coupled mode of interest.

Frequency and damping of each mode of interest will be determined from the decay of that mode. The test procedure will be to select either the flaperon or collective actuator and tune its excitation frequency to the modal frequency, then turn off (the actuators automatically center) and record the decay. This procedure was used in the full-scale test in the 40 x 80 foot wind tunnel, and gave good results. The decays will be monitored and analyzed on the ground for flight safety during flight envelope expansion.

The excitation system will also be used to generate transfer functions by slow-sweeping excitation frequency. These transfer functions will be used for an additional check on the validity of the coupled rotor/airframe stability analysis.

Tests to evaluate the empennage flutter characteristics will excite the empennage modes with doublet inputs to the elevator and rudders. These will be generated through the series SCAS actuators.

CONCLUDING REMARKS

1. For an elastomeric damper such as the one used on the Model 609 blade lead-lag hinge, the characteristics of the material depend on its strain. Since the lead-lag displacement (hence strain) varies with flight conditions, the lead-lag frequency varies throughout the flight test. It was learned from this study that, in the moving block analysis, a good estimate of the assumed frequency of computation could help the convergence.

2. The dynamic and aerodynamic environment of a rotor change as the flight condition changes; hence the steady state one-per-rev and two-per-rev harmonic loads also vary. Therefore it is suggested that the nulling system be retuned whenever the flight condition changes. However this option was not used during the Model 609 test because the rotor synchro was not operational.

3. Because of the limitations on SCAS authority for the Model 609 testing, the signal-to-noise ratio for the modes of interest was relatively low. Therefore, a number of different analog filters were used to clean up the data. Low-pass filters from 3 Hz to 12 Hz, however, made no appreciable difference in damping calculations.

4. The single-mode excitation technique, using the SCAS actuators, produces excellent stability data since the input signal is well under the user's control. Depending on the input magnitude phasing and limitations of the SCAS authority, any mode in a rotary wing aircraft can be excited by the oscillation of the rotor controls in a prescribed manner. But whether the initial condition (mode shape) of the aeroelastic mode of interest is excited properly remains to be seen. The moving block analysis in most cases can be used in conjunction with the single-mode excitation technique to assess the stability information from ground run or flight test with real time computation. This testing and data reduction package is useful for on-line flight flutter testing of rotary wing aircraft.

REFERENCES

1. Anderson, William D.: Investigation of Reactionless Mode Stability Characteristics of a Stiff Inplane Hingeless Rotor System. Preprint No. 734, the 29th Annual National Forum of the American Helicopter Society, May 1973.

2. Lin, Y. K.: Probabilistic Theory of Structural Dynamics. McGraw-Hill Book Company, 1967.

3. Edenborough, Kipling H., Gaffey, Troy M., and Weiberg, James A.: Analysis and Tests Confirm Design of Proprotor Aircraft. AIAA Paper No. 72-803, August 1972.

4. Marr, Roger L., and Neal, Gordon T.: Assessment of Model Testing of a Tilt-Proprotor VTOL Aircraft. The American Helicopter Society Symposium on Status of Testing and Modeling Techniques for V/STOL Aircraft, October 1972.

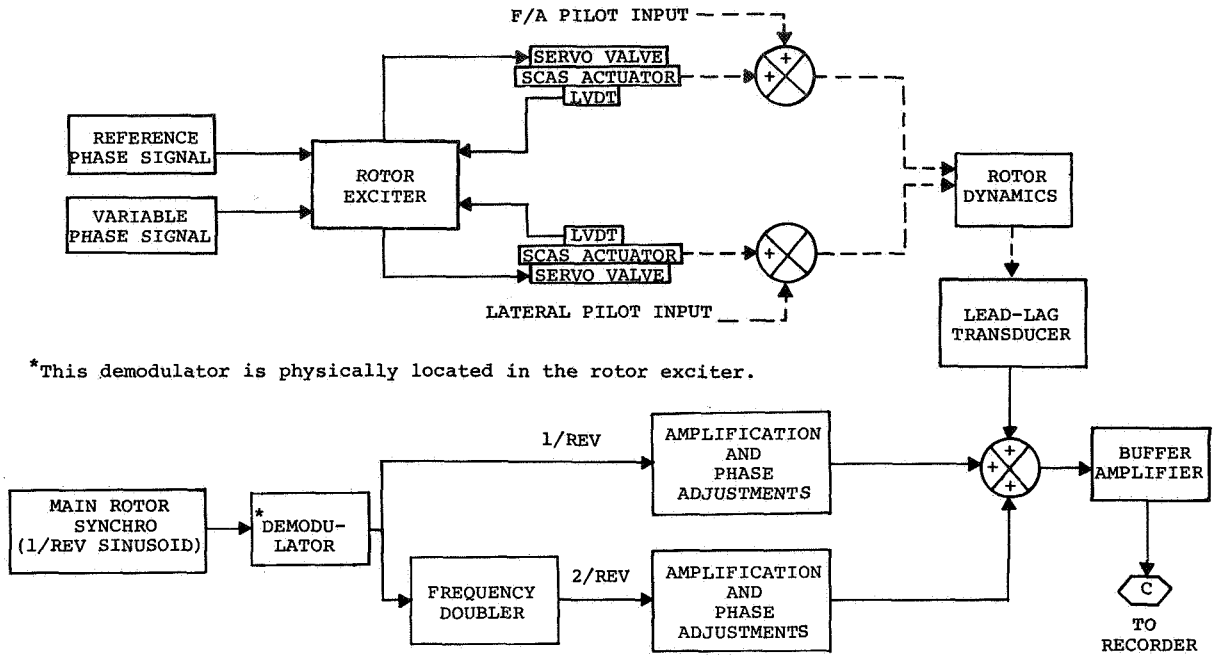

Figure 1. Functional block diagram of rotor excitation system.

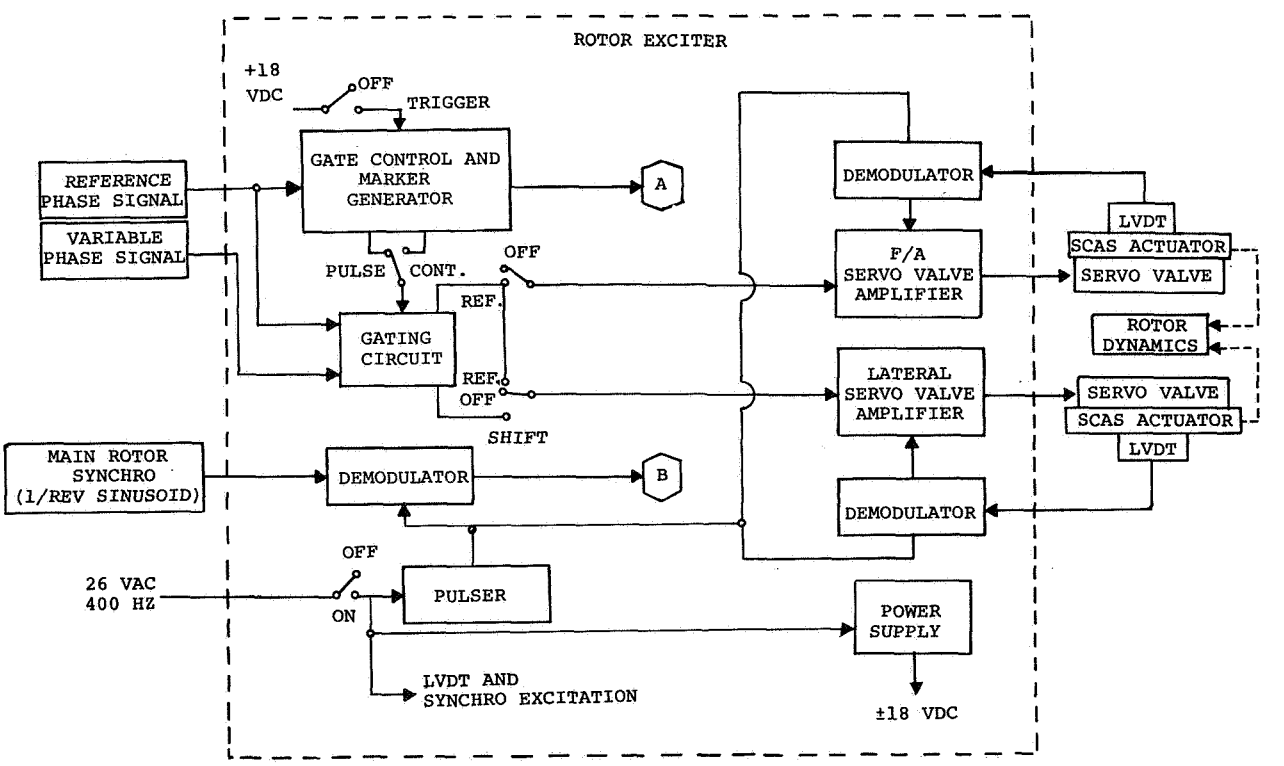

Figure 2. Diagram of rotor exciter.

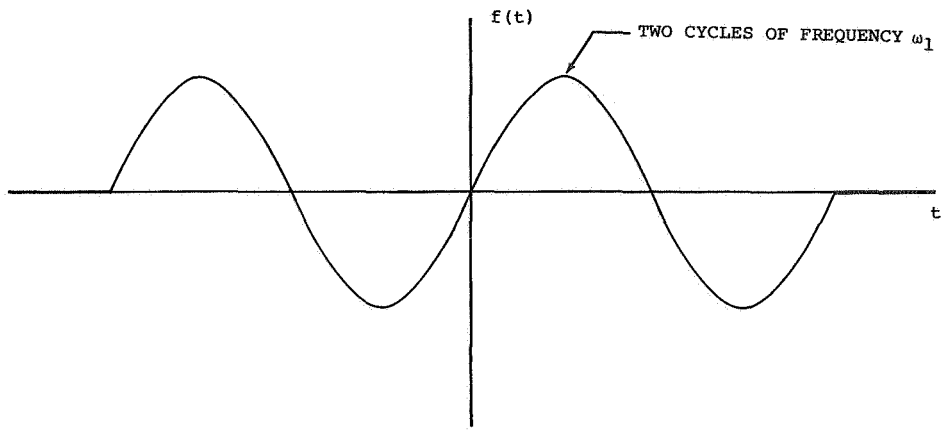

(a) Plot of f(t).

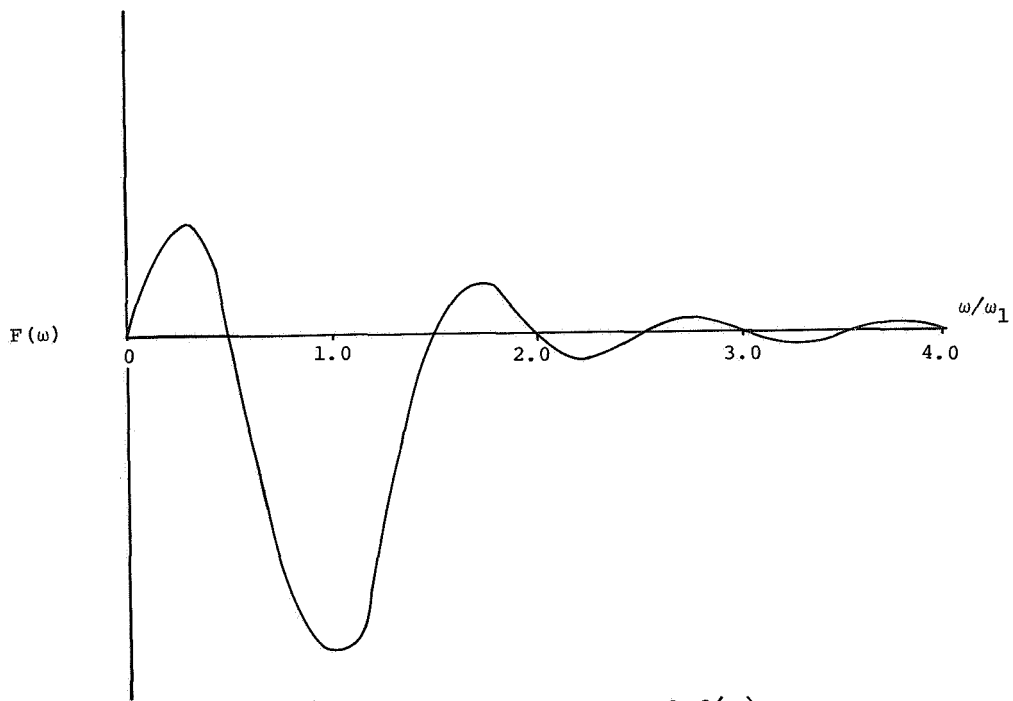

(b) Fourier transform of f(t).

Figure 3. Forcing function f(t).

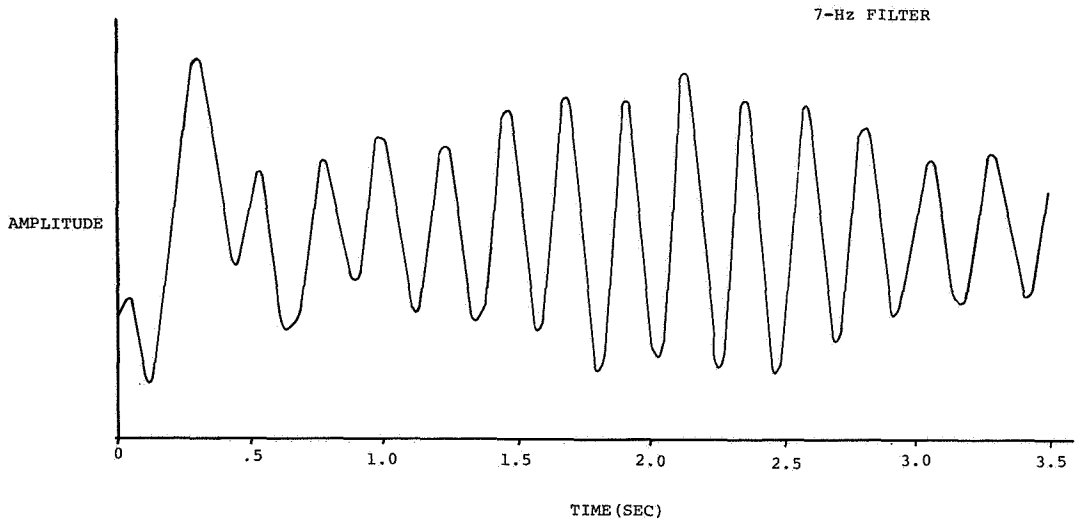

(a) With 7-Hz filter.

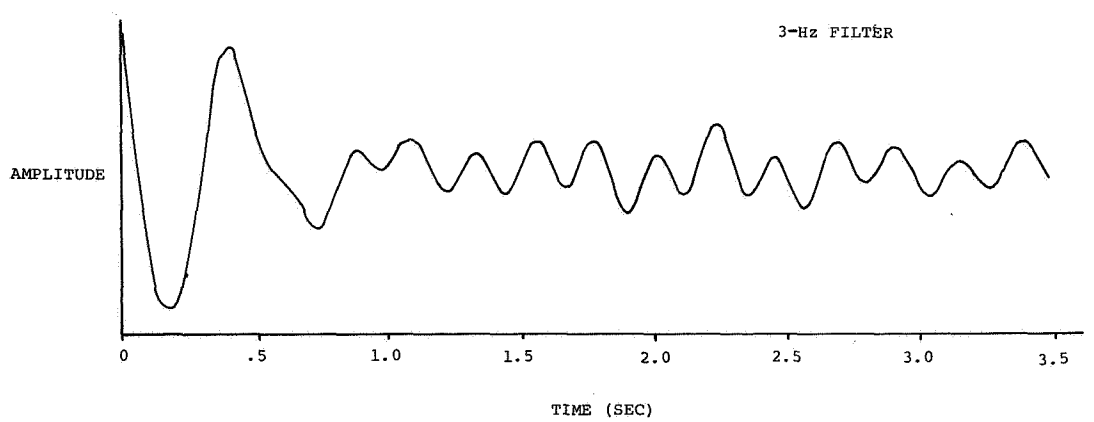

(b) With 3-Hz filter.

Figure 4. Fuselage roll mode decay in ground run. Ω = 260 rpm; low collective.

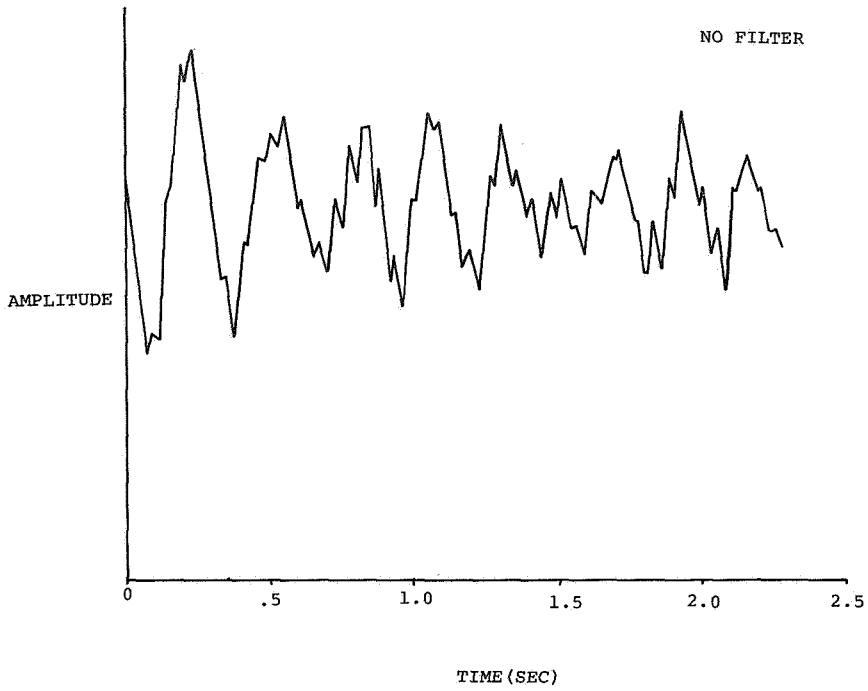

(a) With no filter.

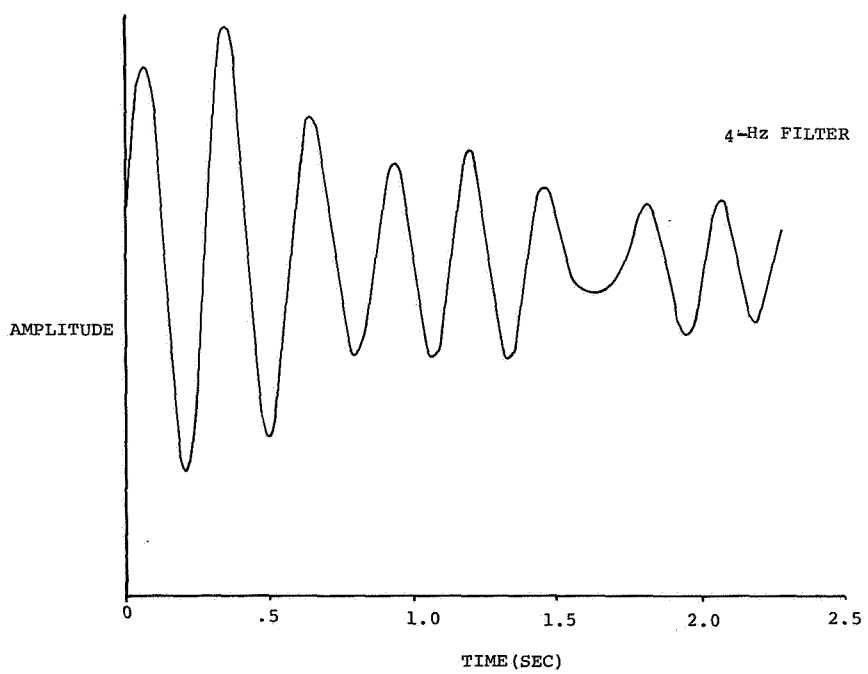

(b) With 4-Hz filter.

Figure 5. Blade lead-lag decay in ground run. Ω = 280 rpm; high collective.

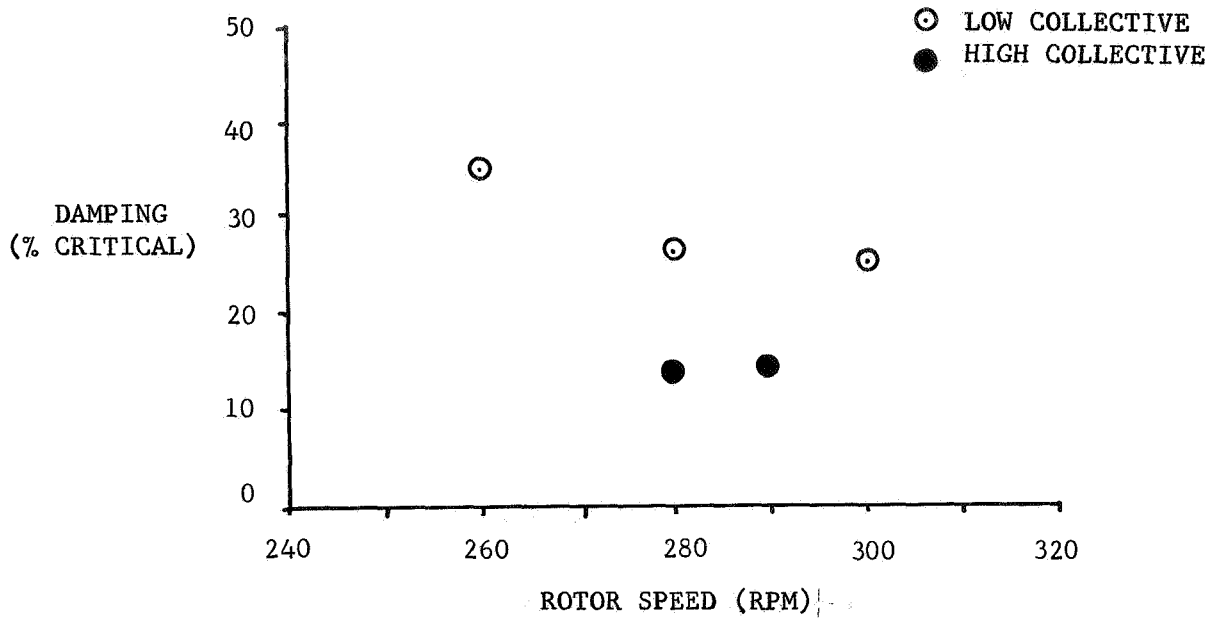

(a) Blade lead-lag damping.

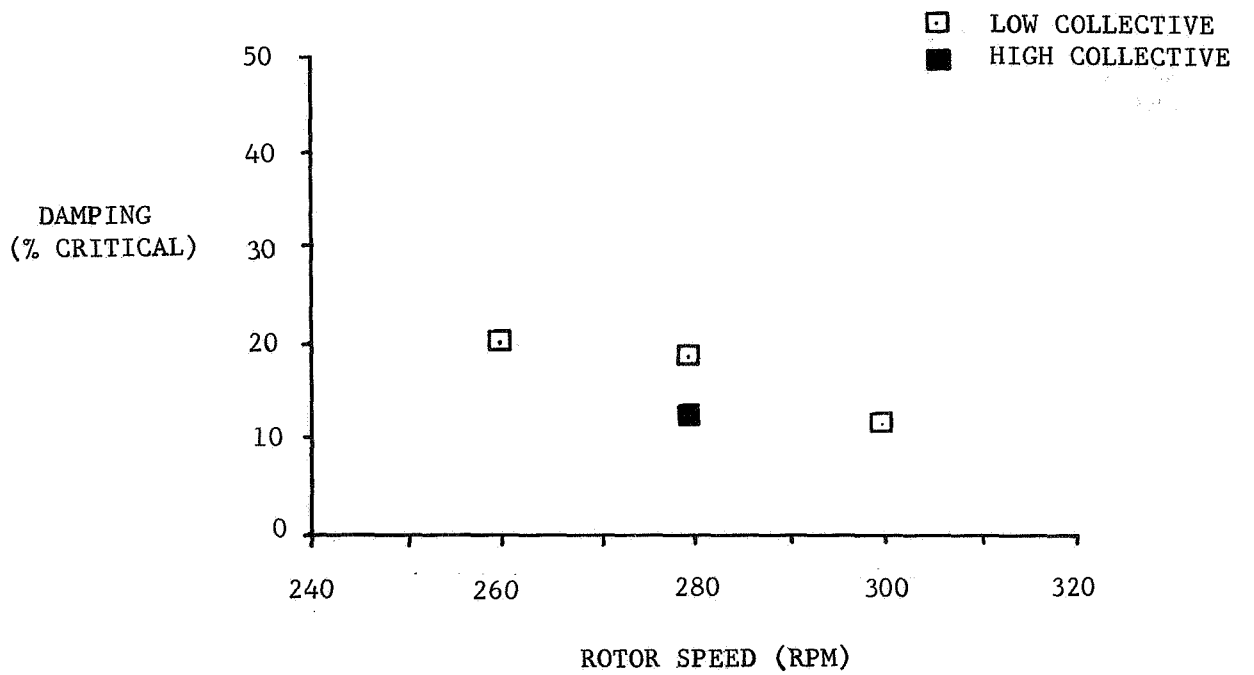

(b) Fuselage roll mode damping.

Figure 6. Damping in fixed system.

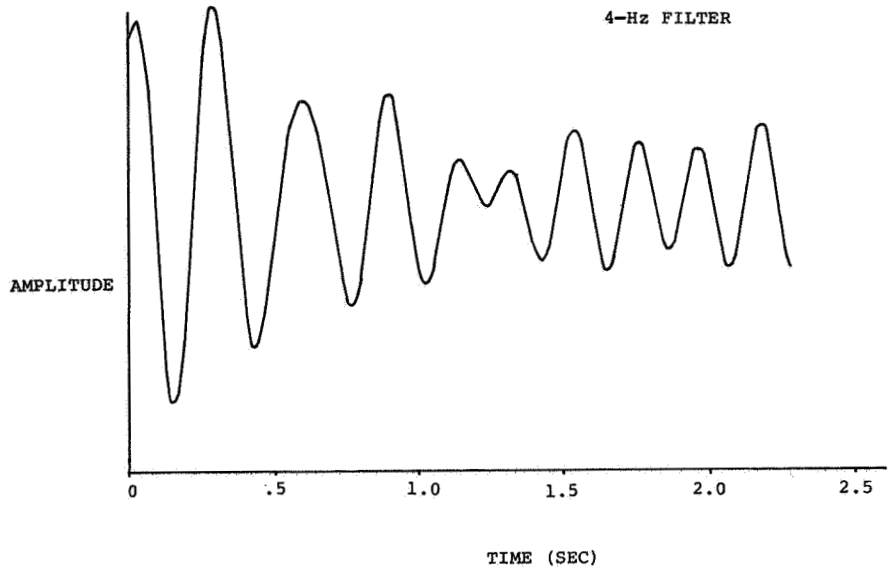

Figure 7. Filtered blade lead-lag decay in hover, Ω = 285 rpm.

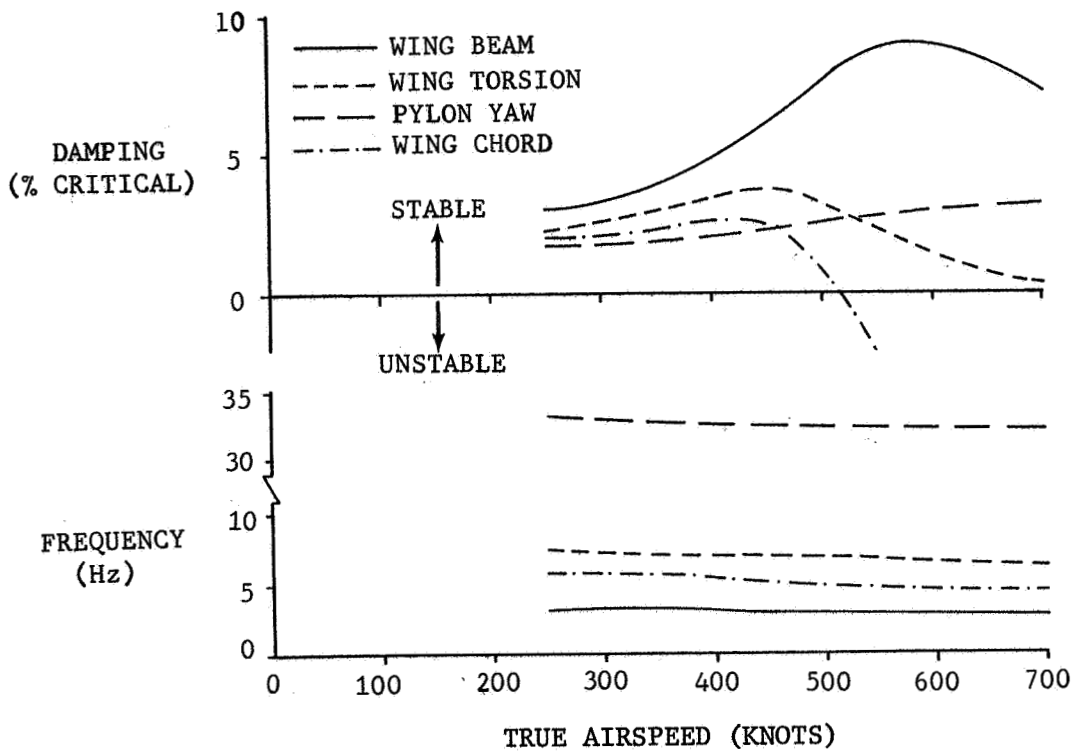

Figure 8. Calculated stability for XV-15 at density altitude 6096 m. (20000 ft).

"The aeronautical and space activities of the United States shall be conducted so as to contribute . . . to the expansion of human knowledge of phenomena in the atmosphere and space. The Administration shall provide for the widest practicable and appropriate dissemination of information concerning its activities and the results thereof."

—NATIONAL AERONAUTICS AND SPACE ACT OF 1958

NASA SCIENTIFIC AND TECHNICAL PUBLICATIONS

TECHNICAL REPORTS: Scientific and technical information considered important, complete, and a lasting contribution to existing knowledge.

TECHNICAL NOTES: Information less broad in scope but nevertheless of importance as a contribution to existing knowledge.

TECHNICAL MEMORANDUMS: Information receiving limited distribution because of preliminary data, security classification, or other reasons. Also includes conference proceedings with either limited or unlimited distribution.

CONTRACTOR REPORTS: Scientific and technical information generated under a NASA contract or grant and considered an important contribution to existing knowledge.

TECHNICAL TRANSLATIONS: Information published in a foreign language considered to merit NASA distribution in English.

SPECIAL PUBLICATIONS: Information derived from or of value to NASA activities. Publications include final reports of major projects, monographs, data compilations, handbooks, sourcebooks, and special bibliographies.

TECHNOLOGY UTILIZATION PUBLICATIONS: Information on technology used by NASA that may be of particular interest in commercial and other non-aerospace applications. Publications include Tech Briefs, Technology Utilization Reports and Technology Surveys.

Details on the availability of these publications may be obtained from:

SCIENTIFIC AND TECHNICAL INFORMATION OFFICE

NATIONAL AERONAUTICS AND SPACE ADMINISTRATION

Washington, D.C. 20546